Endocranial microtomographic study of marine reptiles (Plesiosauria and Mosasauroidea) from the Turonian (Late Cretaceous) of Morocco : palaeobiological and behavioral implications

Rémi Allemand

MUSEUM NATIONAL D'HISTOIRE NATURELLE

Ecole Doctorale Sciences de la Nature et de l'Homme – ED 227

Année 2017 **N° attribué par la bibliothèque**

|_|_|_|_|_|_|_|_|_|_|_|_|_|

THESE

Pour obtenir le grade de

DOCTEUR DU MUSEUM NATIONAL D'HISTOIRE NATURELLE

Spécialité : Paléontologie

Présentée et soutenue publiquement par

Rémi ALLEMAND

Le 21 novembre 2017

Etude microtomographique de l'endocrâne de reptiles marins (Plesiosauria et Mosasauroidea) du Turonien (Crétacé supérieur) du Maroc : implications paléobiologiques et comportementales

---

Sous la direction de **: M^me^ BARDET Nathalie, Directrice de Recherche CNRS**
et les co-directions de **: M^me^ VINCENT Peggy, Chargée de Recherche CNRS**
et **M^me^ HOUSSAYE Alexandra, Chargée de Recherche CNRS**

Composition du jury :

M. JALIL, Nour-Eddine	**Professeur, Muséum national d'Histoire naturelle, Paris**	**Président du jury**
M^me^ WEISBECKER, Vera	**Lecturer, School of Biological Sciences, University of Queensland, Australia**	**Rapporteur**
M. SCHEYER, Torsten	**Research Associate, Palaeontological Institute and Museum, University of Zurich, Switzerland**	**Rapporteur**
M. BRISCHOUX, François	**Chargé de Recherche CNRS, Centre d'Études Biologiques de Chizé, Université de La Rochelle, France**	**Examinateur**
M. BUFFETAUT, Eric	**Directeur de Recherche CNRS, Ecole Normale Supérieure, Paris, France**	**Examinateur**
M^me^ BARDET, Nathalie	**Directrice de Recherche CNRS, Muséum national d'Histoire naturelle, Paris, France**	**Directrice de Thèse**

Remerciements

Cette thèse est le résultat des recherches que j'ai réalisées pendant trois ans au Muséum National d'Histoire Naturelle. Trois ans…ça peut paraitre long mais en réalité c'est assez court et on donne surtout l'impression de courir après le temps (surtout sur la fin !). Le travail que j'ai effectué a été possible grâce à un grand nombre de personnes qui m'ont apporté leur aide et soutien, et avec qui j'ai interagi durant ces trois dernières années. Je tiens donc à prendre le temps ici de remercier toutes ces personnes qui ont, d'une manière ou une autre, permis à ce travail d'être ce qu'il est.

Je voudrais tout d'abord remercier Nathalie Bardet, Alexandra Houssaye et Peggy Vincent, directrice et encadrantes de ma thèse, pour le rôle important que vous avez eu au cours de ces trois ans. Nathalie vous m'avez encadré durant mon stage de Master 2 qui portait sur la description d'un bassin de ptérosaure. Même si ce sujet de Master n'avait rien à voir avec le sujet de thèse, vous avez eu assez confiance en moi pour me proposer de continuer cette aventure. J'ai beaucoup apprécié de travailler sur cette thématique qui m'a permis de m'intéresser à des domaines très variés. Mon seul regret sera de n'avoir pu partir sur le terrain avec vous, j'aurai enfin pu vous tutoyer ! Alexandra, Peggy, si Nathalie a fait figure de "seconde mère" au cours de cette thèse, vous êtes considérées comme les "grandes sœurs". A vous trois, vous formez un "trio de choc". Je pense avoir beaucoup appris à vos côtés, et je ne vous remercierai jamais assez pour votre soutien au quotidien, votre disponibilité, vos conseils, votre patience (surtout quand je dois conclure ou que je suis trop négatif) et votre aide.

Je tiens également à remercier les membres de mon comité de thèse Xavier Pereda Suberbiola, Marc Herbin, Damien Germain, ainsi que mon référent à l'école doctorale du MNHN, Antoine Zazzo, pour leur suivi et les conseils donnés afin de mener à bien ce travail.

Je remercie sincèrement mes rapporteurs, Vera Weisbecker et Torsten Scheyer, ainsi que mes examinateurs, Nour-Eddine Jalil, François Brischoux et Eric Buffetaut d'avoir accepté de lire et d'évaluer le présent travail. J'espère sincèrement qu'il sera à la hauteur de vos attentes.

Je remercie le Labex BCDiv pour le financement de ce travail, et plus particulièrement Myriam Meziou et Anne-Cécile Haussonne pour m'avoir grandement facilité la vie quand il s'agissait de réserver des billets d'avions ou toute autre tâche administrative.

Cette étude sur les endocrânes n'aurait pu être possible sans le matériel adéquat. Un immense merci à Renaud Boistel, Gheylen Daghfous, Anthony Herrel, et Alexandra Houssaye pour m'avoir prêté les nombreux scans qui ont été utilisés au cours de cette thèse. Je tiens également à remercier Erin Maxwell, Michael Polcyn ainsi que le Musée de Rhinopolis pour les prêts des spécimens fossiles. Un très grand merci à Miguel Garcia Sanz et à la plateforme AST-RX du MNHN pour la production des données CT. Toutes ces données ont été traitées à la salle d'imagerie 3D du CR2P. Je tiens vivement à remercier Florent Goussard pour m'avoir formé à l'utilisation de Mimics, pour avoir été présent à chaque fois que j'avais un problème et pour avoir galéré avec moi quand il a fallu exporter un fichier STL à partir de VG Studio Max. Merci également à Damien Germain pour m'avoir formé à l'utilisation de VG, je suis d'accord avec toi, le rendu 3D est bien meilleur que mimics mais ce n'est pas encore au point pour faire un pdf 3D (demande à Florent). Je remercie également Raphaël Cornette pour son aide et ses conseils lors des diverses manipulations sous le logiciel R, quand on te voit faire ça à l'air simple mais une fois qu'on est seul devant son ordi c'est une autre histoire.

Cette thèse a été effectuée au sein du Centre de Recherches sur la Paléobiodiversité et des Paléoenvironnements (CR2P), UMR 7207 et département Histoire de la Terre, et au sein du laboratoire Mécanismes Adaptatifs et Evolution (MECADEV), UMR 7179 et département Adaptations du Vivant du Muséum National d'Histoire Naturelle. Je souhaite donc remercier leurs directrices respectives, Sylvie Crasquin et Fabienne Aujard pour m'avoir accueilli dans leurs laboratoires. Un très grand merci à toutes les personnes avec qui j'ai pu discuter et interagir au cours de ces années, notamment à Arnaud avec qui j'ai pu partager les longues heures à galérer en salle 3D, à Claire, Fabrice, Maxime, Charlène, Malcolm, Constance, François, Valentin, Bérengère, Eli, Donald, Thomas, Julien, Martial (mon premier colocataire de bureau), Séverine, Marion, Léo, Ameline, Ronan, Colas, Yohan, Véronique, Sandrine, Renaud. Je m'excuse par avance pour toute personne qui aurait été oubliée. Ce n'est bien évidement pas volontaire mais plutôt à mettre sur le compte d'une écriture tardive des remerciements (pourtant on m'avait prévenu de tenir une liste…).

Je tiens particulièrement à remercier toute l'équipe de "Palbot". Vous êtes en grande partie responsable du fait que l'on se sente vite comme chez soi dans ce bâtiment. Merci à Dario, Olivier, Eloïse, Marc, Jean, Anaïs, Sandra. Merci pour ces moments partagés. Merci pour votre soutient, vos petits mots d'encouragement. Je me dois de remercier tout particulièrement les thésards, post-doc et membres occasionnels de la "Palbot", mon actuel colocataire de bureau Cédric, Mélanie, Guillaume, Yingying, Julien, Pauline, Hugo. Ces moments partagés avec vous ont été très agréables, j'espère très vite fêter le rendu de thèse au cours d'un "afterwork" que Cédric nous aura planifié.

Je tiens également à remercier mes parents, mes sœurs ainsi que toute ma famille pour votre soutien et l'intérêt que vous avez porté à mon travail. Un très grand merci à tous les amis "hors muséum" avec qui j'ai toujours autant de plaisir à discuter du métier si peu ordinaire de paléontologue. Merci de montrer autant d'intérêt dans ce que je fais. Un très grand merci à Anouck pour ton soutien, ton aide au moment de l'écriture, et pour ta présence tout au long de cette aventure.

TABLE OF CONTENTS

Introduction

Early Permian mesosaurs are considered as the first known reptiles having returned to an aquatic lifestyle (Bardet et al., 2014). Later, during the Mesozoic era, numerous clades of reptiles underwent a spectacular return to an aquatic life, colonizing most marine environments (e.g., Houssaye, 2009; Bardet et al., 2014). These taxa were highly diversified, both systematically, morphologically and ecologically. At least seven clades have formed the major component of Mesozoic marine ecosystems (Benson and Butler, 2011a). They are ichthyosaurs, sauropterygians and thalattosaurs, exclusively marine and only known from the Mesozoic, whereas chelonians, crocodyliforms, rhynchocephalians and squamates included marine representatives at only some periods of their evolutionary history (Bardet et al., 2014).

Marine reptiles show a great diversity in size, ranging from 20 cm to 21 m in total length (Houssaye, 2009; Nicholls and Manabe, 2004). Most of these taxa were carnivorous, their diet might include osteichthyans, chondrychthyans, invertebrates, other marine reptiles (Motani, 2009), however, some "herbivorous" forms have been also reported (e.g., von Huene, 1936; Chun et al., 2016). Marine reptiles display different morphologies and explored many different swimming styles (e.g., Massare, 1988). Generally, most taxa adapted to shallow water environments, such as mesosaurs, exhibit a slender body, an antero-posteriorly elongated skull with a long neck, and long limbs not modified into paddles but with a lengthening of the fingers and a long laterally-compressed tail (Houssaye, 2009), whereas taxa adapted to a pelagic environment, such as most of the ichthyosaurs, usually are best known for their peculiar and unique bauplan resembling that of cetaceans or "fishes" and that includes a fusiform body shape, an elongated snout, limbs modified into compact hydrofoils, as well as dorsal and caudal fins essentially composed of soft-tissue (Bardet et al., 2014). Some marine reptile lineages survived the Cretaceous-Palaeogene boundary, being known in the Cenozoic up to the present time but most of them disappeared during the Mesozoic (Bardet et al., 2014). Nowadays, however, compared to this Mesozoic radiation, marine reptiles are only minor components of the marine biotas, being represented essentially by turtles and snakes (Rasmussen et al., 2011).

Among these Mesozoic marine reptiles, sauropterygians (including plesiosaurians) and mosasauroid squamates constitute two of the major clades. During the Late Cretaceous, they

co-existed and their association has been documented in numerous sites (Vincent et al., 2013). Because it is generally assumed that both mosasauroids and plesiosaurians represented top-predators of these marine environments (Vincent et al., 2013), these associations question their interactions and niche partitioning. Adaptations to the aquatic realm for both mosasauroids and plesiosaurians have been extensively studied from the perspective of modifications of the post-cranial skeleton (e.g., Lingham-Soliar, 1992; Nicholls and Godfrey, 1994; Caldwell, 1997; O'Keefe, 2002; Lindgren et al., 2008, 2011; Araújo et al., 2015), as well as from physiological (i.e., diet, reproduction, locomotion, thermoregulation), micro-anatomical and histological ones (e.g., Massare, 1987, 1988, 1994; Caldwell and Lee, 2001; Bernard et al., 2010; O'Keefe and Chiappe, 2011; Houssaye, 2013; Bardet et al., 2015). However, although few studies have suspected vomerolfaction and a well-developed vision from morphological evidences in both clades (e.g., Cruickshank et al., 1991; Lingham-Soliar, 1994; Everhart, 2002; Schulp et al., 2005), little is known about their sensorial abilities or the sensory changes accompanying their adaptation to life and partitioning in aquatic environments.

How can the sensorial abilities of an extinct species be reconstructed? Despite the relatively abundant fossilized remains of ancient organisms, this task is hard. The brain itself is not preserved in fossil vertebrates (but see the study by Pradel et al., 2009 for a possible exception), but some evidences of its maximal size and shape are available from the endocranial surface of the cranial cavity in most groups (Walsh and Knoll, 2011). A cranial endocast does not represent the actual morphology of the brain and brainstem only, but also the contours of associated brain tissues in contact with the internal surface of the braincase, such as the meninges, the blood vessels and the venous system (Witmer et al., 2008; Witmer and Ridgely, 2009). These tissues may account for significant proportions of the endocranial space (Witmer et al., 2008; Walsh and Knoll, 2011), and the degree of brain accuracy offered by the endocasts varies greatly between clades and over ontogeny (e.g., Jerison, 1973; Hopson, 1979; Macrini et al., 2007; Witmer et al., 2008; George and Holliday, 2013; Hurlburt et al., 2013). However, it is generally admitted that these endocasts may provide important information about the central nervous system in extinct animals (Walsh and Knoll, 2011) and may be used as relevant information about their sensory abilities and behavior (Witmer et al., 2008).

Recent advances in non-invasive imaging have increased the number of taxa for which endocranial morphology is accessible. As a result, many studies focusing on sensory and behavioral inferences have been published for extinct mammals (e.g., Macrini et al., 2007; Silcox et al., 2010; Ahrens, 2014; Orihuela, 2014; Dozo and Martinez, 2016), birds (e.g., Burish et al., 2004; Milner and Walsh, 2009; Picasso et al., 2009, 2010; Gold et al., 2016; Proffitt et al., 2016), non-avian dinosaurs (e.g., Rogers, 1999; Brochu, 2000; Franzosa and Rowe, 2005; Witmer et al., 2008; Knoll et al., 2012; Carabajal and Succar, 2015; Brasier et al., 2017) and pterosaurs (e.g., Witmer et al., 2003; Eck et al., 2011; Codorniú et al., 2016).

However, such techniques have been rarely applied to Mesozoic marine reptiles. Indeed, only few studies have been published about the endocranial anatomy of extinct turtles (e.g., Carabajal et al., 2013), thalattosuchians (e.g., Herrera et al., 2013; Herrera, 2015; Brusatte et al., 2016; Pierce et al., 2017), ichthyosaurians (e.g., Marek et al., 2015; Abele, 2017), basal sauropterygians (e.g., Neenan and Scheyer, 2012; Voeten et al., 2014). Finally, although microtomographic studies have been performed on the inner ear of plesiosaurians and mosasauroids (e.g., Georgi, 2008; Georgi and Sipla, 2008; Cuthbertson et al., 2015; Yi and Norell, 2015; Neenan and Benson, 2017), the endocast of both taxa, which represent the main co-existing clades of apex predatory marine reptiles during the Late Cretaceous, has never been investigated through such approach, and thus used for sensory or behavioral inferences.

The reconstruction of sensory abilities and behavior in extinct species usually begins with an examination of their phylogenetic relationships with extant ones (Rogers, 2005). Indeed, vertebrate brains may differ in their organization (Butler and Hodos, 2005) and comparisons between fossil taxa and their closest living relatives appear more insightful (Rogers, 2005). In this context, the phylogenetic position of mosasauroids shows the relevance to consider extant squamates as a comparative model, especially snakes and monitor lizards that are regarded as their possible sister-group (e.g., Lee, 2005; Conrad, 2008; Reeder et al., 2015) (see Chapter 2). As far as plesiosaurians are concerned, no extant directly-related species exist (Smith, 2008), but as they are generally considered as derived diapsids more closely related to lepidosauromorphs than to archosauromorphs (e.g., Motani et al., 1998), comparisons with extant squamates as well as other living marine reptiles, such as sea-turtles that moreover share a similar mode of locomotion, may also be relevant.

To date, there is an increasing number of endocranial studies performed on extant taxa, mainly mammals (e.g., Lyras and Van der Geer, 2003, Lefebvre et al., 2004, Macrini et al. 2007; Bienvenu et al., 2011; Racicot and Colbert, 2013; Ahrens, 2014; Danilo et al, 2015), and birds (e.g., Kawabe et al., 2013, 2015; Carril et al., 2015; Corfield et al., 2015).

Conversely, endocranial studies are scarcer among non-avian reptiles or even nonexistent (e.g., rhynchocephalians). Only few studies have considered the endocast of extant crocodile (e.g., Rogers, 1999; Witmer et al., 2008; Jirak and Janacek, 2017) and both terrestrial and marine turtles (e.g., Wyneken, 2001; Carabajal et al., 2013; Carabajal et al., in press). As far as squamates are concerned, computed tomography has already been used for different purposes, such as the skull morphology (e.g., Rowe et al., 1999; Bever et al., 2005; Rieppel and Maisano, 2007; Comeaux et al., 2010), the study of the brain itself (e.g., Anderson et al., 2000), the inner ear (e.g., Walsh et al., 2009; Boistel et al., 2011; Christensen et al., 2012; Yi and Norell, 2015; Palci et al., 2017), the vascular network (e.g., Porter and Witmer, 2015), or the lacrimal system (e.g., Souza et al., 2015). However, to date, only a single study has focused on the endocast of the burrowing snake *Uropeltis woodmasoni* Theobald, 1876 (Olori, 2010). Consequently, the endocranial anatomy in extant squamates remains almost unknown and much needs to be done. In this context, snakes, which exhibit a large variability in their lifestyle (fossorial, arboreal, marine, terrestrial, semi-aquatic), constitute an appropriate group for comparisons with fossils studied in this work.

Based on exceptionally preserved specimens of both mosasauroids and plesiosaurians from the Turonian outcrops of Goulmima (Southern Morocco), the aims of this PhD are: 1) to describe for the first time the endocranial anatomy of these coeval major clades of Late Cretaceous apex predators in order to provide clues about their sensory abilities and to interpret them for behavioral inferences; 2) to describe - also for the first time - for a comparative approach the endocranial anatomy of related extant squamates, mainly snakes but also varanids and amphisbaenians in order to understand the form-function relationship associated to endocasts and to apprehend possible phylogenetic and ecological signals; 3) As a result, to discuss about the paleobiological and paleoecological adaptations of both mosasauroids and plesiosaurians in order to understand their cohabitation, interactions and niche partitioning.

The present manuscript is organized as follows:

- **Chapter 1** introduces the deposit of Goulmima, Southern Morocco. It replaces the locality in its stratigraphic and paleoenvironmental context, and paints the faunal assemblages discovered in this area.
- **Chapter 2** depicts the state of knowledge on the paleobiology, paleoecology and systematic of both mosasauroids and plesiosaurians.
- **Chapter 3** aims to define the paleoneurology and the kind of information associated to endocasts.
- **Chapter 4** introduces the material analyzed and the methodology used for endocranial reconstructions.
- **Chapter 5** corresponds to the endocranial study performed on snakes. It provides evidences that snake endocasts reflect both phylogenetic and ecologic signals.
- **Chapter 6** is a preliminary study that aims to introduce the endocranial anatomy of both varanids and amphisbaenians in order to consider the possible signal associated to the structure.
- **Chapter 7** present the endocranial anatomy of the mosasauroid *Tethysaurus nopcsai.*
- **Chapter 8** consist in the anatomical descriptions and identifications of the plesiosaurian skulls studied during this PhD Thesis.
- **Chapter 9** presents the plesiosaurian endocranial antomy through the reconstructions performed for three specimens.
- **Chapter 10** presents the paleoecological reconstruction of the Early Turonian (Late Cretaceous) marine reptile assemblage of Goulmima, Southern Morocco.

Abbreviations of the institutions

AMNH, American Museum of Natural History, New York, U.S.A.

D, Musée de Rhinopolis, Gannat, France

ESRF, European Synchrotron Radiation Facility, Grenoble, France

IC2MP, Institut de Chimie des Milieux et Matériaux, Poitiers, France

IPHEP, Institut de Paléoprimatologie, Paléontologie Humaine; Evolution et Paléoenvironnements, Université de Poitiers, France

LACM, Natural History Museum of Los Angeles County, Los Angeles, California, U.S.A.

MCZ, Museum for Comparative Zoology, Harvard University, U.S.A.

MNHN, Muséum national d'Histoire naturelle, Paris, France

MNHNGr, Muséum d'Histoire naturelle de Grenoble, Grenoble, France

MOR, Museum of the Rockies, Bozeman, Montana, U.S.A.

NHMUK, Natural History Museum, London, UK

PMO, Palaeontological Museum, University of Oslo, Norway

ROM, Royal Ontario Museum, Toronto, Ontario, Canada

SGU, Saratov State University, Saratov, Russia

SMNK, Staatliches Museum für Naturkunde Karlsruhe, Germany

SMNS, Staatliches Museum für Naturkunde, Stuttgart, Germany

SMU SMP, Shuler Museum of Paleontology, Southern Methodist University, Dallas, U.S.A.

UCMP, University of California Museum of Paleontology, Berkeley, U.S.A.

UMO, Urwelt-Museum, Bayreuth, Germany.

UQUAM, Université du Québec à Montréal, Canada

ZRC, Zoological Reference Collections, National University of Singapore

Chapter 1

Mosasauroidea (Squamata) and Plesiosauria (Sauropterygia): Phylogenetical context, paleobiology and paleoecology

Mosasauroidea and Plesiosauria constitute two extinct reptile clades that underwent a spectacular radiation in the aquatic realm during the Mesozoic era (Fig. 1.1). Both clades exhibit different adaptations to an aquatic lifestyle and represent major components, as top-predators, of the marine Mesozoic ecosystems (Bardet et al., 2014). The aim of this section is to report the state of knowledge relative to both mosasauroids and plesiosaurians. For this, their phylogenetic contexts, paleobiologies and paleoecologies are considered.

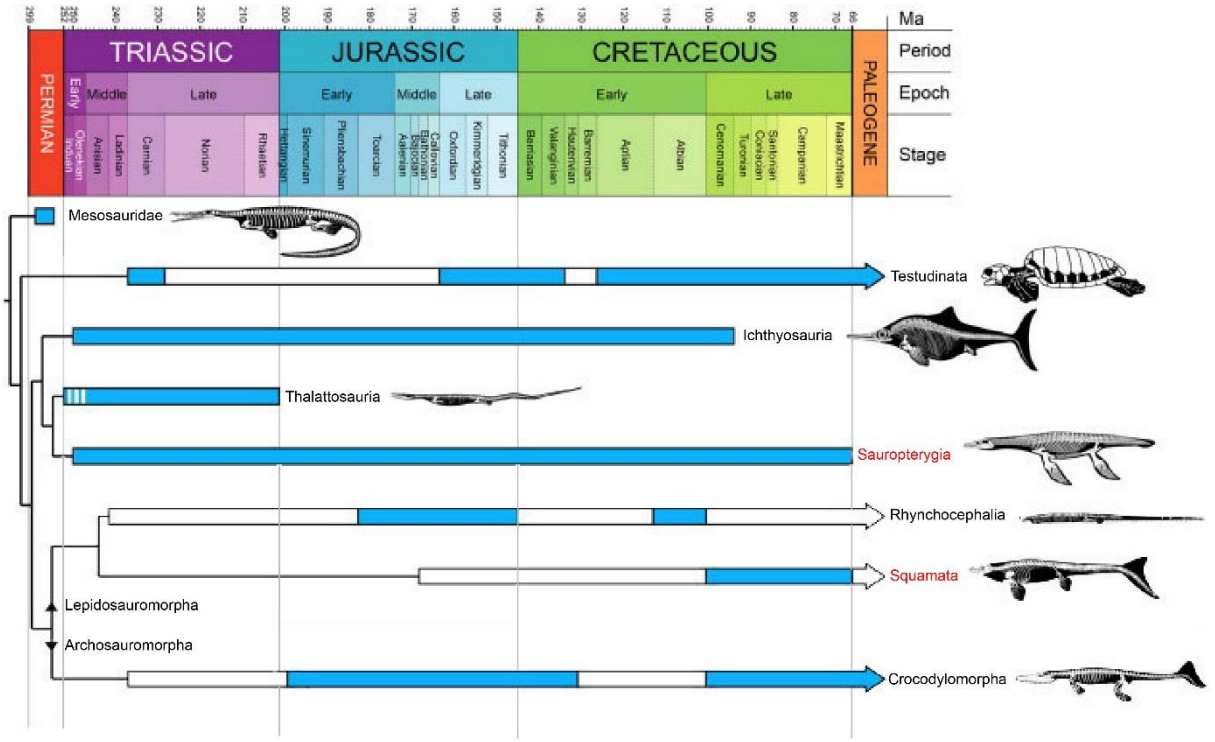

Fig. 1.1. Schematic phylogenetic relationships of Mesozoic marine reptiles. Blue color indicates the presence of marine representatives for each clade (from Bardet et al., 2014).

1.1. Mosasauroidea (Squamata)

Mosasauroids invaded the marine realm, and freshwater habitats (e.g., Makádi et al., 2012), at the beginning of the Late Cretaceous (Cenomanian, 98 Ma) and became extinct at the end of the Maastrichtian (66 Ma). Their remains have been recovered from all continents (Polcyn et

al., 2014) and across a wide range of latitudes, from near the Arctic (Lindgren and Siverson, 2002) to the Antarctic (Martin, 2006; Fernández and Gasparini, 2012).

Since Camper (1800), mosasauroids are universally regarded as squamate reptiles, however, their affinities within other squamates remain questioned and the phylogenetic position of these marine predators has been the subject of an animated scientific debate for centuries. Camper (1800) and Cuvier (1808) were the first scientists to consider mosasauroids as closely related to the living monitor lizards (Varanidae), and this single hypothesis persisted for more than 150 years (e.g., Baur, 1890; Camp, 1923; McDowell and Bogert, 1954). However, since 1869, Cope has recognised several points of similarity between mosasaurs and snakes, leading him to introduce the order Pythonomorpha to include all mosasaur taxa known at that time and snakes (Cope, 1869). Cope argued for a systematic relationship between mosasaurs and snakes based on common traits in their lower jaws, including a free mandibular symphysis and a straight vertical splenial-angular joint, allowing a large gape to facilitate feeding on large preys (Cope, 1869, 1872). Based on similarities in tooth eruption patterns between mosasaurs and snakes, Lee (1997a, b) corroborated that snakes and mosasaurs are derived from a common ancestor characterized by recumbent replacement teeth (Lee, 1997a). Lee (1997b) redefined the clade Pythonomorpha as the most recent common ancestor of mosasauroids and snakes, and all its descendants; and several phylogenetic studies based on morphology (Fig. 1.2A) supported this clade (Lee and Caldwell, 1998; Caldwell, 1999; Lee and Caldwell, 2000; Pierce and Caldwell, 2004; Reeder et al., 2015). Conversely, several studies continue to regarded mosasauroids as sister group of varanoids (e.g., Carroll and DeBraga, 1992; DeBraga and Caroll, 1993; Zaher and Rieppel, 1999; Rieppel and Zaher, 2000a, b, 2001; Schulp et al., 2005; Liu et al., 2016, see Fig. 1.2B).

The descriptions of several fossil hind-limbed snakes were supportive of a marine snake origin and thus to mosasaur-snake affinities (e.g., Caldwell and Lee, 1997; Scanlon et al., 1999; Lee, 2005; Palci and Caldwell, 2007; Lee et al., 2016; Palci et al., 2017). However, the ecology of snake origin remains highly debated and several studies favouring a burrowing snake ancestor placed snakes as the sister group to an (Amphisbaenia, Dibamidae) clade, and thus not as the sister group of mosasauroids, which is rather nested within Varanoidea (e.g., Vidal and Hedges, 2004; Conrad, 2008; Longrich et al., 2012; Hsiang et al., 2015; Martill et al., 2015; Yi and Norell, 2015; Liu et al., 2016).

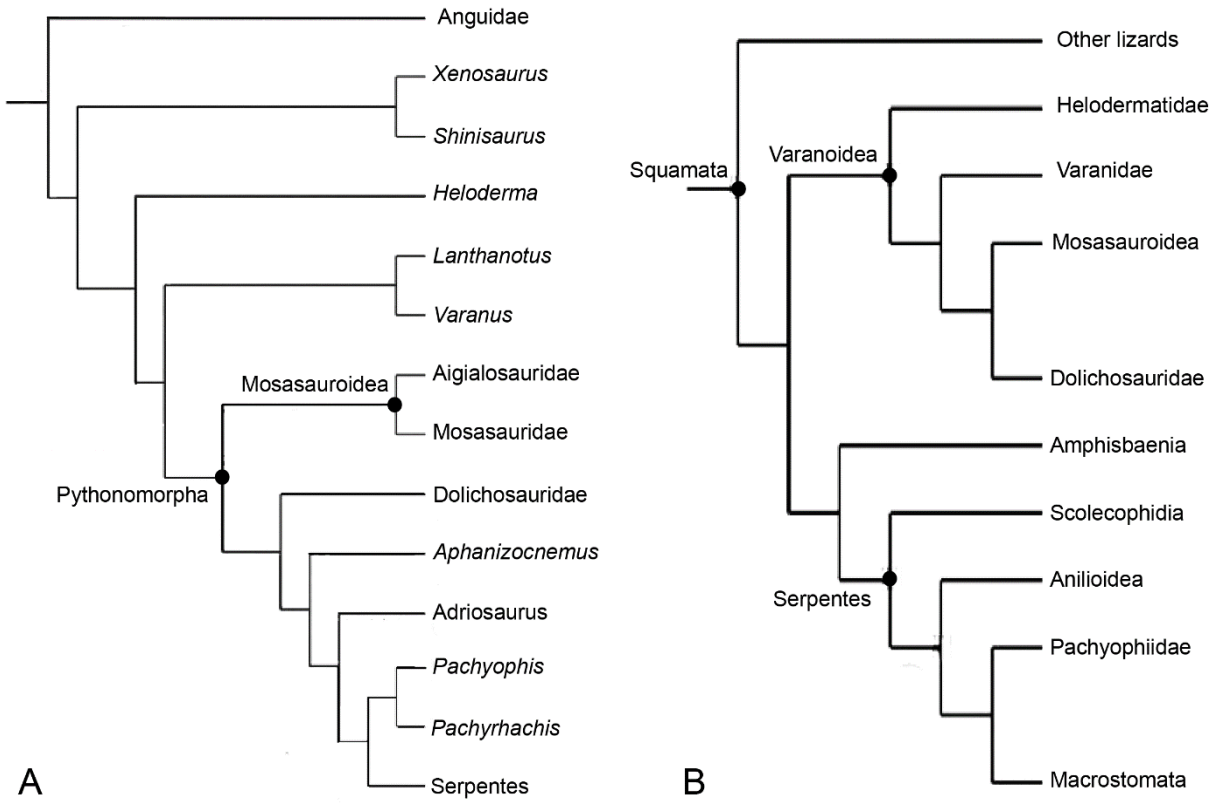

Fig. 1.2. Hypotheses of squamates interrelationships illustrating: (A) Mosasauroids and snakes included among Pythonomorpha (modified from Palci and Caldwell, 2007); (B) Mosasauroids placed within Varanoidea and snakes as the sister group to an (Amphisbaenia, Dibamidae) clade (modified from Zaher, 1998 and Rieppel and Zaher, 2000a).

Although the phylogenetic relationships among this clade are still debated (e.g., Bell and Polcyn, 2005; Caldwell and Palci, 2007; Dutchak and Caldwell, 2009; Palci et al., 2013), the term Mosasauroidea, introduced by Camp (1923), is now defined as including Aigialosauridae and Mosasauridae (e.g., Bell, 1997; Lee, 1997a, b; Bardet et al., 2008; Simões et al., 2017). These Late Cretaceous marine squamates display three main morphotypes along their evolutionary history that illustrate steps in their gradual adaptation to increasing open-sea habitats (e.g., Bell and Polcyn, 2005; Caldwell and Palci, 2007; Bardet et al., 2008). The most basal mosasauroids present plesiopedal (i.e., plesiomorphical "terrestrial-like") limbs (Fig. 1.3A), with elongated propodials generally occupying more than one-half of the limb length, non-expanded mesopodials and short cylindrical epipodials (Bell and Polcyn, 2005). They also display a plesiopelvic anatomy (i.e., typical squamate pelvic girdle in which the ilium is

anchored to the vertebral column via sacral ribs) and their tail is slightly modified for swimming (Fig. 1.3A). These small forms (less than 2 meters long) were living in shallow water and are were probably poorly active swimmers (Houssaye, 2013; Bardet et al., 2014). Plesiopedal and hydropelvic mosasauroids for their part had terrestrial-like limbs but no sacrum, no posterior superior iliac process and a highly developed anterior superior iliac process (Caldwell and Palci, 2007). These taxa are medium-sized forms (from 3 to 6 meters long) and are considered as more active swimmers than the plesiopelvic forms but still not efficient pelagic swimmers (Houssaye et al., 2013; Bardet et al., 2014). Finally, hydropedal and hydropelvic mosasauroids (Fig. 1.3B) display limbs significantly shortened modified as flippers, and no sacrum. These latter forms present limbs highly optimized for marine life and extensive modification of the tail for underwater propulsion (Bell and Polcyn, 2005). It is important to note that these categories defined here refer to ecological grades (Dutchak, 2005) and have no phylogenetic significance.

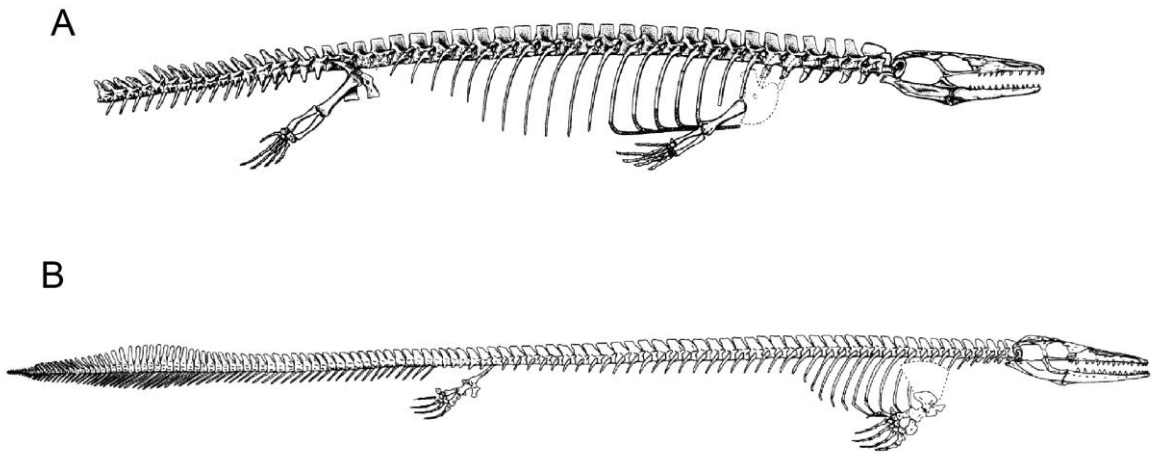

Fig. 1.3. Skeletal reconstructions of **(A)** the plesiopedal and plesiopelvic mosasauroid *Komensaurus carrolli* and of **(B)** the hydropedal and hydropelvic mosasauroid *Clidastes sternbergi* (modified from Caldwell et al., 1995). Not to scale.

Several studies on tooth morphology, jaw function and stomach contents demonstrated a cosmopolitan diet within mosasauroids including invertebrates, osteichthyans, chondrychthyans, birds, turtles and even other marine reptiles such as plesiosaurians or other mosasauroids (e.g., Dollo, 1887; Williston, 1899; Sternberg, 1922; Camp, 1942; Bjork, 1981; Martin and Bjork, 1987; Bell and Martin, 1995; Mulder, 2003; Schulp, 2005; Bardet et al., 2015). Although the breeding ecology of mosasauroids has remained speculative for decades,

discoveries provided evidence supporting mosasauroid viviparity (e.g., Caldwell and Lee, 2001; Field et al., 2015). In addition, histological evidences have shown that mosasauroids had a high growth rate (e.g., Houssaye and Bardet, 2012; Houssaye et al., 2013), which is in accordance with the geochemical ones obtained by Bernard et al. (2010) who suggested that hydropelvic mosasauroids might have been partially homeothermic (i.e., stable internal body temperature regardless of external influence). Based on dental isotopic data, they indeed estimated that these taxa exhibited high body temperatures (between 35±2°C and 39±2°C: Bernard et al., 2010). However, these values were lowered by Motani (2010), who suggested that hydropelvic mosasauroids might have been gigantothermic (i.e., able to maintain elevated body temperature by virtue of large body size and possibly insulation), hypothesis supported by Houssaye (2013). Finally, the recognition of decompression syndrome-related pathology (in the form of avascular necrosis) revealed that some mosasauroids were capable to realize deep, prolonged, or repetitive diving (Rothschild and Martin, 2005).

Little information exists about the sensory abilities in mosasauroids and those that exist are contradictory. Based on the large size of the orbits and the narrow aperture of the vomeronasal organ found in some specimens, Lingham-Soliar (1995) and Polcyn (2010) suggested that vision in mosasauroids was more important than olfaction. This hypothesis has been corroborated by evidences of binocular vision in some mosasauroid species (e.g., halisaurines: Konishi et al., 2016) and possible adaptations to an underwater vision through the presence and shape of sclerotic rings (Yamashita et al., 2015). Conversely, the presence of paired fenestrae in the palate associated with the vomers, as well as the presence of pterygoid teeth led Schulp et al. (2005) to suggest that mosasauroids had a forked tongue, indicating a well-developed vomeronasal chemoreception.

1.2. Plesiosauria (Sauropterygia)

Plesiosaurians represent one of the longest-persisting groups of Mesozoic marine reptiles, ranging stratigraphically from the Late Triassic to the latest Cretaceous (e.g., Sennikov and Arkhangelsky, 2010; Benson et al., 2012; Vincent et al., 2013). Plesiosaurians went extinct during the Cretaceous–Paleogene biotic crisis (Gasparini et al., 2003a; Vincent et al., 2011). However, during the Late Cretaceous, they had a worldwide distribution, including high-

latitude seas surrounding Antarctica (Gasparini et al., 2003b; Novas et al., 2015) and were very diversified (Vincent et al., 2011).

Plesiosaurians are part of the Sauropterygia (Fig. 1.4), with the nothosaurs, pachypleurosaurs, and placodonts (e.g., Neenan et al., 2013). All these taxa are characterized by the presence of a single pair of temporal fenestrae at the rear of the skull (i.e., euryapsid), a condition shared with ichthyosaurs and opposed to the two pairs of temporal fenestrae found in most other diapsids. The Euryapsida clade is variously considered a monophyletic taxon within diapsids (e.g., Caldwell, 1997), or a polyphyletic assemblage (Müller, 2003). In addition, the exact relationships within and among sauropterygian groups are still debated (Neenan et al., 2013).

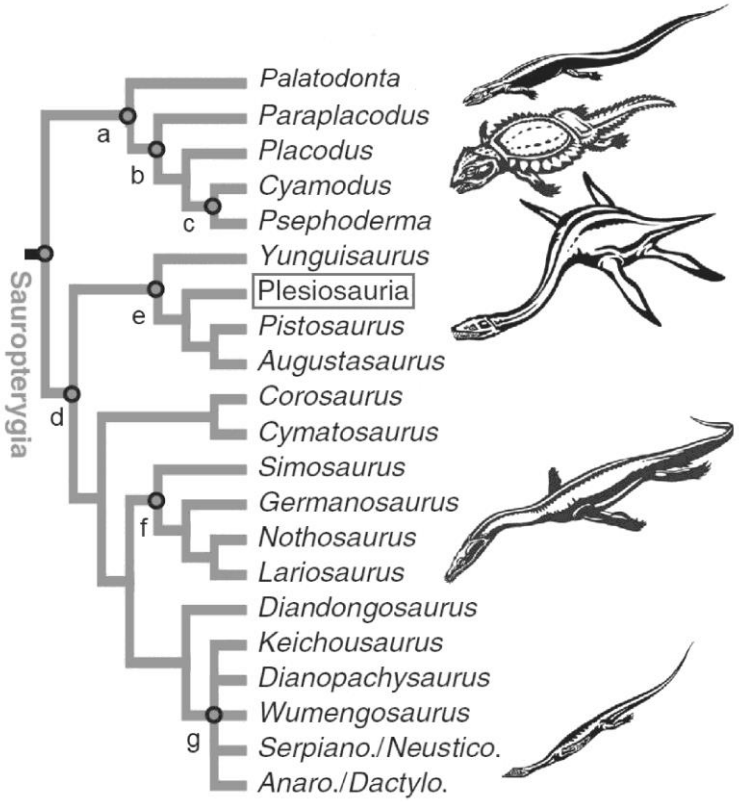

Fig. 1.4. Possible phylogenetic relationships among Sauropterygia (modified from Neenan et al., 2013); **(a)** Placodontiformes, **(b)** Placodontia, **(c)** Cyamodontoidea, **(d)** Eosauropterygia, **(e)** Pistosauroidea, **(f)** Nothosauroidea, **(g)** Pachypleurosauria.

The term Plesiosauria was erected by De Blainville (1835) and has since maintained taxonomic validity. Its monophyly is considered well established in the literature (e.g., Storrs, 1991; O'Keefe, 2001, 2004, 2006; Druckenmiller and Russell, 2008b); however, the process of finding a stable and well-supported phylogeny of Plesiosauria is still in "*its early stages*" (Ketchum and Benson, 2010). O'Keefe (2001, 2004) published the first major analysis of Plesiosauria, incorporating 166 characters and 34 taxa sampled across a wide stratigraphical and morphological range of variation. However, these results called into question longstanding assumptions of higher-level relationships within the clade, including the validity and definition of the two traditional clades, Plesiosauroidea and Pliosauroidea (e.g., O'Keefe, 2001; Druckenmiller and Russell, 2008b; Ketchum and Benson, 2010). Although all existing plesiosaurian classifications split the order Plesiosauria into two clades, there is no consensus regarding species-level relationships within certain clades, such as Elasmosauridae (Sato, 2002; O'Keefe, 2004; Groβmann, 2007; Druckenmiller and Russell, 2008b; Ketchum and Benson, 2010), Pliosauridae (O'Keefe, 2004; Druckenmiller and Russell, 2008b), and Rhomaleosauridae (O'Keefe, 2004; Smith and Dyke, 2008; Ketchum and Benson, 2010) or even between clades, such as Polycotylidae for which the systematic position remains controversial as the group is related either to the pliosauroids (e.g., Persson, 1963; Adams, 1997; Smith and Dyke, 2008) or to the plesiosauroids (e.g., Williston, 1903; Carpenter, 1996, 1997; O'Keefe, 2004),

Plesiosaurians possess an unusual body plan with a short and stiff trunk, a short tail and four enlarged hydrofoil-shaped propulsive flippers for swimming (e.g., Massare, 1994; O'Keefe, 2002; Rieppel et al., 2002; Motani, 2009; Carpenter et al., 2010; Bardet et al., 2014). Two body plans, pending on the proportions between head size and neck length, are variably found among plesiosaurians and evolved independently in different clades (e.g., Carpenter, 1997, O'Keffe, 2002; O'Keefe and Carrano, 2005). Although it exists a large range of intermediate morphologies between these body plans, a long neck and a small head characterize the plesiosauromorph morphotype (Fig. 1.5A), whereas pliosauromorphs present a short neck and a large head (Fig. 1.5B).

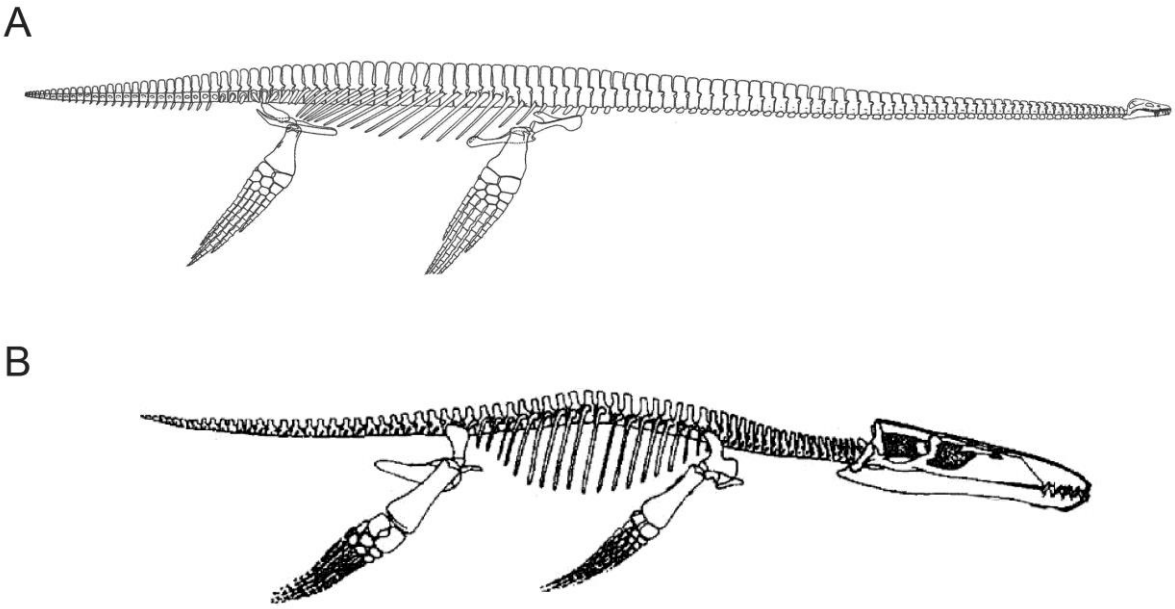

Fig. 1.5. Morphotype examples through the plesiosauromorph *Hydrotherosaurus alexandrae* **(A)** and the pliosauromorph *Liopleurodon ferox* **(B)**. Modified from Welles (1943) and O'Keefe (2002). Not to scale.

All plesiosaurians were obligatory aquatic animals (Rieppel, 2000). The fossil record shows that during the Jurassic and Cretaceous, they were abundant in marine and marginal marine deposits (Benson et al., 2013), but also present in freshwater (e.g., Russell, 1931; Sato et al., 2003; Kear, 2006; Benson et al., 2013). The pattern of locomotion employed by plesiosaurians has been debated for a long time (e.g., Watson, 1924; Robinson, 1975; Chatterjee and Small, 1989; O'Keefe, 2001; Carpenter et al., 2010; Muscutt et al., 2017). Nowadays, it is admitted that plesiosaurians used a mix involving antero-posterior rowing movements for the posterior limbs while anterior limbs performed an "underwater flight" defined by dorso-ventral movements (Carpenter et al. 2010; Liu et al., 2015; Muscutt et al., 2017). Thus, plesiosaurians were possibly forelimb-dominated swimmers using their hind limbs mainly for maneuverability and stability (Liu et al., 2015) and synchronized or nearly synchronized movements to reach higher speed with less effort (Carpenter et al., 2010). The consensus is that pliosauromorphs were specialized for manoeuvrability and pursuit, whereas plesiosauromorphs were specialized for cruising at low to intermediate speeds and able to cover long distances (Carpenter et al., 2010). Their diverse morphologies and locomotor abilities suggest the colonization of numerous feeding guilds (Bardet et al., 2014). Most are presumed to have been piscivorous (Massare, 1987), remains of bony fishes having been observed in stomach contents (Cope,

1871; Brown, 1904; Patterson, 1975; Storrs, 1995), but also cephalopod jaw elements and hooklets (e.g., Tarlo, 1959; Sato and Tanabe, 1998). In addition, tooth marks on isolated bones indicate that some large pliosauromorphs preyed upon other reptiles (Clark and Etches, 1992) and some plesiosauromorphs were specialised predators of invertebrates dwelling on marine sediments (e.g., elasmsoaurid: McHenry et al., 2005). Recent studies showed that plesiosaurians were viviparous with a K-selected reproduction strategy suggesting social behaviour and maternal care (O'Keefe and Chiappe, 2011), able to regulate their body temperature independently of the surrounding water temperature (Bernard et al., 2010), capable to realize deep, prolonged, and/or repetitive diving (Rothschild and Storrs, 2003), and to migrate, at least occasionally, over long distances (Vincent et al., 2017).

Few information has been revealed about the sensory abilities of plesiosaurians. Andrews (1913) suggested that their large orbits and their sclerotic plates indicate that plesiosaurians were primarily visual hunters with a possible binocular vision (e.g., Shuler, 1950; Forrest, 2000). Conversely, the postero-dorsal position of external nostrils of plesiosaurians related to the internal nares led Cruickshank et al. (1991) to suspect adaptation for underwater olfaction (but see Buchy et al., 2006). More recently, the foramina on the dorsal and lateral surfaces of the snout of *Pliosaurus kevani* have been interpreted as a neurovascular system involved in prey detection similar to crocodile pressure receptors or shark electroreceptors (Foffa et al., 2014).

During Late Cretaceous, mosasauroids and plesiosaurians coexist through different associations that illustrate possible ecological partitioning. The association between the long-necked elasmosaurids and large mosasauroids is common in Late Cretaceous marine reptile faunal assemblages and has been documented in numerous sites (see Vincent et al., 2013 for details), such as Montana (Sternberg, 1915), New Mexico (Lucas et al., 1988) and Kansas (Everhart, 2005) in North America, Jordan (Bardet and Pereda Suberbiola, 2002), Angola (Jacobs et al., 2006) and NW Saudi Arabia (Kear et al., 2008) for Africa and Middle-East, and Czech Republic (Kear et al., 2014) in Europe. Such an association illustrates the absence of competition between the gracile and (probably) piscivorous Elasmosauridae and large mosasauroids that occupied the top-predator niches.

In addition, although they remain scarce, associations of mosasaurids and polycotylids have also been reported in North America (e.g., USA: Zangerl, 1953; Canada: Russell, 1967),

New Zealand (Warren and Speden, 1977) and Russia (Nessov, 1995). Because it can reasonably be assumed that some of the largest Mosasauridae and Polycotylidae occupied top-predator niches (Vincent et al., 2013), these contrasted associations highlight marked geographical feeding partitioning between giant marine predators in Late Cretaceous oceans. Indeed, when such associations occur, mosasauroids appear significantly smaller than polycotylids (Vincent et al., 2013) and may indicate that plesiosaurians this time occupied the top-predator niches.

In Goulmima (see Chapter 2), the marine reptile association including polycotylid, elasmosaurid and pliosaurid plesiosaurians and mosasauroid squamates. Such an association is very rare worldwide. Indeed, it includes several taxa that can potentially be considered as top-predators. Such an association has only been reported in the Early-Middle Turonian of Kansas (Fairport Chalk Member of the Carlile Shale) by Schumacher and Everhart (2005) and Schumacher (2011). However, since this formation provided only indeterminate fragmentary specimens, no study could investigate the mosasauroid and plesiosaurians cohabitation (McIntosh et al., 2016). In this PhD thesis, the exceptionally preserved specimens that have permitted to define numerous well known species, provide the rare opportunity to consider the paleoecologic significance of such a marine reptile faunal assemblage.

Chapter 2

Goulmima, an exceptionally preserved outcrop from the Turonian (Late Cretaceous) of Southern Morocco

In North Africa, early Late Cretaceous continental and marine successions widely crop out, forming in the landscape a recognizable cliff named “Hamada” that extends SW–NE, from the Gulf of Agadir (Morocco) to the Gulf of Gabès (Tunisia) (Choubert and Faure-Muret, 1962) (Fig. 2.1A).

In South-eastern Morocco, these deposits are exposed on large distances in the southern slope of the High-Atlas, the Er-Rachidia-Goulmima region, and in the Anti-Atlas zone, around Erfoud and south to this city, in the Kem Kem region. Here, remains of vertebrate fossils have been found in great abundance for more than 70 years, and nowadays about 80 vertebrate taxa are known from this region (see Cavin et al., 2010 for details).

The first record of marine vertebrate remains (consisting of fish fragments) associated with an ammonite assemblage in the early Late Cretaceous of the High-Atlas and Midelt area was made by Dubar (1949). Over the following decades only a few vertebrate fossils from this area were described (Cavin et al., 2010). Since the last 30 years however, local people here have been engaged in active excavation work to collect fossils for commercial purposes (Cavin et al., 2010). Although such practices have negative aspects (e.g., no precise information about the geographical and stratigraphical location of fossils, as well as of the sedimentology), they have also significantly increased the number of fossils discovered in this area and permitted in some cases their scientific study. In parallel, new field campaigns undertaken by institutional paleontologists, often in collaboration with local people, have permitted to recover new *in situ* fossils (e.g., Cavin et al., 2010) and, more notably and interestingly, to show that most marine reptile remains come from a single level excavated by local people and well visible in the landscape (N. Bardet personal communication, see Fig. 2.1B).

As a result, the Turonian deposits of Goulmima represent nowadays a very rich fossiliferous site that has yielded a very diverse marine fauna encompassing ammonites (Kennedy et al., 2008), chondrichthyans (Underwood et al., 2009), bony fishes (Cavin, 1995, 1997, 1999, 2001; Cavin et al., 2001, 2010), as well as large marine reptiles (Bardet et al., 2003a, b; Buchy, 2005; Buchy et al., 2005; Angst and Bardet, 2015). Some of these marine reptiles already described (Bardet et al., 2003b; Buchy, 2005), as well as newly recovered specimens (Allemand et al., 2017a; Allemand et al., in press), are the basement of the studies undertaken in this PhD Thesis. This chapter aims to present the outcrop of Goulmima in order to depict the stratigraphical and paleoenvironmental contexts in which this PhD has been performed.

Fig. 2.1. **A**, General view of the Goulmima region taken from Goulmima city, with in the background the famous early Late Cretaceous "Hamada", topped by the marine Turonian cliff; **B**, detailed view of the main fossiliferous level excavated by local people that can be followed in the landscape for great distances (photos by courtesy of N. Bardet).

2.1. Geographical and stratigraphical contexts

The Goulmima outcrop was named after the city on the southern slope of the Moroccan High-Atlas (Er-Rachidia Province), around which most fossiliferous sites are located, mainly near the villages of Tadirhourst and Asfla, in the North of Goulmima.

The early Late Cretaceous continental and marine successions mentioned above are part of a famous series, originally defined as the "Trilogie Méso-Crétacée" by the French geologist G. Choubert in the Anti-Atlas region of southeastern Morocco. It comprises from the base to the top: the "Grés Infracénomaniens", the "Marnes à gypses cénomaniennes" and the "Calcaires cénomano-turoniens" (Choubert, 1948, Choubert et al., 1952). However, at the same time, G. Dubar, another French geologist in charge on the geological map of this region, recognized a similar tripartite series along the southern slope of the High-Atlas that he named differently as such: Ifezouane, Aoufous and Akrabou Formations (Dubar, 1949). Choubert et al. (1952) interpreted these two series as deposits of two different basins without (or with very few) connections, justifying their different designations. Lavocat (1954) later demonstrated connections between these two series and thus represent the same deposits

Nowadays, there is no sedimentological or palaeogeographical arguments to consider these series formed in the same basin as different (see Fig. 2.2A). Following Ferrandini et al. (1985) and Ettachfini and Andreu (2004), all the early late cretaceous deposits of Southeastern Morocco are currently defined and recognized as such, from the base to the top:

- 1) Ifezouane Formation of Dubar ("Grés Infra-cénomaniens" of Choubert, 1948), consisting of red sandstones with crossed stratifications;

- 2) Aoufous Formation of Dubar ("Marnes a gypses cénomaniennes" of Choubert, 1948), composed of gypsum marl sandstones and green marls;

These two units, now considered as Cenomanian in age and of continental and deltaic origin, are usually informally grouped into the classical "Continental intercalaire" of the French authors or "Kem Kem beds" (see Sereno et al., 1996 and Cavin et al 2010 for details);

- 3) Akrabou Formation of Dubar ("Calcaires cénomano-turoniens" of Choubert, 1948), is a massive calcareous bar that tops the series; it is of coastal passing to open marine origin, and corresponds to the great Cenomanian–Turonian worldwide transgression (Gale, 2000). The marine reptiles found in the Goulmima outcrop all come from this Turonian bar (Fig. 2.2B).

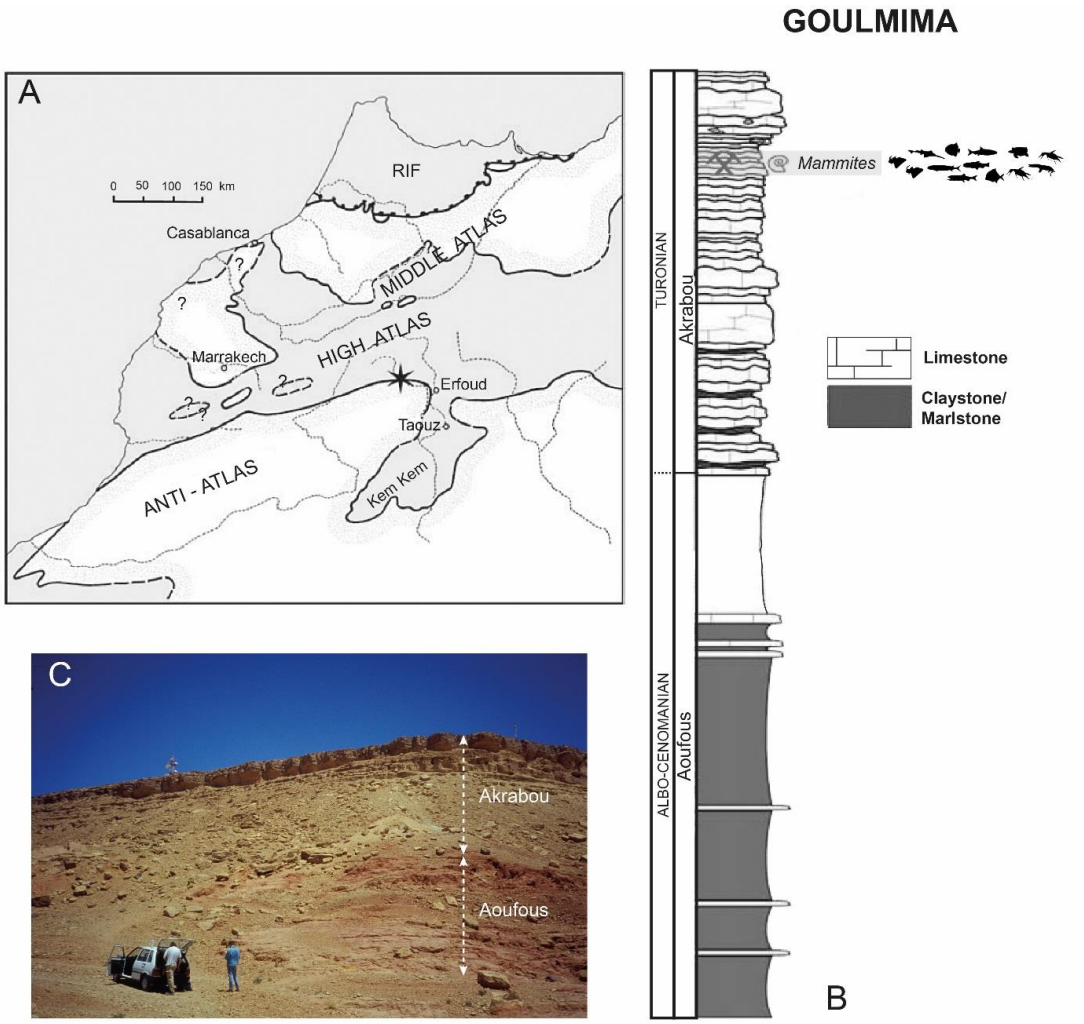

Fig. 2.2. **A**, Palaeogeographical location of the Goulmima (indicated by a star) area in southern Morocco and **B**, probable stratigraphical range (*Mammites* horizon) of the fossil taxa. **C**, detailed view of the two fossiliferous series observed in Goulmima (photos by courtesy of N. Bardet). Paleogeographical map modified from Bardet et al. (2003a) and stratigraphical column from Cavin et al. (2010).

2.2. Preservation

The fossils are usually exceptionally preserved and contained in early diagenetic calcareous nodules (e.g., Terrab, 1996) lying horizontally in marly limestone, in association with the Lower Turonian ammonite *Mammites* (see Cavin et al., 2010 for details). Depending on the size of the taxa preserved (ammonites, “fishes”, marine reptiles), the specimens are either embedded in a

single nodule or preserved in several adjacent ones. The size of these nodules may vary according to specimens, the largest ones can reach one meter in diameter (N. Bardet personal communication). The specimens can be entirely or partially enclosed in the nodules, with a general tendency (not linked to collecting biases) of truncated appendages observable in both "fish" and marine reptile specimens. As a result of the exposures and dissolutions associated to the desert condition, some specimens are preserved as print only (N. Bardet personal communication.).

These nodules can be prepared either mechanically or chemically (with formic acid) but in many case the siliceous nodule core remain impossible to remove, preventing a complete preparation of the specimens (Cavin et al., 2010; N. Bardet personal communication) Ammonites are more frequent than vertebrates and preserved either within nodules, or lie free in the marly beds (Cavin et al, 2010).

Most fossiliferous nodules are concentrated near the top of a Cenomanian–Turonian calcareous succession (Akrabou Formation), in the Unit 4 of Ferrandini et al. (1985), previously considered as Early Turonian in age based on the ammonite assemblage (mainly *Mammites*) (Bardet et al., 2003a, b, 2008). It was later reappraised as Unit T2a of the Akrabou Formation, Middle Turonian in age, by Ettachfini and Andreu (2004), but more recently this unit has been re-dated from the Early Turonian (Kennedy et al., 2008).

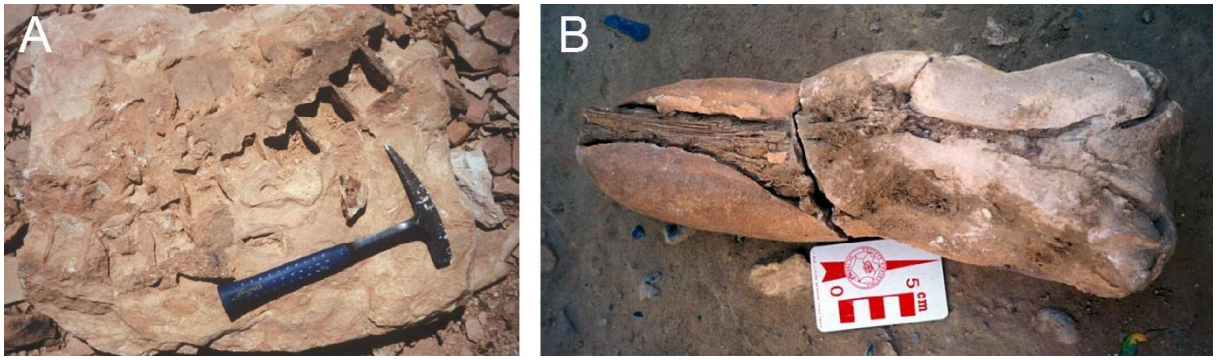

Fig. 2.3. Examples of differential preservation found in the Goulmima fossiliferous nodules. **A**, portion of a plesiosaur vertebral column partly preserved only as a print; **B**, Dorsal view of the indeterminate Polycotylidae (MNHN F-GOU 14) studied in this PhD Thesis (Allemand et al., in press), preserved in a nodule with some part dissolved and other ones obscured by the matrix (photos by courtesy of N. Bardet).

2.3. Paleogeographical and paleoenvironmental contexts

The Goulmima area was the center of a basin exemplifying large subsidence during the Cenomanian–Turonian transgression (Bardet et al., 2003a, b) in a warm, humid and intertropical climate (Lezin et al., 2010; Lebedel et al., 2013, 2015).

These deposits correspond to a deep (mid ramp/outer ramp) and open marine carbonate platform with influences essentially from the Tethys but also from the Central Atlantic (e.g., Cavin et al., 2001; Ettachfini and Andreu, 2004; Bardet et al., 2008) (see Fig. 2.2A).

The redox proxies indicate dysoxic conditions in the bottom waters and a disturbed development of planktonic foraminifera, resulting in a low paleo-productivity at the sea surface (Lebedel et al., 2013, 2015). According to Cavin et al. (2010), the faunal assemblages of Goulmima, isochronous with the *Mammites* ammonite bioevent, show small and poorly diversified microfossil assemblages consisting mainly in buliminid foraminifera. This poorly diversified association might indicate a possible reason for the good quality of preservation of fishes and other vertebrates because of the lack of organisms responsible for the decay of carcasses (Cavin et al., 2010).

2.4. Goulmima faunal assemblages

As previously developed, the Goulmima deposits have yielded a rich and diversified marine faunal assemblage, defined by Cavin et al. (2010) as the "Goulmima assemblage", that provides an overview of the ecosystem associated to the locality.

The Turonian ammonite assemblage in this area is quite diversified through the occurrence of different genus: *Mammites*, *Romaniceras*, *Fagesia*, *Neoptychites*, *Choffaticeras*, *Nannovascoceras*, and *Hoplitoides* (Basse and Choubert, 1959; Kennedy et al., 2008). The composition of the ammonite assemblage shows the predominance of *Mammites* (35%: Kennedy et al., 2008) and characterizes the second bioevent, dated from the late Early Turonian, occurring within the Akrabou Formation (Cavin et al., 2010). In addition, the occurrence of *Romaniceras* ammonites in the upper part of the section may suggest a Middle Turonian age (Cavin et al., 2010).

Goulmima deposits also yielded a rich ichthyofauna including several families: pycnodontids, ichthyodectids, araripichthyids, osmeroidids, pachyrhizodontids and enchodontids (Cavin, 1999). Pycnodontids are known only from microremains (Cavin, 1999), while other families were recorded through complete individual specimens (e.g., the ichthyodectid *Ghrisichthys bardacki*, the osmeroidid *Osmeroides rheris*, the araripichthyid *Araripichthys corytophorus* and the pachyrhizodontid *Goulmimichthys arambourgi*, the most common fish from this assemblage, see Cavin, 1995, 1997) or through indeterminate specimens sometimes preserved as gut contents (e.g., the small enchodontid, *Enchodus* sp., see Cavin, 1999). A simplified network of trophic relationships (see Fig 2.4) between the bony fishes of Goulmima was performed by Cavin (1996). The presence of numerous juvenile *Enchodus* suggested that the environment of deposition might have been used as a nursery ground for this species. Micro-remains of *Enchodus* associated to the body cavity or coprolite in larger bony fishes have shown that small *Enchodus* were preyed on by *G. arambourgi* and *O. rheris* (Cavin, 1997, 1999), which might explain the abundance of piscivorous fishes in Goulmima, in terms of number of species and of individuals (Cavin, 1999).

Associated to the osteichthyan fauna, elasmobranchs are also present in Goulmima but much rarer, and include moderate-sized rays: the platyrhinid (thornback) ray *Tingitanius tenuimandibulus* (Claeson et al., 2013) and the ptychotrigonids *Microprystis* sp. and *Ptychotrigon* sp. (Gale et al., 2017), as well as sharks represented by an undescribed sclerorhynchid saw shark and the small lamniform *Squalicorax* sp. (Gale et al., 2017). It is most likely that sharks in Goulmima preyed upon the different fishes located in the area (Cavin, 1996). *Squalicorax*, at least, may have been in competition with marine reptiles for the consumption of large bony fishes (e.g., Everhart, 2004). This genus, with a body length between 1.5 m and 3 m, is considered as active predators, and opportunistic feeders or scavengers (e.g., Shimada and Cicimurri, 2005). Evidences of shark predation and/or scavenging on marine reptiles are rather commonly recorded (e.g., Everhart, 2004); however, in Goulmima, the possible predator-prey relationships between sharks and marine reptiles remain unknown.

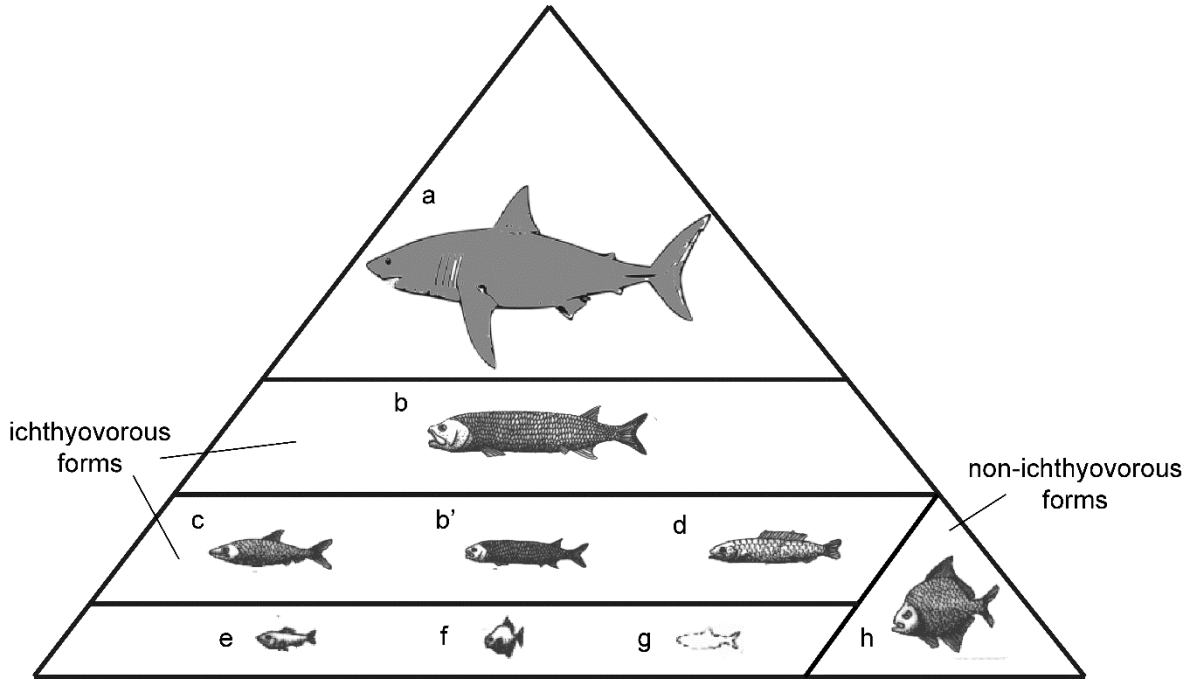

Fig. 2.4. Trophic relationships within the osteichthyan and chondrichthyan faunas of Goulmima (modified from Cavin, 1996). The triangles and the four levels represent supposed trophic relationships based upon size, shape and set of teeth of fishes (Cavin, 1996). **Abbreviations**: **a**, sharks; **b, b'**, Ichthyodectidae sp. (**b**, individuals of large size; **b'**, individuals of middle size); **c**, *Goulmimichthys arambourgi*; **d**, *Osmeroides* sp.; **e**, *Enchodus* sp.; **f**, Pycnodont sp.; **g**, indeterminate teleost; **h**, *Araripichthys* sp.

Finally, various marine reptiles were also discovered in this locality. These latter are represented by a protostegid turtle (Cavin et al., 2010), the basal mosasauroid squamate *Tethysaurus nopcsai* (Bardet et al., 2003b, 2008), and several plesiosaurian specimens belonging to three major Cretaceous families: the elasmosaurid *Libonectes morgani* (specimens SMNK-PAL 3978, SMNS 81783, and D1-8213: Buchy, 2005; Allemand et al., 2017a; Sachs and Kear, 2017; Allemand et al. in press), the polycotylids *Thililua longicolis* (specimen MNHGr.PA.11710: Bardet et al., 2003a), *Manemergus anguirostris* (specimen SMNK-PAL 3861: Buchy et al., 2005), and two indeterminate specimens (PMO201.956: Ronander, 2007; MNHN F-GOU14: Allemand et al., in press), and the pliosaurid *Brachauchenius lucasi* (specimen MNHN GOU 11: Angst and Bardet, 2015).

In addition to being exceptional for the abundance and diversity of the taxa found, the Turonian marine deposits of the Goulmima area represent one of the very few worldwide outcrops in which mosasauroids are preserved with several plesiosaurian taxa (e.g., Schumacher and Everhart, 2005; Schumacher, 2011). The excellent preservation condition of the fossils here unearthed provide the unique opportunity to study, through their endocranial anatomy, the possible behavior of these large marine reptiles and to apprehend their interrelationships and relative positions in the trophic food chain.

Chapter 3

Paleoneurology and endocast

Paleoneurology is the study of the brain and nervous system of fossil taxa (Buchholtz and Seyfarth, 1999) and represents the interface between two broader areas, paleontology and neurology (Sales and Schultz, 2014). Paleoneurological studies provide an indirect access to the brain and its associated nervous system in order to make hypotheses about the behavior and the sensorial activity of extinct species (e.g., Rogers, 2005; Witmer et al., 2008; Witmer and Ridgely, 2009). Fossils generally lack soft tissues, so that inquiries about this area are made by looking at the osteology of the braincase, and by looking at the cavities that in life held the brain and other associated soft tissues. This is done from the reconstruction of endocasts. In the strictest anatomical sense, endocasts are representations (casts) of any enclosed, three-dimensional (3D) space. Although the term may refer to all intracranial cavities (e.g., nasal capsule, semicircular canals and vestibule, bony sinus, neurovascular canals), it is usually reserved for the endocranial cavity housing the brain and the associated tissues (e.g., meninges, venous blood, arteries, cerebrospinal fluid). A standard endocast is generated at the interface between the skeleton (typically bone or cartilage) and the soft tissue (or fluid) lying immediately deep to it (Balanoff et al., 2015). It provides an overview of the shape and the maximal size of the endocranial structures.

Nowadays, more and more endocranial studies are performed for various taxa with different purposes. This chapter aims to provide a brief history of the paleoneurology and its development through selected scientists that have impacted the topic, and to outline the information associated to the endocast.

3.1. Brief history of the paleoneurology

3.1.1. Paleoneurology from 1804 to 1960s

At the beginning of the 19th century, in his book entitled "*Sur les espèces d'animaux dont proviennent les os fossiles répandus dans la pierre à plâtre des environs de Paris*", George Cuvier wrote:

> *"On n'imagine guère que je sois aussi en état de donner quelques traits de la description du cerveau d'un animal qui paroît détruit depuis tant de siècles : un hasard heureux m'a cependant procuré cette faculté. La tête dont je viens de parler étoit toute environnée d'un mélange de glaise et de gypse, et c'est précisément ce qui l'avoit rendue si friable; car les os contenus dans la marne, se brisent généralement quand on veut les en tirer, sans doute parce que cette terre ne les a pas préservés de l'humidité, comme fait le gypse; mais dans ce cas-ci, sa présence a été heureuse: elle s'est moulée dans la cavité du crâne, et comme cette cavité elle- même dans l'animal vivant s'étoit moulée sur le cerveau, la glaise nous représente nécessairement la vraie forme de celui-ci; il étoit peu volumineux à proportion, aplati horizontalement ses hémisphères ne montroient pas des circonvolutions mais on vovoit seulement un enfoncement longitudinal peu profond sur chacun. Toutes les lois de l'analogie nous autorisent à conclure que notre animal étoit fort dépourvu d'intelligence. Il faudroit, pour que la conclusion fût anatomiquement rigoureuse, connoître les formes de la base du cerveau et surtout la proportion de sa largeur avec celle de la moelle alongée; mais cette base n'est pas bien conservée dans notre moule."* [Cuvier, 1804, p. 25]

Thus, in 1804, Cuvier provided this first description of a natural endocast of *Anoplotherium commune*, an artiodactyl of the Late Palaeogene of France, from the gypsum quarries of Montmartre (Paris). The structure dorsally exposed in a broken skull provided an overview of the cerebral hemispheres (Fig. 3.1). Cuvier (1804) realized thus that casts of the

brain cavity in fossil vertebrates could be informative concerning the external anatomy of the brain (Edinger, 1962).

Fig. 3.1. Georges Cuvier (1769-1832) Portrait (engraving) source: Portrait Prints of Men and Women of Science and Technology in the Dibner Library; and the dorsal view of the endocast of *Anoplotherium commune*; illustration modified from Cuvier (1804, p. 25, Pl. XXIX, unscaled).

Throughout the 19th century, the term endocast appears sporadically in the paleontological literature (see Paleoneuroloy 1804-1966: An annotated Bibliography, Edinger, 1975 for details). A large part of the literature concerns the hominid endocasts; however, natural endocasts were occasionally described and used to discuss about the "intelligence", sensory abilities of fossil mammals, birds and dinosaurs. During this period, Othniel Charles Marsh (Fig. 3.2) was one of the first scientists to use endocasts for evolutionary purposes. Although Marsh described numerous endocasts of dinosaurs and extinct birds (e.g., Marsh, 1879, 1880a, b, 1881), his most paleoneurological contribution concerns the series of "laws" he elaborated in 1877 from several previous studies about the endocast of extinct mammals (e.g., Marsh, 1874, 1875, 1877, 1878, 1886, 1887):

> *"The earliest known Tertiary mammals all had very small brains, and in some forms this organ was proportionally less than in certain Reptiles. There was a gradual increase in the size of the brain during this period, and it is interesting to find that this growth was mainly confined to the cerebral hemispheres, or higher portion of the brain. In most groups of mammals, the brain has gradually become more convoluted, and thus increased in quality, as well as quantity. In some, also, the cerebellum, and olfactory lobes, the lower parts of the brain, have even diminished in size. In the long struggle for existence during Tertiary time, the big brains won, then as now; and the increasing power thus gained rendered useless many structures inherited from primitive ancestors, but no longer adapted to new conditions."* [Marsh, 1877, p. 54-55].

These various propositions expressed as "*the general laws of brain growth*" by Marsh (1877) constituted the earliest attempt to recognize the role played by endocasts in understanding the evolutionary history of the taxa. However, these laws were highly challenged by one of the pioneers of modern paleoneurology, Johanna Gabriele Ottilie Edinger (Fig. 3.2) (Buchholtz and Seyfarth, 2001; Franzosa, 2004). During the 1920s, Edinger's first published paper dealt with the description of the natural endocast of the marine reptile *Nothosaurus* (Reptilia, Sauropterygia), a Triassic relative of the plesiosaurians (Edinger, 1921). This paper is the first in a series that focused on fossil brain casts. Edinger provided endocranial descriptions from a wide array of extinct animals, including a large volume of works on flying vertebrates (e.g., Edinger, 1925a; 1926; 1927; 1941; 1951), marine reptiles (e.g., Edinger, 1925b, 1928), and mammals (e.g., Edinger, 1939, 1940, 1948). Additionally, Edinger provided more generalist paleoneurological studies in order to gather together all the widely scattered information on the topic (e.g., Edinger, 1975) and performed different studies a series of brains along a lineage, and to study how the various parts of the brain changed from most primitive taxa to more derived ones (e.g., Edinger, 1941, 1942, 1948, 1955). From her accumulated experience in paleoneurology, Edinger discussed in 1962 the supposed increase of mammal brain size during the Tertiary and the assumption that small brains were a factor of extinction as supposed by Marsh (1877). Marsh's "laws" were scrutinized in detail, and rejected by citing

contradicting data from both extant and extinct taxa. Edinger demonstrated that an increase in relative brain size is not proven through lineages (Edinger, 1962).

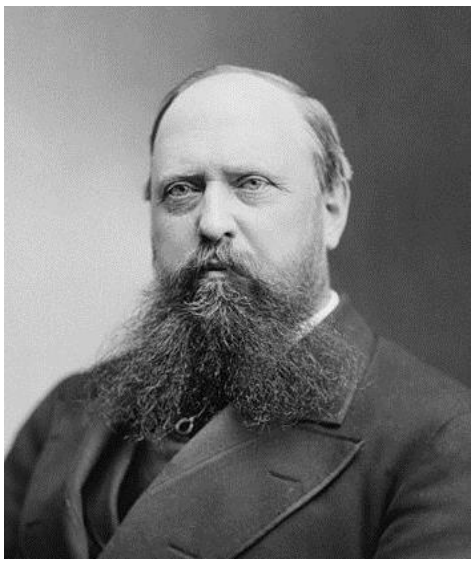

Fig. 3.2. Othniel Charles Marsh (1831-1899) on the left and Johanna Gabriele Ottilie ('Tilly') Edinger (1897-1967) on the right. Source: Library of Congress Prints and Photographs Division. Brady-Handy Photograph Collection.

3.1.2. Paleoneurology from 1960s to present

If Edinger was responsible for establishing the bases of palaeoneurology in the early 20th century, Harry Jerison could arguably be credited for being the most important figure to make the field evolve towards the science we know today (Walsh and Knoll, 2011). He was the first to formulate a relationship between the body size and the brain and to use it to discuss brain evolution and to determine whether fossil taxa, as compared to extant ones, had larger or smaller brains than expected based on their body size. From his results, Jerison showed that "fishes" and non-avian reptiles have smaller brains than mammals and birds of the same body size. Jerison believed this meant birds and mammals ("higher" vertebrates) could process more information, and were therefore more "intelligent" than "lower" vertebrates (Jerison, 1969, 1973). In the conceptualization of Jerison, the term "intelligence" correlates with cognitive ability or other measures of "intelligence" such as innovation rate, i.e. the rate at which novel

behaviors or techniques are acquired (Jerison, 1977), and can be gauged by a measure of encephalization, defined as the brain size relative to the body size (Jerison, 1973). The concept of encephalization was based on some equations that he developed plotting brain weight (in g) against body weight (in kg) for extant "fishes", non-avian reptiles, birds and mammals (Fig. 3.3). From these data, Jerison calculated ratios or encephalization quotients (EQ) of observed brain weight to expected brain weight (Jerison 1973) in order to investigate whether correlations between brain and body size exist, and determine where deviations from the baseline occur in a variety of vertebrate taxa (Walsh and Knoll, 2011). Thus, using this method, it was possible to estimate EQs for extinct taxa, allowing trends in brain size over time to be observed.

Jerison argued that when the encephalization quotient is greater than 1.0, it means the brain is larger than expected for an "average" animal of the inspected animal's size and group. Similarly, EQs lower than 1.0 implies a smaller brain than expected for an average animal of the inspected animal's size and group (Jerison, 1973). Based on his results, he established different conclusions (Jerison, 1985):

> *"(1) A basal lower vertebrate grade of encephalization evolved in the earliest bony fishes, amphibians and reptiles and has be maintained to the present as a steady-state or equilibrium during at least 350 million years. Since about two-thirds of living vertebrate species are members of these three classes of vertebrates, this basal grade is considered as the norm for vertebrates;*
>
> *(2) There are variations in encephalization within the lower vertebrate groups, the most interesting being between herbivorous and carnivorous dinosaurs. The carnivores were apparently significantly more encephalized.*
>
> *(3) The earliest fossil birds and mammals with known endocasts have evolved to a higher grade, representing at least three or four times as much brain as in lower vertebrate species of comparable body size. This progressive or 'anagenetic' evolution occurred at least 150 million years ago, and in the case of the mammals may have begun with their reptilian ancestors at least 50 million years earlier;*
>
> *(4) Within the mammals there is a good fossil record of the brain, which is consistent with a picture of steady-states punctuated by rapid evolution to higher grades. However, many grades of encephalization are represented in living mammalian species, with some (opossum, hedgehog) at the same grade*

as the earliest of the mammals;

(5) Primates have always been a brainy order, perhaps doing with their brains what many other species did by morphological specializations. The evolution of encephalization in the primates followed rather than preceded or even accompanied other adaptations by primates to their niches;

(6) The highest grade of encephalization is shared by humans and bottlenosed dolphins (Tursiops truncatus). The sapient grade was attained about 200 000 years ago, but cetaceans may have reached their highest grade 18 million years ago;

(7) Encephalization in the hominids is a phenomenon of the past three to five million years, and its rapidity appears to have been unique in vertebrate evolution;

(8) These results suggest two complementary conclusions. First, the long steady states that occurred in most groups indicate that, on the whole, encephalization was not a major element in vertebrate evolution. A particular grade of encephalization tended to be maintained once it was achieved. On the other hand, its appearance in many different and distantly related groups is evidence of some Darwinian 'fitness' for encephalization." [Jerison, 1985, p. 24-25]

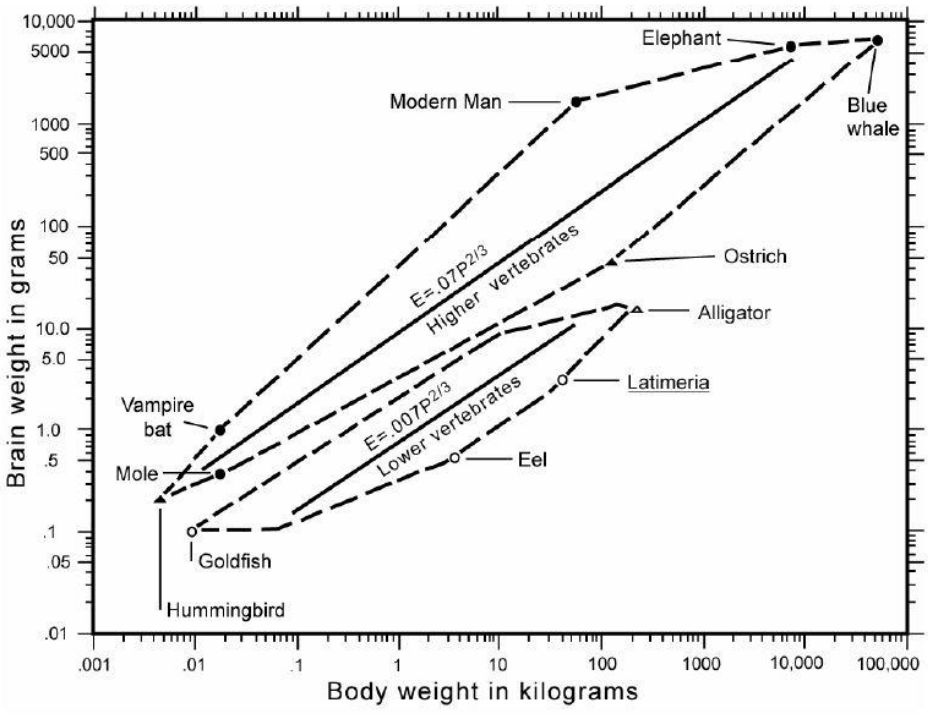

Fig. 3.3. Chart showing the brain weight to body weight ratio of several extant taxa. Redrawn based on Jerison (1969).

Applied to extinct taxa, the EQ method has shown limits that have been largely debated (e.g., Franzosa, 2004). Indeed, the estimation of the EQ was based on different parameters, such as body mass and brain size, which are complicated to evaluate in extinct taxa, or on assumptions, such as that brains in non-avian reptiles only filled 50% of the cranial cavity, which invalidate the method because incorrect. However, although the EQ analysis as put forward by Jerison has been criticized for some of its inherent assumptions (e.g., Hopson 1979; Hurlburt, 1996), the basic approach is still used in current research (Walsh and Knoll, 2011).

Jerison also attempted to establish the "Principle of Proper Mass", specifically that taxa relying more heavily on certain senses (e.g., vision) or engaging in particular activities (e.g., arboreality requiring well-developed balance) will have a greater proportion of processing power devoted to those modalities. The brain regions associated with such processing will possess a greater number of neurons and will consequently be relatively larger (Jerison, 1973). Thus, the relative size of specific brain regions visible on endocranial casts should be able to provide some information about brain functionality and, hence, some information about the

behavior and ecology of the species in question (Jerison, 1973). This principle was the basis for investigations into behavior and sensory abilities in extinct species.

Besides the four people listed above, several other scientists studied endocasts in varying degrees of details. Since the 1960s, it appears that paleoneurological studies are more and more focused on evolutionary questions specific to certain taxonomic groups, rather than address overarching problems in vertebrate brain evolution (Walsh and Knoll, 2011). Nowadays, a high number of scientists contribute to paleoneurology and it would be difficult to cite all authors contributing to the topic. However, it is interesting to note that vertebrates are not equal in terms of papers describing or interpreting endocranial casts; and a quick search on Google Scholar about endocasts reveals a marked bias towards mammal and archosauromorph research.

3.2. Endocranial studies and associated information

Studies on individual braincase bones in multiple extinct taxa can reveal how the organization of foramina and sutures changed through time; however, to elucidate changes occurring in the soft tissues of the brain, the entire endocranial cavity must be examined. To date, as more and more endocranial studies are performed for various taxa with different purposes, it seems important to list the kind of information that such studies reveal.

3.2.1. Endocasts as brain proxies

The brain is not isolated within the endocranial cavity but shares this space with a number of intimately associated structures (Balanoff and Bever, 2017). These structures, as well as the volume ratio between the brain and the cranial cavity, vary between vertebrate lineages and may have a strong impact on the endocast morphology.

The external surface of the brain and the internal surface of the bony and/or cartilaginous endocranial cavity are not in direct contact but separated by meningeal tissues (Butler and Hodos, 2005). These membranes are connective tissues surrounding the central nervous system

(CNS). It is generally assumed that the primary function attributed to meninges is to protect the CNS by forming a barrier that safeguards the sensitive organs against trauma (e.g., Decimo et al., 2012). They also contain an ample supply of blood vessels that deliver blood to CNS tissues and produce the cerebrospinal fluid that fills the cavities of the cerebral ventricles and surrounds the brain as well as the spinal cord. The cerebrospinal fluid protects and nourishes the CNS tissues by acting as a shock absorber, by enabling nutrient circulation, and by getting rid of waste products.

The meninges differ across vertebrates (e.g., Buttler and Hodos, 2005; Balanoff and Bever, 2017). The plesiomorphic condition, observed in "fishes", is a single, undifferentiated layer known as the primitive meninx, which divided "*somewhere along the tetrapod stem lineage*" (Balanoff and Bever, 2017, p. 227) to form an inner layer, the secondary meninx (endomeninx), and the more superficial layer, the *dura mater*. Then, the secondary meninx differentiated to form the *pia mater* (the closest to the brain) and the intermediate arachnoid layer in mammals and birds but also in a non-homologous way in turtles, crocodilians and amphibians (Balanoff and Bever, 2017).

The changes occurring in the meningeal history across chordates need further study to be elucidated. However, this history is of relatively limited importance for the stated goals of this PhD as compared to their variable thickness. Indeed, it is the latter that impacts the endocast morphology. Unfortunately, there has been no attempt yet to provide a systematic survey of vertebrate meningeal thickness (Balanoff and Bever, 2017), and the only information available is that birds possess thin meninges as compared to the thick ones of mammals (e.g., Iwaniuk and Nelson, 2002).

The brain is surrounded at its surface by veins that drain blood in different cerebral region through the cranial venous sinus system (Kilic and Akakin, 2008). It is assumed that some of the sinuses reach a large size and can influence the endocast morphology and thus reduce the size and shape correspondence between the endocast and brain (Balanoff and Bever, 2017). Some studies have shown for example that non-avian reptiles display a large occipital sinus along the sagittal midline of the cerebellum and produce a prominent dural peak over this region (Goodrich, 1930). However, information about the place occupied by the venous sinus system in an endocranial reconstruction remain scarce and preclude any generalization (Morhardt et al., 2012).

Although their influence on the size and shape of an endocast is not typically large (Balanoff and Bever, 2017), certain cranial nerves and arteries do course through the endocranial cavity and thus diminish the place occupied by the brain (see the example of the trigeminal ganglion in Balanoff and Bever, 2017). Finally, another important predictor of brain-endocast correspondence is the structural architecture of the braincase itself. In many vertebrate groups, the endocranial cavity is only partially delineated by bones, the rest being surrounded by cartilage, which can represent an obstacle to the reconstruction and the interpretation of the endocasts.in fossils, whose cartilage is not preserved.

The impact of these structures on both reconstruction and interpretation of endocasts has long been recognized (e.g., Edinger, 1951; Hopson, 1979; Witmer et al., 2008) and was recently taken into consideration in the definition of the brain-to-endocranial cavity (BEC) index (Balanoff et al., 2015). This index reflects the degree to which the brain fills the cranial cavity. High BEC values can be expected to produce an endocast that reflects the brain volume and morphology with high fidelity, whereas low BEC values are associated with an endocast bearing less resemblance to the actual brain (Balanoff et al., 2015). No rule exists today about the BEC values across vertebrate evolution (Balanoff and Bever, 2017). This factor can vary widely between lineages (e.g., Jerison, 1973; Hopson, 1979; Macrini et al., 2007; Witmer et al., 2008; George and Holliday, 2013) but also over ontogeny (e.g., Macrini et al., 2007; Hurlburt et al., 2013). For example, the brain of the marsupial *Monodelphis domestica* fills from 67.8% to 86.6% of the endocranial volume according of age increasing (Macrini et al., 2007), whereas in alligators, the smallest forms' brain occupies 68% of the endocranial space, and the largest's only 32% (Hurlburt et al., 2013). As a general tendance and independently of ontogeny, mammals and birds, which are generally considered as highly encephalized taxa, tend to have brains that nearly fill the cranial cavity, resulting in a strong correlation between the volume and morphology of the endocast and those of the brain (Balanoff et al., 2015). Among other vertebrates, it is generally admitted that the brain incompletely fills the cranial cavity (Balanoff et al., 2015). Originally, the common estimation was that the brain occupies only 50% of the endocranial space (e.g., Jerison, 1973; Hopson, 1979). However, this ratio was only based on the observation of only one *Sphenodon* and one *Iguana* specimens (Hurlburt et al., 2013), and is thus far from representing a general pattern in non-endotherms. For example, it has been shown that the brain almost entirely fills the endocranial space in some extant chondrichthyans

and teleost fishes (Northcutt, 2002; Balanoff et al., 2015). Within Squamata (lizards, snakes and amphisbaenians), a wide range of brain versus endocranial cavity proportions were found (Kim and Evans, 2014). The lowest brain–endocranial volume ratio being found in the tokay gecko (*Gecko gecko*: 0.35), whereas the Spotted false monitor lizard (*Callopistes maculatus*) exhibits a brain that nearly fills the endocranial cavity (0.97). Moreover, snakes and amphisbaenians are known to have a brain that fills most of the endocranial space (Starck, 1979; Nieuwenhuys et al., 1998). A recent study estimated that the brain in snakes fills around 90 percent of the endocranial cavity (Triviño et al., in press). The brain thus fills the intracranial cavity in some squamates, though not all, indicating that endocasts within these species may reflect the external morphology of the brain with a certain degree of accuracy.

The percentage of the endocranial cavity filled by the brain (BEC index) is an important metric for assessing the explanatory potential of endocast (Balanoff and Bever, 2017); however, it does not take into account the anatomical reality that the spatial relationship between the brain and the endocranial wall is not uniform but may vary widely between neuroanatomical regions. The cerebrum of extant crocodilians, for example, fills most of the associated portion of the endocranial cavity, whereas the hindbrain of these taxa does not (Osmolska, 2004; Evans, 2005). This feature is not limited to archosaurs. The description of the brain and endocranial cavity of the Australian lungfish (*Neoceratodus forsteri*) showed that some of the brain regions are similar to the endocast, except in the areas of the diencephalon and the hindbrain/anterior spinal cord (Clement et al., 2015).

It is thus important to be aware and to remind that an endocast is not a perfect reflect of the brain. There is no rule allowing to determine in advance the proportions of the cranial cavity occupied by the brain, and comparisons that mix brains and endocasts can lead to erroneous interpretations.

3.2.2. Endocasts as sources of phylogenetic information

As windows into the deep history of neuroanatomy, endocasts may provide information about the brain's evolutionary history through its consideration/analysis in extinct lineages and may help to understand the modern neurological disparity (Balanoff and Bever, 2017). From this idea, the endocasts can be used as sources of systematic information and provide additional

features that would help to establish phylogenetic relationships. Such studies have already been performed from endocasts in both living and extinct Carnivora (e.g., Radinsky, 1973a, b, 1975, 1978; Willemsen, 1980; Lyras and Van der Geer, 2003; Ahrens, 2014) but remain very scarce for other clades (e.g., Friedman, 2007; Clement et al., 2016: lungfishes). Characters defined and coded from endocasts may be directly used or added to matrix taken other morphological features into account, in order to perform phylogenetic analysis (e.g., Clement et al., 2016). However, as endocasts correspond to replica of the braincase, great care must be taken in order not to score the same character twice (Clement et al., 2016). Indeed, the incorporation of these new characters requests the prior knowledge of the braincase/endocast relationships in order to take into consideration only endocranial features that vary irrespective of the braincase. Such relationships have not been studied, which probably partially explains why endocast features are rarely incorporated in phylogenetic analyses despite the potential for new suites of characters (Macrini et al., 2006).

3.2.3. Endocasts as sources of sensory and behavioral information

Since the definition of the encephalization quotient (EQ) by Jerison, endocasts have been used to assess the "intelligence" of extinct taxa (e.g., Jerison 1973; Hopson 1977, 1980) and to illustrate the idea that birds and mammals may have a complex cognitive behavior (e.g., Lefebvre et al. 2002; Marino 2002). However, although several attempts were made to improve Jerison's equations (e.g., Radinsky, 1978; Hurlburt, 1996; Larsson et al., 2000; Hurlburt et al., 2013), advances on the topic have seriously questioned the utility of the EQ to infer on the behavior of extinct taxa (Franzosa, 2004). Additional measures have been used to infer cognitive abilities in vertebrates, such as estimations of brain region size relative to total brain size (Krebs et al., 1989), or the resort to brain surface instead of brain volume (e.g., Sultan, 2002; Güntürkün et al., 2017). However, all these attempts were criticized as not being able to convincingly explain the distribution of higher cognitive abilities in vertebrates (Healy and Rowe, 2007). Nowadays, whole endocast volume is not necessary to make behavioral inferences. The development of digital technologies has improved the quality of endocranial reconstructions, allowing the partitioning of endocasts into functional neuroanatomical regions.

It enables to perform sensory inferences from the structure, independently from both total brain values and body size estimation (Balanoff and Bever, 2017).

3.2.3.1. Correlations between brain regions and functions

The relative size and morphology of the brain regions (e.g., olfactory bulbs, optic lobes, cerebellum) greatly varies across vertebrate clades and can reflect different functions associated to particular abilities (Iwaniuk, 2017). Such correlation between brain regions and functions is derived from the Principle of Proper Mass defined by Jerison (1973), which states that the mass of neural tissues controlling a particular function is appropriate to the amount of information processing involved in performing the function (Jerison, 1973, p.8). According to Iwaniuk (2017), the examination of the variability in the relative size of individual brain regions may be more informative and biologically relevant than comparisons of whole brain size. The rationale for this argument is that the brain is a heterogeneous organ comprised of numerous, functionally distinct regions that can and do vary in size independently of one another and are more directly linked to specific capacities (Iwaniuk, 2017).

The vertebrate brain can be divided into five main regions (Hopson, 1979). These are the telencephalon, diencephalon, mesencephalon, metencephalon, and myelencephalon (Fig. 3.4). The telencephalon and diencephalon make up what is commonly called the prosencephalon (or forebrain), the mesencephalon is the midbrain, and the metencephalon and myelencephalon make up the rhombencephalon (or hindbrain) (Hopson, 1979).

Telencephalon—The telencephalon is the most anterior division of the brain and consists in the main olfactory bulbs (MOB), accessory olfactory bulbs (AOB), olfactory tracts (peduncles), olfactory nerves (CN I), vomeronasal nerve (VN) and cerebral hemispheres (see Fig. 3.4). The olfactory nerves (CN I) have receptors located in the mucous membranes of the nose and travel through openings in the roof of the nasal passage to the MOB (Butler and Hodos, 2005). The vomeronasal nerve (VN) is functionally similar to the olfactory nerve. It arises from a sensory area inside the nose called the organ of Jacobson and projects to the AOB that lies next to the MOB. In non-avian reptiles, the main olfactory bulbs are responsible for the sense of smell and the accessory olfactory bulbs are associated to the vomeronasal organ and the pheromones-

based communications (Güntürkün et al., 2017). The olfactory bulb size varies greatly among and within non-avian reptiles and is often used as a proxy for olfactory abilities (e.g., Zelenitsky et al., 2011: non-avian dinosaurs). The length of the tract depends on the length of the animal's snout (Nieuwenhuys et al., 1998). In animals with a long snout, in which the nostrils are located relatively far anterior to the eyes, such as alligators, the olfactory tract can be quite long. In short-snouted animals, such as turtles, the tract is rather short. The cerebral hemispheres integrate information from both motor and sensory systems and deal with olfactory and visual integrations, memory and spatial behavior (Butler and Hodos, 2005). Although there are little neuroanatomical comparisons in non-avian reptiles (Wilkinson and Huber, 2012), the few studies existing on snakes and lizards have shown a correlation between the size of some cerebral hemisphere structures (i.e., dorsal and medial cortex) and the home range, as well as the spatial behavior (Day et al. 1999a, b; Ladage et al., 2009; Holding et al., 2012). The interspecific comparison performed by Day et al. (1999a) has shown that both dorsal and medial cortex were larger in an active foraging lizard compared with a congeneric sit-and-wait predator, despite no species difference in spatial memory (Day et al., 1999b). Within snake species, the relative size of the medial cortex is larger in individuals that have larger home ranges and/or move greater distances (Roth et al., 2006; Holding et al., 2012). Similarly, in side-blotched lizards (*Uta stansburiana*), the relative size of the dorsal cortex is larger in males that defend large territories compared with non-territorial males that occupy much smaller home ranges (Ladage et al., 2009).

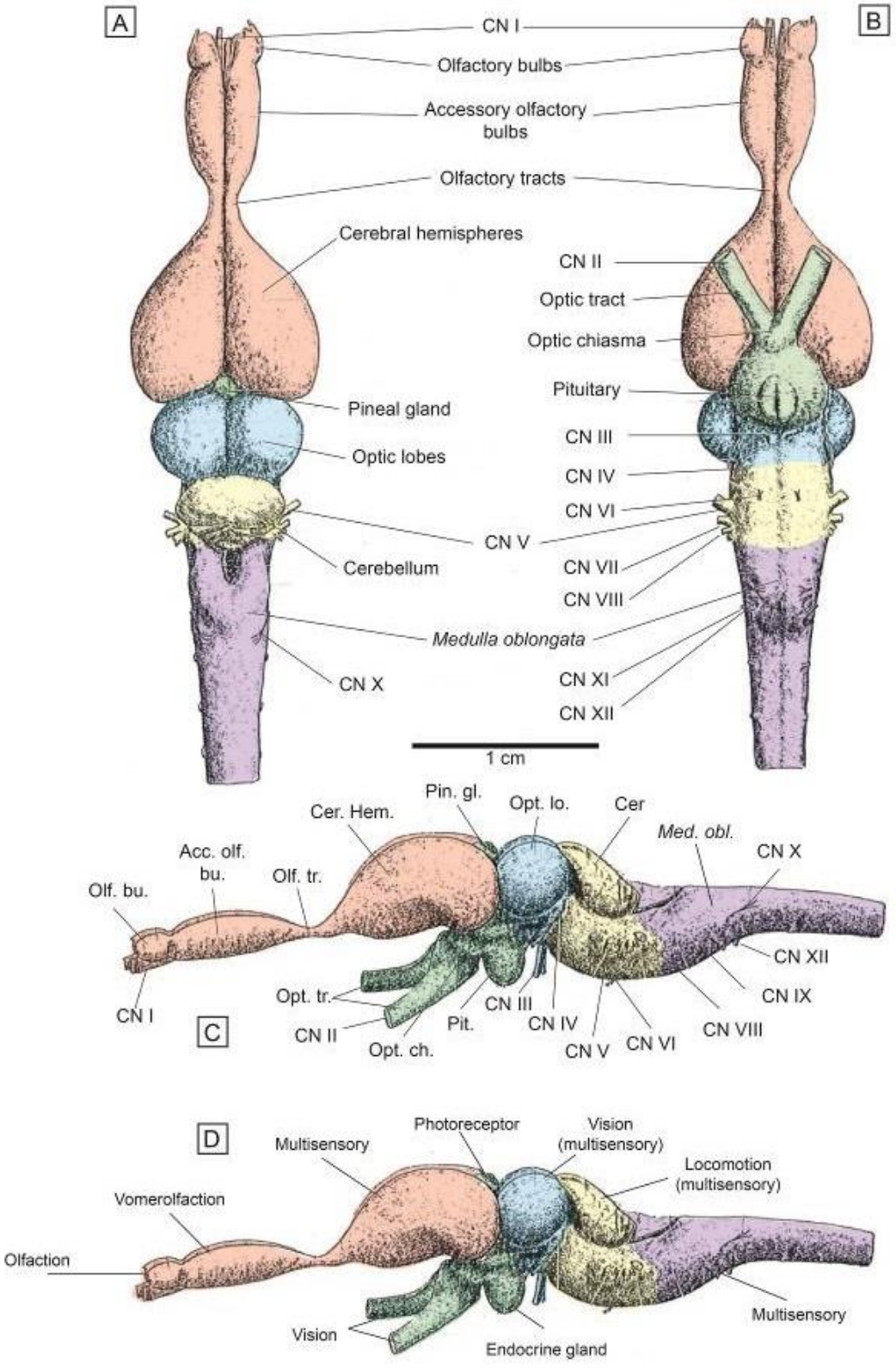
A
B
CN I
Olfactory bulbs
Accessory olfactory bulbs
Olfactory tracts
Cerebral hemispheres
CN II
Optic tract
Optic chiasma
Pituitary
Pineal gland
Optic lobes
CN III
CN IV
CN VI
CN V
Cerebellum
CN VII
CN VIII
Medulla oblongata
CN X
CN XI
CN XII
1 cm
Cer. Hem.
Pin. gl.
Opt. lo.
Cer
Med. obl.
CN X
Acc. olf. bu.
Olf. tr.
Olf. bu.
CN XII
CN IX
Opt. tr.
CN III
CN I
C
CN II
Pit.
CN IV
CN VIII
Opt. ch.
CN V
CN VI
D
Photoreceptor
Vision (multisensory)
Multisensory
Locomotion (multisensory)
Vomerolfaction
Olfaction
Multisensory
Vision
Endocrine gland

Fig. 3.4. Brain of the yellow monitor (*Varanus flavescens*, Varanidae) showing the telencephalon (red), diencephalon (green), mesencephalon (blue), metencephalon (yellow) and myencephalon (purple) in dorsal **(A)**, ventral **(B)**, left lateral views **(C)**, and principal sensory associated to each structures **(D)**. **Abbreviations**: **Acc. olf. bu.**, accessory olfactory bulbs; **Cer**, Cerebellum; **Cer. Hem.**, Cerebral hemispheres; ***Med. obl.***, *medulla oblongata*; **Olf. bu.**, Olfactory bulbs; **Olf. tr.**, Olfactory tracts; **Opt. ch.**, Optic chiasma; **Opt. lo.**, Optic lobes; **Opt. tr.**, Optic tracts; **Pin. gl.**, Pineal gland; **Pit.**, Pituitary; **CN I**, Olfactory nerves; **CN II**, Optic nerves; **CN III**, Occulomotor nerves; **CN IV**, Trochlear nerves; **CN V**, Trigeminal nerves; **CN VI**, Abducens nerves; **CN VII**, Facial nerve; **CN VIII**, Vestibulocochlear nerve; **CN IX**, Glossopharyngeal nerve; **CN X**, Vagus nerve; **CN XI**, Accessory nerve; **CN XII**, Hypoglossal nerve. Modified from Senn, 1966.

Diencephalon—The diencephalon is defined as "the more caudal of the two divisions of the forebrain, between the telencephalon and the mesencephalon" (Moreno et al., 2017). It includes several structures in vertebrates: the optic tracts, the optic nerves (CN II), the pretectum, the posterior tuberculum, the epithalamus, the dorsal and ventral thalamus, the hypothalamus and the hypophysis (or pituitary) (Butler and Hodos, 2005). However, as most of these structures correspond to nuclei assemblages within the diencephalon (e.g., Butler and Northcutt, 1973), there are not visible from the external morphology of the brain, and therefore from endocasts. When the external morphology of the brain is considered, only the more superficial structures can be observed (Fig. 3.4): the optic nerves (CN II), the optic chiasm, the most dorsal part of the epithalamus, the epiphysis (or pineal complex) and the most ventral part, the hypophysis (or pituitary).

The retinal cells of the eyes communicate signals from the receptors (rods and/or cones) to brain through the optic nerves that converge in an optic chiasm (Wyneken, 2007). The optic nerve tracts primarily project to the contralateral side (i.e., opposite side) of the optic tectum but also may have limited ipsilateral (i.e., same side) projections in turtles, snakes and lizards, whereas *Sphenodon* and crocodilians lack ipsilateral nerve tract components (Repérant et al., 1992). The binocular vision (i.e., perception of depth) has been related by various investigators (e.g., Polyak, 1957) to the development of an ipsilateral projection. However, the absence of such ipsilateral projections in the snapping turtle (*Chelydra serpentina*), for which the binocular

vision would profit for striking its prey, leads Knapp and Kang (1968) to doubt that the existence of ipsilateral projections is significant for depth perception.

The epiphysis (pineal complex) is composed of the pineal gland in turtles, squamates and *Sphenodon* but not in crocodiles, and the parietal eye in *Sphenodon* and some species of lizards (e.g., Quay, 1979; Tosini, 1997). The role of the epiphysis in the regulation of circadian and other biological rhythms is well established (Butler and Hodos, 2005). Both pineal gland and parietal eye are photoreceptive, in particular the parietal eye is a highly organized photoreceptive structure, with a well-defined lens, cornea and retina (Tosini, 1997). Both structures synthesize the melatonin hormone. The pineal complex may influence the thermoregulation, circadian rhythms, and reproduction in reptiles affecting the animal's physiology and/or behavior (Butler and Hodos, 2005). The size of this organ largely differs from non-avian reptile taxa; however, the ecological functions of such variability are still unclear since Labra et al. (2010) have shown that the size of the structure is not related with the habitat of taxa and show a weak association with thermal tolerances.

The hypophysis (or pituitary gland) is an endocrine gland found in all non-avian reptiles, but its internal organization as well as its size largely vary according to taxa (Saint Girons, 1970). The hypophysis is associated to the production of several hormones acting for different purposes, such as the reproductive cycles (e.g., Eyeson, 1971a, b: ovulatory and testicular cycles in snakes), the growth (e.g., Edinger, 1942), the skin pigmentation (e.g., Butler and Hodos, 2005); and controls the functions of many other glands, such as the pineal complex (Moreno et al., 2017). However, it is unclear how the size of the hypohysis may impact its function (Butler and Hodos, 2005).

Mesencephalon—The mesencephalon can be divided into three major regions: the tectum, the tegmentum, and the isthmus (Butler and Hodos, 2005). However, when the external morphology of the brain is considered, only the optic tectum (part of the tectum) can be visualized because its more superficial position, the other structures being more internal. The optic tectum forms two lobes on the dorsal surface of the brain (see Fig. 3.4) and is involved in integrating the spatial aspects of visual and auditory inputs (Butler and Hodos, 2005). One of the major functions of the optic lobes is to localize a stimulus in space and to cause the involuntary reflex allowing the animal to turn its head and/or eyes in the direction of the source of the stimulus (Knudsen and Schwarz, 2017). Such reflex is of great immediate importance for

animals. Their survival depending upon the speed and accuracy with which appropriate behaviors are executed in case of feeding or escape from a predator. In addition, the optic lobes should contribute to the control of spatial attention by signaling which stimulus, among all current stimuli, is of greatest immediate importance (Knudsen and Schwarz, 2017). In non-avian reptiles, the size and shape of the optic tectum differs among species (Ulinski et al., 1992). There is some correlation between the size of the tectum, the size of the eyes and the visual abilities; within snakes the tectum is relatively largest in diurnal and arboreal taxa and smallest in burrowing forms with reduced eyes (Masai, 1973).

In addition to the optic tectum, the mesencephalon encompasses the oculomotor nerves (CN III), and trochlear nerves (CN IV) (see Fig. 3.4). Both are related to movements of the eyeballs. The oculomotor nerves go from the brain to the extraocular muscles of the eyes, as well as the *levator* muscle of the upper eyelid and the trochlear nerves control the dorsal oblique eye muscle.

Metencephalon—The metencephalon is composed of the cerebellum (dorsally) and several cranial nerves: trigeminal nerve (CN V), abducens nerve (CN VI), facial nerve (CN VII), and vestibulocochlear nerve (CN VIII) (Butler and Hodos, 2005). The functions of the cerebellum are very complex. It does not only coordinate movement and positioning, but also controls muscle tone (Pearson, 1972; Breazile and Hartwig, 1989) and "*has a close relationship with the vestibular, somatosensory, visual, and auditory systems*" according to Butler and Hodos (2005: p.262). In addition, the cerebellum plays a role in motor learning and is a major sensory organ. Among non-avian reptiles, the shape of the cerebellum varies between taxa, from the flat one in turtles to the posteriorly curved one in crocodiles and anteriorly curved one in lizards (see Butler and Hodos, 2005: p.244). The size of the cerebellum also greatly varies within non-avian reptiles and particularly with locomotor behavior (Wyneken, 2007). It tends to be smaller in ground-dwelling species and larger in aquatic and climbing species.

Among the cranial nerves located on the metencephalon, the trigeminal nerve (CN V) is both a sensory and a motor nerve (Butler and Hodos, 2005). It is composed of three main branches: the ophthalmic (V1) branch, the maxillary (V2) branch, and the mandibular (V3) branch. All three branches emanate from the trigeminal ganglion. The ophthalmic branch (V1) is the principal sensory nerve of the orbit and nasal cavity. The maxillary branch innervates the eyelids, the skin of the dorsal orbital and infraorbital regions, the palate, and the nasal cavity.

The mandibular branch innervates jaw adductor muscles, lower eyelid muscles, salivary glands, and the skin of the intranasal region. The facial nerve (CN VII), like the trigeminal nerve, is both motor and sensory, and has several branches. This nerve innervates the skin and muscles around the ear, upper jaw, and pharynx; and controls the superficial neck muscles and mandibular depressor (Wyneken, 2007). Finally, the vestibulocochlear nerve deals with the hearing and balance of the animal (Butler and Hodos, 2005). It is composed of two vestibular branches; both enter the osseous labyrinth and innervate the ampullae of the semicircular canals, utricular macula and sacculus, and one cochlear branch that innervates the basilar membrane and the macula of the lagena.

Myelencephalon—The myelencephalon consists in the *medulla oblongata* and several cranial nerves: glossopharyngeal nerve (CN IX), vagus nerve (CN X), accessory nerve (CN XI), and hypoglossal nerve (CN XII) (Butler and Hodos, 2005). The medulla oblongata in non-avian reptiles is fairly conservative and appears to function as in other vertebrates (Wyneken, 2007). It houses the visceral, auditory, proprioceptive, and respiratory centers; controls basic heart rate; and regulates gastrointestinal mobility and secretion (Butler and Hodos, 2005; Wyneken, 2007).

The glossopharyngeal nerve (CN IX) is related to the taste and sensation in the pharynx; and controls the tongue muscles. The vagus nerve (CN X) provides general viscero-sensory functions for the thorax and digestive tract (Butler and Hodos, 2005). It also provides visceromotor control for the heart, lungs, and digestive tract, usually via peripheral ganglia (Jerison, 1973). The accessory nerve (CN XI) is motor and innervates portions of the neck and upper body (Jerison, 1973). Finally, the hypoglossal nerve (CN XII) is a motor that controls portions of the tongue, pharynx, larynx and trachea.

3.2.3.2. Does size matter ?

In vertebrates, the relative sizes of the brain and brain regions vary in a fairly consistent pattern with behavior and sensory abilities (Iwaniuk, 2017). However, several studies have recognized the complex functional and structural organization of the brain. There is indeed significant evidence that specific interconnected neural systems, rather than isolated localized structures, share a given function and that they tend to evolve as an integrated unit (Barton et al., 1995; Barton and Harvey, 2000; De Winter and Oxnard, 2001). Analyzing the relative size and

morphology of different functional divisions within the brain revealed correlations with numerous behavioral and ecological traits. For example, studies on olfactory bulb size of birds revealed a correlation between olfactory ratios (i.e., the ratio of the greatest diameter of the olfactory bulb to the greatest diameter of the cerebral hemisphere) and foraging method, diet, nesting and breeding habits (e.g., Bang 1971; Bang and Wenzel, 1985). In addition, species with convergent skeletal morphology and ecology may possess convergent brain proportions (e.g., mammals: De Winter and Oxnard, 2001). Thus, it is important to understand which specific interconnected neural systems within the brain differ between taxa that possess different behaviors, sensorial abilities and ecologies (Barton and Harvey, 2000) in order to clearly associate functions and brain regions.

Recent studies have suggested to use the numbers of neurons to provide a more accurate proxy to infer behavior and sensory abilities of taxa (e.g., Herculano-Houzel, 2011: mammals; Ngwenya et al., 2016: crocodiles; Olkowicz et al., 2016: birds). In fact, both neuron size and connectivity between neurons could be considered because they both can impact the behavior and sensory abilities of taxa (Iwaniuk, 2017). However, these methods may appear difficult to realize because are more time consuming than measuring volumes and are dependent on appropriate fixation of brains (Iwaniuk, 2017). Finally, the most inconvenient point, especially in the case of this PhD work, is that neurons do not fossilize and there is no mean of determining the number or size of neurons in an endocast. To understand how the brain of extinct species evolved and how endocast morphology relates to behavior and sensory abilities, it is necessary to establish first the link between behavior and sensory abilities and brain region sizes in extant species (e.g., Zelenitsky et al., 2011; Walsh and Knoll, 2011).

Notably because of one specific brain region is not necessarily associated to a unique function, the understanding of the relationships between brain regions, behavior and sensory abilities is complicated. This is even truer when we consider endocasts instead of brains for inferring behavior and sensory abilities in fossil taxa. However, despite the difficulties and limits related to the use of endocasts, the information gleaned from the structure appears as a relevant opening of new pathways for constructing and testing evolutionary and functional hypotheses that must not be neglected but rather developed.

Chapter 4

Material and Methods

The reconstruction of an endocast is dependent on the state of preservation of the specimen. Although it is possible to rebuild in its original organization a disarticulated skull thanks to different software of 3D imaging, skulls preserved in three dimensions give a better chance to avoid any possible "reconstruction" bias about the endocranial morphology. In the case of mosasauroids and plesiosaurians, this parameter strongly restricts the number of specimens used. Indeed, because mosasauroids exhibit a kinetic skull where elements of the dorsal skull roof and palate move relative to the braincase (Russell, 1967), the skull remains are often preserved disarticulated and are difficult to use for an endocranial reconstruction. Similarly, although the plesiosaurian skull is more rigid than that of mosasauroids, it appears more fragile and is often badly crushed (e.g., Kear, 2005; Vincent et al., 2011), preventing the access of the endocranial anatomy.

The exceptional three-dimension preserved marine reptile specimens of the Turonian marine deposits of Goulmima permit such endocranial study. This section introduces the specimens sampled for this work and the methods used to access the endocranial anatomy. In addition to these fossil specimens, several squamate taxa (snakes, varans and amphisbaenes) have been used as comparative data to interpret fossil endocasts in order to test the existence of phylogenetic and / or ecological signals and to provide palaebiological and behavioral inferences (cf. Chapter Introduction for details of the aims of this work).

4.1. Material

The list of the material analysed is presented in Table 4.1 and Table 4.2.

4.1.1. Fossil taxa

Mosasauroidea - *Tethysaurus nopcsai* Bardet et al., 2003b

In Goulmima, mosasauroids are represented by only one species, *Tethysaurus nopcsai*. This species was originally considered as a basal mosasauroid, sister-group of the Mosasauridae (Bardet et al., 2003b). However, its phylogenetic position varies according to authors and it has

been also reported as a basal mosasaurid forming a clade with *Yaguarasaurus* and *Russellosaurus*, being inferred sister-group of either the russellosaurines (Bell and Polcyn, 2005) or the halisaurines (Caldwell and Palci, 2007).

In the collections of the Muséum National d'Histoire Naturelle (Paris, France), this species is known through five specimens (MNHN GOU1-5: Bardet et al., 2003b; Houssaye and Bardet, 2013). The holotype MNHN GOU1 is a complete slightly crushed skull with the mandible in occlusion and the atlas-axis complex. The skull measures 30 cm long, up to 9 cm wide and 7 cm high.

The other specimens are preserved in the collections of the Southern Methodist University of Dallas (USA) and data provided by prof. Michael Polcyn with which collaborations are made. Among the five specimens, GM1, GM2 and GM3 specimens consist only in braincase whereas SMU 76335 and SMU 75 486 correspond to complete skulls.

Fig. 4.1. *Tethysaurus nopcsai*, MNHN GOU 1, holotype, Early Turonian, Goulmima region, Morocco. Articulated skull, mandible and associated first cervical vertebrae in left dorsolateral and right ventrolateral views (modified from Bardet et al., 2003b).

Plesiosauria

Plesiosaurians in Goulmima are known through eight specimens belonging to three major Cretaceous families (see Chapter 2). During this PhD, it has been possible to study one published specimens but also unpublished ones for which both osteological and endocranial anatomy are described here for the first time.

Elasmosauridae - *Libonectes morgani* (Carpenter, 1997) - SMNS 81783

This specimen was referred to the elasmosaurid *Libonectes atlasense* by Buchy (2005) but not described. SMNS 81783 is currently housed in the collections of the Stuttgart Museum (SMNS). It is preserved in a nodule about 40 cm long, up to 11 cm wide and 13 cm high (Fig. 4.2), which encompasses a skull with the mandible in occlusion and the atlas-axis complex. The specimen is incompletely prepared. Its anterior half shows bones incompletely dissolved and exposed, surrounded by a light beige matrix (Fig. 2.3 A, B). The posterior half of the fossil is still embedded in the matrix and thus not observable. This specimen has been reviewed and re-assigned to *Libonectes morgani* (Allemand et al., 2017a; see Chapter 8).

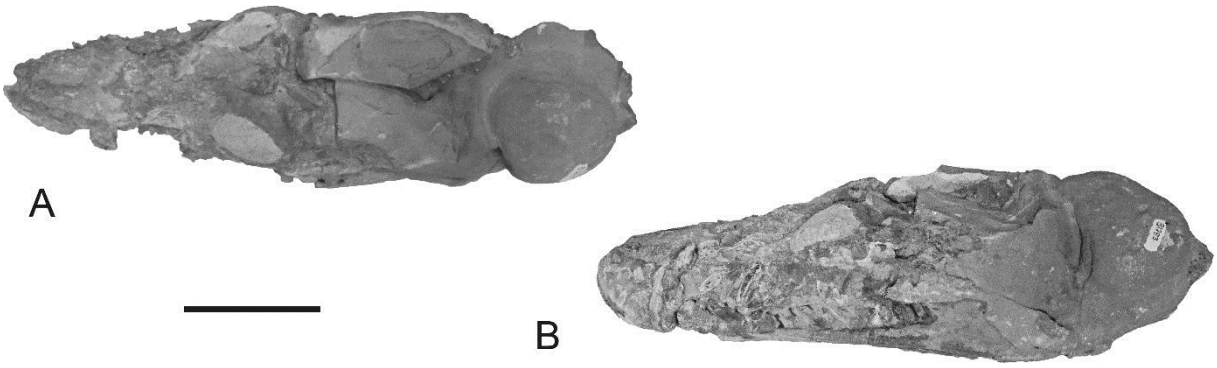

Fig. 4.2. *Libonectes morgani*, specimen SMNS 81783 in dorsal (A) and left lateral (B) views, Early Turonian, Goulmima region, , Morocco. Scale bar equals 10 cm.

Elasmosauridae - *Libonectes morgani* - D1-8213

This undescribed specimen is housed in the collections of the Rhinopolis Museum (Gannat, France). It is preserved in a nodule in two pieces that fit perfectly. The complete nodule enclosing D1-8213 measures 41 cm long, up to 15 cm wide and 12 cm high (Fig. 4.3). D1-8213 is incompletely prepared, the anterior half of the nodule shows bones incompletely dissolved and/or exposed, surrounded by a light beige matrix. The posterior half of the fossil is still embedded in the matrix and not observable. This specimen has been described in this PhD Thesis (see Chapter 8) and attributed to *Libonectes morgani* (Allemand et al., in press)

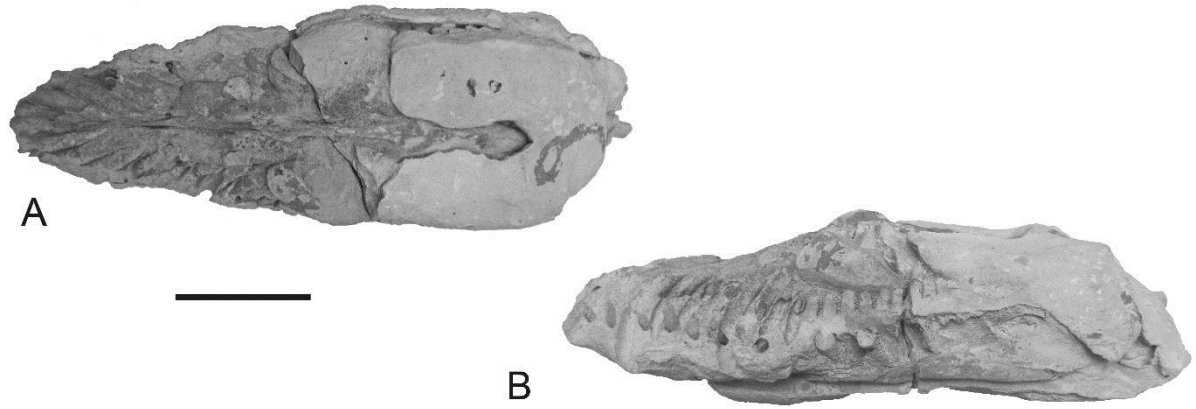

Fig. 4.3. *Libonectes morgani*, specimen D1-8213 in dorsal (A) and left lateral (B) views, Early Turonian, Goulmima region, , Morocco. Scale bar equals 10 cm.

Polycotylidae indet - MNHN F-GOU14

MNHN F-GOU 14 is an undescribed specimen housed in the paleontological collections of the Muséum National d'Histoire Naturelle (Paris, France). It has been collected several years ago by N. Bardet during fieldwork in the Goulmima region. The specimen is preserved in a nodule in two pieces that fit perfectly. The complete nodule measures 36 cm long, up to 12 cm wide and 11 cm high (Fig. 4.4). MNHN F-GOU 14 is still mostly embedded in the matrix, only the dorsal part of the anterior part of the skull is visible. This specimen has been described in this PhD Thesis (see Chapter 8) and assigned to an indeterminate Polycotylidae (Allemand et al., in press)

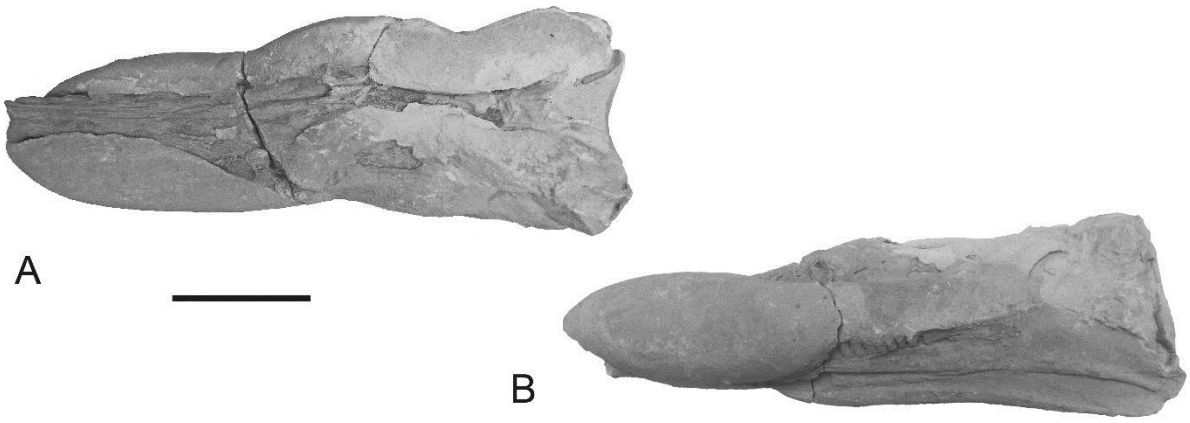

Fig. 4.4. Polycotylidae indet., specimen MNHN F-GOU14 in dorsal (A) and left lateral (B) views, Early Turonian, Goulmima region, , Morocco. Scale bar equals 10 cm.

Table 4.1. List of fossil specimens analyzed and scan parameters.

	Taxon	**Collection reference**	**Voxel size (in µm)**
Mosasauroidea	*Tethysaurus nopcsai*	MNHN GOU1	81.3
		GM1	97.5
		GM2	85.3
		GM3	85.3
		SMU75486	77.8
		SMU76335	81
Plesiosauria	*Libonectes morgani*	SMNS 81783	134
		D1-8213	115
	Polycotylidae indet.	MNHN F-GOU14	93.4

4.1.2. Extant taxa

The sample includes μCT scans of 52 squamate specimens (45 snakes, 4 monitor lizards and 3 amphisbaenians; see Table 4.2). Snake specimens have been selected in order to represent a wide diversity in terms of phylogeny and ecology (i.e., habitats: fossorial, terrestrial, arboreal, semi-aquatic and marine; see Chapter 5). The dataset is divided into six fossorial, seven arboreal, thirteen terrestrial, nine semi-aquatic and ten marine species (Heatwole, 1999; Houssaye et al., 2013; A. Herrel personnal communication). The semi-aquatic group encompasses species that spend most of their time in freshwater without contact with the sea. Three specimens of a single species, *Python regius*, were analyzed in order to evaluate the intraspecific variation.

Table 4.2. List of the material of extant squamates analyzed. Abbreviations: Personal collections of AH, Anthony Herrel; GD, Gheylen Daghfous; RB, Renaud Boistel. Ha represents the categories based on habitat: A, arboreal; G, Generalist; F, fossorial; M, marine; T, terrestrial; SA, semi-aquatic.

	Family	Taxon	Collection reference	Voxel size (in µm)	Ab.	Ha
SNAKES	Boidae	*Rhinotyphlops schlegelii* Roux-Estève, 1974	AH Unnumb	13.3	Rs	F
	Anomalepididae	*Typhlophis squamosus* Schlegel, 1839	MNHN 1997.2042	5.1	Ts	F
	Uropeltidae	*Uropeltis pulneyensis* Beddome, 1863	MNHN 1994.0753	5.0	Up	F
	Cylindrophiidae	*Cylindrophis ruffus* Laurenti, 1968	MNHN 1998.0201	20.1	Cy	F
	Aniliidae	*Anilius scytale* Linnaeus, 1758	MNHN 1997.2106	10.1	An	F
	Pythonidae	*Python regius* Shaw, 1802	AH Unnumb	33.3	P3	T
			AH Unnumb	28.9	P2	T
			AH MS 37	21.6	P1	T
	Boidae	*Boa constrictor* Linnaeus, 1758	MNHN 1989.0177	7.6	Bc	A
		Candoia sp. Gray, 1842	AH Unnumb	33.3	Cd	T
		Corallus hortulanus Linnaeus, 1758	AH MS 62	32	Ch	A
		Eunectes murinus Linnaeus, 1758	MNHN 1996.7898	7.6	Em	SA
	Acrochordidae	*Acrochordus granulatus* Schneider, 1799	ZRC 2.2334	24.2	Ag	SA
	Pareatidae	*Pareas margaritophorus* Jan, 1866	MNHN 1974.1469	7.5	Pm	A
	Viperidae	*Crotalus atrox* Baird and Girard, 1853	AH MS 31	28.5	Cr	T
		Agkistrodon contortrix Linnaeus, 1766	AH MS 56	23.4	Ac	T

SNAKES	Homalopsidae	*Enhydris enhydris* Schneider, 1799	ZRC 2.5507b	24.2	Ee	SA
		Enhydris punctata Gray, 1849	ZRC 2.3554	24.2	Ep	SA
		Cerberus rynchops Schneider, 1799	MNHN-RA-1998.8583	35.3	Ce	SA
		Homalopsis buccata Linnaeus, 1758	ZRC 2.6411	24.2	Hb	SA
		Erpeton tentaculatum Lacépède, 1800	GD Unnumb	7.5	Et	SA
		Bitia hydroides Gray, 1842	ZRC 2.4374	20.9	Bh	M
		Fordonia leucobalia Schlegel, 1837	MNHN-RA-1912.26	33.2	Fl	SA
		Cantoria violacea Girard, 1857	ZRC 2.3672	20.8	Cv	SA
	Lamprophiidae	*Mimophis mahfalensis* Grandidier, 1867	MRSN R3171	24.7	Mm	T
		Atractaspis irregularis Reinhardt, 1843	MNHN 1999.9129	7.6	Ai	F
	Elapidae	*Micrurus lemniscatus* Linnaeus, 1758	MNHN 1997.2353	7.6	Ml	T
		Naja nivea Linnaeus, 1758	AH MS 68	28.5	Nn	T
		Hydrophis elegans Gray, 1842	MNHN-RA-0.1879	30.7	He	M
		Enhydrina schistosa Daudin, 1803	ZRC 2.2043	20.8	Es	M
		Astrotia stokesii Gray, 1846	ZRC 2.2032	20.8	As	M
		Hydrophis major Kharin, 1984	MNHN 1990 4557	44.8	Hm	M
		Hydrophis ornatus Gray, 1842	MNHN-RA-1994.6997	36	Ho	M
		Pelamis platurus Linnaeus, 1766	AH MS 64	31.9	Pp	M
		Aipysurus duboisii Bavay, 1869	MNHN-RA-1990.4519	41	Ad	M
		Aipysurus eydouxii Gray, 1849	MNHN-RA-0.7704	40.2	Ae	M
		Microcephalophis gracilis Shaw, 1802	ZRC 2.2155	20.8	Mg	M

	Natricidae	*Thamnophis sirtalis* Linnaeus, 1758	GD Unnumb	7.5	Ta	T
SNAKES	Colubridae	*Chrysopelea ornate* Shaw, 1802	MCZ R-177291	14.9	Co	A
		Hierophis gemonensis Laurenti, 1768	AH Unnumb	23.4	Hg	T
		Hierophis viridiflavus Lacépède, 1789	AH Unnumb	19.2	Hv	T
		Dispholidus typus Smith, 1829	AH Unnumb	32	Dt	A
		Boiga dendrophila Boie, 1827	AH MS 102	18.2	Bd	A
		Dasypeltis sp. Wagler, 1830	MCZ 71877	14.9	Ds	A
		Coronella austriaca Laurenti, 1768	AH MS 51	21.6	Ca	T
LIZARDS	Varanidae	*Varanus prasinus* Schlegel, 1839	AH Unnumb	48.08	Vp	A
		Varanus salvator Laurenti, 1768	AH Unnumb	39.9	Vs	SA
		Varnus niloticus Linnaeus, 1758	AH Unnumb	14.8	Vn	G
		Varanus exanthematicus Bosc, 1792	AH Unnumb	45	Ve	G
AMPHISBAENIA	Amphisbaenidae	*Amphisbaena gonavensis* Gans and Alexander, 1962	AH Unnumb	7.46	/	F
		Amphisbaena kingii Bell, 1833	AH Unnumb	12.64	/	F
		Amphisbaena vanzolini Gans, 1963	MNHN 1998.02.02	7.46	/	F

4.2. Methods

4.2.1. Computed Microtomography scan

During this PhD Thesis, computed microtomography was performed in order to non-destructively digitize the endocranial anatomy of the specimens.

The holotype of *Tethysaurus nopcsai* (MNHN GOU1: complete skull, Fig. 4.1) has been scanned at the AST-RX platform of the MNHN (Paris) using a GEphoenix|Xray|v|tome|x L240. In addition, scans of five other unpublished *T. nopcsai* specimens (GM 1; GM 2; GM 3; SMU 75486; SMU 76335), performed at the University of Texas High-Resolution X-ray CT Facility, have been loaned by Michael J. Polcyn (Southern Methodist University, Dallas, Texas) were scanned at the University of Texas High-Resolution X-ray CT Facility by Matthew Colbert in 2010.

As far as extant squamates are concerned, the digitized data have been obtained from different sources: (1) at the University of Poitiers (France), Institut de Chimie des Milieux et Matériaux of Poitiers (IC2MP, Poitiers, France) using a X8050-16 Viscom model (resolution between 16.7 and 32.3 µm; reconstructions performed using Feldkamp algorithm with DigiCT software, version 1.15 [Digisens SA, France]); (2) at the European Synchrotron Radiation Facility (ESRF, Grenoble, France) using third generation synchrotron microtomography (Tafforeau et al. 2006), on beamlines ID 19 and BM5 (resolution between 5.0 and 14.9 µm). reconstructions performed using filtered back-projection algorithm with the ESRF PyHST software), and have been loaned by A. Herrel (MNHN), A. Houssaye (MNHN), R. Boistel (IPHEP) and G.Daghfous (UQAM).

4.2.2. Morphometric approaches

In order to compared quantitatively the snake endocasts, three different approaches were performed from descriptive characters, linear measurements and the outline curves (see Chapter 5 for detail explanations).

4.2.3. Data processing

Image segmentation and visualization were performed using VGStudioMax 2.2 (Volume Graphics Inc., Heidelberg, Germany) and MIMICS (Materialise Interactive Medical Image Control System) Innovation Suite software (Materialise®, release 18) at the Palaeontology Imaging Unit of the MNHN/UMR 7207 CR2P; and Avizo 7.0 (VSG, Burlington MA, USA) at the MNHN/UMR 7179 MECADEV. The segmentation tools of these software packages were utilized to reconstruct the skull and the endocast.

Chapter 5

Comparative morphology of snake (Squamata) endocasts: evidence of phylogenetic and ecologic signals

The present contribution proposes the first endocast comparative study in squamates. It will focus on snakes that are of particular interest since they show a great diversity in morphology, and occupy a wide range of ecologies with e.g., fossorial, aquatic, and arboreal species (e.g., Heatwole, 1999; Greene et al., 2000). Here, we propose to provide a quantitative anatomical description of the endocast of a wide sample of snake species using different morphometric approaches in order to: 1) bring new information about this structure, its general traits within snakes and the variation occurring; 2) test if, as in mammals and birds, the endocast of snakes reflects a phylogenetic and/or ecologic signal.

This chapter has been published in Journal of Anatomy:
Allemand, R., R. Boistel, Z. Blanchet, R. Cornette, N. Bardet, P. Vincent, and A. Houssaye. 2017b. Comparative morphology of snake (Squamata) endocasts: evidence of phylogenetical and ecological signals. Journal of Anatomy 2017:doi: 10.1111/joa.12692.

5.1. Material and Methods

5.1.1. Material

The material consists of the skull of 45 snake specimens (38 genera and 43 species; see Chapter 4 Material and Methods); illustrating the diversity of snakes in both phylogenetic and ecological (i.e., habitat) perspectives (see Fig. 5.1).

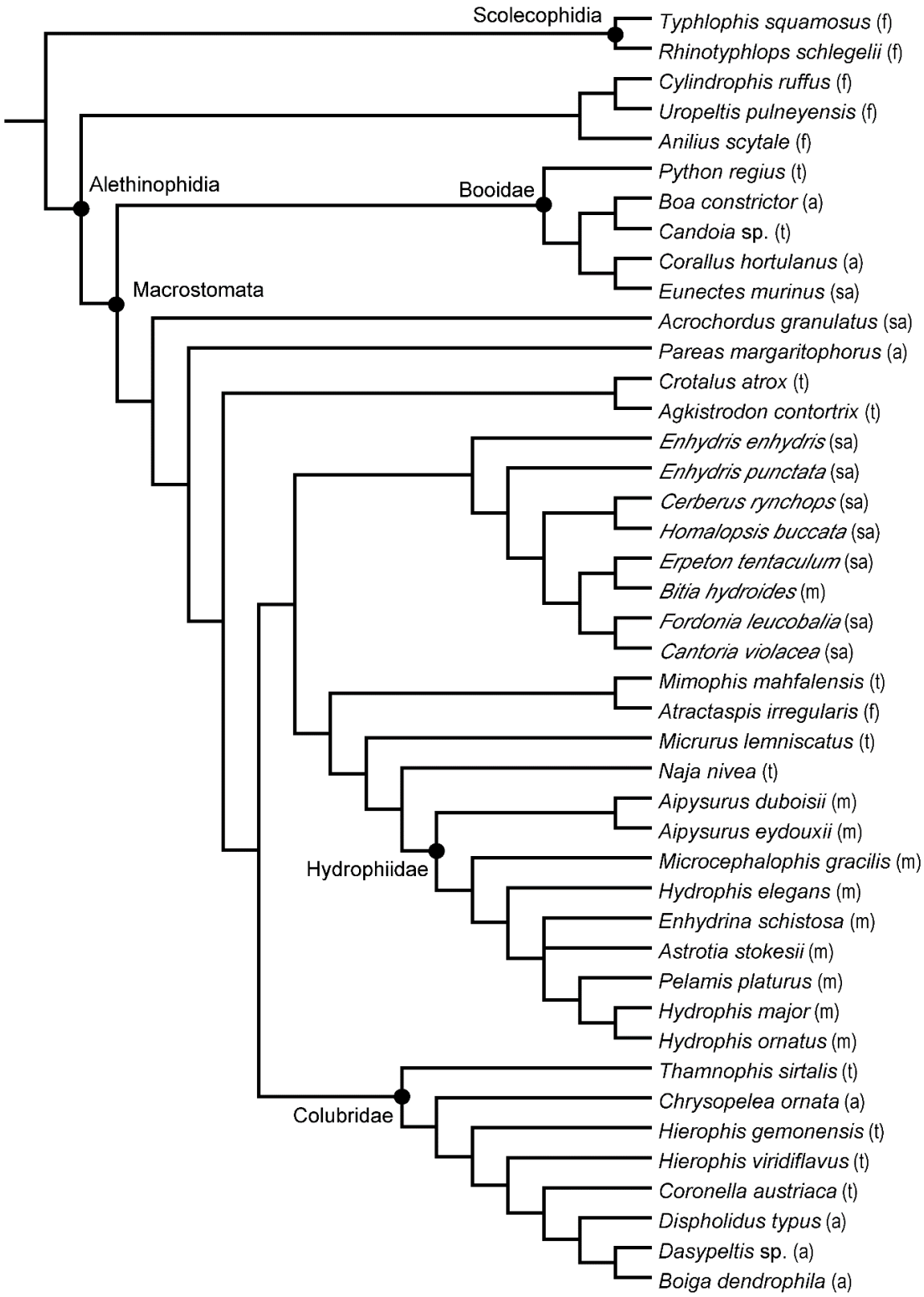

Fig. 5.1. Schematic phylogenetic relationships of snakes sampled in the study (modified from Lee and Scanlon, 2002; Pyron et al., 2011; Hsiang et al., 2015). Principal ecology/habitat: fossorial (f), terrestrial (t), arboreal (a), semi-aquatic (sa), marine (m).

5.1.2. Methods

Microtomography was performed in order to non-destructively digitize the brain endocast of the specimens (see Chapter 4 Material and Methods). Image segmentation and visualization were performed using VGStudioMax 2.2 (Volume Graphics Inc., Heidelberg, Germany) at the Palaeontology Imaging Unit of the MNHN/UMR 7207 CR2P and Avizo 7.0 (VSG, Burlington MA, USA) at the UMR 7179 MECADEV. The segmentation tools of these software packages were used to select the endocranial space of the specimens thereby allowing separation of the skull from the endocranial space, and to reconstruct the endocast (see Appendix 1 to visualize all snake endocasts reconstructed).

5.1.2.1. Measurements

For each specimen, 21 measurements were defined and taken to illustrate the whole 3D shape, volume and surface of the endocast (see Fig. 5.2B). All the measurements made on the endocast were measured point-to-point and obtained with the digital caliper of VGStudioMax 2.2 and the measuring tool of Avizo 7.0, both with accuracy of 0.01mm (see Appendices 2 and 3). The print of the sutures between the different skull bones visible on the endocast surface were used to define homologous distances. The following list introduces the measurements taken on the endocast. The different parts of the endocast are named with the same terms as those used for the brain itself (see Fig. 5.2A), following Butler and Hodos (2005); however the terms used here do not have a neurological significance and are not related to neural structures.

(a) *Length of the endocast* **(LE)**: distance between the anteriormost part of the olfactory bulbs still entirely surrounded by the frontal bone and the tip of the suture left by the contact of the supraoccipital with the two exoccipitals on the dorsal surface of the endocast;

(b) *Length of the olfactory bulbs* **(LOB)**: distance between the anteriormost part of the olfactory peduncles still entirely surrounded by the frontal bone and the fronto-parietal suture;

(c) *Length of the groove between the olfactory bulbs* **(LG)**: distance between the anteriormost end of the groove between the olfactory peduncles and the fronto-parietal suture;

(d) *Height of the main olfactory bulb* **(HOB)**: at the level of the anteriormost part of the main olfactory bulb still entirely surrounded by the frontal bone;

(e) *Height of the olfactory peduncle* **(HOP)**: at the level of the fronto-parietal suture;

(f) *Width of the olfactory peduncles* **(WOP)**: at the level of the fronto-parietal suture;

(g) *Length of the fissura interhemispherica* **(LFI)**: distance between the fronto-parietal suture and the virtual limit made by the groove between the cerebral hemispheres and the optic tectum;

(h) *Maximal width of the cerebral hemispheres* **(WCH)**;

(i) *Lateral expansion of the cerebral hemispheres* **(LCH)**: distance between the fronto-parietal suture and the posterior end of the lateral margin of the cerebral hemispheres;

(j) *Maximal height of the cerebral hemispheres* **(HCH)**;

(k) *Maximal width of the optic tectum* **(WOR)**;

(l) *Length of the optic tectum* **(LOR)**: distance between the virtual limit made by the groove separating the cerebral hemispheres of the optic tectum (see Fig. 5.2B) and the tip of the V-shaped suture between the parietal and the supraoccipital (see Fig. 5.2A);

(m) *Height of the optic tectum* **(HOR)**: distance between the dorsal surface of the optic tectum and the triple point formed by the suture between the parietal, prootic and basisphenoid (see Fig. 5.2A);

(n) *Length of the pituitary gland* **(LP)**: distance between the fronto-parietal suture and the most posterior point of the pituitary bulb;

(o) *Height of the pituitary gland* **(HP)**: distance between the most ventral point of the pituitary gland and the triple point formed by the sutures between the parietal, prootic and basisphenoid;

(p) *Width of the inner ear region* **(WIE)**: distance between the two triple points formed by the sutures of the supraoccipital, prootic and exoocipital;

(q) *Dorsal width of the posterior end of the endocast* **(DWPE)**: distance taken at the level of the suture between the supraoccipital and the two exoccipitals seen on the dorsal surface of the endocast;

(r) *Length of the posterior part of the endocast* **(LPE)**: distance between the tip of the V-shaped suture between the parietal and the supraoccipital, and the tip of the V-shaped suture between the supraoccipital and the two exoccipitals;

(s) *Height of the posterior part of the endocast* **(HPE)**: distance between the maximum of concavity of the inner ear region and the ventral margin of the endocast;

(t) *Width of the ventral part of the endocast* **(WPE)**: distance between the two triple points formed by the suture between the prootic, basisphenoid and basioccipital on the ventral margin;

(u) *Width in the pituitary gland region* **(WP)**: distance taken on the ventral surface of the brain endocast, between the triple points formed by the sutures between the parietal, prootic and basisphenoid.

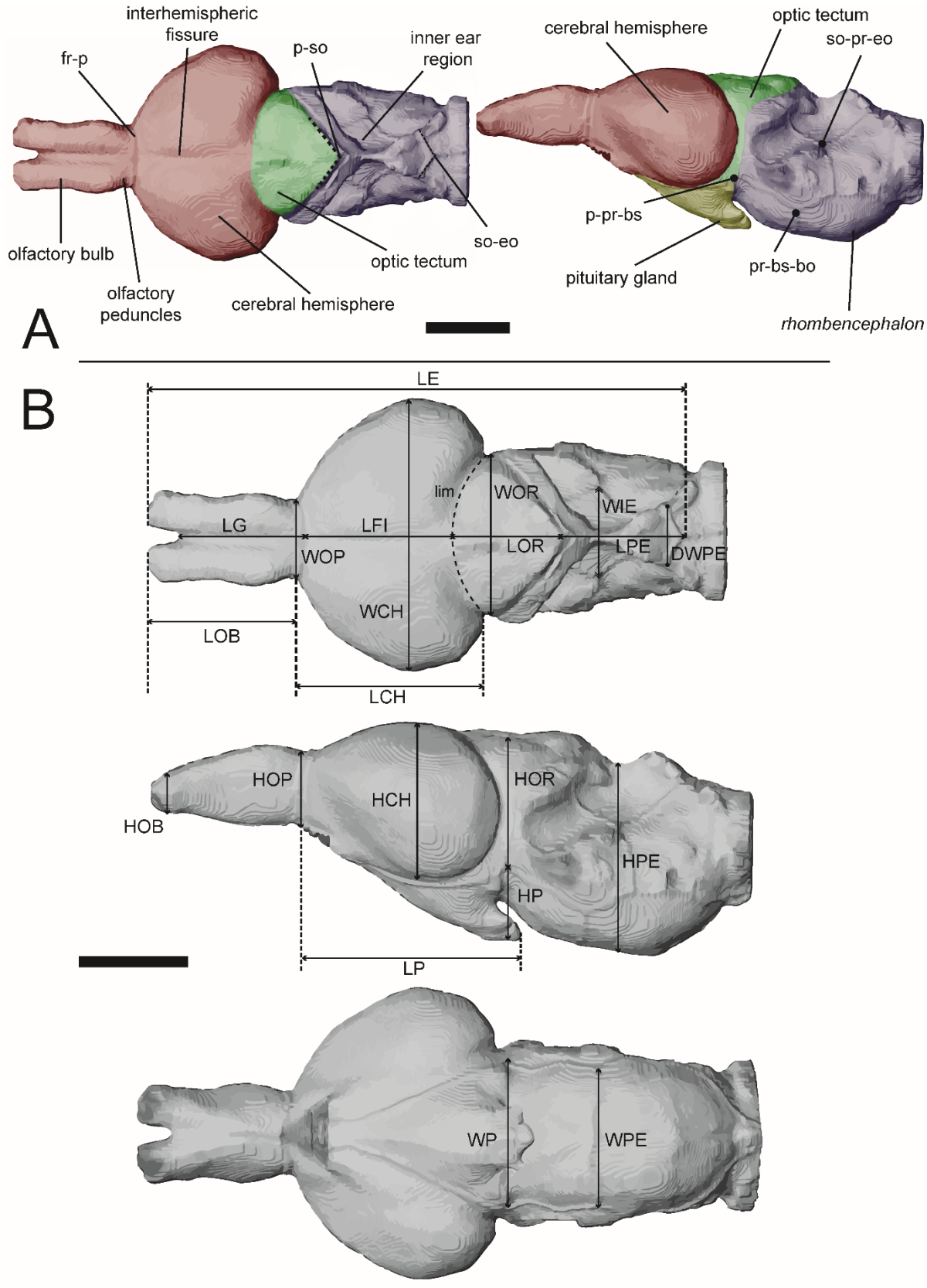
A
interhemispheric fissure
fr-p
p-so
inner ear region
olfactory bulb
olfactory peduncles
optic tectum
so-eo
cerebral hemisphere
cerebral hemisphere
optic tectum
so-pr-eo
p-pr-bs
pituitary gland
pr-bs-bo
rhombencephalon
B
LE
lim
WOR
WIE
LG
LFI
LOR
LPE
DWPE
WOP
WCH
LOB
LCH
HOP
HCH
HOR
HOB
HPE
HP
LP
WP
WPE

Fig. 5.2. Reconstructed endocast of *Enhydris punctata* (Homalopsidae) **(A)**, Illustration of the major structures seen in dorsal and left lateral views: telencephalon (red), diencephalon (yellow), mesencephalon (green), rhombencephalon (purple); **(B)**, Illustration of the various measurements defined in Material and Method and taken in dorsal, left lateral and ventral views. **Abbreviations: fr-p**, fronto-parietal suture; **lim**, groove between the optic tectum and the cerebral hemispheres; **p-pr-bs**, triple point formed by the sutures between the parietal, prootic and basisphenoid; **p-so**, parietal-supraoccipital suture; **pr-bs-bo**, triple point formed by the suture between the prootic, basisphenoid and basioccipital; **so-eo**, supraoccipital-exoccipital suture; **so-pr-eo**, triple point formed by the sutures of the supraoccipital, prootic and exoocipital; **DWPE**, Dorsal width of the posterior end of the endocast; **HCH**, Maximal height of the cerebral hemisphere; **HOB**, Height of the main olfactory bulb; **HOP**, Height of the olfactory peduncle; **HOR**, Height of the optic tectum; **HP**, Height of the pituitary bulb; **HPE**, Height of the posterior part of the endocast; **LCH**, Lateral expansion of the cerebral hemispheres; **LE**, Length of the endocast; **LFI**, Length of the interhemispheric fissure; **LG**, Length of the groove between olfactory bulbs; **LOB**, Length of the olfactory bulbs; **LOR**, Length of the optic tectum; **LP**, Length of the pituitary bulb; **LPE**, Length of the posterior part of the endocast; **WCH**, Maximal width of the cerebral hemispheres; **WIE**, Width in the inner ear region; **WOP**, Width of the olfactory peduncles; **WOR**, Maximal width of the optic tectum; **WP**, Width in the pituitary gland region; **WPE**, Width of the ventral part of the endocast. Scale bar equals to 2 mm.

5.1.2.2. Quantitative analyses

In order to provide complementary information, three different approaches were used to study the endocranial variability occurring in snakes.

Descriptive character analysis

The differences observed between the various snake endocasts were listed and coded (see Appendix 4: List of the characters and Matrix). We used the coded characters to run a principal

coordinate analysis (PCoA) in order to evaluate the distances between the taxa and thus to identify which taxa are similar in endocast morphology based on these coded characters: the closest the species, the more similar are the endocast morphologies.

Measure analysis

All data (see Appendices 2 and 3) were log10-transformed prior to analysis to meet assumptions of normality and homoscedasticity required for parametric analyses. All the analyses were performed using the statistic software R (R Development Core Team, 2008). To analyze shape components independently from size, the log-shape ratios (Mosimann and James, 1979) were calculated based of the raw log10-transformed linear dimensions of the brain endocast.

In order to take into account the biases induced by measurement repeatability, three specimens of *Python regius* showing the lowest shape variation were selected. According to the data published by Aubret et al. (2005), the comparison of their jaw length seems to differentiate a neonate specimen (P1; jaw length = 25.4 mm) from a juvenile (P3; jaw length = 31.4 mm) and an adult (P2; jaw length = 40.3 mm) ones. Ten repetitions were performed for each measure on these three specimens. Then, to quantify and visualize the differences between repetitions, a Principal Component Analysis (PCA) was performed. Shape differences between specimens were much higher than shape differences induced by repetitions.

To evaluate the phylogenetic signal in the shape of the endocast in snakes, we used a multivariate generalization of the K statistic of Blomberg et al. (2003): the *K*mult (Adams, 2014). The phylogenetic signal is based on a phylogenetic consensus tree derived from several published phylogenies (Lee and Scanlon, 2002; Pyron et al., 2011; Hsiang et al., 2015, Fig. 5.1). Adams (2014) demonstrated that values of *K*mult <1 imply that taxa resemble each other phenotypically less than expected under Brownian motion whereas values of *K*mult >1 imply that close relatives are more similar to one another phenotypically than expected under Brownian motion. A PCA was also performed on the data obtained from the measurements made on the 45 snake specimens; the mean of the 10 measurements taken on each of the *Python regius* specimens was used.

To test the relationships between the habitat/ecology and the morphology of the endocast, the sampled taxa were classified into five habitat categories (see Fig. 5.1): fossorial,

terrestrial, arboreal, semi-aquatic, and marine (Heatwole, 1999; Houssaye et al., 2013; A. Herrel personnal communication). We performed a standard and phylogenetic MANOVA, to respectively evaluate whether the endocast variability could reflect the ecology, taking or not the phylogenetic relationships into consideration.

Outline curve analysis

For each brain endocast, the ventral and lateral views were selected to perform an outline curve analysis using geometric morphometrics (Zelditch et al., 2004). We used 2D sliding semi-landmarks (Gunz and Mitteroecker, 2013) that permit accurate description of homologous anatomical curves devoid of anatomical landmarks. Sliding semi-landmarks are allowed to slide, minimizing the bending energy between each specimen and the mean shape of the data set. This step creates a geometric homology between specimens that permits all classical geometric morphometric analyses. We performed a General Procrustes Superimposition to work on shape (Rohlf and Slice, 1990) and PCAs for each view.

The dorsal view was not used here because of the difficulty to distinguish homologous outline curves on the posterior part of the structure at the level of the inner ear position. In ventral view, the 45 endocasts of our dataset were used. In lateral view, we used the posterior crest formed by the inner ear and three homologous points as landmarks to facilitate the placement of the curve semilandmarks. The sutures between the different skull bones visible on the posterior part of the endocast surface were used to define homologous points. The first point corresponds to the triple point formed by the sutures between the basioccipital, exoccipital and prootic. The second is the triple point formed by the prootic, the basioccipital and the basisphenoid. The last point represents the most ventral point of the suture between the basioccipital and the basisphenoid. In lateral view, we used 38 specimens because the sutures are not visible and did not allow the placement of the same landmarks on *Aipysurus eidouxii*, *Cerebrus rynchops*, *Corallus hortulanus*, *Dispholidus typus*, *Mimophis mahfalensis*, the smallest specimen of *Python regius* and *Uropeltis pulneyensis*.

5.2. General description of snake endocast and variability

Here, only a description of the endocast will be provided, without considering the cranial nerves or the inner ear (data in Boistel et al., 2011; Yi and Norell, 2015). The cast of the endocranial space does not only reflect the brain itself: associated tissues (e.g., venous system) are also reconstructed during segmentation and may hide some parts of the brain. The endocast morphology resulting from the segmentation of the endocranial space is described below as a whole. The endocast in snakes is surrounded dorsally by the frontal and parietal (anteriorly) and the supraoccipital and exoccipital (posteriorly), laterally by the prootics, and ventrally by the basioccipital and para-basisphenoid (Fig. 5.3). The surface of the endocast of snakes is smooth.

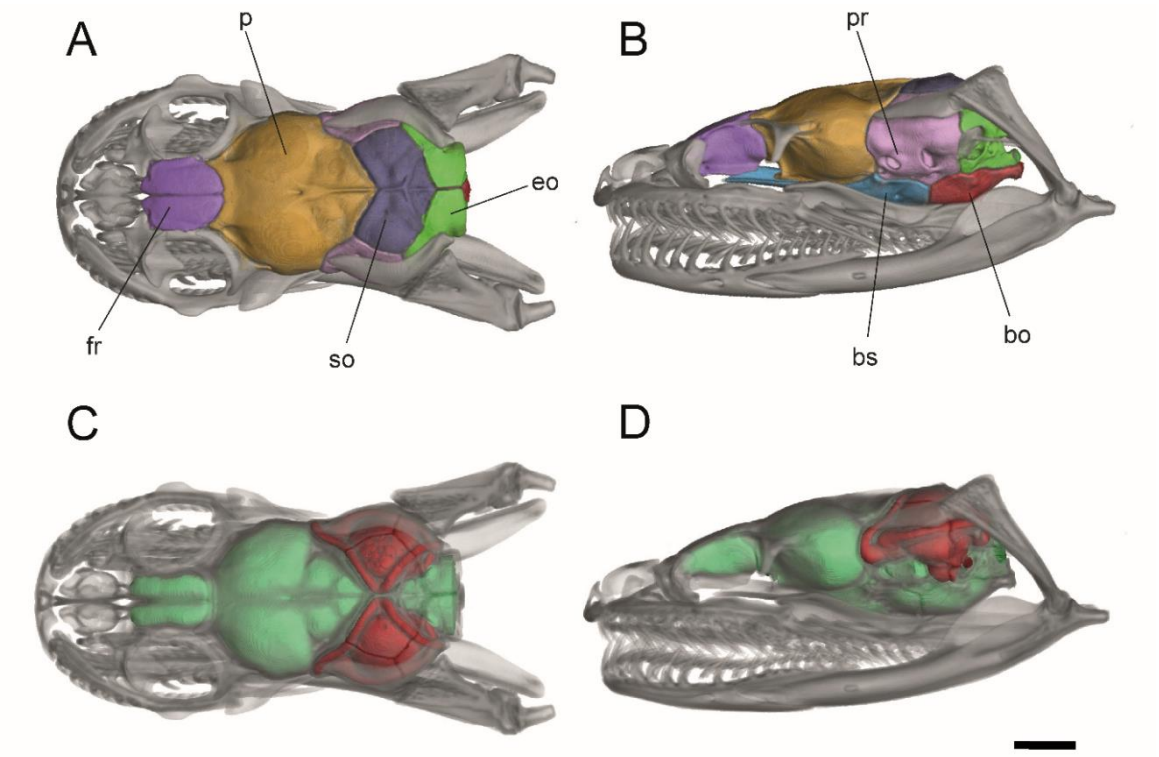

Fig. 5.3. Skull of *Enhydris punctata* (Homalopsidae) in dorsal (A) and left lateral (B) views showing the bones surrounding the endocast; (C-D) with bones rendered transparent to reveal the endocast (green) and the inner ear (red). **Abbreviations: bo**, basioccipital; **bs**, basisphenoid; **eo**, exoccipitals; **fr**, frontal; **p**, parietal; **pr**, prootics; **so**, supraoccipitals. Scale bar equals 2 mm.

5.2.1. Telencephalon

The telencephalon includes the olfactory bulbs, the olfactory peduncles and the cerebral hemispheres (see Fig. 5.2A). The main and accessory olfactory bulbs correspond to the anteriormost structure of the brain endocast (see Fig. 5.2A); however, from the endocast only it is not possible to distinguish one from another. They are attached to the rostral pole of the cerebral hemisphere by short olfactory peduncles. In dorsal view, a groove is visible running between the two olfactory bulbs. Posteriorly, the cerebral hemispheres represent the largest part of the endocast and gradually widen laterally. An interhemispheric fissure may be visible on the dorsal surface of the endocast, as attested by a groove between the cerebral hemispheres. The length of the interhemispheric fissure and the depth of the groove vary according to taxa.

Some taxa may exhibit olfactory bulbs wider than long, giving a short and stout aspect (e.g., width/length aspect ratio superior to one in *Typhlophys squamosus*, see Fig. 5.4A) in dorsal view, while most taxa have an olfactory structure longer than wide (e.g., width/length aspect ratio inferior to one in *Hierophis viridiflavus*, see Fig. 5.4B). The lateral margin of this structure may be mediolaterally convex (e.g., *Acrochordus granulatus*, see Fig. 5.4D), relatively straight (e.g., *Eunectes murinus*, see Fig. 5.4E) or mediolaterally concave (e.g., *Hierophis viridiflavus*, see Fig. 5.4B) in dorsal view. Most species possess in dorsal view a system composed of two parallel olfactory bulbs and peduncles (e.g., *Eunectes murinus*, see Fig. 5.4E). Some others show a projection that diverges laterally from the fronto-parietal suture (e.g., *Homalopsis buccata*, see Fig. 5.4F), whereas others share the two conditions with parallel olfactory bulbs and peduncles diverging laterally at their anterior end (e.g., *Hierophis viridiflavus*, see Fig. 5.4B). In lateral view, the ventral margin may be ventrodorsally concave (e.g. *Mimophis mahfalensis*, see Fig. 5.5D), convex (e.g., *Boiga dendrophila*, see Fig. 5.5B) forming a bulge, or straight (e.g., *Homalopsis buccata*, see Fig. 5.5C). Some taxa (e.g., *Typhlophys squamosus*, see Fig. 5.4A) do not show any separation over the whole length of the olfactory peduncles in dorsal view. Most taxa have olfactory peduncles diverging only at their anterior end (e.g., *Hierophis viridiflavus*, see Fig. 5.4B). Some species have a large space between the two olfactory structures, separating them along almost their entire length (e.g., *Acrochordus granulatus*, see Fig. 5.4D). The width of the olfactory bulbs may vary antero-posteriorly. At the level of the fronto-parietal suture and in dorsal view, some taxa possess a

posterior part as wide (e.g., *Eunectes murinus*, see Fig. 5.4E) or wider (e.g., *Cylindrophis ruffus*, see Fig. 5.4C) than the anterior end. However, others have olfactory bulbs with an anterior end wider than the posterior part (e.g., *Hierophis viridiflavus*, see Fig. 5.4B).

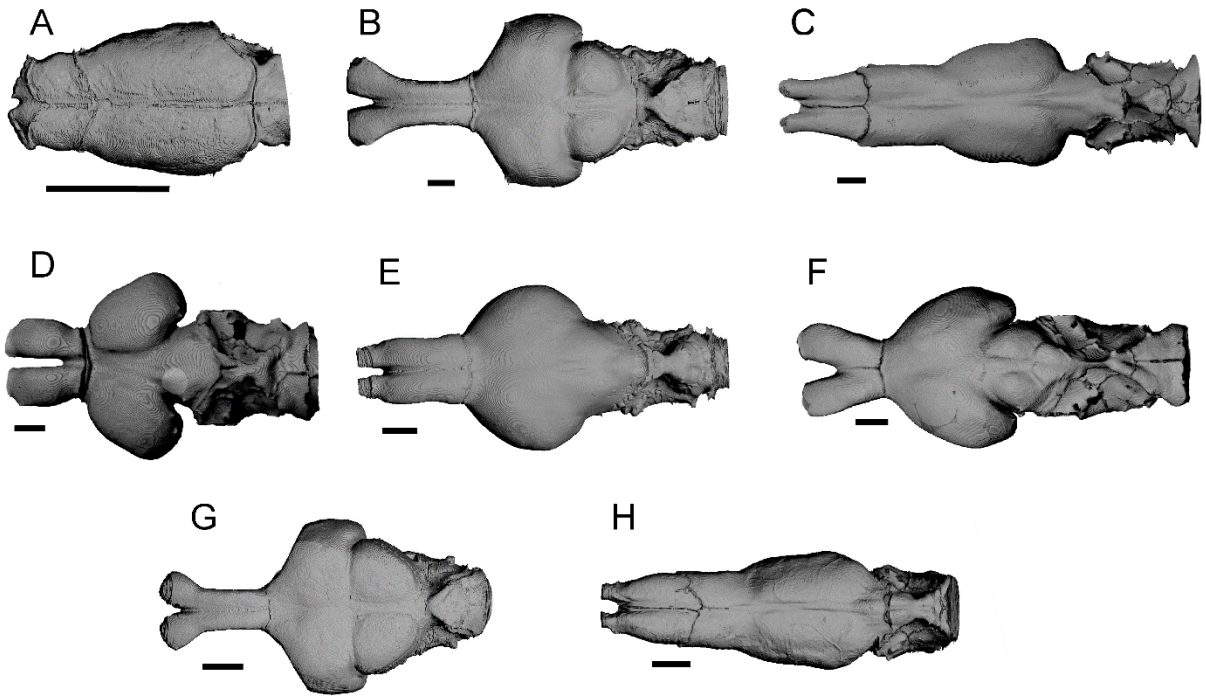

Fig. 5.4. Endocasts in dorsal view of **(A)** *Typhlophys squamosus* (Typhlopidae); **(B)** *Hierophis viridiflavus* (Colubridae); **(C)** *Cylindrophis ruffus* (Cylindrophiidae); **(D)** *Acrochordus granulatus* (Acrochordidae); **(E)** *Eunectes murinus* (Boidae); **(F)** *Homalopsis buccata* (Homalopsidae); **(G)** *Chrysopelea ornata* (Colubridae); **(H)** *Anilius scytale* (Aniliidae). Scale bars equal 1mm.

The relative size of the cerebral hemispheres varies between taxa. A distinction is seen between those that have hemispheres wider than long (e.g., width/length aspect ratio close to 1.4 in *Chrysopelea ornata*, see Fig. 5.4G) and those that have a structure as long as wide (e.g., width/length aspect ratio close to one in*Typhlophys squamosus*, see Fig. 5.4A). A few taxa are exceptions with cerebral hemispheres longer than wide (e.g., width/length aspect ratio close to 0.3 in *Cylindrophis ruffus*, see Fig. 5.4C). The lateral extension in dorsal view generally begins

just posterior to the fronto-parietal suture (e.g., *Eunectes murinus*, see Fig. 4E) but two taxa (*Cylindrophis ruffus* [Fig. 5.4C] and *Anilius scytale* [Fig. 5.4H]) exhibit cerebral hemispheres with an anterior part as wide as the fronto-parietal suture, the lateral extension occurring more posteriorly. In dorsal view, the lateral margin may be rounded (e.g., *Eunectes murinus*, see Fig. 5.4E) or relatively straight (e.g., *Chrysopelea ornata*, see Fig. 5.4G), providing a square appearance to the cerebral hemispheres. In lateral view, differences occur between taxa with cerebral hemispheres developed only along the horizontal axis (e.g., *Typhlophys squamosus*, see Fig. 5.5A), taxa with cerebral hemispheres developed in the horizontal plane but with a posterior part directed ventrally (e.g., *Homalopsis buccata*, see Fig. 5.5C) and taxa with a dorso-ventral extension at least as long as the horizontal one (e.g., *Boiga dendrophila*, see Fig. 5.5B). The limit between the cerebral hemispheres and the optic tectum depends on the lateral extension of the cerebral hemispheres. Species that do not have an important lateral extension (e.g., *Anilius scytale*, see Fig. 5.4H) do not show a clear delimitation between the optic tectum and the cerebrum, contrary to those that have a groove between the two structures and have laterally extended cerebral hemispheres (e.g., *Chrysopelea ornata*, see Fig. 5.4G).

5.2.2. Diencephalon

The pituitary gland, located ventrally to the cerebral hemispheres, is the only structure of the diencephalon seen on the endocast (see Fig. 5.2A); the pineal gland is not visible. In addition, the external morphology of the endocast does not allow the hypothalamus and the hypophysis to be delimited.

The pituitary gland may be marked by the presence in lateral view of a small bulge on the ventral surface of the endocast (e.g., *Anilius scytale*, see Fig. 5.5E). But generally the system shows a structure more developed ventrally, displaying (e.g., *Hierophis viridiflavus*, see Fig. 5.5F) or not (e.g., *Eunectes murinus*, see Fig. 5.5G) a posterior projection. Among those displaying a posterior projection, a distinction is made between those presenting a tilted system (e.g., *Enhydrina schistosa*, see Fig. 5.5H) and those having a posterior projection in the horizontal plane (e.g., *Hierophis viridiflavus*, see Fig. 5.5F). Differences relative to the ventral

margin of the posterior projection also occur, between a curved (e.g., *Thamnophis sirtalis*, see Fig. 5.5J) and a flat (e.g., *Dispholidus typus*, see Fig. 5.5I) shape.

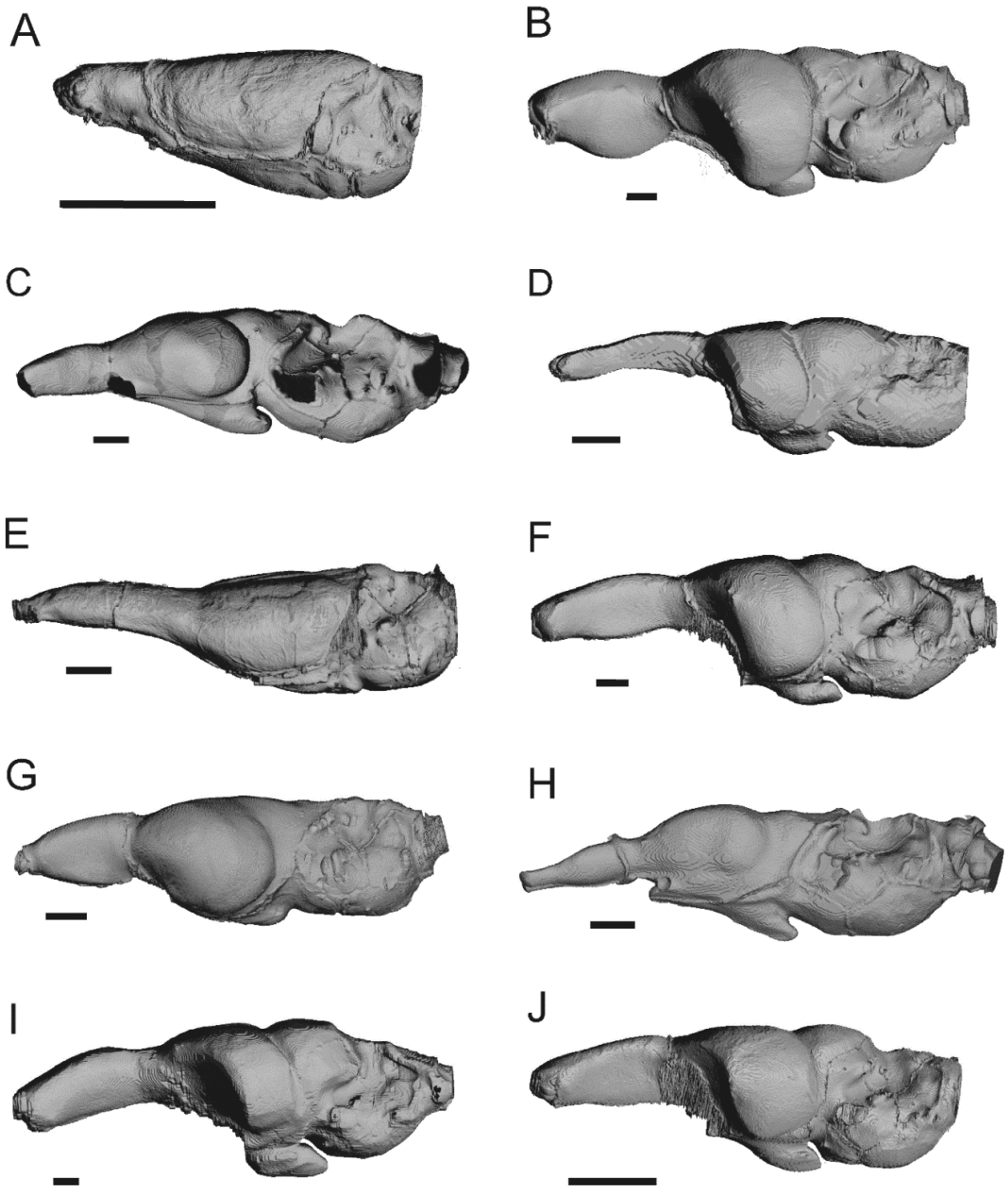

Fig. 5.5. Endocasts in left lateral view of **(A)** *Typhlophys squamosus* (Typhlopidae); **(B)** *Boiga dendrophila* (Colubridae); **(C)** *Homalopsis buccata* (Homalopsidae); **(D)** *Mimophis mahfalensis* (Lamprophiidae); **(E)** *Anilius scytale* (Aniliidae); **(F)** *Hierophis viridiflavus* (Colubridae); **(G)** *Eunectes murinus* (Boidae); **(H)** *Enhydrina schistosa* (Elapidae); **(I)** *Dispholidus typus* (Colubridae); **(J)** *Thamnophis sirtalis* (Natricidae). Scale bars equal 1mm.

5.2.3. Mesencephalon

The mesencephalon lies posterior to the cerebral hemispheres. The optic tectum forms the roof of the mesencephalon (see Fig. 5.2A). From the endocast, the distinction between the optic tectum and the tegmentum, which is located more ventrally in the mesencephalon, is not possible. In dorsal view, the mesencephalon is less wide than the cerebral hemispheres.

In a few taxa this structure is not distinguishable from the cerebral hemispheres (e.g., *Typhlophys squamosus*, see Fig. 5.4A). In some others, the structure is visible in dorsal view only thanks to its decrease in width as compared to the cerebral hemispheres (e.g., *Eunectes murinus*, see Fig. 5.4E), and its surface appears smooth and flattened. However, in other species, the optic tectum exhibits in dorsal view a pair of domes separated by a median sulcus (e.g., *Thamnophis sirtalis*, see Fig. 5.6A). Some taxa show (in dorsal view) a distinct optic tectum as wide as the rhombencephalon (e.g. *Homalopsis buccata*, see Fig. 5.4F). The others have an optic tectum wider (e.g., *Chrysopelea ornata*, see Fig. 5.4G) or narrower (e.g., *Acrochordus granulatus*, see Fig. 5.4D) than the ventral margin of the rhombencephalon. In lateral view, most taxa possess a dorsal margin of the optic tectum located at the same height as the cerebral hemispheres (e.g., *Eunectes murinus*, see Fig. 5.5G), except *Erpeton tentaculatum*, in which the margin is located more dorsally (see Fig. 5.6D).

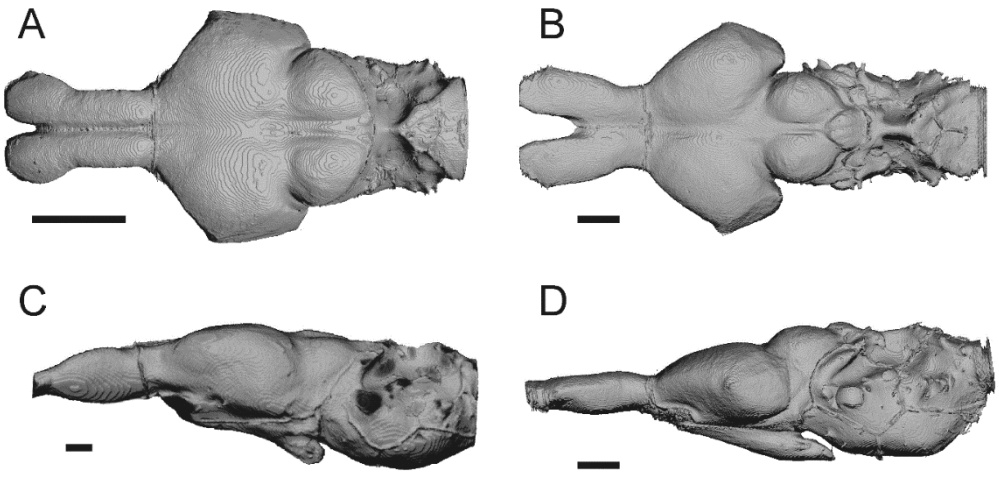

Fig. 5.6. Endocasts in dorsal (upper row) and left lateral (lower row) views of **(A)** *Thamnophis sirtalis* (Natricidae); **(B)** *Erpeton tentaculatum* (Homalopsidae); **(C)** *Hydrophis major* (Elapidae); **(D)** *Erpeton tentaculatum*. Scale bars equal 1mm.

5.2.4. Rhombencephalon

Posterior to the optic tectum, the cerebellum is not visible on the dorsal surface of the endocast. According to Aurboonyawat et al. (2008), the dorsal longitudinal vein located on the mid-dorsal surface of the endocast must cover it. On the lateral sides of the endocast, the large and round impressions indicate the position of the inner ear (see Fig. 5.2A). The *medulla oblongata* is located ventral to the inner ear region, and represents the ventral margin of the posterior part of the endocast.

Most species exhibit a rhombencephalon in lateral view with a rounded (e.g., *Boa constrictor*, see Fig. 5.7A) or straight (e.g., *Erpeton tentaculatum*, see Fig. 5.6D) ventral margin, but in some taxa (e.g., *Crotalus atrox*, see Fig. 5.7B) the ventral margin is triangular, pointing ventrally. The ventral extension of the *rhombencephalon* may correspond to the most ventral surface of the endocast in lateral view (e.g., *Boa constrictor*, see Fig. 5.7A) or not (e.g., *Dispholidus typus*, see Fig. 5.5I).

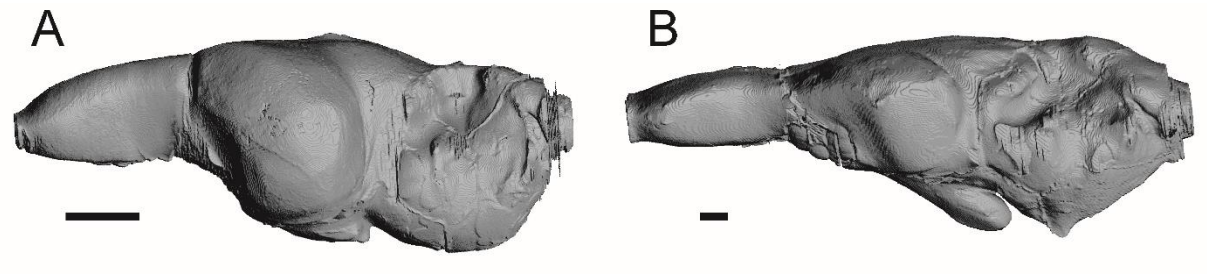

Fig. 5.7. Endocasts in left lateral view of **(A)** *Boa constrictor* (Boidae); **(B)** *Crotalus atrox* (Viperidae). Scale bars equal 1mm.

5.3. Quantitative analyses

Snake endocasts show a great variability. This variability is characterized by different relative proportions between the structures visible on the endocasts (e.g., size of the optic tectum compared to that of the cerebral hemispheres), giving a wide range of shapes, from stout (e.g.,

Typhlophis squamosus), to elongated and gracile (e.g., *Pelamis platurus*) or elongated and wide (e.g., *Boa constrictor*) endocasts. Below, this variability is analyzed quantitatively.

5.3.1. Descriptive character analysis

The results obtained (Fig. 5.8) show that 50.3 % of the variance is explained by the two main principal components (29.4 % and 20.9 % respectively). The distribution of the taxa indicates that fossorial and marine snakes are both distinct from those with other ecologies. Among the fossorial species, *Atractaspis irregularis* is quite distinct from two groups: the first one including *Uropeltis pulneyensis*, *Cylindrophis ruffus*, and *Anilius scytale*, and the second one made by *Typhlophis squamosus* and *Rhinotyphlops schlegelii*. *Micrurus lemniscatus* and *Acrochordus granulatus*, a terrestrial and a semi-aquatic snakes, respectively, tend toward the endocast morphology found in the fossorial taxa. Among the marine species of our dataset, *Enhydrina schistosa* and *Microcephalophis gracilis* are close to each other and distinct from other marine snakes. The terrestrial species show a wide distribution. The isolated position of *M. lemniscatus* was already cited above. *Hierophis gemonensis*, *Hierophis viridiflavus*, and *Thamnophis sirtalis* are close together and located near the two arboreal snakes *Dispholidus typus* and *Chrysopelea ornata*. These species are distinct from *Mimophis mahfalensis*, *Crotalus atrox, Agkistrodon contortrix*, *Coronella austriaca* and *Naja nivea*, which are close together and possess a brain endocast morphology similar to the arboreal snakes *Boiga dendrophila* and *Dasypeltis* sp. In addition, the three specimens of *Python regius* and *Candoia* sp., are distinct from the other terrestrial taxa with an endocast morphology tending towards those found in marine ones. Among the arboreal taxa not cited above, *Corallus hortulanus, Boa constrictor* and *Pareas margaritophorus* are close to the semi-aquatic snake *Cantoria violacea*. The distribution of the semi-aquatic species overlaps those of the terrestrial and arboreal snakes. The endocast of *Enhydris enhydris* is similar to that of *M. mahfalensis* and distinct from those of *Erpeton tentaculum*, *Fordonia leucobalia*, *Homalopsis buccata*, and *Enhydris punctata*, which are grouped together. The two species *Cerberus rynchops* and *Eunectes murinus* are respectively close to *Candoia* sp. and to the three specimens of *P. regius*, and tend towards the marine taxa.

The species distribution suggests the existence of phylogenetic and ecological signals. Phylogenetically close species show more similarities than with other species (e.g., *Typhlophis squamosus* and *Rhinotyphlops schlegelii*). However, an ecological signal is also perceived, meaning that species sharing the same ecology show more endocranial similarities than species with a different ecology.

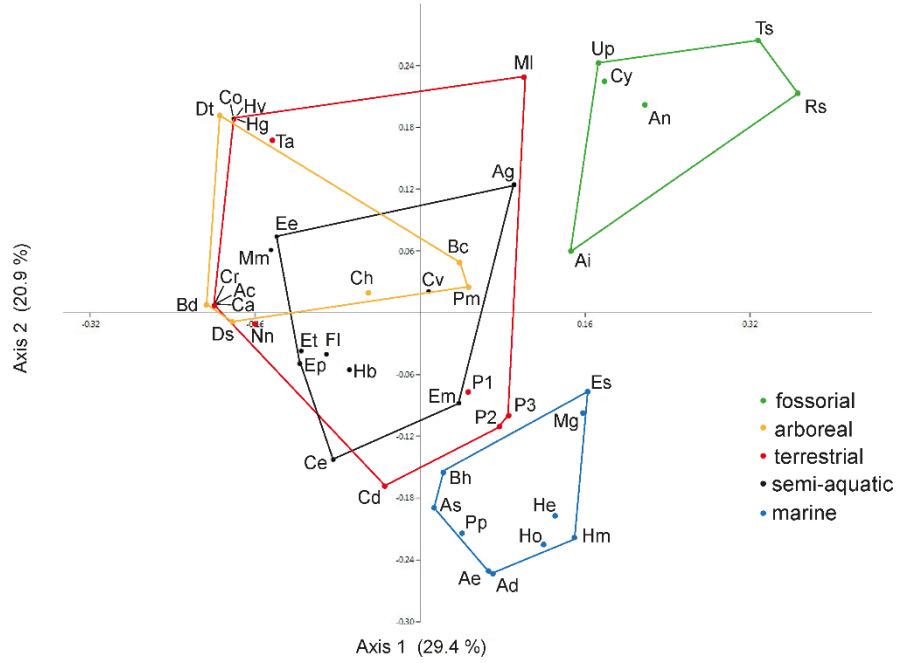

Fig. 5.8. Results of the principal coordinate analysis performed on the snake endocast characters (Appendix 4). See Material and Methods (Chapter 4, p. 61) for name abbreviations.

5.3.2. Measure analysis

5.3.2.1. Intraspecific variability in Python regius

The PCA (see Fig. 5.9) shows that the two main axes explain 93 % of the variance (80 % and 13 % respectively). The repeatability test is positive as the ten iterations for each specimen are clearly grouped and the three specimens clearly distinct, indicating that the variability caused by the measurement acquisition is inferior to the variability between the specimens. All variables seem to act on the distribution of the specimens (though the impact of LP (Length of the pituitary bulb) on the second axis appears significantly more important than that of the other

variables). The first principal component mostly separates the specimens based on size. The variables principally acting on PCA1 are the height of the olfactory bulbs (HOB), the length of the optic tectum (LOR) and the length of the pituitary gland (LP). The smaller specimen (P1) has the greatest height of the olfactory bulbs, the greatest length of the pituitary bulb, and the smallest length of the optic tectum. The second principal component separates the intermediate specimen (P3) from the two others. The main variable acting along the second axis is still the length of the pituitary gland (LP). The intermediate specimen (P3) shows the smallest height of the olfactory bulb, the greatest length of the optic tectum and an intermediate value for the length of the pituitary gland. Finally, the largest specimen (P2) possesses the greatest length of the pituitary gland, and intermediate values for the height of the olfactory bulb and for the length of the optic tectum.

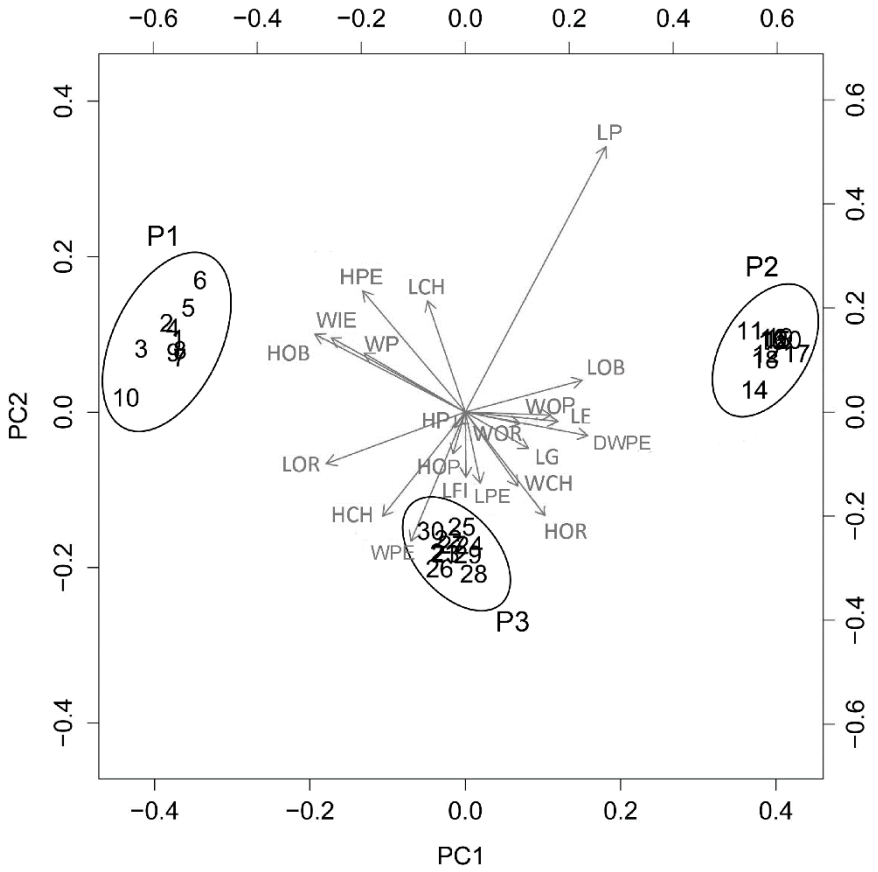

Fig. 5.9. Results of the principal component analysis performed on the endocast variables for three *Python regius* specimens, (P1) smaller specimen, (P3) intermediate specimen, (P2) largest specimen. Scatter plot illustrating the position of the different specimens on the first two principal components. **Abbreviations: DWPE**, Dorsal width of the posterior end of the endocast; **HCH**, Maximal height of the cerebral hemisphere; **HOB**, Height of the main olfactory bulb; **HOP**, Height of the olfactory peduncle; **HOR**, Height of the optic tectum; **HP**, Height of the pituitary bulb; **HPE**, Height of the posterior part of the endocast; **LCH**, Lateral expansion of the cerebral hemispheres; **LE**, Length of the endocast; **LFI**, Length of the interhemispheric fissure; **LG**, Length of the groove between olfactory bulbs; **LOB**, Length of the olfactory bulbs; **LOR**, Length of the optic tectum; **LP**, Length of the pituitary gland; **LPE**, Length of the posterior part of the endocast; **WCH**, Maximal width of the cerebral hemispheres; **WIE**, Width in the inner ear region; **WOP**, Width of the olfactory peduncles; **WOR**, Maximal width of the optic tectum; **WP**, Width in the pituitary gland region; **WPE**, Width of the ventral part of the endocast.

5.3.2.2. Interspecific variability

The PCA obtained with all snake specimens (see Fig. 5.10) shows that 60 % of the variance is explained by the two first axes (44.7% and 15.3% respectively). Fossorial species are clearly distinct from the others, with a great distribution along the first axis, contrary to the snakes with other ecologies, that all display a more limited distribution. The PCA shows some overlap between the snakes with arboreal, terrestrial, semi-aquatic and marine habitats, but a gradation is clearly visible. The arboreal and terrestrial taxa appear distinct (with no overlap) from the marine ones. All variables seem to act on the repartition of the species (see Appendix 5). However, along the first axis, two variables mostly act on the distribution of the taxa: the width at the optic tectum level (WOR) and the dorsal width of the posterior end of the endocast (DWPE). The first axis seems to separate species that have an optic tectum as wide as the posterior end of the endocast (e.g., *Typhlophis squamosus*) from the ones in which the optic tectum is much wider than the posterior end of the endocast (e.g., *Pelamis platurus*). Along the second axis, the width of the olfactory peduncles (WOP) and the width of the cerebral hemispheres (WCH) explain most of the variability. These variables allow to distinguish

species presenting a large difference between the width of the olfactory peduncles and the width of the cerebral hemispheres (e.g., *Boa constrictor*), from those that have a smaller difference between these two widths (e.g., *Cylindrophis ruffus*).

The MANOVA performed on the data indicates significant differences between endocasts depending on ecology (MANOVA: Wilks $\lambda = 0.751$, $F_{2, 22} = 8.75$, $P = 0.013$). The Kmult test indicates that endocast shape in snakes exhibits a significant phylogenetic signal (Kmult = 0.814; P.value = 0.001), showing the importance to consider the phylogeny in studies of snake endocasts. The phylogenetic MANOVA still indicates significant differences pending on ecology (phylogenetic MANOVA: Wilks $\lambda = 0.0074$, $F_{2, 22} = 81.748$, Pphyl = 0.0087).

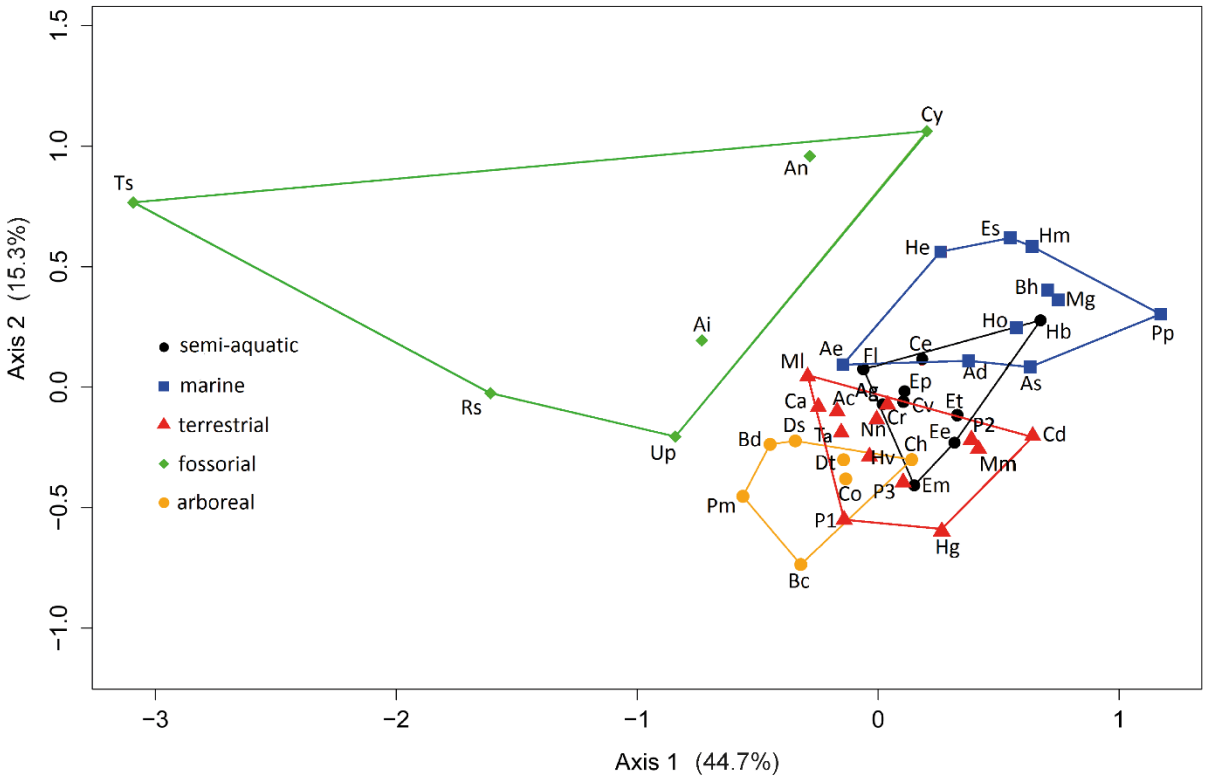

Fig. 5.10. Results of the principal component analyses performed on the snake endocast variables of the 45 specimens. Scatter plot illustrating the position of the different species on the first and second principal components and figuring the different ecologies. See Material and Methods (Chapter 4, p. 61) for name abbreviations.

5.3.3. Outline curve analysis

The results obtained by the outline curve analyses (Fig. 5.11 and 5.12) enable to comment on the shape of snake endocasts according to the different ecologies.

The first PCA is obtained from the endocast outline curves in ventral view (Fig. 5.11) and shows that 61.9% of total variance is explained by the two first axes (44.6% and 17.3% respectively). The first axis separates proportionally stout endocasts, wide at the level of the olfactory bulbs and of the cerebral hemispheres (blue dotted line, Fig. 5.11, Axis 1), from longer and narrower endocasts (black dotted line, Fig. 5.11, Axis 1). Thus, endocasts of semi-aquatic, arboreal and terrestrial snakes are mostly wide, whereas the fossorial and marine species have an extended distribution along this first axis, encompassing both wide and narrow endocasts. However, the distribution of marine taxa is mainly concentrated towards narrow endocasts and only two species, *Aipysurus duboisii* and *Aipysurus eydouxii*, move towards wide endocasts. Along the second axis, the shape of the forebrain (olfactory bulbs and cerebral hemispheres) principally drives the distribution. Endocasts with wide olfactory bulbs have cerebral hemispheres located more anteriorly (dark dotted line, Fig. 5.11, Axis 2) than those with thinner olfactory bulbs (blue dotted line, Fig. 5.11, Axis 2). Semi-aquatic, fossorial and marine species all exhibit an endocast with wide olfactory bulbs and anteriorly located cerebral hemispheres, contrary to the arboreal and terrestrial snakes that are distributed all along the axis and thus express the two conditions.

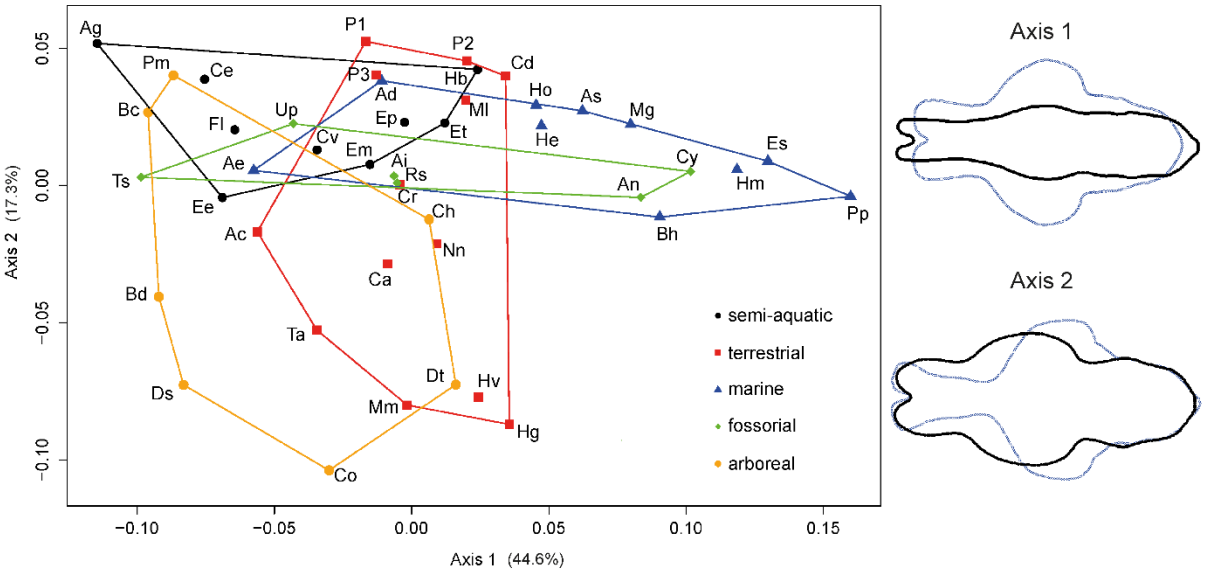

Fig. 5.11. Results of the principal component analyses performed on the snake endocast outline curves in ventral view. The blue and dark dotted lines indicate respectively the low and high values along the two axes. See Material and Methods (Chapter 4, p. 61) for names abbreviations.

The second PCA is obtained from the endocast outline curves in lateral view (Fig. 5.12) and shows that 65.8% of total variance is explained by the two first axes (48% and 17.8% respectively). The first axis illustrates endocasts with well dorsoventrally developed and ventrally oriented olfactory bulbs, and a posterior part characterized by a rounded dorsal surface more developed dorsally than the anterior part (blue dotted line in Fig. 5.12, Axis 1). These endocasts differ from those in which the olfactory bulbs are less developed dorsoventrally and dorsally oriented, and the posterior part presents a flat dorsal surface located at the same level as the anterior part (dark dotted line Fig. 5.12, Axis 1). The endocast of the fossorial species *Rhinotyphlops schlegelii* is well distinct from those of other taxa, with a structure very developed dorsoventrally and the posterior region higher than the anterior one. Arboreal and terrestrial species may show a mix between the two morphologies, with a well dorsoventrally developed endocast but a flat posterior region located at the same level as the anterior one. Marine snakes tend to have a flat endocast, whereas semi-aquatic and fossorial taxa show a large distribution presenting the two endocast morphologies. The second axis separates stout

endocasts well developed dorsoventrally, with a slight dorsal constriction at the limit between the olfactory bulbs and the cerebral hemispheres (blue dotted line Fig. 5.12, Axis 2) from longer but less dorsoventrally developed endocasts (dark dotted line Fig. 5.12, Axis 2), with a ventral constriction at the limit between the olfactory bulbs and the cerebral hemispheres. The distribution of the taxa seems to indicate that the two morphologies are variably found in all ecologies. However, the dorsoventrally compressed endocast found in both marine (*Pelamis platurus*) and terrestrial (*Candoia* sp.) snakes, differs from the more dorsoventrally developed endocasts found in other taxa sharing their ecologies.

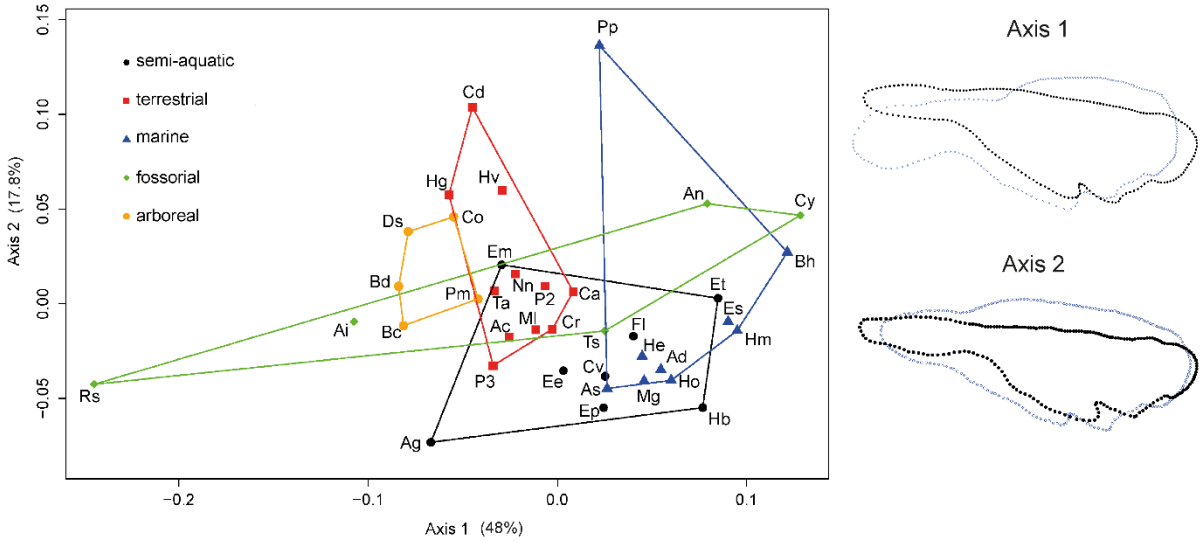

Fig. 5.12. Results of the principal component analyses performed on the snake endocast outline curves in lateral view. The blue and dark dotted lines indicate respectively the low and high values along the two axes. See Material and Methods (Chapter 4, p.61) for names abbreviations.

5.4. Discussion

5.4.1. Phylogenetic signal

We detected a significant phylogenetic signal in the snake endocast variability, meaning that it is at least partly constrained by shared ancestry. Indeed, some patterns or main trends in the brain endocast morphology reflect snakes' systematics. The scolecophidian snakes (*R.*

schlegelii and *T. squamosus*, see Fig. 5.1) are the only ones presenting an endocast where the optic tectum is not visible (see Fig. 5.4A). Within the Booidae (see Fig. 5.1), the surface of the optic roof is smooth (e.g., *Eunectes murinus*, see Fig. 5.4E), and the pituitary gland is only developed ventrally. The Hydrophiidae (see Fig. 5.1) have cerebral hemispheres poorly developed laterally (e.g., *Enhydrina schistosa*, see Fig. 5.5H), contrary to the Colubridae (see Fig. 5.1) that possess cerebral hemispheres very developed both laterally and ventrally (e.g., *Hierophis viridiflavus*, see Fig. 5.4B, 5.5F), as well as an optic roof clearly visible with two distinct domes, and the olfactory bulbs widening on their anterior part. As the multivariate K was lower than one, species resemble each other less than expected under a Brownian motion model of evolution, which shows that, though significant, the phylogenetic signal remains weak. This suggests that other factors, such as ecology, do affect the snake endocast morphology.

5.4.2. Ecological signal

We also detected an ecological signal in the endocast of snakes, even when the phylogenetic relationships were taken into account. Though the different ecologies tested here are thus associated with morphological trends of the endocast, it nevertheless appears difficult to associate one structure with one ecology. Both standard and phylogenetic MANOVAs indicate significant differences between the ecologies, with an impact of all variables on the distribution of snakes. Thus, fossorial species have an endocast with a poor lateral development of the cerebral hemispheres, and not visible or absent optic tectum and pituitary gland. Marine species exhibit an endocast more elongated, with cerebral hemispheres poorly developed laterally and projected only in the antero-posterior plan, but the optic tectum is clearly visible and the pituitary gland is developed ventrally. Endocasts of terrestrial and arboreal snakes differ from marine ones' by the great lateral extension of the cerebral hemispheres. Finally, it appears difficult to distinguish a common pattern for semi-aquatic snakes.

Within the same ecology, a great variability in the endocast morphology can be observed. The results obtained from the outline curve analysis (Fig. 5.11 and 5.12) provide some examples. The cerebral hemispheres of *Aipysurus duboisii* and *Aipysurus eydouxii* are

wider than long and developed ventrally on their posterior part, whereas in the other marine taxa of our dataset, the cerebral hemispheres are as long as wide and only directed in the horizontal plane. The endocasts of *Pelamis platurus* and *Candoia* sp. appear more flattened than those respectively found in other marine and terrestrial species. Finally, the morphology, the proportions and the orientation of the endocast of *Rhinotyphlops schlegelii* appear very distinct from those found in other fossorial snakes. It appears difficult to interpret these differences. It has been demonstrated that constraints imposed by the environment (e.g., habitat) and activity pattern have an impact in snake head shape, irrespective of the phylogenetic relationships (Fabre et al., 2016; Segall et al., 2016). These ecological constraints affect the endocranial morphology in snakes as well. However, it is difficult to determine with certainty which ecological parameters mostly affect the endocranial morphology. The two marine species, *A. duboisii* and *A. eydouxii*, have an endocast quite different from other marine taxa. It is unclear if these differences are related to changes in their skull morphology due to the fish-egg dietary specialization (Sanders et al., 2012) or if the particular morphology of their cerebral hemispheres has a sensory meaning. Similarly, the flattened endocast of *Pelamis platurus*, not found in any other marine specimen from our dataset, could be related to modifications in the skull morphology associated with its pelagic condition, only known in this species, or to its unique foraging strategy at the oceanic surface through labile features such as slicks or drift lines (Brischoux and Lillywhite, 2011). It will be interesting to decompose the ecology in different factors (e.g., locomotion, prey capture mode) to determine which parameters mostly influence the snake brain endocast morphology.

5.4.3. Sensory inferences

Studies in mammals and birds have shown that the endocast morphology, like the brain morphology, may give some information about species sensory abilities (Sakai et al., 2011a, b; Corfield et al., 2012, 2015; Carril et al., 2015). Several studies on snake brain have shown a link between structure and function (e.g., Kubie et al., 1978; Halpern and Frumin, 1979; Halpern and Kubie, 1980; Friedman and Crews, 1985; Krohmer and Crews, 1987; Crews et al., 1988; Miller and Gutzke, 1999; Wyneken, 2007; Krohmer et al., 2010) but the link between

sensory abilities and endocasts has never been investigated in snakes. According to Starck (1979) and Nieuwenhuys et al. (1998), the brain of snakes could fill the majority of the endocranial space, and thus reflect the brain anatomy. If it is the case, endocasts could provide information about their sensory abilities. The relationships between the brain and the endocast is currently untested in snakes (Olori, 2010), and was not the goal of this study.

In snakes, the main olfactory bulb (MOB) is responsible for capturing smells at the level of the olfactory epithelium, and transmitting them to the olfactory bulb; the accessory olfactory bulb (AOB) is responsible for pheromone processing related to chemical social communication and prey capture (Bales, 2014). The MOB projects mainly to the lateral cortex and the AOB mainly to the *nucleus sphericus* (Lanuza and Halpern, 1997), two structures localized in the cerebral hemispheres. The MOB and AOB are involved in different behavioral activities, such as predation, mating and courtship (Bales, 2014). It is difficult to clearly identify the two structures and their limits from the endocast. However, morphological differences are perceived between the sampled taxa and they may imply differences in their sensory abilities. All snakes have a very developed vomeronasal system (Kubie and Halpern, 1979; Bales, 2014); however in hydrophiinae sea snakes the main olfactory bulbs are considered to be functionless and it seems that they use the AOB for smelling underwater (Schwenk, 2008; Schichida et al., 2013). Endocasts of hydrophiidae are indeed the only ones to show olfactory bulbs with a width increasing along the antero-posterior axis (e.g., *Enhydrina schistosa*, see Fig. 5.5H), which could correspond to a reduced MOB and a more developed AOB.

The cerebral hemispheres of snakes are composed of different structures (e.g., cortex, nucleus sphericus, anterior ventricular ridge, amygdala), each being considered as a link between the sources of sensory information and the brain structures that control and modulate the behavior (Halpern, 1980; Bales, 2014). Different studies about the lizard brain have shown that the medial dorsal cortices are relatively bigger in active foragers (Day et al., 1999a,b; 2001; Ladage et al., 2009). In snakes, males, which have a larger average territory than females, possess a significantly larger medial cortex than females (Roth et al., 2006). However, all these internal structures are not distinguishable on endocasts. Moreover, no comparative studies on snake endocasts have been performed to correlate size variation of these inner neural structures with endocast morphology. It is thus difficult to evaluate whether the different morphologies exhibited by the cerebral hemispheres of snakes involve differences in their sensory abilities.

The optic tectum in snakes is involved in the production of natural orienting movements in response to somatosensory, visual, and auditory stimuli (Nieuwenhuys et al., 1998; Wyneken, 2007), and to signals from the infrared sensory system found in some snake families (Boidae, Pythonidae, and Crotalinae) (Goris, 2011). Several authors have shown that the size of the optic tectum is correlated to some behavioral traits and ecologies (Masai, 1973; Nieuwenhuys et al., 1998). For instance diurnal species have a larger optic tectum than burrowing species. From snake endocasts, it actually appears that all fossorial species have a reduced optic tectum, (e.g., *Cylidrophis ruffus*, see Fig. 5.4C), contrary to terrestrial and arboreal taxa, which have a large optic tectum (e.g., *Chrysopelea ornata*, see Fig. 5.4G). According to Lillywhite (2014), vision is better developed in arboreal snakes, and poorly developed in burrowing species and some aquatic species living in turbid waters. It seems thus possible to connect the size of the optic tectum to the development of vision. According to Masai (1973), the optic tectum of diurnal snakes is, as a rule, larger than that of nocturnal ones. However, the correlation between large optic tectum and diurnal activity is not clear. Some exceptions exist: the endocast of *Boiga dendrophila* (see Fig. 5.5B), a nocturnal snake (Rodda et al., 1999; Shivik et al., 2000), also shows a large optic tectum. There seems also to be no correlation between the occurrence of an infrared sensory system and the size of the optic tectum on endocasts. Specimens that have infrared organs (e.g., *Crotalus atrox*, see Fig. 5.7B) do not exhibit a larger optic tectum than specimens without infrared organs (e.g., *Boa constrictor*, see Fig. 5.7A). There is however one exception: *Erpeton tentaculatum* (see Fig. 5.6B-D), the only specimen which has an endocast with the dorsal margin of the optic tectum located more dorsally than the dorsal margin of the cerebral hemispheres. Such features can be correlated to the special nature of *E. tentaculatum*, which is the only snake presenting a pair of appendages that protrude from the face (Catania, 2011; 2012). The tentacles, useful to detect and locate preys, are innervated by trigeminal fibers to the optic tectum and could be responsible for its large size in *E. tentaculatum*.

Snake endocasts also show a great variability in the pituitary gland. This structure is generally considered to be structurally and functionally the most complex organ of the endocrine system (Harris and Donovan, 1966). Among vertebrates, the pituitary of snakes possesses some unique features: an asymmetrical structure flattened dorsoventrally and a pars tuberalis never developed (Schreibman, 1986). From the observation of endocasts only, a large

variability is observed. However, it is not possible to determine whether this variability has a sensory significance. For example, endocasts of fossorial specimens have a clearly reduced pituitary gland but it is not clear whether this morphology is an adaptation reflecting the specialization of the skull due to fossorial activity (Rieppel, 1979; Rieppel & Zaher, 2000b) or if this morphology has a sensory implication.

It is tempting to interpret the brain endocast variability in snakes through differences in sensory abilities between species; however, it is necessary to be very careful in the sensory inferences brought by an endocast study, which gives only an overview of the external morphology of the brain, and the complexity of the structure(s) must be taken into account.

5.5. Perspectives

The rapidly expanding interest in, and availability of, digital tomography data to visualize casts of the vertebrate endocranial cavity housing the brain (endocasts) represent new opportunities and challenges to the field of comparative neuroanatomy (Balanoff et al., 2015). In snakes, the endocast is still poorly known and the information associated with this structure remains untested. The different approaches used here have shown that snake endocasts contain both phylogenetic and ecological signals. However, the degree of influence of these two signals on the brain endocast morphology is difficult to interpret. It will be interesting to dissociate the variability due to each signal. Moreover, to fully understand the brain endocast structure and its variability among snakes, it appears necessary to decompose the ecology in different parameters (e.g., locomotion, prey capture mode) in order to test whether one is particularly associated to one endocranial structure.

Beyond the methodological approaches that we used in this study, the resort to three-dimensional geometric morphometrics (3DGM) would be interesting to improve the amount of shape changes taken into consideration. However, the difficulty of finding homologous anatomical landmarks would impose the use of sliding semi landmarks on surfaces (Gunz and Mitteroecker, 2013).

Cranial endocasts also represent a potentially large amount of unexplored phylogenetic data. Most morphological data for phylogenetic analyses of vertebrates come from the exterior

shape of the skull (e.g., Gauthier et al., 2012). Internal cranial morphology is poorly represented in phylogenetic analyses because of the difficulty in visualizing and studying this anatomy. The advent of CT technology provides the potential to incorporate these new data into phylogenetic analyses.

Finally, in the context of the strong debate about the phylogenetic and ecological origin of snakes (e.g., Lee et al., 1999; Conrad, 2008; Hsiang et al., 2015; Martill et al., 2015; Reeder et al., 2015; Yi and Norell, 2015), endocranial studies might be of strong interest. Their application on crown snakes and lineages closely related to snakes (i.e., varanids, dibamids, mosasauroids) would provide major complementary information.

5.6. Conclusion

We used different methods to describe the endocast of snakes: descriptive characters, outline curve analysis, measurement series, and we observed a great variability in the brain endocast morphology of snakes. These methods provided different complementary information but all have shown that the shape of this structure contains, as in mammals and birds, a phylogenetic signal but also an ecological one. The different trends observed in the endocranial morphology distinguish the different ecologies, notably fossorial and marine snakes. The great diversity observed in the snake endocast, even within the same ecology, appears difficult to interpret and further analyses on the relation between endocast and ecological and sensory factors will be required. Biological inferences based on this structure should thus be made with caution and it is important to understand the complexity of this structure in order to avoid quick potentially wrong assumptions.

Chapter 6

Endocranial anatomy in varanids and amphisbaenians

The snake endocast reflects both phylogenetic and ecologic signals. This could be related to the fact that the brain in snakes fills around 90% of the endocranial space (Starck, 1979; Nieuwenhuys et al., 1998; Triviño et al., in press). Thus, there is a good correlation between the brain and the endocast in snakes. Within squamates, a wide range of brain versus endocranial cavity proportions were found (Kim and Evans, 2014). The lowest brain–endocranial volume ratio is found in *Gecko gecko* (0.35), whereas the false monitor lizard *Callopistes maculatus* exhibits a brain that nearly fills the endocranial cavity (0.97). Such variability might have an impact on the signal reflected by the endocast that could be different according to taxa.

This chapter aims to provide information about the endocranial anatomy of varanids and amphisbaenians. Considering the strong involvement of both taxa in the context of the still debated phylogenetic position of mosasauroids among squamates, this chapter introduces their endocranial anatomy through the study of a few specimens. This preliminary contribution focuses on the description of their endocasts in order to compare them with the endocranial anatomy found in mosasauroids and to provide the first elements to discuss if, as in snakes, the varanid and amphisbeanian endocasts reflect phylogenetic and/or ecologic signals, as well as possible sensory inferences associated to their endocast morphology.

6.1. Material and Methods

Four varanid and three amphisbaenian specimens belonging to different species and representing several ecological adaptations (arboreal, fossorial, aquatic, generalist) have been studied (see Table 6.1).

The endocranial reconstructions were performed using the MIMICS (Materialise Interactive Medical Image Control System) Innovation Suite software (Materialise®, release 18) at the Palaeontology Imaging Unit of the CR2P UMR 7207 CNRS/MNHN/UPMC. The segmentation tools of these software packages were used to select the endocranial space of the specimens thereby allowing separation of the skull from the endocranial space and to reconstruct the endocast.

The braincase of amphisbaenians, as in snakes, is completely ossified and provides a complete cast of the endocranial cavity. In contrast, the ventral and anterior part of the varanid braincase is cartilaginous; however, the preservation of the soft tissues in the four varanid specimens analyzed here provided the limits of the endocranial cavity permitting thus to have a good idea of its size and morphology.

Family	Taxon	Collection reference	Voxel size (in µm)	Habitat
Varanidae	*Varanus prasinus*	AH Unnumb	48.08	Arboreal
	Varanus salvator	AH Unnumb	39.9	Aquatic
	Varanus niloticus	AH Unnumb	14.8	Generalist
	Varanus exanthematicus	AH Unnumb	45	Generalist
Amphisbaenidae	*Amphisbaena gonavensis*	AH Unnumb	7.46	Fossorial
	Amphisbaena kingii	AH Unnumb	12.64	Fossorial
	Amphisbaena vanzolinii	MNHN 1998.02.02	7.46	Fossorial

Table 6.1. List of the varanid and amphisbaenian specimens analyzed in this chapter. **Abbreviations:** AH, Anthony Herrel personal collections.

6.2. Descriptions

6.2.1. Varanids

The endocast in varanids is surrounded dorsally by, from front to back the frontal, the parietal and the supraoccipital. Its posterior part is enclosed laterally by the prootics and the opisthotic-exoccipitals, and ventrally by the basioccipital and basisphenoid. The anterior part of the endocast, however, is cartilaginous. The endocranial pattern found in the four specimens is similar. The proportions occupied by the endocast are similar and represent about two thirds of the skull length (Fig. 6.1).

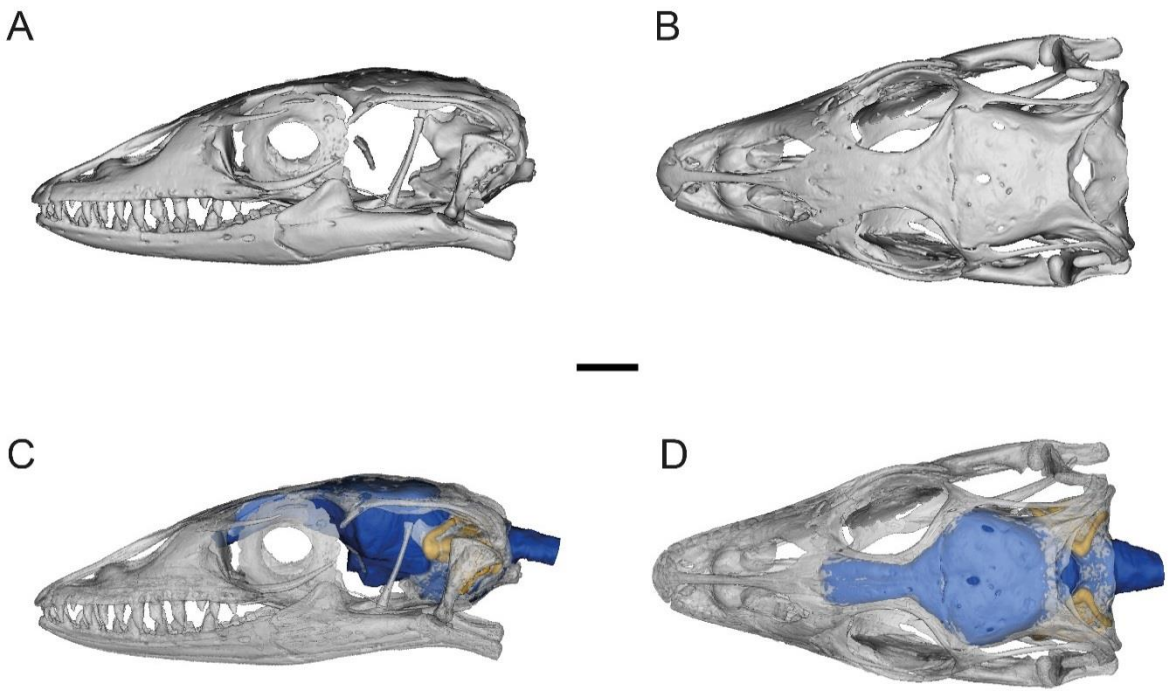

Fig. 6.1. Skull of *Varanus niloticus* in left lateral (A, C) and dorsal (B, D) views with bones rendered transparent to reveal the endocast (blue) and the inner ear (orange). Scale bar equals 5 mm.

The olfactory bulbs correspond to the anteriormost structure of the endocast (Fig. 6.2) and are attached to the anterior part of the cerebral hemispheres through the olfactory tracts. The distinction between the olfactory bulbs and the olfactory tracts is difficult to establish from the endocast only. In dorsal view, the width of the olfactory structure (bulbs and tracts) decreases laterally up to the two thirds of their anteroposterior length, where it forms a small constriction, and then widens laterally up to the fronto-parietal suture. *Varanus exanthematicus* is the only specimen that exhibits, in dorsal view, an olfactory structure made of two parallel olfactory bulbs and tracts (Fig. 6.2A, B) with a less marked constriction. The three other taxa (*V. salvator*, *V. niloticus*, *V. prasinus*) show a projection that diverges laterally from the constriction observed on the olfactory tracts (Fig. 6.2C-H). The length of the olfactory structure is about two third that of the endocast. In lateral view, the anterior part of the olfactory structure is projected ventrally from the main axis of the endocast.

Posterior to the fronto-parietal suture, the dorsal surface of the endocast appears rather flat. Two anterior bulges observed in dorsal view, less delimited in *V. prasinus* (Fig. 6.2G), correspond to the cerebral hemispheres and represent the largest part of the endocast. In lateral view, the cerebral hemispheres seem to be developed only along the horizontal axis.

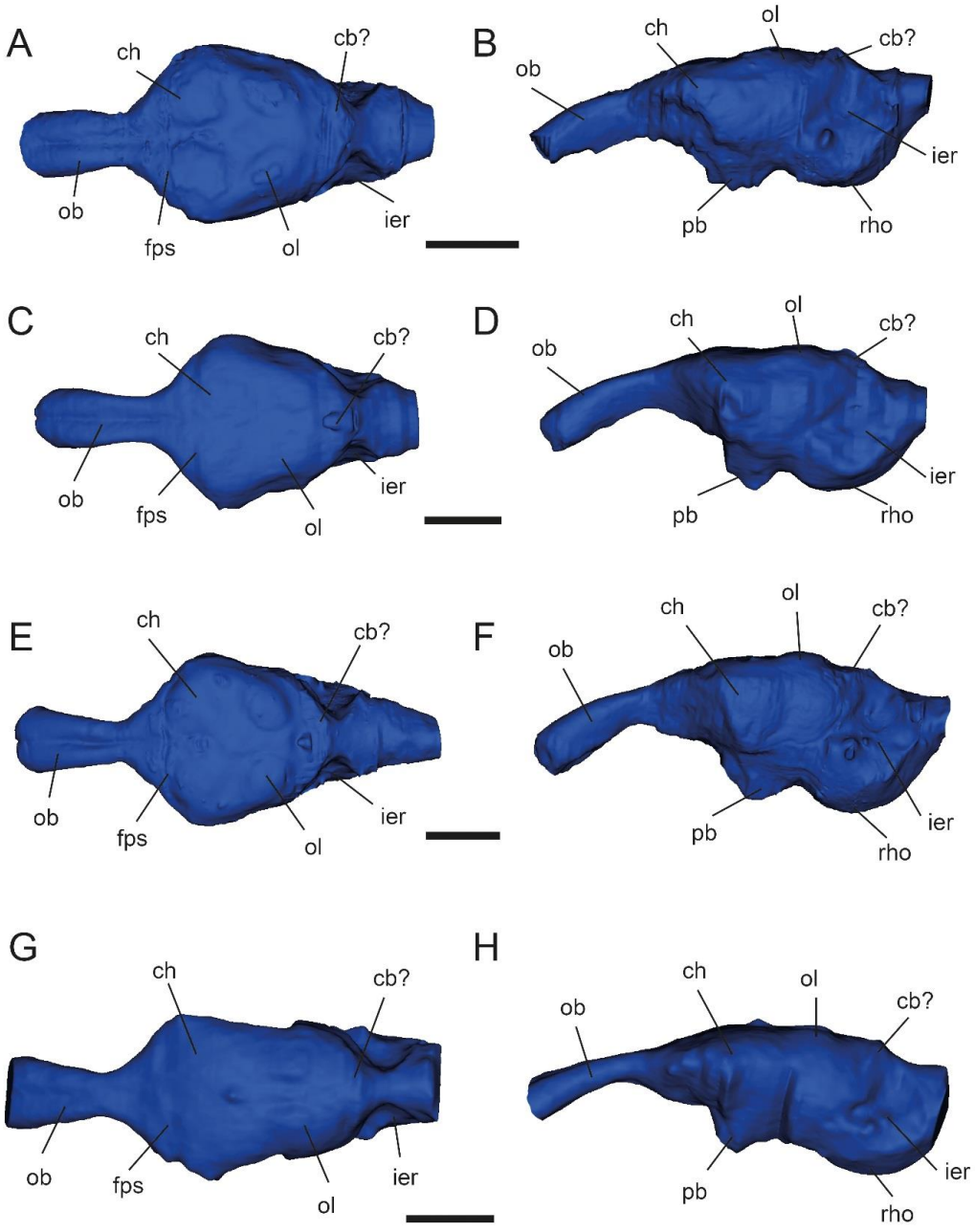

Fig. 6.2. Digital endocasts in dorsal (left) and left lateral (right) views of *Varanus exanthematicus* (A, B), *Varanus salvator* (C, D), *Varanus niloticus* (E, F) and *Varanus prasinus* (G, H). **Abbreviations: cb**, cerebellum, **ch**, cerebral hemispheres; **fps**, fronto-parietal suture; **ier**, inner ear region; **ob**, olfactory bulbs; **ol**, optic lobes; **pb**, pituitary bulb; **rho**, rhombencephalon. Scale bars equal 5 mm.

Ventral to the cerebral hemispheres the pituitary bulb is marked by the presence in lateral view of a projection on the ventral surface of the endocast. In *V. prasinus* (Fig. 6.2H) the space between the pituitary bulb and the rhombencephalon is more extended and less concave than in the others (Fig. 6.2B, D, and F).

Posterior to the cerebral hemispheres, the optic lobes forms the roof of the mesencephalon and appears, in dorsal view, less wide than the cerebral hemispheres. Their position is indicated by two bulges on the dorsal surface of the endocast.

Posterior to the optic lobes, a small bulge on the dorsal surface of the endocast may indicate the cerebellum; however, as the venous system located on the mid-dorsal surface of the endocast may cover it (Aurboonyawat et al., 2008) its extension is difficult to determine.

On the postero-lateral sides of the endocasts, the large and round impressions indicate the position of the inner ear. This part corresponds to the rhombencephalon and exhibits a convex ventral margin. In lateral view, the ventral extension of the rhombencephalon in *V. salvator* and *V. prasinus* is vertically at the same level as the ventral projection of the pituitary bulb (Fig. 6.2B, D, and F). In *V. niloticus* and *V. prasinus*, however, the ventral margin of the rhombencephalon is projected more ventrally than the pituitary bulb (Fig. 6.2H)

6.2.2. Amphisbaenians

In amphisbaenians, the endocast is completely enclosed by the skull bones. Its anterior part is surrounded dorsally by the frontal and parietal. Its posterior part is enclosed laterally and dorsally by the occipital complex, and ventrally by the parabasisphenoid. The three specimens

studied here exhibit a similar endocranial pattern. The endocasts in all cases represent about two thirds of the skull length (Fig. 6.3).

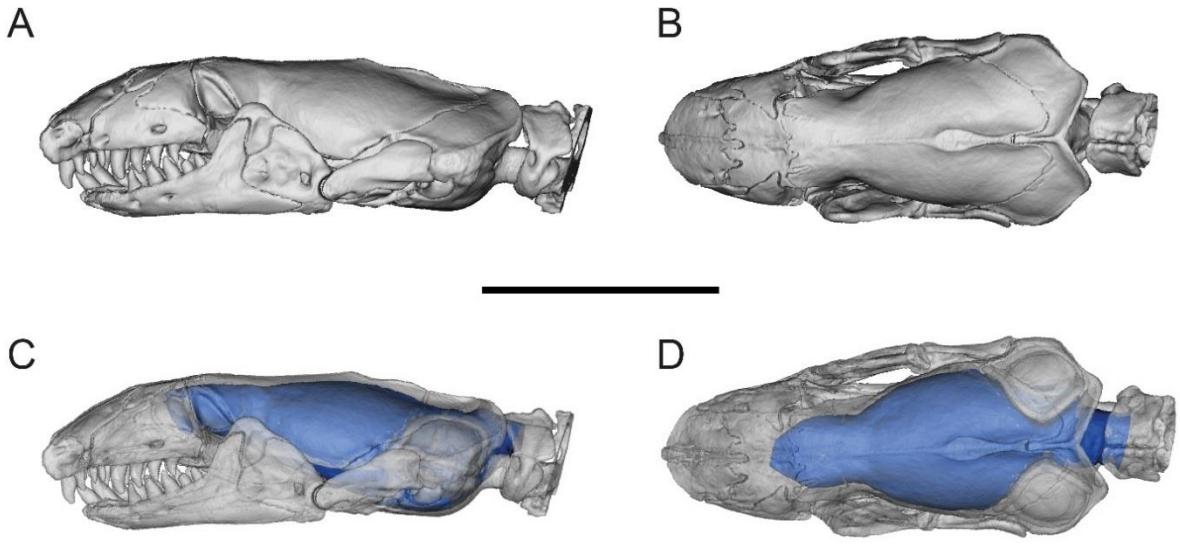

Fig. 6. 3. Skull of *Amphisbaena kingii* in left lateral (A, C) and dorsal (B, D) views with bones rendered transparent to reveal the endocast (blue). Scale bar equals 5 mm.

At the anteriormost part, the olfactory structures (bulbs and tracts) are ovoid, anteroposteriorly elongated. The length of the olfactory structures is about one third that of the whole endocast. In dorsal view, a medial groove runs between the anterior part of the olfactory casts. In dorsal and lateral views, the olfactory region is separated from the rest of the endocast by a small constriction forming a distinct neck. This constriction is less pronounced in *Amphisbaenia gonavensis* (Fig. 6.4C). In lateral view, the olfactory bulbs and tracts are projected horizontally, along the axis of the rest of the endocast.

The cerebral hemispheres casts are located immediately posterior to the olfactory region. In the dorsal view, the cerebral hemispheres are anteroposteriorly elongated and smooth (Fig. 6.4A, C, E). The posterior part of the cerebral hemispheres represents the maximal width of the endocast, except in *Amphisbaena sleveni* for which the maximal width is reached more anteriorly (Fig. 6.4E). A small ridge divides medially the posterior part of the cerebral hemispheres and may correspond to the dorsal longitudinal vein (Aurboonyawat et al., 2008). In lateral view, the cerebral hemisphere appears anterioposterioly elongated.

The ventral surface of the endocast in amphisbaenians is smooth (Fig. 6.4B, D, F) and there is no evidence of a pituitary bulb. Similarly, the optic lobes and cerebellum are not discernible from the endocast (Fig. 6.4A, C, E). These structures may be covered by the dorsal longitudinal vein located on the mid-dorsal surface of the endocast (Aurboonyawat et al., 2008).

On the posterior part of the endocasts, the lateral sides exhibit large and round impressions for the position of the inner ear. The rhombencephalon is located ventral to the inner ear region, and shows a convex ventral margin. At the posterior end of the endocast, the spinal cord is located dorsally.

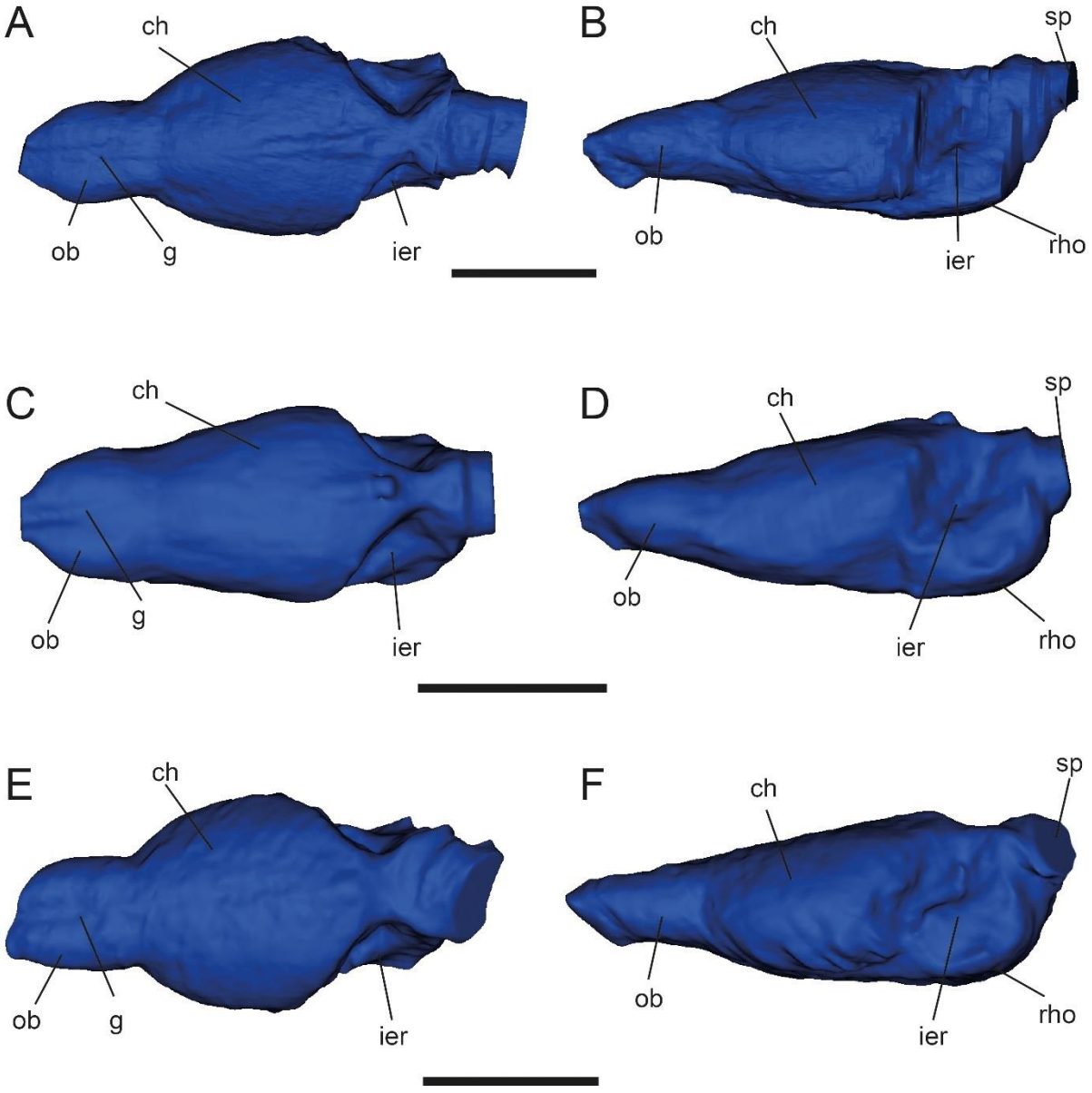

Fig. 6. 4. Digital endocasts in dorsal (left) and left lateral (right) views of *Amphisbaena kingii* (A, B), *Amphisbaena gonavensis* (C, D), and *Amphisbaena vanzolinii* (E, F). **Abbreviations: ch**, cerebral hemispheres; **g**, medial groove separating the olfactory casts; **ier**, inner ear region; **ob**, olfactory bulbs; **rho**, rhombencephalon; **sp**, spinal cord. Scale bars equal 2 mm.

6.3. Endocranial comparisons

Here, each structure composing the endocast of varanids, amphisbaenians and snakes is compared individually between all taxa.

The shape of the olfactory complex (olfactory bulbs and tracts) in varanids clearly differs from in amphisbaenians and in most snakes whose complex is short and wide (e.g., *Amphisbaenia kingi* and *Python regius*). Although some terrestrial snakes (e.g., *Hierophis viridiflavius*) exhibit also an elongated olfactory complex, the most-anterior part is separated in two independent structures, whereas in varanids the olfactory complex is in contact along the entire length. Only varanids exhibit, in lateral view, an olfactory complex projected ventrally antero-posteriorly, whereas in snakes and amphisbaenians the complex is projected horizontally, along the axis of the rest of the endocast.

In lateral view, the cerebrum in varanids is only projected along the horizontal axis similarly to the condition observed in amphisbaenians and in both fossorial and marine snakes. This condition differs from that observed in terrestrial, arboreal and semi-aquatic snakes, in which the cerebrum is also projected ventrally. In dorsal view, the width of the cerebrum in varanids decreases gradually to the optic lobes whereas in all snakes, the transition between the two structures is more abrupt as the width of the optic lobes is significantly narrower than that of the cerebrum. The optic lobes in varanids are wide, similarly to what is observed in terrestrial and arboreal snakes. However, the two bulges forming the structure are more differentiated in snakes than in varanids.

In lateral view, the pituitary bulb in varanids forms a prominent bulge on the ventral surface of the endocast. This structure is not visible from endocasts of amphisbaenians; however, in snakes, most species exhibit a structure directed posteriorly, which differs from

varanids' condition. Only *Python regius* exhibits a pituitary bulb similar in shape to that of varanids but less ventrally extended.

On the posterior part of the endocast, the rhombencephalon of varanids shows a rounded ventral margin that differs from the slightly convex ventral margin observed in snakes and amphisbaenians.

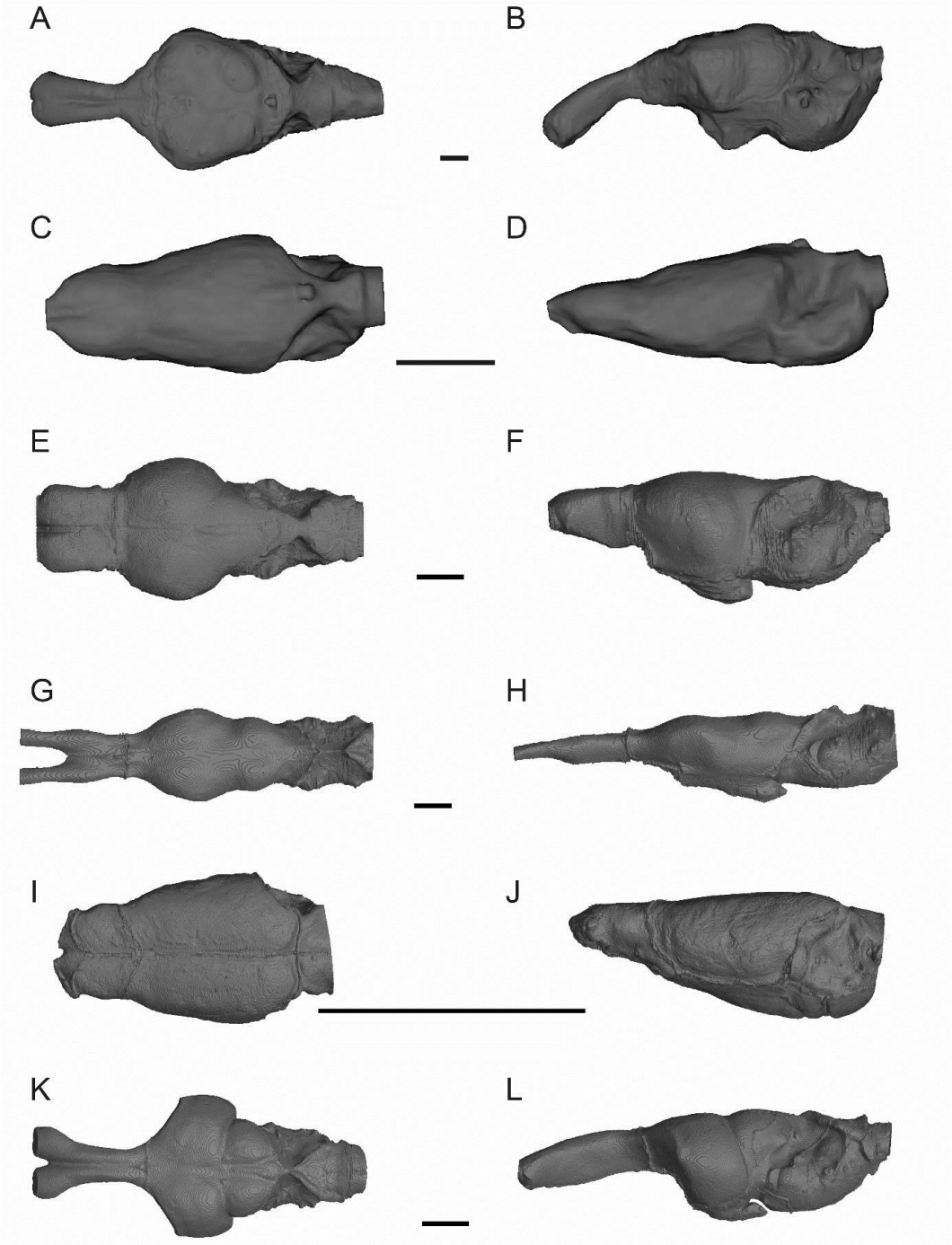

Fig. 6.5. Digital endocasts in dorsal (left) and lateral (right) views of **(A-B)**) the varanid *Varanus niloticus*, **(C-D)** the amphisbaenian *Amphisbaena gonavensis*, and the snakes **(E-F)** *Python regius*, **(G-H)** *Pelamis platurus*, **(I-J)** *Typhlophis squamosus*, **(K-L)** *Hierophis gemonensis.* Scale bars equal 2 mm.

6.4. Discussion

6.4.1. Varanid endocast

Several studies have shown that varanids exhibit considerable variation in body size (e.g., Pianka, 1995; Clemente et al., 2011), relative limb proportions (e.g., Thompson and Withers, 1997), skull and teeth morphologies (e.g., Estes and Williams, 1984; Stayton, 2005; Openshaw and Keogh, 2014). This diversity is also reflected by a large range of habitats and behaviors during prey capture and processing (McCurry et al., 2015). Among the varanid species used here, *Varanus exanthematicus* and *V. niloticus* have a high ecological plasticity and are found in terrestrial, arboreal and aquatic environments (Pianka and King, 2004), whereas *V. salvator* appears more aquatic and *V. prasinus* highly arboreal (Pianka and King, 2004). In addition, the four taxa show a large range of diets, from the generalized carnivorous *V. salvator* and *V. niloticus*, to the insectivorous *V. prasinus*, and *V. exanthematicus* that shows adaptations for crushing hard preys, such as snails (Pianka and King, 2004).

Despite this great variability, their endocranial anatomies exhibit a globally similar pattern. This differs completelly from the observations made on snakes, in which endocasts of arboreal and aquatic taxa greatly differ according to these respective ecologies (Allemand et al., 2017b; see Chapter 5). Openshaw and Keogh (2014) stated that in varanids with different ecologies, most of the shape variation is related to changes in the snout and head width rather than in the braincase. Our results corroborate this hypothesis as a similar endocranial pattern is found in varanids with different ecologies. Thus, the similar endocranial pattern found in varanids could be related to a strong phylogenetic signal and a weak ecological variability. The absence of a clear ecologic signal in the endocranial shape of varanids could be related to their high ecological plasticity, revealing that most of the varanids are generalist and not specialized

to a specific habitat. Indeed, among the specimens studied here, *V.exanthematicus* and *V. niloticus* are found in terrestrial, arboreal and aquatic environments (Pianka and King, 2004) and show more endocranial similarities with the semi-aquatic *V. salvator* than with the highly arboreal *V. prasinus*. Another possibility that could explain the absence of clear ecological signal in the varanid endocast could be related to the fact that the brain in these taxa does not fill the endocranial cavity (contrary to snakes, e.g., Triviño et al., in press). Thus, assuming that the brain shape may vary according to ecology (e.g., Aristide et al., 2016), the endocranial reconstruction in varanids would reflect only the braincase shape, which is somewhat conservative in varanids (Openshaw and Keogh, 2014). It would be interesting to determine the relationships between the brain and the braincase (endocast) in varanids in order to determine whether the brain reflects an ecologic signal or not, and to compare the signal differences perceived in the brain and in the endocast.

6.4.2. Amphisbaenian endocast

Amphisbaenians are highly specialized fossorial squamates. Most amphisbaenians are believed to be dietary generalists (e.g., Colli & Zamboni, 1999; Kearney, 2003; Bernardo-Silva et al., 2006; Gomes et al. , 2009; Balestrin & Cappellari, 2011), although some species appear more selective and limited to specific small-size arthropods (Lopez et al., 1991; Webb et al., , 2000; Bernardo-Silva et al., 2006).

The endocast shape in amphibaenians shows similarities with that of fossorial snakes. All these taxa exhibit an endocast with a poor lateral development of the cerebral hemispheres, and both the optic tectum and the pituitary bulb are not visible. Fossorial squamates may exhibit convergences in their skull morphology (e.g., Roscito and Rodrigues, 2010) and sensory abilities (e.g., Foureaux et al., 2010). Thus, it is unclear whether the endocranial similarities perceived between snakes and amphisbaenians are related to changes in their skull morphologies due to the fossorial specialization, and thus reflect an ecological signal, or if the particular morphology of their endocast has a phylogenetic meaning. Indeed, some phylogenetic hypotheses obtained from the morphological data place snakes and amphisbaenians into a sister group (e.g., Estes and Pregill, 1988; Hallermann, 1998; Kearney,

2003; Conrad, 2008) and the endocranial similarities perceived between these taxa could corroborate this hypothesis.

6.5. Conclusions

Though the number of specimens used in this work precludes any generalization, it seems however that the signal associated to the endocast in squamates can vary according to the taxa and could be dependent to the degree of ecological plasticity. Thus, endocasts of specialized species in which ecologies are well differentiated are more likely to exhibit an ecological signal, whereas the endocast of more generalist species reflect mainly a phylogenetic signal. The place occupied by the brain in the endocranial cavity could also impact the perceptibility of both ecologic and phylogenetic signals. In snakes and amphisbaenians, it is generally admitted that the brain nearly fills the endocranial cavity (e.g., Starcks, 1979; Nieuwenhuys et al., 1998; Triviño et al., in press). In varanids, however, the brain-endocranial space relationships remains untested and additional data, obtained from MRI imaging for example, could allow to test this hypothesis.

Chapter 7

Endocranial anatomy of the basal mosasauroid *Tethysaurus nopcsai*

Little information exists about the endocast of mosasauroids. These structures are only known through the reconstructions performed by Camp (1942) for one specimen of the russellosaurine *Platecarpus* Cope, 1869 and one of the basal mosasaurine *Clidastes* Cope, 1868 (Turonian of Smoky Hill, Kansas, U.S.A.) (Fig.7.1). The reconstruction for *Platecarpus* was made by joining its dissociated braincase elements and filling the brain cavity "with liquid rubber backed with sawdust" (Camp, 1942, p. 40). For *Clidastes*, the olfactory bulbs and tracts were supplied from a "latex mold" of the ventral olfactory wall in the frontal (Camp, 1942 p. 40); however, these are the only details given by Camp, and no additional information was provided about the reconstruction of the rest of the endocast. Camp (1942) compared the endocasts of both *Platecarpus* and *Clidastes* with the brain of a juvenile *Varanus niloticus*. However, as it is generally assumed that the brain in non-avian reptiles does not fill the cranial cavity (Nieuwenhuys et al., 1998), it should be mentioned that such comparison between brain and endocast might introduce bias (e.g., Jirak and Janacek, 2017). From these endocasts, Camp (1942) did not provide any sensory or behavioral inference for mosasauroids. However, as he noticed a strong similarity between mosasauroid endocasts and the brain of a juvenile *Varanus*, he suggested a close phylogenetic relationship between mosasauroids and varanids (Camp, 1942).

Camp (1942) also performed the reconstruction from latex liquid injection of the inner ear of both specimens. Once again, the similarities noticed between the inner ears of mosasauroids and varanids led Camp to conclude that these taxa are closely related (Camp, 1942). Although this hypothesis has been taken up by some authors (e.g., Russell, 1967), more recent studies performed on CT images of the inner ear of *Platecarpus* and *Tylosaurus* Marsh, 1872 revealed differences in the shape of the semicircular canals between these mosasauroids and varanids (Georgi, 2008; Georgi and Sipla, 2008), refuting the hypothesis of Camp (1942).

Finally, Cuthbertson et al. (2015) suggest from the digital reconstruction of the inner ear in *Plioplatecarpus* Dollo, 1882 that this taxon was an agile predator with high locomotor abilities that might have engaged in acrobatic, spatially complex behaviors during foraging.

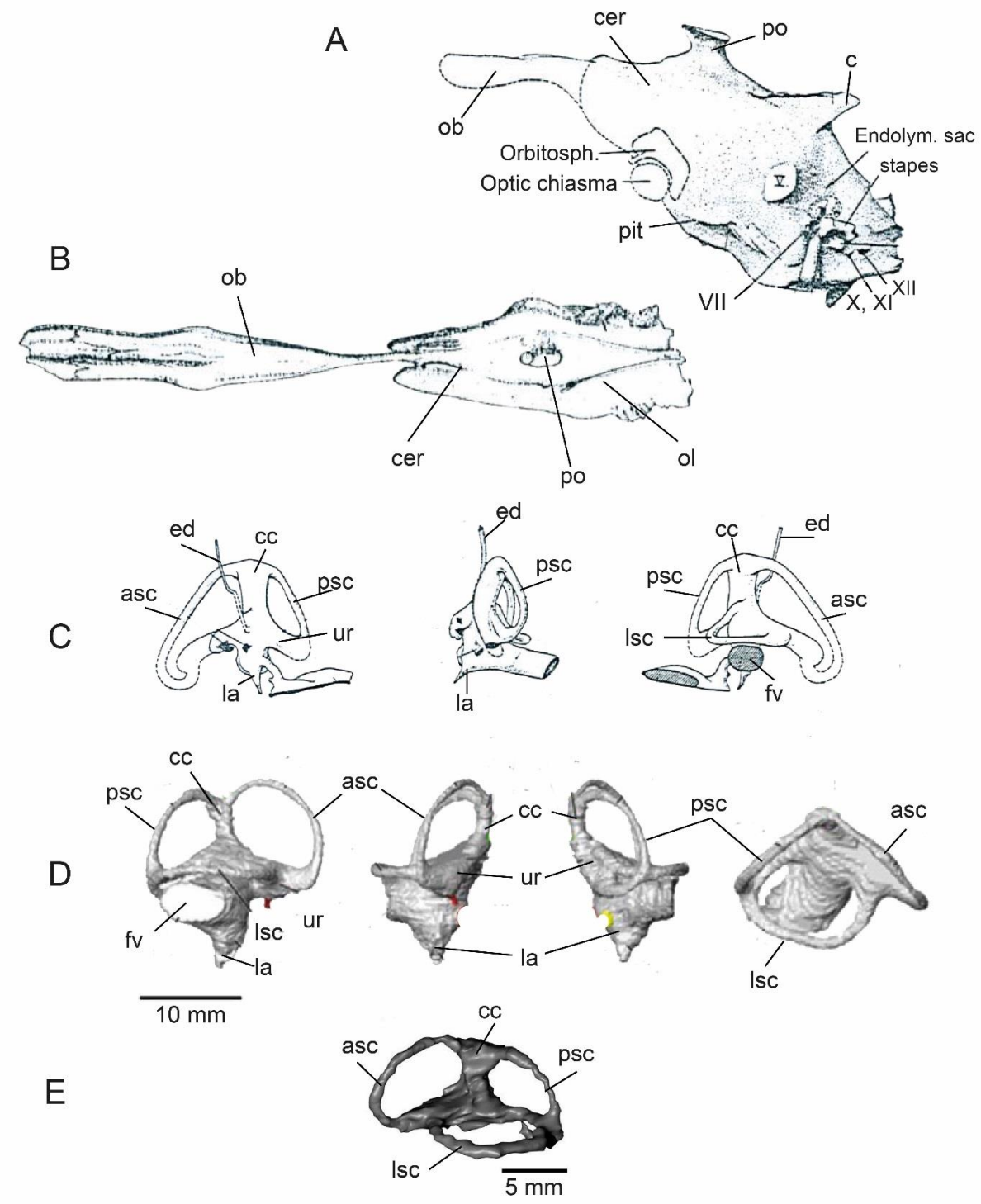
A
cer
po
c
ob
Endolym. sac
Orbitosph.
stapes
Optic chiasma
pit
VII
X, XI
XII
B
ob
cer
po
ol
C
ed
cc
asc
psc
ur
la
ed
psc
la
cc
ed
psc
asc
lsc
fv
D
cc
psc
asc
fv
lsc
ur
la
cc
ur
la
psc
asc
lsc
10 mm
E
cc
asc
psc
lsc
5 mm

Fig. 7.1. Endocasts of **(A)** *Platecarpus tympaniticus* (UCMP 32136) in left lateral view and **(B)** *Clidastes tortor* (UCMP 34535) in dorsal view, modified from Camp (1942) (No scale bar available). **(C)** Right inner ear of *Platecarpus tympaniticus* (UCMP 32136) in medial, posterior and lateral views, modified from Camp (1942) (No scale bar available). **(D)** Right inner ear of *Plioplatecarpus peckensis* (MOR 1062) in lateral, anterior, posterior and dorsal views, modified from Cuthbertson et al. (2015). **(E)** Lateral view of the incomplete inner ear of *Platecarpus tympaniticus* (AMNH 1645), modified from Georgi (2008). **Abbreviations: asc**, anterior semicircular canal; **c**, cartilage between the parietal and the supraoccipital; **cc**, common crus; **cer**, cerebrum; **ed**, endolymphatic duct; **fv**, fenestra vestibule; **ier**, inner ear region; **la**, lagena; **lsc**, lateral semicircular canal; **mo**, medulla oblongata; **ob**, olfactory bulbs; **ol**, optic lobes; **ot**, olfactory tracts; **po**, pineal organ; **pit**, pituitary bulb; **psc**, posterior semicircular canal; **ur**, utricular region; **V**, trigeminal nerve;; **VII**, facial nerve; **X, XI**, vagus and accessory nerves; **XII**, hypoglossal nerves.

In this chapter is qualitatively and quantitatively analyzed the endocranial anatomy of several specimens belonging to the basal mosasauroid *Tethysaurus nopcsai* that had been reconstructed thanks to computed tomography. The aim is to provide new anatomical information about this poorly known region within mosasauroids. Comparisons with other mosasauroid endocasts, and with endocasts of snakes and varanids, have been performed in order to discuss the possible ecologic and phylogenetic signal associated to the structure. Finally, the endocast of *Tethysaurus* has been used to perform sensory and behavioral inferences for this taxon that shows intermediate adaptations between the optionally terrestrial "aigialosaurids" (e.g., Caldwell and Palci, 2007) and the obligatory aquatic mosasauroids.

7.1. Material and Methods

7.1.1. Material

Among the six specimens used in this work (see Chapter 4), MNHN GOU1 (holotype specimen), SMU 76335, SMU 75 486 correspond to complete skulls whereas GM1, GM2 and GM3 (juvenile, M. Polcyn personal communication) specimens consist only in braincase and encompass the basioccipital and the basisphenoid ventrally, the prootics and the exoccipitals-opisthotics laterally, and the supraoccipital dorsally.

Specimens	**Scans**	**Voxel size (in µm)**
MNHN GOU1 (Holotype)	AST-RX platform (MNHN, Paris), this work	81.3
GM1	University of Texas High-Resolution X-ray CT Facility (scans lent by M. Polcyn, Southern Methodist University, Dallas, Texas)	97.5
GM2		85.3
GM3		85.3
SMU75486		77.8
SMU76335		81

Table 7.1. List of the *Tethysaurus nopcsai* specimens studied in this PhD Thesis.

7.1.2. Methods

7.1.2.1. Endocranial reconstructions

The endocranial reconstructions for the six specimens were performed using the multiple 2D cross-sectional slices edit tool of MIMICS (Materialise Interactive Medical Image Control System) Innovation Suite software (Materialise®, release 18) at the Palaeontology Imaging Unit of the CR2P UMR 7207 CNRS/MNHN/UPMC (see Chapter 4 for details).

The reconstructions performed from GM1, GM2 and GM3 provide an overview of the posterior part of the endocast, as well as the pathways for the cranial nerves (see Appendix 7.1). In the holotype specimen MNHN GOU1, the segmentation allows to reconstruct the posterior part of the endocast, the cranial nerves and the inner ears. Finally, endocasts for both SMU 76335 and SMU 75 486 specimens have been reconstructed but the resolution of the scans is not sufficient to observe the cranial nerves and the inner ears.

7.1.2.2. Quantitative comparisons

In order to quantitatively compare the endocast of *T. nopcsai* to those of extant relatives, we used the linear measurements defined from snake endocasts (see Chapter 5). These measurements were performed on varanid endocasts and for one specimen of *T. nopcsai* (SMU 76335) because of the incompleteness of the other mosasauroid endocranial reconstructions (see Appendix 6 for measures).

Due to the cartilaginous parts of the braincase of *T. nopcsai* that prevents the complete reconstruction of the endocast, it was only possible to take 14 of the 21 measurements defined for snakes and varanids (see Chapter 5): **(1)** length of the endocast (LE), **(2)** length of the olfactory bulbs (LOB), **(3)** length of the groove between the olfactory bulbs (LG), **(4)** height of the main olfactory bulb (HOB), **(5)** height of the olfactory tracts (HOP), **(6)** width of the olfactory tracts (WOP), **(7)** maximal width of the optic lobes (WOR), **(8)** length of the pituitary gland (LP), **(9)** height of the pituitary gland (HP), **(10)** width of the inner ear region (WIE), **(11)** dorsal width of the posterior end of the endocast (DWPE), **(12)** height of the posterior part of the endocast (HPE), **(13)** width of the ventral part of the endocast (WPE), **(14)** width in the pituitary gland region (WP).

The data were log10-transformed and the log-shape ratios (Mosimann and James, 1979) were calculated based on the log10-transformed raw linear dimensions of the endocast. Then a Principal Component Analysis (PCA) was performed from the data obtained for the 45 snake specimens, the four varanids and *Tethysaurus nopcsai*. The amphisbaenians were not included in the analysis in order to prevent the loss of informative characters. Indeed, as both the pituitary bulb and the optic tectum are not distinguishable from the endocast in these taxa, the associated measurements cannot be “taken”.

7.2. Neuroanatomical description

7.2.1. Endocast

In *Tethysaurus nopcsai*, the posterior part of the braincase is fully surrounded by bones, which enables an accurate reconstruction of the endocast. However, the anterior part is cartilaginous and absence of bone prevents the ventral and lateral delimitations of the cerebrum. The following description is based only on the reconstruction performed for SMU 76335 and SMU 75486, whose endocasts are the most complete ones (Fig. 7.2).

The endocranial pattern found in the two specimens is similar. Endocasts are elongated and mediolaterally wide, the proportions of the skull occupied by this structure are comparable in both specimens (about 50%). In SMU 76335 and SMU 75486, the anterior and posterior parts of the endocast are nearly situated along the same horizontal plane (Fig. 7.2) and do not exhibit the pronounced flexure illustrated by Camp (1942) for *Platecarpus*, in which the posterior part of the endocast is clearly ventral to the anterior part (Fig. 7.1)

The olfactory bulbs are the anteriormost structures and are located on the ventral surface of the frontal. The olfactory bulbs appear wider than the elongated olfactory tracts, which are projected through the ventral wall of the frontal. The anteroposterior length of the olfactory tracts is approximately 30 mm in SMU 76335 and corresponds to about half of the endocast length (Fig. 7.2B). In SMU 75486, the anteriormost part of the olfactory bulbs is missing and prevents its measurements (Fig. 7.2A). The olfactory tracts are mediolaterally compressed in the middle of their length, and widen at the level of the contact with the cerebrum. There is no separation between the olfactory tracts, except on the anteriormost part, at the level of the olfactory bulbs (Fig. 7.2B). The olfactory the tract continues posteriorly until it meets the cast of the cerebrum, on the ventral surface of the parietal. In lateral view, the olfactory tracts are projected horizontally, along the axis of the rest of the endocast. The comparisons indicate that the olfactory bulbs and tracts in *T. nopcsai* are similar to those exhibited by *Clidastes* (Fig. 7.1), but differ from the proportionally short ones found in *Platecarpus* (Camp, 1942).

Posterior to the olfactory tracts, the dorsal surface of the endocast appears rather flat and the anterior part corresponds to the cerebrum. However, due to the open condition of the braincase anteriorly to the prootic, the reconstructions performed for SMU 76335 and SMU

75486 provide only an overview of the dorsal surface of the cerebrum. The ventral and lateral extensions of the cerebrum were not reconstructed in order to avoid over-interpretation (Fig. 7.2). Posteriorly to the cerebrum, a small dorsal bulge may correspond to the pineal organ. The same structure was reported in *Platecarpus* and *Clidastes* (Camp, 1942). Both *Tethysaurus* and *Clidastes* exhibit a relatively small pineal organ and differ from *Platecarpus* (Fig. 7.1), in which the pineal organ appears relatively larger and more elongated antero-posteriorly (Camp, 1942). This structure indicates the limit between the cerebrum and the optic lobes. However, the true extension and the limits of the latter are difficult to determine from the endocast.

In lateral view and ventrally to the optic lobes, a ventral projection corresponds to the pituitary bulb. This structure is expanded more ventrally than the ventral surface of the *medulla oblongata* in both specimen of *Tethysaurus*; however, in SMU 75486, the pituitary bulb seems to be located more posteriorly than in SMU 76335 (Fig. 7.2). The pituitary bulb in *Tethysaurus* largely differs from in *Platecarpus*, in which the structure only forms a small bulge on the ventral surface of the endocast (Fig. 7.1).

The position of the cerebellum is not visible from the endocast. The posterior part of the endocast, the rhombencephalon, is thin and laterally constricted, enclosed by the prootics and the exoccipitals. Ventrally, the surface can be reconstructed with reasonable accuracy, as it is framed by the dorsal surfaces of the basisphenoid and basioccipital. The lateral sides exhibit large and round impressions for the position of the inner ear. Dorsally to the inner ear region, the cartilage between the parietal and supraoccipital covers the endocast, as in *Platecarpu*s (Camp, 1942).

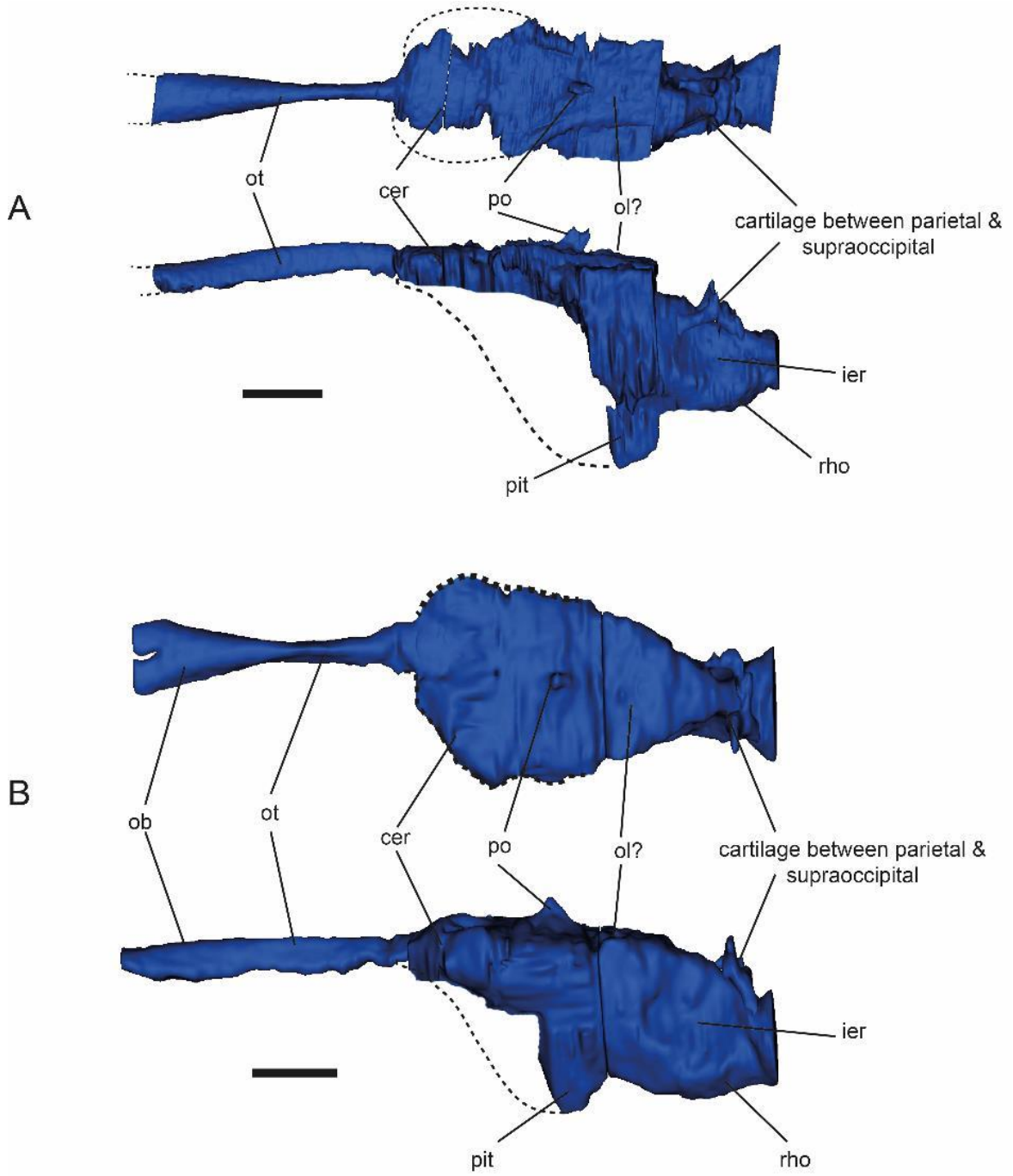

Fig. 7.2. Virtual endocasts of the two *Tethysaurus nopcsai* specimens (Early Turonian, Goulmima, Morocco) SMU 75486 (**A)** and SMU 76335 **(B)** in dorsal (up) and left lateral (down) views. **Abbreviations**: **cer**, cerebral hemispheres; **ier**, inner ear region; **ob**, olfactory bulbs; **ol**, optic lobes; **ot**, olfactory tracts; **po**, pineal organ; **pit**, pituitary bulb; **rho**, rhombencephalon. The dotted lines indicate unknown limits of the endocasts. Scale bars equal 20 mm.

7.2.2. Cranial nerves

The cranial nerves were reconstructed for GM1, GM2, GM3 (see Appendix 7) and MNHN GOU1 (Fig. 7.3) specimens. The identification of the different cranial nerves is based on the information given in the description of mosasauroid braincases (e.g., Russell, 1967; Rieppel and Zaher, 2000a) and on the endocranial reconstructions performed by Camp (1942). The optic (II), oculomotor (III), and trochlear (IV) nerves could not be traced due to the cartilaginous nature of the skull part enclosing the endocast antero-ventrally. The canal for the trigeminal nerve (V) can be identified as it corresponds to the prootic fenestra (e.g., Russell, 1967); however, its true extension could not be determined (Fig. 7.3). The abducens nerve (VI) is anteriorly projected and exits by the dorsolateral foramina of the pituitary fossa (Fig. 7.3). The facial nerve (VII) projected posteriorly exits from the foramen on the prootic and is located just anterior to the inner ear (Fig. 7.3). The width of the facial nerve is similar to that of the abducens nerve. Two branches located on the medial surface of the prootics correspond to the vestibulocochlear nerve (VIII) and contact the medial surface of the inner ear (Fig. 7.3B). Just posterior to the inner ear, the glossopharyngeal nerve (IX) pierces the medial surface of the exoccipital-opisthotic and represents the largest cranial nerve (Fig. 7.3). Posteriorly, the vagus-accessory nerves (X + XI) are located dorsally form the three branches of the hypoglossal nerve (XII).

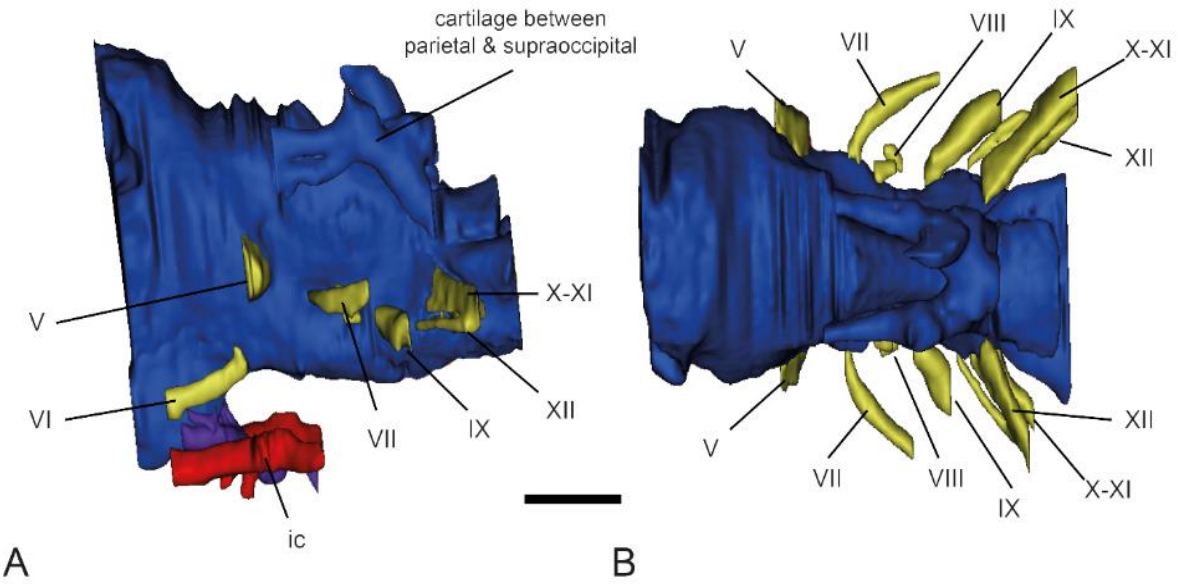

Fig. 7.3. Posterior part of the endocast of the *Tethysaurus nopcsai* holotype specimen MNHN GOU 1, Early Turonian, Goulmima, Morocco, in left lateral (A) and dorsal (B) views. **Abbreviations**: **ic**, internal carotid; **V**, trigeminal nerve; **VI**, abducens nerve; **VII**, facial nerve; **VIII**, vestibulocochlear nerve; **IX**, glossopharyngeal nerve; **X-XI**, vagus and accessory nerves; **XII**, hypoglossal nerves. Scale bar equals 10 mm.

7.2.3. Inner ear

Left and right inner ears of MNHN GOU1 were reconstructed (Fig. 7.4). They seem complete and slightly crushed. The otic capsule is a tripartite structure formed by the prootic, the opisthotic portion of the exoccipital-opisthotic and the supraoccipital (Fig. 7.4A). The endosseous labyrinth is enclosed at the confluence of these three elements. The prootic forms the anteroventral portion of the otic capsule (Fig. 7.4B), enclosing within it most of the anterior semicircular canal, the anterior half of the horizontal semicircular canal, and the anterior portion of the lagenar region. On the lateral surface, the prootic forms the anterior margin of the ovoid fenestra vestibuli. The opisthotic portion forms the posteroventral portion of the otic capsule (Fig. 7.4D), enclosing most of the posterior semicircular canal, the posterior half of the horizontal semicircular canal and the posterior portion of the lagenar region. The opisthotic completes the posterior margin of the fenestra vestibuli. The supraoccipital forms the dorsal portion of the otic capsule (Fig. 7.4C), enclosing the medial portions of the anterior and posterior semicircular canals, as well as the common duct (common crus).

All three canals composing the endosseous labyrinth are very similar to each other in both size and shape (Fig. 7.4E-H). They are very thin as reported for *Platecarpus* and *Plioplatecarpus* (Georgi, 2008; Cuthbertson et al., 2015). The angles formed between the anterior and posterior semicircular canals is approximately 88°, 66° between the anterior and lateral semicircular canals and 71° between the posterior and lateral semicircular canals. The anterior and posterior canals meet medially at a narrow common crus, and all three canals are connected to the triangular utricular region (Fig. 7.4).

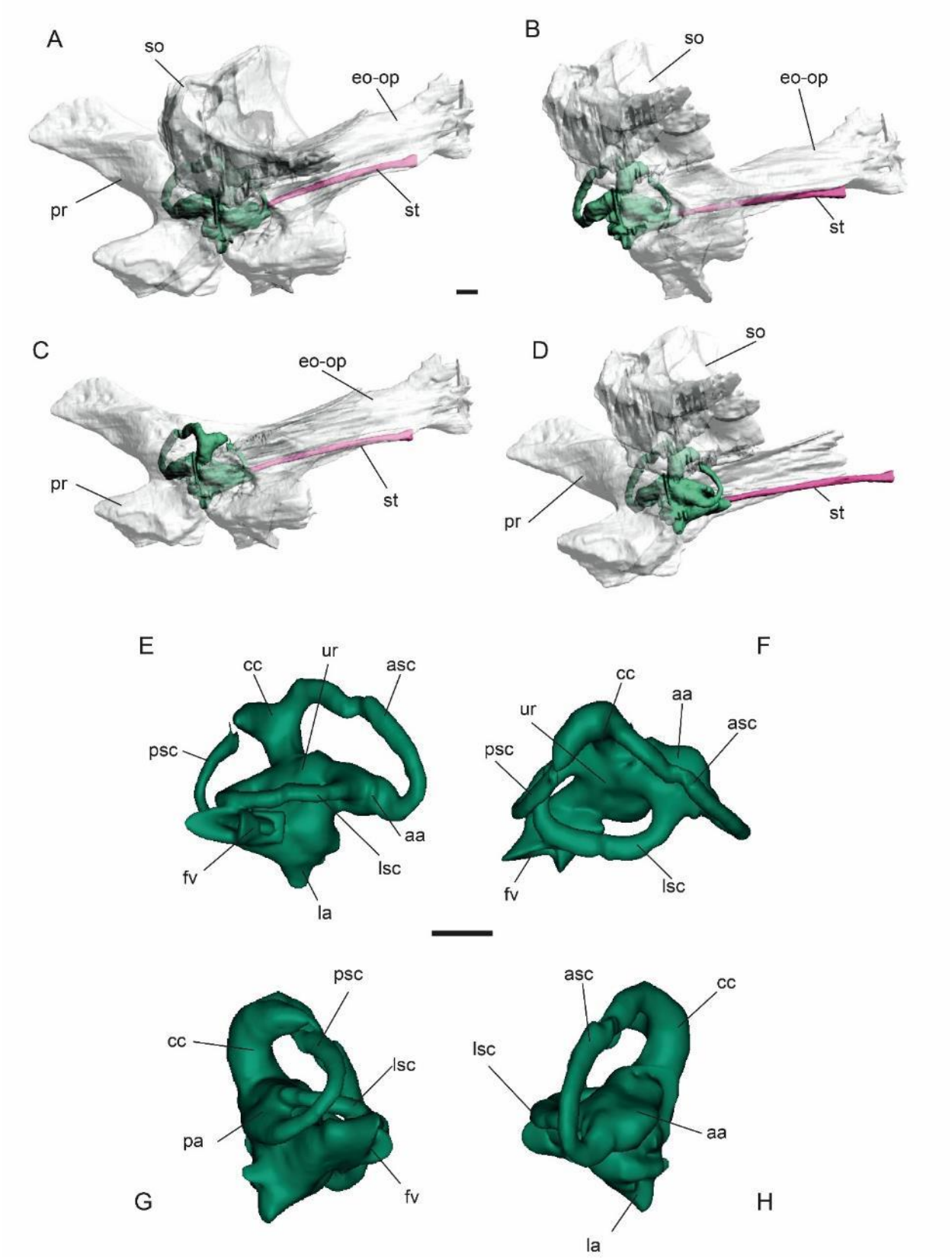
A
so
eo-op
pr
st
B
so
eo-op
st
C
eo-op
pr
st
D
so
pr
st
E
cc
ur
asc
psc
aa
fv
lsc
la
F
cc
aa
ur
asc
psc
fv
lsc
G
psc
cc
lsc
pa
fv
H
asc
cc
lsc
aa
la

Fig. 7.4. Braincase and endosseous labyrinth of the *Tethysaurus nopcsai* holotype specimen MNHN GOU1, Early Turonian, Goulmima, Morocco. (A), the location of the labyrinth revealed with the braincase rendered transparent in medial view. (B–D), the contributions of the three elements of the braincase to enclosing the labyrinth revealed when the prootic (B), supraoccipital (C), and exoccipital-opisthotic (D) are digitally removed in medial view. (E-H) Right inner ear of in lateral (E), dorsal (F), posterior (G) and anterior (H) views. **Abbreviations**: **aa**, anterior ampulla; **asc**, anterior semicircular canal; **cc**, common crus; **eo-op,** exoccipital-opisthotic; **fv**, fenestra vestibuli; **la**, lagena; **lsc**, lateral semicircular canal; **pa**, posterior ampulla; **pr,** prootic; **psc**, posterior semicircular canal; **so,** supraoccipital; **st,** stapes; **ur**, utricular region. Scale bars equal 5 mm.

When the labyrinth is oriented so that the lateral semicircular canal is horizontal, the anterior canal is taller than the posterior one. The anterior and posterior canals are ovoid and similar to the oblong condition seen in *Platecarpu*s and *Tylosaurus* (Georgi, 2008; Georgi and Sipla, 2008) but differ from the strongly arced canals found in *Plioplatecarpus* (Cuthbertson et al., 2015). In addition, only a small section of the posterior canal in *Tethysaurus* is ventral to the plane of the lateral canal (Fig. 7.4G), a condition similar to *Tylosaurus* but differing from *Platecarpus* (Georgi, 2008). All three canals lack conspicuous ampullar expansions, as in *Platecarpu*s, *Tylosaurus* and *Plioplatecarpus* (Georgi, 2008; Cuthbertson et al., 2015). The conical lagena is ventrally oriented and appears shorter than the lagena reported for *Plioplatecarpus* (Cuthbertson et al., 2015). The fenestra vestibuli is located near the posterodorsal limit of the lagena.

7.3. Comparisons with snake and varanid endocasts

7.3.1. Qualitative comparisons

Although the endocast of *Tethysaurus nopcsai* is incomplete, the general shape presents some similarities with that of varanids but also with some snakes, especially some terrestrial ones (Fig. 7.5). Here, each distinguishable structure is compared between these taxa.

The shape of the olfactory complex (olfactory bulbs and tracts) in *T. nopcsai* clearly differs from most snakes in which the complex is short and wide (e.g., *Python regius* and *Pelamis platurus*, Fig. 7.5E, G). However, some terrestrial snakes (e.g., *Mimophis mahfalensis*, Fig. 7.5I) exhibit an elongated and thin olfactory complex comparable to that of *T. nopcsai*. On the contrary, although the olfactory complex in varanids is also elongated (Fig. 7.5C), the latter appears wider than that observed in *T. nopcsai*. In addition, only varanids exhibit an olfactory complex projected ventrally antero-posteriorly, whereas in snakes and *T. nopcsai* the complex is projected horizontally, along the axis of the rest of the endocast.

The cerebrum and the optic lobes in *T. nopcsai* are no clearly delimited and do not allow to discuss about each other separately. Nevertheless, the flat surface that encompasses both structure in *T. nopcsai* is more similar to that of varanids and differs from all snakes. Indeed, in *T. nopcsai* and varanids, the width decrease gradually from the cerebrum to the optic lobes in dorsal view (Fig. 7.5A, C), whereas in snakes, the transition between the two structures is more abrupt since the width of the optic lobes is significantly narrower than that of the cerebrum (Fig. 7.5 E, G, I, K).

In lateral view, the pituitary bulb in *T. nopcsai* forms a prominent bulge on the ventral surface of the endocast. In varanids, the shape of the structure is comparable to that of *T. nopcsai* but the ventral extension is less developed and do not extend beyond the ventral marge of the medulla oblongata. In snakes, most of the species exhibit a structure directed posteriorly that differ from *T. nopcsai* (e.g., *Pelamis platurus*, Fig.7.5H). However, some taxa (e.g., *Python regius*, Fig. 7.5F) have a pituitary bulb similar in shape to that of *T. nopcsai* but less extended ventrally.

On the posterior part of the endocast, the rhombencephalon of *T. nopcsai* shows a slightly convex ventral margin in lateral view, as in most snakes (e.g., *Hierophis gemonensis*,

Fig. 7.5L), but differs from the varanid condition, in which the ventral margin of the rhombencephalon is rounded (Fig. 7.5D)

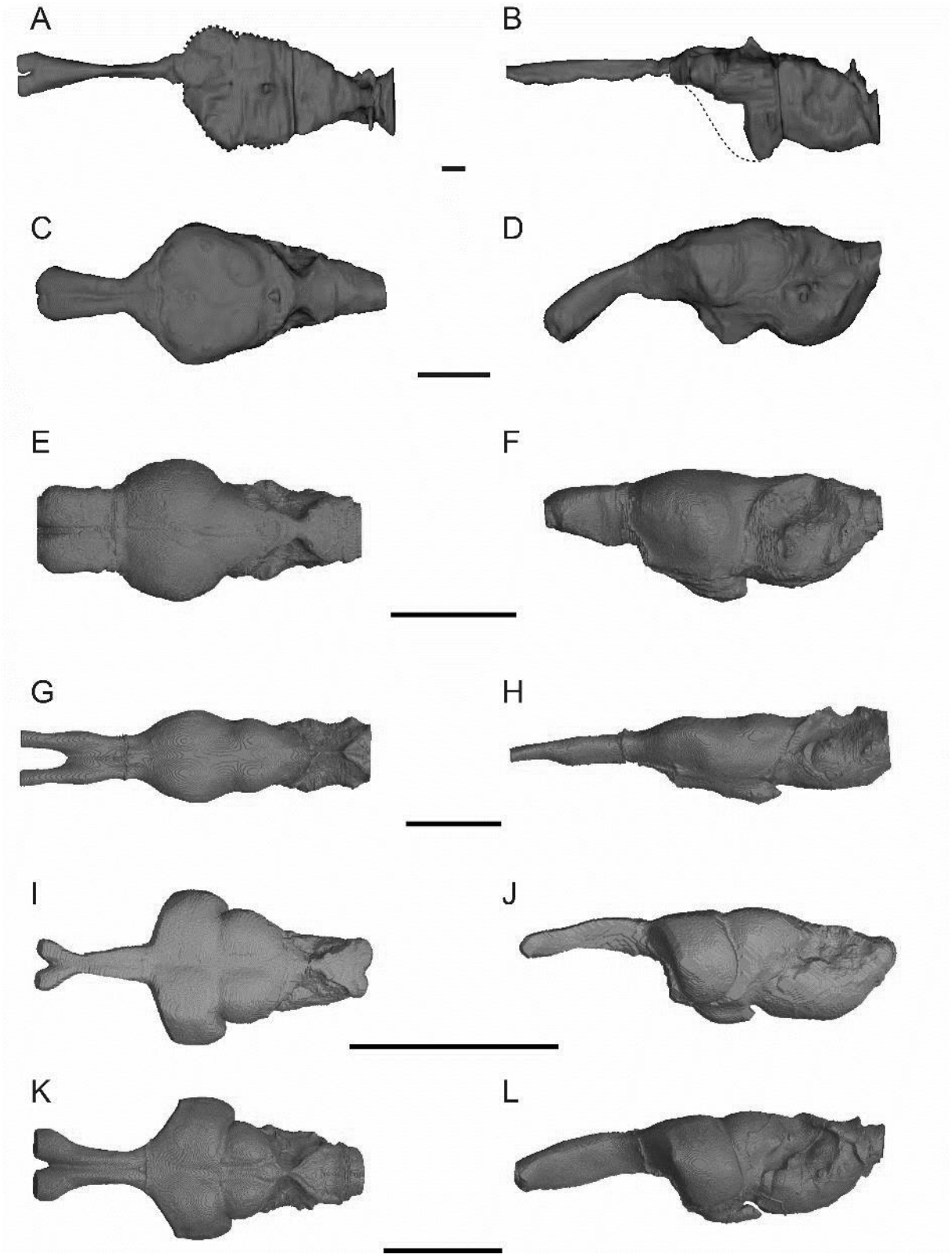

Fig. 7.5. Digital endocasts in dorsal (left) and lateral (right) views of **(A-B)** the mosasauroid *Tethysaurus nopcsai*, **(C-D)** the varanid *Varanus niloticus*, and the snakes **(E-F)** *Python regius*, **(G-H)** *Pelamis platurus*, **(I-J)** *Mimophis mahfalensis*, **(K-L)** *Hierophis gemonensis.* Scale bars equal 5 mm.

7.3.2. Quantitative comparisons

The PCA obtained with all specimens (see Fig. 7.6A) shows that 64% of the variance is explained by the two first axes (44% and 20% respectively). All variables seem to act on the repartition of the species. Along the first axis, *Tethysaurus nopcsai* is separated to both snakes and varanids without being closer to one or the other. One variable mostly acts on the distribution of the taxa along the first axis: the maximal width of the optic lobes. The first axis seems to separate taxa according to the width of the optic lobes. Along the second axis, varanids and *Tethysaurus* are close to each other and distinct from all snakes. This distribution is mainly caused by one variable: the length of the olfactory bulbs. This variable separates taxa according to the length of the olfactory tracts.

A second analysis has been performed by removing the two snake specimens (*Typhlophis squamosus* and *Rhinotyphlops schlegelii*) responsible for the extended distribution of snakes along the first axis. The second PCA obtained from the remaining specimens (see Fig. 7.6B) shows that 57% of the variance is explained by the two first axes (35% and 22% respectively). Along the first axis, *T. nopcsai* is separated from both snakes and varanids, but closer to the latter. Two variables act on this distribution: the width of the olfactory tracts and their length. The first axis separates taxa with short and wide olfactory tracts from those that exhibit long and narrow olfactory tracts. Along the second axis, the height of the olfactory bulbs acts on the taxa distribution. This variable allows to separate *T. nopcsai* from varanids, in which the olfactory bulbs are developed dorso-ventrally, but not from snakes that exhibit a great variability in size.

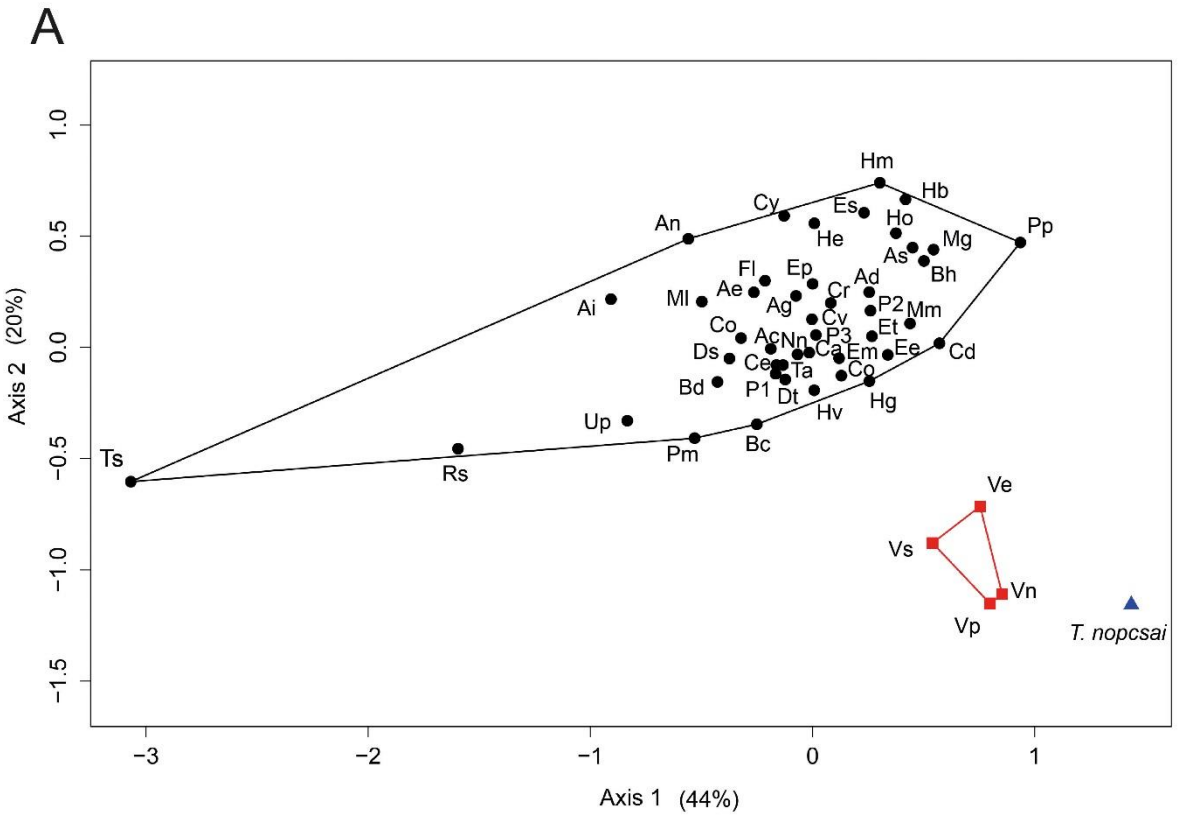
A
Axis 2 (20%)
Axis 1 (44%)
Hm
Hb
Cy
Es
An
Ho
Pp
He
Mg
As
Bh
Fl
Ep
Ad
Ae
Cr
Ai
Ml
Ag
P2
Mm
Cv
Co
Et
Ac
Nn
P3
Ds
Ca
Em
Ee
Cd
Ce
Ta
Co
Bd
P1
Dt
Hg
Hv
Up
Ts
Rs
Pm
Bc
Ve
Vs
Vn
Vp
T. nopcsai

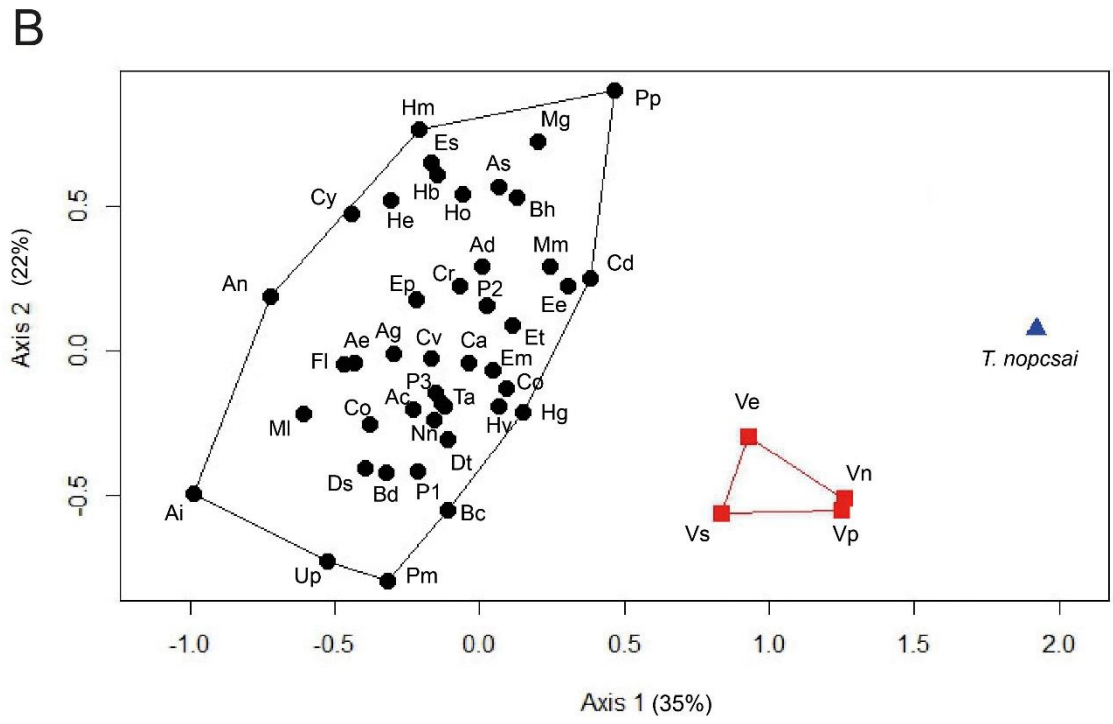
B
Axis 2 (22%)
Axis 1 (35%)
Hm
Pp
Mg
Es
As
Cy
Hb
Ho
Bh
He
Ad
Mm
Cd
An
Ep
Cr
P2
Ee
Ae
Ag
Cv
Ca
Et
Fl
Em
P3
Co
Ac
Ta
Co
Hg
Ml
Hv
Nn
Dt
Ds
Bd
P1
Ai
Bc
Up
Pm
Ve
Vn
Vs
Vp
T. nopcsai

Fig. 7.6. Scatter plots illustrating the position of the different specimens on the first two principal components. Results of the principal component analyses based on the measurements taken on the endocast of the *Tethysaurus nopcsai* (SMU 76335), snake (black circles), and varanid (red squares) specimens **(A)** and after removing the two snake specimens *Typhlophis squamosus* and *Rhinotyphlops schlegelii* **(B)**. See Material and Methods (Chapter 4, p. 57) for taxon name abbreviations.

7.4. Discussion

Similarly to in mammals and birds, the squamate endocast and inner ear seem to reflect both phylogenetic and ecologic signals (e.g., Boistel et al., 2011a; Yi and Norell, 2015; Allemand et al., 2017b; Palci et al., 2017; Chapters 5 and 6). In the following discussion, both signals are considered without distinction.

7.4.1. Mosasauroid endocasts

The endocranial comparisons between *Tethysaurus nopcsai*, *Clidastes* and *Platecarpus* do not reveal a common pattern for mosasauroids. Endocasts of both *Tethysaurus* and *Clidastes* have elongated and mediolaterally compressed olfactory tracts and a small pineal organ. However, as Camp (1942) only figured the dorsal view of the endocast of *Clidastes*, comparisons are limited. Conversely, the endocranial pattern of *Tethysaurus* greatly differs from that of *Platecarpus*. Indeed, the short olfactory tracts, the large pineal organ, the small pituitary bulb not projected ventrally and the pronounced ventral flexure on the posterior part of the endocast figured by Camp (1942) for *Platecarpus* differ from *Tethysaurus* and *Clidastes*.

Among these differences, Camp figured short olfactory tracts in dotted line; however, as this structure is in fact unknown, comparisons with *Tethysaurus* and *Clidastes* are not relevant. The most noticeable differences are the small pituitary bulb and the pronounced ventral flexure observed in *Platecarpus*, differing from the ventrally developed pituitary bulb and the nearly straight endocast in *Tethysaurus*. As Camp (1942) does not provide any clue

about the state of preservation of *Platecarpus*, it is difficult to evaluate the impact of this factor on these differences. However, a bias caused by the use of dissociate braincase elements for the endocranial reconstruction in *Platecarpus* (Camp, 1942) could explain why the latter is so different from that of *Tethysaurus*.

A similar ventral flexure has been reported in other groups, such as archosaurs (Giffin, 1989) and plesiosaurians (see Chapter 9). According to Giffin (1989), this characteristic could be directly correlated to: 1) the size of the specimens, the endocast of smaller taxa have a more pronounced flexure than those of larger taxa; 2) the ontogeny: young individuals have a more pronounced flexure than older ones of the same species; and 3) the size of the eyes: large eyes relative to the skull length could increase the flexure. Such hypotheses are difficult to verify as no information about the size or the ontogenetic stage in *Platecarpus* were given by Camp (1942). However, indirect evidences from another adult specimen of *Platecarpus tympaniticus* (LACM 128319, Konishi et al., 2012) suggest that the body size is not correlated to the pronounced flexure as the adult *Tethysaurus* (MNHN GOU1: 3m, Bardet et al., 2003b) appears smaller than *Platecarpus* (LACM 128319: 5m, Konishi et al., 2012). On the contrary, the ratio between the orbit length and the skull length estimated to 20% for *Platecarpus tympaniticus* (LACM 128319, Konishi et al., 2012) and to 15% in *Tethysaurus* corroborate the hypothesis that the eye size may influence the endocranial shape.

Tethysaurus nopcsai was originally considered a basal mosasauroid, sister-group of Mosasauridae (Bardet et al., 2003b; see Fig. 7.7C). However, its phylogenetic position varies according to authors and it has been also reported as a basal mosasaurid (forming a clade with *Yaguarasaurus* and *Russellosaurus*) being inferred sister-group of either the Russellosaurinae (Bell and Polcyn, 2005; see Fig. 7.7A) or of the Halisaurinae (Caldwell and Palci, 2007; see Fig. 7.7.B); in both case, it has never been considered as close to the Mosasaurinae. Among the two other mosasauroid taxa for which the endocast is known, *Platecarpus* is included in the Russellosaurina (Polcyn and Bell, 2005) whereas *Clidastes* is considered a basal Mosasaurinae (Polcyn and Bell, 2005; Caldwell and Palci, 2007).

The endocasts of *Tethysaurus* and *Platecarpus* differ significantly, whereas that of *Clidastes* exhibits some endocranial structures (olfactory tracts, pineal organ) similar to those found in *Tethysaurus*. Based on these preliminary comparisons, *Tethysaurus* could be

considered as more closely related to *Clidastes* than to *Platecarpus*, suggesting an alternative phylogenetical position to those already suggested (Bardet et al, 2003b; Bell and Polcyn, 2005; Caldwell and Palci, 2007), that is a basal Mosasaurinae possibly close to *Clidastes*.

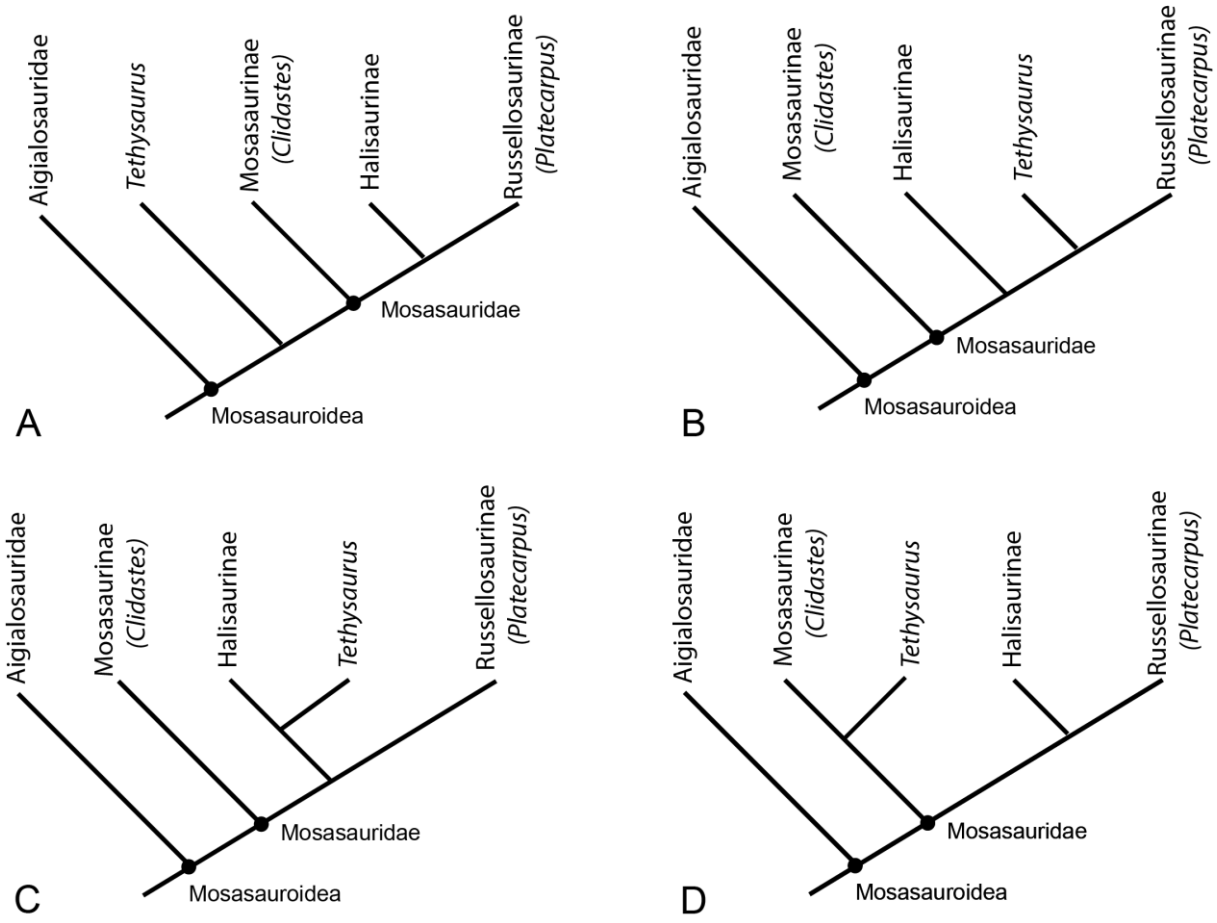

Fig. 7.7. Simplified cladograms showing the variable phylogenetic position of *Tethysaurus nopcsai* as (A) sister-group of Mosasauridae (Bardet et al., 2003b); (B) sister-group of the Russellosaurinae (Bell and Polcyn, 2005); (C) sister-group of the Halisaurinae (Caldwell and Palci, 2007); (D) as basal Mosasaurinae possibly close to *Clidastes* on the basis of the endocranial morphology.

On an ecological point of view, *Tethysaurus* is regarded as a plesiopedal and hydropelvic taxon (see Chapter 1). The anatomy of *Tethysaurus* pelvis suggests no possibility

for a facultative quadrupedal locomotion on earth (Caldwell and Palci, 2007). This taxon is thus considered as obligatory aquatic, adapted to an intermediate life between the shallow-water plesiopedal-plesiopelvic mosasauroids, which have facultative terrestrial limbs and a sacrum, and the open-sea hydropedal-hydropelvic ones that exhibit a pelvis highly modified and paddles (e.g., Caldwell and Palci, 2007).

From an endocast perspective, the implications of such ecological grades are difficult to discern. The hydropelvic and hydropedal conditions in *Platecarpus* suggests that this species was adapted to an open-sea lifestyle (e.g., Russell, 1967; Lingham-Soliar, 1991; Konishi et al., 2012) and may explain why its endocast greatly differs from that of *Tethysaurus*. Although *Clidastes* is also regarded as a hydropelvic and hydropedal mosasauroid (e.g., Lindgren and Siverson, 2004), the habitat of this species is still uncertain as several authors have noticed its occurrence in shallow-water environments (e.g., Williston, 1897; Russell, 1967; Erlström and Gabrielson, 1992) whereas Sheldon (1997) stated that its reduced bone density reflects an adaptation to deeper-water environments (but see Houssaye and Bardet, 2012). Thus, the similar endocranial structure between *Clidastes* and *Tethysaurus* could be, in addition to a phylogenetic signal, also the reflect of comparable intermediate life between shallow-water and open-sea.

7.4.2. Mosasauroid inner ear

The general shape of *Tethysaurus* inner ear is similar to that reported for other mosasauroids (Georgi, 2008; Georgi and Sipla, 2008; Cuthbertson et al., 2015), with the exception of *Platecarpus* (UCMP 32136) inner ear illustrated by Camp (1942) that is difficult to compare with *Tethysaurus*'s as several regions are "unclear". A qualitative comparison indicates more similarities between *Tethysaurus* and *Tylosaurus* than with *Platecarpus* (MOR 1062) and *Plioplatecarpus* (Georgi, 2008; Georgi and Sipla, 2008; Cuthbertson et al., 2015). The inner ear of *Clidastes* remains unfortunately unknown, preventing any comparisons as those made with the endocasts. This similarity could reflect a phylogenetic signal revealing close affinities between *Tethysaurus* and russellosaurines (*Platecarpus*, *Tylosaurus*, *Plioplatecarpus*), as suggested by Bell and Polcyn (2005), which in this case would differ from the data obtained

from the endocasts. However, the lack of comparative data in both halisaurines (other possible sister-group of *Tethysaurus*, Caldwell and Palci, 2007), as well as with mosasaurines prevents any conclusion.

In vertebrates, the semicircular canals were described to perceive orientation and balance providing accurate information on the body movement, which are transmitted to the brain for participation in muscular reflex in order to stabilize the trunk, head, and visual field during postural and locomotor activities (Sipla and Spoor, 2008). Based on the shape of the semicircular canals, Cuthbertson et al. (2015) suggested that *Plioplatecarpus* was an agile predator with high locomotor abilities and may have engaged in acrobatic, spatially complex behaviors during foraging. Additionally, the authors stated that the differences observed among the mosasauroid semicircular canals might be related to different swimming behaviors despite sharing similar body proportions and close phylogenetic relationships (Cuthbertson et al., 2015). Thus, the semicircular canal in *Tethysaurus* would reveal different locomotor abilities than *Plioplatecarpus*. However, such differences are difficult to evaluate as the inner ear in both hydropelvic and hydropedal *Tylosaurus* and *Platecarpus* show similarities with *Tethysaurus*.

7.4.3. Sensory inferences

More and more studies use the endocranial anatomy of extinct species as a source of sensory information (e.g., Witmer and Ridgely, 2009; Lautenschlager et al., 2012; Holloway et al., 2013; Pierce et al., 2017). As for mosasauroids, the shift from a terrestrial to a marine habit should be reflected in the sense organs; however, still little information exists about their sensory abilities.

The olfactory bulb size has been used as an indicator of olfactory acuity in archosaurs and mammals (e.g., Gittlemen, 1991; Healy and Guildford, 1990; Zelenitsky et al., 2009). Zelenitsky et al. (2009) proposed to quantify the olfactory acuity in extinct theropod dinosaurs from the ratio of the greatest diameter of the olfactory bulb to the greatest diameter of the cerebrum (Zelenitsky et al., 2009).

Camp (1942) and Polcyn (2010) noticed that the olfactory bulbs in mosasauroids are rather small and suggested a diminished sense of olfaction. However, as the cerebrum is incomplete in mosasauroids, it is not possible to use the ratio previously mentioned and to determine the olfactory acuity of *Tethysaurus*. However, qualitative comparisons with extant taxa, especially with crocodiles that share a similar organization with long olfactory tracts differentiated from large olfactory bulbs (Jirak and Janacek, 2017), suggest that the olfactory bulbs were small in *Tethysaurus* and corroborate the hypothesis of a diminished sense of olfaction.

The paired fenestrae in the palate associated with the vomers (e.g. Russell, 1967) is indicative of the presence of vomeronasal organs and vomerolfaction in mosasauroids (Schulp et al., 2005). Additionally, the presence of vomeronasal organs with openings on the mouth is correlated with tongue-flicking behavior for chemical retrieval (Schulp et al. 2005). According to Schulp et al. (2005), the endocast reconstruction illustrated by Russell (1967, text-fig. 16) shows well-developed accessory olfactory bulbs. It is, therefore, a strong evidence that mosasauroids used tongue-flicking and vomerolfaction in life, probably in the same way as living squamates do during foraging and courtship (Schulp et al., 2005). Contrary to this hypothesis, Polcyn (2010) suggested that the small size of the Jacobson organ housing the vomeronasal system in mosasauroids indicates diminished vomerolfaction abilities. From the endocast of *Tethysaurus*, it is not possible to differentiate the accessory olfactory bulbs (AOB) associated to the vomerolfaction from the main olfactory bulbs (MOB) associated to the sense of smell. However, the relative small size of the whole olfactory bulbs (MOB+AOB) argues for the hypothesis suggested by Polcyn (2010), that is, diminished vomerolfaction abilities.

A relatively small pineal organ is visible on the endocasts of *Tethysaurus* (this work) and *Clidastes* (Camp, 1942). This differs from the large one illustrated for *Platecarpus* by Camp (1942). The pineal organ has important physiological functions (Holloway et al., 2013) and is involved in the production of melatonin, which plays a role in the regulation of the circadian rhythm and seasonal cycles (Hopson, 1979) but it has also different functions according to taxa (see Holloway et al., 2013 for details). The exact functions of a small pineal organ in mosasauroids is thus difficult to determine. Connolly (2016) have shown no correlation

between the size of the pineal organ and latitudinal preferences as a large pineal organ can be observed in individuals living through diverse latitudinal habitats. The same study suggested that there may also be a relationship between the size of the pineal organ and the ability to dive deeply in mosasauroids (Connolly, 2016), large pineal organ could be related for deep diving in mosasauroids, helping to orient themselves at depth.

On the opposite way, the small pineal organ in *Tethysaurus* and its occurrence in shallow-water environment could corroborate this hypothesis. This could also indicate that *Clidastes*, which exhibits a similarly small pineal organ, could live in shallow-water rather than in deeper environments (e.g., Erlström and Gabrielson, 1992). However, the significance of a large versus small pineal foramen should be further tested and investigate since the opposite condition strangely occur in Sauropterygia, for which the shallow-water *Placodus gigas* exhibits a larger pineal organ (Neenan and Scheyer, 2012) than deep diving elasmosaurids (see Chapter 9).

7.4.4. Comparisons with extant squamates

Different authors consider mosasauroids as closely related to varanids (e.g., Rieppel and Zaher, 2000a, b; Schulp et al., 2005; Liu et al., 2016), while others argue for phylogenetical relationship between mosasauroids and snakes (e.g., Lee, 1996, 1997b; Caldwell and Lee, 1997).

Based on the endocasts reconstructed for *Platecarpus* and *Clidastes*, Camp (1942) suggested that the endocranial configuration seen in the two mosasauroid specimens is close to the condition found in varanids, which demonstrates their phylogenetic affinities.

In this work, quantitative and qualitative comparisons show similarities between *Tethysaurus* and varanids, especially about the organization of their cerebrum, optic lobes and pituitary bulbs. However, as some snakes may also present similar endocranial organization, the hypothesis of close affinities between varanids and mosasauroids does not appear so clear and has to be tested further. For this, the consideration of additional taxa, among basal mosasauroids, varanoids, “primitive” snakes and “dolichosaurs” (possible sister-group of the ophidian crown group: e.g., Pierce and Caldwell, 2004) appears necessary.

The reconstruction performed on *Tethysaurus* shows that its inner ear has the typical shape found in mosasauroids. According to Camp (1942) and Russell (1967) the inner ear of mosasauroids is practically identical to that of varanids and testifies a close phylogenetic relationship between these two clades. However, more recent studies performed on CT images of the inner ear of *Platecarpus* and *Tylosaurus* revealed differences between mosasauroids and varanids (Georgi, 2008; Georgi and Sipla, 2008), questioning the hypothesis of Camp (1942) and Russell (1967). Indeed, varanids exhibit in lateral view a more triangular inner ear, with anterior and posterior semicircular canals nearly straight, than mosasauroids, for which the curved semicircular canal gives a more rounded aspect to the inner ear. In snakes, although they exhibit a large range of inner ear morphologies (e.g., Boistel et al., 2011; Yi and Norell, 2015; Palci et al., 2017), a similar to varanid triangular shape is also perceived and differs thus from the mosasauroid condition. From these preliminary data, it seems that the morphology of the mosasauroid inner ear differs from both snakes and varanids and does not reveal preferential affinities with any of these taxa. Quantitative comparisons from measurements illustrating the shape and the size of the inner ear could provide additional data to interpret this variability.

7.5. Conclusion

The interpretation of the endocranial anatomy of *Tethysaurus nopcsai* is difficult as the lack of comparative data prevents to evaluate the impact of the phylogenetic and ecologic signals. However, several hypotheses have been performed during this work. On one hand, the endocast of *Tethysaurus* could suggest an alternative phylogenetical position, as a basal Mosasaurinae, differing from those already stated (Bardet et al, 2003b; Bell and Polcyn, 2005; Caldwell and Palci, 2007) and could reflect an ecological signal related to an intermediate life between shallow-water and open-sea. On the other hand, the inner ear morphology of *Tethysaurus* could reveal close affinities between *Tethysaurus* and russellosaurines, as suggested by Bell and Polcyn (2005), which in this case would differ from the data obtained from the endocasts. The endocranial anatomy of *Tethysaurus* shows some similarities with both varanids and snakes, whereas the inner ear of *Tethysaurus* differs from both varanids and snakes. These preliminary results show no indication that could suggest closer phylogenetic affinities with one or another

group of these extant squamates. Although it has been difficult to delimit the different structures composing the endocast of *Tethysaurus* the relative small size of the olfactory bulbs suggests poor olfactory abilities and could corroborate the hypothesis that mosasauroids relied more on visual clues than olfactory ones to interact with their environment.

Chapter 8

Cranial anatomy of three plesiosaurian specimens from the Late Cretaceous (Turonian) of Goulmima, Morocco

Fossils coming from Goulmima are included in ovoid calcareous nodules (see Chapter 4 Material and Methods) that are difficult to prepare as bones may be partially or totally dissolved, making their study difficult. This particular preservation can often prevent a complete access to the fossil anatomy and the use of computed microtomography represents a suitable solution to circumvent these technical issues. In this work, the microtomography was used to reconstruct and describe the cranial anatomy in three different specimens.

The two sections of this chapter (8.1 and 8.2) corresponds to two different articles:

Allemand, R., N. Bardet, A. Houssaye and P. Vincent. 2017a. *Virtual re-examination of a plesiosaurian specimen (Reptilia, Plesiosauria) from the Late Cretaceous (Turonian) of Goulmima (Southern Morocco) thanks to computed tomography*. Journal of Vertebrate Paleontology 37: e1325894.

Allemand, R., P. Vincent, A. Houssaye, and N. Bardet. In press. *New plesiosaurian specimens (Reptilia, Plesiosauria) from the Late Cretaceous (Turonian) of Goulmima (Southern Morocco)*. Cretaceous Research.

8.1. Virtual reexamination of a plesiosaurian specimen (Reptilia, Plesiosauria) from the Late Cretaceous (Turonian) of Goulmima, Morocco, using computed tomography

8.1.1. Material and Methods

The plesiosaurian specimen (SMNS 81783), poorly preserved in an incompletely prepared nodule (Fig. 8.1B), was previously referred to *Libonectes atlasense* (Buchy, 2005). The specimen was scanned at the AST-RX platform of the MNHN (Paris) using a GEphoenix|Xray|v|tome|x L240 with a voxel size of 134 μm (see Chapter 4 Material and Methods). A virtual three-dimensional reconstruction of the skull was then performed at the Palaeontology Imaging Unit of the MNHN Département Histoire de la Terre/UMR 7207 CR2P CNRS/MNHN/UPMC using the MIMICS (Materialise Interactive Medical Image Control System) Innovation Suite software (Materialise®, release 18).

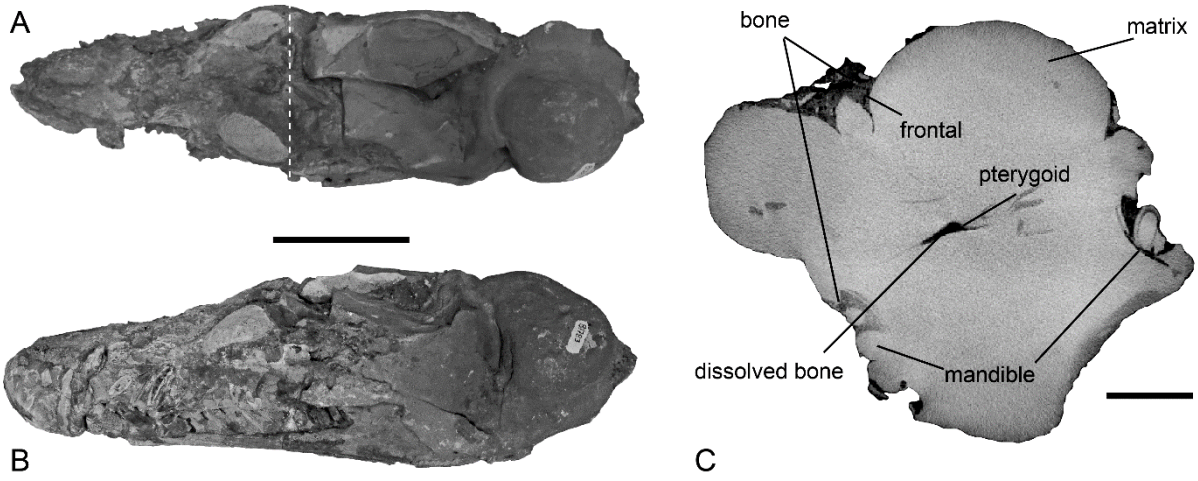

Fig. 8.1. A, B. Photographs of SMNS 81783 in dorsal **(A)** and left lateral **(B)** views. The dotted line indicates the location of the transverse section. **C**. Transverse section in the middle of the skull of SMNS 81783 showing the general state of preservation. Scale bars equal 10 cm **(A, B)** and 2 cm **(C)**.

During segmentation work, bony elements appeared generally with darker grayscale values than the matrix (Fig. 8.1C) due to the different X-ray absorption coefficients. However, no unique threshold value could accurately describe the boundary between bone and the matrix. The shape of some bones that appeared completely dissolved at the surface of the nodule has been reconstructed using their natural cast encased in the matrix. This was the case for the mandible, for which only the cast of the medial margin is preserved (Fig. 8.1C) so that the lateral margin was reconstructed by an approximate extension of its contour (see Fig. 8.5, hatched area). The same method was performed for reconstruction of the lateral margins of the jugal and squamosal (see Fig. 8.1, hatched area).

8.1.2. Systematic Paleontology

SAUROPTERYGIA Owen, 1860

Order PLESIOSAURIA de Blainville, 1835

Family ELASMOSAURIDAE Cope, 1869

LIBONECTES MORGANI Carpenter, 1997

Holotype—SMUSMP 69120, skull and mandible, atlas-axis complex, 48 successive cervical vertebrae, fragmentary thoracic ribs, gastralia and associated gastroliths (Sachs and Kear, 2015); late Cenomanian; Britton Formation, Eagle Ford Group, Near Cedar Hill, Dallas County, Texas, U.S.A.

Referred Specimen—SMNS 81783, skull and mandible, atlas-axis complex. Middle Turonian (Upper Cretaceous) Unit T2a (Ettachfini and Andreu, 2004) of the Cenomanian–Turonian limestone bar, north of Goulmima, Er-Rachidia Province, Southern Morocco.

8.1.3. Description

8.1.3.1. General Preservation

The skull of SMNS 81783 is slightly laterally crushed but most of the bones remain in their natural arrangement and only some parts are missing, including the most dorsal part of the parietal crest, the left lateral margin of the temporal fenestra, and both squamosal arches. The right maxilla is almost dissolved, so that only a small part is preserved. The left part of the palate is broken and disarticulated but much of the right side, posterior to the internal nares is well preserved. The identification of the sutures between palatal bones is difficult and the narial region is crushed and difficult to interpret. The mandible is almost completely preserved except its lateral margin and the posterior part of the right dentary, and it is in occlusion with the cranium.

8.1.3.2. Skull

We estimate that the original cranial length was about 295 mm long from the tip of the premaxilla to the occipital condyle (see measurements and skull proportions in Table 8.1). The beak index (percentage of the preorbital length to the entire length of the skull; Welles, 1952) represents 42% of the skull length. In most elasmosaurids, this value is close to 40%, whereas it is close to 55% in Polycotylidae (Buchy et al., 2005). The temporal fossae are estimated to have occupied about 40% of the skull length. A similar ratio (35–40%) is observable in Cretaceous Elasmosauridae (Sato et al., 2006).

Skull length	295
Preorbital length (tip of the snout/ anterior margin of the orbit)	124
Orbit length *	53.4
Temporal fenestra length **	128
Paraoccipital process length **	30
Mandibular symphysis length	44.5

Table 8.1. Measurements in mm of the skull and mandible of SMNS 81783. Measurements taken on the left (*) or the right (**) side.

Premaxillae—Each premaxilla bears five teeth and participates to the external naris (Fig. 8.2B), constituting its anterior and medial margins. The flat dorsal surface of the premaxilla is slightly pitted and bears a clearly visible suture between both premaxillae (Fig. 8.2A). SMNS 81783 possesses a slight transverse 'rostral' constriction between the premaxilla and the maxilla (Fig. 8.2A), as observed in many large-headed plesiosaurians (e.g., Taylor, 1992; O'Keefe, 2001; Druckenmiller and Russell, 2008a; Smith and Dyke, 2008) and in some elasmosaurids (e.g., Vincent et al., 2011). A small diastema forms a small concavity between the last premaxillary and the first maxillary teeth (Fig. 8.2C). The premaxilla-maxilla suture originates posterior to the fifth premaxillary alveolus and extends posterodorsally to a point just anterodorsal to the external naris (Fig. 8.2C). The posterolateral extension of the premaxilla at the level of the posterior narial border is unclear (Fig. 8.2A, C) and it is impossible to confirm the presence of a prefrontal and its possible extension. In dorsal view, at the level of the interorbital region, the posterior process of the premaxilla forms a shallow concavity separating the frontals (Fig. 8.2A). The posterior extension of the premaxillae is long and shows a small contact with the parietal at the level of the last third of the orbital length (Fig. 8.2A). This feature is seen in many Late Cretaceous elasmosaurids (Sato et al., 2006), polycotylids and some pliosaurids (Ketchum and Benson, 2010). A small isolated piece of bone, located dorsally in the interorbital region, is preserved dorsally to the concavity of the posterior processes of the premaxillae (Fig. 8.2A). It is tentatively interpreted as part of the premaxilla, since it matches perfectly with the concavities of the posterior processes of the premaxillae, and covers the sutures between the premaxillae and the frontal. In ventral view, the palatal surface of the premaxillae exhibit an alveolar channel connecting the replacement alveoli (Fig. 8.2B).

Maxillae—The right maxilla is severely damaged; only a small piece of its preorbital part is present (Fig. 8.2C). The left maxilla is well-preserved and shows 15 alveoli (Fig. 8.2C). The maxilla forms the lateral, ventral and posteroventral margins of the external naris, and the anterior corner of the orbit (Fig. 8.2A, C) as in *Libonectes morgani* (Carpenter, 1997). Anterior to the orbit, the sutures between the maxilla and the frontal-prefrontal are not observable (Fig. 8.2A, C). Laterally, the maxilla extends beneath the orbit and underlaps the jugal ventrally (Fig. 8.2C). The maxilla-jugal suture is long and posteroventrally directed as in other elasmosaurids (e.g., *Futabasaurus suzukii* Sato et al., 2006) and it extends posteriorly to about half the length

of the temporal fenestra. Its suture with the squamosal is unclear (Fig. 8.2C), as is the participation of the maxilla in the margin of the internal naris in palatal view (Fig. 8.2B).

Nares—The external nares are located above the third to fifth maxillary teeth (Fig. 8.2C), just anterior to the orbits. The anterior extension of the external nares is difficult to determine (Fig. 8.2A, C). The internal nares (Fig. 8.2B) largely overlap the external ones but are located slightly anteriorly to them, as in *Libonectes morgani* (Carpenter, 1997).

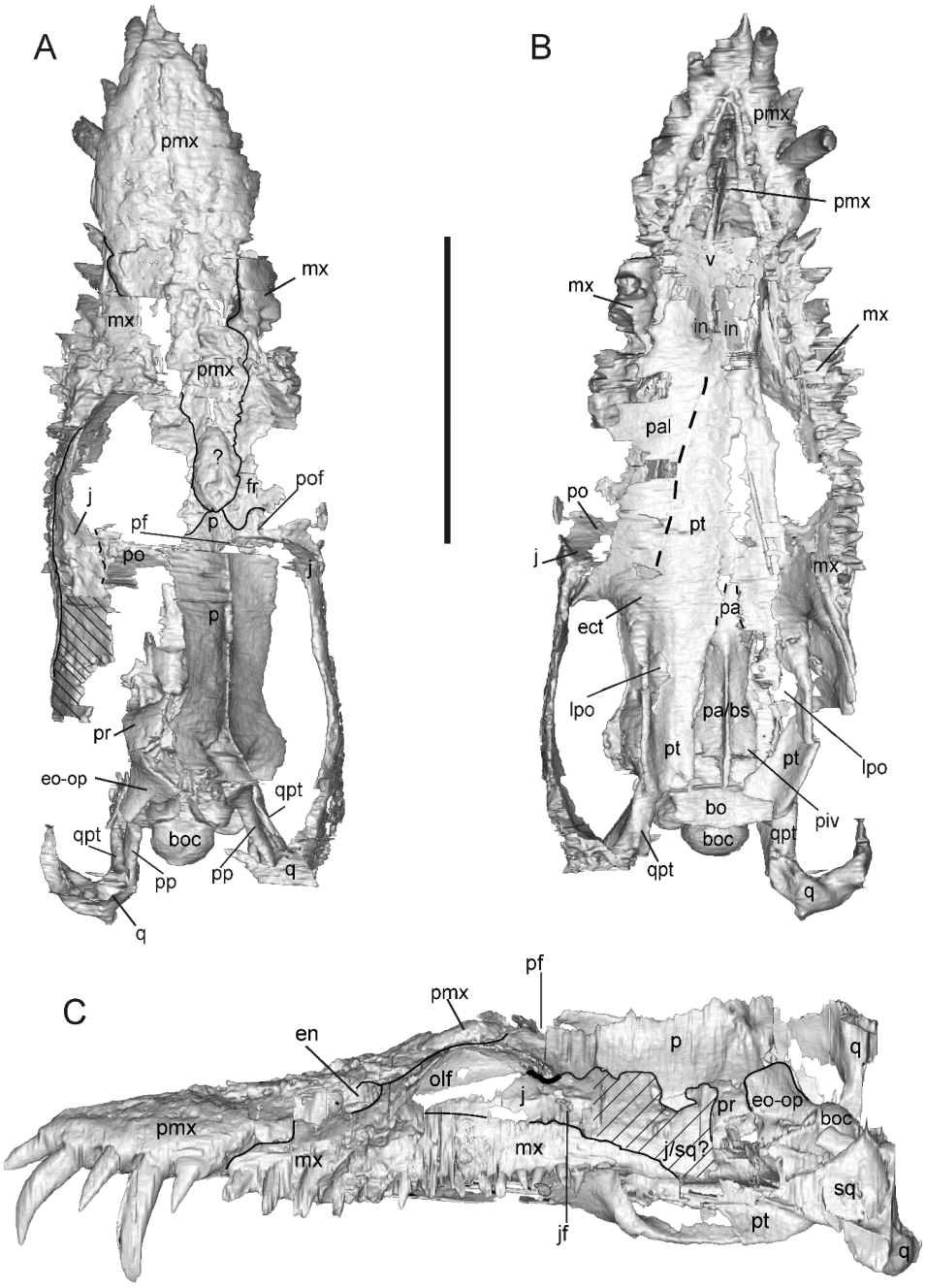

Fig. 8.2. Digital reconstruction of the skull of SMNS 81783, Early Turonian, Goulmima, Morocco, in dorsal **(A)**, ventral **(B)**, and left lateral **(C)** views. **Abbreviations**: **bo**, basioccipital; **boc**, occipital condyle; **ect**, ectopterygoid; **en**, external naris; **eo-op**, exoccipital-opisthotic; **fr**, frontal; **in**, internal nares; **j**, jugal; **jf**, jugal foramen; **lpo**, lateral pterygoid opening; **mx**, maxilla; **olf**, lateral wall of the olfactory canal; **p**, parietal; **pa**, parasphenoid; **pa/bs**, parabasisphenoid; **pal**, palatine; **pf**, pineal foramen; **piv**, posterior interpterygoid vacuities; **pmx**, premaxillae; **po**, postorbital; **pof**, postfrontal; **pp**, paraoccipital process; **pr**, prootic; **pt**, pterygoid; **q**, quadrate; **qpt**, quadrate ramus of the pterygoid; **sq**, squamosal; **v**, vomer; **?**, undetermined bone. Scale bar equals 10 cm.

Frontal—The frontal forms the roof of the orbit (Fig. 8.2A). It contacts the premaxillae medially and the postfrontal posterolaterally (Fig. 8.2A). It does not seem to contribute to the temporal fenestra but, because of the bad preservation of this area, it is not possible to comment on its contact with the maxillae. The frontals are separated by the long dorsal processes of the premaxillae along their entire length, as in most elasmosaurids (Vincent et al., 2011), but unlike the condition of all Jurassic and a few Cretaceous taxa (*Brancasaurus brancai* Wegner, 1914 and *Callawayasaurus colombiensis* Carpenter, 1999) that exhibit frontals in contact all along their length (Carpenter, 1997, 1999; Sato, 2003; Kear, 2005; Brown et al., 2013). Around the posterior orbital margins, the sutural relationships between the frontal, premaxillae, parietal, postfrontal and postorbital are difficult to interpret (Fig. 8.2A). Ventrally, the frontals form the lateral wall of the olfactory sulcus (Fig. 8.2C).

Orbits—The maxilla forms the anterolateral corner of the orbit (Fig. 8.2A, C) but it is not clear whether the maxilla or the prefrontal form their anteromedial corner. The frontal and the jugal form respectively its dorsal and ventral edges (Fig. 8.2A, C), as in *Libonectes morgani*, *Styxosaurus snowii* Williston, 1890 and *Thalassomedon haningtoni* Welles, 1943 (Carpenter, 1997). The ventral margin formed by the maxillae appears convex in lateral view (Fig. 8.2C), as in many elasmosaurids (Sato et al., 2006). Similarly as in most known elasmosaurid skulls (e.g., *Terminonatator ponteixensis* Sato, 2003), the sclerotic ring is not preserved.

Postorbital Bar—The postorbital bar is partially preserved on both sides (Fig. 8.2A). The exact of its contacts with the frontal and postfrontal, as well as its relationships with the posterior rim of the orbits, and its possible contact with the squamosal posteriorly are unclear.

Jugal—The jugal is a plate-like, transversely thin bone that forms the most part of the ventral margin of the orbit (Fig. 8.2C), as in *Libonectes morgani* and *Futabasaurus suzukii* (Carpenter, 1997; Sato et al., 2006). The left jugal is rather well preserved, contrary to the right, but the suture with the postorbital is not easily observable (Fig. 8.2A). Posterior to the orbit, a large foramen perforates the lateral surface of the jugal (Fig. 8.2C), as in *Libonectes morgani* (Welles, 1949). It is not possible to differentiate the squamosal from the posterior part of the jugal (Fig. 8.2C).

Parietal—The closed parietals form a median dorsal roof over the endocranial cavity, with lateral surfaces weakly concave. The exact height of the parietal crest is unknown because of partial dissolution (Fig. 8.2C). Anteriorly, the parietal contacts the frontal at the level of the posterior margin of the orbit (Fig. 8.2A). A small pineal foramen is present anteriorly and totally enclosed within the parietals at the level of the postorbital bar (Fig. 8.2A). The pineal foramen is absent in most elasmosaurids (*Futabasaurus suzukii*, *Libonectes morgani*, *Styxosaurus snowii*, *Terminonatator ponteixensis*, *Tuarangisaurus keyesi* Wiffen and Moisley, 1986, *Zarafasaura oceanis* Vincent et al., 2011) but present in *Callawayasaurus colombiensis* (Welles, 1952). Its loss is considered as a synapomorphy of Late Cretaceous Elasmosauridae and Polycotylidae by Carpenter (1997), but recent phylogenetic data sets suggest that the pineal foramen was lost independently in some Cretaceous elasmosaurids (e.g., *Eromangasaurus carinognathus* Kear, 2005) and some polycotylids (O'Keefe, 2001; Kear, 2005; Druckenmiller and Russell, 2008a; Ketchum and Benson, 2010). The posterior end of the parietal overlaps the supraoccipital.

Squamosal—Both squamosals are partially preserved (Fig. 8.2A, C); their medial contact is not preserved. The left dorsal ramus has been lost, along with the medial dorsal portion of the right ramus. The anterior and ventral rami are preserved on the right side and show that the suspensorium was only slightly inclined anterodorsally (Fig. 8.2A), in contrast to the straight suspensorium present in *Terminonatator ponteixensis* (Sato, 2003) or the curved one (posterior margin is convex in lateral view) of *Styxosaurus snowii* and *Thalassomedon haningtoni* (Carpenter, 1999). The right anterior ramus of the squamosal forms the temporal

bar, contacting the jugal anteriorly (Fig. 8.2A). The sutural relationships of the ventral ramus of the squamosal with the quadrate remains unclear. On the right side, medial to the quadrate, the squamosal is overlain by the quadrate ramus of the pterygoid.

Quadrate—The right quadrate is poorly preserved but the left one is almost complete (Fig. 8.2A, C), though its most posterior surface is dissolved. The left quadrate seems to be mediolaterally convex in posterior view and concave in anterior view. It extends anteromedially to contact the quadrate ramus of the pterygoid (Fig. 8.2A, B). Ventrally, the quadrate extends well ventral to the tooth row (Fig. 8.2C), being the thickest at the articulation with the mandible to form a large quadrate condyle. The latter is divided into two parts by an oblique, anteroposteriorly oriented intercondylar depression. Both quadrates have a small depression on their medial surface corresponding to the facet of the paraoccipital process (Fig. 8.2A).

Vomer—The vomer is poorly preserved; its anteriormost part is missing (Fig. 8.2B), and the occurrence of a vomeronasal foramen cannot be determined. The vomer forms the anterior and medial margins of the internal naris (Fig. 8.2B). Its posterior extension and its sutural relationships with the pterygoid are unclear. The median suture between the two vomers is clearly seen in the median sheet of bone separating the internal nares (Fig. 8.2B).

Palatine—The palatine is well-preserved on the right side of the palate (Fig. 8.2B), though some parts are partially broken and its sutural relationships with the pterygoid are not visible. On the left side the palatine is strongly damaged (Fig. 8.2B). The anterior extension of the palatine, as well as its participation to the naris margin are unclear (Fig. 8.2B).

Pterygoid—The right pterygoid is well preserved, while the left one is damaged in a similar manner to the left palatine (Fig. 8.2B). The pterygoids form the central plate-like portion of the palate, posterior to the vomers and anterior to the posterior interpterygoid vacuities (Fig. 8.2B). Both pterygoids are broken anterior to the posterior interpterygoid vacuities, obscuring their midline suture. Our interpretation is that there is no anterior interpterygoid vacuity and that the pterygoids are closed along their median suture (Fig. 8.2B), as in the Jurassic microcleidids, *Microcleidus* (=*Occitanosaurus) tournemirensis* (Sciau et al., 1990) and *Microcleidus homalospondylus* (Owen, 1865) (Benson et al., 2012; Brown et al., 2013), as well as in the Cretaceous elasmosaurids (Bardet et al., 1999; Großmann, 2007). Lateral to the narrow and elongated posterior interpterygoid vacuities, the ventral surface of the pterygoid is slightly concave and its lateral margin is projected ventrolaterally, forming a curved prominent flange

that contacts posteriorly the quadrate ramus (Figs. 8.2B, 8.3). On the right side, the pterygoid bears an anteroposteriorly extended opening located laterally to the posterior interpterygoid vacuity (Figs. 8.2B, 8.3). Despite a poor preservation of this area on the left side, an opening on the left pterygoid appears present as well. These openings are exactly mirrored on the left and right pterygoids (Fig. 8.2B), which suggests that they are most likely not taphonomic artefacts. Such openings were reported in *Zarafasaura oceanis* as a possible autopomorphy of the taxon (Vincent et al., 2011). Posterior to the interpterygoid vacuities, the bones are dissolved and it is not possible to comment on the medial contact between the pterygoids covering the basioccipital (Fig. 8.2B).

Epipterygoid—The epipterygoid forms a thin vertical process lateral to the parabasisphenoid (Fig. 8.3). The epipterygoid seems to extend dorsally from the anterior dorsal edge of the vertical pterygoid process, similarly to that observed in *Libonectes morgani* (Carpenter, 1997).

Ectopterygoid—The ectopterygoid is a C-shaped bone located posterolaterally to the palatines and laterally to the pterygoids (Fig. 8.2B, 8.3). The suture between the pterygoid and ectopterygoid, though unclear, appears possibly located near the bump formed by the ectopterygoid (Fig. 8.2B). A facet is visible on the lateral margin of the ectopterygoid and seems to contact the posterior elongation of the maxillary (Fig. 8.3). At the juncture of the right palatine with the ectopterygoid and pterygoid, a small fenestra is present and may correspond to the suborbital fenestra (Fig. 8.2B), as seen in *Libonectes morgani* (Carpenter, 1997). The poor preservation of the left pterygoid precludes observation of this fenestra on that side.

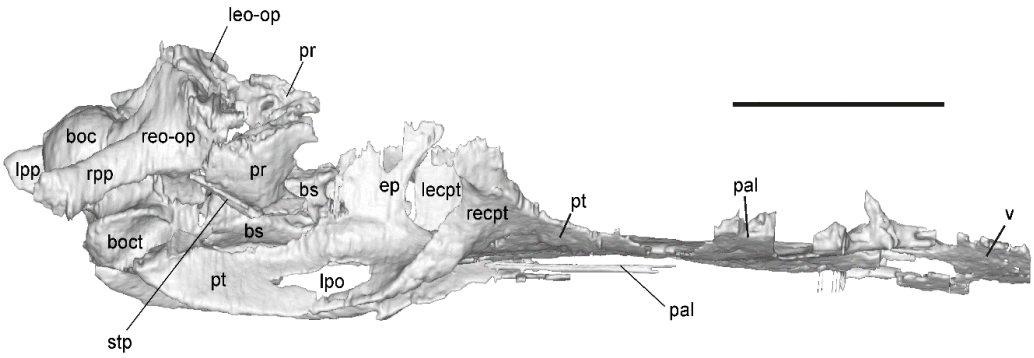

Fig. 8.3. Digital reconstruction of the braincase and the palate of SMNS 81783, Early Turonian, Goulmima, Morocco, in right lateral view. **Abbreviations**: **boct**, basioccipital tuber; **boc**, occipital condyle; **bs**, basisphenoid; **ep**, epipterygoid; **lecpt**, left ectopterygoid; **leo-op**, left exoccipital-opisthotic; **lpo**, lateral pterygoid opening; **lpp**, left paraoccipital process; **pal**, palatine; **pr**, prootic; **pt**, pterygoid; **recpt**, right ectopterygoid; **reo-op**, right exoccipital-opisthotic; **rpp**, right paraoccipital process; **stp**, stapes; **v**, vomer. Scale bar equals 5 cm.

8.1.3.3. Braincase

The braincase is formed by the supraoccipital, the fused exoccipital-opisthotics, the basioccipital, the prootic, and the parabasisphenoid. The elements are slightly displaced from their natural position. The foramen magnum is taller than wide and seems to be slightly constricted at the level of the supraoccipital-exoccipital-opisthotic sutures.

Parabasisphenoid—The parasphenoid and the basisphenoid form the anterior floor of the braincase and there is no trace of suture between the dorsal part of the parasphenoid and the ventral part of the basisphenoid. Anteriorly, the cultriform process of the parasphenoid is visible on the palatal surface (Fig. 8.4A, B, C) where it terminates between the posterior ends of the anterior rami of the pterygoids. The parasphenoid carries a prominent ventral keel that divides the posterior interpterygoid vacuities (Figs. 8.2B, 8.4B), as in Cretaceous elasmosaurids and in the Jurassic forms *Microcleidus (=Occitanosaurus) tournemirensis* and *Microcleidus homalospondylus* (Bardet et al., 1999; Brown et al., 2013). The ventral keel continues slightly posterior to the posterior margins of the interpterygoid vacuities and tapers posteriorly along the ventral surface of the basioccipital (Fig. 8.2B). In dorsal view, just posterior to the cultriform

process, the sella turcica is open anteriorly (Fig. 8.4A). The pituitary fossa occupies about one-third of the braincase floor, which is comparable to the condition in *Tricleidus seeleyi* Andrews, 1909 (see Sato et al., 2011). The sella turcica posteriorly terminates with the dorsum sellae (Fig. 8.4A, C). A prominent pila antotica extends anterodorsally from this region, and a pila metoptica is present more anteriorly (Fig. 8.4A, B, C), as in *Thalassiodracon hawkinsi* (Owen, 1938) (Storrs and Taylor, 1996; Benson et al., 2011b). In lateral view and ventrally to the pila antotica, a process extends from the lateral surface of the basisphenoid (Fig. 8.4B) and forms a facet that contacts the pterygoid (basipterygoid process). The lateral surface of the parabasisphenoid is pierced by a large foramen for the internal carotid located ventral to the pila antotica and just posterior to the basipterygoid process of the basisphenoid (Fig. 8.4B). In anterior view, a pair of internal carotid foramina penetrates the posterior wall of the sella turcica (Fig. 8.4C), as in *Libonectes morgani* (Carpenter, 1997:fig. 5) but differs from *Alexandronectes zealandiensis* Otero et al., 2016 in which there is only a single foramen in the floor of the sella turcica (Otero et al., 2016). The dorsolateral side of the pituitary fossa bears a foramen visible in anterior view (Fig. 8.4C) that probably carried the abducens nerve (Carpenter, 1997).

Basioccipital—The basioccipital is a stout element. Its dorsal surface bears two facets (Fig. 8.4C) for articulation with the exoccipitals (otooccipital facets: Evans, 2012). A small portion of the basioccipital median ridge seems to be present in dorsal view (Fig. 8.4A, C). Ventrolaterally, the basioccipital tubers show two ovoid facets for contact with the pterygoids (Fig. 8.4B, D). In ventral view, the basioccipital contacts the parabasisphenoid anteriorly and the pterygoids laterally. Contrary to what is reported among pliosaurids and cryptoclidids (e.g., Andrews, 1913; Brown, 1993), in which the exoccipital-opisthotic forms part of the occipital condyle, the basioccipital appears here to form the entire rounded occipital condyle (Fig. 8.4D). A groove surrounds the occipital condyle forming a distinct neck ventrally and laterally (Fig. 8.4D) as in elasmosaurids (Brown, 1993), but differing from the condition of *Thalassiodracon hawkinsi* (Benson et al., 2011b), in which the occipital condyle is a shallow dome lacking a groove between the condyle and the body of the basioccipital.

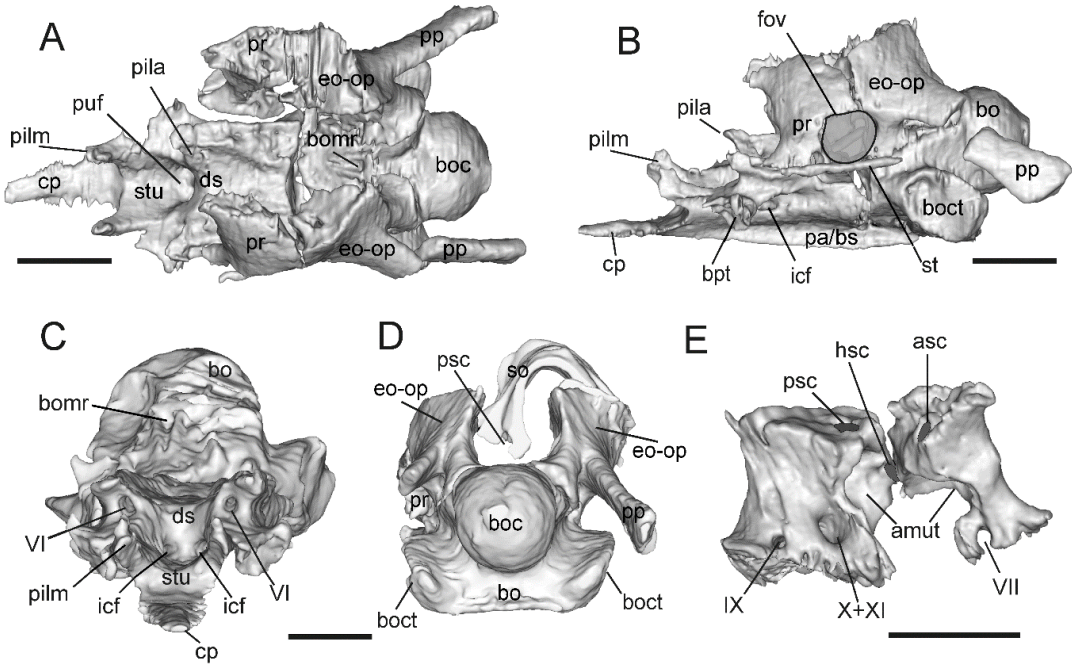

Fig. 8.4. Digital reconstruction of the braincase of SMNS 81783, Early Turonian, Goulmima, Morocco, in dorsal **(A)**, left lateral **(B)**, anterior **(C)** and posterior **(D)** views and of the left exoccipital-opisthotic and prootic in medial view **(E)**. **Abbreviations**: **amut**, chamber for ampulla and utriculus; **asc**, anterior semicircular canal; **bo**, basioccipital; **boc**, occipital condyle; **boct**, basioccipital tuber; **bomr**, basioccipital median ridge; **bpt**, basipterygoid process of the basisphenoid; **cp**, cultriform process; **ds**, dorsum sellae; **eo-op**, exoccipital-opisthotic; **fov**, fenestra ovalis; **hsc**, horizontal semicircular canal; **icf**, internal carotid foramen; **IX**, foramen for glossopharyngeal nerve; **pa/bs**, parabasisphenoid; **pila**, pila antotica; **pilm**, pila metoptica; **pp**, paraoccipital process; **pr**, prootic; **psc**, posterior semicircular canal; **puf**, pituitary fossa; **so**, supraoccipital; **st**, stapes; **stu**, sella turcica; **VI**, foramen for the abducens nerve; **VII**, foramen for the facial cranial nerve; **X+XI**, foramen for the vagus and accessory nerves. Scale bars equal 2 cm.

Exoccipital-opisthotics—Both exoccipital-opisthotics are well preserved and are fused as in most plesiosaurians (e.g., Sato et al., 2011; Sachs et al., 2015). On the anterior surface, a deep chamber for the ampulla and utriculus is visible (Fig. 8.4E). Dorsally and laterally to these structures, two openings are preserved and correspond to the caudal part of the posterior and

horizontal semicircular canals, respectively (Fig. 8.4E). Two foramina pierce the medial surface of the exoccipital adjacent to its ventral surface (Fig. 8.4E). The more anterior foramen is larger and might have served for passage of the glossopharyngeal nerve (IX) and possibly also for the perilymphatic duct (Sachs et al., 2015). The smaller one may be considered as a foramen for the vagus and accessory nerves (X + XI) as well as the jugular vein (Sachs et al., 2015). Anteriorly, the opisthotic forms the posterior margin of the fenestra ovalis (Fig. 8.4B). This character differs from the hypothesis proposed by Maisch (1998) for *Muraenosaurus leedsii* Seeley, 1874 in which the opisthotics did not contribute to the fenestra ovalis. The straight paroccipital process has an anteroposteriorly oval cross section and is ventrally inclined (Fig. 8.4A, B, D). Its distal end is a little expanded but does not form a spatulate terminus as observed in pliosaurids and basal plesiosaurians (e.g., Smith and Dyke, 2008; Benson et al., 2011b).

Prootic—The prootic occurs anteriorly to the exoccipital-opisthotic, and forms the anterior margin of the keyhole-shaped fenestra ovalis seen in lateral view (Fig. 8.4B). The prootic is a rectangular element, containing the anterior part of the vestibule of the inner ear dorsomedially (Fig. 8.4E). The facet for the supraoccipital faces posterodorsally and is pierced by an opening for the anterior semicircular canal (Druckenmiller, 2002; Sato et al., 2011). A much larger foramen on the exoccipital-opisthotic facet (Fig. 8.4E) is the exit for the horizontal semicircular canal (Sato et al., 2011). A foramen at the posterior part of the prootic base may represent the exit for cranial nerve VII (Carpenter, 1997).

Supraoccipital—The supraoccipital is a small arch-shaped element lying above the braincase (Fig. 8.4D) and below the parietal, enclosing the dorsal and dorsolateral margins of the foramen magnum. The supraoccipital contacts the parietal dorsally. Its ventrolateral portions are expanded anteroposteriorly to accommodate part of the semicircular canals, as in *Muraenosaurus leedsii* (Maisch, 1998) and *Thalassiodracon hawkinsi* (Benson et al., 2011b). It also contacts the prootic anteroventrally and the exoccipital-opisthotic posteroventrally.

Stapes—Ventrally to the exoccipital-opisthotics and prootics, two anteroposteriorly oriented rods may correspond to the stapes (Fig. 8.4B). The two elements are 28 mm in length but the right one is broken in the middle. Stapes are commonly preserved in Lower Jurassic plesiosaurians (e.g., Brown et al., 2013), but rarely reported among Middle–Upper Jurassic or Cretaceous taxa (Sato et al., 2011), and some authors hypothesized that these taxa may have lacked stapes (e.g., Carpenter, 1997). Contrary to the stapes identified by Storrs and Taylor

(1996) that contacts the anterior surface of the opisthotic (Benson et al., 2011b), the stapes in SMNS 81783 does not contact any other element and its anterior end reaches the anterior extremity of the prootic base.

8.1.3.4. Mandible

Dentary—The dentary is a long and straight bone that occupies most of the lateral surface of the mandible. In dorsal view, the left and right dentaries unite at their anterior ends near alveoli positions 4 (Fig. 8.5A), to form a narrow, gracile and slightly elongated mandibular symphysis, as observed in *Callawayasaurus colombiensis* (bearing three to five pairs of teeth) and *Hydrotherosaurus alexandrae* Welles, 1943 (bearing three pairs). The symphysis, which represents 15% of the total skull length, is not laterally expanded and straight in lateral view (Fig. 8.5C). The dentary seems to be the only component of the symphysis, and it seems that the coronoid extends anteriorly up to the last third of the mandibular ramus. The suture between the dentary and the splenial are only visible anteriorly to the coronoid (Fig. 8.5C); however, the anterior extension of the splenial is unclear. The tooth number is difficult to define since only the medial margin is preserved; however, we estimate the original presence of 16 teeth on the dentary (Fig. 8.5A). Medially to these teeth, the alveoli for the replacement teeth are visible (Fig. 8.5A).

Coronoid—The coronoid (preserved on both sides) lies in tight contact with the dentary, on the medial surface of the mandible (Fig. 8.5A, C). It is a thin and triangular bone with a large dorsal inflation (Fig. 8.5C), comparable to that described in *Zarafasaura oceanis* (Vincent et al., 2011). It contacts the dentary anteriorly, the prearticular ventrally, and the surangular posteriorly.

Prearticular—The prearticular is a narrow bone that contacts the coronoid dorsally and the dentary ventrally; its anterior end is not preserved (Fig. 8.5C). Medially, the prearticular covers the posterior part of the Meckelian canal. The cast of the Meckelian canal visible in lateral view seems to be narrow anteriorly and to expand posteriorly (Fig. 8.5C). The mandibular foramen is only visible medially, located between the coronoid and the prearticular (Fig. 8.5C), where it opens largely posteriorly although the termination of the foramen cannot

be confidently traced posterior to this region, due to the poor preservation of the bones in the posterior part of the mandible. The glenoid fossa appears just posterior to the occipital condyle.

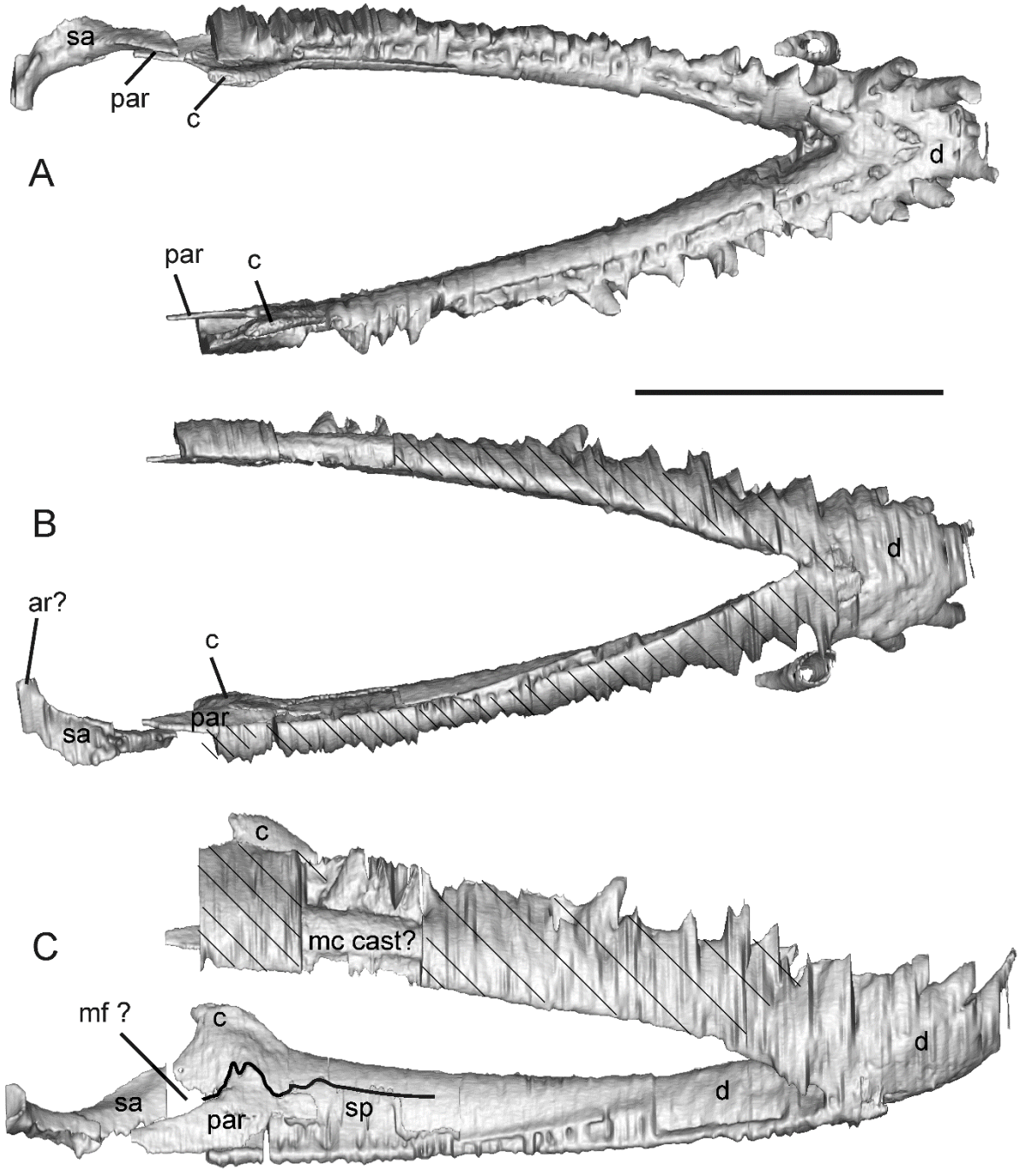

Fig. 8.5. Digital reconstruction of the mandible of SMNS 81783, Early Turonian, Goulmima, Morocco, in dorsal **(A)**, ventral **(B)** and right ventrolateral **(C)** views. **Abbreviations**: **ar**, articular; **c**, coronoid; **d**, dentary; **mc cast**, cast of the Meckelian canal; **mf**, mandibular foramen; **par**, prearticular; **sa**, surangular; **sp**, splenial. Scale bars equal 10 cm.

Surangular—Only the left surangular is partially preserved (Fig. 8.5C). Its anterior part is developed dorsoventrally and forms a ridge that becomes flattened on its posterior part. In the posterior part of the mandible and posterior to the coronoid, the surangular descends to the glenoid cavity.

8.1.3.5. Teeth

The teeth (Fig. 8.2) are slightly flattened and oval in cross-section as in *Callawayasaurus colombiensis*, *Terminonatator ponteixensis*, *Styxosaurus snowii* and *Libonectes morgani* (Sachs and Kear, 2015). The two first teeth on the premaxillae are small and procumbent, as in *L. morgani* and *Dolychorhynchops osborni* Williston, 1902 (Carpenter, 1997). The second and fourth premaxillary teeth are the largest. Several alveoli for replacement teeth are observable on the premaxillae and the left maxilla in palatal view. The maxillary teeth are poorly preserved, but appear to diminish in size from anterior to posterior, in contrast to the condition in both *Aristonectes parvidens* Cabrera, 1941 and *Aristonectes quiriquinensis* Otero et al, 2014 (Gasparini et al., 2003b; Otero et al., 2014), and *Kaiwhekea katiki* Cruickshank and Fordyce, 2002 (Cruickshank and Fordyce, 2002).

8.1.3.6. Atlas-Axis Complex

The conjoined atlas-axis centrum (Fig. 8.6) is cylindrical and distinctly longer than high, as illustrated in a number of other elasmosaurids (e.g., Welles, 1943; Sachs, 2005; Kubo et al., 2012; Otero et al., 2014; Sachs and Kear, 2015). The atlantal cotyle is circular and deeply concave. The cotylar rim is surrounded by a thin edge that is damaged along its left lateral

margin; a posteriorly tapering notch incises its dorsal midline. Ventrally, the atlas intercentrum bears a prominent hypophyseal ridge similar to that reported in *Elasmosaurus platyurus* Cope, 1868 (Sachs, 2005), *Eromangasaurus australis* (Kear, 2005), *Albertonectes vanderveldei* Kubo et al., 2012 (Kubo et al., 2012), *Libonectes morgani* (Sachs and Kear, 2015) and *Vegasaurus molyi* O'Gorman et al., 2015 (O'Gorman et al., 2015). The anteroventral extremity of the hypophyseal ridge is flattened and elliptical in outline, as recorded in *A. vanderveldei* (Kubo et al., 2012) and *L. morgani* (Sachs and Kear, 2015). Posteriorly, the hypophyseal ridge forms a narrow crest merging with the articular face of the axis centrum. The atlas neural spine is oriented posteriorly, narrow on its base and flared dorsally. Only the ventral part of the neural spine is preserved. The exact height is unknown, and the contact between the atlas and axis neural arches seems perforated by a large intervertebral foramen, similar to that depicted in *Libonectes atlasense* (Buchy, 2005), *L. morgani* (Sachs and Kear, 2015) but also in *V. molyi* (O'Gorman et al., 2015) and *Tuarangasaurus keyesi* (Wiffen and Moisley, 1986). The atlas ribs, situated at the approximate mid-section of the atlas-axis complex, are fused to the axis ribs so that they cannot be distinguished from each other. The rib complex is projected laterally posteroventrally (about 45° from the horizontal), beyond the articular face of the axis centrum. The concave and rounded articular face of the axis is partially preserved. It seems surrounded by a thickened convex rim.

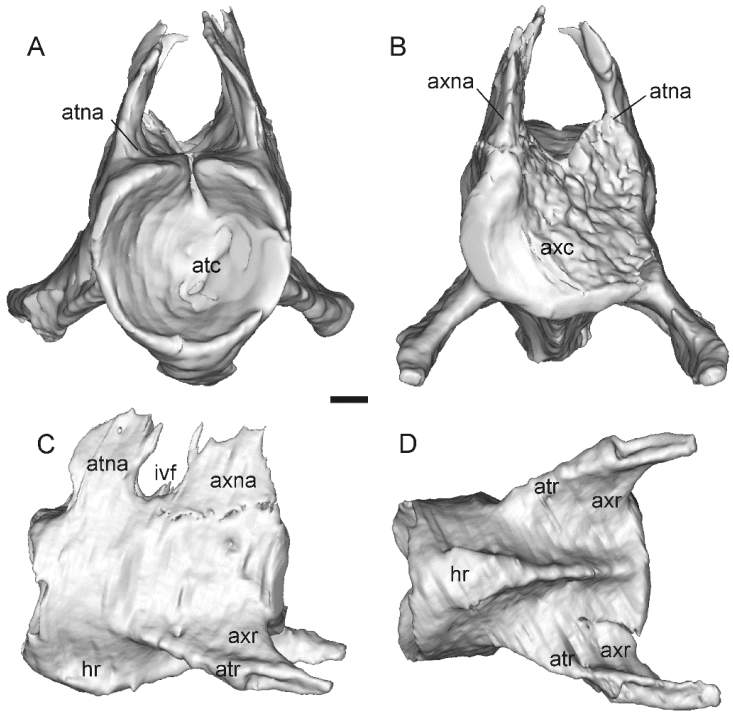

Fig. 8.6. Digital reconstruction of the atlas-axis complex of SMNS 81783, Early Turonian, Goulmima, Morocco, in anterior **(A)**, posterior **(B)**, left lateral **(C)** and ventral **(D)** views. **Abbreviations**: **atc**, atlas centrum; **atna**, atlas neural arch; **atr**, atlas rib; **axc**, axis centrum, **axna**, axis neural arch; **axr**, axis rib; **ivf**, intervertebral foramen; **hr**, hypophyseal ridge. Scale bar equals 1 cm.

8.1.4. Phylogenetic analysis

In order to infer the phylogenetic relationships of SMNS 81783 within Plesiosauria, a cladistic analysis was performed using the datasets of Benson and Druckenmiller (2014), plus two additional OTUs: SMNS 81783 and the type specimen of *Libonectes atlasense* (see Appendix 8). The scores of *Libonectes morgani* were modified following Sachs and Kear (2015). *Yunguisaurus liae* Cheng et al., 2006 was specified as the outgroup taxon and all characters were coded as unordered and unweighted.

A heuristic search for the most parsimonious trees was performed using TNT 1.1 (Goloboff et al., 2008). The search resulted in 100 parsimonious trees; the strict consensus is

shown in Figure 8.7. The consensus tree has a tree length of 1345 steps, an ensemble consistency index of 0.24, and an ensemble retention index of 0.62. Bremer indices higher than one are indicated for each node shown in Figure 8.

The results of the phylogenetic analysis place SMNS 81783 within the Elasmosauridae (Bremer index = 3), as sister taxon to *Libonectes morgani* and *Libonectes atlasense*. Two synapomorphies (ACCTRAN) unite the three taxa: the posterior extent of maxillary tooth row ventral to the postorbital bar and the heterodont maxillary dentition. SMNS 81783 presents three autapomorphies (ACCTRAN): the presence of a transverse constriction of the rostrum at the premaxillae-maxilla suture, the absence of a dorsomedian ridge on the premaxillae and the short anterior extension of the parietal to the level of the temporal bar. The clade formed by *L. morgani* and *L. atlasense* is supported by one autapomorphy (ACCTRAN): the absence of a pineal foramen.

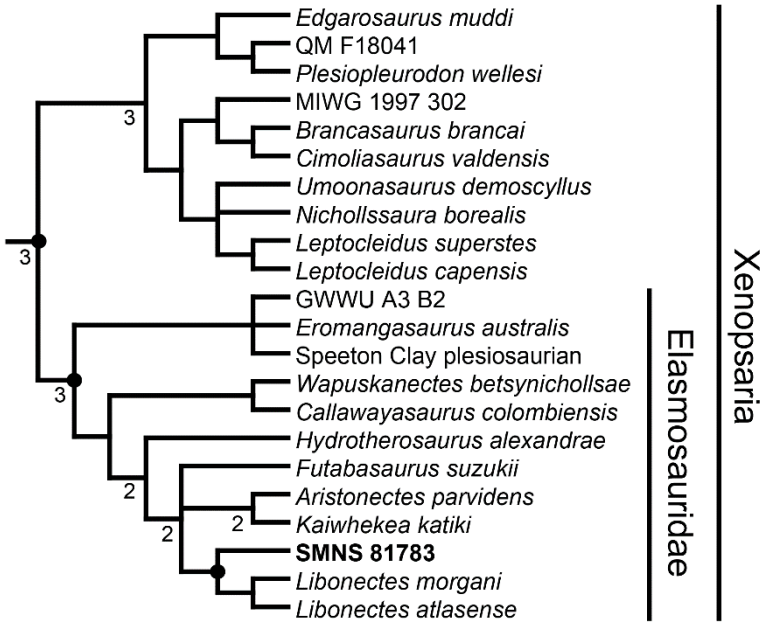

Fig. 8.7. Strict consensus tree showing the relationships of the specimen SMNS 81783 among xenopsarians. Strict consensus of the 100 most parsimonious trees; tree length = 1345 steps; CI = 0.24; RI = 0.62. Bremer indices higher than one are indicated for each node.

8.1.5. Discussion

8.1.5.1. Comparisons with other elasmosaurids

SMNS 81783 presents several elasmosaurid characters: (1) the anterior tooth with an oval cross section (Ketchum and Benson, 2010: character 109); (2) absence of an anterior interpterygoid vacuity (Bardet et al., 1999: character 12; Vincent et al., 2011: character 23); (3) high coronoid eminence (Vincent et al., 2011: character 39); (4) a keyhole-shaped foramen magnum (Druckenmiller and Russell, 2008a: character 67). In addition, SMNS 81783 displays a combination of characters variably found in other elasmosaurids: (1) five premaxillary teeth (Brown, 1993; Sato, 2002); (2) a dorsomedial process of the premaxilla contacting the anterior extension of the parietal (Kear, 2005); (3) a pineal foramen present but not bordered by the frontal (Kear, 2005); (4) a convex ventral margin of the orbit (Sachs and Kear, 2015); (5) a keel on the ventral surface of the parabasisphenoid (Kear, 2005). Comparisons with the available elasmosaurid skulls show that the flat dorsal surface of the premaxillae in SMNS 81783 differs from the prominent dorsomedial bump situated anteriorly to the orbit in *Futabasaurus*, *Styxosaurus snowii*, and *Terminonatator ponteixensis* (Sato, 2003; Sato et al., 2006), the prominent dorsomedian ridge present in *Eromangasaurus* (Kear, 2005) or the low keel reported dorsally along the midline of the premaxillae in *Elasmosaurus carinognathus* (Sachs, 2005). Moreover, in SMNS 81783 the premaxillae bear in total 10 teeth, contrary to the conditions in *E. carinignathus* (7), *E. platyrus* (12), *T. ponteixensis* (9), *Kaiwhekea katiki* (7) or *Aristonectes parvidens* (10–13 teeth) (Carpenter, 1999; Cruickshank and Fordyce, 2002; Gasparini et al., 2003b; Sato, 2003; Kear, 2005). In SMNS 81783, the external nares are oval and located above the third to fifth maxillary tooth, just anterior to the orbit. This condition differs from the circular external nares found in *Thalassomedon haningtoni* (Carpenter, 1999), and from the position of the external nares located above the sixth and seventh maxillary teeth in *S. snowii* or above the second and third ones in *Tuarangisaurus keyesi* (Carpenter, 1999). The size variability in the maxillary dentition that incorporates teeth with an oval cross-section in SMNS 81783 contrasts with the relatively small and consistently sized dentition occurring in *A. parvidens* and *K. katiki* (Cruickshank and Fordyce, 2002; Gasparini et al., 2003b), and the rounded tooth cross sections of *E. carinognathus* (Kear, 2005) and *T. ponteixensis* (Sato, 2003). The ventral margin of the orbit in SMNS 81783 is convex and mainly formed by the jugal, in

contrast to that reported for *T. haningtoni* and *Zarafasaura oceanis*, in which the jugal forms only one-third of the ventral margin of the orbit (Carpenter, 1999; Vincent et al., 2011), or *Hydrotherosaurus alexandrae*, in which the jugal is excluded from the orbital margin (Welles, 1943) and *F. suzukii* that has a straight ventral margin of the orbit (Sato et al., 2006). The pineal foramen present in SMNS 81783 is absent in *F. suzukii*, *H. alexandrae*, *S. snowi*, *T. keyensi*, *T. ponteixensis* and *Z. oceanis* (Welles, 1943; Sato, 2003; Vincent et al., 2011). Moreover, in SMNS 81783, the pineal foramen is totally enclosed by the parietals, contra that observed in *Callawayasaurus colombiensis* where the frontal forms the anterior border of the pineal foramen (Welles, 1952). In SMNS 81783, the anterior margin of the parietal contacts the frontal at the level of the posterior margin of the orbit, differing from the situation in *A. parvidens*, in which the parietal terminates more anteriorly between the orbits (Gasparini et al., 2003b). The mandible of SMNS 81783 presents a Meckelian canal not open for most of its length contrary to the conditions in *C. colombiensis* and *T. ponteixensis* (Welles, 1962; Sato, 2003), and a high coronoid, in contrast to that observed in *E. carinognathus* (Kear, 2005). The mandibular symphysis in SMNS 81783 reaches the fourth tooth pair, unlike in *H. alexandrae* (3 pairs), *T. ponteixensis*, *F. suzukii* (2–3 pairs) and *A. parvidens* (one pair). Moreover, the mandibular symphysis represents 15% of the total skull length, contrary to the condition in *E. carinognathus* (23% of the skull length), *T. keyensi* (6%) and *Z. oceanis* (8%) (Vincent et al., 2011). The characters presented by SMNS 81783 differentiate this specimen from most of the elasmosaurid taxa, except the genus *Libonectes*, with which many similarities have been found.

8.1.5.2. Comparison with *Libonectes*

The diagnosis for *Libonectes* established by Carpenter (1997) is principally based on postcranial characters and difficult to apply for SMNS 81783, which presents only a skull and the atlas-axis complex. The only diagnostic cranial character proposed by Carpenter (1997) concerns the preorbital length/skull length ratio, but according to the author, this character has a limited taxonomic utility (Carpenter, 1997:214). The anatomical comparisons between SMNS 81783 and the other elasmosaurids allow its referal to *Libonectes*. Moreover, the phylogenetic result

obtained in this study recovers a sister group relationship with the two species of *Libonectes*, supporting the hypothesis proposed by Buchy (2005).

The comparison with the holotypes of *Libonectes morgani* and *Libonectes atlasense* reveals only a few differences between the three specimens. A pineal foramen is present in SMNS 81783 but not in *L. morgani* and *L. atlasense*. The virtual reconstruction of SMNS 81783 reveals the presence of this structure, but it appears hardly visible because of its small size (diameter = 5 mm) as well as its limited depth (4 mm). This structure is possibly not observable in *L. morgani* and *L. atlasense* because of the poor preservation of the interorbital region (see Carpenter, 1997; Buchy, 2005). Lateral to the posterior interpterygoid vacuities, the ventral surface of the pterygoid in SMNS 81783 is dorsally concave and its lateral margin is projected ventrolaterally, forming a curved prominent flange. This contrasts with the description of *L. morgani* given by Carpenter (1997), in which the pterygoids are plate-like structures (Carpenter, 1997:203). However, the illustrations of Welles (1949:pl. 3) and Druckenmiller and Russell (2008a:12, fig. 6), as well as the revised character score performed by Sachs and Kear (2015:char. 100), show that the pterygoids of *L. morgani* are dorsally concave and similar to those of SMNS 81783. The pterygoids are not visible in *L. atlasense* (Buchy, 2005). The openings situated on the pterygoids lateral to the posterior interpterygoid vacuities found in SMNS 81783 are absent in *L. morgani* and not observed in *L. atlasense*. A reasonable doubt remains concerning the real nature of these openings that could correspond to an artefact of preservation. The dorsomedian ridge found on the dorsal surface of the premaxillae in *L. morgani* (Sachs and Kear, 2015) and *L. atlasense* (Buchy, 2005:fig. 2) is not present in SMNS 81783, in which the premaxillae appear flattened on their dorsal surface. The dorsomedian ridge found in *L. morgani* was not reported in the description of Carpenter (1997), while Welles (1949:8) and Sachs and Kear (2015:696) described the prominent dorsomedian ridge on the premaxillae as a feature distinguishing *L. morgani* from other Elasmosauridea. The ventral emargination between the third premaxillary and the third maxillary teeth is concave in *L. atlasense* (Buchy, 2005) but straight in *L. morgani* (Carpenter, 1997:fig. 2) and SMNS 81783. The mandibular symphysis comprises six teeth in *L. atlasense* (Buchy, 2005) but eight in *L. morgani* (Carpenter, 1997:fig. 2) and SMNS 81783.

It appears difficult to state if SMNS 81783 is more related to *Libonectes morgani* or to *Libonectes atlasense*. Buchy (2005) proposed four diagnostic cranial characters allowing to

differentiate *L. atlasense* from *L. morgani*: (1) the ventral emargination between the third premaxillary and the third right (fifth on the left) maxillary teeth is concave; (2) the external naris is situated at the level of the fourth to fifth maxillary teeth, which are the largest teeth in the maxillary tooth row; (3) the mandibular symphysis comprises three teeth; (4) the mandibular symphysis is flat, posteroventrally oriented and extends to the anterior end of the maxilla. SMNS 81783 differs from *L. atlasense* on all these characters and is thus more similar to *L. morgani*. Based on the differential diagnosis proposed by Sachs and Kear (2015), SMNS 81783 nevertheless differs from *L. morgani*, based on two characters: the presence of a pineal foramen and the absence of a prominent dorsomedian ridge on the premaxillae. These differences might however be related to different states of preservation for the specimens of these taxa, the intraorbital region being not well preserved in *L. morgani*. Similarly a doubt remains about the prominent dorsomedian ridge on the premaxillae, the absence or presence of such a structure being possibly part of an intraspecific variability (e.g., sexual dimorphism), which is still unknown among plesiosaurians.

The relationships among the different OTUs referred to this genus remain unresolved. Based on the limited differences, we refer SMNS 81783 to *Libonectes morgani*, but the comparison between *L. morgani* and *L. atlasense* is not clear because of the lack of comparative data. The type specimen of *L. morgani* is essentially known from its cranial characters and presents 24% of missing cranial data in the phylogenetic analysis of Benson and Druckenmiller (2014). Conversely, *L. atlasense* presents 80% of missing cranial data and SMNS 81783 has an intermediate value with 50% of missing cranial data. The use of computed tomography on the type specimen of *L. atlasense* would enable to provide new information about its cranial characters, and to clarify the relationships among the specimens referred to *Libonectes*.

8.1.5.3. Paleobiogeography and Paleoecological Interpretations

The assignation of SMNS 81783, from the Turonian of Morocco, to *Libonectes morgani*, a North American taxon previously only known from the Late Cenomanian of Texas (Sachs and Kear, 2015), greatly enlarges the palaeobiogeographical distribution of this species. Some affinities between North American and North African faunas have already been noted for other Turonian vertebrate taxa, more specifically between teleostean fishes (Cavin et al., 2010), but

also for a pliosaurid specimen referred to *Brachauchenius lucasi* Williston, 1903 (Angst and Bardet, 2015).

Thanks to the particular preservation of the fossil (nodule) and the use of computed microtomography, some structures that are rarely preserved and difficult to observe, such as the pineal foramen and the stapes, could be identified in SMNS 81783. The pineal foramen is considered as lacking in many derived elasmosaurids (e.g., Wiffen and Moisley, 1986; Carpenter, 1997; Bardet et al., 1999; Sato, 2003). Its condition (small and shallow) in SMNS 81783 raises questions relative to its true or artefactual absence in advanced elasmosaurids. In addition, the absence of stapes was considered as a synapomorphy of Elasmosauridae (Carpenter, 1997) but its occurrence in the elasmosaurids *Tuarangisaurus keyesi* (O'Gorman et al., 2017) and SMNS 81783 challenges this hypothesis. According to Sato et al. (2011), it is possible that some plesiosaurians lacked an ossified stapes. However, the morphology of the thin and fragile stapes found in SMNS 81783 likely suggests that its supposed absence in most elasmosaurid specimens is possibly due to their poor state of preservation.

8.1.6. Conclusion

The use of computed microtomography provides new anatomical information of a Moroccan plesiosaurian specimen difficult to study by direct observation because of its particular mode of preservation. The digital reconstruction of SMNS 81783 confirms its position within Elasmosauridae and its assignment to *Libonectes*, as previously suggested by Buchy (2005). The specimen was referred to *Libonectes atlasense* (Buchy, 2005), but our study indicates greater similarity to the North American taxon *Libonectes morgani*. A reexamination of the holotype of *Libonectes atlasense* using computed microtomography will help to clarify the morphological disparity with *L. morgani*.

8.2. New plesiosaurian specimens (Reptilia, Plesiosauria) from the Upper Cretaceous (Turonian) of Goulmima (Southern Morocco)

8.2.1. Material and Methods

The present work examines two new plesiosaurian specimens (D1-8213 and MNHN F-GOU14, see Fig. 8.8) from the area of Goulmima in Southern Morocco (see Chapter 4 Material and Methods).

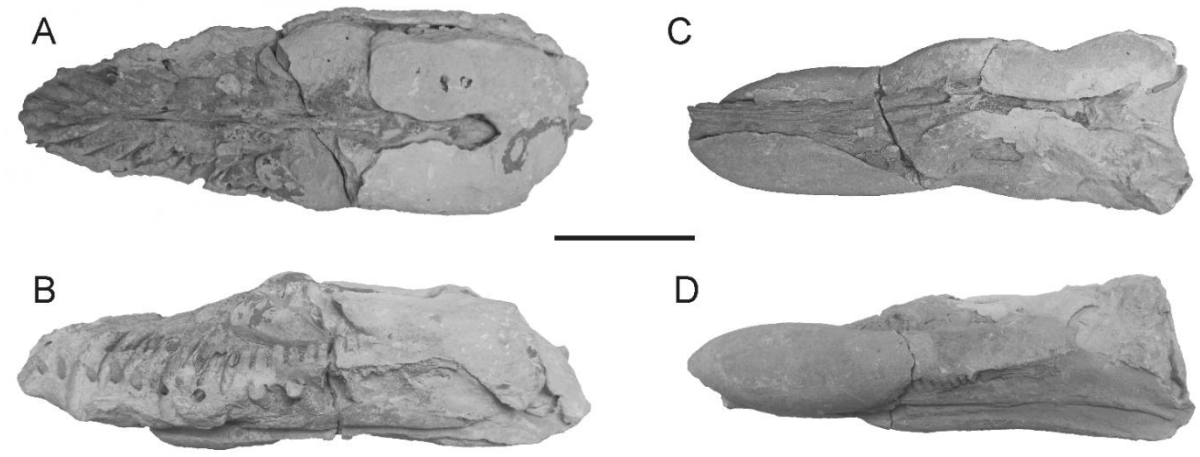

Fig. 8.8. Photographs of *Libonectes morgani* specimen D1-8213 (left) and the undetermined Polycotylidae MNHN F-GOU14 (right) from the lower Turonian of Goulmima (Morocco) in dorsal **(A, C)** and left lateral **(B, D)** views. Scale bars equal 10 cm.

The two specimens were scanned at the AST-RX platform of the MNHN (Paris) using a GEphoenix|Xray|v|tome|x L240 with a different voxel size, voltage and intensity for each piece (see Chapter 4 Material and Methods). A virtual three-dimensional reconstruction of each specimen was then performed at the Palaeontology Imaging Unit of the UMR 7207 CR2P CNRS/MNHN/UPMC using MIMICS (Materialise Interactive Medical Image Control System) Innovation Suite software (Materialise®, release 18).

8.2.2. Systematic Palaeontology

SAUROPTERYGIA Owen, 1860

Order PLESIOSAURIA de Blainville, 1835

Super Family PLESIOSAUROIDEA Welles, 1943 (sensu Ketchum and Benson, 2010)

Family ELASMOSAURIDAE Cope, 1869

Genus *LIBONECTES* Carpenter, 1997

Type species ELASMOSAURUS MORGANI Welles, 1949

Synonym—*Libonectes atlasense* Buchy, 2005 (sensu Sachs and Kear, 2017).

Holotype—SMU SMP 69120, skull and mandible, atlas-axis complex, 48 successive cervical vertebrae, fragmentary thoracic ribs, gastralia and associated gastroliths (Welles, 1949; Sachs and Kear, 2015); upper Cenomanian; Britton Formation, Eagle Ford Group, Near Cedar Hill, Dallas County, Texas, USA.

Referred specimens—SMNK-PAL 3978, articulated skull and postcranial skeleton (Buchy, 2005; Sachs and Kear, 2017); SMNS 81783, skull, mandible and atlas-axis complex (Allemand et al., 2017a); and D1-8213, skull and mandible, as well as the atlas-axis complex (see below). Early Turonian (Upper Cretaceous) Unit T2a (Ettachfini and Andreu, 2004; Kennedy et al., 2008) of the Cenomanian-Turonian limestone bar, north of Goulmima, Er-Rachidia Province, Southern Morocco.

8.2.2.1. Description and comparison of D1-8213

General preservation

The skull of D1-8213 is incomplete, several elements are not preserved (e.g., jugal, squamosal, quadrate) and others are only partially preserved (e.g., premaxillae, coronoid) because of dissolution. The braincase is well preserved and the bones are in their natural arrangement. The mandible is in occlusion with the cranium, but only the dentary, the coronoid and a small part of the prearticular are preserved. The atlas-axis complex is also preserved posterior to the basioccipital. The original cranial length is about 350 mm from the tip of the premaxilla to the occipital condyle. The beak index (ratio of the distance from the tip of the snout to the anterior

orbital margin, Welles, 1952) represents 45% of the skull length, and is thus similar to the values found in most Elasmosauridae (close to 40%), whereas it is higher (close to 55%) in Polycotylidae (Buchy et al., 2005).

Skull

Premaxillae—The dorsal surface of the premaxillae is completely dissolved (Fig. 8.9A). Its posterior extension is not preserved and its contacts with the parietal, frontal and prefrontal are not visible. A small part of the maxillae is maybe preserved anterolaterally but it is not possible to differentiate it from the premaxillae. On the virtual reconstruction of the skull, only partial casts of the anterior teeth alveoli are visible (Fig. 8.9A). However, nine teeth on each side were counted anteriorly to the orbit on the premaxillae-maxillae part visible on the surface of the nodule. In ventral view of the virtual reconstruction, the palatal surface of the premaxillae exhibits an alveolar channel connecting the replacement teeth alveoli (Fig. 8.9B).

Maxillae—Only a small portion of the left maxilla is preserved (Fig. 8.9A). Four teeth alveoli are visible, however, no more details are visible.

Frontal—A small isolated piece of the frontal is preserved, and forms ventrally the lateral wall of the olfactory canal (Fig. 8.9A, C).

Parietal—The parietal crest is not preserved (Fig. 8.9A, C). The lateral extension of the parietal is more developed on its anterior and posterior parts, giving an hourglass shape to the bone in dorsal view (Fig. 8.9A). The anterior end of the parietal is dissolved. The posterior end of the parietal overlaps the supraoccipital.

Vomer— The anteriomost part of the vomer is missing (Fig. 8.9B), and the occurrence of a vomeronasal foramen cannot be evidenced. The vomer constitutes the medial margins of the internal nares (Fig. 8.9A, B). At the level and posterior to the internal nares, its dorsal surface forms a gutter with its lateral margin that is dorsally directed (Fig. 8.9A). Its posterior extension and its sutural relationships with the pterygoid are undetermined. The median suture between the two vomers is visible in ventral view (Fig. 8.9B), forming a low ridge at the level of the internal nares.

Palatine—Only a small part of the right palatine is preserved. Its dorsal surface appears slightly concave (Fig. 8.9A, B), as in *Libonectes morgani* (Sachs and Kear, 2017). It forms a

large, subrectangular sheet of bone as in *Libonectes morgani* (Carpenter, 1997). Posteriorly, at the conjuncture of the palatine, ectopterygoid and pterygoid, the bone is partially dissolved and it is not possible to observe the suborbital fenestra.

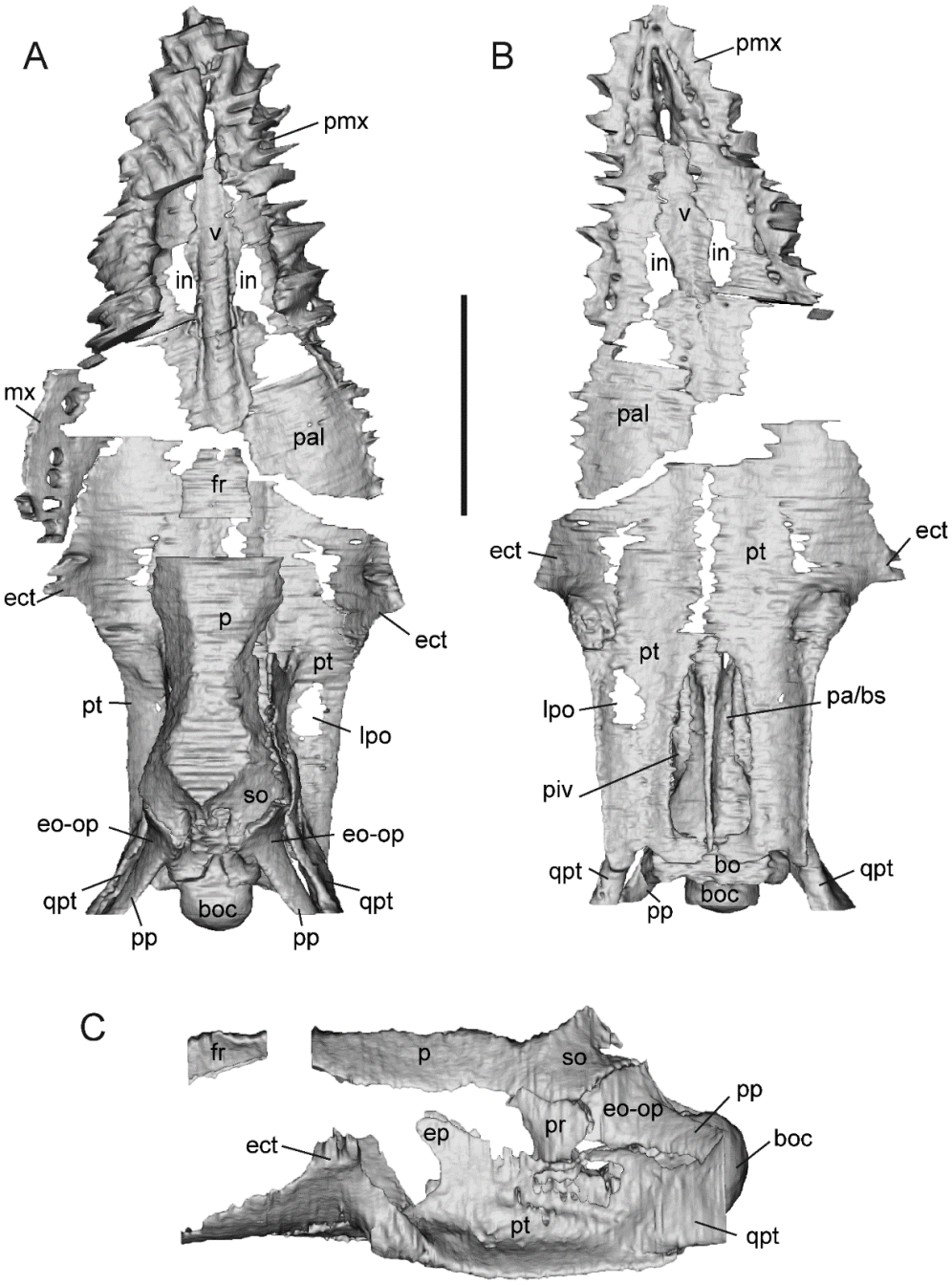

Fig. 8.9. Digital reconstruction of the skull of the *Libonectes morgani* specimen D1-8213 from the lower Turonian of Goulmima (Morocco) in dorsal **(A)**, ventral **(B)**, and left lateral **(C)** views. **Abbreviations**: **bo**, basioccipital; **boc**, occipital condyle; **ect**, ectopterygoid; **ep**, epipterygoid; **eo-op**, exoccipital-opisthotic; **fr**, frontal; **in**, internal nares; **lpo**, lateral pterygoid opening; **mx**, maxilla; **p**, parietal; **pa/bs**, parabasisphenoid; **pal**, palatine; **piv**, posterior interpterygoid vacuities; **pmx**, premaxillae; **pp**, paraoccipital process; **pr**, prootic; **pt**, pterygoid; **qpt**, quadrate ramus of the pterygoid; **so**, supraoccipital; **v**, vomer. Scale bar equals 10 cm.

Pterygoid— The anterior extension of the pterygoids is partially preserved and its contact with the vomer is undetermined (Fig. 8.9A, B). Anterior to the posterior interpterygoid vacuity, the median suture of the pterygoids is damaged but it seems that they contacted each other along the midline (Fig. 8.9B), as in the Jurassic microcleidids, *Microcleidus* (= *Occitanosaurus) tournemirensis* and *Microcleidus homalospondylus* (Benson et al., 2012; Brown et al., 2013), as well as in the Cretaceous elasmosaurids (Bardet et al., 1999; Großmann, 2007). Lateral to the narrow and elongated posterior interpterygoid vacuity, the ventral surface of the pterygoid is slightly concave and its lateral margin projects latero-ventrally (Fig. 8.9B), forming a curved flange less prominent than that found in SMNS 81783 (Allemand et al., 2017a). Posterior to the epipterygoid, the pterygoid forms a dorsal blade extending along the sides of the basisphenoid and basioccipital (Fig. 8.9C), as in *Libonectes morgani* (Carpenter, 1997). A large opening, leaving only a thin rod of bone at the level of the contact between the prootic and the exoccipital-opisthotics, perforates this dorsal blade. On the right pterygoid and ventrally, an anteroposteriorly extended opening is visible and situated lateral to the anterior part of the posterior interpterygoid vacuity (Fig. 8.9B). This large opening is not found on the left pterygoid, and only a small pit occurs at the same level. The opening and the pit are exactly mirrored on the left and right pterygoids as in *Zarafasaura oceanis* (Vincent et al., 2011). Posterior to the posterior interpterygoid vacuity, the pterygoids are partially dissolved and cover the basioccipital ventrally (Fig. 8.9B); however, it seems that there is no medial contact between them, as in SMNS 81783 (Allemand et al., 2017a), but differing from the condition in *Libonectes morgani* (Carpenter, 1997; Sachs and Kear, 2015).

Epipterygoid—Lateral to the parabasisphenoid, a vertical process of the pterygoid, the epipterygoid, rises dorsally (Fig. 8.9C). The epipterygoid seems to extend dorsally from the anterior dorsal edge of the vertical pterygoid process, as in *Libonectes morgani* (Carpenter, 1997).

Ectopterygoid—The ectopterygoid is a C-shaped bone located posterolaterally to the palatines and lateral to the anterior end of the posterior interpterygoid vacuity (Fig. 8.9A, B, C). The suture between the pterygoid and ectopterygoid is located posteriorly to the small bulge formed by the ectopterygoid on the right side. The same bulge is visible on the left side but the suture between the pterygoid and ectopterygoid is not visible. On both sides, the symmetrical dissolution seems to follow the suture line between the pterygoid and ectopterygoid.

Braincase

The occiput is formed by the supraoccipital, the fused exoccipital-opisthotics, the basioccipital, the prootic, and the parabasisphenoid. The elements are in their natural position. The foramen magnum is taller than wide and is constricted at the level of the supraoccipital-exoccipital-opisthotic suture (Fig. 8.10C).

Parabasisphenoid—The parasphenoid and the basisphenoid form the anterior floor of the braincase and contact the basioccipital posteriorly. There is no trace of a suture between the dorsal part of the parasphenoid and the ventral part of the basisphenoid. Anteriorly, the clinoid process of the parasphenoid is visible on the palatal surface but not preserved on its entire length (Fig. 8.10A, B, D). The parasphenoid carries a prominent ventral keel that divides the posterior interpterygoid vacuity, as in Cretaceous Elasmosauridae and the Jurassic forms *Microcleidus* (= *Occitanosaurus) tournemirensis* and *Microcleidus homalospondylus* (Bardet et al., 1999; Brown et al., 2013). The ventral keel that is wider anteriorly than posteriorly, continues slightly posterior to the posterior margin of the interpterygoid vacuity (Fig. 8.9B) and tapers along the ventral surface of the basioccipital (Fig. 8.9B). In dorsal view, just posterior to the clinoid process, the sella turcica opens anteriorly and houses the pituitary gland (Fig. 8.10A, D). The sella turcica in D1-8213 is longer than that of *L. morgani* SMNS 81783 specimen (Allemand et al., 2017a). The sella turcica posteriorly terminates with the dorsum sellae (Fig. 4A, D). A prominent pila antotica extends anterodorsally from this region, and a pila metoptica is present

more anteriorly (Fig. 8.10A, B, C), as in *Thalassiodracon hawkinsii* (Benson et al., 2011) and SMNS 81783 (Allemand et al., 2017a). In lateral view and ventrally to the pila antotica, a process extends from the lateral surface of the basisphenoid (Fig. 8.10B) and forms a facet that contacts the pterygoid (basipterygoid process). In anterior view, the pair of internal carotid foramina penetrates the posterior wall of the sella turcica (Fig. 8.10D), as in *Libonectes morgani* holotype (Carpenter, 1997: Fig. 5) but differently from in the elasmosaurid specimen SGU 251/1 (Zverkov et al., 2017) and in *Alexandronectes zealandiensis*, in which only a single foramen on the floor of the sella turcica is observed (Otero et al., 2016; Zverkov et al., 2017). On the lateral surface of the parabasisphenoid, the large carotid foramina exit ventrally to the pila antotica and just posterior to the basipterygoid process of the basisphenoid (Fig. 8.10B). The dorsolateral side of the pituitary fossa bears bilateral foramina. These are visible in anterior view (Fig. 8.10D) and carried the abducens nerves (Carpenter, 1997).

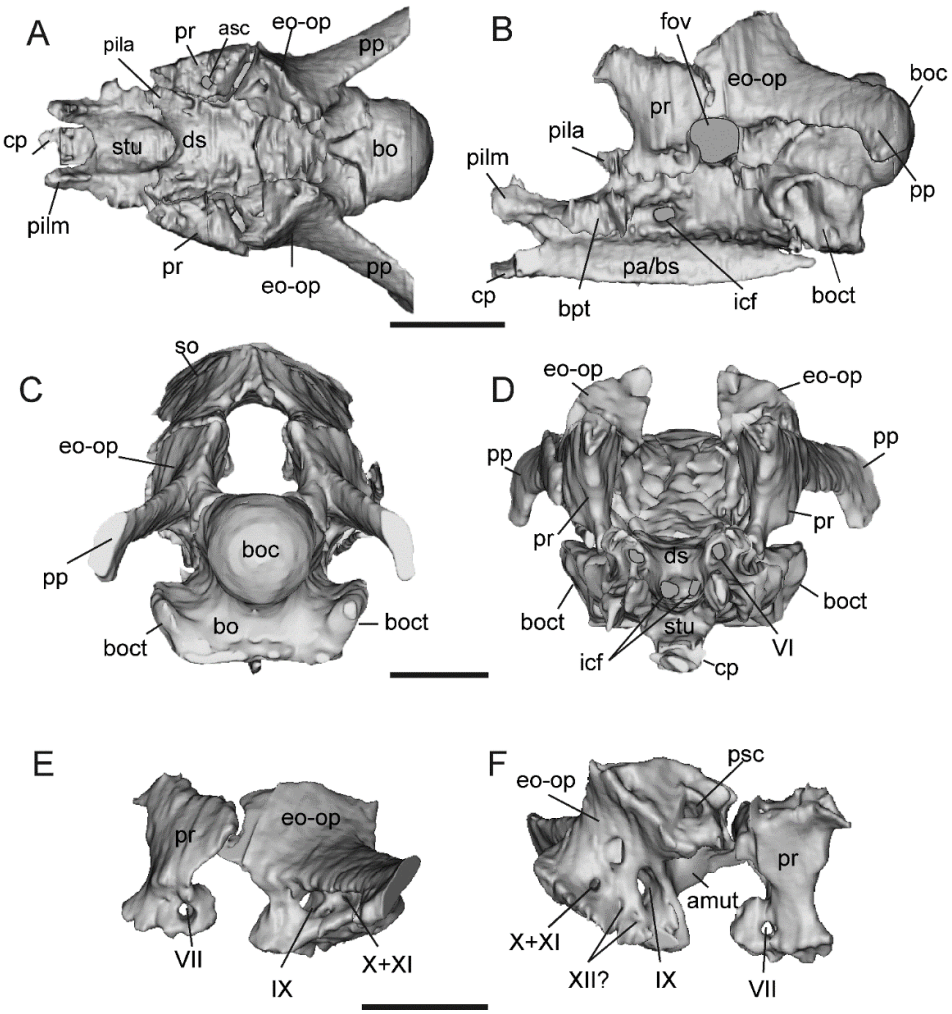

Fig. 8.10. Digital reconstruction of the braincase of *Libonectes morgani* specimen D1-8213 from the lower Turonian of Goulmima (Morocco) in dorsal **(A)**, left lateral **(B)**, posterior **(C)** and anterior **(D)** views and of the left exoccipital-opisthotic and prootic in lateral **(E)** and medial **(F)** views. **Abbreviations**: **amut**, chamber for ampulla and utriculus; **asc**, anterior semicircular canal; **bo**, basioccipital; **boc**, occipital condyle; **boct**, basioccipital tuber; **bpt**, basipterygoid process of the basisphenoid; **cp**, clinoid process; **ds**, dorsum sellae; **eo-op**, exoccipital-opisthotic; **fov**, fenestra ovalis; **icf**, internal carotid foramen; **pa/bs**, parabasisphenoid; **pila**, pila antotica; **pilm**, pila metoptica; **pp**, paraoccipital process; **pr**, prootic; **psc**, posterior semicircular canal; **so**, supraoccipital; **stu**, sella turcica; **VI**, foramen for the abducens nerve; **VII**, foramen for the facial cranial nerve; **IX**, foramen for glossopharyngeal nerve; **X+XI**, foramen for the vagus and accessory nerves; **XII?**, foramina for the hypoglossal nerves. Scale bars equal 2 cm.

Basioccipital—The basioccipital is a stout element. Two large facets for the exoccipital-opisthotics occupy its dorsal surface (otooccipital facets: Evans, 2012). The basioccipital contacts anteriorly the parabasisphenoid and has a pair of distinct basioccipital processes that contact the pterygoid at the posterior edge of the braincase. These processes are projected ventrolaterally and show two ovoid facets for contact with the pterygoids (Fig. 8.10B, D). Contrary to what is reported among pliosaurids and cryptoclidids in which the exoccipital-opisthotic forms part of the occipital condyle (e.g., Andrews, 1913; Brown, 1993), the basioccipital appears here to form the entire rounded occipital condyle (Fig. 8.10C). A groove surrounds the occipital condyle forming a distinct neck ventrally and laterally as in elasmosaurids (Brown, 1993), but differing from the condition in *Thalassiodracon hawkinsii* (Benson et al., 2011b), in which the occipital condyle is a shallow dome with no groove between the condyle and the body of the basioccipital.

Exoccipital-opisthotics—Both exoccipital-opisthotics are well preserved and are fused, as in most plesiosaurians (e.g. Sato et al., 2011; Sachs et al., 2015). On the anterior surface, a deep chamber for the ampulla and utriculus is visible (Fig. 8.10F). Dorsal and lateral to these structures, the preserved opening corresponds to the caudal part of the posterior semicircular canals. Four foramina pierce the medial surface of the exoccipital-opisthotics adjacent to its ventral surface. The more anterior foramen is larger and might have served for

the glossopharyngeal nerve (IX) and possibly also for the perilymphatic duct (Sachs et al., 2015). The smaller one may be considered as a foramen for the vagus and accessory nerves (X+XI) as well as the jugular vein (Sachs et al., 2015). Both exit at the base of the paraoccipital process, as in *Libonectes morgani* (Sachs et al., 2015). The smallest foramina, located close to one another, served for branches of the hypoglossal nerve (XII). Anteriorly, the exoccipital-opisthotic forms the dorsal and posterior margins of the fenestra ovalis. This character differs from the hypothesis proposed by Maisch (1998) for *Muraenosaurus leedsii* in which the opisthotics did not contribute to the fenestra ovalis. The straight paroccipital process has an anteroposteriorly oval cross-section and is ventrally inclined. Its distal end is more expanded than in SMNS 81783 (Allemand et al., 2017a) but does not form a spatulate terminus as in pliosaurids and basal plesiosaurians (e.g., Smith and Dyke, 2008; Benson et al., 2011b).

Prootic—The prootic occurs anterior to the exoccipital-opisthotic, and forms the anterior margin of the keyhole shaped fenestra ovalis seen in lateral view (Fig. 8.10B). The prootic is a rectangular element, containing the anterior part of the vestibule of the inner ear dorsomedially. The facet for the supraoccipital faces posterodorsally and is pierced by an opening for the anterior semicircular canal (Fig. 8.10A). A foramen at the posterior part of the prootic base may represent the exit for cranial nerve VII (Carpenter, 1997).

Supraoccipital—The supraoccipital is a small arch-shaped element forming the dorsal roof of the braincase (Fig. 8.10C) and ventral to the parietal, enclosing the dorsal and dorsolateral margins of the keyhole-shaped foramen magnum. The supraoccipital contacts the parietal dorsally; the suture between the two bones is visible ventrally through a difference of thickness. The ventrolateral portions of the supraoccipital are expanded anteroposteriorly to accommodate part of the semicircular canals, as in *Muraenosaurus leedsii* (Maisch, 1998) and *Thalassiodracon hawkinsii* (Benson et al., 2011b). It contacts the prootic anteroventrally and the exoccipital-opisthotic posteroventrally. In posterior view, the supraoccipital presents a median process projecting ventrally into the midline of the foramen magnum, similarly to in *Libonectes morgani* (Welles, 1949; Carpenter, 1997) and *Thalassiodracon hawkinsii* (Storrs and Taylors, 1996), giving a heart shape to the dorsal part of the foramen magnum. According to Carpenter (1997), this projection served for the nuchal ligament.

Mandible

Dentary—In dorsal view, the left and right dentaries unite at their anterior ends at the level of the fourth alveoli teeth (Fig. 8.11A), as in *Libonectes morgani* (Carpenter, 1997; Allemand et al., 2017a), to form a narrow, gracile and slightly elongated mandibular symphysis. The dentaries seem to be the only component of the symphysis. The left dentary bears 18 teeth but is incomplete (Fig. 8.11A). Medially to these teeth, the alveoli for the replacement teeth are visible (Fig. 8.11A).

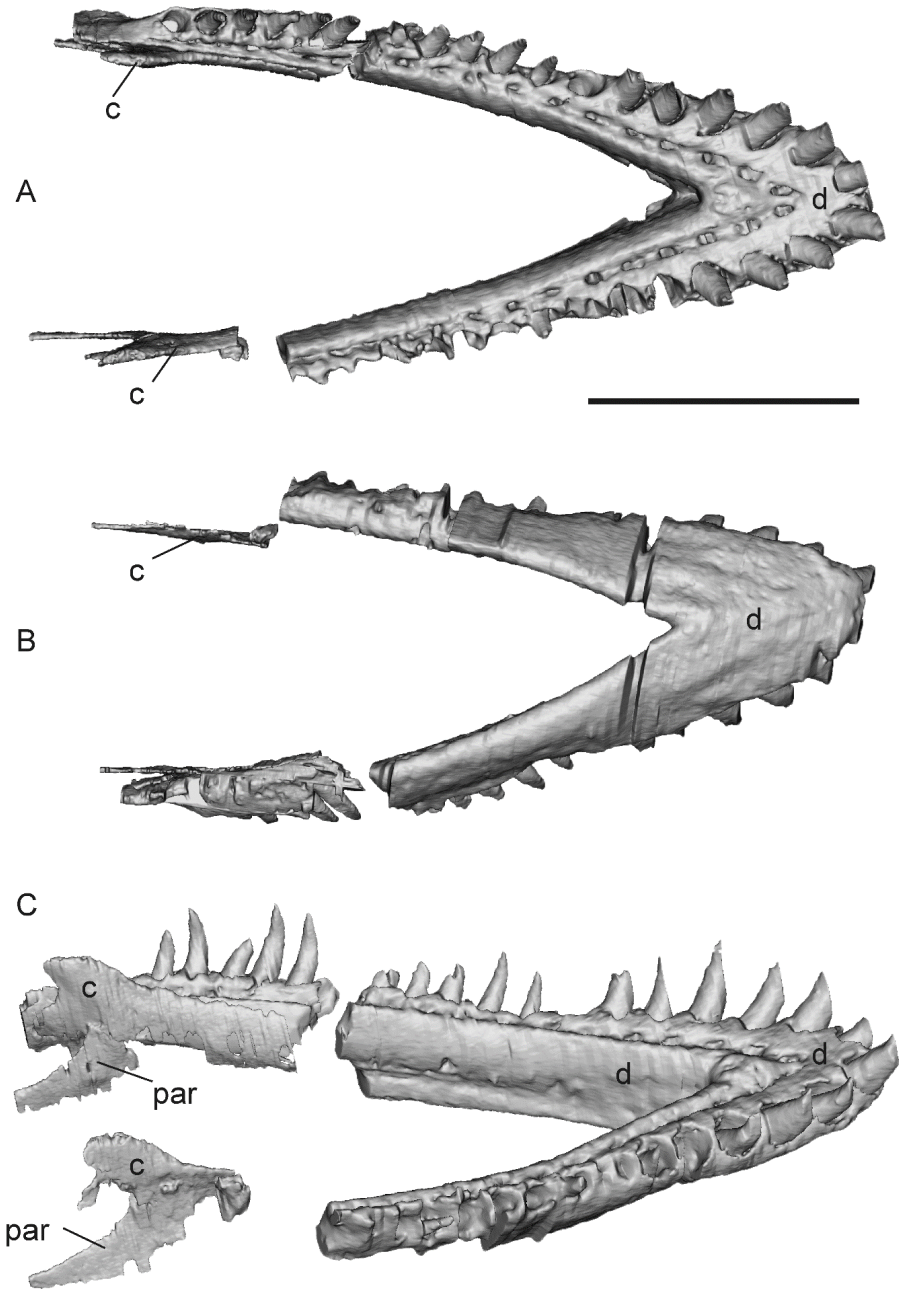

Fig. 8.11. Digital reconstruction of the mandible of *Libonectes morgani* specimen D1-8213 from the lower Turonian of Goulmima (Morocco) in dorsal **(A)**, ventral **(B)** and right ventrolateral **(C)** views. **Abbreviations**: **c**, coronoid; **d**, dentary; **par**, prearticular. Scale bars equal 10 cm.

Coronoid—The coronoid (preserved on both sides) is pressed against the dentary, on the medial surface of the mandible (Fig. 8.11). It is a roughly thin triangular bone with a large dorsal inflation (Fig. 5C), comparable to that described in *Zarafasaura oceanis* (Vincent et al., 2011), and *Libonectes morgani* (Sachs and Kear, 2015; Allemand et al., 2017a). It contacts the dentary anteriorly but its extension is unknown.

Prearticular—A small part of the prearticular is preserved on both sides (Fig. 8.11C). It contacts the coronoid dorsally but its anterior and posterior ends are not preserved.

Teeth

The teeth are slightly flattened and oval in cross-section as in *Callawayasaurus colombiensis*, *Terminonatator ponteixensis*, *Styxosaurus snowii* and *Libonectes morgani* (Williston, 1890; Welles, 1962; Sato, 2003; Sachs and Kear, 2015; Allemand et al., 2017a). Preservation precludes any observation of an eventual ornamentation. The maxillary teeth are not reconstructed but appear to diminish in size anteroposteriorly, contrary to the condition in *Aristonectes* specimens (Gasparini et al., 2003b; Otero et al., 2014) and *Kaiwhekea katiki* (Cruickshank and Fordyce, 2002). Similarly, the teeth on the dentary are larger on the symphysis than posteriorly.

Atlas-axis complex

The conjoined atlas and axis form the atlas-axis complex with no suture visible between the two elements (Fig. 8.12). The atlas-axis complex is cylindrical and distinctly longer than high as illustrated in a number of other Elasmosauridae (e.g., Welles, 1943; Sachs, 2005; Kubo et al., 2012; Otero et al. 2014; Sachs and Kear, 2015). The atlantal cotyle is circular and deeply

concave (Fig. 8.12A). The cotylar rim is surrounded by a thin edge and its dorsal midline is incised by a tapered notch. Ventrally, the atlas intercentrum bears a prominent hypophyseal ridge (Fig. 8.12C, D) similar to that reported in *Elasmosaurus platyurus* (Sachs, 2005), *Eromangasaurus australis* (Kear, 2005), *Albertonectes vanderveldei* (Kubo et al., 2012), *Libonectes morgani* (Sachs and Kear, 2015), *Thalassomedon haningtoni* (Sachs et al., 2016a) and *Vegasaurus molyi* (O'Gorman et al., 2015). The anteroventral extremity of the hypapophyseal ridge is flattened and elliptical in outline (Fig. 8.12D), as recorded in *Albertonectes vanderveldei* (Kubo et al., 2012) and *Libonectes morgani* (Sachs and Kear, 2015). Posteriorly, the hypophyseal ridge forms a narrow crest merging with the articular face of the axis centrum. The atlas neural arch is narrow on its basis, flared dorsally and posteriorly oriented. The axis neural arch is wider on its ventral part than on its dorsal one (Fig. 8.12B). Its exact height is unknown, and the contact between the atlas and axis neural arch is perforated by a large foramen (Fig. 8.12C), typical to the elasmosaurid condition (Sachs and Kear, 2017). The atlas ribs, situated at the approximate mid-section of the atlas-axis complex, are separated from the axis ribs (contrary to what is observed on the SMNS 81783 specimen of *L. morgani*, see Allemand et al., 2017a) but in contact with their posterior ends (Fig. 8.12C). The rib complex is projected laterally posteroventrally (about 45° from the horizontal), beyond the border of the cotyle of the axis centrum. A thickened rim (Fig. 8.12B) surrounds the slightly concave and rounded articular face of the axis.

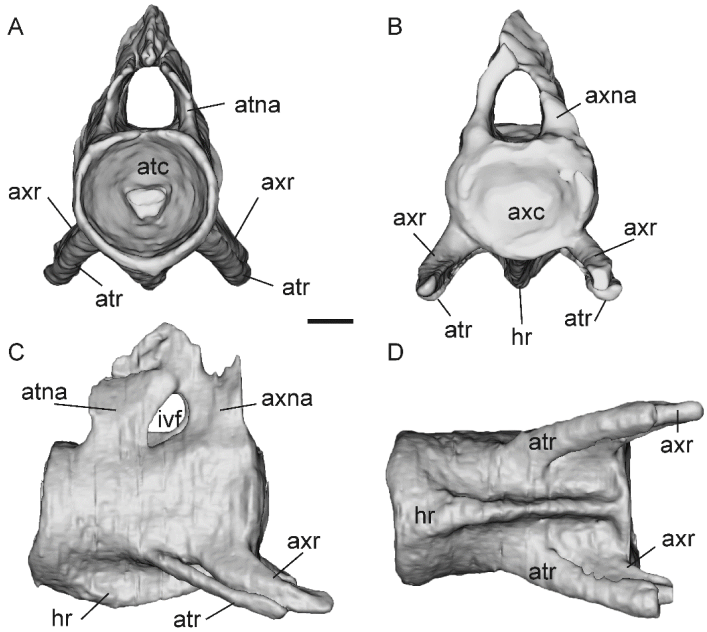

Fig. 8.12. Digital reconstruction of the atlas-axis complex of *Libonectes morgani*, specimen D1-8213 from the lower Turonian of Goulmima (Morocco) in anterior **(A)**, posterior **(B)**, left lateral **(C)** and ventral **(D)** views. **Abbreviations**: **atc**, atlas centrum; **atna**, atlas neural arch; **atr**, atlas rib; **axc**, axis centrum, **axna**, axis neural arch; **axr**, axis rib; **ivf**, intervertebral foramen; **hr**, hypophyseal ridge. Scale bar equals 10mm.

8.2.2.2. Systematic attribution of D1-8213

D1-8213 presents two characters allowing to assign it to the Elasmosauridae: a high coronoid eminence on the mandible (Vincent et al., 2011: character 39); a keyhole-shaped foramen magnum (Druckenmiller and Russell, 2008b: character 67). In addition, D1-8213 displays features that are variably found in other elasmosaurids (O'Keefe, 2001; Kear, 2005; Kubo et al., 2012): a keel on the ventral surface of the parabasisphenoid, a ventral keel (hypophysis) on the atlas-axis complex, an occipital condyle formed exclusively by the basioccipital (shared with polycotylids), an absence of anterior interpterygoid vacuity, and a maxillary tooth count similar to most of the elasmosaurids (except aristonectines).

Only a few comparisons are possible between D1-8213 and other Elasmosauridae since the braincase is poorly known among this clade despite several relatively complete and well-studied specimens. Detailed descriptions and/or illustrations of the braincase are only available for a limited number of taxa: *Libonectes morgani*, *Tuarangisaurus keyesi*, *Alexandronectes zealandiensis*, (Carpenter, 1997; Sachs et al., 2015; Otero et al., 2016; Allemand et al., 2017a) and some undetermined Elasmosauridae (Sachs et al., 2015; Zverkov et al., 2017). In D1-8213, the ectopterygoid is directed laterally and the parabasisphenoid covers only one third of the basioccipital body contrary to the condition of *T. keyesi*, in which the ectopterygoid is directed posteriorly and the parabasisphenoid covers all the ventral surface of the basioccipital body (Otero et al., 2016). Lateral to the posterior interpterygoid vacuity, the ventral surface of the pterygoid is slightly concave in D1-8213 and differs from the horizontal projection found in *A. zealandiensis* (Otero et al., 2016). The mandible of D1-8213 bears a slightly elongated symphysis reaching the fourth tooth pair, as in *L. morgani*, *Callawayasaurus columbiensis*, and *Zarafasaura oceanis* but unlike in other Cretaceous taxa that bear less teeth: *Hydrotherosaurus*

alexandrae (3 pairs), *Terminonatator ponteixensis* and *Futabasaurus suzukii* (2–3 pairs) (Carpenter, 1997; Gasparini et al., 2003; Sato, 2003; Sato et al., 2006; Vincent et al., 2011). The mandibular symphysis of D1-8213 represents 19% of the skull length, which is close to the conditions in *Eromangasaurus australis* (23% of skull length), *L. morgani* and *Plesiosaurus dolichodeirus* (18%), *H. alexandrae* (16%) and *T. ponteixensis* (15%) (Sato, 2003; Kear, 2005; Vincent et al., 2011) but different from in *Z. oceanis* (approximately 8% of the total skull length) and *T. keyesi* (6%) (Kear, 2005; Vincent et al., 2011).

D1-8213 differs from all Elasmosauridae for which the braincase is known except *L. morgani*. The comparison shows many similarities, especially with specimen SMNS 81783 that comes from the same deposit of Goulmima (Allemand et al., 2017a), and allows to assign D1-8213 to *L. morgani*. The unique difference between the two specimens concerns the absence of stapes in D1-8213. In SMNS 81783, two rods located lateroventrally to the exoccipital-opisthotics and oriented anteroposteriorly, were interpreted as stapes (Allemand et al., 2017a). Similarly, in D1-8213 two rod-like bones were also identified in the same position as those in SMNS 81783. However, they appear to be part of a dorsal blade of the pterygoids. It seems that the dissolution of the dorsal wall creates a hole on its surface, leaving only a thin rod-like bone at the level of the contact between the prootic and the exoccipital. Thus, due to an advanced dissolution, the stapes found in SMNS 81783 could be a misinterpretation of the rest of the dorsal wall formed by the pterygoid, laterally to the posterior interpterygoid vacuity.

SAUROPTERYGIA Owen, 1860

Order PLESIOSAURIA de Blainville, 1835

Super Family PLESIOSAUROIDEA Welles, 1943 (sensu Ketchum and Benson, 2010)

Family POLYCOTYLIDAE Williston, 1908

Polycotylidae indet.

Material—MNHN F-GOU14, skull and mandible. Early Turonian (Upper Cretaceous) Unit T2a (Ettachfini and Andreu, 2004) of the Cenomanian-Turonian limestone bar, north of Goulmima, Er-Rachidia Province, Southern Morocco.

8.2.2.3. Description and comparison of MNHN F-GOU14

General Preservation

The skull seems to be slightly compressed laterally. In dorsal aspect, it is narrowly triangular in outline. Its snout is similarly thin and elongated to that of Polycotylidae and Leptocleididae (e.g., Bardet et al., 2003a; Buchy et al., 2005; Ronander, 2007; Druckenmiller and Russell, 2008a), but differs from the ovoid skull shape found in the Elasmosauridae, in which the preorbital segment is broad and short (e.g., Carpenter, 1997). The anterior tip of the snout is not preserved and it is difficult to evaluate the length of the missing part.

Skull

Premaxillae— The anterior extension of the premaxillae is not preserved. It is difficult to assess the length of the missing part. The dorsal surface of the premaxillae is completely dissolved (Fig. 8.13), making it impossible to determine the presence of a dorsomedian ridge. The posterior extension of the premaxillae is badly preserved and the sutures with the maxillae, frontal, and prefrontal are not visible. On the ventral surface of the premaxillae/maxillae, six alveoli are present on the right side and five on the left one (Fig. 8.13B). Anterior alveoli are broadly spaced (8 mm) with respect to posterior alveoli (separated by 6 mm) (Fig. 8.13B).

Maxillae—The sutural relationships of the maxillae with the premaxillae are undetermined. The relationships between the maxilla, the prefrontal and the frontal are not visible. The maxilla extends posteriorly as a narrow, tapering edge bordered dorsally by the jugal (Fig. 8.13C). It is unclear whether the maxilla participates to the orbital margin. Ventrally, the posterior part of the maxilla bears seven alveoli (Fig. 8.13B).

Frontal—In the interorbital region, the badly preserved frontal forms the prominent lateral wall of the olfactory sulcus (Fig. 8.13C).

Parietal—The parietal is poorly preserved and crushed ventrally. Its contacts with the frontal and prefrontal are not clear because of the bad preservation of this region. A large ovoid pineal foramen is visible (Fig. 8.13A). The state of preservation does not allow determining the presence of a parietal table just posterior to the pineal foramen. Posteriorly, the parietal contacts the supraoccipital but it not possible to determine the level of potential recovery.

Jugal—The jugal, bounded ventrally along its entire length by the maxilla, forms the concave posterolateral margin of the orbit (Fig. 8.13C). Its posterior extension, as well as its contact with the squamosal and prefrontal are not preserved.

Vomer—Only the anterior portion of the vomer is preserved. However, its sutural relationships with the premaxillae, maxillae and pterygoid are undetermined. On the right side, a small alveolus is visible and may correspond to the anterior margin of the primary alveolus (Fig. 8.13B), found also in *Nichollsaura borealis* Druckenmiller and Russell, 2008a anteriorly to the internal nares (Druckenmiller and Russell, 2008a). The dorsal margins of the dorsal surface of the vomers project dorsally for most of their length.

Palatine—Only a small part of the right palatine is preserved. Posteriorly, at the conjuncture of the palatine, ectopterygoid and pterygoid, the bone is dissolved and it is not possible to observe the suborbital fenestra.

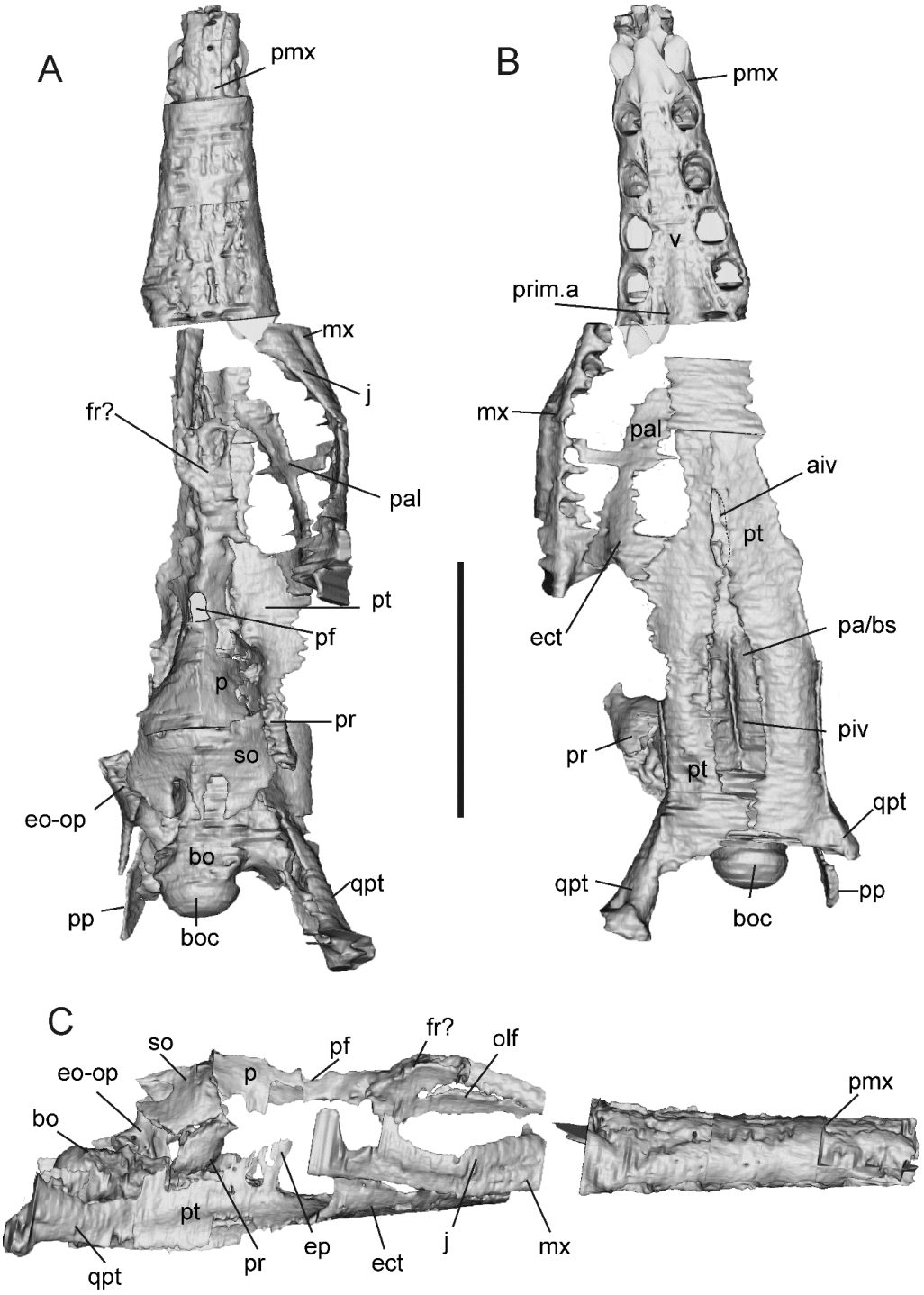
A
pmx
mx
j
fr?
pal
pt
pf
p
pr
so
eo-op
bo
qpt
pp
boc
B
pmx
v
prim.a
mx
pal
aiv
pt
ect
pa/bs
piv
pr
pt
qpt
qpt
pp
boc
C
so
pf
fr?
olf
eo-op
p
pmx
bo
pt
ep
j
mx
pr
ect
qpt

Fig. 8.13. Digital reconstruction of the skull of the Polycotylidae indet. MNHN F-GOU14 from the Turonian of Goulmima (Morocco) in dorsal **(A)**, ventral **(B)**, and right lateral **(C)** views. **Abbreviations**: **aiv**, anterior interpterygoid vacuity; **bo**, basioccipital; **boc**, occipital condyle; **ect**, ectopterygoid; **ep**, epipterygoid; **eo-op**, exoccipital-opisthotic; **fr?**, frontal; **j**, jugal; **mx**, maxilla; **olf**, olfactory wall; **p**, parietal; **pa/bs**, parabasisphenoid; **pal**, palatine; **pf**, pineal foramen; **piv**, posterior interpterygoid vacuities; **pmx**, premaxillae; **pp**, paraoccipital process; **pr**, prootic; **prim.a**, primary alveolus; **pt**, pterygoid; **qpt**, quadrate ramus of the pterygoid; **so**, supraoccipital; **v**, vomer. Scale bar equals 10 cm.

Pterygoid—The sutural relationships between the pterygoid, the vomer and the palatine are undetermined (Fig. 8.13B). In front of the posterior interpterygoid vacuity, the pterygoids appeared united together (Fig. 8.13B). However, this seems to be due to the medial displacement of the left pterygoid. Indeed, transversal slides in this region show a thickening that seems to be the result of the stack between the palatine and pterygoid. However, due to the poor contrast, it is not possible to distinguish the two elements. This could imply the presence of an anterior interpterygoid vacuity just anterior of the clinoid process (Fig. 8.13B); however, it is difficult to observe because of its obstruction by the pterygoid displacement. The presence of the anterior interpterygoid vacuity and its posteriorly displaced position would be similar to the condition seen in polycotylids (e.g., Williston, 1908; Druckenmiller, 2002) and differs from elasmosaurids which lack such trait (e.g., Carpenter, 1997). It also differs from leptocleidids that possess an anterior interpterygoid vacuity anteriorly shifted compared to that of polycotylids (e.g., Druckenmiller and Russell, 2008a). Lateral to the triangular and elongated openings of the posterior interpterygoid vacuity (Fig. 8.13B), the ventral surface of the pterygoid is concave, a feature regarded as a synapomorphy for polycotylids (O'Keefe, 2004) but also found in the leptocleidids *Umoonasaurus demoscyllus* Kear et al., 2006 and *Nichollsaura borealis* (Kear and Barrett, 2011), and in the elasmosaurid *Libonectes morgani* (Allemand et al., 2017a; Sachs and Kear, 2017). At the level of the posterior interpterygoid vacuity, the lateral margin of the pterygoid in MNHN F-GOU14 appears straight, as in the polycotilids *Trinacromerum bentonianum* Cragin, 1888 and *Edgarosaurus muddi* Druckenmiller, 2002 (Williston, 1908; Druckenmiller, 2002). In addition, posterior to the

posterior interpterygoid vacuity, the pterygoids are partially dissolved; however, a midline contact between both pterygoids, covering the entire body of the basioccipital is possible (Fig. 8.13B).

Epipterygoid—In lateral view, the right epipterygoid is better preserved than the left one, and rises dorsally, having a triangular outline (Fig. 8.13C). Its ventral part contacts the parabasisphenoid laterally to the sella turcica.

Ectopterygoid—The ectopterygoid is a triangular bone in ventral view, located posterolateral to the palatine and laterally to the pterygoid. Its lateral end is dorsally recurved. The incomplete right ectopterygoid is in its original anatomical position (Fig. 8.13B, C), whereas the left one is not preserved. The sutures between the right ectopterygoid, pterygoid and palatine are not visible.

Braincase

Parabasisphenoid— Anteriorly, the clinoid process of the parabasisphenoid is visible on the palatal surface but not really differentiable from the pterygoids (Fig. 8.14A, B). Its entire length is unknown. The ventral surface of the parabasisphenoid forms a median keel along its entire length (Fig. 8.13B), as in *Nichollsaura borealis*, *Edgarosaurus muddi* and *Libonectes morgani* (Carpenter, 1997; Druckenmiller, 2002; Druckenmiller and Russell, 2008a) but contrary to in *Leptocleidus capensis* Andrews, 1911 (Cruickshank, 1997). However, the parabasisphenoid keel does not contact the basioccipital body in MNHN F-GOU14 unlike in elasmosaurids (e.g., Carpenter, 1997; Kear, 2005; Allemand et al., 2017a). In dorsal view, just posterior to the clinoid process, the sella turcica is open anteriorly (Fig. 8.13A). The sella turcica posteriorly terminates with the dorsum sellae (Fig. 8.13A, B). A prominent pila antotica extends anterodorsally from this region, and a pila metoptica is present more anteriorly (Fig. 8.13A, B). The posterior wall of the anteriorly opened sella turcica is pierced by a pair of internal carotid foramens (Fig. 8.13A, B), which arise posteriorly through the lateral surface of the parabasisphenoid. The two foramina for nerve VI are located on the dorsolateral side of the pituitary fossa.

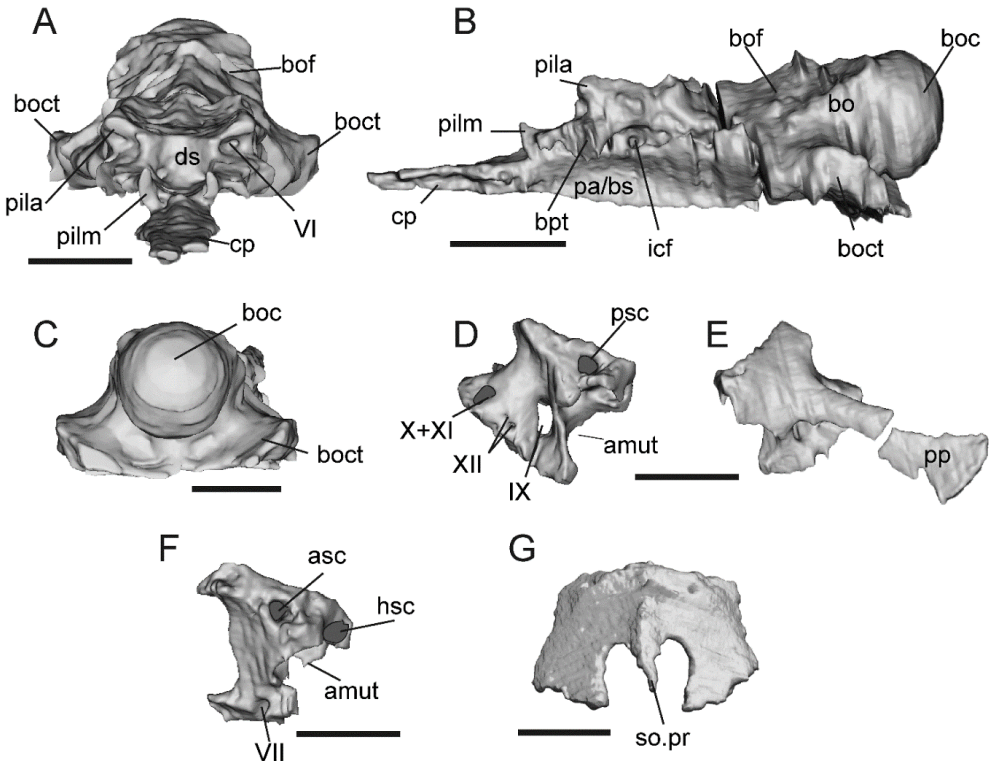

Fig. 813. Digital reconstruction of the parabasisphenoid and basioccipital of the Polycotylidae indet. MNHN F-GOU14 from the Turonian of Goulmima (Morocco) in anterior **(A)**, left lateral **(B)** views; basioccipital in posterior view **(C)**; left exoccipital-opisthotic in medial **(D)** and antero-lateral **(E)** views; prootic in medial view **(F)** and supraoccipital in dorsal view **(G)**. **Abbreviations**: **amut**, chamber for ampulla and utriculus; **asc**, anterior semicircular canal; **bo**, basioccipital; **boc**, occipital condyle; **boct**, basioccipital tuber; **bof**, basioccipital facet for the exoccipital-opisthotic; **bpt**, basipterygoid process of the basisphenoid; **cp**, clinoid process; **ds**, dorsum sellae; **hsc**, horizontal semicircular canal; **icf**, internal carotid foramen; **pa/bs**, parabasisphenoid; **pila**, pila antotica; **pilm**, pila metoptica; **pp**, paraoccipital process; **psc**, posterior semicircular canal; **so.pr**, median process of the supraoccipital; **VI**, foramen for the abducens nerve; **VII**, foramen for the facial cranial nerve; **IX**, foramen for glossopharyngeal nerve; **X+XI**, foramen for the vagus and accessory nerves; **XII**, foramina for the hypoglossal nerves. Scale bars equal 2 cm.

Basioccipital—The basioccipital forms the ventral margin of the foramen magnum and bears large facets, inclined laterally for the exoccipital-opisthotic along most of its dorsolateral surface (Fig. 8.13A, B). A dorsomedian ridge is visible between the two facets (Fig. 8.13A). The basioccipital forms the entire rounded occipital condyle, contrary to what is reported among pliosaurids and cryptoclidids in which the exoccipital-opisthotic forms part of the occipital condyle (e.g., Andrews, 1913; Brown, 1993). The occipital condyle lacks a notochordal pit (Fig. 8.13C). A slight constriction forms a neck surrounding the occipital condyle but it is less pronounced than in elasmosaurids (Carpenter, 1997; Allemand et al., 2017a). The basioccipital tubers in MNHN F-GOU14 are oriented more ventrally (Fig. 8.13C) than in elasmosaurids (Allemand et al., 2017a).

Exoccipital-opisthotics—Only the left exoccipital-opisthotic is preserved in MNHN F-GOU14 (Fig. 8.13D, E). A deep chamber for the ampulla and utriculus is visible on the anterior surface and two openings, corresponding to the caudal parts of the posterior and horizontal semicircular canals, respectively, are located dorsally and laterally to the chamber. Four foramina pierce the medial surface of the exoccipital-opisthotics. The large more anterior foramen (Fig. 8.13D) might have served for the glossopharyngeal nerve (IX) and possibly for the perilymphatic duct (Sachs et al., 2015). The smallest foramina (Fig. 8.13D), located ventrally and close to one another, served for branches of the hypoglossal nerve (XII). The more posterior foramen (Fig. 8.13D) corresponds to the vagus and accessory nerves (X+XI) as well as the jugular vein (Sachs et al., 2015). The paraoccipital process of MNHN F-GOU14 is ventrally inclined (Fig. 8.13E) as in most xenopsarians (e.g., Carpenter, 1997; Druckenmiller, 2002; Allemand et al., 2017a). Its distal end is expanded and thin, forming a spatulate terminus, similar to the condition observed in the leptocleidids and polycotylids (e.g., Smith and Dyke, 2008; Benson et al., 2011), as well as in the elasmosaurids *Callawayasaurus colombiensis* and *Alexandronectes zealandiensis* (Welles, 1962; Otero et al., 2016).

Prootic—Only the right prootic is preserved in MNHN F-GOU14, and it is not in its anatomic position. The prootic contains the anterior part of the vestibule of the inner ear (Fig. 8.13F), with the ventrolateral edge forming the rim of the fenestra ovalis. The two foramen on the supraoccipital and exoccipital-opithotic facets represent the exits for the anterior and horizontal semicircular canals, respectively (Fig. 8.13F). The foramen at the posterior part of

the prootic base represents the exit for the cranial nerve VII (Carpenter, 1997). The dorsal edge of the process is wide and smoothly notched for the trigeminal nerve (V).

Supraoccipital—The supraoccipital in MNHN F-GOU14 encloses the dorsal and dorsolateral margins of the keyhole-shaped foramen magnum and contacts the parietal dorsally, the prootic anteroventrally, and the exoccipital-opisthotic posteroventrally. The supraoccipital in MNHN F-GOU14 has a midline process (Fig. 8.13G) projecting ventrally into the foramen magnum, giving to the supraoccipital an M-shape in dorsal view, as in D1-8213, *Nichollsaura borealis* (Druckenmiller and Russell, 2008a), *Thalassiodracon hawkinsi* (Benson et al., 2011), *Dolichorhynchops osborni* (Carpenter, 1997), *Muraenosaurus leedsi* (Maisch, 1998) and *Plesiopterys wildi* (O'Keefe, 2004).

Mandible

The anterior part of the mandible is missing. The right mandibular ramus is straight along its entire length (Fig. 8.14), its posterior end as well as the posterior part of the left ramus are not preserved. No visible sutures differentiate the components of the mandible. There is no longitudinal groove occurring anteriorly on the lateral surface of the dentary (Fig. 8.14C), unlike in *Nichollsaura* (Druckenmiller and Russell, 2008a). In dorsal view, the left and right dentaries unite to form a long mandibular symphysis (about 10 cm, see Fig. 8.14A), which is straight in lateral view, with no keel along its ventral surface. The alveoli are more spaced and larger on the symphyseal part of the mandible, than posteriorly (Fig. 8.14A). The mandibular symphysis bears at least five teeth.

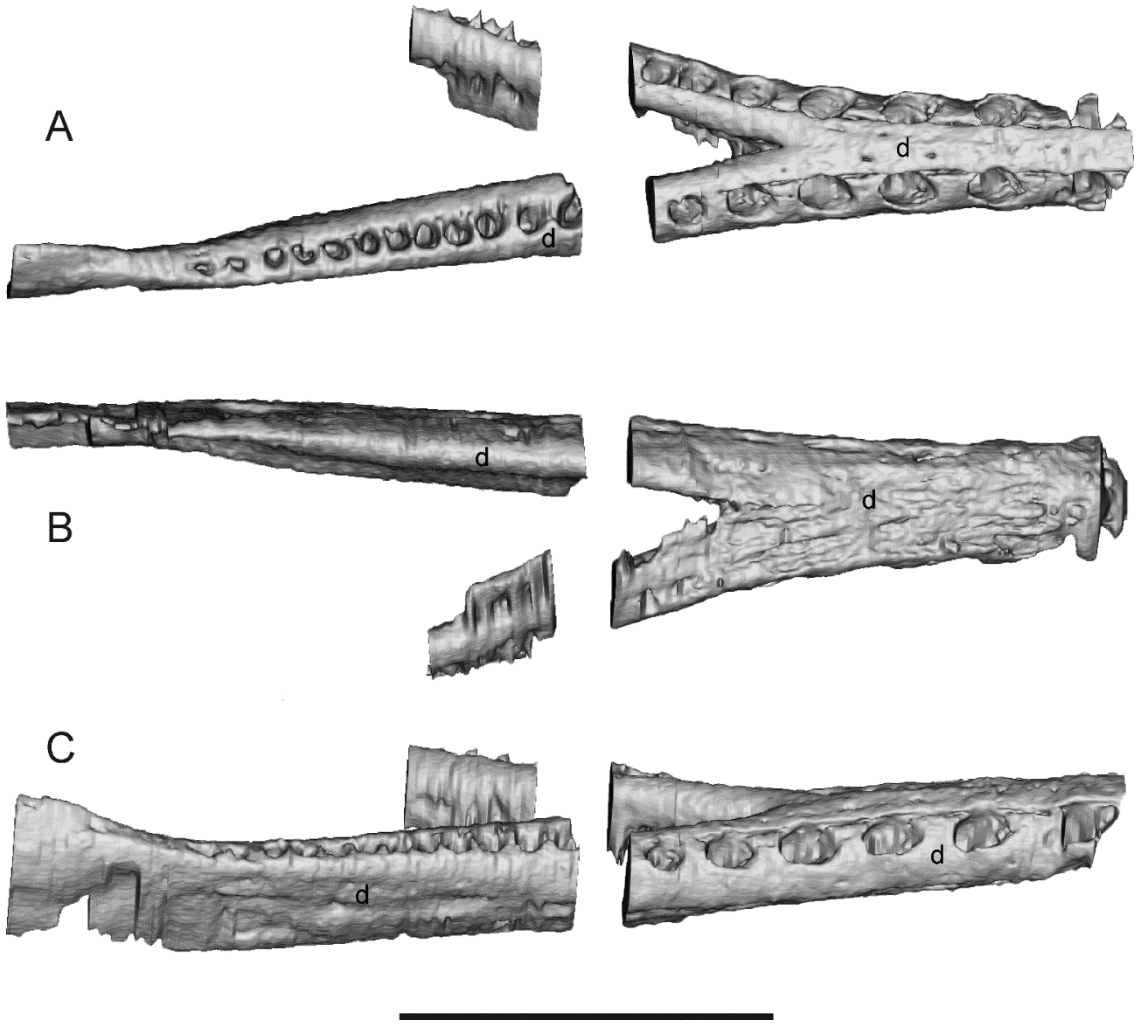

Fig 8.14. Digital reconstruction of the dentary of the Polycotylidae indet. MNHN F-GOU14 from the Turonian of Goulmima (Morocco) in dorsal (A), ventral (B) and right ventrolateral (C) views. Scale bars equal 10 cm.

8.2.2.4. Systematic attribution of MNHN F-GOU14

Among Cretaceous plesiosaurians in general, the thin and elongated rostrum of MNHN F-GOU14 allows to distinguish it from the elasmosaurids and from the Jurassic plesiosaurids, in which the snout is wider and relatively shorter (Carpenter, 1997; Bardet et al., 1999; Gasparini et al., 2003; Sato, 2003; Benson et al., 2011, 2013; Vincent et al., 2011; Brown et al., 2013).

Among taxa presenting a similar long snout, MNHN F-GOU14 differs from the pliosaurids in the absence of a prominent ridge on the ventral surface of the pterygoid. This ridge follows the perimeter of the subtemporal fenestra anteromedially, then extends posteromedially towards the midline at the base of the posterior ramus of the pterygoid. The posterior contact of these ridges forms the posterior wall of a midline fossa at the posterior end of the interpterygoid vacuity (Ketchum and Benson, 2011). This structure is present in all pliosaurids (e.g., Williston, 1903; Andrews, 1913; Taylor and Cruickshank, 1993; Albright et al., 2007; Schumacher et al., 2013) and is considered a synapomorphy of the clade (Druckenmiller and Russell, 2008b; Ketchum and Benson, 2010).

Among the Leptocleidia, clade that unites leptocleidids and polycotylids (Ketchum and Druckenmiller, 2010), the skull of MNHN F-GOU14 measures 350 mm and differs from the lengths found in the leptocleidids *Nichollsaura borealis* (285 mm, Druckenmiller and Russell, 2008a), *Leptocleidus superstes* Andrews, 1922 (242.8 mm but incomplete, Kear and Barrett, 2011), *Umoonasaurus demoscyllus* (222 mm, Kear et al., 2006) and *Brancasaurus brancai* (237 mm, Sachs et al., 2016b). In addition, the anterior interpterygoid vacuity in MNHN F-GOU14, located just anterior to the clinoid process of the parabasisphenoid, differs from the condition observed in leptocleidids, in which the anterior interpterygoid vacuity is located more anteriorly on the palate, and contacts the vomer (Druckenmiller and Russell, 2008a; Kear and Barrett, 2011). Among polycotylids, the straight lateral margins of the pterygoids at the level of the posterior interpterygoid vacuity in MNHN F-GOU14 contrasts with the curved lateral margins (kidney-shaped) found in *Dolichorynchops* specimens (Druckenmiller, 2002; O'Keefe, 2004; Sato et al., 2011). The straight lateral margin of the pterygoids in MNHN F-GOU14 is very similar to those of basal polycotylids such as *Edgarosaurus muddi* and *Trinacromerum bentonianum* (Williston, 1908; Druckenmiller, 2002). However, MNHN F-GOU14 presents a pineal foramen and thus differs from *T. bentonianum* that does not (Morgan, 2016). Comparisons among the polycotylids known from Goulmima, *Thililua longicollis* Bardet et al., 2003a, *Manemergus anguirostris* Buchy et al., 2005 and the undetermined specimen PMO 201.956 (Bardet et al., 2003a; Buchy et al., 2005; Ronander, 2007) are difficult because of the lack of overlapping preserved elements. Only the posterior portion of the posterior interpterygoid vacuity is preserved in *M. anguirostris.* According to Morgan (2016), the pterygoids in *M. anguirostris* resemble the condition seen in *E. muddi*, rather than in

Dolychorhynchops, with straight and narrow pterygoids, and hence are similar to those of MNHN F-GOU14. However, in the absence of comparative data for the palate of *T. longicollis* and for the undetermined specimen PMO 201.956, we decided to assign MNHN F-GOU14 to an undetermined Polycotylidae, waiting to the re-evaluation of Moroccan polycotylids.

The description of the new polycotylid specimen MNHN F-GOU14 emphasizes the importance to have access and to consider the braincase in order to identify plesiosaurian taxa and to confirm their affinities. Indeed, *Thililua longicollis* was first assumed to be a polycotylid (Bardet et al., 2003a; O'Keefe, 2008) but this affiliation is controversial (O'Keefe 2001; Druckenmiller and Russell 2008a; Ketchum and Benson 2010; Kear and Barrett 2011) and the results obtained by Ketchum and Benson (2010) reported *T. longicollis* as a leptocleidid.

8.2.3. Discussion

8.2.3.1. Diagnostic features and paleobiological implications

According to Sato et al. (2011), it is usually difficult in plesiosaurians to determine whether a particular feature of the braincase is diagnostic to a species or shared within a higher taxonomic rank because of the difficulties to access this region. Here, the description of two plesiosaurian specimens provides additional knowledge about their braincases. We considered their variability and, as in the study performed by Sato et al. (2011), to focus on their potential phylogenetic signal and possible functional meaning.

Vincent et al. (2011) considered the openings located on the ventral surface of the pterygoids of *Zarafasaura oceanis* as a possible autapomorphy. Their presence in D1-8213 and SMNS 81783 (Allemand et al., 2017a) suggests that these openings are not specific to *Z. oceanis* but also found in *Libonectes morgani* and could be a synapomorphy of both taxa or a feature that could change during the elasmosaurid ontogeny. However, a doubt remains about the possible taphonomic reason to these openings. Indeed, the difference in size observed between each side in D1-8213, could indicate that this structure corresponds to a delicate zone of the pterygoids, more affected by the dissolution.

The absence of a stapes in many plesiosaurians has often been attributed to postmortem loss, primarily due to taphonomic causes (Druckenmiller and Russell, 2008a). However, this

structure has been described in *Rhomaleosaurus zetlandicus* Seeley, 1874 (Taylor, 1992), *Thalassiodracon hawkinsii* (Storrs and Taylor, 1996), *Plesiosaurus dolichodeirus* (Storrs, 1997), *Microcleidus homalospondylus* (Brown et al., 2013), *Alexandronectes zealandiensis* (Otero et al., 2016) and *Tuarangisaurus keyesi* (O'Gorman et al., 2017). Here, the stapes are missing in both specimens. In addition, the reconstruction of D1-8213 reveals that the stapes observed in SMNS 81783 (Allemand et al., 2017a) is a misinterpretation and corresponds rather to the rest of the dorsal wall formed by the pterygoid. Although the stapes are absent in *Libonectes morgani*, their description in several plesiosaurian taxa contradict the Taylor's hypothesis (1992) about the non-tympanic nature of the plesiosaurian ear. However, as the dorsal wall of the pterygoid may prevent the stapes from direct communication between the outer ear and the fenestra ovalis (Druckenmiller and Russell, 2008a), especially if the stapes are attached to the quadrate as in *Rhomaleosaurus zetlandicus* and *Thalassiodracon hawkinsii* (Taylor, 1992; Storrs and Taylor, 1996), it thus questions the position of the stapes and the hearing mechanisms associated to them. The exact method of sound transmission to the inner ear in plesiosaurians is unclear and the range of variation in the morphology of the ear region (Sato et al., 2011) warns against an easy generalization on the morphology and function of the structure.

Sato et al. (2011) noted variation in the longitudinal length of the sella turcica relative to the rest of the braincase in all plesiosaurians and suggested that a short sella turcica would be a derived condition in polycotylids, cryptoclidids and elasmosaurids. In Triassic sauropterygians, the sella turcica constitutes 25% of the braincase floor, 20% in the lower Jurassic plesiosaurian specimen NHMUK 39514 and 36% in the pliosauroid *Thalassiodracon hawkinsii* (Zverkov et al., 2017). Although its absolute size is not equal in the elasmosaurids SMNS 81783 (14mm) and D1-8213 (18mm), the sella turcica occupies about 25% of the braincase floor in both specimens of *Libonectes morgani*. In addition, the sella turcica in the undetermined polycotylid MNHN F-GOU14 represents 20% of the braincase floor. These proportions are similar to those reported by Zverkov et al. (2017, see supplementary data) for several elasmosaurids, polycotylids and cryptoclidids. However, contrary to the hypothesis of Sato et al. (2011), these values indicate a great variability in the proportions of the sella turcica, even within the same family, and no general evolutional trend can be noticed about the size of the sella turcica in sauropterygians. Thus, scoring the length of the sella turcica as character

calls for caution because of its variability among plesiosaurian taxa. To avoid misinterpretation, the examination of additional taxa is required to better constrain its range of variation.

8.2.3.2. Palaeobiogeographical conclusions

Goulmima represents the richest plesiosaurian site known from Africa with a high taxonomic diversity. As far as plesiosaurians are concerned, these deposits have already yielded specimens referred to Elasmosauridae, Polycotylidae and Pliosauridae (Angst and Bardet, 2015).

Here the description of a new specimen of *Libonectes morgani*, a species previously known from the Late Cenomanian of North-America (Carpenter, 1997) and recently reported in Goulmima (Sachs and Kear, 2017; Allemand et al., 2017a), reinforces the idea of a trans-Atlantic faunal connectivity, already revealed by the coeval occurrence of the pliosaurid *Brachauchenius lucasis* (Angst and Bardet, 2015) and teleostean fishes (the araripichthyid *Araripichthys corytophorus* and the pachyrhizodontid *Goulmimichthys arambourgi*, see Cavin et al., 2010), between Goulmima and the Western Interior Seaway of North America (as discussed by Sachs and Kear, 2017). In addition, the distribution of *Libonectes morgani* agrees that elasmosaurids were able to exploit open marine habitats, through different modes of dispersion (i.e., seasonal migration), similarly to pliosauroids (Kear, 2004).

8.2.4. Conclusion

The plesiosaurian braincase is a part of the skull poorly known due to either poor preservation and/or insufficient preparation. Here, the use of computed microtomography provides new anatomical information about the braincase and the palate of two Moroccan plesiosaurian specimens difficult to study by direct observation because of their particular mode of preservation. This contribution emphasizes the importance to have access and consider these regions in order to identify plesiosaurian taxa, particularly in Moroccan polycotylids, for which this part of the skull is still unknown.

Chapter 9

Endocranial anatomy of plesiosaurian specimens (Reptilia, Plesiosauria) from the Late Cretaceous (Turonian) of Goulmima (Southern Morocco)

The current understanding of the plesiosaurian paleoneurology is poor. Partial endocasts were described and illustrated only for *Brancasaurus brancai* (Edinger, 1921; see Hopson, 1979) and *Libonectes morgani* (Carpenter, 1997) (Fig. 9.1), and the inner ear morphology for *Muraenosaurus leedsii* (Evans, 1999); however, no inference about their sensorial abilities were provided.

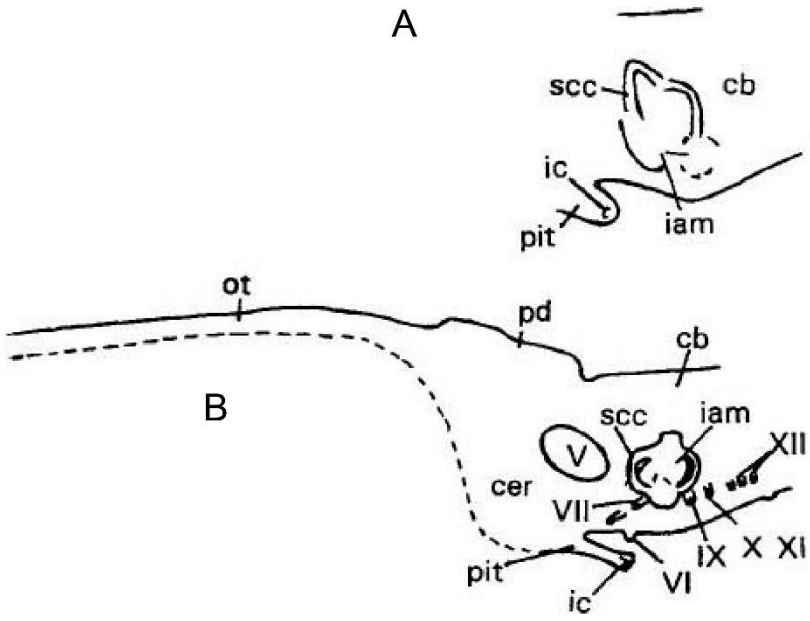

Fig. 9. 1. Endocasts of *Brancasaurus brancai* (A) and *Libonectes morgani* SMUMP 69120 (B) in lateral view (from Carpenter, 1997). **Abbreviations**: **cb**, cerebellum; **cer**, cerebral hemispheres; **iam**, internal auditory meatus; **ic**, internal carotid; **ot**, olfactory tracts; **pd**, pineal organ; **pit**, pituitary bulb; **scc**, semicircular canal; **V**, trigeminal nerve; **VI**, abducens nerve; **VII**, facial nerve; **IX**, glossopharyngeal nerve; **X-XI**, vagus and accessory nerves; **XII**, hypoglossal nerves.

In this chapter, the endocranial anatomy of three plesiosaurian specimens has been reconstructed thanks to computed tomography in order to provide new anatomical information about this region poorly known within plesiosaurians. Such reconstructions provide the opportunity to discuss about the possible difference of sensorial capabilities between the two

plesiosaurians bauplans and about the link between the shape of the endocast regions and the biology of these organisms.

9.1. Material and Methods

The two specimens SMNS 81783 and D1-8213 were referred to *Libonectes morgani* (Allemand et al., 2017; Allemand et al., in press) and the third one, MNHN F-GOU14, was referred to as an undetermined Polycotylidae (Allemand et al., in press) (Table 9.1).

Taxon	Collection reference	Voxel size (in µm)	Voltage (in kV)	Intensity (in µA)
Libonectes morgani	SMNS 81783	134	230	500
	D1-8213	115	240	400
Polycotylidae indet.	MNHN F-GOU14	93.4	220	400

Table 9.1. Scan parameters for the plesiosaurian specimens analyzed in this chapter.

All specimens were scanned at the AST-RX platform of the MNHN (Paris) (see Chapter 4, Material and Methods). A virtual three-dimensional reconstruction of endocasts, cranial nerves and inner ears was then performed at the Palaeontology Imaging Unit of the CR2P UMR 7207 CNRS/MNHN/UPMC using the MIMICS (Materialise Interactive Medical Image Control System) Innovation Suite software (Materialise®, release 18). The isolation of the endocranial cavity was performed thanks to the difference of contrast between the bones, which appear with darker grayscale values, and the matrix.

9.2. Description

An almost complete cranial endocast for D1-8213 was reconstructed, together with the cranial nerves and the inner ear (Fig. 9.2A). The olfactory bulbs located at the anteriormost part of the endocast and the ventral extent of the brain cast, anterior to the pituitary bulb, were not reconstructed due the absence of bony limit. The dorsal surface of the brain cast in SMNS 81783 was reconstructed from the olfactory bulbs to the cerebellum; however, the ventral part anterior to the pituitary bulb, as well as the inner ears, are missing (Fig. 9.2B). The brain cast of MNHN F-GOU14 is the less complete and the more crushed one (Fig. 9.2C). Only its dorsal surface could be partially reconstructed; and both the anteriormost and posteriormost parts, as well as the inner ears, are missing.

The posterior part of the endocast is surrounded dorsally by the supraoccipital, laterally by the prootics (anteriorly) and the exoccipital-opisthotic (posteriorly), and ventrally by the basioccipital and parabasisphenoid. Anterior to the prootic and ventral to the parietal, the absence of bones in this region prevent the delimitation of the endocast (Fig. 9.2). Thus, in this region, the ventral extension of the endocast was unknown and not reconstructed in order to avoid over-interpretation.

The endocranial pattern found in the three plesiosaurian specimens is similar. Although endocasts are incomplete, proportions of the skull occupied by this structure seem to be similar for the three specimens (50%). Endocasts are elongated and mediolaterally narrow. The three specimens exhibit a slight ventral flexure in lateral view at the level of the contact between the olfactory tracts and the cerebrum (Fig. 9.2A, B, C). The flexure found in the *Libonectes morgani* specimens examined here (D1-8213 and SMNS 81783) is less pronounced than the flexure illustrated in another specimen of *L. morgani* (SMUSMP 69120) by Carpenter (1997) (see Fig. 9.1B).

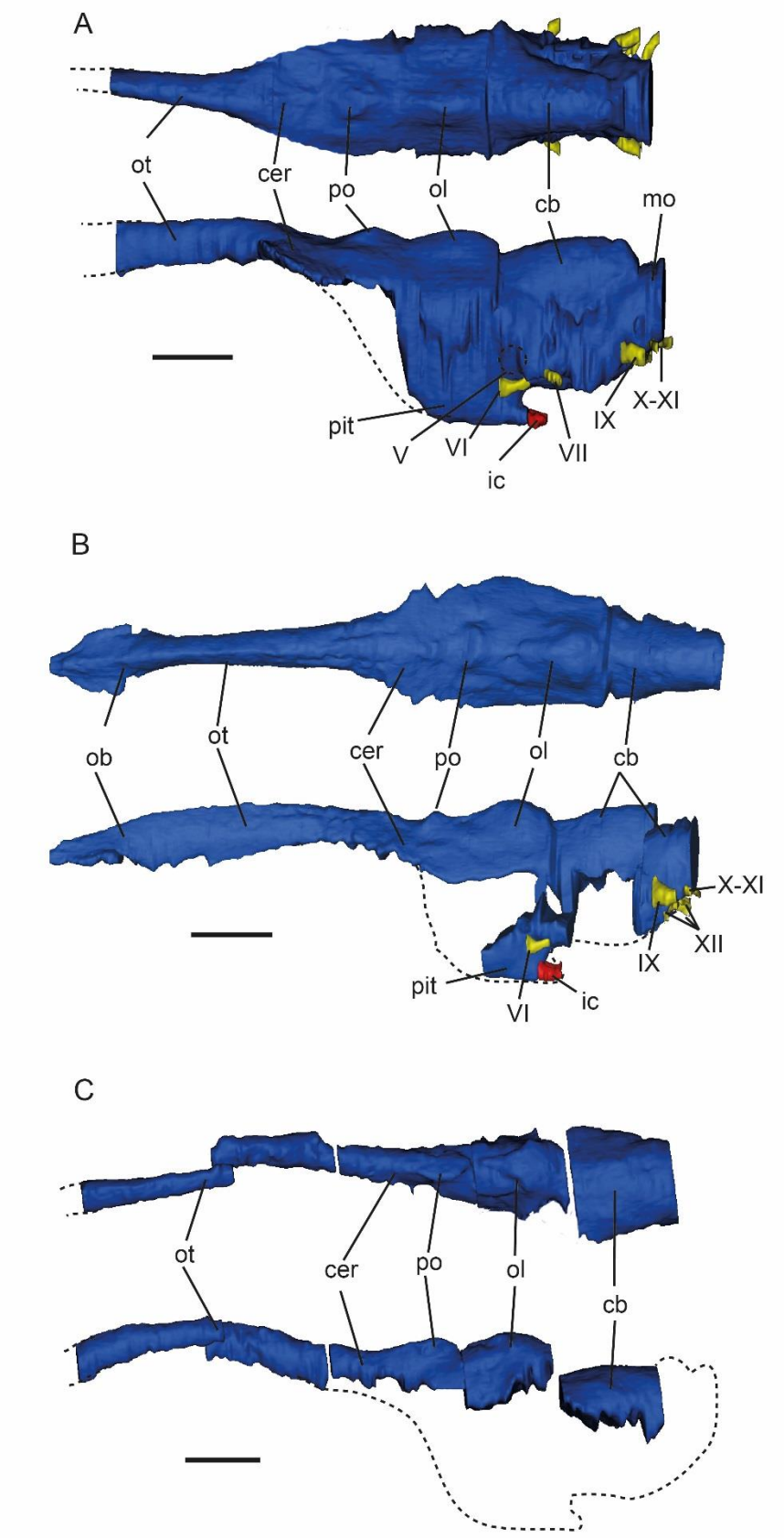
A
ot
cer
po
ol
cb
mo
pit
V
VI
ic
VII
IX
X-XI
B
ob
ot
cer
po
ol
cb
X-XI
XII
IX
pit
VI
ic
C
ot
cer
po
ol
cb

Fig 9.2. Virtual plesiosaurian endocasts of the *Libonectes morgani* specimens D1-8213 **(A)** and SMNS 81783 **(B)**; and the undetermined Polycotylidae MNHN F-GOU14 **(C)**, both Early Turonian, Goulmima, Morocco, in dorsal (up) and left lateral (down) views. **Abbreviations**: **cb**, cerebellum; **cer**, cerebral hemispheres; **ic**, internal carotid; **mo**, *medulla oblongata*; **ob**, olfactory bulbs; **ol**, optic lobes; **ot**, olfactory tracts; **po**, pineal organ; **pit**, pituitary bulb; **V**, trigeminal nerve; **VI**, abducens nerve; **VII**, facial nerve; **IX**, glossopharyngeal nerve; **X-XI**, vagus and accessory nerves; **XII**, hypoglossal nerves. Scale bars equal 20 mm. The dotted-lines indicate the missing parts.

9.2.1. Endocast

The digital reconstructions performed for the three plesiosaurian specimens allow to discern the different structures composing their brain (Butler and Hodos, 2005). The most anterior part of the brain cast corresponds to the olfactory bulbs. They have been reconstructed only in SMNS 81783 (Fig. 9.2B), in which the ventral surface of the dorsomedian ridge of the premaxilla and the anterior part of the frontal show impressions of them. Despite a partial reconstruction that does not allow to observe their ventral surface, the olfactory bulbs appear wider than the olfactory tracts (Fig. 9.2B). These are projected through the ventral wall of the frontal and appear anteroposteriorly elongated. The olfactory tracts become more mediolaterally compressed at their mid-length, and widen at the level of the contact with the cerebrum (Fig. 9.2B). The anteroposterior length of the olfactory tracts is approximately 76 mm in SMNS 81783, which corresponds to about half of the brain cast length. No separation between the olfactory tracts is visible (Fig. 9.2A, B, C). The cast of the tracts continues posteriorly until it meets the cast of the cerebrum, visible on the ventral surface of the parietal. The cerebrum extends anteroposteriorly; however, due to the open condition of the braincase anteriorly to the prootic, its lateral and ventral extensions are not preserved and difficult to determine. The dorsal surface of the cerebrum appears dorsoventrally concave just posterior to the contact with the olfactory tracts. The concavity is more marked in both *Libonectes morgani* specimens (Fig. 9.2A, B) than in the undetermined polycotylid (Fig. 9.2C), and appears more extended antero-posteriorly in D1-8213 than in SMNS 81783. Posteriorly to the concavity

observed on the dorsal surface of the cerebrum, a bulge may correspond to the pineal organ (Fig. 9.2A, B, C). Posteriorly to the possible pineal organ, a more pronounced bulge on the dorsal surface of the brain cast indicates the position of the optic lobes (Fig. 9.2A, B, C), which are enclosed dorsally by the parietal. Ventrally to the optic lobes, the pituitary bulb is projected more ventrally than the ventral surface of the posterior part of the brain cast (Fig. 9.2A, B). Its ventral surface is horizontal and a pair of internal carotid foramen is visible at the posterior end of the pituitary bulb. The posterior part of the brain cast, the rhombencephalon, consists of the cerebellum and the *medulla oblongata* (Fig. 9.2A, B). The cerebellum is incomplete in SMNS 81783 and MNHN F-GOU14 but, in the three specimens it forms an anteroposteriorly developed bulge on the dorsal surface of the endocast (Fig. 9.2A, B). Its dorsal surface slopes posterodorsally and constitutes the main structure of the plesiosaurian brain cast. The medulla oblongata visible in D1-8213 is thin and laterally constricted (Fig. 9.2A), enclosed by the prootics and the exoccipitals. Ventrally, the surface can be reconstructed with reasonable accuracy, as it is framed by the dorsal surfaces of the basisphenoid and basioccipital.

9.2.2. Cranial nerves

The identification of the different cranial nerves has been performed from the information given in the description of plesiosaurian braincases (e.g., Carpenter, 1997; Sato et al., 2011; Sachs et al., 2015). The optic (II), oculomotor (III), and trochlear (IV) nerves could not be traced due to the cartilaginous nature of the skull part enclosing the endocast antero-ventraly. The canal for the trigeminal nerve (V) can be identified as it corresponds to the prootic fenestra (Carpenter, 1997); however, its true extension cannot be determined (Fig. 9.2A). The abducens nerve (VI) is anteriorly projected and exits by the dorsolateral foramen of the pituitary fossa (Fig. 9.2A, B and Fig. 9.3A). The canal for the facial nerve (VII) exits from the foramen on the prootic, posterioriorly to the abducens nerve and just anterior to the inner ear (Fig. 9.2A and Fig. 9.3A). The width of the facial nerve is similar to that of the abducens nerve. The vestibulocochlear nerve (VIII) is not visible on the endocast reconstructions. Just posterior to the inner ear, two foramina pierce the medial surface of the exoccipital adjacent to its ventral surface. The most anterior one is for the exit of the glossopharyngeal nerve (IX), which represents the largest

cranial nerve (Fig. 9.2A, B and Fig. 9.3A), and the dorso-posteriorly foramen is for the vagus-accessory nerves (X + XI). Branches of the hypoglossal nerve (XII) pass through the three foramina in each of the exoccipitals, ventrally to the vagus-accessory nerves. The branches of the hypoglossal nerve are thin and arranged in a triangular pattern on each side of the *medulla oblongata.*

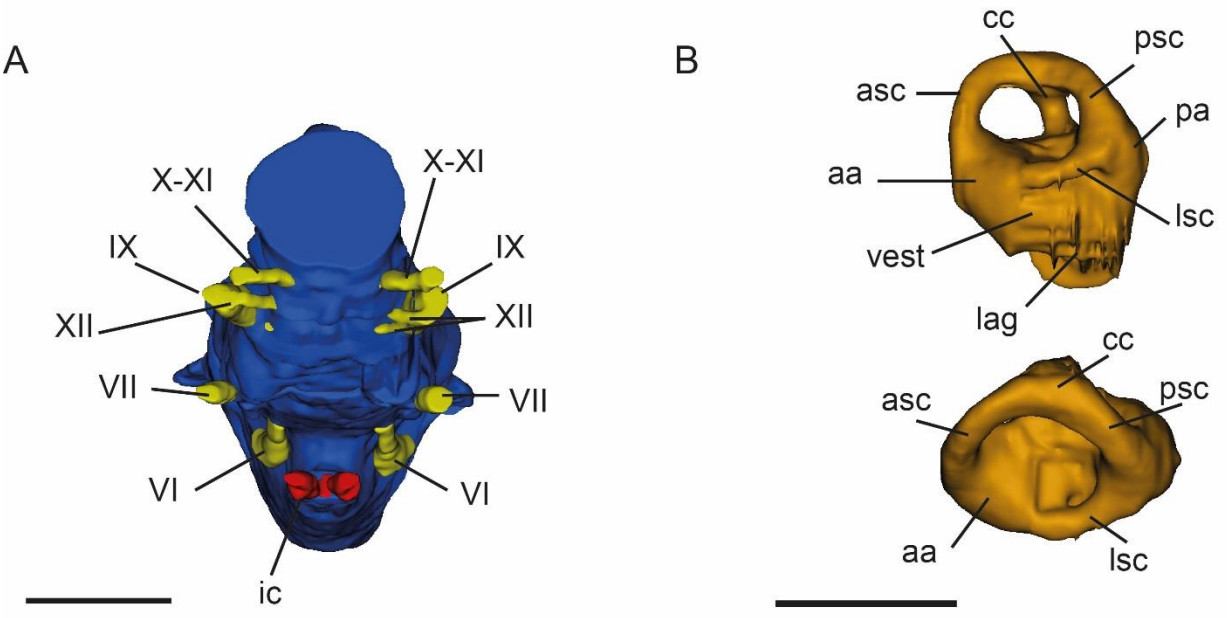

Fig. 9.3. (A) Endocast of the more complete *Libonectes morgani* specimen D1-8213, Early Turonian, Goulmima, Morocco, in ventroposterior view. **(B)**, Left inner ear of D1-8213 in lateral and dorsal views. **Abbreviations**: **aa**, anterior ampulla; **asc**, anterior semicircular canal; **cc**, common crus; **ic**, internal carotid; **lag**, lagena; **lsc**, lateral semicircular canal; **pa**, posterior ampulla; **psc**, posterior semicircular canal; **vest**, vestibule; **VI**, abducens nerve; **VII**, facial nerve; **IX**, glossopharyngeal nerve; **X-XI**, vagus and accessory nerves; **XII**, hypoglossal nerves. Scale bars equal 20 mm.

9.2.3. Inner ear

Left and right inner ears of D1-8213 are preserved, except the most ventral part of the lagena (Fig. 9.3B). The inner ear is positioned ventrally to the cerebellum and its general aspect is

similar to the inner ear of the cryptoclidid *Muraenosaurus leedsii* (Evans, 1999), the only plesiosaurian specimen for which the inner ear is known. The vestibule is rounded and the semicircular canals are square-shaped in lateral view, robust and low (Fig. 9.3B). Even if the true ventral extent of the lagena is unknown, it seems to be relatively short, robust and uncoiled. The inner ear is approximately 24 mm tall and has a maximum width of 20 mm at the level of the semi-circular canals. The anterior semicircular canal (asc) is longer than the two other ones, which seem to be similar in length. The comparison of the diameters shows that the posterior semicircular canal (psc) is the thickest (psc>asc>lsc). The dorsal margins of both anterior and posterior semicircular canals are at the same level (Fig. 9.3B), unlike the condition in *Muraenosaurus leedsii* (Evans, 1999) in which the anterior semicircular canal is more dorsally extended than the posterior one. The angles formed between the anterior and posterior semicircular canals is approximately 113°; 96° between the anterior and lateral semicircular canals and 84° between the posterior and lateral semicircular canals. The anterior and posterior canals meet at the common crus (Fig. 9.3B), which is approximately of similar diameter as the canals themselves.

9.3. Discussion

9.3.1. Endocranial comparisons with extinct and extant marine reptiles

The reconstructions of the endocranial morphologies of extant reptilian taxa that live in marine ecosystems are scarce. The endocast of several aquatic snakes, among which the only extant pelagic snake, *Pelamis platurus*, have been studied recently (Allemand et al., 2017b). Within sea-turtles, only endocast of *Dermochelys* (Dermochelyidae) has been examined (Wyneken, 2001) and Georgi (2008) gave some elements of its inner ear morphology.

Among extinct reptilian taxa, those considered as marine inhabitants are numerous but the data availables concerning their endocasts that could be used for comparisons are scarce. The endocranial information in ichthyosaurs is limited to the latex casts made by McGowan (1973) for an *Ichthyosaurus* sp., a digital brain cast of an indeterminate juvenile specimen (Marek et al., 2015) and the endocranial reconstruction for *Platypterygius longmanni* Wade,

1990 (Abele, 2017). The neuroanatomy of thalattosuchians appears the most studied and is known for at least seven species that are *Metriorhynchus superciliosus* de Blainville, 1853 (Wenz, 1968), *Cricosaurus* (=*Geosaurus*) *araucanensis* Gasparini and Dellapé, 1976 (Herrera et al., 2013; Herrera, 2015), *Dakosaurus* cf. *D. andiniensis* Vignaud and Gasparini, 1996 (Herrera, 2015), *Teleosaurus eucephalus* (Seely, 1880), *Steneosaurus pictaviensis* Vignaud, 1998 (Wharton, 2000), *Steneosaurus* cf. *gracilirostric* Westphal, 1961 (Brusatte et al., 2016), *Pelagosaurus typus* Bronn, 1841 (Pierce et al., 2017). Among squamates, Camp (1942) figured the endocasts of the two mosasauroids, *Platecarpus* sp. and *Clidastes* sp., and during this PhD thesis the endocast of *Tethysaurus nopcsai* has been studied (see Chapter 7). As for the inner ear morphology, it is also known in mosasauroids for *Plioplatecarpus peckensis* (Cuthbertson et al., 2015), *Platecarpus coryphaleus*, *Platecarpus tympaniticus*, *Tylosaurus neopaeolicus* (Georgi, 2008; Georgi and Sipla, 2008) and *Tethysaurus nopcsai* (see Chapter 7).

Comparisons with these marine reptiles show that plesiosaurians exhibit an unique combination of endocranial characteristics. The plesiosaurian olfactory tracts are elongated anteroposteriorly and not separated along their length, as in the mosasauroid *Tethysaurus nopcsai* (Fig. 9.4F). This condition differs from the short olfactory tracts observed in turtles (Fig. 9.4D) and the more or less separated olfactory tracts found in snakes (Fig. 9.4C), the thalattosuchian *Pelagosaurus typus* (Fig. 9.4E) and the indeterminate ichthyosaur (Fig. 9.4G). In addition, plesiosaurians exhibit a large cerebellum. Indeed, for the other marine reptiles, this structure is not always distinguishable from endocasts (e.g., the snake *Pelamis platurus*, Fig. 9.4C) or, when visible, it is not as developed as in plesiosaurians (e.g., the thalattosuchian *Pelagosaurus typus*, Fig. 9.4E). At last, the plesiosaurian pituitary projected horizontally differs from the tilted one seen in *Pelamis platurus* (Fig. 9.4C) and *Pelagosaurus typus* (Fig. 9.4E), and also from the bulge exhibited by *Tethysaurus nopcsai* (Fig. 9.4F)

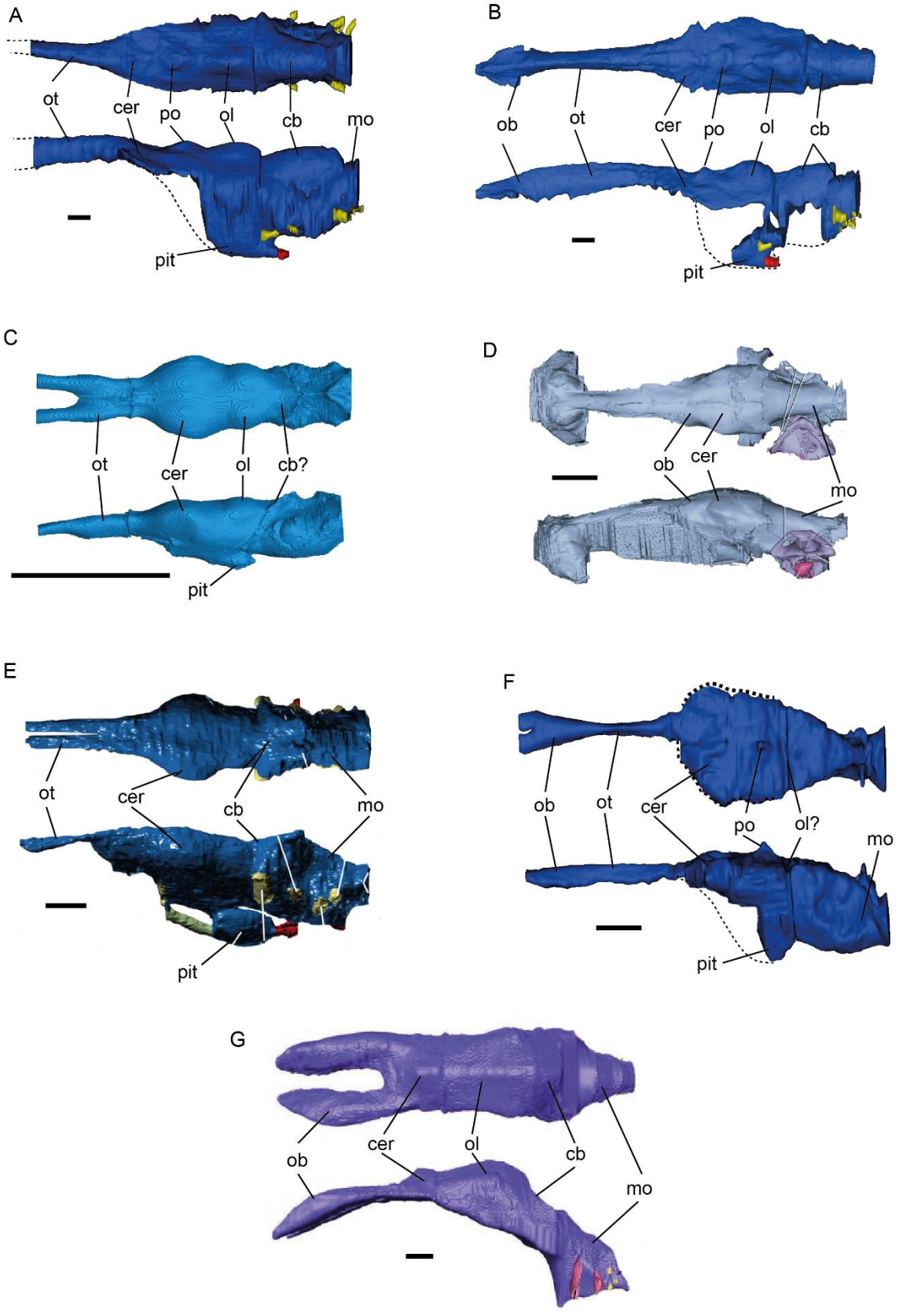
A
ot
cer
po
ol
cb
mo
pit
B
ob
ot
cer
po
ol
cb
pit
C
ot
cer
ol
cb?
pit
D
ob
cer
mo
E
ot
cer
cb
mo
pit
F
ob
ot
cer
po
ol?
mo
pit
G
ob
cer
ol
cb
mo

Fig 9.4. Virtual endocasts of the *Libonectes morgani* specimens **(A)** D1-8213 and **(B)** SMNS 81783, Early Turonian, Goulmima, Morocco, compared to **(C)** the extant snake *Pelamis platurus* (Allemand et al., 2017b; see Chapter 5); **(D)** the extinct marine turtle *Plesiochelys etalloni* (modified from Carabajal et al., 2013); **(E)** the thalattosuchian *Pelagosaurus typus* (modified from Pierce et al., 2017); **(F)** the mosasauroid *Tethysaurus nopcsai*, Early Turonian, Goulmima, Morocco (see Chapter 7); and **(G)** an indeterminate juvenile ichthyosaur (modified from Marek et al., 2015) in dorsal (up) and left lateral (down) views. **Abbreviations**: **cb**, cerebellum; **cer**, cerebrum; **mo**, *medulla oblongata*; **ob**, olfactory bulbs; **ol**, optic lobes; **ot**, olfactory tracts; **po**, pineal organ; **pit**, pituitary bulb. Scale bars equal 10 mm.

9.3.2. Endocranial comparisons with other sauropterygians

Endocranial studies among Triassic Sauropterygia are still limited; however, information exists for *Nothosaurus mirabilis* Münster, 1834 (Edinger, 1921; figured by Hopson, 1979), *Nothosaurus marchicus* Koken, 1893 (Voeten et al., 2014) and *Placodus gigas* Agassiz, 1833 (Neenan and Scheyer, 2012).

The most complete endocast of *Placodus gigas* known shows only the hindbrain cavity posterior to the pineal foramen (specimen UMO BT13; Neenan and Scheyer, 2012). The structure appears strongly anteroposteriorly inclined by about 70° from the skull roof table and is very sigmoidal (Neenan and Scheyer, 2012). This condition clearly differs from the horizontal orientation of the posterior part of the endocast observed in the specimens of *Libonectes* and polycotilid examined here. This difference could be linked to the size of the braincase of *Placodus* that is shorter than those of other sauropterygians (Neenan and Scheyer, 2012). The short and solid skull of *Placodus* could correspond to a functional adaptation that helps to dissipate the strains when the animal crushes its hard-shelled food (Neenan and Scheyer 2012). When the cranial cavity is restricted, the brain could present a more or less flexured shape, with an anterior part higher than the posterior part (Hopson, 1979). The difference in endocast flexure observed between *Placodus* and the plesiosaurians examined here could thus correspond to a morphological adaptation to different ecological constraints.

The endocasts of both species of *Nothosaurus* are straight with long olfactory tracts (Hopson, 1979; Voeten et al., 2014), similar to the plesiosaurian endocasts described in this study and contra that observed in *Placodus*. In *Nothosaurus*, the skull is more elongated than that of *Placodus* in a similar way than that observed in Plesiosauria, giving more place for the accommodation of the brain.

Although it is impossible to evaluate the phylogenetic signal of the sauropterygian endocast morphology in the current state of the art, the similarity between the endocasts of *Nothosaurus* and plesiosaurians could be assessed as a reflection of their close phylogenetic relationships (e.g., Neenan et al., 2013). However, as the phylogenetic relationships within sauropterygian groups are still debated (Neenan et al., 2013), additional endocranial information could be useful in order to include endocranial characters in phylogenetic studies and hopefully better resolve the phylogenetic relationships in this clade.

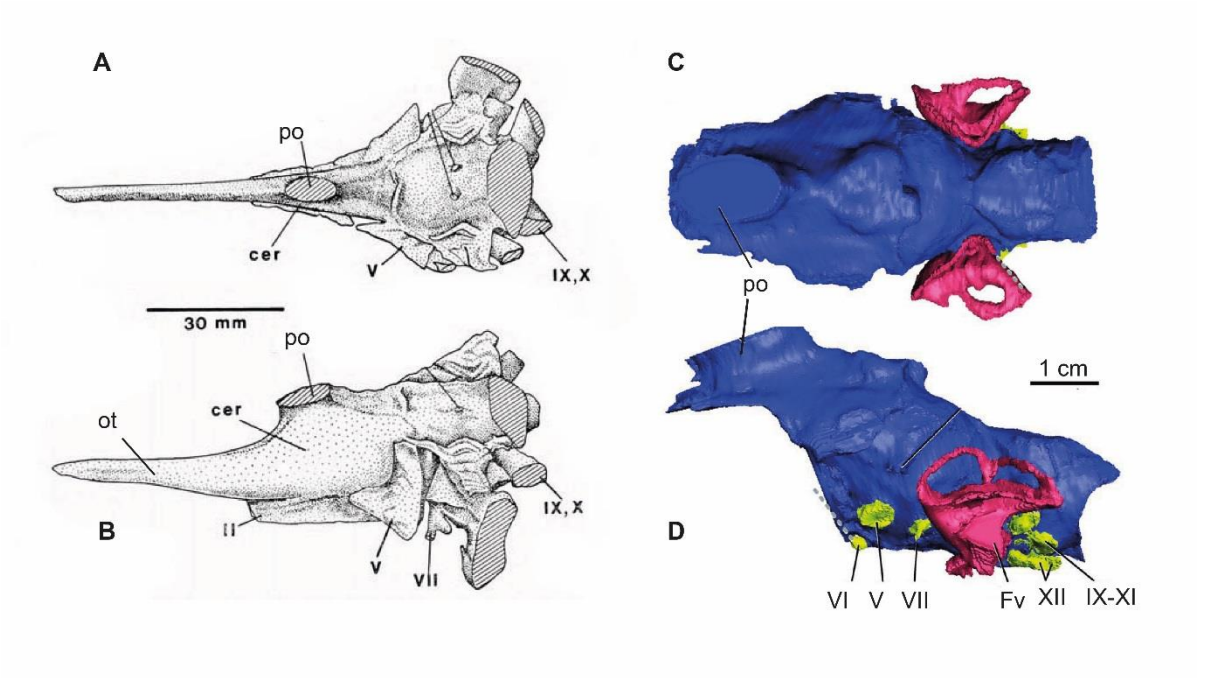

Fig. 9. 5. Endocasts of **(A, B)** *Nothosaurus mirabilis* (modified from the redrawn of Hopson, 1979) and **(C, D)** *Placodus gigas* (modified from Neenan and Scheyer, 2012) in dorsal **(A, C)** and lateral views **(B, D)**. **Abbreviations**: **cer**, cerebral hemispheres; **fv**, fenestra vestibule; **ot**, olfactory tracts; **po**, pineal organ; vest; **II**, optic nerve; **V**, trigeminal nerve; **VI**, abducens nerve; **VII**, facial nerve; **IX**, glossopharyngeal nerve; **X**, vagus nerve; **XI**, accessory nerves; **XII**, hypoglossal nerves.

9.3.3. Endocranial comparisons with other plesiosaurians

Both elasmosaurid and polycotylid specimens seem to share a similar pattern: the nearly straight endocasts are characterized by long olfactory tracts, a reduced pineal organ, a pituitary bulb projected horizontally, developed optic lobes and a large cerebellum that represents the main endocranial structure in relative size.

The endocast of the holotype of *Libonectes morgani*, SMUMP 69120 (Carpenter, 1997) shows a similar pattern to that of the two other specimens of *L. morgani* studied here. Although the endocranial proportions are similar, there is, however, one noticeable difference in the ventral flexure of the endocast. The reconstruction of Carpenter (1997) shows that the cerebellum in SMUMP 69120 is located more ventrally than the plane defined by the olfactory tracts in lateral view, whereas in D1-8213 and SMNS 81783, both olfactory tracts and the cerebellum are in the same plane, resulting in a nearly horizontal endocast. Thus, among the three specimens of *Libonectes morgani* examined here, SMUMP 69120 shows the more pronounced flexure of its endocast, whereas the skull of SMNS 81783 and D1-8213 show a more horizontal development of their brain cavities. This difference seems not to correspond to artefacts of preservation, as the specimens do not show taphonomical deformations. Both of them (SMNS 81783 and D1-8213) are preserved in nodules that probably formed fast after the death of the individuals. The third one was not observed directly but the author who described it (Carpenter in 1997) does not mention any deformation for this fossil. Examination of the endocast flexure of additional specimens exhibiting different skull size is necessary to confirm that this character is not specific to this individual. Some additional specimen are available for such a study (e.g., *Libonectes morgani* specimen SMNK-PAL 3978). According to Giffin (1989), the main causes of the endocranial flexures are the absolute size of the skull and the relative size of the eyes. Smaller taxa tend to show an endocast with a more pronounced flexure than large ones, the same pattern is observed in young individuals compared to older ones of the same species (Giffin, 1989). The loss of the flexures is thus, within individuals, a consequence of the increase in skull size, the skull growing at a higher speed than the brain, the latter has thus relatively more space in the larger individuals and "unfolds" (Hopson, 1979). On the contrary, when the cranial cavity is restricted, the brain presents a more or less pronounced "S" shape, with an anterior part higher than the posterior part (Hopson, 1979). In addition, large

eyes, that could be related to a juvenile trait within a same species or an ecologic adaptation to a particular lifestyle (e.g., nocturnal, see Konishi et al., 2016), compress the occipital region as well as the brain could increase the flexures (Starck, 1979). Surprisingly, the specimen of *Libonectes* that presents the longest skull (SMUMP 69120: about 500 mm in length, see Carpenter, 1997) shows the more pronounced flexure. The two other specimens (SMNS 81783 and D1-8213) are smaller (they measure respectively 295 and 350 mm long) but show no flexure of the endocast. Size being usually correlated with the age of individuals, this observation thus questions the assumption of Giffin (1989). This difference in endocast flexures does probably not correspond to an ontogenetical variation within the species. It could however possibly correspond to sexual dimorphism. Total brain size is reported to differ between males and females of different mammalian taxa, including human (e.g., Nopoulos et al., 2000; Iwaniuk, 2001). Similarly, the size of structures composing the brain in lizards may differ between male and females (e.g., size of the olfactory bulbs; Sampedro et al., 2008). Thus, the gender of plesiosaur having the largest brain could also present a more pronounced flexure of its endocast than the other one.

9.3.4. Plesiosaurian pineal foramen

The endocranial reconstructions show that a small pineal organ is visible on the endocast of the three plesiosaurian specimens. However, the pineal foramen is considered as absent in most of the elasmosaurid and polycotylid species. Indeed, the loss of the pineal foramen has long been considered as a synapomorphy of Late Cretaceous Elasmosauridae and Polycotylidae by Carpenter (1997), but recent phylogenetic data have suggested that this structure had been lost independently in some taxa of both families (O'Keefe, 2001; Kear, 2005; Druckenmiller and Russell, 2008a; Ketchum and Benson, 2010). In the skull reconstructions of *Libonectes morgani* specimen D1-8213 and the undetermined polycotylid MNHN F-GOU14 performed here, the pineal foramen was not observed (Allemand et al., in press), but the examination of the endocasts reveals its presence. Such observation suggests that the non-visible pineal foramen in some elasmosaurids and polycotylids specimens could be due to the weakness of their skull, as most elamosaurid and polycotylid skulls are often preserved crushed (e.g., Kear, 2006;

Vincent et al., 2011); the small pineal foramen could thus be hidden or closed by the displacement of the skull roof bone elements. The possibility of an evolutionary tendency to a loss of a pineal organ beginning with the closure of the pineal foramen should however not be excluded,

The pineal organ has important physiological functions (Holloway et al., 2013) and is involved in the production of melatonin, which plays a role in the regulation of the circadian rhythm and seasonal cycles (Hopson, 1979) but has also different functions according to taxa (see Holloway et al., 2013 for details). The exact functions of a pineal organ in plesiosaurians are difficult to determine. Nevertheless, this organ is possibly present in the entire clade of Sauropterygia (a pineal foramen at least is easily observable in almost all the species of sauropterygians) and has thus certainly an important biological function. Comparisons with other sauropterygians show that *Placodus gigas* and *Nothosaurus mirabilis* both exhibit a large pineal organ (Hopson, 1979; Neenan and Scheyer, 2012), whereas, in the tree specimens of plesiosaurians examined here, the pineal organ is reduced. Elasmosaurids and polycotylids being considered as more derived taxa than placodont and nothosaurs, the functional benefit of pineal organ reduction is questionable. The same trends of reductions in pineal organ size appear independently in other clades of reptiles and have been observed in pseudosuchians, theropods, and sauropods (Holloway et al., 2013). However, this trend does not seems associated to the size of the animal, as the contrary has been reported in mosasauroids (see Chapter 7), in which larger species exhibit larger pineal organ than smaller ones. Thus, the functional implications for the reduction are difficult to understand and it is not possible to determine whether it occurred for the same or different reasons in each of these clades.

9.3.5. Plesiosaurian inner ear

The inner ear reconstructed here for the elasmosaurid *Libonectes morgani* specimen (D1-8213) is similar to that of the cryptoclidid *Muraenosaurus leedsii* illustrated by Evan (1999). Both exhibit a square appearance in lateral view with short semicircular canals, a well-developed common crus and a rounded vestibule. However, one difference is noticed in the configuration of the semicircular canals. In *Libonectes morgani*, the dorsal margins of both anterior and

posterior semicircular canals are at the same level (Fig. 9.3B), unlike the condition in *Muraenosaurus leedsii* (Evans, 1999) in which the anterior semicircular canal is more dorsally extended than the posterior one. It is important to notice that morphological differences exist between the inner ear of *Muraenosaurus* and *Libonectes* thus indicating that the inner ear morphology is not homogenous among this clade. These differences could be related to phyologenetical or ecological traits and the study of the inner ear morphology of plesiosaurians is thus a crucial issue to better characterise their life history or ecological evolution.

Among sauropterygians, only another inner ear, that of *Placodus gigas*, has been described (Fig. 9.5C, D modified from Neenan and Scheyer, 2012). *Placodus gigas* exhibits a dorsoventrally flattened labyrinth extended anteroposteriorly, with gracile semicircular canals that form a "M"-shaped morphology at the crus communis (Neenan and Scheyer, 2012). This morphology differs from the compact and bulbous labyrinth found in *Libonectes morgani*, in which the short and thick semicircular canals appear more elliptical and rounded, with a horizontal junction between the anterior and posterior canals (Fig. 9.3B). The differences between *Libonectes* and *Placodus* are more important than between *Libonectes* and *Muraenosaurus*. Although the inner ear in *Muraenosaurus* appears more robust aspect than that of *Placodus*, both exhibit an anterior semicircular canal more dorsally extended than the posterior one. Such features could reflect an ecological adaptation and reveal an adaptation to nearshore to open-sea lifestyle transition.

The plesiosaurian inner ear differs from most extinct and extant non-avian reptiles for which the labyrinth may show a triangular shape (e.g., snakes, lizards: Yi and Norell, 2015; Palci et al., 2017), an oblong shape (e.g., mosasauroids: Cuthbertson et al., 2015; see Chapter 7) or a "M"-shape (e.g., crocodilians, thalattosuchians, rhynchocephalians: Walsh et al., 2009; Pierce et al., 2017). However, strong similarities are perceived when the plesiosaurian inner ear is compared to that of turtles. Both exhibit low and short semicircular canals, as well as a short and robust common crus and a horizontal junction between the anterior and posterior canals (e.g., Carabajal et al., 2013, Carabajal et al., in press). Such similarities could be the reflect of phylogenetic affinities between plesiosaurians and turtles. Indeed, several studies have shown the stong imprint of phylogenetic history on the shape of the bony labyrinth in mammals (e.g., Billet et al., 2015; Grohé et al., 2015; Mennecart and Costeur, 2016), but also within squamates (e.g., Boistel et al., 2011). However, if such phylogenetic signal is expressed, it is surprising

that *Placodus gigas*, the most closely related species to plesiosaurians, exhibits this difference in inner ear morphology. Boistel et al. (2011) revealed that the dimensions of the vestibular system show clear differences among animals with different lifestyles. This could explain the differences perceived between the inner ear of the nearshore *Placodus gigas* (Neenan and Scheyer, 2012) and the offshore plesiosaurians, and the similarity between the latter and turtles could be related to the fact that they share a similar mode of locomotion, both swim without using an axial undulatory locomotion and rely completely on paraxial propulsion (e.g., O'Keefe, 2001).

9.3.6. Sensory inferences

Several studies have suggested that plesiosaurians were visual hunters, with a more or less developed binocular vision (e.g., Shuler, 1950; Forrest, 2000; Cruickshank and Fordyce, 2002), and possibly adapted to the vomerolfaction (e.g., Cruickshank et al., 1991; but see Buchy et al., 2006). In this contribution, the lack of endocranial data in plesiosaurians prevents any generalization to the clade; however, it is possible to discuss about some functional inferences from endocranial features availables.

The olfactory bulb size has been used as an indicator of olfactory acuity in archosaurs and mammals (e.g., Gittlemen, 1991; Healy and Guildford, 1990; Zelenitsky et al., 2009). Zelenitsky et al. (2009) proposed the first quantitative evaluation of the olfactory acuity in extinct theropod dinosaurs based on an olfactory ratio between the greatest diameter of the olfactory bulb to the greatest diameter of the cerebral hemispheres. However, considering data available for plesiosaurians, the endocranial reconstructions do not provide information about the cerebral hemispheres; it is thus not possible to calculate this ratio, preventing inferences about the olfactory acuity of these taxa. Nevertheless, qualitative comparisons with extant taxa, especially with crocodiles that share a similar organization with long olfactory tracts differentiated from large olfactory bulbs (Jirak and Janacek, 2017), suggest plesiosaurian olfactory bulbs are small and corroborate the hypothesis of diminished sense of olfaction. Same inferences have been performed from the *Nothosaurus* endocast in which the restricted olfactory bulges suggest limited in vivo olfactory performances (Voeten et al., 2014).

Endocranial reconstructions for the three plesiosaurian specimens indicate that both the optic lobes and the cerebellum are developed. However, there is still no measurement allowing to quantify their development. The optic lobes receive both visual and auditory input (Wyneken, 2007) and their size is correlated with the importance of visual stimuli (Butler and Hodos, 2005). The cerebellum integrates touch, proprioception, vision, hearing, and motor input and has a role in maintaining postural equilibrium (Wyneken, 2007). Although it is important to take into account that these structures may be covered dorsally by the venous system (Aurboonyawat et al., 2008) and have a strong impact on the size of these structures, the prominent optic lobes could indicate an important role of the vision in these taxa. In addition, the large cerebellum in plesiosurians, which differs from all non-avian reptiles, including turtles that share a similar mode of locomotion (e.g., Carabajal et al., 2013; in press), or other highly aquatic extinct taxa such as ichthyosaurs (e.g., Marek et al., 2015), could be related to the particular mode of locomotion, using asynchronous movements (e.g., Carpenter et al., 2010; Liu et al., 2015) with their anterior and posterior limbs. Thus, the large cerebellum could be related to limb coordination requirements for more efficient swimming, however, such enlargement could be also related to the length of the neck and its role in maintaining postural equilibrium and consideration of the endocast of short-necked taxa should allow to consider this hypothesis.

9.4. Conclusions

Despite the open condition of the plesiosaurian braincase, it is possible to reconstruct their endocasts and the different structures appear well differentiated. Plesiosaurians exhibit unique endocranial morphology with an organisation that clearly differ from that of all the extant and extinct known taxa. The interpretation of this unique morphology is difficult as the lack of comparative data prevents to evaluate the impact of the phylogenetic and ecologic signals. However, several hypotheses have been performed during this work. The plesiosaurian endocast has been considered as a reflect of a morphological adaptation to different ecological constraints (see comparison with *Placodus gigas*). The differences perceived in the plesiosaurians inner ear could reflect adaptation to life in open-sea. Indeed, some features, such

as the dorsal margins of both anterior and posterior semicircular canals in the same level, could be related to diving habits and the study of the inner ear morphology in plesiosaurians appears necessary to better characterise their life history or ecological evolution. Sensory inferences from the plesiosaurian endocast suggest that they might rely more on vision than olfaction to interact with their environment. The study of additional taxa among sauropterygians could provide an evolutive aspect to this first work in order to consider the sensory evolution that had accompanied the secondary adaptation to life in marine environments.

Chapter 10

Paleoecological reconstruction of the Early Turonian (Late Cretaceous) marine reptile assemblage of Goulmima, Southern Morocco

In Morocco, the Turonian deposits of Goulmima have yielded a diverse marine fauna (see Chapter 2) among which large marine reptiles constitute an important component, in terms of both diversity and number of taxa. Although the coeval and abundant fauna of bony fishes and invertebrates also found in this area (see Chapter 2) could explain such a rich marine reptile assemblage, the presence of numerous large predators in a same place, including marine reptiles but also sharks, questions their cohabitation, interactions and niche partitioning.

As species' lifestyle is reflected by the central nervous system (Nieuwenhuys et al., 1998), endocasts in extinct taxa may be used as additional information to reconstruct their paleobiology and paleoecology. By adding the new endocast data to informations already available in the literature concerning the general morphology (e.g., Massare, 1987, 1988; Noè et al., 2017) of the marine reptiles found here as well as the associated faunas and paleoenvironnement (e.g., Cavin et al., 2010; Lebedel et al., 2013), this work aims to depict the ecological options available for each marine reptile taxon and to discuss the marine vertebrate trophic structure characterizing the marine environment of Goulmima.

Among the marine reptile assemblage of Goulmima, the elasmosaurid *Libonectes morgani* exhibits a large size that may reach 7-8 meters (Buchy, 2005), whereas polycotylids and the basal mosasauroid *Tethysaurus nopcsai* appear smaller with a size-estimate of 5-6 meters (e.g., *Thililua longicollis*: Bardet et al., 2003a) and of 3-4 meters respectively (Bardet et al., 2003b). Besides, although the pliosaurid *Brachauchenius lucasi* is only known through the description of its mandible, its length (1500 mm, see Angst and Bardet, 2015) suggests, from comparisons with more complete specimens (McHenry, 2009), a large animal with a body size of about 5-6 meters. If such size diversity may suggest primarily that ingested preys were different in size and that possible prey-predator relationships may occur however, it does not provide any information about how these taxa may have coexisted.

It is possible that, in order to avoid direct competition, marine reptiles in Goulmima have occupied different positions in the water column. The avascular necrosis observed on plesiosaurian limbs led Rothschild and Storrs (2003) to suggest that elasmosaurids, pliosaurids and polycotylids were able to perform deep or repetitive diving (but see Farke, 2007). In addition, the large quantities of gastroliths mainly associated to elasmosaurid remains (Cicimurri and Everhart, 2001) and the probable function of these stomach stones as a buoyancy

compensation mechanism (Storrs, 1993), may suggest that elasmosaurids occupied a deeper position in the water column than polycotylids and pliosaurids. However, as no avascular necrosis or gastroliths have been reported in taxa of Goulmima, such hypothesis cannot be refuted or confirmed here.

It is highly probable that Goulmima marine reptiles were prey-specialized and might have exhibited different foraging behaviors in order to coexist. To find food in their natural habitat, the organisms have to orient towards potential food sources, detect and localize possible prey items, analyze the nature of these items to classify them as edible, and finally move toward these preys to ingest them (Von Der Emde and Bleckmann, 1998). Such processes are directly related to the abilities of each taxon and can be considered through different structures which are analyzed below.

10.1. Prey preferences via skull and tooth morphoguilds

The most commonly used skeletal components to define diet and prey preferences are teeth (Bardet et al., 2015). Massare (1987) used contrasting dental morphologies in Mesozoic marine amniotes to define seven feeding guilds based on analogies with modern marine mammals. The resulting morphospaces - now an interpretive standard (Bardet et al., 2015) – is materialized by a triangular diagram showing gradational and/or overlapping guilds distributed along axes connecting three apex categories (Fig. 10.1): 1) the “Pierce” guild, corresponding to predators feeding on small, soft-bodied preys such as small fishes and invertebrates; 2) the “Crush” guild, feeding on medium sized, hard-shelled invertebrates; 3) and the “Cut” guild, which includes opportunistic top-predators feeding on bony vertebrates. The “Pierce” guild corresponds to the most restricted prey item diversity, whereas the “Cut” guild includes predators able to feed on the broadest range of organisms. In the following section, the size and shape of both teeth and skull of each marine reptile taxon from Goulmima are discussed and put together with the coeval marine faunas, in order to consider their possible prey preferences.

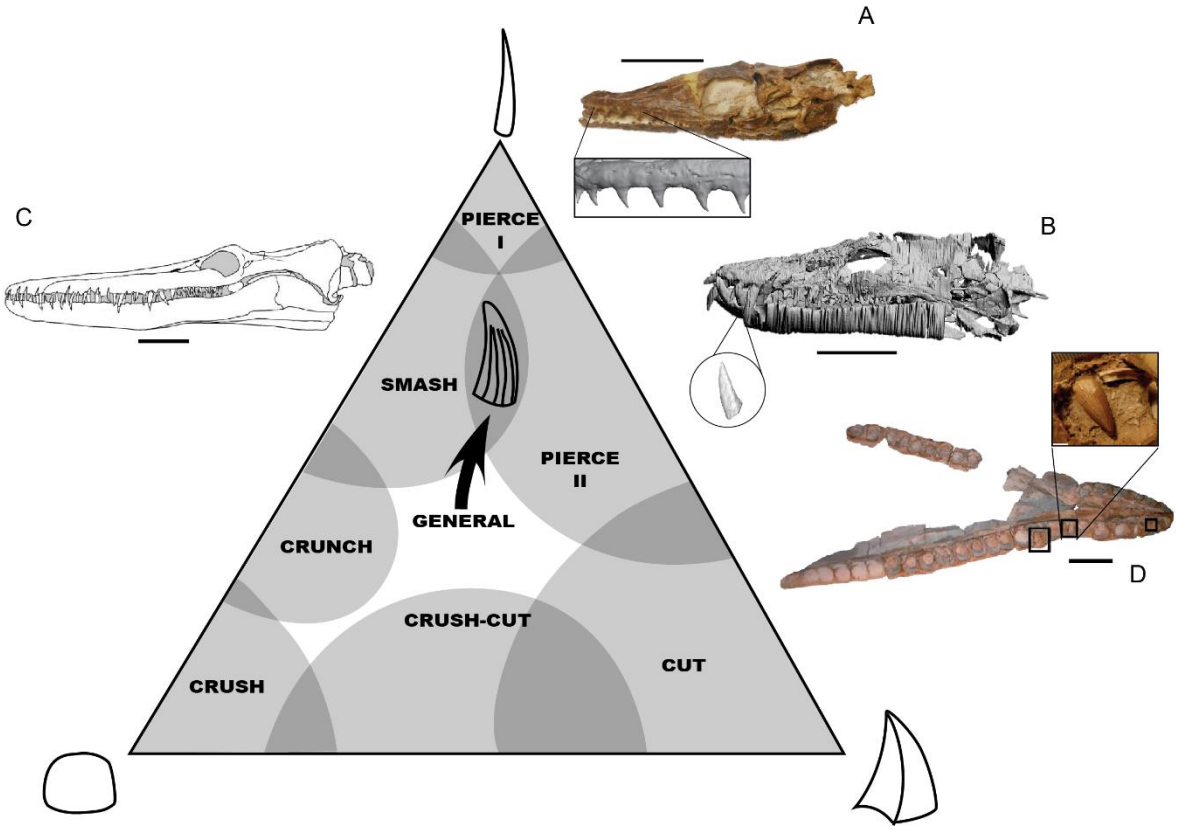

Fig. 10.1. Triangular diagram illustrating the tooth morphoguilds (based on Bardet et al., 2015) of the marine reptile assemblage of Goulmima. **A**, Pierce I: the mosasauroid *Tethysaurus nopcsai* (MNHN GOU 1; from Bardet et al., 2003b); **B**, Smash-Pierce II : the elasmosaurid *Libonectes morgani* (SMNS 81783; from Allemand et al, 2017a); C, Smash-Pierce II : the polycotylid *Thililua longicollis* (MHNGr.PA.11710; from Bardet et al., 2003a); **D**, Smash-Pierce II : the pliosaurid *Brachauchenius lucasi* (MNHN GOU 11; from Angst and Bardet, 2015). Scale bars equal 10 cm.

Tethysaurus nopcsai teeth are small and slender (Fig. 10.1A), strongly posteromedially recurved and slightly laterally compressed (Bardet et al., 2003b). This morphology ranges into the "Pierce I" guild (Massare, 1987). Although Gale et al. (2017) suggested that *T. nopcsai* would be capable of biting through an ammonite test, this dentary morphology, associated to the small and gracile skull morphology (about 30 cm long), indicates rather a diet of soft-bodied small preys (Massare, 1987). In Goulmima, *Tethysaurus* may have been specialized in the capture of soft-bodied invertebrates and small bony fishes located at the basis of the trophic

chain, such as *Enchodus* and *Pycnodont* sp. (total length estimated to about 100 mm; Cavin and Dutheil, 1999), although the flexible, kinetic skull characterizing the mosasauroids (Russell, 1967) could allow it to swallow larger preys.

Among the plesiosaurians, the teeth of both elasmosaurids and polycotylids are simple long and slender cones slightly recurved posteriorly (Fig.10.1B, C). This generalist morphology ranges into the "Smash and Pierce II" guilds of Massare (1987) and is adapted to catch bony fishes and invertebrates, however, both groups would have been relatively harmless to larger fish and other marine reptiles (Everhart, 2004). The main difference, however, is perceived on the morphology and size of their skull.

The brevirostrine skull in *L. morgani* (about 40 cm long) and the teeth may suggest specialization for filter- or sieve-feeding niche on a large range of mesoscopic prey from the water column, the interface between the water and the sediments, or within the sediments, which are trapped behind the teeth and then shallowed in their entirety (Noè et al., 2017). Indeed, the simple open-and-shut jaws of elasmosaurids (Noè et al., 2017), associated to the dentition, suggest that these taxa were unable of complex oral processing and preys had to be swallowed in their entirety because of the inability of elasmosaurids to reduce large prey items into smaller pieces (Noè et al., 2017). The tooth spacing suggests an approximate minimum prey width in the order of 10-20 mm for most adult elasmosaurids and the space between the jaw articulations indicates an approximate maximum width close to 200 mm (Brown, 1981; Cicimurri and Everhart, 2001). In Goulmima, as *Tethysaurus*, *Libonectes* may have been also specialized in the capture of soft-bodied invertebrates and small bony fishes located at the basis of the trophic chain, such as *Enchodus* and *Pycnodont* sp.

Contrary to *L. morgani*, the polycotylid skull appears longer (e.g., *Thililua longicollis*: 66 cm, Buchy et al., 2005) with a longirostrine condition, the snout representing 60% of the total skull length in *T. longicollis* (Buchy et al., 2005) contra 40% in *L. morgani*. Such difference may involve different preys. Indeed the longirostrine condition could indicate a more pronounced adaptation for piscivory in polycotylids, which might have "sacrificed" skull strength for high velocity in jaw closure, similarly to some crocodilians (Pierce et al., 2008), in order to successfully feed on fast and agile preys. However, according to Testin (2011), the thick and structured enamel on teeth of polycotylids would suggest also that shell was an

important part of their diet. In Goulmima, the elongated and large skull of the polycotylids found may suggest these taxa fed on the ammonites present in this area but also on medium-sized bony fishes, such as *Goulmimichthys arambourgi* and/or *Osmeroides* sp. (body length estimated to about 300 mm; Cavin, 2001).

Finally, the large caniniform teeth exhibited by the pliosaurid *Brachauchenius lucasi* (Fig. 10.1D) also range into the "Smash and Pierce" guild of Massare (1987), however, their size associated to the large skull would indicate a more macrophagous diet, including large bony fishes (Hampe, 2005), and probably other marine reptiles or sharks (Massare, 1987). *Brachauchenius* was probably the apex predator of the Goulmima area, and might feed on the largest bony fishes, such as *Ichthyodectidae* sp. (body length estimated to 800 mm, Cavin, 1996), but also on other marine reptiles.

To sum up, although some overlaps are perceived (e.g., *L. morgani* and *Tethysaurus*), the skull and tooth morphoguilds reflect distinct prey preferences in the Goulmima marine reptile assemblage. However, such morphological evidences provide information about how taxa may catch their prey just before to ingest them and which kind of prey preferences they could had, without considering the first steps of the foraging behavior, that are to detect and to move forward the prey. These steps, detailed below, may differ according to taxa and their sensorial and locomotory abilities, which can be apprehended in part through endocranial studies.

10.2. Prey detection via endocranial studies

The first step of the foraging behavior consists in the detection of possible preys. For this, it is generally admitted that animals mainly use their chemical senses and/or vision (e.g., Atema, 1980). Several studies have suggested that both mosasauroids and plesiosaurians were visual hunters, with a more or less developed binocular vision (e.g., Shuler, 1950; Lingham-Soliar, 1995; Forrest, 2000; Cruickshank and Fordyce, 2002; Yamashita et al., 2015; Konishi et al., 2016), and possibly adapted to the vomerolfaction (mosasauroids: Schulp et al., 2005;

plesiosaurians: Cruickshank et al., 1991; but see Buchy et al., 2006). These hypotheses will be hereafter discussed in the light of the endocranial reconstructions performed in this work.

10.2.1 Chemical senses (olfaction, vomerolfaction, gustation)

In vertebrates, the chemical senses include the olfaction, the vomerolfaction and the gustation (Hemilä and Reuter, 2008). In vertebrates, the olfactory system is involved in detecting chemicals emanating from distant sources, whereas the vomeronasal system and the gustation are involved in close-range detection (Eisthen and Schwenk, 2008). Olfaction is associated to the nasal capsules whereas the vomerolfaction is related to the vomeronasal organ (Jacobson's organ). Sensory epithelia of both systems are innervated by different branches of the olfactory nerve (I) to the main and accessory olfactory bulbs located at the anteriormost part of the brain (Schwenk, 2008). Gustation is mediated by taste buds located within the oral and pharyngeal cavities, and innervated by the facial (VII), glossopharyngeal (IX) and vagus (X) nerves to the hindbrain (Reiss and Eisthen, 2008).

From endocasts, such distinction between the main and accessory olfactory bulbs (olfaction/vomerolfaction) is not possible as only the external morphology is perceived. Thus, only the size and shape of the whole structure is available in extinct taxa. The size of the olfactory bulbs in vertebrates has been used as an indicator of olfactory acuity (i.e., ability to discriminate between different odors, Zelenitsky et al., 2009). Among non-avian reptiles, both crocodylians and turtles are known to have relative large olfactory bulbs (e.g., Parson, 1959; Starck, 1979; Carabajal et al., in press) that can be associated to their developed sense of smell (e.g., Pooley and Gans, 1976; Rogers, 1999; Hays et al., 2003). From snake endocasts, the size of the olfactory bulbs greatly vary between taxa (Allemand et al., 2017b; see Chapter 5) and may indicate variable olfactory abilities according to their ecology. However, as the olfaction is involved in different activities, such as predation, mating and courtship (Bales, 2014), it is difficult to determine behavioral inferences from the size of the olfactory bulbs.

In order to measure the olfactory abilities in non-avian dinosaurs, Zelenitsky et al. (2009) used the ratio of the greatest diameter of the olfactory bulb to the greatest diameter of the cerebrum. Unfortunately, this measurement is not applicable from the endocasts of

plesiosaurians and *Tethysaurus* because the lateral and ventral limits of the cerebrum are not preserved. However, qualitative comparisons with crocodiles that share a similar olfactory organization (long olfactory tracts with well-differentiated olfactory bulbs: Jirak and Janacek, 2017) show that both *Tethysaurus* and *Libonectes* have rather small olfactory bulbs compared to the rest of the endocast, that may suggest that these taxa no rely heavily on olfactory cues to detect their prey.

In fossil taxa, the gustation cannot be evaluated from taste buds, as they are not preserved (Schulp et al., 2005). However, because of a correlation between the size of the cranial nerves in vertebrates and their sensory development (Buttler and Hodos, 2005), the size of the cranial nerves associated to the gustation (VII, IX and X) could provide some clues about this sense in mosasauroids and plesiosaurians. Thus, the relative larger sizes of both facial (VII) and vagus (X) nerves in the mosasauroid *Tethysaurus* may suggest that gustation is more developed in this latter than in *Libonestes.* As gustation in reptiles is involved in the discrimination of palatable from unpalatable food once mouth or tongue contact occurs (Schwenk, 2008), such hypothesis could involve that *Tethysaurus* was a more specialist feeder than the supposed non-selective *Libonectes* (Noè et al., 2017).

10.2.2. Vision

It is generally admitted that optic lobes reconstructions offer the opportunity to consider the vision acuity in vertebrates (e.g., Nieuwenhuys et al., 1998; Wyneken, 2007). Indeed, as these structures receive mainly visual inputs from the retina through the optic (II) nerves (Butler and Hodos, 2005), the optic lobe size has been correlated to the importance of vision in different taxa (e.g., Pearson, 1972; Jerison, 1973; Butler and Hodos 2005; Franzosa, 2004).

From snake endocasts, it appears that all fossorial species have reduced optic lobes contrary to terrestrial and arboreal specimens (Allemand et al., 2017b, see Chapter 5). Since vision is better developed in arboreal snakes, and poorly developed in burrowing species as well as some aquatic species living in turbid waters (Lillywhite, 2014), the new snake data tend to confirm the link between the size of the optic tectum and the development of vision. In addition, several studies suggested that only the superficial layers of the optic lobes are related

to vision, whereas more internal layers are involved in auditory and somatosensory inputs (e.g., Buttler and Hodos, 2005). Thus, one of the major functions of the optic lobes is to localize a stimulus in space and to cause the involuntary reflex allowing the animal to turn its head and/or eyes in the direction of the source of the stimulus (Knudsen and Schwarz, 2017). Such reflex is of great immediate importance for animals. Their survival depending upon the speed and accuracy with which appropriate behaviors are executed in case of feeding or escape from a predator. In addition, the optic lobes should contribute to the control of spatial attention by signaling which stimulus, among all current stimuli, is of greatest immediate importance (Knudsen and Schwarz, 2017).

From endocast study, it is not possible to determine which layer of the optic lobe is more developed than another as only the external morphology of the structure is visible. The optic lobes in the mosasauroid *Tethysaurus* are not clearly differentiated and it is not possible to determine their limits and size. It seems thus difficult to discuss about any sensory inference in this species. On the contrary, the optic lobes in the plesiosaurian taxa studied here (*Libonectes* and a polycotylid) are well differentiated, forming a distinct bulge, from the rest of the endocast. Their relative large size would suggest well-developed abilities to localize preys or predators, from vision and/or auditory inputs.

Both *Tethysaurus* and *Libonectes* seem to rely mainly on vision to detect their prey rather than the olfaction. This could be related to the small size of their preys, more easily distinguishable from visual clues rather than olfactory ones. It would be interesting to reconstruct the endocast of the pliosaurid *Brachauchenius* in order to determine whether this large opportunist predator and possibly scavengers rely on the same clues to detect its prey.

The detection of food is the first step until its introduction in the mouth. Once the prey is detected, it is necessary to catch it. This next step involves the locomotor abilities. It is highly likely that the locomotor performance differs between plesiosaurians with their four paddle-limbs and the plesiopedal and hydropelvic mosasauroid *T. nopcsai*.

10.3. Prey approach via locomotion

10.3.1. Post-cranial skeleton evidences

In plesiosaurians, there has been a great deal of speculation about how they swam (Muscutt et al., 2017). Early work suggested that these taxa used a single forward-and-backward antero-posterior rowing stroke (e.g., Watson, 1924); however, it is today admitted that plesiosaurians used a mix involving antero-posterior rowing movements for the posterior limbs while anterior limbs performed an "underwater flight" defined by dorso-ventral movements (Carpenter et al. 2010; Muscutt et al., 2017). According to Carpenter et al. (2010), plesiosaurians swam with synchronized or nearly synchronized movements of the anterior and posterior limbs allowing to reach higher speed with less effort.

Although all plesiosaurians share a similar mode of locomotion based on hydrofoil-shaped limbs, differences about swimming speed, locomotor efficiency and manoeuvrability have been suggested between plesiosauromorph (i.e., long neck and small head) and pliosauromorph (i.e., short neck and large head) (e.g., Massare, 1988, 1994; O'Keefe, 2001). Thus, plesiosauromorphs have been inferred as cruising specialists rather than ambush predators, covering long distances while hunting at low to intermediate speeds, whereas pliosauromorphs have been presumed as pursuit predator possessing high speed, high manoeuvrability, but relatively low efficiency (O'Keefe, 2001). However, as the "dichotomy" between plesiosauromorph and pliosauromorph is actually a continuum (O'Keefe, 2001), and plesiosaurians body proportions vary between the two extremes, no generalization can be made through plesiosaurians taxa.

In Goulmima, the pliosaurid *Brachauchenius* reflects the pliosauromorph condition, and was probably able to reach high speed with a high manoeuvrability in order to pursue preys that were able to escape the attack. The elasmosaurid *Libonectes* illustrates the plesiosauromorph condition and may be considered as a cruising specialist, hunting at low to intermediate speed. This mode of locomotion might had allow to *Libonectes* to approach school of small bony fishes. Finally, as polycotylids in Goulmima have also an elongated neck (e.g., 30 cervical vertebrae in *Thililua*, Bardet et al., 2003a, they may have exhibited intermediate locomotor performances between *Brachauchenius* and *Libonectes*.

Among mosasauroids, the different morphotypes that have been recognized (see Chapter 1) illustrate progressive steps in the mosasauroid abilities for more energy-efficient swimming (Houssaye et al., 2013). Due to its hydropelvic and plesiopedal condition, *Tethysaurus* could be considered as an undulatory (anguilliform) swimmer or an axial subundulatory (subcarangiform) swimmer (Houssaye, 2013) and able to perform rapid acceleration for ambushed predation (Lingham-Soliar, 1991; Massare, 1994).

10.3.2. Endocranial evidences

Endocasts, as they offer the possibility to observe the cerebellum, could provide additional and complementary informations to the morphological study of the postcranial skeleton, about the locomotor abilities in fossil taxa. Indeed, although the cerebellum is multisensory and plays an important role in cognitive functions, such as integrates touch, proprioception, vision, hearing, and has a role in maintaining postural equilibrium (e.g., Wyneken, 2007), it also has a critical role in the locomotor behavior (e.g., Thach and Bastian, 2004; Buttler and Hodos, 2005). Among vertebrates, the cerebellum shows a great variability in size, shape and organization (Butler and Hodos, 2005). In non-avian reptiles, this structure generally has a modest size and forms a flat plate just posterior to the optic lobes. However, no explanation of the variation in relative size has been analyzed.

The cerebellum in *Tethysaurus* is not visible from its endocast. This characteristic is similar to that observed in varanids and snakes, for which this structure is covered by the venous system.

On the contrary, all plesiosaurian taxa here studied (*Libonectes*, polycotylid) (see Chapter 9) show a very large cerebellum that constitutes the main component of the brain endocast. The plesiosaurian cerebellum differs from all non-avian reptiles, including turtles that share a similar mode of locomotion (e.g., Carabajal et al., 2013; in press), or other highly aquatic extinct taxa such as ichthyosaurs (e.g., Marek et al., 2015). Since plesiosaurians probably used asynchronous movements (e.g., Carpenter et al., 2010; Liu et al., 2015) with their anterior and posterior limbs, the large cerebellum could be related to limb coordination requirements for more efficient swimming. However, such enlargement could be also related to the length of the

neck and its role in maintaining postural equilibrium and consideration of the endocast of short-necked taxa should allow to verify this hypothesis.

10.4. Trophic relationships in Goulmima

From morphological and endocranial evidences, it is possible to reconstruct the possible trophic relationships characterizing Goulmima (Fig. 10. 2). Marine reptiles in this area were nektonic predators and highly located in the trophic network. The pliosaurid *Brachauchenius* was probably the top-level predator (Fig. 10.1) due to its ability to hunt large-sized prey items and may have shared this place with large sharks (e.g., *Squalicorax* sp.). The elasmosaurid *Libonectes*, polycotylids, mosasauroid *Tethysaurus* and small sharks (e.g., sclerorhynchid saw sharks) were all primarily piscivores, belonging to the next level in the trophic structure, the quaternary consumers (Fig. 10.2). In this level, marine reptiles seem to exploit a wide range of food, including ammonites, soft-bodied invertebrates and bony fishes. The results obtained from the skull and tooth morphoguilds, indeed, reflect differences in prey preferences according to taxa. The mosasauroid *Tethysaurus* and the elasmosaurid *Libonectes* may have been specialized in the capture of soft-bodied invertebrates and small bony fishes located at the basis of the trophic chain, whereas the polycotylids may have fed on ammonites and medium-sized bony fishes. The avoidance of competition between *Libonectes* and *Tethysaurus* for small bony fishes could be related mainly to their different mode of locomotion and hunting techniques. Both taxa seem to rely more on visual clues than olfactory ones to interact with their environment (see Chapter 7 and 9). The generalist long-necked *Libonectes* was possibly a cruising specialist, hunting at low to intermediate speed, and using its long neck to approach and catch school of small bony fishes. Conversely, the more specialized mosasauroid *Tethysaurus* might have been an ambush predator, able to detect preys at close-range and to perform rapid acceleration to capture them. Integrative studies could be envisaged (e.g., geochemistry, Schulp et al., 2013, 2017; Martin et al., 2015) on the entire vertebrate fauna (osteichthyans, chondrichthyans, marine reptiles) and would allow to refine our knowledge of the trophic network of this exceptional Early Late outcrop.

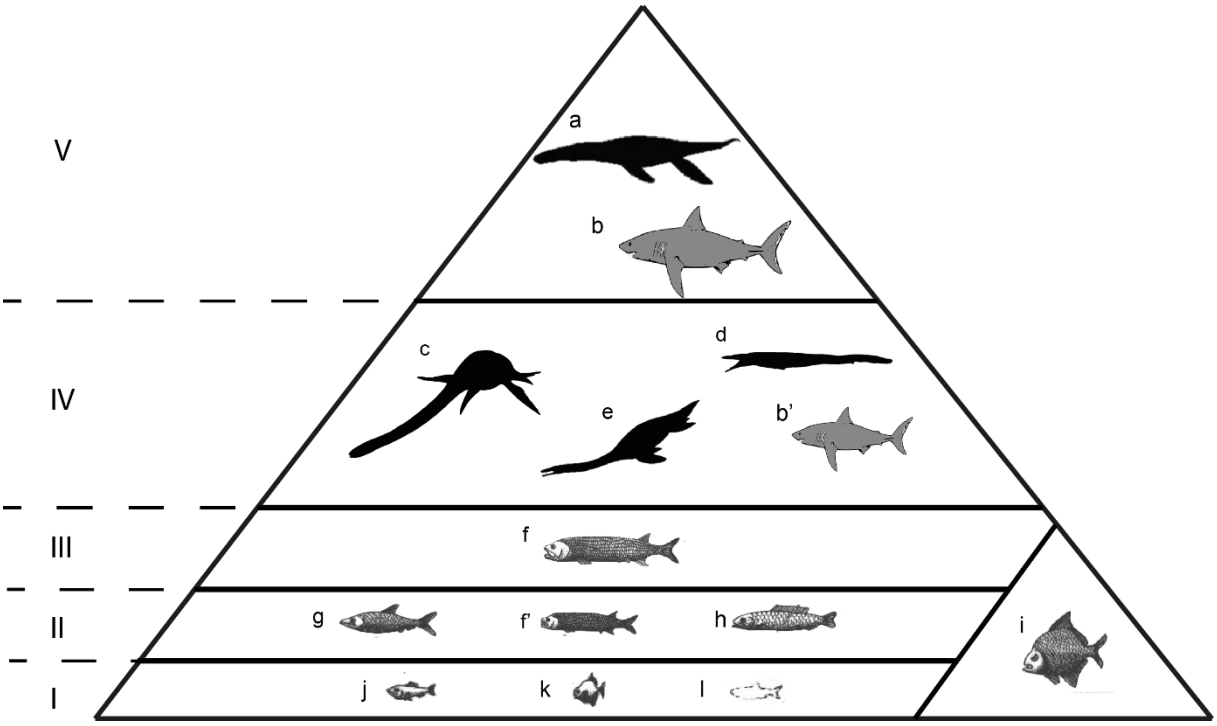

Fig. 10.2. Potential trophic relationships within the faunal assemblage of Goulmima (modified from Cavin, 1996). The triangles and the three levels represent the supposed trophic relationships and levels. **Abbreviations**: **a**, *Brachauchenius lucasi*; **b, b'**, sharks sp. (**b**, individuals of large size; **b'**, individuals of middle-small size); **c**, *Libonectes morgani*; **d**, *Tethysaurus nopcsai*; **e**, polycotylids; **f, f'**, Ichthyodectidae sp. (**f**, individuals of large size; **f'**, individuals of middle size); **g**, *Goulmimichthys arambourgi*; **h**, *Osmeroides* sp.; **i**, *Araripichthys* sp.; **j**, *Enchodus* sp.; **k**, Pycnodont sp.; **l**, indeterminate teleost.

Conclusions and Perspectives

Thanks to computed tomography, the endocranial anatomy of both mosasauroids and plesiosaurians, almost unknown until now, has been performed in details for the first time on the basis of exceptionally preserved specimens coming from the Turonian outcrop of Goulmima, Southern Morocco. These data set has been used to provide insights about their sensory abilities and thus to understand their cohabitation, interactions and niche partitioning. For comparative purpose, the endocranial anatomy of related extant squamates, mainly snakes but also varanids and amphisbaenians, also almost unknown until now, has been performed for the first time also and used to illustrate the form-function relationships associated to endocasts and to apprehend possible phylogenetic and ecological signals.

Concerning extant squamates, different methods were used to qualitatively and quantitatively describe the variability found in snake endocasts. Results show that, similarly as in mammals and birds, the snake endocast exhibits both phylogenetic and ecologic signals. Indeed, although phylogenetically related taxa share several similarities between each other in their endocranial morphologies, the shape of the endocast reflects some notable ecological trends: e.g., 1) fossorial species possess both reduced optic tectum and pituitary gland compared to arboreal and terrestrial species; 2) both fossorial and marine species have cerebral hemispheres poorly developed laterally compared to arboreal and terrestrial species; 3) cerebral hemispheres and optic tectum are more developed in arboreal and terrestrial species than in fossorial and marine species (Chapter 5). The amphisbaenian endocasts exhibit similar features as fossorial snakes, which could have either a phylogenetic meaning and/or reflect similar ecologic constraints (Chapter 6). In varanids, despite different ecologies, the endocranial anatomies exhibit a globally similar pattern (Chapter 6). This could be related to a strong phylogenetic signal and a weak ecological variability. The absence of a clear ecologic signal in the endocranial shape of varanids could be associated to their high ecological plasticity, two specimens studied here being found in terrestrial, arboreal and aquatic habitats).

Beyond the endocast shape-habitat relationships, the relative size of each structure composing the endocast has been used in order to perform sensory inferences. The large optic lobes observed in terrestrial and arboreal snakes were associated to the importance of vision for

these ecologies, whereas the absence of such a structure on the endocasts of fossorial taxa (snakes and amphisbaenians) was tentatively related to a poor development of their sight. The small olfactory bulbs in marine snakes were associated to their reduced olfactory abilities.

The mosasauroid endocranial and inner ear anatomy was studied for several specimens of the basal taxon *Tethysaurus nopcsai* (Chapter 7). The possible phylogenetic and ecologic signals associated to the mosasauroid endocast and inner ear were discussed based on comparisons with the little information available in the literature. The similarities observed between the endocasts of *Tethysaurus* and the mosasaurine *Clidastes* are assumed to reflect phylogenetic affinities between these two taxa, suggesting an alternative phylogenetic position (as a basal Mosasaurinae) from those already hypothesized (Bardet et al, 2003b; Bell and Polcyn, 2005; Caldwell and Palci, 2007); however, they could also reflect comparable lifestyle associated to habitat transition between nearshore and offshore environments. Conversely, the similarities observed in the inner ear morphology of *Tethysaurus* compared to that of *Platecarpus*, *Tylosaurus* and *Plioplatecarpus* could indicate a different phylogenetic signal that contradicts the results obtained from the endocast, revealing close phylogenetic affinities between *Tethysaurus* and russellosaurines such as suggested by Bell and Polcyn (2005). The growing number of studies on the vertebrate inner ear morphology (e.g., Mennecart and Costeur, 2016) has shown that this structure is strongly phylogenetically driven. Thus, in mosasauroids, the inner ear could reflect more a phylogenetic signal, whereas the endocast could reflect more an ecological signal.

The debate on the phylogenetic position of mosasaurs within squamates - lizards versus snakes - originated in the 19th century with the pioneering works of, on one hand, Camper (1800) and Cuvier (1808) and, on the other hand, Cope (1869) that brought mosasaurs closer to snakes and grouped them in a taxon he named Pythonomorpha. Since that time, some authors consider mosasauroids as closely related to varanids (e.g., Rieppel and Zaher, 2000a, b), while others argue for mosasauroids and snakes being phylogenetically close (e.g., Lee, 1997; Caldwell and Lee, 1997). In this context, quantitative and qualitative comparisons were performed between the endocast of *Tethysaurus* and those of both extant snakes and varanids. Our results show more similarities between *Tethysaurus* and varanids, especially on the organization of their cerebrum, optic lobes and pituitary bulbs. However, as some snakes may

also present a similar endocranial organization, the hypothesis of close affinities between varanids and mosasauroids based on endocranial data, stated by Camp (1942) has to be further tested. In addition, qualitative comparisons between the inner ear of *Tethysaurus* snakes and varanids revealed a morphology in *Tethysaurus* as distinct from snakes as from varanids.

Finally, although it has been difficult to delimit the different structures composing the endocast of *Tethysaurus*, comparisons with extant semi-aquatic crocodiles that show similar endocranial organization but large olfactory bulbs with a good sense of smell (Jirak and Janacek, 2017), could indicate that the relative small size of the olfactory bulbs in *Tethysaurus*, is related to poor olfactory abilities. This corroborates the hypothesis that mosasauroids relied more on visual clues (e.g., Polcyn, 2010) than on olfactory ones to interact with their environment.

During this PhD thesis, computed tomography was used to reconstruct and describe in detail the cranial morphology of three unpublished plesiosaurian specimens (Chapter 8). The new anatomical characters recorded for the specimen SMNS 81783, originally referred to *Libonectes atlasense* (Buchy, 2005), have allowed to re-assign it to *Libonectes morgani*, a North American taxon previously only known from the Late Cenomanian of Texas (Sachs and Kear, 2015). This greatly enlarges the palaeobiogeographical distribution of this species and reinforces the idea of the existence of a trans-Atlantic faunal connectivity between Goulmima and the Western Interior Seaway of North America (e.g., Cavin et al., 2010; Angst and Bardet, 2015). Additionally, the cranial morphology of D1-8213 and MNHN F-GOU14, have been reconstructed and their descriptions have allowed assigning them to *Libonectes morgani* and to an undetermined Polycotylidae respectively. It provides, furthermore, additional information about the plesiosaurian braincase, which remains generally poorly known due to either poor preservation and/or insufficient preparation, but which offers potentially a large number of characters to be used in phylogenetical analyses.

The plesiosauran endocranial anatomy was performed for the two elasmosaurid specimens referred to *Libonectes morgani* and the indeterminate polycotylid (Chapter 9). Plesiosaurians exhibit an endocranial morphology clearly differing from that of all other vertebrates. The interpretation of this unique morphology is difficult due to the lack of comparative data. Indeed, as no extant directly-related species exist for plesiosaurians and little

information has been published on the endocranial anatomy of sauropterygians, the impact of phylogenetic and ecologic signals cannot be considered in details. The unusual inner ear morphology observed in *Libonectes morgani* differing from that of the nearshore placodont *Placodus gigas* and possibly the plesiosaurian *Muraenosaurus leedsii*, could be associated to a more open-sea lifestyle. This hypothesis corroborates the large palaeobiogeographical distribution of *Libonectes morgani*.

Sensory inferences were deducted from the endocast of these three plesiosaurian specimens representing two different taxa of moderate- to long-necked plesiosaurians (elasmosaurids and polycotylids). The small size of the olfactory bulbs and the large relative size of the optic lobes could suggest that these plesiosaurian taxa might rely more on vision than on olfaction to interact with their environment. Their large cerebellum could be either related to their particular mode of locomotion, i.e., asynchronous movements with their anterior and posterior limbs, or associated to the length of their neck, playing a role in maintaining postural equilibrium.

These exceptionally preserved specimens of both mosasauroids and plesiosaurians from the Turonian outcrops of Goulmima have provided the opportunity to discuss the marine vertebrate trophic structure characterizing this marine environment (Chapter 10). Indeed, the new endocast data were added to information already available in the literature concerning the general morphology (skull shape, tooth morphoguilds, locomotion) of the marine reptiles and the associated fauna present in Goulmima, in order to depict the ecological options available for each marine reptile taxon. As a result, the pliosaurid *Brachauchenius* was probably the top-level predator due to its ability to hunt large-sized prey items, and may have share this place with large sharks also discovered in Goulmima. The elasmosaurid *Libonectes*, polycotylids, the mosasauroid *Tethysaurus* and small sharks, all primarily piscivores, belong to the next level in the trophic structure, the quaternary consumers. In this level, the results obtained from the skull shape and tooth morphoguilds reflect differences in prey preferences according to taxa. The mosasauroid *Tethysaurus* and the elasmosaurid *Libonectes* may have been specialized in the capture of soft-bodied invertebrates and small bony fishes located at the basis of the trophic chain, whereas the polycotylids may have fed on ammonites and medium-sized bony fishes. Although both the mosasauroid *Tethysaurus* and the elasmosaurid *Libonectes* probably show

preferences for small-sized bony fishes, they would be able to avoid direct competition thanks to different mode of locomotion and hunting techniques. The large cerebellum observed in the long-necked *Libonectes* (but also in the indeterminate polycotylid) could be related to high abilities in spatial orientation, navigation, prey detection and tracking allowing them to approach and catch school of small bony fishes. In the mosasauroid *Tethysaurus*, the size of cranial nerves related to gustation could suggest this species had a good sense of taste. Although this hypothesis is difficult to associate to a particular behavior, it could indicate that *Tethysaurus* detected preys mainly at close-range and corroborate an ambush predator lifestyle with abilities to perform rapid acceleration to capture preys.

The works performed during this PhD Thesis have permitted to obtain first results, on one hand about the endocranial anatomy of both mosasauroids and plesiosaurians, which constitute with the ichthyosaurians (e.g., Marek et al., 2015), the main clades of Mesozoic marine reptiles, and, on the other hand, about three different groups of extant squamates, for which the endocast has never been considered.

One of the first perspectives I proposed will be the inclusion of additional endocranial data for both extant and extinct groups.

Indeed, among fossil taxa, additional data would allow to replace the endocast in an evolutionary context. *Tethysaurus* being a basal moasauroid, it would be interesting to reconstruct the endocast of derived ones and "aigialosaurids" to consider the evolution of the endocast through their secondary adaptation of aquatic life. For the same purpose, the endocranial reconstructions of different taxa among sauropterygians, including plesiosaurians and Triassic forms, which both exhibit a wide range of different morphologies and habitats, would allow larger scale comparisons in order to distinguish which structures are preserved along the evolutionary history and which ones are modified for a specific ecologic adaptation. Such perspective could be expanded to several Mesozoic marine reptile taxa (e.g., mesosaurids, ichthyosaurians, turtles, crocodyliforms) in order to reinforce our knowledge about secondary adaptation to an aquatic environment, one of the most remarkable processes in Tetrapod evolution.

In extant taxa, additional endocranial data among squamates, but also within other non-avian reptiles (e.g., turtles, crocodiles) could allow large-scale endocranial comparisons, which

coupled to data on the skeletal morphology, could help to perform behavioral inferences and to interpret the endocast in fossil taxa. In addition to the endocast, it would be very interesting to simultaneously access to the brain. Indeed, a previously commonly estimation considers that the brain in non-avian reptiles occupies only 50% of the endocranial space (Hopson, 1979). Nowadays, though it is admitted that this ratio is far from representing a general pattern among these taxa (e.g., Kim and Evans, 2014), it has never been tested. Such relationships could be highlighted for different taxa but also through different ontogenetic stages. Because the morphological configuration of the brain is not fully reflected in the endocast, knowledge of the brain/endocast relationship should therefore provide important additional information to interpret the fossil endocasts.

Résumé étendu en français

Au cours du Mésozoïque, divers groupes de reptiles ont entrepris un spectaculaire retour à la vie aquatique et ont formé une composante importante des écosystèmes marins. Les mosasaures (Squamata) et plésiosaures (Sauropterygia) constituent deux clades majeurs au sein de ces reptiles marins. Durant le Crétacé supérieur, ces deux groupes de super-prédateurs marins ont coexisté comme l'atteste de nombreux gisements fossiles (e.g., Vincent et al., 2013). Ainsi leurs interactions et leurs places au sein des niches écologiques peuvent être questionnées. Bien que les adaptations des mosasaures et plésiosaures au milieu aquatique aient été largement étudiés au travers des modifications de leur squelette postcrânien, de leur physiologie (alimentation, reproduction, locomotion et thermorégulation) ou d'études micro-anatomiques et histologiques, très peu d'informations existent à propos de leurs capacités sensorielles accompagnant ce retour à la vie aquatique.

Durant ce travail doctoral, l'anatomie endocrânienne de spécimens exceptionnellement préservés de mosasaures et plésiosaures provenant des dépôts turoniens de Goulmima (Crétacé supérieur) a été reconstruite grâce à la microtomographie. L'anatomie endocrânienne de squamates actuels, principalement des serpents mais aussi des varans et amphisbènes, a également été étudiée afin d'apporter des nouvelles données sur cette structure également peu connue chez les reptiles non-aviens actuels, et de servir de base comparative.

Au sein des squamates actuels, différentes méthodes ont été utilisées afin de décrire qualitativement et quantitativement la variabilité trouvée dans les morphologies endocrâniennes. Les résultats montrent que la forme de l'endocrâne chez les serpents (Chapitre 5) reflète un signal phylogénétique mais également un signal écologique. Bien que les espèces proches phylogénétiquement présentent des endocrânes morphologiquement similaires, certaines tendances écologiques sont également décelées. Ainsi les endocrânes des serpents fouisseurs sont tous caractérisés par l'absence des lobes optiques et de l'hypophyse. Seules les espèces fouisseuses et marines présentent des hémisphères cérébraux peu étendus latéralement, alors que chez les espèces terrestres et arboricoles, les hémisphères cérébraux et les lobes optiques sont très développés. L'endocrâne des amphisbènes présente des similitudes avec les

serpents fouisseurs (Chapitre 6) qui pourraient suggérer d'étroites relations phylogénétique mais pourrait également être le reflet de contraintes écologiques similaires. Chez les varans, les endocrânes présentent un patron commun sans différences significatives bien que les taxons étudiés aient des écologies variables (Chapitre 6). Ceci pourrait refléter le fort impact du signal phylogénétique sur la morphologie de l'endocrâne des varans au dépend du signal écologique. Cependant l'absence d'un tel signal écologique pourrait être également dû au fait que les taxons étudiés présentent une forte plasticité écologique, étant capable de vivre à la fois dans des environnements terrestres, arboricoles et aquatiques.

La taille relative des structures composant l'endocrâne des squamates actuels a également été utilisé pour proposer des inférences sur leurs capacités sensorielles. Ainsi le développement des lobes optiques chez les serpents terrestres et arboricoles pourrait être associé à l'importance d'une bonne acuité visuelle pour ces écologies, alors que l'absence de tels lobes chez les espèces fouisseuses de serpents et d'amphisbènes pourrait être le reflet d'une acuité visuelle moindre. La petite taille des lobes olfactifs chez les serpents marins serait à associer avec des capacités olfactives peu développées.

L'anatomie endocrânienne et l'oreille interne des mosasaures a été étudiée au travers des reconstructions faites pour l'espèce basale *Tethysaurus nopcsai* (Chapitre 7). L'impact possible des signaux phylogénétiques et écologiques sur la morphologie de l'endocrâne et de l'oreille interne ont été discuté à partir du peu d'information déjà disponible sur ce sujet dans la littérature et du référentiel actuel développé dans cette thèse. Les similarités morphologiques observées entre les endocrânes de *Tethysaurus* et le mosasaurine *Clidastes* pourraient refléter une affinité phylogénétique entre ces deux taxons, suggérant une position phylogénétique alternative de ce qui a déjà été proposé (Bardet et al, 2003b; Bell and Polcyn, 2005; Caldwell and Palci, 2007). Cependant, une telle similarité pourrait être également le reflet d'un mode de vie similaire, à la fois côtiers et de pleine mer. Les ressemblances observées dans la morphologie de l'oreille interne de *Tethysaurus* avec les taxons *Platecarpus*, *Tylosaurus* et *Plioplatecarpus* sont en faveur d'une relation phylogénétique différente de celle exprimée par l'étude de l'endocrâne. En effet une telle ressemblance morphologique suggère de proches relations phylogénétiques entre *Tethysaurus* et les russellosaurines, et corroborent l'hypothèse déjà émise par Bell et Polcyn (2005).

Différentes études réalisées sur l'oreille interne des vertébrés ont montré que cette structure est fortement associée à un signal phylogénétique. Ainsi, chez les mosasaures, l'oreille interne refléterait plus un signal phylogénétique, alors que la morphologie de l'endocrâne exprimerait un signal plus écologique.

Le débat sur la position phylogénétique des mosasaures au sein des squamates trouve ses origines au cours du 19ème siècle. Les travaux pionniers de Camper (1800) et Cuvier (1808) proposèrent de placer les mosasaures en proche parents des varans, tandis que Cope (1869) suggéra une affinité phylogénétique entre les mosasaures et les serpents. Cette question n'est toujours pas résolue, les deux hypothèses étant encore soutenue dans la littérature (Lee, 1997 ; Caldwell and Lee, 1997 ; Rieppel and Zaher, 2000a, b,). Dans ce contexte, l'endocrâne de *Tethysaurus* a été comparé quantitativement et qualitativement à ceux des varans et des serpents. Nos résultats montrent que des ressemblances existent entre les morphologies endocrâniennes de *Tethysaurus* et des varans. Cependant, certains serpents présentent également une morphologie très ressemblante à celle de l'endorâne de *Tethysaurus*. Nos résultats montrent qu'une relation phylogénétique étroite entre les mosasaures et les varans argumentée par l'étude seule de l'endocrâne n'est pas envisageable ce qui contredit les hypothèses de Camp (1942). De plus, les comparaisons qualitatives entre les oreilles internes de *Tethysaurus*, serpents et varans montrent que l'oreille interne de *Tethysaurus* diffère autant de celles des varans que de celles des serpents.

Finalement, bien qu'il soit difficile de délimiter les différentes structures composant l'endocrâne de *Tethysaurus*, des comparaisons avec les crocodiles actuels présentant une organisation similaire est possible. Cependant, les crocodiles possèdent des bulbes olfactifs de grande taille associés à un sens de l'odorat développé contrairement à *Tethysaurus* où la petite taille des bulbes olfactifs serait par comparaison associée à des capacités olfactives diminuées. Cette hypothèse corrobore l'hypothèse que les mosasaures utilisent plus leur vision que l'olfaction pour interagir avec leur environnement.

Au cours de cette thèse, la microtomographie a été utilisée pour reconstruire et décrire en détail la morphologie crânienne de trois nouveaux spécimens de plésiosaures (Chapitre 8). Les nouveaux caractères anatomiques mis en évidence pour le spécimen SMNS 81783, auparavant référé à l'espèce *Libonectes atlasense* (Buchy, 2005), ont permis de réassigner ce

spécimen à *Libonectes morgani*, une espèce Nord-Américaine seulement connu dans le Cénomanien supérieur du Texas (Sachs and Kear, 2015). Un tel changement permet ainsi de grandement agrandir la distribution paleobiogéographique de cette espèce et renforce l'hypothèse d'une connexion transatlantique entre Goulmima et la mer intérieure nord-américaine (e.g., Cavin et al., 2010; Angst and Bardet, 2015). L'usage de la microtomographie a également permis de reconstruire l'anatomie crânienne de deux spécimens supplémentaires, D1-8213 et MNHN F-GOU14, dont la description a permis de les assigner respectivement à *Libonectes morgani* et à un polycotylidé indéterminé. De telles descriptions, fournissent des informations supplémentaires sur la boite crânienne des plésiosaures, une structure qui reste généralement assez méconnue car souvent mal préservée et/ou insuffisamment préparée, mais qui offre un grand nombre de caractères pouvant potentiellement être utilisés dans des analyses phylogénétiques.

L'anatomie endocrânienne des plésiosaures a été étudiée à partir des spécimens d'élasmosaures référés à *Libonectes morgani* et d'un polycotylidé indéterminé (Chapitre 9). Les plésiosaures présentent une morphologie endocrânienne très différente de tous les autres vertébrés qu'ils soient actuels ou fossiles. L'interprétation de cette morphologie unique est de ce fait difficile à cause de l'absence de données comparatives. Ceci peut s'expliquer par l'absence de descendant ou proche parent des plésiosaures dans le registre actuel ainsi que la pauvreté de la littérature associée à l'étude de l'anatomie endocrânienne des sauroptérygiens, il est difficile d'évaluer l'impact du signal phylogénétique et écologique sur la morphologie de l'endocrâne. L'oreille interne observée chez *Libonectes morgani* révèle une morphologie peu commune qui diffère de celle retrouvée chez le placodonte côtier *Placodus gigas* ainsi que celle reconstruite pour le plésiosaure *Muraenosaurus leedsii*. La morphologie de l'oreille interne chez *Libonectes* pourrait correspondre à un signal écologique différent et être associé à un mode de vie plus pélagique, en accord avec la grande répartition paléobiogéographique de cette espèce.

Des inférences sensorielles ont également été proposées à partir de leur morphologie endocrânienne. Ainsi, la petite taille des bulbes olfactifs et la présence de lobes optiques développés suggèrent que ces plésiosaures dépendaient plus de leur vision que de l'olfaction pour interagir avec leur environnement. L'important développement du cervelet chez ces taxons pourrait être associé à leur mode assez particulier de locomotion, caractérisé par des

mouvements asynchrones des membres antérieurs et postérieurs. Cependant, la taille de cette structure pourrait également être liée à la longueur du cou, les spécimens étudiés ici ayant tous un cou moyennement ou très allongé, le cervelet pouvant avoir un rôle dans le maintien de l'équilibre.

Ces spécimens exceptionnellement préservés de mosasaures et de plésiosaures ont fourni l'opportunité de discuter du réseau trophique caractérisant Goulmima au Turonien (Crétacé supérieur). Les données endocrâniennes ont été associées aux informations déjà disponibles concernant la morphologie générale (forme du crâne, morphologie des dents, locomotion) des reptiles marins et des faunes associées de Goulmima afin de présenter les options écologiques disponibles pour chaque taxon de reptiles marins. Nos résultats montrent que le pliosaure *Brachauchenius* était probablement le super-prédateur de cet environnement, capable d'ingurgiter des proies de grandes tailles. Il est probable que ce reptile marin ait partagé sa place de super-prédateur avec les grands requins qui ont été également retrouvés à Goulmima. L'élasmosaure *Libonectes*, les polycotylidés, le mosasaure *Tethysaurus*, ainsi que les plus petites formes de requins apparaissent tous piscivores et appartiennent au niveau suivant dans la chaine trophique. Les résultats obtenus à partir de l'étude de la forme du crâne et des morphologies dentaires montrent des préférences différentes dans les proies consommées selon les taxons. Le mosasaure *Tethysaurus* et l'élasmosaure *Libonectes* semblent spécialisés dans la capture d'invertébrés à corps mou et de petits poissons osseux retrouvés à la base de leur alimentation, alors que les polycotylidés semblent se nourrir d'ammonites et de proies de plus grosses tailles. Bien que le mosasaure *Tethysaurus* et l'élasmosaure *Libonectes* aient eu probablement une préférence pour le même type de proie, il est également possible qu'ils aient évité une compétition entre eux grâce à des modes de locomotion et de chasse différents. L'imposant cervelet retrouvé chez *Libonectes* suggère de hautes capacités dans l'orientation et la navigation permettant la détection et la poursuite des bancs de petits poissons. Le mosasaure *Tethysaurus*, pourrait avoir eu un sens du gout développé par rapport aux plésiosaures. Bien qu'une telle information soit difficile à associer à un comportement en particulier, cela pourrait indiquer que *Tethysaurus* détectait ses proies à une distance assez proche, et pourrait indiquer un mode de chasse basé sur l'embuscade.

Bibliography

Abele, A. 2017. Digital reconstruction of skull and endocranium of the Cretaceous ichthyosaur Platypterygius longmani from Australia, regarding sensory perception and internal structures. In O. Hampe, D. Schwarz and M. Voss (eds), 8th International meeting Secondary adaptation of Tetrapods to life in water, Berlin, Germany. Abstract book, pp. 41.

Adams, D. 1997. Trinacromerum bonneri, new species, last and fastest pliosaur of the Western Interior Seaway. Texas Journal of Science 49:179–198.

Adams, D. C. 2014. A generalized K statistic for estimating phylogenetic signal from shape and other high-dimensional multivariate data. Systematic Biology 63:685–697.

Agassiz, L. 1833. Recherches sur les Poissons Fossiles, Vol. I–V. Neuchâtel: Imprimaire de Petitpierre.

Ahrens, H. E. 2014. Morphometric study of phylogenetic and ecologic signals in Procyonid (Mammalia: Carnivora) endocasts: morphometrics of Procyonid endocasts. The Anatomical Record 297:2318–2330.

Albright III, L. B., D. D. Gillette, and A. L. Titus. 2007. Plesiosaurs from the Upper Cretaceous (Cenomanian–Turonian) tropic shale of southern Utah, part 2: polycotylidae. Journal of Vertebrate Paleontology 27:41–58.

Allemand, R., N. Bardet, A. Houssaye and P. Vincent. 2017a. Virtual re-examination of a plesiosaurian specimen (Reptilia, Plesiosauria) from the Late Cretaceous (Turonian) of Goulmima (Southern Morocco) thanks to computed tomography. Journal of Vertebrate Paleontology 37: doi:10.1080/02724634.2017.1325894.

Allemand, R., R. Boistel, Z. Blanchet, R. Cornette, N. Bardet, P. Vincent, and A. Houssaye. 2017b. Comparative morphology of snake (Squamata) endocasts: evidence of phylogenetical and ecological signals. Journal of Anatomy 2017:doi: 10.1111/joa.12692.

Allemand, R., P. Vincent, A. Houssaye, and N. Bardet. In press. New plesiosaurian specimens (Reptilia, Plesiosauria) from the Late Cretaceous (Turonian) of Goulmima (Southern Morocco). Cretaceous Research.

Anderson, C. L., G. W. Kabalka, D. G. Layne, J. P. Dyke, and G. M. Burghardt. 2000. Non-invasive high field MRI brain imaging of the Garter Snake (Thamnophis sirtalis). Copeia 2000:265–269.

Andrews, C. W. 1909. On some new Plesiosauria from the Oxford Clay of Peterborough. Annals and Magazine of Natural History, London 48:418–429.

Andrews, C. W. 1911. Description of a new plesiosaur (Plesiosaurus capensis, sp. nov.) from the Uitenhage Beds of Cape Colony. Annals of the South African Museum 1:309–322.

Andrews, C. W. 1913. A descriptive catalogue of the Marine Reptiles of the Oxford Clay. Based on the Leeds Collection in British Museum (Natural History), Part II. British Museum (Natural History), London, 206 pp.

Andrews, C. W. 1922. Description of a new plesiosaur from the Weald Clay of Berwick (Sussex). Quarterly Journal of the Geological Society of London 78:285–295.

Angst, D., and N. Bardet. 2015. A new record of the pliosaur Brachauchenius lucasi Williston, 1903 (Reptilia: Sauropterygia) of Turonian (Late Cretaceous) age, Morocco. Geological Magazine 153:449–459.

Araújo, R., M. J. Polcyn, A. S. Schulp, O. Mateus, L. L. Jacobs, A. O. Gonçalves, and M. L. Morais. 2015. A new elasmosaurid from the early Maastrichtian of Angola and the implications of girdle morphology on swimming style in plesiosaurs. Netherlands Journal of Geosciences 94:109–120.

Aristide, L., S. F. Dos Reis, A. C. Machado, I. Lima, R. T. Lopes, and S. I. Perez. 2016. Brain shape convergence in the adaptive radiation of New World monkeys. Proceedings of the National Academy of Sciences 113:2158–2163.

Atema, J. 1980. Chemical senses, chemical signals and feeding behavior in fishes. Fish Behaviour and its Use in the Capture and Culture of Fishes 12:57–101.

Aubret, F., X. Bonnet, M. Harris, and S. Maumelat. 2005. Sex differences in body size and ectoparasite load in the ball python, Python regius. Journal of Herpetology 39:315–320.

Aurboonyawat, T., V. Pereira, T. Kring, F. Toulgoat, A. Churojana, and P. Lasjaunias. 2008. Patterns of the Cranial Venous System from the Comparative Anatomy in Vertebrates: Part II. The Lateral-Ventral Venous System. Interventional Neuroradiology 14:21–31.

Balanoff, A. M., G. S. Bever, M. W. Colbert, J. A. Clarke, D. J. Field, P. M. Gignac, D. T. Ridgely, N. A. Smith, C. R. Torres, S. Walsh, and L. M. Witmer. 2015. Best practices for digitally constructing endocranial casts: examples from birds and their dinosaurian relatives. Journal of Anatomy 229:173–190.

Balanoff, A.M., and G. S. Bever. 2017. The Role of Endocasts in the Study of Brain Evolution, pp. 223–241. In J. Kaas (ed.), Evolution of Nervous Systems 2e. vol. 1, Oxford: Elsevier.

Bales, T. B. 2014. Proliferation, migration and survival of cells in the telencephalon of the ball python, Python regius. PhD Thesis, 131pp.

Balestrin, R. L., and L. H. Cappellari. 2011. Reproduction and feeding ecology of Amphisbaena munoai and Anops kingi (Amphisbaenia, Amphisbaenidae) in the Escudo Sul-Rio-Grandense, southern Brazil. Iheringia. Série Zoologia 101:93–102.

Bang, B. G. 1971. Functional anatomy of the olfactory system in 23 orders of birds. Acta anatomica 79:1–76.

Bang, B. G., and B. M. Wenzel. 1985. Nasal cavity and olfactory system. Form and function in birds 3:195–225.

Bardet, N., P. Godefroit, and J. Sciau. 1999. A new elasmosaurid plesiosaur from the Lower Jurassic of Southern France. Palaeontology 42:927–952.

Bardet, N., X. Pereda Suberbiola. 2002. Marine reptiles from the Late Cretaceous Phosphates of Jordan: palaeobiogeographical implications. Geodiversitas 24:831–839.

Bardet, N., and X. Pereda Suberbiola, and N. E. Jalil. 2003a. A new polycotylid plesiosaur from the Late Cretaceous (Turonian) of Morocco. Comptes Rendus Palevol 2:307–315.

Bardet, N., X. Pereda Suberbiola, and N. E. Jalil. 2003b. A new mosasauroid (Squamata) from the Late Cretaceous (Turonian) of Morocco. Comptes Rendus Palevol 2:607–616.

Bardet, N., A. Houssaye, J.-C. Rage, and X. Pereda Suberbiola. 2008. The Cenomanian–Turonian (Late Cretaceous) radiation of marine squamates (Reptilia): the role of the Mediterranean Tethys. Bulletin de la Société Géologique de France 179:605–22.

Bardet, N., J. Falconnet, V. Fischer, A. Houssaye, S. Jouve, X. Pereda Suberbiola, A. Pérez-Garcia, J.-C Rage, and P. Vincent. 2014. Mesozoic marine reptile palaeobiogeography in response to drifting plates. Gondwana Research 26:869–887.

Bardet, N., A. Houssaye, P. Vincent, X. Pereda Suberbiola, M. Amaghzaz, E. Jourani, and S. Meslouh. 2015. Mosasaurids (Squamata) from the Maastrichtian Phosphates of Morocco: Biodiversity, palaeobiogeography and palaeoecology based on tooth morphoguilds. Gondwana Research 27:1068–1078.

Barton, R. A., A. Purvis, and P. H. Harvey. 1995. Evolutionary radiation of visual and olfactory brain systems in primates, bats and insectivores. Philosophical Transactions of the Royal Society B 348:381–392.

Barton, R. A., and P. H. Harvey. 2000. Mosaic evolution of brain structure in mammals. Nature 405:1055–1058.

Basse, E., and G. Choubert. 1959. Les faunes d'ammonites du Cénomano-Turonien de la partie orientale du domaine Atlasique marocain et de ses annexes sahariennes. In L. B. Kellum (ed), El sistema cretácico. International Geological Congress 20:59–81.

Baur, G. H. 1890. On the characters andsystematic position of the large sea-lizards, Mosasauridae. Science 16:262–273.

Bell Jr, G. L., and J. E. Martin. 1995. Direct evidence of aggressive intraspecific competition in Mosasaurus conodon (Mosasauridae: Squamata). Journal of Vertebrate Paleontology 15:25–33.

Bell Jr, G. L. 1997. A phylogenetic revision of North American and Adriatic Mosasauroidea pp. 293–332 in J. M. Callaway and E. L. Nicholls (eds.), Ancient Marine Reptiles. San Diego Academic Press, California.

Bell Jr, G. L., and M. J. Polcyn. 2005. Dallasaurus turneri, a new primitive mosasauroid from the Middle Turonian of Texas and comments on the phylogeny of Mosasauridae (Squamata). Netherlands Journal of Geosciences 84:177–194.

Benson, R. B., and R. J. Butler. 2011a. Uncovering the diversification history of marine tetrapods: ecology influences the effect of geological sampling biases. Geological Society, London, Special Publications 358:191–208.

Benson, R. B. J., K. T. Bates, M. R. Johnson, and P. J. Withers. 2011b. Cranial anatomy of Thalassiodracon hawkinsii (Reptilia, Plesiosauria) from the Early Jurassic of Somerset, United Kingdom. Journal of Vertebrate Paleontology 31:562–574.

Benson, R. B. J., M. Evans, and P. S. Druckenmiller. 2012. High diversity, low disparity and small body size in Plesiosaurs (Reptilia, Sauropterygia) from the Triassic–Jurassic boundary. PLoS One 7: e31838.doi:10.1371/journal.pone.0031838.

Benson, R. B. J., H. F. Ketchum, D. Naish, and L. E. Turner. 2013. A new leptocleidid (Sauropterygia, Plesiosauria) from the Vectis Formation (Early Barremian–early Aptian; Early Cretaceous) of the Isle of Wight and the evolution of Leptocleididae, a controversial clade. Journal of Systematic Palaeontology 11:233–250.

Benson, R. B. J., and P. S. Druckenmiller. 2014. Faunal turnover of marine tetrapods during the Jurassic–Cretaceous transition. Biological Reviews 89:1–23.

Bernard, A., C. Lécuyer, P. Vincent, R. Amiot, N. Bardet, E. Buffetaut, G. Cuny, F. Fourel, F. Martineau, J. M. Mazin, and A. Prieur. 2010. Regulation of body temperature by some Mesozoic marine reptiles. Science 328:1379–1382.

Bernardo-Silva, J. S., E. M. Von-Mühlen, M. Di-Bernardo, and J. Ketterl. 2006. Feeding ecology in the small neotropical amphisbaenid Amphisbaena munoai (Amphisbaenidae) in southern Brazil. Iheringia. Série Zoologia 96:487–489.

Bever, G. S., C. J. Bell, and J. A. Maisano. 2005. The ossified braincase and cephalic osteoderms of Shinisaurus crocodilurus (Squamata, Shinisauridae). Palaeontologia Electronica 8:1–36.

Bienvenu, T., F. Guy, W. Coudyzer, E. Gilissen, G. Roualdes, P. Vignaud, and M. Brunet. 2011. Assessing endocranial variations in great apes and humans using 3D data from virtual endocasts. American Journal of Physical Anthropology 145:231–246.

de Blainville, H. D. 1835. Description de quelques espèces de reptiles de la Californie, précédée de l'analyse d'un système général d'Erpétologie et d'Amphibiologie. Nouvelles Annales du Muséum (national) d'Histoire Naturelle de Paris 4:233–296.

de Blainville, H. D. 1853. Lettre de Monsieur de Blainville, p.103–138. In E. Deslongchamps, Lettres sur les Crocodiles vivants et fossiles. Mémoires Société Linnéenne de Normandie 9, Caen.

Billet, G., L. Hautier, and R. Lebrun. 2015. Morphological diversity of the bony labyrinth (inner ear) in extant xenarthrans and its relation to phylogeny. Journal of Mammalogy 96:658–672.

Bjork, R. R. 1981. Food habits of mosasaurs from the Pierre Shale of South Dakota. Rocky Mountain Section, Geological Society of America, Abstracts with Programs 13:191–202.

Blomberg, S. P., T. Garland, and A. R. Ives. 2003. Testing for phylogenetic signal in comparative data: behavioral traits are more labile. Evolution 57:717–745.

Boistel, R., A. Herrel, R. Lebrun, R. Daghfous, P. Tafforeau, J. B. Losos, and B. Vanhooydonck. 2011. Shake rattle and roll: the bony labyrinth and aerial descent in Squamates. Integrative and Comparative Biology 51:957–968.

Brasier, M. D., D. B. Norman, A. G. Liu, L. J. Cotton, J. E. Hiscocks, R. J. Garwood, J. B Antcliffe, and D. Wacey. 2017. Remarkable preservation of brain tissues in an Early Cretaceous iguanodontian dinosaur. Geological Society, London, Special Publications 448:383–398.

Breazile, J. E., and H. G. Hartwig. 1989. Central nervous system, pp. 485–566. In: A. S. King, J. McLelland (eds) Form and function in birds. Academic, London.

Brischoux, F., and H. B. Lillywhite. 2011. Light- and flotsam-dependent 'float-and-wait' foraging by pelagic sea snakes (Pelamis platurus). Marine Biology 158:2343–2347.

Brochu, C. A. 2000. A digitally-rendered endocast for Tyrannosaurus rex. Journal of Vertebrate Paleontology 20:1–6.

Bronn, H. G. 1841. Über die fossilen Gaviale der Lias-Formation und der Oolithe. Archiv für Naturgeschichte, Berlin 8:77–82.

Brown, B. 1904. Stomach stones and food of plesiosaurs. Science 20:184–185.

Brown, D. S. 1981. The English Upper Jurassic Plesiosauroidea (Reptilia) and a review of the phylogeny and classification of the Plesiosauria. Bulletin of the British Museum (Natural History), Geology 35:253–347.

Brown, D. S. 1993. A taxonomic reappraisal of the families Elasmosauridae and Cryptoclididae (Reptilia: Plesiosauria). Revue de Paléobiologie 7:9–16.

Brown, D. S., P. Vincent, and N. Bardet. 2013. Osteological redescription of the skull of Microcleidus homalospondylus (Sauropterygia, Plesiosauria) from the Lower Jurassic of England. Journal of Paleontology 87:537–549.

Brusatte, S. L., A. Muir, M. T. Young, S. Walsh, L. Steel, and L. M. Witmer. 2016. The braincase and neurosensory anatomy of an Early Jurassic marine crocodylomorph: Implications for crocodylian sinus evolution and sensory transitions. The Anatomical Record 299:1511–1530.

Buchholtz, E. A., and E. A. Seyfarth. 1999. The gospel of the fossil brain: Tilly Edinger and the science of paleoneurology. Brain research bulletin 48:351–361.

Buchy, M. C. 2005. An elasmosaur (Reptilia: Sauropterygia) from the Turonian (Upper Cretaceous) of Morocco. Carolinea 63:5–28.

Buchy, M. C., F. Métayer, and E. Frey. 2005. Osteology of Manemergus anguirostris n. gen. et sp., a new plesiosaur (Reptilia, Sauropterygia) from the Upper Cretaceous of Morocco. Palaeontographica, Abteilung A 272:97–120.

Buchy, M. C., E. Frey, and S. W. Salisbury. 2006. The internal cranial anatomy of the Plesiosauria (Reptilia, Sauropterygia): evidence for a functional secondary palate. Lethaia 39:289–303.

Burish, M. J., H. Y. Kueh, and S. S. H. Wang. 2004. Brain architecture and social complexity in modern and ancient birds. Brain, Behavior and Evolution 63:107–124.

Butler, A. B., and R. G. Northcutt. 1973. Architectonic studies of the diencephalon of Iguana iguana (Linnaeus). Journal of Comparative Neurology 149:439–461.

Butler, A. B., and W. Hodos. 2005. Comparative Vertebrate Neuroanatomy: Evolution and Adaptation. John Wiley & Sons, Inc., Hoboken, NJ, USA, 744 pp.

Cabrera, A. 1941. Un plesiosaurio nuevo del Cretáceo del Chubut. Revisita del Museo de la Plata (Neuvo Serio) 2:113–130.

Caldwell, M. W., R. L. Carroll, and H. Kaiser. 1995. The pectoral girdle and forelimb of Carsosaurus marchesetti (Aigialosauridae), with a preliminary phylogenetic analysis of mosasauroids and varanoids. Journal of Vertebrate Paleontology 15:516–531.

Caldwell, M. W. 1997. Modified perichondral ossification and the evolution of paddle-like limbs in ichthyosaurs and plesiosaurs. Journal of Vertebrate Paleontology 17:534–547.

Caldwell, M. W., and M. S. Lee. 1997. A snake with legs from the marine Cretaceous of the Middle East. Nature 386:705–709.

Caldwell, M. W. 1999. Squamate phylogeny and the relationships of snakes and mosasauroids. Zoological Journal of the Linnean Society 125:115–147.

Caldwell, M. W., and M. S. Lee. 2001. Live birth in Cretaceous marine lizards (mosasauroids). Proceedings of the Royal Society of London B: Biological Sciences 268:2397–2401.

Caldwell, M. W., and A. Palci. 2007. A new basal mosasauroid from the Cenomanian (U. Cretaceous) of Slovenia with a review of mosasauroid phylogeny and evolution. Journal of Vertebrate Paleontology 27:863–883.

Camp, C. L. 1923 Classification of lizards. Bulletin of American Museum of Natural History 48:289–481.

Camp, C. L. 1942. California Mosasaurs. University of California Press, Berkeley and Los Angeles pp. 67.

Camper, A. G. 1800. Lettre de A.G. Camper à G. Cuvier, Sur les ossemens fossiles de la montagne de St. Pierre, à Maëstricht. J. Phys. Chim. Hist. Nat. 51:278–291.

Carabajal, A. P., J. Sterli, J. Müller, and A. Hilger. 2013. Neuroanatomy of the marine Jurassic turtle Plesiochelys etalloni (Testudinata, Plesiochelyidae). PLoS One 8:e69264.

Carabajal, A. P., and C. Succar. 2015. The endocranial morphology and inner ear of the abelisaurid theropod Aucasaurus garridoi. Acta Palaeontologica Polonica 60:141–144.

Carabajal, A. P., J. Sterli, J. Georgi, S. F. Poropat, and B. P. Kear. In press. Comparative neuroanatomy of extinct horned turtles (Meiolaniidae) and extant terrestrial turtles

(Testudinidae), with comments on the palaeobiological implications of selected endocranial features. Zoological Journal of the Linnean Society.

Carroll, R. L., and M. Debraga. 1992. Aigialosaurs: mid-Cretaceous varanoid lizards. Journal of Vertebrate Paleontology 12:66–86.

Carpenter, K. 1996. A review of short-necked plesiosaurs from the Cretaceous of the Western Interior, North America. Neues Jahrbuch für Geologie und Palaontologie 201:259–287.

Carpenter, K. 1997. Comparative cranial anatomy of two North American Cretaceous plesiosaurs; pp. 191–216 in J. M. Callaway and E. L. Nicholls (eds.), Ancient Marine Reptiles. San Diego Academic Press, California.

Carpenter, K. 1999. Revision of North American elasmosaurs from the Cretaceous of the Western Interior. Paludicola 2:148–173.

Carpenter, K., F. Sanders, B. Reed, J. Reed, and P. Larson. 2010. Plesiosaur swimming as interpreted from skeletal analysis and experimental results. Transactions of the Kansas Academy of Science 113:1–34.

Carril, J., C. P. Tambussi, F. J. Degrange, M. J. Benitez Saldivar, and M. B. J. Picasso. 2015. Comparative brain morphology of Neotropical parrots (Aves, Psittaciformes) inferred from virtual 3D endocasts. Journal of Anatomy 229:1–13.

Catania, K. C. 2011. The brain and behavior of the tentacled snake. Annals of the New York Academy of Sciences 1225:83–89.

Catania, K. C. 2012. Tactile sensing in specialized predators–from behavior to the brain. Current Opinion in Neurobiology 22:251–258.

Cavin, L. 1995. Goulmimichthys arambourgi n. g., n. sp., un Pachyrhizodontidae (Actinopterygii, Teleostei) d'une nouvelle localité a nodules fossilifères du Turonien inferieur marocain. Comptes Rendus de l'Académie des Sciences, Paris, Série IIa 32:1049–1054.

Cavin, L. 1996. Supposed and direct evidence of trophic relationships within the marine fish community from the Lower Turonian of Goulmima, Morocco. DGF Online Series, Geological Society of Denmark.

Cavin, L. 1997. Nouveaux Teleostei du gisement du Turonien inférieur de Goulmima (Maroc). Compte Rendus de l'Académie des Sciences de Paris 325:19–24.

Cavin, L. 1999. Occurrence of a juvenile teleost, Enchodus sp., in a fish gut content from the Upper Cretaceous of Goulmima, Morocco. Palaeontology 60:57–72.

Cavin, L., and D. B. Dutheil. 1999. A new Cenomanian ichthyofauna from southeastern Morocco and its relationships with other early Late Cretaceous Moroccan faunas. Geologie en Mijnbouw, 78:261–266.

Cavin, L. 2001. Osteology and phylogenetic relationships of the teleost Goulmimichthys arambourgi Cavin, 1995 from the Upper Cretaceous of Goulmima, Morocco. Eclogae Geologicae Helvetica 133:25–52.

Cavin, L., L. Boudad, S. Duffaud, L. Kabiri, J. Le Loeuff, I. Rouget, and H. Tong. 2001. L'évolution paléoenvironnementale des faunes de poissons du Crétacé supérieur du bassin du Tafilalt et des régions avoisinantes (Sud-Est du Maroc): implications paléobiogéographiques. Compte Rendu de l'Académie des Sciences de Paris, Sciences de la Terre et des planètes 333:677–683.

Cavin, L., H. Tong, L. Boudad, C. Meister, A. Piuz, J. Tabouelle, M. Aarab, R. Amiot, E. Buffetaut, G. Dyke, S. Hua, and J. Le Loeuff. 2010. Vertebrate assemblages from the early Late Cretaceous of southeastern Morocco: An overview. Journal of African Earth Sciences 57:391–412.

Chatterjee, S., and B. J. Small. 1989. New plesiosaurs from the Upper Cretaceous of Antarctica. Geological Society, London, Special Publications 47:197–215.

Cheng, Y. N., T. Sato, X. C. Wu, and C. Li. 2006. First complete pistosaurid from the Triassic of China. Journal of Vertebrate Paleontology 26:501–504.

Choubert, G. 1948. Essai sur la paléogéographie du Mésocrétacé marocain. Volume Jubilaire de la Société des Sciences Naturelles du Maroc 1:307–329.

Choubert, G., L. Clariond, and J. Hindermeyer. 1952. Livret-guide de l'excursion C 36. Anti-Atlas central et oriental. Congrès Géologique International, XIXe Session (Alger 1952), Série: Maroc, No. 11. Rabat, 89 p.

Choubert, G., and A. Faure-Muret. 1962. Évolution du domaine atlasique marocain depuis les temps paléozoïques. Livre à la mémoire du professeur Paul Fallot, tome 1. Bulletin de la Société Géologique de France Mémoire hors série 1–657.

Christensen, C. B., J. Christensen-Dalsgaard, C. Brandt, and P. Teglberg Madsen. 2012. Hearing with an atympanic ear: good vibration and poor sound-pressure detection in the royal python, Python regius. The Journal of Experimental Biology 215:331–342.

Chun, L., O. Rieppel, C. Long, and N. C. Fraser. 2016. The earliest herbivorous marine reptile and its remarkable jaw apparatus. Science Advances 25:e1501659.

Cicimurri, D. J., and M. J. Everhart. 2001. An elasmosaur with stomach contents and gastroliths from the Pierre Shale (Late Cretaceous) of Kansas. Transactions of the Kansas Academy of Science 104:129–143.

Claeson, K. M., C. J. Underwood, and D. J. Ward. 2013. † Tingitanius tenuimandibulus, a new platyrhinid batoid from the Turonian (Cretaceous) of Morocco and the cretaceous radiation of the Platyrhinidae. Journal of Vertebrate Paleontology 33:1019–1036.

Clarke, J., and S. Etches. 1992. Predation among Jurassic reptiles. Proceedings of the Dorset Natural History and Archaeological Society 113:202–205.

Clement, A. M., J. Nysjö, R. Strand, and P. E. Ahlberg. 2015. Brain–endocast relationship in the Australian lungfish, Neoceratodus forsteri, elucidated from tomographic data (Sarcopterygii: Dipnoi). PloS One 10:e0141277.

Clement, A. M., T. J. Challands, J. A. Long, and P. E. Ahlberg. 2016. The cranial endocast of Dipnorhynchus sussmilchi (Sarcopterygii: Dipnoi) and the interrelationships of stem-group lungfishes. PeerJ 4:e2539 https://doi.org/10.7717/peerj.2539.

Clemente, C. J., P. C. Withers, G. Thompson, and D. Lloyd. 2011. Evolution of limb bone loading and body size in varanid lizards. Journal of Experimental Biology 214:3013–3020.

Codorniú, L., A. P. Carabajal, D. Pol, D. Unwin, and O. W. Rauhut. 2016. A Jurassic pterosaur from Patagonia and the origin of the pterodactyloid neurocranium. PeerJ 4:e2311.

Colli, G. R., and D. S. Zamboni. 1999. Ecology of the worm-lizard Amphisbaena alba in the Cerrado of Central Brazil. Copeia 733–742.

Comeaux, R. S., J. C. Olori, and C. J. Bell. 2010. Cranial osteology and preliminary phylogenetic assessment of Plectrurus aureus Beddome, 1880 (Squamata: Serpentes: Uropeltidae). Zoological Journal of the Linnean Society 160:118–138.

Connolly, A. 2016. Exploring the Relationship between Paleobiogeography, Deep-Diving Behavior, and Size Variation of the Parietal Eye in Mosasaurs. Unpublished Master Thesis, University of Kansas.

Conrad, J. L. 2008. Phylogeny and systematics of Squamata (Reptilia) based on morphology. Bulletin of the American Museum of Natural History 310:1–182.

Cope, E. D. 1868. On new species of extinct reptiles. Proceedings of the Academy of Natural Sciences of Philadelphia 20:250–266.

Cope, E. D. 1869. Synopsis of the extinct Batrachia and Reptilia of North America. Transactions of the North American Philosophical Society 14:1–252.

Cope, E. D. 1871. Extinct Batrachia, Reptilia and Aves of North America. Transactions of the American Philosophical Society 14:1–253.

Cope, E. D. 1872. Note of some Cretaceous Vertebrata in the State Agricultural College of Kansas. Proc. Am. Phil. Soc. 12:168–170.

Corfield, J. R., J. M. Wild, S. Parsons, and M. F. Kubke. 2012. Morphometric analysis of telencephalic structure in a variety of Neognath and Paleognath bird species reveals regional differences associated with specific behavioral traits. Brain, Behavior and Evolution 80:181–195.

Corfield, J. R., K. Price, A. N. Iwaniuk, C. Gutierrez-Ibanez, T. Birkhead, and D. R. Wylie. 2015. Diversity in olfactory bulb size in birds reflects allometry, ecology and phylogeny. Frontiers in Neuroanatomy 9:doi:10.3389/fnana.2015.00102.

Cragin, F. W. 1888. Preliminary description of a new or little known saurian from the Benton of Kansas. American Geologist 2:404–407.

Crews, D., V. Hingorani, and R. J. Nelson. 1988. Role of the pineal gland in the control of annual reproductive behavioral and physiological cycles in the Red-Sided Garter Snake (Thamnophis sirtalis parietalis). Journal of Biological Rhythms 3:293–302.

Cruickshank, A. R I., P. G. Small, and M. A. Taylor. 1991. Dorsal nostrils and hydrodynamically driven underwater olfaction. Nature 352:62–64.

Cruickshank, A. R. I. 1997. A Lower Cretaceous pliosauroid from South Africa. Annals of the South African Museum 105:207–226.

Cruickshank, A. R., and R. E. Fordyce. 2002. A new marine reptile (Sauropterygia) from New Zealand: further evidence for a Late Cretaceous austral radiation of cryptoclidid plesiosaurs. Palaeontology 45:557–575.

Cuthbertson, R. S., H. C. Maddin, R. B. Holmes, and J. S. Anderson. 2015. The braincase and endosseous labyrinth of Plioplatecarpus peckensis (Mosasauridae, Plioplatecarpinae), with functional implications for locomotor behavior. The Anatomical Record 298:1597–1611.

Cuvier, G. 1804. Sur les espèces d'animaux dont proviennent les os fossiles répandus dans la pierre a plâtre des environs de Paris. Premier mémoire. Restitution de la tête. Annales du Museum National d'Histoire Naturelle 3:275–303.

Cuvier, G. 1808. Sur le grand animal fossile des carrières de Maestricht. Annales du Muséum d'Histoire naturelle 12:145–176.

Danilo, L., J. Remy, M. Vianey-Liaud, S. Mérigeaud, and F. Lihoreau. 2015. Intraspecific variation of endocranial structures in extant Equus: A prelude to endocranial studies in fossil Equoids. Journal of Mammalian Evolution 22:561–582.

Day, L. B., D. Crews, and W. Wilczynski. 1999a. Relative medial and dorsal cortex volume in relation to foraging strategy in congeneric lizards. Brain, Behavior and Evolution 54:314–322.

Day, L. B., D. Crews, and W. Wilczynski. 1999b. Spatial and reversal learning in congeneric lizards with different foraging strategies. Animal Behaviour 57:395–407.

Day, L. B., D. Crews, and W. Wilczynski. 2001. Effects of medial and dorsal cortex lesions on spatial memory in lizards. Behavioural Brain Research 118:27–42.

DeBraga, M., and R. L. Carroll. 1993. The origin of mosasaurs as a model of macroevolutionary patterns and processes, pp. 245–322. In M. K. Hecht, R. J. MacIntyre, and M. T. Clegg (eds) Evolutionary Biology, Evolutionary Biology, Springer US, Boston.

Decimo, I., G. Fumagalli, V. Berton, M. Krampera, and F. Bifari. 2012. Meninges: from protective membrane to stem cell niche. American journal of stem cells 1:92–105.

De Winter, W., and C. E. Oxnard. 2001. Evolutionary radiations and convergences in the structural organization of mammalian brains. Nature 409:710–714.

Dollo, L. 1882. Note sur l'ostéologie des Mosasauridae. Bulletin du Musée Royal d'Histoire Naturelle de Belgique 1:55–80.

Dollo, L. 1887. Le hainosaure et les nouveaux vertébrés fossiles du Musée de Bruxelles. Revue du Questions de Science 1:70–112.

Dozo, M. T., and G. Martínez. 2016. First digital cranial endocasts of Late Oligocene Notohippidae (Notoungulata): implications for endemic South American ungulates brain evolution. Journal of Mammalian Evolution 23:1–16.

Druckenmiller, P. S. 2002. Osteology of a new plesiosaur from the Lower Cretaceous (Albian) Thermopolis Shale of Montana. Journal of Vertebrate Paleontology 22:29–42.

Druckenmiller, P. S., and A. P. Russell. 2008a. Skeletal anatomy of an exceptionally complete specimen of a new genus of plesiosaur from the Early Cretaceous (Early Albian) of northeastern Alberta, Canada. Palaeontographica Abteilung A 283:1–33.

Druckenmiller, P. S., and A. P. Russell. 2008b. A phylogeny of Plesiosauria (Sauropterygia) and its bearing on the systematic status of Leptocleidus Andrews, 1922. Zootaxa 1863:1–120.

Dubar, G. 1949. Carte géologique provisoire du Haut Atlas de Midelt, échelle au 1/200 000e. Notice explicative, Notes et Mémoires du Service Géologique du Maroc, 59bis pp.1–60.

Dutchak, A. R. 2005. A review of the taxonomy and systematics of aigialosaurs. Netherlands Journal of Geosciences 84:221–229.

Dutchak, A. R., and M. W. Caldwell. 2009. A redescription of Aigialosaurus (= Opetiosaurus) bucchichi (Kornhuber, 1901) (Squamata: Aigialosauridae) with comments on mosasauroid systematics. Journal of Vertebrate Paleontology 29:437–452.

Eck, K., R. A. Elgin, and E. Frey. 2011. On the osteology of Tapejara wellnhoferi Kellner 1989 and the first occurrence of a multiple specimen assemblage from the Santana Formation, Araripe Basin, NE-Brazil. Swiss Journal of Palaeontology 130:1–16.

Edinger, T. 1921. Über Nothosaurus. I. Ein Steinkern der Schädelhöhle. Senckenbergiana 3:121–129.

Edinger, T. 1925a. Die Archaeopteryx. Natur und Museum 55:491–496.

Edinger, T. 1925b. Das Zentralnervensystem von Placodus gigas Ag. Abh. senckenb. naturf. Ges. 88:311–318.

Edinger, T. 1926. The brain of Archaeopteryx. Annals and Magazine of Natural History, Series 9 18:151–156.

Edinger, T. 1927. Das Gehirn der Pterosaurier. Zeitschrift für Anatomie und Entwicklungsgeschichte 83:105–112.

Edinger, T. 1928. Über einige fossile Gehirne. Paläontologische Zeitschrift 9:379–402.

Edinger, T. 1939. Two notes on the central nervous system of fossil Sirenia. Bull. Fac. Sci. Fouad I Univ. (Cairo) 19:43–57.

Edinger, T. 1940. The brains of three Pontian ovibovinae from China. Bull. Geol Inst. Uppsala 28:133–140.

Edinger, T. 1941. The brain of Pterodactylus. American Journal of Science 239:665–682.

Edinger, T. 1942. The pituitary body in giant animals fossil and living: a survey and a suggestion. The Quarterly Review of Biology 17:31– 45.

Edinger, T. 1948. Evolution of the horse brain. Geological Society of America Memoir 25:1–177.

Edinger, T. 1951. The brains of the Odontognathae. Evolution 5:6–24.

Edinger, T. 1955. Hearing and smell in cetacean history. Monatsschr. Psychiatrie Neurologie [Festschrift E. Grunthal] 129:37–58.

Edinger, T. 1962. Anthropocentric misconceptions in paleoneurology. Proceedings of the Rudolf Virchow Medical Society in the City of New York 19:55–107.

Edinger, T. 1975. Paleoneurology 1804-1966. An annotated bibliography. Advances in Anatomy, Embryology, and Cell Biology 49:1–258.

Eisthen, H. L., and K. Schwenk. 2008. The chemical stimulus and its detection, pp. 35–41 In J. G. M. Thewissen, and S. Nummela (eds.) Sensory evolution on the threshold: adaptations in secondarily aquatic vertebrates. University of California Press, Berkeley.

Erlström, M. and J. Gabrielson. 1992. Petrology, fossil composition and depositional history of the Ignaberga limestone, Kristianstad Basin, Scania. Sveriges Geologiska Undersökning Ca 80:1–30.

Estes, R., and E. E. Williams. 1984. Ontogenetic variation in the molariform teeth of lizards. Journal of Vertebrate Paleontology 4:96–107.

Estes, R., and G. K. Pregill. 1988. Phylogenetic Relationships of the Lizard Families: Essays Commemorating Charles L. Camp. Stanford, CA: Stanford University Press, pp. 631.

Ettachfini, E. M., and B. Andreu. 2004. Le Cénomanien et le Turonien de la plate-forme Préafricaine du Maroc. Cretaceous Research 25:277–302.

Evans, M. 1999. A new reconstruction of the skull of the Callovian elasmosaurid plesiosaur Muraenosaurus leedsii Seeley. Mercian Geologist 14:191–198.

Evans, D. C. 2005. New evidence on brain−endocranial cavity relationships in ornithischian dinosaurs. Acta Palaeontologica Polonica 50: 617–622.

Evans, M. 2012. A new genus of plesiosaur (Reptilia: Sauropterygia) from the Pliensbachian (Early Jurassic) of England, and a phylogeny of the Plesiosauria. Ph.D. dissertation, University of Leicester, 397 pp.

Everhart, M. J. 2002. New data on cranial measurements and body length of the mosasaur, Tylosaurus nepaeolicus (Squamata; Mosasauridae), from the Niobrara Formation of western Kansas. Transactions of the Kansas Academy of Science 105:33–43.

Everhart, M. J. 2004. Late Cretaceous interaction between predators and prey. Evidence of feeding by two species of shark on a mosasaur. PalArch, vertebrate palaeontology series 1:1–7.

Everhart, M. J. 2005. Oceans of Kansas—A Natural History of the Western Interior Sea. Indiana University Press, 320 pp.

Eyeson, K. N. 1971a. The role of the pituitary gland in testicular function in the lizard Agama agama. General and comparative endocrinology 16:342–355.

Eyeson, K. N. 1971b. Pituitary control of ovarian activity in the lizard, Agama agama. Journal of Zoology 165:367–372.

Fabre, A. C., D. Bickford, M. Segall, and A. Herrel. 2016. The impact of diet, habitat use, and behaviour on head shape evolution in homalopsid snakes. Biological Journal of the Linnean Society 118:634–647.

Farke, A. A. 2007. Reexamination of paleopathology in plesiosaurs and implications for behavioral interpretations. Journal of Vertebrate Paleontology 27:724–726.

Fernández, M. S., and Z. Gasparini. 2012. Campanian and Maastrichtian mosasaurs from Antarctic Peninsula and Patagonia, Argentina. Bulletin de la Société Géologique de France 183:93–102.

Ferrandini, M., J. Philip, J. F. Babinot, and G. Tronchetti. 1985. La plate-forme carbonatée du Cénomano–Turonien de la région d'Erfoud-Errechidia (Sud-Est marocain): stratigraphie et paléoenvironement. Bulletin de la Société Géologique de France 8:559–564.

Field, D. J., A. LeBlanc, A. Gau, and A. D. Behlke. 2015. Pelagic neonatal fossils support viviparity and precocial life history of Cretaceous mosasaurs. Palaeontology 58:401–407.

Foffa, D., J. Sassoon, A. R. Cuff, M. N. Mavrogordato, and M. J. Benton. 2014. Complex rostral neurovascular system in a giant pliosaur. Naturwissenschaften 101:453–456.

Forrest, R. 2000. A large rhomaleosaurid pliosaur from the Upper Lias of Rutland. Mercian Geologist 15:37–40.

Foureaux, G., M. I. Egami, C. Jared, M. M. Antoniazzi, R. C. Gutierre, and R. L. Smith. 2010. Rudimentary eyes of squamate fossorial reptiles (Amphisbaenia and Serpentes). The anatomical record 293:351–357.

Franzosa, J. W. 2004. Evolution of the brain in Theropoda (Dinosauria). Unpublished Ph.D. dissertation, The University of Texas at Austin, 381 pp.

Franzosa, J. W., and T. Rowe. 2005. Cranial endocast of the Cretaceous theropod dinosaur Acrocanthosaurus atokensis. Journal of Vertebrate Paleontology 25:859–864.

Friedman, D., and D. Crews. 1985. Role of the anterior hypothalamus–preoptic area in the regulation of courtship behavior in the male Canadian red-sided garter snake (Thamnophis sirtalis parietalis): Lesion experiments. Behavioral neuroscience 99:942–949.

Friedman, M. 2007. The interrelationships of Devonian lungfishes (Sarcopterygii: Dipnoi) as inferred from neurocranial evidence and new data from the genus Soederberghia Lehman, 1959. Zoological Journal of the Linnean Society 151:115–171.

Gale, A. S. 2000. The Cretaceous world, pp. 4–19. In: S. J. Culver, and P. F. Rawson (eds.) Biotic Response to Global Change: The Last 145 Million Years. Cambridge University Press, Cambridge.

Gale, A. S., W. J. Kennedy, and D. Martill. 2017. Mosasauroid predation on an ammonite–Pseudaspidoceras–from the Early Turonian of south-eastern Morocco. Acta Geologica Polonica 67:31–46.

Gasparini, Z. L., and D. Dellapé. 1976. Un nuevo cocodrilo marino (Thalattosuchia, Metriorhynchidae) de la Formacion Vaca Muerta (Jurasico, Titoniano) de la provincia de Neuquen. Actas I Congreso Geologico Chileno 1:1–21.

Gasparini, Z., L. Salgado, and S. Casadi. 2003a. Maastrichtian plesiosaurs from northern Patagonia. Cretaceous Research 14:157–170.

Gasparini, Z., N. Bardet, J. E. Martin, and M. Fernandez. 2003b. The elasmosaurid plesiosaur Aristonectes Cabrera from the latest Cretaceous of South America and Antarctica. Journal of Vertebrate Paleontology 23:104–115.

Gauthier, J. A., M. Kearney, J. A. Maisano, O. Rieppel, and A. D. B. Behlke. 2012. Assembling the squamate tree of life: Perspectives from the phenotype and the fossil record. Bulletin of the Peabody Museum of Natural History 53:3–308.

George, I. D., and C. M. Holliday. 2013. Trigeminal nerve morphology in Alligator mississippiensis and its significance for Crocodyliform facial sensation and evolution. The Anatomical Record 296:670–680.

Georgi, J. A. 2008. Semicircular canal morphology as evidence of locomotor environment in amniotes. PhD dissertation, New York: Stony Brook University, 235p.

Georgi, J. A., and J. Sipla. 2008. Comparative and functional anatomy of balance in aquatic reptiles and birds, pp. 233–256. In J. M. G. Thewissen, and S. Numella (eds) Sensory Evolution on the

Threshold: Adaptations in Secondarily Aquatic Vertebrates, Berkeley: University of California Press.

Giffin, E. B. 1989. Pacycephalosaur Paleoneurology (Archosauria: Ornithischia). Journal of Vertebrate Paleontology 9:67–77.

Gittleman, J. L. 1991. Carnivore olfactory bulb size: allometry, phylogeny and ecology. Journal of Zoology 225:253–272.

Gold, M. E. L., E. Bourdon, and M. A. Norell. 2016. The first endocast of the extinct dodo (Raphus cucullatus) and an anatomical comparison amongst close relatives (Aves, Columbiformes). Zoological Journal of the Linnean Society 177:950–963.

Goloboff, P. A., J. M. Carpenter, J. S. Arias, and D. R. M. Esquivel. 2008. Weighting against homoplasy improves phylogenetic analysis of morphological datasets. Cladistics 24:1–16.

Gomes, J. O., A. O. Maciel, J. C. Costa, and G. V. Andrade. 2009. Diet composition in two sympatric amphisbaenian species (Amphisbaena ibijara and Leposternon polystegum) from the Brazilian Cerrado. Journal of Herpetology 43:377–384.

Goodrich, E. S. 1930. Studies on the Structure and Development of Vertebrates. The University of Chicago Press, Chicago reprint 1986, 837 pp.

Goris, R. C. 2011. Infrared organs of snakes: An integral part of vision. Journal of Herpetology 45:2–14.

Greene, H. W., M. Fogden, and P. Fogden. 2000. Snakes: The Evolution of Mystery in Nature. University of California Press, 365pp.

Groβmann, F. 2007. Preliminary description and phylogenetic position of a new plesiosaur (Reptilia: Sauropterygia) from the Toarcian of Holzmaden, Germany. Journal of Paleontology 78:973–988.

Grohé, C., Z. J. Tseng, R. Lebrun, R. Boistel, and J. J. Flynn. 2016. Bony labyrinth shape variation in extant Carnivora: a case study of Musteloidea. Journal of anatomy 228:366–383.

Güntürkün, O., M. Stacho, and F. Ströckens. 2017. The Brains of Reptiles and Birds, pp. 171–221. In J. Kaas (ed.), Evolution of Nervous Systems 2e. vol. 1, Oxford: Elsevier.

Gunz, P., and P. Mitteroecker. 2013. Semilandmarks: a method for quantifying curves and surfaces. Hystrix, the Italian Journal of Mammalogy 24:103–109.

Hallermann, J. 1998. The ethmoidal region of Dibamus taylori (Squamata: Dibamidae), with a phylogenetic hypothesis on dibamid relationships within Squamata. Zoological Journal of the Linnean Society 122:385–426.

Halpern, M. 1980. The telencephalon of snakes, pp. 257–295. In S. O. E. Ebbesson (ed) Comparative Neurology of the telencephalon. Springer US.

Halpern, M., and N. Frumin. 1979. Roles of the vomeronasal and olfactory system in prey attack and feeding garter snakes. Physiology & Behavior 22:1183–1189.

Halpern, M., and J. L. Kubie. 1980. Chemical access to the vomeronasal organs of Garter snakes. Physiology & Behavior 24:367–371.

Hampe, O. 2005. Considerations on a Brachauchenius skeleton (Pliosauroidea) from the lower Paja Formation (late Barremian) of Villa de Leyva area (Colombia). Fossil record 8:37–51.

Harris, G. W., and B. T. Donovan. 1966. The pituitary gland: anterior pituitary. University of California Press, pp. 444–459.

Hays, G. C., S. Åkesson, A. C. Broderick, F. Glen, B. J. Godley, F. Papi, and P. Luschi. 2003. Island-finding ability of marine turtles. Proceedings of the Royal Society of London B: Biological Sciences 270:S5–S7.

Healy, S., and T. Guilford. 1990. Olfactory-bulb size and nocturnality in birds. Evolution 44:339–346.

Healy, S. D., and C. Rowe. 2007. A critique of comparative studies of brain size. Proceedings of the Royal Society of London B: Biological Sciences 274:453–464.

Heatwole, H. 1999. Sea snakes. Krieger Publishing Company, 148pp.

Hemilä, S., and T. Reuter. 2008. The physics and biolo gy of olfaction and taste, pp. 292–333. In J. G. M. Thewissen, and S. Nummela (eds.) Sensory evolution on the threshold: adaptations in secondarily aquatic vertebrates. University of California Press, Berkeley.

Herculano-Houzel, S. 2011. Scaling of brain metabolism with a fixed energy budget per neuron: implications for neuronal activity, plasticity and evolution. PloS One 6:e17514.

Herrera, Y., M. S. Fernández, and Z. Gasparini. 2013. The snout of Cricosaurus araucanensis: a case study in novel anatomy of the nasal region of metriorhynchids. Lethaia 46:331–340.

Herrera, Y. 2015. Metriorhynchidae (Crocodylomorpha: Thalattosuchia) from Upper Jurassic–Lower Cretaceous of Neuquén Basin (Argentina), with comments on the natural casts of the brain. Publicación Electrónica de la Asociación Paleontológica Argentina 15:159–171.

Holding, M. L., J. A. Frazier, E. N. Taylor, and C. R. Strand. 2012. Experimentally altered navigational demands induce changes in the cortical forebrain of free-ranging Northern Pacific Rattlesnakes (Crotalus o. oreganus). Brain, behavior and evolution 79:144–154.

Holloway, W. L., K. M. Claeson, and F. R. O' Keefe. 2013. A virtual phytosaur endocast and its implications for sensory system evolution in archosaurs. Journal of Vertebrate Paleontology, 33:848–857.

Hopson, J. A. 1977. Relative brain size and behavior in archosaurian reptiles. Annual Review of Ecology and Systematic 8:429–448.

Hopson, J. A. 1979. Paleoneurology, pp. 39–146. In C. Gans, R.G. Northcutt and P. Ulinski (eds) Biology of the Reptilia (Neurology A) vol 9. Academic Press, New York.

Hopson, J. A. 1980. Relative brain size in dinosaurs – implications for dinosaurian endothermy, pp. 211–236. In: R. D. Thomas, E. C. Olson (eds.), A Cold Look at the Warm-Blooded Dinosaurs. Westview Press, New Heaven.

Houssaye, A. 2009. "Pachyostosis" in aquatic amniotes: a review. Integrative Zoology, 4:325–340.

Houssaye, A., and N. Bardet. 2012. Rib and vertebral micro-anatomical characteristics of hydropelvic mosasauroids. Lethaia 45:200–209.

Houssaye, A., and N. Bardet. 2013. A baby mosasauroid (Reptilia, Squamata) from the Turonian of Morocco–Tethysaurus 'junior'discovered?. Cretaceous Research 46:208–215.

Houssaye, A. 2013. Palaeoecological and morphofunctional interpretation of bone mass increase: an example in Late Cretaceous shallow marine squamates. Biological Reviews 88:117–139.

Houssaye, A., R. Boistel, W. Böhme, and A. Herrel. 2013. Jack-of-all-trades master of all? Snake vertebrae have a generalist inner organization. Naturwissenschaften 100:997–1006.

Hsiang, A. Y., D. J. Field, T. H. Webster, A. D. Behlke, M. B. Davis, R. A. Racicot, and J. A. Gauthier. 2015. The origin of snakes: revealing the ecology, behavior, and evolutionary history of early snakes using genomics, phenomics, and the fossil record. BMC Evolutionary Biology 15:1–22.

Huene von F. 1936. Henodus chelyops, ein neuer Placodontier. Palaeontogr. Abt. A 84:99–147.

Hurlburt, G. R. 1996. Relative brain size in recent and fossil amniotes: determination and interpretation. Ph.D. dissertation, University of Toronto, Toronto, Canada, 250 pp.

Hurlburt, G. R., R. C. Ridgely, and L. M. Witmer. 2013. Relative size of brain and cerebrum in tyrannosaurid dinosaurs: an analysis using brain-endocast quantitative relationships in extant

alligators pp. 1–21. In J. M. Parrish, R. E. Molnar, P. J. Currie, and E. B. Koppelhus (eds) Tyrannosaurid Paleobiology, Bloomington: Indiana University Press.

Iwaniuk, A. N. 2001. Interspecific variation in sexual dimorphism in brain size in Nearctic ground squirrels (Spermophilus spp.). Canadian Journal of Zoology 79:759–765.

Iwaniuk, A. N., and J. E. Nelson. 2002. Can endocranial volume be used as an estimate of brain size in birds? Canadian Journal of Zoology 80:16–23.

Iwaniuk, A. N. 2017. Functional Correlates of Brain and Brain Region Sizes in Nonmammalian Vertebrates, pp. 335–348. In J. Kaas (ed.), Evolution of Nervous Systems 2e. vol. 1, Oxford: Elsevier.

Jacobs, L.L., O. Mateus, M. J. Polcyn, A. S. Schulp, M. T. Antunes, M. L. Morais, and T. Da Silva Tavares. 2006. The occurrence and geological setting of Cretaceous dinosaurs, mosasaurs, plesiosaurs, and turtles from Angola. Journal of the Paleontological Society of Korea 22:91–110.

Jerison, H. J. 1969. Brain evolution and dinosaur brains. The American Naturalist 103:575–588.

Jerison, H. 1973. Evolution of the brain and intelligence. Academic Press, New York, 482 pp.

Jerison, H. J. 1977. The theory of encephalization. Annals of the New York Academy of Sciences 299:146–160.

Jerison, H. J. 1985. Animal intelligence as encephalization. Philosophical Transactions of the Royal Society of London. Series B, Biological Sciences 308:21–34.

Jirak, D., and J. Janacek. 2017. Volume of the crocodilian brain and endocast during ontogeny. PloS one 12:e0178491.

Kawabe, S., T. Shimokawa, H. Miki, S. Matsuda, and H. Endo. 2013. Variation in avian brain shape: relationship with size and orbital shape. Journal of Anatomy 223:495–508.

Kawabe, S., S. Matsuda, N. Tsunekawa, and H. Endo. 2015. Ontogenetic shape change in the chicken brain: Implications for paleontology. PLoS One 10:e0129939.

Kear, B. P. 2004. Biogeographic and biostratigraphic implications of Australian Mesozoic marine reptiles. Australian Biologist 17:4–22.

Kear, B. P. 2005. A new elasmosaurid plesiosaur from the Lower Cretaceous of Queensland, Australia. Journal of Vertebrate Paleontology 25:792–805.

Kear, B. P. 2006. Plesiosaur remains from Cretaceous high-latitude non-marine deposits in southeastern Australia. Journal of Vertebrate Paleontology 26:196–199.

Kear B.P., N. I. Schroeder, and M. S. Y. Lee. 2006. An archaic crested plesiosaur in opal from the Lower Cretaceous high-latitude deposits of Australia. Biology Letters 2:615–619.

Kear, B. P., T. H. Rich, M. A. Ali, Y. A. Al-Mufarrih, A. H. Matiri, A. M. Masary, and Y. Attia. 2008. Late Cretaceous (Campanian–Maastrichtian) marine reptiles from the AdaffaFormation, NW Saudi Arabia. Geological Magazine 145:648–654.

Kear, B. P., and P. M. Barrett. 2011. Reassessment of the Lower Cretaceous (Barremian) pliosauroid Leptocleidus superstes Andrews, 1922 and other plesiosaur remains from the nonmarine Wealden succession of southern England. Zoological Journal of the Linnean Society 161:663–691.

Kear, B. P., B. Ekrt, J. Prokop, and G. L. Georgalis. 2014. Turonian marine amniotes from the Bohemian Cretaceous Basin, Czech Republic. Geological Magazine 151:183–198.

Kearney, M. 2003. Systematics of the Amphisbaenia (Lepidosauria: Squamata) based on morphological evidence from recent and fossil forms. Herpetological Monographs 17:1–74.

Kennedy, W. J., A. S. Gale, D. J. Ward, and C. J. Underwood. 2008. Early Turonian ammonites from Goulmima, southern Morocco. Bulletin de l'Institut Royal des Sciences Naturelles de Belgique 78:149–177.

Ketchum, H. F., and R. B. J. Benson. 2010. Global interrelationships of Plesiosauria (Reptilia, Sauropterygia) and the pivotal role of taxon sampling in determining the outcome of phylogenetic analyses. Biological Reviews 85:361–392.

Ketchum, H. F., and R. B. Benson. 2011. The cranial anatomy and taxonomy of Peloneustes philarchus (Sauropterygia, Pliosauridae) from the Peterborough Member (Callovian, middle Jurassic) of the United Kingdom. Palaeontology 54:639–665.

Kiliç, T., and A. Akakin. 2008. Anatomy of cerebral veins and sinuses. Frontiers of Neurology and Neuroscience 23:4–15.

Kim, R., and D. Evans D. 2014. Relationships among brain, endocranial cavity, and body sizes in reptiles. Society of Vertebrate Paleontology 74th Annual Meeting, Berlin, Germany pp.159.

Knapp, H., and D. S. Kang. 1968. The visual pathways of the snapping turtle (Chelydra serpentina). Brain, Behavior and Evolution 1:19–42.

Knoll, F., L. M. Witmer, F. Ortega, R. C. Ridgely, and D. Schwarz-Wings. 2012. The braincase of the basal sauropod dinosaur Spinophorosaurus and 3D reconstructions of the cranial endocast and inner ear. PLoS One 7:e30060.

Knudsen, E. I., and J. S. Schwarz. 2017. The Optic Tectum: A Structure Evolved for Stimulus Selection pp. 387–408, In J. Kaas (ed.), Evolution of Nervous Systems 2e. vol. 1, Oxford: Elsevier.

Koken, E. 1893. Beiträge zur Kenntnis der Gattung Nothosaurus. Zeitschrift der Deutschen Geologischen Gesellschaft 45:337–377.

Konishi, T., J. Lindgren, M. W. Caldwell, and L. Chiappe. 2012. Platecarpus tympaniticus (Squamata, Mosasauridae): osteology of an exceptionally preserved specimen and its insights into the acquisition of a streamlined body shape in mosasaurs. Journal of Vertebrate Paleontology 32:1313–1327.

Konishi, T., M. W. Caldwell, T. Nishimura, K. Sakurai, and K. Tanoue. 2016. A new halisaurine mosasaur (Squamata: Halisaurinae) from Japan: the first record in the western Pacific realm and the first documented insights into binocular vision in mosasaurs. Journal of Systematic Palaeontology 14:809–839.

Krebs, J. R., D. F. Sherry, S. D. Healy, V. H. Perry, and A. L. Vaccarino. 1989. Hippocampal specialization of food-storing birds. Proceedings of the National Academy of Sciences 86:1388–1392.

Krohmer, R. W., and D. Crews. 1987. Temperature activation of courtship behavior in the male red-sided garter snake (Thamnophis sirtalis parietalis): Role of the anterior hypothalamus-preoptic area. Behavioral neuroscience 101:228–236.

Krohmer, R. W., M. H. Boyle, D. I. Lutterschmidt, and R. T. Mason RT. 2010. Seasonal aromatase activity in the brain of the male red-sided garter snake. Hormones and Behavior 58:485–492.

Kubie, J. L., and M. Halpern. 1979. Chemical senses involved in Garter snake prey trailing. Journal of Comparative and Physiological Psychology 93:648–667.

Kubo, T., M. T. Mitchell, and D. M. Henderson. 2012. Albertonectes vanderveldei, a new elasmosaur (Reptilia, Sauropterygia) from the Upper Cretaceous of Alberta. Journal of Vertebrate Paleontology 32:557–572.

Labra, A., K. L. Voje, H. Seligmann, and T. F. Hansen. 2010. Evolution of the third eye: a phylogenetic comparative study of parietal-eye size as an ecophysiological adaptation in Liolaemus lizards. Biological journal of the Linnean Society 101:870–883.

Ladage, L. D., B. J. Riggs, B. Sinervo, and V. V. Pravosudov. 2009. Dorsal cortex volume in male side-blotched lizards (Uta stansburiana) is associated with different space use strategies. Animal behaviour 78:91–96.

Lanuza, E., and M. Halpern. 1997. Afferent and efferent connections of the nucleus sphericus in the snake Thamnophis sirtalis: Convergence of olfactory and vomeronasal information in the lateral cortex and the amygdala. The journal of Comparative Neurology 385:627–640.

Larsson, H. C., P. C. Sereno, and J. A. Wilson. 2000. Forebrain enlargement among nonavian theropod dinosaurs. Journal of Vertebrate Paleontology 20:615–618.

Lautenschlager, S., E. J. Rayfield, P. Altangerel, L. E. Zanno, and L. M. Witmer. 2012. The endocranial anatomy of Therizinosauria and its implications for sensory and cognitive function. PLoS One 7:e52289.

Lavocat, R. 1954. Reconnaissance géologique dans les Hammadas des confins algéro-marocains du Sud. Notes et Mémoires du Service Géologique du Maroc 2:116–147.

Lebedel, V., C. Lezin, B. Andreu, M. J. Wallez, E. M. Ettachfini, and L. Riquier. 2013. Geochemical and palaeoecological record of the Cenomanian–Turonian Anoxic Event in the carbonate platform of the Preafrican Trough, Morocco. Palaeogeography, Palaeoclimatology, Palaeoecology 369:79–98.

Lebedel, V., C. Lézin, B. Andreu, E. M. Ettachfini, and D. Grosheny. 2015. The upper Cenomanian–lower Turonian of the Preafrican Trough (Morocco): Platform configuration and palaeoenvironmental conditions. Journal of African Earth Sciences 106:1–16.

Lee, M. S. Y. 1997a. On snake-like dentition in mosasaurian lizards. Journal of Natural History 31:303–314.

Lee, M. S. 1997b. The phylogeny of varanoid lizards and the affinities of snakes. Philosophical Transactions of the Royal Society of London B: Biological Sciences 352:53–91.

Lee, M. S., and M. W. Caldwell. 1998. Anatomy and relationships of Pachyrhachis problematicus, a primitive snake with hindlimbs. Philosophical Transactions of the Royal Society B: Biological Sciences 353:1521–1552.

Lee, M. S., G. L. Bell Jr., and M. W. Caldwell. 1999. The origin of snake feeding. Nature 400:655–659.

Lee, M. S., and M. W. Caldwell. 2000. Adriosaurus and the affinities of mosasaurs, dolichosaurs, and snakes. Journal of Paleontology 74:915–937.

Lee, M. S., and J. D. Scanlon. 2002. Snake phylogeny based on osteology, soft anatomy and ecology. Biological Review 77:333–401.

Lee, M. S. 2005. Molecular evidence and marine snake origins. Biology Letters 1:227–230.

Lee, M. S., A. Palci, M. E. Jones, M. W. Caldwell, J. D. Holmes, and R. R. Reisz. 2016. Aquatic adaptations in the four limbs of the snake-like reptile Tetrapodophis from the Lower Cretaceous of Brazil. Cretaceous Research 66:194–199.

Lefebvre, L., N. Nicolakakis, and D. Boire. 2002. Tools and brains in birds. Behaviour 139:939–973.

Lefebvre, L., S. M. Reader, and D. Sol. 2004. Brains, innovations and evolution in birds and primates. Brain, Behavior and Evolution 63:233–246.

Lezin, C., B. Andreu, E. M. Ettachfini, M. J. Wallez, and V. Lebedel. 2010. Evolution biosédimentaires au Cénomanien supérieur et au Turonien dans le Sillon Préafricain (Maroc). Réunion des Sciences de la Terre. Bordeaux, France.

Lillywhite, H. B. 2014. How snakes work: structure, function, and behavior of the world's snakes. Oxford University Press, 256pp.

Lindgren, J., and M. Siverson. 2002. Tylosaurus ivoensis: a giant mosasaur from the early Campanian of Sweden. Earth and Environmental Science Transactions of the Royal Society of Edinburgh 93:73–93.

Lindgren, J., an M. Siverson. 2004. The first record of the mosasaur Clidastes from Europe and its palaeogeographical implications. Acta Palaeontologica Polonica 49:219–234.

Lindgren, J., M. W. Caldwell, and J. W. Jagt. 2008. New data on the postcranial anatomy of the California mosasaur Plotosaurus bennisoni (Camp, 1942) (Upper Cretaceous: Maastrichtian), and the taxonomic status of P. tuckeri (Camp, 1942). Journal of Vertebrate Paleontology 28:1043–1054.

Lindgren, J., M. J. Polcyn, and B. A. Young. 2011. Landlubbers to leviathans: evolution of swimming in mosasaurine mosasaurs. Paleobiology 37:445–469.

Lingham-Soliar, T. 1991. Mosasaurs from the upper Cretaceous of Niger. Palaeontology 34:653–670.

Lingham-Soliar, T. 1992. The tylosaurine mosasaurs (Reptilia, Mosasauridae) from the upper Cretaceous of Europe and Africa. Bulletin de l'Institut Royal des Sciences naturelles de Belgique, Sciences de la Terre 62:171–194.

Lingham-Soliar, T. 1994. The mosasaur Plioplatecarpus (Reptilia, Mosasauridae) from the Upper Cretaceous of Europe. Bulletin-Institut royal des sciences naturelles de Belgique. Sciences de la terre 64:177–211.

Lingham-Soliar, T. 1995. Anatomy and functional morphology of the largest marine reptile known, Mosasaurus hoffmanni (Mosasauridae, Reptilia) from the Upper Cretaceous, Upper Maastrichtian of the Netherlands. Philosophical Transactions of the Royal Society of London B: Biological Sciences 347:155–172.

Liu, S., A. S. Smith, Y. Gu, J. Tan, C. K. Liu, and G. Turk. 2015. Computer simulations imply forelimb-dominated underwater flight in plesiosaurs. PLoS computational biology 11:e1004605.

Liu, M., D. A. Reed, G. M. Cecchini, X. Lu, K. Ganjawalla, C. S. Gonzales, R. Monahan, X. Luan, and T. G. H. Diekwisch. 2016. Varanoid Tooth Eruption and Implantation Modes in a Late Cretaceous Mosasaur. Frontiers in physiology 7:doi:10.3389/fphys.2016.00145.

Longrich, N. R., B. A. S. Bhullar, and J. A. Gauthier. 2012. A transitional snake from the Late Cretaceous period of North America. Nature 488 :1–13.

López, P., A. Salvador, and J. Martín. 1998. Soil temperature, rock selection, and the thermal ecology of the amphisbaenian reptile Blanus cinereus. Canadian Journal of Zoology 76:673–679.

Lucas, S. G., A. P. Hunt, and R. Pence. 1988. Some Late Cretaceous reptiles from New Mexico. Contributions to Late Cretaceous paleontology and stratigraphy of New Mexico part III. New Mexico Bureau of Mines & Mineral Resources 122:49–60.

Lyras, G. A., and A. A. E. Van Der Geer. 2003. External brain anatomy in relation to the phylogeny of Caninae (Carnivora: Canidae). Zoological Journal of the Linnean Society 138:505–522.

Macrini, T. E., T. Rowe, and M. Archer. 2006. Description of a cranial endocast from a fossil platypus, Obdurodon dicksoni (Monotremata, Ornithorhynchidae), and the relevance of endocranial characters to monotreme monophyly. Journal of Morphology 267:1000–1015.

Macrini, T. E., T. Rowe, and J. L. VandeBerg. 2007. Cranial endocasts from a growth series of Monodelphis domestica (Didelphidae, Marsupialia): A study of individual and ontogenetic variation. Journal of Morphology 268:844–865.

Maisch, M. 1998. Notes on the cranial osteology of Muraenosaurus Seeley, 1874 (Sauropterygia, Jurassic), with special reference to the neurocranium and its implications for sauropterygian phylogeny. Neues Jahrbuch für Geologie und Paläontologie, Abhandlungen 207:207–253.

Makádi, L., M. W. Caldwell, and A. Ősi. 2012. The first freshwater mosasauroid (Upper Cretaceous, Hungary) and a new clade of basal mosasauroids. PLoS One 7:e51781.

Marek, R. D., B. C. Moon, M. Williams, and M. J. Benton. 2015. The skull and endocranium of a Lower Jurassic ichthyosaur based on digital reconstructions. Palaeontology 58:723–742.

Marino, L. 2002. Convergence of complex cognitive abilities in cetaceans and primates. Brain, Behavior and Evolution 59:21–32.

Marsh, O. C. 1872. Note on Rhinosaurus. American Journal of Science 4, 147pp.

Marsh, O. C. 1874. Small size of the brain in Tertiary mammals. American Journal of Science and Arts, Series 3 8:66–67.

Marsh, O. C. 1875. Notice of new Tertiary mammals, IV. American Journal of Science 51:239–250.

Marsh, O. C. 1877. Introduction and Succession of Vertebrate Life in America. American Journal of Science and Arts (1820-1879) 14:337–378.

Marsh, O. C. 1878. Brain of a Fossil Mammal. Nature 17:340–340.

Marsh, O. C. 1879. History and Methods of Paloeontological Discovery. American Journal of Science and Arts 18:323–359.

Marsh, O. C. 1880a. Odontornithes: a monograph on the extinct toothed birds of North America. Memoirs of the Peabody Museum of Yale College 1:1–201.

Marsh, O. C. 1880b. Principal characters of American Jurassic dinosaurs. III. American Journal of Science, Series 3 19:253–259.

Marsh, O. C. 1881. Principal characters of American Jurassic dinosaurs. IV. Spinal cord, pelvis, and limbs of Stegosaurus. American Journal of Science, Series 3 21:167–170.

Marsh, O. C. 1886. Dinocerata: a monograph of an extinct order of gigantic mammals. United States Geological Survey Monograph 10:1–243.

Marsh, O. C. 1887. American Jurassic Mammals. Geological Magazine 4:289–299.

Martill, D. M., H. Tischlinger, and N. R. Longrich. 2015. A four-legged snake from the Early Cretaceous of Gondwana. Science 349:416–419.

Martin, J. E., and R. R. Bjork. 1987. Gastric residues associated with a mosasaur from the late Cretaceous (Campanian) Pierre Shale in South Dakota. Dakoterra 3:68–72.

Martin, J. E. 2006. Biostratigraphy of the Mosasauridae (Reptilia) from the Cretaceous of Antarctica. Geological Society, London, Special Publications 258:101–108.

Martin, J. E., T. Tacail, S. Adnet, C. Girard, and V. Balter. 2015. Calcium isotopes reveal the trophic position of extant and fossil elasmobranchs. Chemical Geology 415:118–125.

Masai, H. 1973. Structural patterns of the optic tectum in Japanese snakes of the family Colubridae in relation to habit. Journal Für Hirnforschung 14:367–374.

Massare, J. A. 1987. Tooth morphology and prey preference of Mesozoic marine reptiles. Journal of Vertebrate Paleontology 7:121–137.

Massare, J. A. 1988. Swimming capabilities of Mesozoic marine reptiles: implications for method of predation. Paleobiology 14:187–205.

Massare, J. A. 1994. Swimming capabilities of Mesozoic marine reptiles: a review, pp. 133-149, in L. Maddock, Q. Bone and J. M. V. Rayner (eds) Mechanics and Physiology of Animal Swimming, Cambridge University Press.

McCurry, M. R., M. Mahony, P. D. Clausen, M. R. Quayle, C. W. Walmsley, T. S. Jessop, S. Wroe, H. Richards, and C. R. McHenry. 2015. The relationship between cranial structure, biomechanical performance and ecological diversity in varanoid lizards. PloS One 10:e0130625.

McDowell, S. B., and C. M. Bogert. 1954 The systematic position of Lanthanotus and the affinities of the anguinomorph lizards. Bulletin of the American Museum of Natural History 105:1–142.

McGowan, C. 1973. The cranial morphology of the Lower Liassic latipinnate ichthyosaurs of England. Bulletin of the British Museum (Natural History), Geology 24 :1–109.

McHenry, C. R., A. G. Cook, and S. Wroe. 2005. Bottom-feeding plesiosaurs. Science 310:75.

McHenry, C.R. 2009. "Devourer of Gods": the palaeoecology of the Cretaceous pliosaur Kronosaurus queenslandicus. PhD thesis, University of Newcastle.

McIntosh, A. P., K. Shimada, and M. J. Everhart. 2016. Late Cretaceous marine vertebrate fauna from the Fairport Chalk Member of the Carlile Shale in southern Ellis County, Kansas, USA. Transactions of the Kansas Academy of Science 119:222–230.

Mennecart, B., and L. Costeur. 2016. Shape variation and ontogeny of the ruminant bony labyrinth, an example in Tragulidae. Journal of anatomy 229:422–435.

Miller, L. R., and W. H. N. Gutzke. 1999. The role of the vomeronasal organ of crotalines (Reptilia: Serpentes: Viperidae) in predator detection. Animal Behaviour 58:53–57.

Milner, A. C., and S. A. Walsh. 2009. Avian brain evolution: new data from Palaeogene birds (Lower Eocene) from England. Zoological Journal of the Linnean Society 155:198–219.

Moreno, N., R. Morona, J. M. Lopez, and A. Gonzalez. 2017. The Diencephalon and Hypothalamus of Nonmammalian Vertebrates: Evolutionary and Developmental Traits pp. 409–426, In J. Kaas (ed.), Evolution of Nervous Systems 2e. vol. 1, Oxford: Elsevier.

Morgan III, D. J. 2016. Revision of polycotylid plesioaur systematics (sauropterygia, plesiosauria) and description of the axial osteology of a juvenile polycotylid. Theses, Dissertation and Capstones, Paper 1015, 141pp.

Morhardt, A.C., R. C. Ridgley, and L. M. Witmer. 2012. From endocast to brain: assessing brain size and structure in extinct archosaurs using gross anatomical brain region approximation (GABRA). Journal of Vertebrate Paleontology 32 Supplement Program and Abstracts, pp. 145.

Mosimann, J. E., and F. C. James. 1979. New Statistical Methods for Allometry with Application to Florida Red-Winged Blackbirds. Evolution 33:444–459.

Motani, R., N. Minoura, and T. Ando. 1998. Ichthyosaurian relationships illuminated by new primitive skeletons from Japan. Nature 393:255–257

Motani, R. 2009. The evolution of marine reptiles. Evolution: Education and Outreach, 2:224–235.

Motani, R. 2010. Warm-blooded “sea dragons”? Science 328:1361–1362.

Mulder, E. W. A. 2003. On latest Cretaceous tetrapods from the Maastrichtian type area. Publicaties van het Natuurhistorisch Genootschap in Limburg 44:1–188.

Müller, J. 2003. Early loss and multiple return of the lower temporal arcade in diapsid reptiles. Naturwissenschaften 90:473–476.

Münster, G. 1834. Vorläufige Nachrichtüber einigeneue Reptilien im Muschelkalke von Baiern. Neues Jahrbuch für die Mineralogie, Geognosie, Geologie und Petrefactenkunde 1834:521–527.

Muscutt, L. E., G. Dyke, G. D. Weymouth, D. Naish, C. Palmer, and B. Ganapathisubramani. 2017. The four-flipper swimming method of plesiosaurs enabled efficient and effective locomotion. In Proceeding of the Royal Society B 284:20170951.

Neenan, J. M., and T. M. Scheyer. 2012. The braincase and inner ear of Placodus gigas (Sauropterygia, Placodontia)—a new reconstruction based on micro-computed tomographic data. Journal of Vertebrate Paleontology 32:1350–1357.

Neenan, J. M., N. Klein, and T. M. Scheyer. 2013. European origin of placodont marine reptiles and the evolution of crushing dentition in Placodontia. Nature Communications 4:16–21.

Neenan, J. M., and R. B. J. Benson. 2017. Evolution of the Sauropterygian inner ear during the nearshore to open water transition. In O. Hampe, D. Schwarz and M. Voss (eds), 8th International meeting Secondary adaptation of Tetrapods to life in water, Berlin, Germany. Abstract book, pp. 33.

Nessov, L. A. 1995. Dinozavri severnoi Yevrazii: Novye dannye o sostave kompleksov, ekologii i paleobiogeografii. Institute for Scientific Research on the Earth's Crust, St. Petersburg State University, St. Petersburg, pp. 156.

Ngwenya, A., N. Patzke, P. R. Manger, and S. Herculano-Houzel. 2016. Continued growth of the central nervous system without mandatory addition of neurons in the Nile crocodile (Crocodylus niloticus). Brain, behavior and evolution 87:19–38.

Nicholls, E. L., and S. J. Godfrey. 1994. Subaqueous flight in mosasaurs-a discussion. Journal of Vertebrate Paleontology 14:450–452.

Nicholls, E. L., and M. Manabe. 2004. Giant ichthyosaurs of the Triassic, a new species of Shonisaurus from the Pardonet Formation (Norian: Late Triassic) of British Columbia. Journal of Vertebrate Paleontology 24:838–849.

Nieuwenhuys, R., H. J. ten Donkelaar, and C. Nicholson. 1998. The Central Nervous System of Vertebrates. Berlin: Springer, 2214pp.

Noè, L. F., M. A. Taylor, and M. Gómez-Pérez. 2017. An integrated approach to understanding the role of the long neck in plesiosaurs. Acta Palaeontologica Polonica 62:137–162.

Nopoulos, P., M. Flaum, D. O'Leary, andN. C. Andreasen. 2000. Sexual dimorphism in the human brain: evaluation of tissue volume, tissue composition and surface anatomy using magnetic resonance imaging. Psychiatry Research: Neuroimaging 98:1–13.

Northcutt, R. G. 2002. Understanding Vertebrate Brain Evolution. Integrative and Comparative Biology 42:743–756.

Novas, F. E., J. S. D'Angelo, J. P. O'Gorman, F. L. Agnolín, J. M. Lirio, and M. P. Isasi. 2015. First record of Polycotylidae (Sauropterygia, plesiosauria) from the Upper Cretaceous of Antarctica. Cretaceous Research 56:563–568.

O'Gorman, J. P., L. Salgado, E. B. Olivero, and S. A. Marenssi. 2015. Vegasaurus molyi, gen. et sp. nov. (Plesiosauria, Elasmosauridae), from the Cape Lamb Member (lower Maastrichtian) of the

Snow Hill Island Formation, Vega Island, Antarctica, and remarks on Wedellian Elasmosauridae. Journal of Vertebrate Paleontology 35:e931285. 2015.

O'Gorman, J. P., R. A. Otero, N. Hiller, J. Simes, and M. Terezow. 2017. Redescription of Tuarangisaurus keyesi (Sauropterygia; Elasmosauridae), a key species from the Uppermost Cretaceous of the Weddellian province: internal skull anatomy and phylogenetic position. Cretaceous Research 71:118–136.

O'Keefe, R. F. 2001. A cladistic analysis and taxonomic revision of the Plesiosauria (Reptilia: Sauropterygia). Acta Zoologica Fennica 213:1–63.

O'Keefe, F. R. 2002. The evolution of plesiosaur and pliosaur morphotypes in the Plesiosauria (Reptilia: Sauropterygia). Paleobiology 28:101–112.

O'Keefe, R. F. 2004. On the cranial anatomy of the polycotylid plesiosaurs, including new material of Polycotylus latipinnis, Cope, from Alabama, Journal of Vertebrate Paleontology 24:326–340.

O'Keefe, F. R., and M. T. Carrano. 2005. Correlated trends in the evolution of the plesiosaur locomotor system. Paleobiology 31:656–675.

O'Keefe, R. F. 2006. Morphologic and ontogenetic patterns in elasmosaur neck length, with comments on the taxonomic utility of neck length variables. Paludicola 5:207–229.

O'Keefe, F. R. 2008. Cranial anatomy and taxonomy of Dolichorhynchops bonneri new combination, a polycotylid (Sauropterygia: Plesiosauria) from the Pierre Shale of Wyoming and South Dakota. Journal of Vertebrate Paleontology 28:664–676.

O'Keefe, F. R., and L. M. Chiappe. 2011. Viviparity and K-selected life history in a Mesozoic marine plesiosaur (Reptilia, Sauropterygia). Science 333:870–873.

Olkowicz, S., M. Kocourek, R. K. Lučan, M. Porteš, W. T. Fitch, S. Herculano-Houzel, and P. Němec. 2016. Birds have primate-like numbers of neurons in the forebrain. Proceedings of the National Academy of Sciences 113:7255–7260.

Olori, J. C. 2010. Digital Endocasts of the Cranial Cavity and Osseous Labyrinth of the Burrowing Snake Uropeltis woodmasoni (Alethinophidia: Uropeltidae). Copeia 2010:14–26.

Openshaw, G. H., and J. S. Keogh 2014. Head shape evolution in monitor lizards (Varanus): interactions between extreme size disparity, phylogeny and ecology. Journal of evolutionary biology 27:363–373.

Orihuela, J. 2014. Endocranial morphology of the extinct Antillean shrew Nesophontes (Lipotyphla: Nesophontidae) from natural and digital endocasts of Cuban taxa. Palaeontologia Electronica 17:1–12.

Osmólska, H. 2004. Evidence on relation of brain to endocranial cavity in oviraptorid dinosaurs. Acta Palaeontologica Polonica 49:321–324.

Otero, R. A., S. Soto-Acuña, F. R. O'Keefe, J. P. O'Gorman, W. Stinnesbeck, M. E. Suárez, D. Rubilar-Rogers, C. Salazar, and L. A. Quinzio-Sinn. 2014. Aristonectes quiriquinensis, sp. nov., a new highly derived elasmosaurid from the upper Maastrichtian of central Chile. Journal of Vertebrate Paleontology 34:100–125.

Otero, R.A., J. P. O'Gorman, N. Hiller, F. R. O'Keefe, and R. E. Fordyce. 2016. Alexandronectes zealandiensis gen. et sp. nov., a new aristonectine plesiosaur from the lower Maastrichtian of New Zealand. Journal of Vertebrate Paleontology 36: e1054494.

Owen, R. 1838. A description of a specimen of the Plesiosaurus macrocephalus, Conybeare, in the collection of Viscount Cole. Transactions of the Geological Society of London, series 2 5:515–535.

Owen, R. 1860. On the orders of fossil and Recent Reptilia, and their distribution through time. Report of the British Association for the Advancement of Science 1859:153–166.

Owen, R. 1865. Monograph on the fossil Reptilia of the Liassic formations, Part.1: Sauropterygia. The Palaeontographical Society, London, 40 p.

Palci, A., and M. W. Caldwell. 2007. Vestigial forelimbs and axial elongation in a 95 million-year-old non-snake squamate. Journal of Vertebrate Paleontology 27:1–7.

Palci, A., M. W. Caldwell, and C. A. Papazzoni. 2013. A new genus and subfamily of mosasaurs from the Upper Cretaceous of northern Italy. Journal of Vertebrate Paleontology 33:599–612.

Palci, A., M. N. Hutchinson, M. W. Caldwell, and M. S. Lee. 2017. The morphology of the inner ear of squamate reptiles and its bearing on the origin of snakes. Open Science 4:10.1098/rsos.170685.

Parsons, T. S. 1959. Nasal anatomy and the phylogeny of reptiles. Evolution 13:175–187.

Patterson, C. 1975. The braincase of pholidophorid and leptolepid fishes, with a review of the actinopterygian braincase. Philosophical Transactions of the Royal Society of London B 269:282–283.

Pearson, R. G. 1972. The Cerebellum, pp. 235–279. In: R. G. Pearson (ed) The Avian Brain, New York: Academic Press.

Persson, P. O. 1963. A revision of the classification of the Plesiosauria with a synopsis of the stratigraphical and geographical distribution of the group. Lunds Universitets Arsskrift, N. F. Avdelningen 2:1–59.

Pianka, E. R. 1995. Evolution of body size: varanid lizards as a model system. The American Naturalist 146:398–414.

Pianka, E., and King. 2004. Varanoid lizards of the world. Indiana University Press, 577pp.

Picasso, M. B., C. Tambussi, and M. T. Dozo. 2009. Neurocranial and brain anatomy of a Late Miocene eagle (Aves, Accipitridae) from Patagonia. Journal of Vertebrate Paleontology 29:831–836.

Picasso, M. B., C. Tambussi, and F. J. Degrange. 2010. Virtual reconstructions of the endocranial cavity of Rhea americana (Aves, Palaeognathae): postnatal anatomical changes. Brain, behavior and evolution 76:176–184.

Pierce, S. E., and M. W. Caldwell. 2004. Redescription and phylogenetic position of the Adriatic (Upper Cretaceous; Cenomanian) dolichosaur Pontosaurus lesinensis (Kornhuber, 1873). Journal of Vertebrate Paleontology 24:373–386.

Pierce, S. E., K. D. Angielczyk, and E. J. Rayfield. 2008. Patterns of morphospace occupation and mechanical performance in extant crocodilian skulls: a combined geometric morphometric and finite element modeling approach. Journal of Morphology 269:840–864.

Pierce, S. E., M. Williams, and R. B. Benson. 2017. Virtual reconstruction of the endocranial anatomy of the early Jurassic marine crocodylomorph Pelagosaurus typus (Thalattosuchia). PeerJ 5:e3225.

Polcyn, M. J. 2010. Sensory adaptations in mosasaurs. Journal of Vertebrate Paleontology 30:146A.

Polcyn, M. J., L. L. Jacobs, R. Araújo, A. S. Schulp, and O. Mateus. 2014. Physical drivers of mosasaur evolution. Palaeogeography, Palaeoclimatology, Palaeoecology 400:17–27.

Pooley, A. C., and C. Gans. 1976. The nile crocodile. Scientific American, 234:114–125.

Polyak, S. L. 1957. The vertebrate visual system. University of Chicago Press.

Porter, W. R., and L. M. Witmer. 2015. Vascular Patterns in Iguanas and Other Squamates: Blood Vessels and Sites of Thermal Exchange. PLoS One 10:e0139215.

Pradel, A., M. Langer, J. G. Maisey, D. Geffard-Kuriyama, P. Cloetens, P. Janvier, and P. Tafforeau. 2009. Skull and brain of a 300-million-year-old chimaeroid fish revealed by synchrotron holotomography. Proceedings of the National Academy of Sciences 106:5224–5228.

Proffitt, J. V., J. A. Clarke, and R. P. Scofield. 2016. Novel insights into early neuroanatomical evolution in penguins from the oldest described penguin brain endocast. Journal of anatomy 229:228–238.

Pyron, R. A., F. T. Burbrink, G. R. Colli, A. N. Montes de Oca, L. J. Vitt, C. A. Kuczynski, and J. J. Wiens. 2011. The phylogeny of advanced snakes (Colubroidea), with discovery of a new subfamily and comparison of support methods for likelihood trees. Molecular Phylogenetics and Evolution 58:329–342.

Quay, W. B. 1979. The parietal eye-pineal complex, pp. 245–406 In Gans, C., Northcutt, R.G., Ulinski, P. (eds) Biology of the Reptilia (Neurology A), Academic Press, London, New York and San Francisco.

R Development Core Team. 2008. R: A language and environment for statistical computing. R Foundation for Statistical Computing, Vienna, Austria. ISBN 3-900051-07-0, http://www.R-project.org.

Racicot, R. A., and M. W. Colbert. 2013. Morphology and Variation in Porpoise (Cetacea: Phocoenidae) Cranial Endocasts. The Anatomical Record 296:979–992.

Radinsky, L. B. 1973a. Evolution of the canid brain. Brain, Behavior and Evolution 7:169 –202.

Radinsky, L. B. 1973b. Are stink badgers skunks? Implications of neuroanatomy for mustelid phylogeny. Journal of Mammalogy 54:585–593

Radinsky, L. B. 1975. Viverrid neuroanatomy: phylogenetic and behavioral implications. Journal of Mammalogy 56:130–150.

Radinsky, L. 1978. Evolution of brain size in carnivores and ungulates. The American Naturalist 112:815–831.

Rasmussen, A. R., J. C. Murphy, M. Ompi, J. W. Gibbons, and P. Uetz. 2011. Marine Reptiles. PLoS One 6:doi:10.1371/journal.pone.0027373.

Reeder, T. W., T. M. Townsend, D. G. Mulcahy, B. P. Noonan, P. L. Wood Jr, J. W. Sites Jr, and J. J. Wiens. 2015. Integrated analyses resolve conflicts over squamate reptile phylogeny and reveal unexpected placements for fossil taxa. PLoS One 10:e0118199.

Reiss, J. O., and H. L. Eisthen. 2008. Comparative anatomy and physiology of chemical senses in amphibians, pp. 43–63. In J. G. M. Thewissen, and S. Nummela (eds.) Sensory Evolution on the Threshold: Adaptations in Secondarily Aquatic Vertebrates. University of California Press, California.

Réperant, J., J. P. Rio, R. Ward, S. Hergueta, D. Micell, and M. Lemire. 1992. Comparative Analysis of the Primary Visual System of Reptiles pp. 175–240. In C. Gans and P. S. Ulinski (eds) Sensory Integration. Biology of Reptilia, (Neurology 7C). The University of Chicago Press.

Rieppel, O. 1979. The braincase of Typhlops and Leptotyphlops (Reptilia: Serpentes). Zoological Journal of the Linnean Society 65:161–176.

Rieppel, O. 2000. Sauropterygia I: Placodontia, Pachypleurosauria, Nothosauria, Pistosauroidea, pp. 1–134. In P. Wellnhofer (ed) Encyclopedia of palaeoherpetology, vol 12A, Munich.

Rieppel, O., and H. Zaher. 2000a. The braincases of mosasaurs and Varanus, and the relationships of snakes. Zoological Journal of the Linnean Society 129:489–514.

Rieppel, O. and H. Zaher. 2000b. The intramandibular joint in squamates, and the phylogenetic relationships of the fossil snake Pachyrhachis problematicus Haas. Fieldiana (Geology) New Serie 43:1–69.

Rieppel, O., and H. Zaher. 2001. Re-building the bridge between mosasaurs and snakes. Neues Jahrbuch fur Geologie und Palaontologie Abhandlungen 221:111–132.

Rieppel, O., P. M. Sander, and G. W. Storrs. 2002. The skull of the pistosaur Augustasaurus from the Middle Triassic of northwestern Nevada. Journal of Vertebrate Paleontology 22:577–592.

Rieppel, O., and J.A. Maisano. 2007. The skull of the rare Malaysian snake Anomochilus leonardi Smith, based on high-resolution X-ray computed tomography. Zoological Journal of the Linnean Society 149:671–685.

Robinson, J. A. 1975. The locomotion of plesiosaurs. Neues Jahrbuch fur Paläontologie, Abhandlugen 149:286–332.

Rodda, G. H., T. H. Fritts, M. J. McCoid, and E. W. Campbell III. 1999. An Overview of the Biology of the Brown Treesnake (Boiga irregularis), a Costly Introduced Pest on Pacific Islands. In G. H. Rodda, Y. Sawai, D. Chiszar, and H. Tanaka (eds) Problem snake management: the habu and the brown treesnake. Cornell University Press, Ithaca, NY, 534pp.

Rogers, S. W. 1999. Allosaurus, crocodiles, and birds: evolutionary clues from spiral computed tomography of an endocast. The Anatomical Record 257:162–173.

Rogers, S. W. 2005. Reconstructing the behaviors of extinct species: an excursion into comparative paleoneurology. American Journal of Medical Genetics Part A 134:349–356.

Rohlf, F.J., and D. Slice. 1990. Extensions of the Procrustes method for the optimal superimposition of landmarks. Systematic Biology 39:40–59.

Ronander, P. 2007. A description and phylogenetic relationship of a polycotylid plesiosaur (Reptilia: Sauropterygia) from the Upper Cretaceous (Turonian) of Goulmima, Morocco. Master Thesis, University of Oslo, Sweden, 49p.

Roscito, J. G., and M. T. Rodrigues. 2010. Comparative cranial osteology of fossorial lizards from the tribe Gymnophthalmini (Squamata, Gymnophthalmidae). Journal of morphology 271:1352–1365.

Roth, E. D., W. I. Lutterschmidt, and D.A. Wilson. 2006. Relative Medial and Dorsal Cortex Volume in Relation to Sex Differences in Spatial Ecology of a Snake Population. Brain Behavior and Evolution 67:103–110.

Rothschild, B. M., and G. W. Storrs. 2003. Decompression syndrome in plesiosaurs (Sauropterygia: Reptilia). Journal of Vertebrate Paleontology 23:324–328.

Rothschild, B. M., and L. D. Martin. 2005. Mosasaur ascending: the phytogeny of bends. Netherlands Journal of Geosciences 84:341–344.

Rowe, T., C. A. Brochu, M. Colbert, J. W. Merck, K. Kishi, E. Saglamer, and S. Warrens. 1999. Introduction to Alligator: Digital atlas of the skull. Journal of Vertebrate Paleontology 19:1–8.

Russell, L. S. 1931. Fresh-water plesiosaurs. Canadian Field-Naturalist 45:135–137.

Russell, D. A. 1967. Cretaceous vertebrates from the Anderson River N. W. T. Canadian Journal of Earth Sciences 4:21–38.

Sachs, S. 2005. Redescription of Elasmosaurus platyurus Cope 1868 (Plesiosauria: Elasmosauridae) from the Upper Cretaceous (lower Campanian) of Kansas, U. S. A. Paludicola 5:92–106.

Sachs, S., and B. P. Kear. 2015. Postcranium of the paradigm elasmosaurid plesiosaurian Libonectes morgani (Welles, 1949). Geological Magazine 152:694–710.

Sachs, S., J. Lindgren, and M. Siversson. 2015. A partial plesiosaurian braincase from the Upper Cretaceous of Sweden. Geological Society, London, Special Publications 434:293–301.

Sachs, S., J. Lindgren, and B. P. Kear. 2016a. Re-description of Thalassomedon haningtoni an elasmosaurid from the Cenomanian of North America. In 5th Triennial Mosasaur Meeting - A Global Perspective on Mesozoic Marine Amniotes - Abstracts and Program, pp. 38–40.

Sachs, S., J. J. Hornung, and B. P. Kear. 2016b. Reappraisal of Europe's most complete Early Cretaceous plesiosaurian: Brancasaurus brancai Wegner, 1914 from the "Wealden facies" of Germany. PeerJ, 4:e2813 https://doi.org/10.7717/peerj.2813.

Sachs, S., and B. P. Kear. 2017. Redescription of the elasmosaurid plesiosaurian Libonectes atlasense from the Upper Cretaceous of Morocco. Cretaceous Research 74:205–222.

Saint Girons, H. 1970. The pituitary gland, pp. 245–406, In C. Gans and T. S. Parsons (eds) Biology of the Reptilia 3, London: Academic Press.

Sakai, S. T., B. M. Arsznov, B. L. Lundrigan, and K. E. Holekamp. 2011a. Brain Size and Social Complexity: A Computed Tomography Study in Hyaenidae. Brain, Behavior and Evolution 77:91–104.

Sakai, S. T., B. M. Arsznov, B. L. Lundrigan, and K. E. Holekamp. 2011b. Virtual endocasts: an application of computed tomography in the study of brain variation among hyenas: Hyena endocasts. Annals of the New York Academy of Sciences 1225:160–170.

Sales, M. A., and C. L. Schultz. 2014. Paleoneurology of Teyumbaita sulcognathus (Diapsida: Archosauromorpha) and the sense of smell in rhynchosaurs. Palaeontologia Electronica 17:1–10.

Sampedro, C., E. Font, and E. Desfilis. 2008. Size variation and cell proliferation in chemosensory brain areas of a lizard (Podarcis hispanica): effects of sex and season. European Journal of Neuroscience 28:87–98.

Sanders, K. L., A. R. Rasmussen, J. Elmberg, S. Mumpuni, M. Guinea, P. Blias, M. S. Lee, and B. G. Fry. 2012. Aipysurus mosaicus, a new species of egg-eating sea snake (Elapidae: Hydrophiinae), with a redescription of Aipysurus eydouxii (Gray, 1849). Zootaxa 3431:1–18.

Sato, T., and K. Tanabe. 1998. Cretaceous plesiosaurs ate ammonites. Nature 394:629–630.

Sato, T. 2002. Description of plesiosaurs (Reptilia: Sauropterygia) from the Bearpaw Formation (Campanian–Maastrichtian) and a phylogenetic analysis of the Elasmosauridae. Unpublished Ph.D. dissertation, University of Calgary, Alberta, Canada, 391 pp.

Sato, T. 2003. Terminonatator ponteixensis, a new elasmosaur (Reptilia: Sauropterygia) from the Upper Cretaceous of Saskatchewan. Journal of Vertebrate Paleontology 23:89–103.

Sato, T., C. Li, and X.-C. Wu. 2003. Restudy of Bishanpliosaurus youngi Dong, 1980, a fresh-water plesiosaurian from the Jurassic of Chongqing. Vertebrata PalAsiatica 41:17–33.

Sato, T., Y. Hasegawa, and M. Manabe. 2006. A new elasmosaurid plesiosaur from the Upper Cretaceous of Fukushima, Japan. Palaeontology 49:467–484.

Sato, T., X. C. Wu, A. Tirabasso, and P. Bloskie. 2011. Braincase of a polycotylid plesiosaur (Reptilia: Sauropterygia) from the Upper Cretaceous of Manitoba, Canada. Journal of Vertebrate Paleontology 31:313–329.

Scanlon, J. D., M. S. Lee, M. W. Caldwell, and R. Shine. 1999. The palaeoecology of the primitive snake Pachyrhachis. Historical Biology 13:127–152.

Shichida, Y., T. Yamashita, H. Imai, and T. Kishida. 2013. Evolution and Senses: Opsins, Bitter Taste, and Olfaction. Springer Japan.

Schreibman, M. P. 1986. The Pituitary Gland, pp.11–55. In: P. K. T. Pang, and M. P. Schreibman (eds) Vertebrate Endocrinology: Fundamentals and Biomedical Implications, Vol. I. Academic Press, New York.

Shuler, E. W. 1950. A new elasmosaur from the Eagle Ford Shale of Texas. Fondren Science Series 1:1–33.

Schumacher, B. A., and M. J. Everhart. 2005. A stratigraphic and taxonomic review of plesiosaurs from the old "Fort Benton group" of Central Kansas. Paludicola 5:33–54.

Schumacher, B. A. 2011. A “woollgari-zone mosasaur” (Squamata; Mosasauridae) from the Carlile Shale (lower Middle Turonian) of central Kansas and the stratigraphic overlap of early mosasaurs and pliosaurid plesiosaurs. Transactions of the Kansas Academy of Science 114:1–14.

Schumacher, B. A., K. Carpenter, and M. J. Everhart. 2013. A new Cretaceous Pliosaurid (Reptilia, Plesiosauria) from the Carlile Shale (middle Turonian) of Russell County, Kansas, Journal of Vertebrate Paleontology 33:613–628.

Schulp, A. S. 2005. Feeding the mechanical mosasaur: what did Carinodens eat? Netherlands Journal of Geosciences 84:345–357.

Schulp, A. S., E. W. A. Mulder, and K. Schwenk. 2005. Did mosasaurs have forked tongues?. Netherlands Journal of Geosciences 84:359–371.

Schulp, A. S., H. B. Vonhof, J. H. J. L. Van der Lubbe, R. Janssen, and R. R. Van Baal. 2013. On diving and diet: resource partitioning in type-Maastrichtian mosasaurs·. Netherlands Journal of Geosciences 92:165–170.

Schulp, A. S., R. Janssen, R. R. van Baal, J. W. Jagt, E. W. Mulder, and H. B. Vonhof. 2017. Stable isotopes, niche partitioning and the paucity of elasmosaur remains in the Maastrichtian type area. Netherlands Journal of Geosciences 96:29–33.

Schwenk, K. 2008. Comparative anatomy and physiology of chemical senses in nonavian aquatic reptiles, pp. 65–81. In J. G. M. Thewissen, and S. Nummela (eds.) Sensory Evolution on the Threshold: Adaptations in Secondarily Aquatic Vertebrates. University of California Press, California.

Sciau, J., J. Y. Crochet, and J. Mattei. 1990. Le premier squelette de Plesiosaure de France sur le Causse du Larzac (Toarcien, Jurassique inférieur). Géobios 23:111–116.

Seeley, H. G. 1874. On Muraenosaurus leedsii, a plesiosaurian from the Oxford Clay. Part I. Quarterly Journal of the Geological Society 30:197–208.

Seeley, H. G. 1880. Note on the cranial characters of a large teleosaur from the Whitby Lias preserved in the Woodwardian museum of the University of Cambridge, indicating a new species, Teleosaurus eucephalus. Quarterly Journal of the Geological Society 36:627–634.

Segall, M., R. Cornette, A. C. Fabre, R. Godoy-Diana, and A. Herrel. 2016. Does aquatic foraging impact head shape evolution in snakes? Proceedings of the Royal Society B 283:1–7.

Senn, D. G. 1966. Uber das optische System im Gehirn squamater Reptilien. Eine vergleichend-morphologische Untersuchung, unter besonderer Berücksichtigung einiger Wühlschlangen. Acta Anatomica. Supplementum 52:1–87.

Sennikov, A. G., and M. S. Arkhangelsky. 2010. On a typical Jurassic sauropterygian from the Upper Triassic of Wilczek Land (Franz Josef Land, Arctic Russia). Paleontological Journal 44:567–572.

Sereno, P. C., D. B. Dutheil, M. Iarochène, H. C. E. Larsson, G. H. Lyon, P. M. Magwene, C. A. Sidor, D. J. Varricchio, and J. A. Wilson. 1996. Predatory Dinosaurs from the Sahara and Late Cretaceous Faunal Differentiation. Science 272:986–991.

Sheldon, M. A. 1997. Ecological implications of mosasaur bone microstructure, p. 333–354. In: J.M. Callaway, and E.L. Nicholls (eds.), Ancient Marine Reptiles, Academic Press, San Diego.

Shimada, K., and D. J. Cicimurri. 2005. Skeletal anatomy of the Late Cretaceous shark, Squalicorax (Neoselachii: Anacoracidae). Palaeontologische Zeitschrift 79:241–261.

Shivik, J. A., W. G. Wright, and L. Clark. 2000. Seasonal variability in brown tree snake (Boiga irregularis) response to lures. Canadian Journal of Zoology 78:79–84.

Shuler, E. W. 1950. A new elasmosaur from the Eagle Ford Shale of Texas. Fondren Science Series 1:1–33.

Simões, T. R., M. W. Caldwell, A. Palci, and R. L. Nydam. 2017. Giant taxon-character matrices: quality of character constructions remains critical regardless of size. Cladistics 33:198–219.

Silcox, M. T., A. E. Benham, and J. I. Bloch. 2010. Endocasts of Microsyops (Microsyopidae, Primates) and the evolution of the brain in primitive primates. Journal of human evolution 58:505–521.

Smith, A. S. 2008. Plesiosaurs. Geology Today 24:71–75.

Smith, A. S., and G. J. Dyke. 2008. The skull of the giant predatory pliosaur Rhomaleosaurus cramptoni: Implications for plesiosaur phylogenetics. Naturwissenschaften 95:975–980.

Souza, N. M., D. J. Maggs, S. A. Park, S. M. Puchalski, C. M. Reilly, J. Paul-Murphy, and C. J. Murphy. 2015. Gross, histologic, and micro-computed tomographic anatomy of the lacrimal system of snakes. Veterinary Ophthalmology 18:15–22.

Starck, D. 1979. Cranio-Cerebral Relations in Recent Reptiles. In Gans, C., Northcutt, R.G., Ulinski, P. (eds) Biology of the Reptilia (Neurology A), Academic Press, London, New York and San Francisco, 462 pp.

Stayton, C. T. 2005. Morphological evolution of the lizard skull: a geometric morphometrics survey. Journal of Morphology 263:47–59.

Sternberg, C. H., 1915. Evidence proving that the Belly River beds of Alberta are equivalent with the Judith River beds of Montana. Science 42:131–133.

Sternberg, C. H. 1922. Explorations of the Permian of Texas and the chalk of Kansas, 1918. Kansas Academy of Science Transactions 30:119–120.

Storrs, G. W. 1991. Anatomy and relationships of Corosaurus alcovensis (Diapsida: Sauropterygia) and the Triassic Alcova Lime stone of Wyoming. Bulletin of the Peabody Museum of Natural History, Yale University 44:1–151.

Storrs, G. W. 1993. Function and phylogeny in sauropterygian (Diapsida) evolution. American Journal of Science 293:63–90.

Storrs, G. 1995. A juvenile specimen of ?Plesiosaurus sp. from the Lias (Lower Jurassic, Pliensbachian) near Charmouth, Dorset, England. Proceedings of the Dorset Natural History and Archaeological Society 116:71–76.

Storrs, G. W., and M. A. Taylor. 1996. Cranial anatomy of a new plesiosaur genus from the lowermost Lias (Rhaetian/Hettangian) of Street, Somerset, England. Journal of Vertebrate Paleontology 16:403–420.

Storrs, G. W. 1997. Morphological and taxonomic clarification of the genus Plesiosaurus in J. M. Callaway and E. L. Nicholls (eds.), Ancient Marine Reptiles. San Diego Academic Press, California pp. 145–190.

Sultan, F. 2002. Brain evolution (Communication arising): Analysis of mammalian brain architecture. Nature 415:133–134.

Tarlo, L. B. 1959. Pliosaurus brachyspondylus (Owen) from the Kimeridge Clay. Palaeontology 1:283–291.

Taylor, M. A. 1992. Functional anatomy of the head of the large aquatic predator Rhomaleosaurus zetlandicus (Plesiosauria; Reptilia) from the Toarcian (Lower Jurassic) of Yorkshire, England. Philosophical Transactions of the Royal Society of London, Series B 335:247–280.

Taylor, M. A., and A. R. I Cruickshank. 1993. Cranial anatomy and functional morphology of Pliosaurus brachyspondylus (Reptilia: Plesiosauria) from the Upper Jurassic of Westbury, Wiltshire. Philosophical Transactions of the Royal Society of London B: Biological Sciences 341:399–418.

Terrab, S. 1996. Le Cénomanien-Turonien d'Agadir. Stratigraphie et diagenèse (nodulisation). Unpublished PhD dissertation, Centre de Géotechnique et d'exploitation du sous-sol, sédimentologie, Ecole des Mines de Paris, France, 255 pp.

Testin, J. J. 2011. Dental Microstructure in Polycotylid Plesiosaurs. Unpublished Master Thesis, Geology and Geological Engineering, South Dakota School of Mines and Technology.

Thach, W. T., and A. J. Bastian. 2004. Role of the cerebellum in the control and adaptation of gait in health and disease. Progress in brain research 143:353–366.

Theobald, W. 1876. Descriptive Catalogue of the Reptiles of British India. Calcutta: Thacker, London, 135 pp.

Thompson, G. G., and P. C. Withers. 1997. Comparative morphology of western Australian varanid lizards (Squamata: Varanidae). Journal of Morphology 233:127–152.

Tosini, G. 1997. The pineal complex of reptiles: physiological and behavioral roles. Ethology Ecology & Evolution 9:313–333.

Triviño, L. N., A. M. Albino, M. T. Dozo, and J. D. Williams. In press. First natural endocranial cast of a fossil snake (Cretaceous of Patagonia, Argentina). The Anatomical Record.

Ulinski, P. S., D. M. Dacey, and M. I. Sereno. 1992. Optic tectum, pp. 241–366. In: C. Gans, P. S. Ulinski (eds) Sensorimotor integration: biology of the Reptilia, vol 17. University of Chicago Press, Chicago.

Underwood, C., K. M. Cleason, and D. J. Ward. 2009. Batoids from the Turonian of SE Morocco. In N. E. Jalil (ed.), 1st International Congress on North African Vertebrate Palaeontology, Program and Abstracts, Marrakech, 25–27 May 2009, pp. 43.

Vidal, N., and S. B. Hedges. 2004. Molecular evidence for a terrestrial origin of snakes. Proceedings of the Royal Society of London B: Biological Sciences 271:S226–S229.

Vignaud, P., and Z. B. Gasparini. 1996. New Dakosaurus (Crocodylomorpha, Thalattosuchia) from the Upper Jurassic of Argentina. Comptes Rendus de l'Académie des Sciences, Paris 2 322: 245–250.

Vignaud, P. 1998. Une Nouvelle espece de Steneosaurus (Thalattosuchia, Teleosauridae) dans le Callovien du Poitou (France) et la systematique des Steneosaurus longirostres du Jurassique moyen d'Europe occidentale. Palaeovertebrata 27:19–44.

Vincent, P., N. Bardet, X. Pereda Suberbiola, B. Bouya, M. Amaghzaz, and S. Meslouh, 2011. Zarafasaura oceanis, a new elasmosaurid (Reptilia: Sauropterygia) from the Maastrichtian Phosphates of Morocco and the palaeobiogeography of latest Cretaceous plesiosaurs. Gondwana Research 19:1062–1073.

Vincent, P., N. Bardet, A. Houssaye, M. Amaghzaz, and S. Meslouh. 2013. New plesiosaur specimens from the Maastrichtian Phosphates of Morocco and their implications for the ecology of the latest Cretaceous marine apex predators. Gondwana Research 24:796–805.

Vincent, P., R. Allemand, P. D. Taylor, G. Suan, and E. E. Maxwell. 2017. New insights on the systematics, palaeoecology and palaeobiology of a plesiosaurian with soft tissue preservation from the Toarcian of Holzmaden, Germany. The Science of Nature 104:51.

Voeten, D., P. Tafforeau, D. Nieweg, and S. Bures. 2014. Endocranial aspects of Nothosaurus marchicus (Diapsida, Sauropterygia) from the lower Muschelkalk of Winterswijk (the Netherlands) revealed through propoagation phase contrast X-ray synchrotron microtomography. In E. Maxwell and J. Miller-Camp (eds), Society of Vertebrate Paleontology 74th Annual Meeting, Berlin, Germany. Abstract book, pp. 249.

Von der Emde, G., and H. Bleckmann. 1998. Finding food: senses involved in foraging for insect larvae in the electric fish Gnathonemus petersii. Journal of Experimental Biology 201:969–980.

Wade, M. 1990. A review of the Australian Cretaceous longipinnate ichthyosaur Platypterygius (Ichthyosauria: Ichthyopterygia). Memoirs of the Queensland Museum 28:115–137.

Walsh, S. A., P. M. Barrett, A. C. Milner, G. Manley, and L. M. Witmer. 2009. Inner ear anatomy is a proxy for deducing auditory capability and behaviour in reptiles and birds. Proceedings of the Royal Society B: Biological Sciences 276:1355–1360.

Walsh, S. A., and M. A. Knoll. 2011. Directions in Palaeoneurology. The Palaeontological Association 86:263–279.

Warren, G., and I. Speden. 1977. The Piripauan and Haumurian stratotypes (Mata Series, Upper Cretaceous) and correlative sequences in the Haumuri Bluff District, South Marlborough. New Zealand Geological Survey Bulletin 92:1–60.

Watson, D. M. S. 1924. The elasmosaurid shoulder-girdle and fore-limb. Proceedings of the Zoological Society of London 28:85–95.

Webb, J. K., R. Shine, W. R. Branch, and P. S. Harlow. 2000. Life underground: food habits and reproductive biology of two amphisbaenian species from southern Africa. Journal of Herpetology 510–516.

Wegner, T. H. 1914. Brancasaurus brancai n.g. n.sp., ein Elasmosauride aus dem Wealden Westfalens, pp. 235–305, In: Festschrift für Wilhelm Brancazum, Geburtstage. Leipzig: Borntraeger,

Welles, S. P. 1943. Elasmosaurid plesiosaurs with a description of new material from California. Memoirs of the University of California 13:125–254.

Welles, S. P. 1949. A new elasmosaur from the Eagle Ford Shale of Texas. Fordren Science, Series 1:1–28.

Welles, S. P. 1952. A review of the North American Cretaceous elasmosaurs. University of California, Publications in Geological Sciences 29:47–144.

Welles, S. P. 1962. A new species of elasmosaur from the Aptian of Columbia and a review of the Cretaceous plesiosaurs. University of California Publications in Geological Sciences 44:1–96.

Wenz, S. 1968. Contribution à l'étude du genre Metriorhynchus. Crâne et moulage endocrânien de Metriorhynchus superciliosus. Annales de Paléontologie (Vertébrés) 54:149–183.

Westphal, F. 1961. Zur Systematik der deutschen und englischen Lias Krokodilier.– Neues Jahrbuch. für Geologie und Paläontologie, Abhandlungen 113:207-218.

Wharton, D. S. 2000. An enlarged endocranial venous system in Steneosaurus pictaviensis (Crocodylia: Thalattosuchia) from the Upper Jurassic of Les Lourdines, France. Comptes Rendus de l'Académie des Sciences-Series IIA-Earth and Planetary Science 331:221–226.

Wiffen, J., and W. L. Moisley. 1986. Late Cretaceous reptiles (families Elasmosauridae and Pliosauridae) from the Mangahouga Stream, North Island, New Zealand. Journal of Geology and Geophysics, New Zealand 29:205–252.

Wilkinson, A., and L. Huber. 2012. Cold-blooded cognition: reptilian cognitive abilities. The Oxford Handbook of Comparative Evolutionary Psychology. Oxford University Press, New Jersey pp.129-143.

Willemsen, G. F. 1980. Comparative study of the functional morphology of some Lutrinae, especially Lutra lutra. Lutrogale perspicillata and the Pleistocene Isolalutra cretensis. Proceedings of the Koniklijke Nederlandse Akademie van Wetenschappen, Series B 83:289–326.

Williston, S. W. 1889. A New Plesiosaur from the Niobrara Cretaceous of Kansas. Transactions of the Annual Meetings of the Kansas Academy of Science 12:174-178.

Williston, S. W. 1890. A new plesiosaur from the Niobrara Cretaceous of Kansas. Transactions of the Kansas Academy of Sciences 12:174–178.

Williston, S. W. 1897. The Kansas Niobrara Cretaceous. The University Geological Survey of Kansas 2:235–246.

Williston, S. W. 1899. Some additional characters of the mosasaurs. University of Kansas Quarterly 8:39–41.

Williston, S. W. 1902. Restoration of Dolichorhynchops osborni, a new Cretaceous plesiosaur. Kansas University Science Bulletin 1:241–244.

Williston, S. W. 1903. North American plesiosaurs. Part I. Field Columbian Museum Publication 2:1–79.

Williston, S. W. 1908. North American Plesiosaurs Trinacromerum. The Journal of Geology, University of Chicago Press 16:715–736.

Witmer, L. M., S. Chaterjee, J. Franzosa, and T. Rowe. 2003. Neuroanatomy of flying reptiles and implications for flight, posture and behaviour. Nature 425:950–953.

Witmer, L. M., R. C. Ridgely, D. L. Dufeau, and M. C. Semones. 2008. Using CT to Peer into the Past: 3D Visualization of the Brain and Ear Regions of Birds, Crocodiles, and Nonavian Dinosaurs, pp. 67–87 In: R. Frey, and H. Endo (eds) Anatomical Imaging: Towards a New Morphology, Tokyo, Springer-Verlag,.

Witmer, L. M., and R. C. Ridgely. 2009. New insights into the brain, braincase, and ear region of tyrannosaurs (Dinosauria, Theropoda), with implications for sensory organization and behavior. The Anatomical Record 292:1266–1296.

Wyneken, J. 2001. The anatomy of sea turtles. U.S. Department of Commerce NOAA Technical Memorandum 470:1–172.

Wyneken, J. 2007. Reptilian Neurology: Anatomy and Function. Veterinary Clinics of North America: Exotic Animal Practice 10:837–853.

Yamashita, M., T. Konishi, and T. Sato. 2015. Sclerotic rings in mosasaurs (Squamata: Mosasauridae): structures and taxonomic diversity. PloS One 10:e0117079.

Yi, H., and M. A. Norell. 2015. The burrowing origin of modern snakes. Science Advances 1:e1500743.

Zaher, H. 1998. The phylogenetic position of Pachyrhachis within snakes (Squamata, Serpentes). Journal of Vertebrate Paleontology 18:1–3.

Zaher, H., and O. Rieppel. 1999. Tooth implantation and replacement in squamates, with special reference to mosasaur lizards and snakes. American Museum of Natural History Novitates 3271:1–19.

Zangerl, R. 1953. The vertebrate fauna of the Selma Formation of Alabama. Part III. The turtles of the family Protostegidae. Fieldiana: Geology Memoirs 3:63–133.

Zelditch, M. L., D. L. Swiderski, H. D. Sheets, and W. L Fink. 2004. Geometric morphometrics for biologists: a primer. Academic Press, 443pp.

Zelenitsky, D. K., F. Therrien, and Y. Kobayashi. 2009. Olfactory acuity in theropods: palaeobiological and evolutionary implications. Proceedings of the Royal Society of London B: Biological Sciences 276:667–673.

Zelenitsky, D. K., F. Therrien, R. C. Ridgely, A. R. McGee, and L. M. Witmer. 2011. Evolution of olfaction in non-avian theropod dinosaurs and birds. In Proceedings of the Royal Society B 278:3625–3634.

Zverkov, N.G., A. O. Averianov, and E. V. Popov. 2017. Basicranium of an elasmosaurid plesiosaur from the Campanian of European Russia. Alcheringa: An Australasian Journal of Palaeontology 7:doi: 10.1080/03115518.2017.1302508.

Appendices

Appendix 1

Digital snake endocast reconstructed during this PhD Thesis in dorsal (up), left lateral (middle) and ventral (down) views. Scale bars equal 2 mm (Chapter 5 snake endocasts).

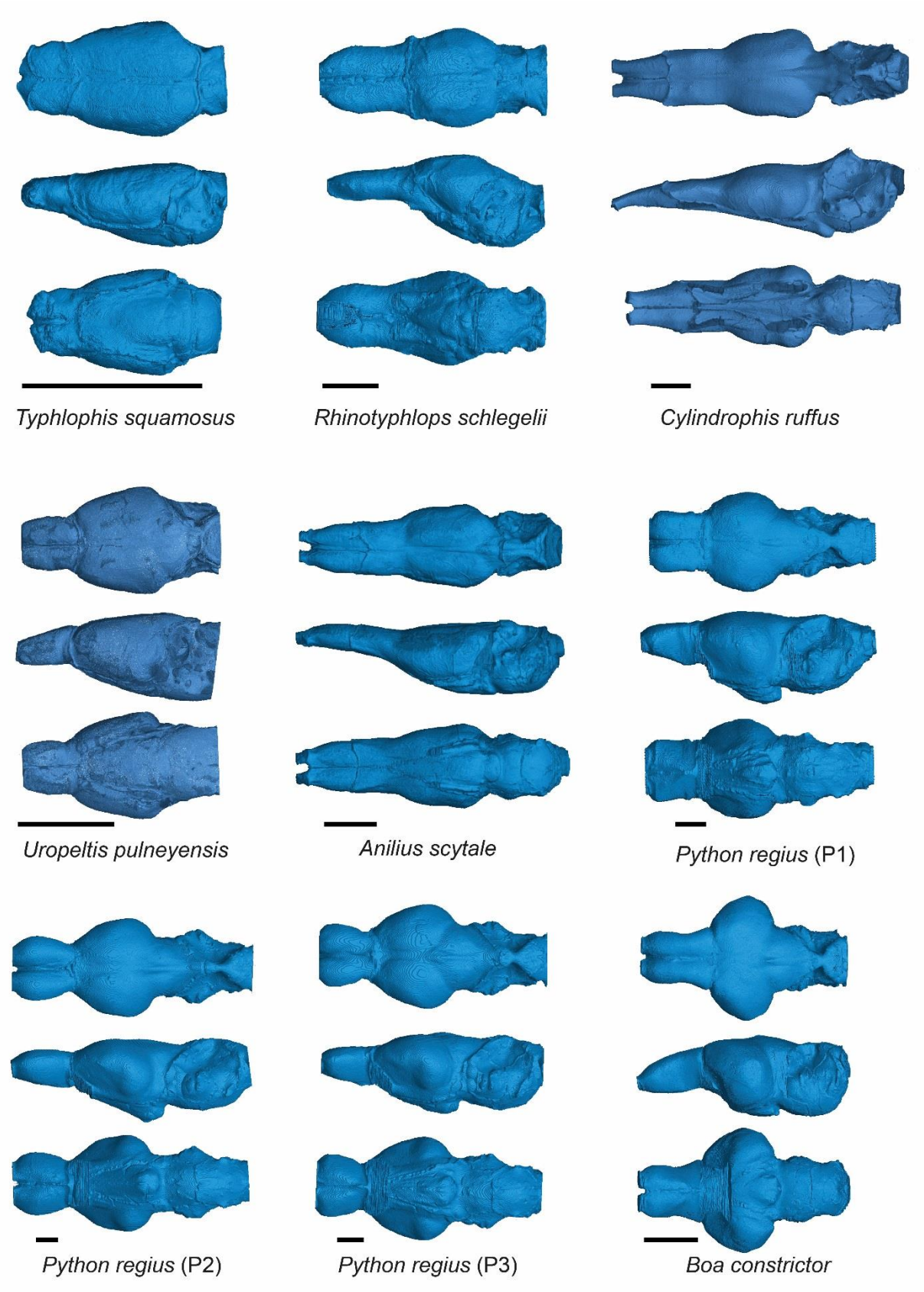
Typhlophis squamosus
Rhinotyphlops schlegelii
Cylindrophis ruffus
Uropeltis pulneyensis
Anilius scytale
Python regius (P1)
Python regius (P2)
Python regius (P3)
Boa constrictor

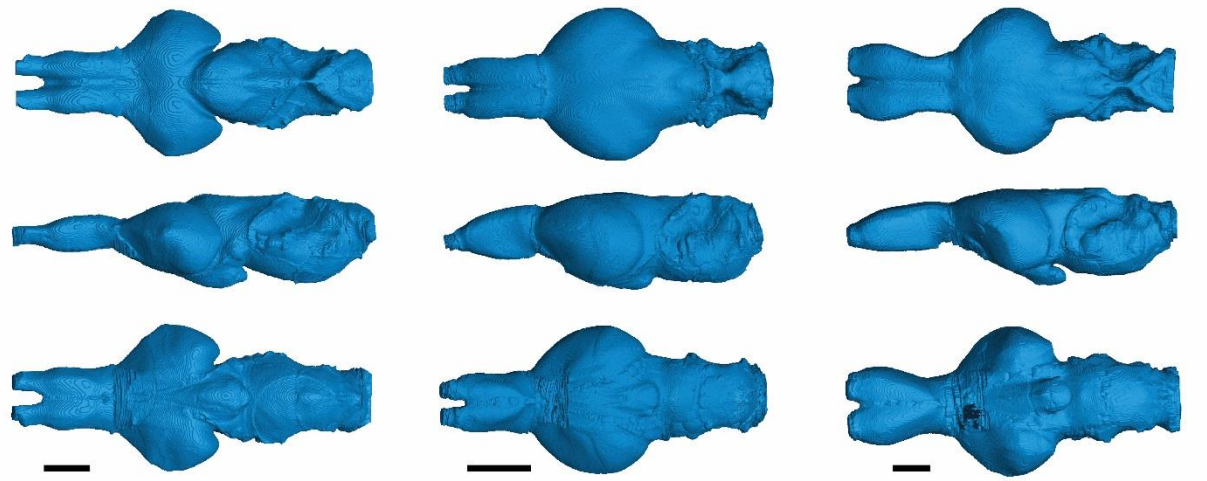

Candoia sp. | *Eunectes murinus* | *Corallus hortulanus*

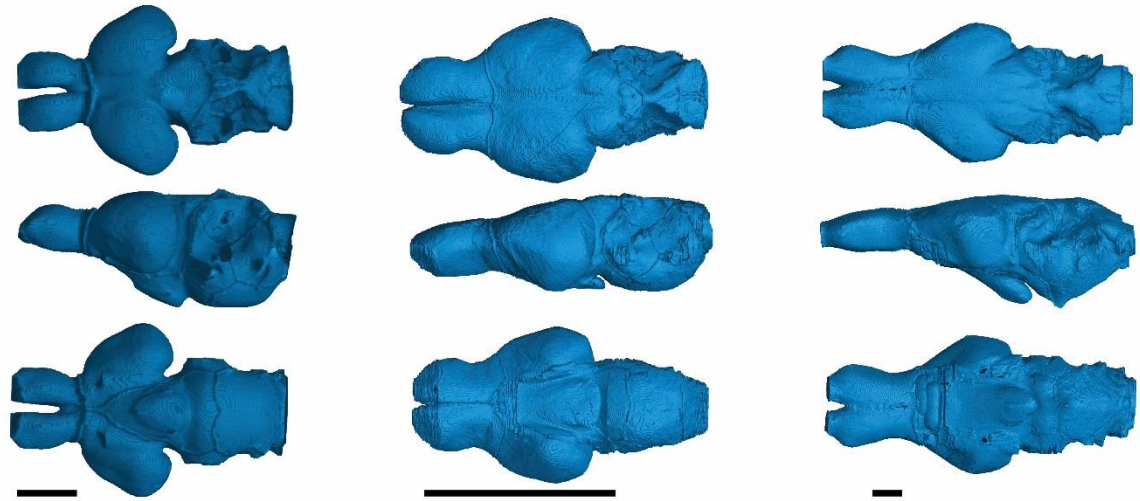

Acrochordus granulatus | *Pareas margaritophorus* | *Crotalus atrox*

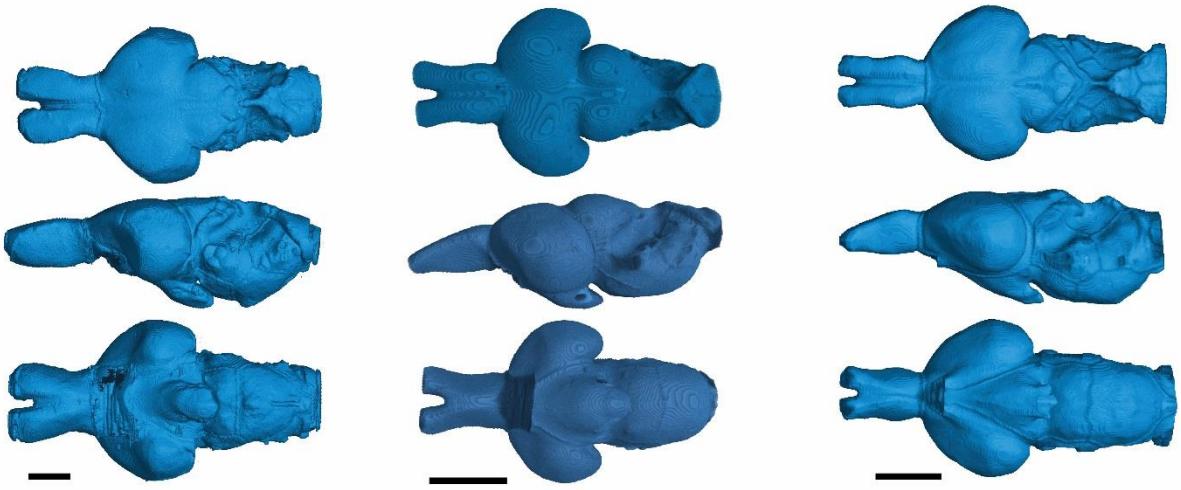

Agkistrodon contortrix | *Enhydris enhydris* | *Enhydris punctata*

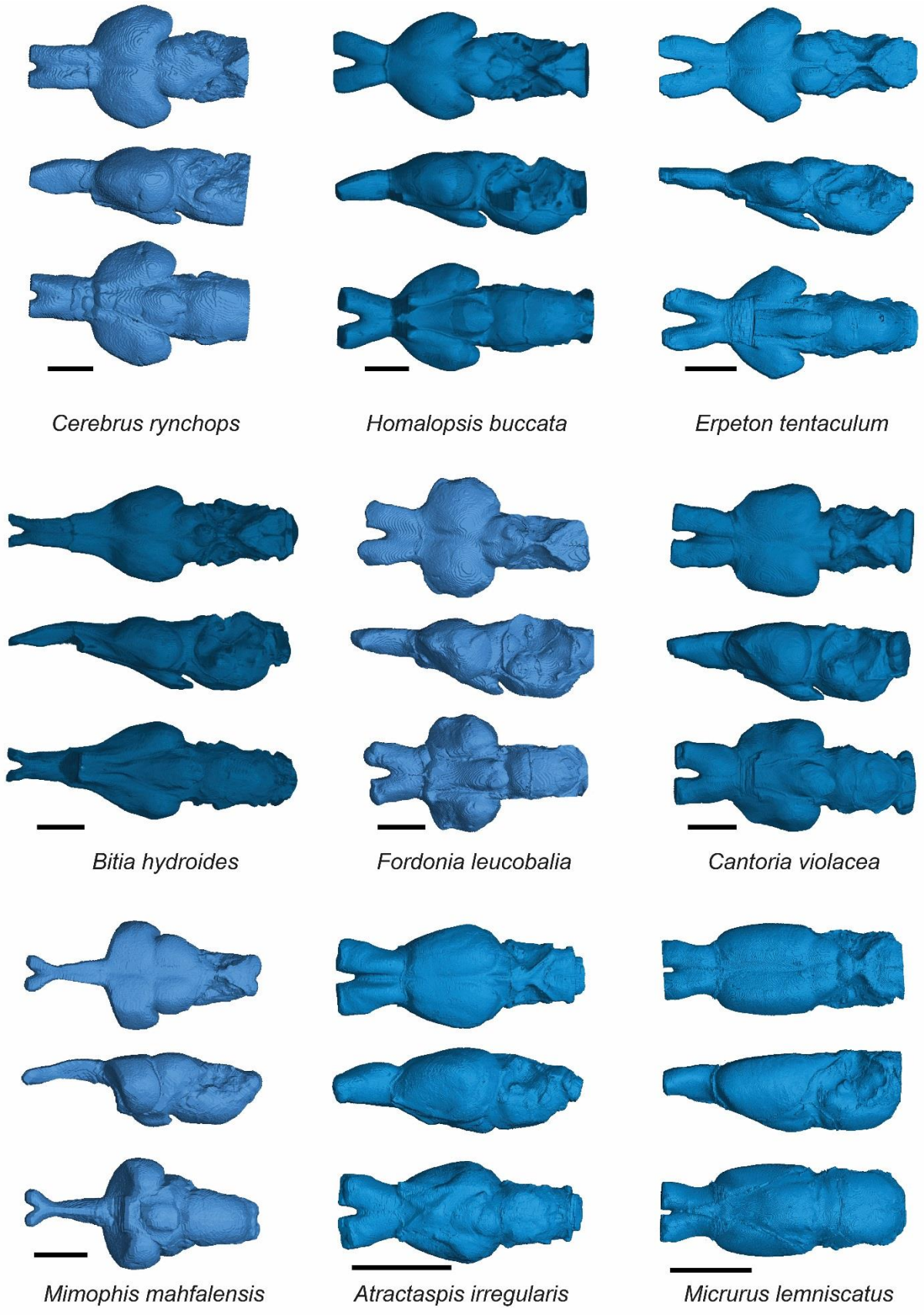
Cerebrus rynchops
Homalopsis buccata
Erpeton tentaculum
Bitia hydroides
Fordonia leucobalia
Cantoria violacea
Mimophis mahfalensis
Atractaspis irregularis
Micrurus lemniscatus

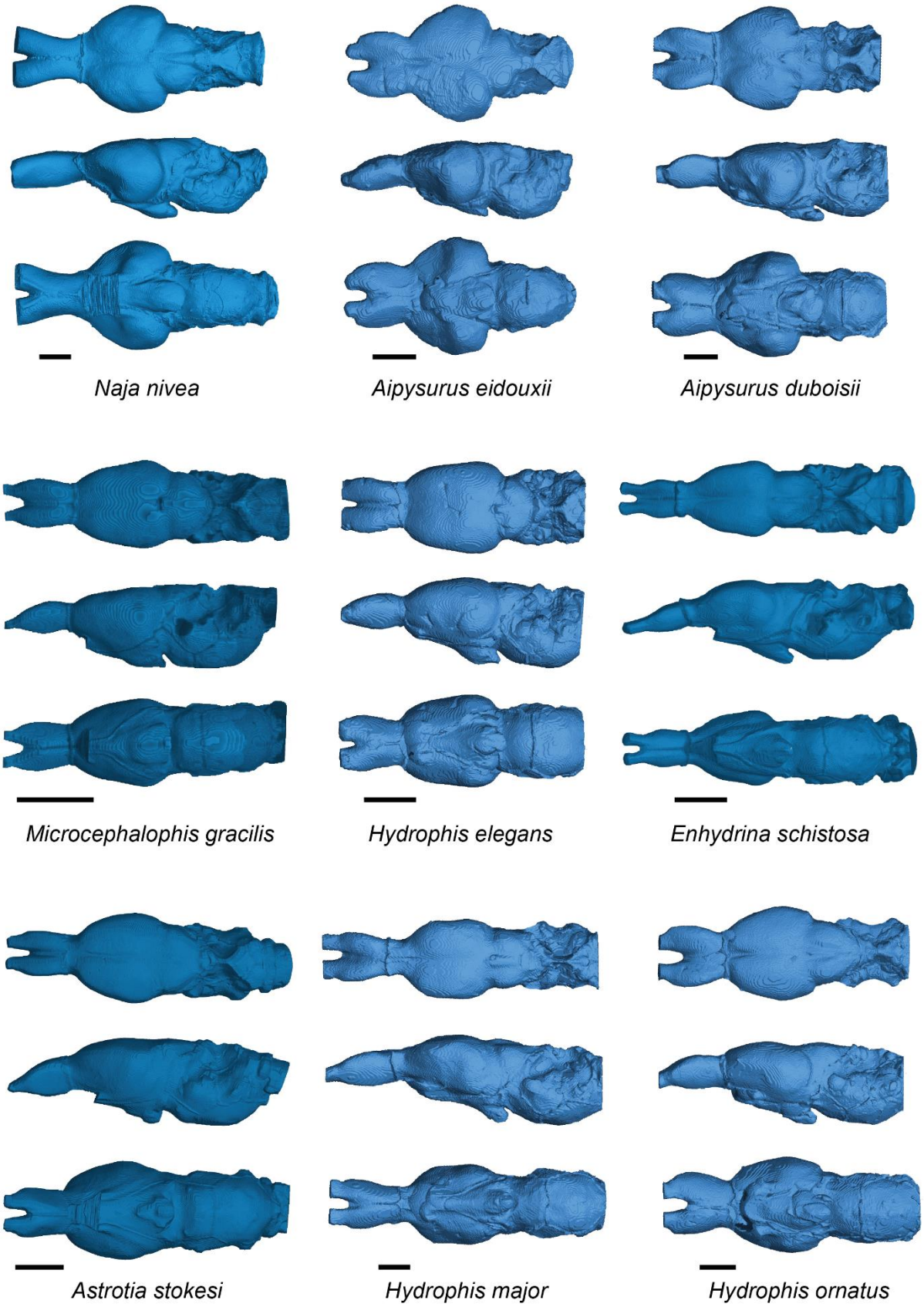
Naja nivea
Aipysurus eidouxii
Aipysurus duboisii
Microcephalophis gracilis
Hydrophis elegans
Enhydrina schistosa
Astrotia stokesi
Hydrophis major
Hydrophis ornatus

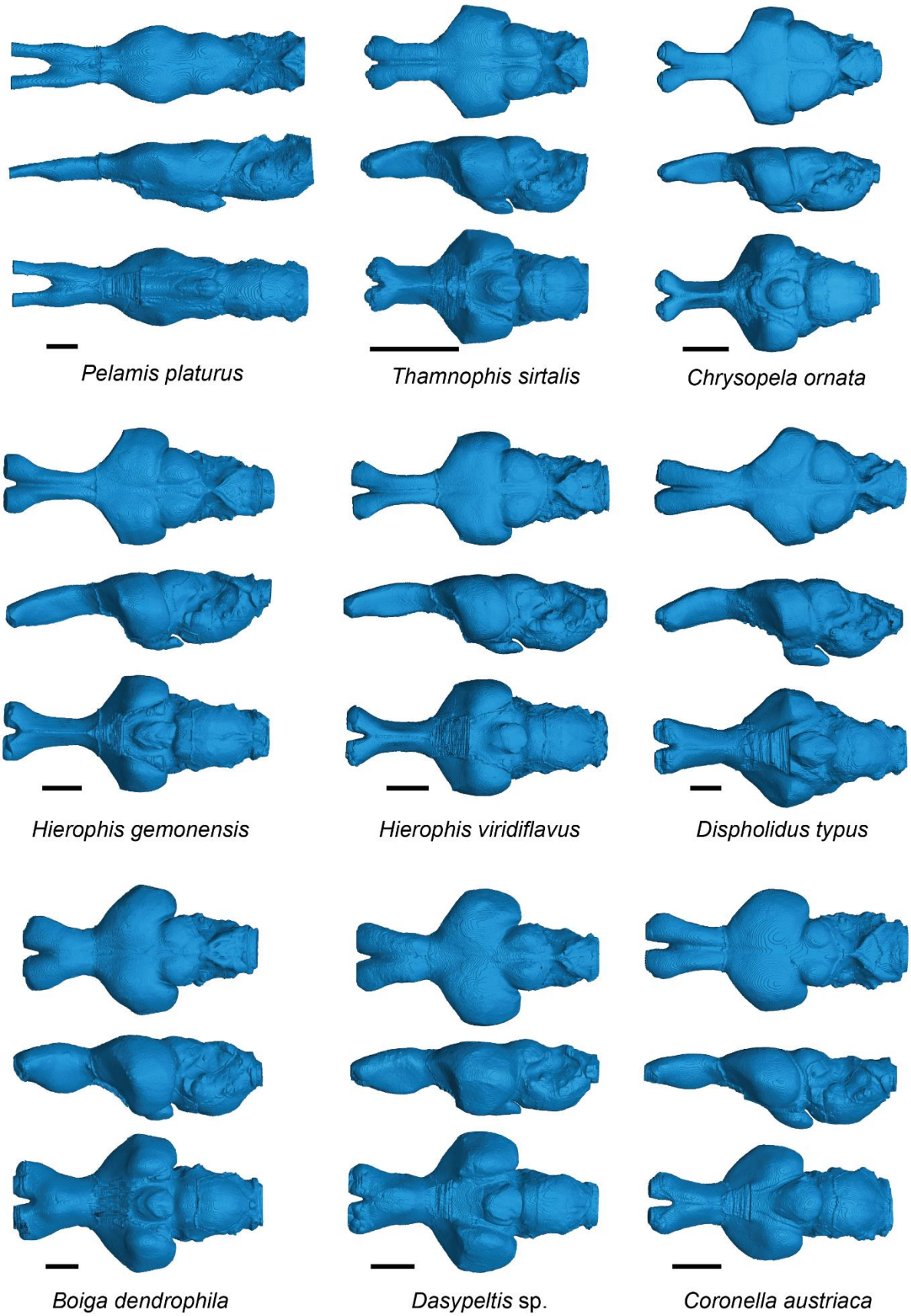
Pelamis platurus
Thamnophis sirtalis
Chrysopela ornata
Hierophis gemonensis
Hierophis viridiflavus
Dispholidus typus
Boiga dendrophila
Dasypeltis sp.
Coronella austriaca

Appendix 2

Table of measurements (in mm) taken on snake endocasts

(Chapter 5 snake endocasts)

Taxa	LE	LOB	LG	HOB	HOP	WO	LFI	WC	LCH	HC	WO	LOR	HO	LP	HP	WIE	DWP	LPE	HPE	WP	WP
E. punctata	9,75	2,44	2,41	0,86	1,57	3,12	5,24	3,52	2,83	3,02	2,31	2,53	3,94	1,25	1,55	3,01	1,18	1,95	2,49	2,62	1,84
H. buccata	11,6	2,52	2,09	1,14	1,78	3,61	5,85	4,91	2,80	3,11	3,39	2,62	5,71	1,99	1,75	3,05	1,10	4,14	2,88	3,08	2,05
E. enhydris	7,46	2,45	2,02	0,57	1,26	1,76	4,59	2,43	2,16	2,52	2,00	1,87	3,04	1,60	1,23	1,75	0,83	1,37	2,03	2,45	1,59
A. granulatus	8,77	2,12	1,23	1,17	1,61	2,28	6,21	3,36	2,84	2,34	2,32	2,63	3,91	1,65	1,79	2,88	1,33	2,21	2,87	2,58	2,44
C. violacea	9,56	2,69	1,89	0,94	1,81	2,53	5,13	4,11	2,90	2,38	2,77	2,36	4,73	1,33	1,77	2,26	1,40	1,76	2,24	2,53	2,42
M. gracilis	6,99	1,93	1,46	0,31	0,89	1,84	2,26	2,64	1,45	1,64	1,85	1,30	2,78	1,29	0,87	1,60	0,91	1,35	1,59	1,82	1,01
B. hydroides	11,9	3,05	2,43	1,05	1,06	3,49	4,40	5,15	2,20	2,55	3,17	2,10	5,76	1,74	1,57	2,96	1,17	2,44	1,98	2,39	1,56
A. stokesii	11,5	2,76	2,03	0,68	1,54	2,88	4,14	3,60	2,77	2,88	3,50	2,35	4,21	1,98	1,81	2,68	1,58	2,25	2,14	2,96	1,76
E. schistosa	10,9	2,47	2,01	0,82	1,19	3,98	3,18	4,03	1,91	2,22	2,57	1,98	4,79	1,92	1,77	2,82	1,33	2,14	2,24	2,33	1,41
T. sirtalis	4,58	1,26	1,29	0,61	0,82	1,34	2,67	1,87	1,41	1,74	1,11	1,17	2,06	0,70	0,95	0,94	0,53	0,75	1,16	1,45	1,02
T. squamosus	2,25	0,49	0,59	0,49	0,70	1,67	1,67	1,15	0,97	1,07	0,08	0,83	1,46	0,31	0,88	0,52	0,66	0,08	0,93	1,29	1,07
R.schlegelii	7,97	3,01	3,01	1,11	1,93	3,17	4,06	3,50	2,76	2,78	0,57	2,65	2,92	0,64	2,20	1,44	2,16	1,12	2,57	2,77	3,29
P. regius 3	16,8	4,37	4,37	1,49	3,23	3,80	7,87	5,71	4,62	4,83	4,75	4,38	6,26	1,77	2,72	4,51	2,79	3,27	3,33	4,55	4,07
P. regius 2	20,0	5,77	5,27	1,50	3,66	5,11	8,54	6,53	5,43	4,50	5,92	4,24	7,16	2,41	3,05	5,31	2,64	4,17	3,74	3,62	4,37
P. regius	13,4	3,58	3,58	1,55	2,75	3,38	6,62	4,74	4,56	4,10	3,98	4,24	4,90	1,35	2,43	3,70	2,93	2,39	3,33	3,51	4,11
P. platurus	18,0	5,56	3,11	0,59	1,52	4,30	4,87	5,13	2,47	3,81	5,99	2,22	7,33	1,91	1,64	2,96	1,39	2,58	2,69	2,92	2,38
P. margaritophorus	3,04	0,76	0,96	0,64	0,68	0,93	2,08	1,27	1,12	1,11	0,83	0,72	1,36	0,46	0,65	0,73	0,49	0,49	0,95	1,05	1,42
N. nivea	15,4	4,11	3,74	2,40	2,28	4,48	7,78	6,62	4,61	4,69	4,30	3,87	7,75	2,30	2,25	2,85	2,67	2,75	3,47	4,16	3,52
M. lemniscatus	5,71	1,41	1,32	0,73	1,14	2,42	2,53	2,35	1,76	1,67	1,57	1,36	2,51	0,81	1,08	1,22	1,30	0,89	1,54	2,04	1,51
H. veridiflavus	12,5	4,19	3,76	1,38	1,49	3,19	6,59	4,40	3,65	4,60	2,73	3,03	5,21	1,51	1,72	2,38	1,96	1,97	2,83	3,75	2,22
E. murinus	10,3	3,14	2,90	0,76	1,83	2,42	5,13	3,29	3,15	2,66	2,97	2,12	3,72	1,02	1,50	2,02	1,27	1,51	2,24	2,83	2,17
E. tentaculum	9,97	2,84	1,76	0,72	1,21	2,40	5,17	3,24	2,13	2,71	2,96	2,06	4,10	1,36	1,10	1,94	1,43	1,41	2,06	2,20	2,53
D. typus	15,8	5,15	5,15	2,45	2,49	4,99	8,94	6,23	4,67	6,82	3,69	4,67	7,26	2,18	1,66	2,95	2,52	2,62	3,60	4,74	3,46
Dasypeltis	10,7	3,05	3,25	1,60	1,96	3,50	7,08	4,75	3,77	3,49	2,28	2,81	5,08	1,14	1,58	2,17	1,89	1,83	2,47	2,39	2,50
C. ruffus	13,6	2,72	2,62	0,77	1,37	6,56	4,57	2,95	7,85	2,11	2,49	2,25	9,05	1,29	1,50	2,89	1,10	1,83	2,70	2,46	2,81
C.austriaca	10,1	2,86	2,53	1,24	1,33	3,36	5,70	3,99	2,89	3,06	2,16	2,90	4,60	1,05	1,97	2,46	2,00	1,90	2,40	2,52	2,36
C. atrox	18,5	5,67	4,70	1,65	2,71	5,16	9,36	6,55	4,66	5,25	4,09	4,35	7,74	2,66	3,13	3,99	2,47	3,50	3,76	5,53	5,38
C. hortulanus	17,2	5,58	5,58	1,51	2,38	4,76	8,63	5,83	4,84	4,29	4,40	3,58	6,42	1,90	1,67	3,29	2,34	2,52	3,43	4,00	4,11
C. ornata	9,64	3,10	2,90	0,97	1,43	2,72	5,83	3,49	2,89	4,50	2,47	2,45	3,91	1,00	1,87	1,52	1,65	1,53	2,61	3,43	1,73
Candoia	15,4	4,60	3,78	0,82	1,83	3,19	7,33	5,07	3,45	3,11	5,32	2,81	6,17	2,00	2,13	3,11	2,14	2,61	2,88	3,71	3,38

B. constrictor	7,43	2,48	2,48	0,61	1,57	1,73	4,70	2,33	2,55	2,33	1,95	2,16	2,40	0,73	1,38	1,49	1,69	1,17	1,71	2,22	2,91
A. irregularis	4,63	1,10	1,10	0,83	1,01	1,90	2,44	2,22	1,79	1,30	0,56	1,25	2,38	0,54	0,57	0,97	1,19	1,12	0,94	1,23	1,39
A. scytale	9,38	2,05	2,05	0,61	1,06	4,65	3,40	2,27	5,31	2,36	1,13	1,97	5,59	0,88	1,24	1,69	1,32	1,57	2,22	2,04	2,10
B. dendrophila	13,6	3,84	3,84	2,14	2,30	4,24	9,02	5,70	5,13	4,78	2,67	3,47	5,40	2,03	2,83	3,16	2,54	2,34	3,27	3,53	3,57
H. gemonensis	13,4	4,61	4,61	1,70	2,10	3,54	7,23	4,72	4,85	3,51	5,86	3,49	5,86	1,59	2,07	2,47	2,50	2,25	3,19	4,12	2,55
A. contortrix	13,2	3,54	2,81	1,76	2,30	3,62	8,20	5,35	4,19	4,67	2,98	3,71	6,68	1,87	2,48	3,25	1,68	2,45	3,56	3,23	3,43
H. ornatus	13,3	3,42	2,16	0,77	1,60	3,78	4,99	4,72	2,92	3,33	3,33	2,70	5,05	1,66	1,40	3,20	1,49	2,82	2,74	2,80	2,50
A. duboisii	13,2	3,66	2,70	0,84	1,65	3,77	6,07	4,81	3,60	3,68	3,50	2,58	5,85	1,92	1,71	3,10	1,97	2,42	2,59	3,01	3,15
A. eydouxii	10,5	2,42	1,75	0,90	1,74	3,45	6,41	4,84	3,50	3,59	2,85	2,79	5,29	1,31	1,93	2,13	1,76	1,69	2,96	3,14	3,16
F. leucobalia	9,48	2,10	1,50	0,89	1,21	2,89	5,60	3,71	2,82	2,30	2,18	2,27	4,02	1,03	1,89	2,87	1,86	2,23	2,26	2,10	2,93
H. elegans	9,32	2,30	1,75	0,52	1,16	3,53	3,52	3,73	2,50	2,31	1,82	1,75	4,03	1,46	1,35	1,89	1,49	1,88	2,09	2,32	1,83
H. major	16,6	3,96	2,73	0,80	2,07	5,53	4,83	5,87	3,66	3,38	3,66	2,35	6,88	2,31	1,76	3,74	2,21	3,22	2,87	3,17	2,28
M. mahfalensis	8,41	2,69	2,59	0,62	0,91	2,13	4,45	2,51	2,35	3,25	2,01	2,10	3,27	0,93	1,01	1,52	0,89	1,65	1,74	1,84	1,16
U. pulneyensis	3,93	1,19	1,19	0,40	0,77	1,43	2,14	1,72	1,37	1,37	0,92	1,32	1,81	0,34	0,97	0,95	0,86	0,37	1,47	1,44	1,41
C. rynchops	9,63	2,63	2,27	0,72	1,37	2,87	5,46	3,74	2,70	2,64	2,18	2,06	4,24	1,36	1,83	2,39	1,09	2,01	2,55	2,41	2,26

Appendix 3

Table of measurements (in mm) taken on the three Python regius specimens

(Chapter 5 snake endocasts)

Specimens	**LE**	**LOB**	**LG**	**HOB**	**HOP**	**WOP**	**LFI**	**WCH**	**LCH**	**HCH**	**WOR**	**LOR**	**HOR**	**LP**	**HP**	**WIE**	**DWPE**	**LPE**	**HPE**	**WPE**	**WP**
P. regius 1.1	13,52	3,55	3,55	1,55	2,77	3,25	6,68	4,57	4,40	4,20	4,16	4,06	4,92	1,61	2,43	3,32	2,90	2,57	4,42	3,39	3,96
P. regius 1.2	13,63	3,58	3,58	1,54	2,8	3,24	6,66	4,58	4,37	4,09	4,24	4,10	4,88	1,64	2,49	3,40	2,97	2,47	4,58	3,52	4,03
P.regius 1.3	13,61	3,63	3,63	1,57	2,91	3,29	6,67	4,50	4,27	4,14	4,30	4,22	4,81	1,58	2,39	3,59	3,01	2,33	4,63	3,37	3,97
P.regius 1.4	13,52	3,59	3,59	1,60	2,83	3,25	6,72	4,65	4,28	4,16	4,33	4,12	4,86	1,66	2,33	3,44	2,94	2,52	4,61	3,46	4,01
P.regius 1.5	13,65	3,61	3,61	1,56	2,83	3,38	6,70	4,51	4,42	3,99	4,22	4,09	4,82	1,66	2,35	3,52	2,96	2,54	4,65	3,51	4,01
P. regius 1.6	13,60	3,59	3,59	1,60	2,81	3,37	6,69	4,66	4,35	3,95	4,23	4,13	4,86	1,77	2,48	3,36	2,93	2,51	4,63	3,48	3,96
P. regius 1.7	13,57	3,55	3,55	1,53	2,81	3,46	6,64	4,72	4,21	4,01	4,13	4,21	4,96	1,60	2,31	3,43	2,84	2,38	4,64	3,44	4,01
P. regius 1.8	13,51	3,56	3,56	1,57	2,90	3,45	6,68	4,71	4,22	3,97	4,12	4,22	4,87	1,62	2,38	3,47	2,85	2,45	4,65	3,40	4,02
P. regius 1.9	13,62	3,55	3,55	1,54	2,83	3,36	6,70	4,73	4,26	4,05	4,29	4,16	4,95	1,61	2,36	3,36	2,95	2,36	4,71	3,41	3,98
P.regius 1.10	13,45	3,58	3,58	1,55	2,75	3,38	6,62	4,74	4,56	4,10	3,98	4,24	4,90	1,35	2,43	3,70	2,93	2,39	4,70	3,33	3,51
P. regius 2.1	20,92	5,75	5,21	1,53	3,63	5,16	8,67	6,54	5,12	4,60	5,88	4,02	7,28	2,74	3,05	5,51	3,17	3,88	6,15	3,73	4,81
P. regius 2.2	20,92	5,81	5,30	1,52	3,66	5,14	8,70	6,73	5,08	4,39	6,01	4,10	7,30	2,68	3,00	5,38	3,10	3,86	6,20	3,64	4,84
P. regius 2.3	20,97	5,75	5,24	1,52	3,51	5,14	8,67	6,56	5,07	4,54	5,95	4,14	7,34	2,75	3,11	5,38	2,98	3,96	6,11	3,69	4,78
P. regius 2.4	21,02	5,74	5,21	1,53	3,58	5,08	8,69	6,71	5,15	4,42	5,95	4,32	7,33	2,51	2,98	5,62	2,95	4,06	6,23	3,62	4,68
P. regius 2.5	21,02	5,74	5,14	1,53	3,49	4,99	8,63	6,60	5,24	4,66	6,12	4,18	7,44	2,78	3,02	5,59	2,92	3,97	6,17	3,60	4,68
P .regius 2.6	20,95	5,83	5,28	1,52	3,63	4,89	8,65	6,74	5,30	4,50	6,22	4,15	7,41	2,76	3,02	5,48	3,05	4,01	6,20	3,65	4,79
P. regius 2.7	21,03	5,71	5,16	1,51	3,44	5,12	8,71	6,72	5,12	4,46	6,01	4,11	7,44	2,76	3,13	5,43	2,85	3,92	6,17	3,59	4,79
P. regius 2.8	20,94	5,76	5,23	1,53	3,62	5,17	8,64	6,60	5,28	4,60	6,03	4,13	7,46	2,64	3,05	5,48	2,99	3,94	6,09	3,61	4,69
P. regius 2.9	21,06	5,72	5,16	1,53	3,55	4,95	8,73	6,60	5,34	4,59	6,07	4,15	7,38	2,76	2,98	5,66	2,89	4,07	6,18	3,64	4,69
P. regius 2.10	20,09	5,77	5,27	1,50	3,66	5,11	8,54	6,53	5,43	4,50	5,92	4,24	7,16	2,41	3,05	5,31	2,64	4,17	6,15	3,74	3,62
P. regius 3.1	16,61	4,36	4,36	1,47	3,26	4,09	7,89	5,70	4,26	4,45	5,01	4,31	6,35	1,70	2,69	4,27	2,79	3,00	5,49	3,32	4,58
P. regius 3.2	16,76	4,35	4,35	1,48	3,26	3,99	7,84	5,78	4,36	4,55	5,00	4,23	6,33	1,76	2,75	4,32	2,88	3,10	5,49	3,21	4,65
P. regius 3.3	16,73	4,41	4,41	1,48	3,28	4,16	7,86	5,69	4,29	4,56	5,06	4,28	6,30	1,71	2,66	4,46	2,93	3,17	5,47	3,27	4,72
P. regius 3.4	16,77	4,34	4,34	1,50	3,21	4,15	7,89	5,83	4,38	4,52	5,01	4,24	6,35	1,76	2,72	4,54	2,81	3,23	5,55	3,23	4,68
P. regius 3.5	16,61	4,35	4,35	1,49	3,24	4,17	7,91	5,83	4,49	4,52	5,10	4,29	6,35	1,78	2,75	4,57	2,83	3,16	5,48	3,25	4,59
P. regius 3.6	16,63	4,36	4,36	1,46	3,25	4,12	7,89	5,71	4,42	4,66	5,02	4,35	6,40	1,71	2,62	4,23	2,75	2,97	5,64	3,26	4,71
P. regius 3.7	16,60	4,42	4,42	1,51	3,23	4,18	7,88	5,83	4,39	4,52	5,02	4,24	6,36	1,72	2,80	4,55	2,85	3,14	5,43	3,28	4,65
P. regius 3.8	16,75	4,39	4,39	1,39	3,26	4,05	7,91	5,74	4,34	4,69	5,11	4,29	6,31	1,73	2,69	4,45	2,73	3,18	5,68	3,33	4,72
P. regius 3.9	16,78	4,42	4,42	1,45	3,24	3,93	7,90	5,67	4,41	4,56	5,12	4,30	6,28	1,73	2,75	4,53	2,71	3,20	5,49	3,25	4,65
P. regius 3.10	16,88	4,37	4,37	1,49	3,23	3,80	7,87	5,71	4,62	4,83	4,75	4,38	6,26	1,77	2,72	4,51	2,79	3,27	5,67	3,33	4,55

Appendix 4

List of characters and matrix used for the PCoA (Chapter 5 snake endocasts)

1/ Lateral margin of the olfactory peduncles in dorsal view

(1) Mediolaterally convex
(2) Straight
(3) Mediolaterally concave

2/ Antero-posterior projection of the olfactory peduncles in dorsal view

(1) Parallel
(2) Diverging laterally from the fronto-parietal suture
(3) Diverging laterally at the anterior end

3/ Ventral margin of the olfactory peduncles in lateral view

(1) Straight
(2) Ventrodorsally convex forming a bulge
(3) Ventrodorsally concave

4/ Separation between each olfactory peduncle in dorsal view

(1) No separation
(2) Olfactory peduncles diverging only at their anterior end
(3) Large space between the two olfactory peduncles

5/ Comparison between anterior and posterior widths of the olfactory peduncles

(1) Posterior part wider than the anterior end
(2) Posterior part as wide as the anterior end
(3) Anterior end wider than the posterior part

6/ Relative size of the cerebral hemispheres

(1) Cerebral hemispheres are wider than long
(2) Cerebral hemispheres are as long as wide
(3) Cerebral hemispheres are longer than wide

7/ Beginning of the lateral extension of the cerebral hemisphere

(1) Just posterior to the fronto-parietal suture
(2) Extension more posteriorly, the anterior part of the cerebral hemisphere is as wide as the fronto-parietal suture.

8/ Lateral margin of the cerebral hemispheres in dorsal view

(1) Rounded
(2) Straight

9/ Antero-posterior development of the cerebral hemisphere lateral view

(1) Cerebral hemisphere developed only along the horizontal axis

(2) Cerebral hemispheres developed in the horizontal plane but with a posterior part directed ventrally

(3) Dorso-ventral development of the cerebral hemisphere as important as the horizontal development

10/ Separation between the cerebral hemispheres and the optic tectum

(1) No delimitation between the two structures

(2) Presence of a groove between the two structures

11/ Pituitary gland development

(1) Presence only of a small bulge

(2) Pituitary gland only developed ventrally

(3) Pituitary gland developed both ventrally and posteriorly

12/ Posterior projection of the pituitary gland

(1) Tilted posterior projection

(2) Posterior projection in the horizontal plane

13/ Optic tectum

(1) Not distinguished on the endocast

(2) Visible only thanks to its decrease in width compared to the cerebral hemispheres

(3) Represented by a pair of domes and separated by a median sulcus

14/ Comparison between the widths of the optic tectum and the rhombencephalon

(1) Optic tectum as wide as the rhombencephalon

(2) Optic tectum wider than the rhombencephalon

(3) Rhombencephalon wider than the optic tectum

15/ Dorsal extension of the optic tectum

(1) Dorsal margin of the optic tectum located at the same height as the cerebral hemispheres

(2) Dorsal margin of the optic tectum located more dorsally than the cerebral hemispheres

16/ Ventral margin of the rhombencephalon

(1) Rounded

(2) Straight

(3) Triangular-shaped, pointing downward

17/ Ventral expansion of the rhombencephalon

(1) Corresponds to the most ventral surface of the brain endocast

(2) Does not correspond to the most ventral surface of the brain endocast

Rhinotyphlops schlegelii	1	1	1	1	1	2	1	1	1	1	1	NA	1	NA	NA	1	2
Typhlophis squamosus	1	1	1	1	2	2	1	2	1	1	1	NA	1	NA	NA	1	1
Uropeltis pulneyensis	1	1	1	1	2	2	1	2	1	1	1	NA	2	3	2	2	1
Cylindrophis ruffus	2	1	1	2	1	3	2	2	1	1	1	NA	2	3	1	1	1
Anilius scytale	1	1	1	2	1	3	2	2	1	1	1	NA	2	3	1	1	1
Atractaspis irregularis	2	2	1	2	2	2	1	1	2	1	1	NA	2	1	1	1	1
Python regius 3	1	1	2	1	2	1	1	1	2	1	2	NA	2	1	1	1	1
Python regius 2	1	1	2	2	2	1	1	1	2	1	2	NA	2	1	1	1	1
Python regius 1	2	1	2	1	2	1	1	1	2	1	2	NA	2	1	1	1	1
Candoia sp	2	1	2	2	1	1	1	1	2	2	3	2	2	1	2	1	1
Crotalus atrox	3	1	1	2	3	1	1	1	2	2	3	1	3	1	1	3	2
Agkistrodon contortrix	3	1	1	2	3	1	1	1	2	2	3	1	3	1	1	3	2
Mimophis mahfalensis	3	3	3	1	2	1	1	2	2	2	3	2	3	2	2	2	1
Micrurus lemniscatus	3	1	1	2	2	2	1	2	1	1	2	NA	2	3	1	1	2
Naja nivea	3	3	1	2	2	1	1	1	2	2	3	1	3	1	1	1	1
Thamnophis sirtalis	3	3	1	2	3	2	1	2	3	2	3	1	3	2	2	1	1
Hierophis gemonensis	3	3	1	2	3	1	1	2	3	2	3	2	3	2	1	2	1
Hierophis viridiflavus	3	3	1	2	3	1	1	2	3	2	3	2	3	2	1	2	1
Coronella austriaca	3	3	2	2	3	1	1	2	3	2	3	2	3	1	2	1	1
Boa constrictor	2	1	1	1	2	1	1	1	2	1	2	NA	2	1	1	1	2
Corallus hortulanus	3	1	2	2	3	1	1	1	3	1	2	NA	2	1	1	1	1
Pareas margaritophorus	1	1	1	1	2	1	1	1	2	1	2	NA	3	1	1	1	2
Chrysopelea ornata	3	3	1	2	3	1	1	2	3	2	3	2	3	2	1	2	1
Dispholidus typus	3	3	1	2	3	1	1	2	3	2	3	2	3	2	2	1	1
Boiga dendrophila	3	3	2	2	3	1	1	2	3	2	3	2	3	1	2	1	1
*Dasypeltis*sp	2	3	2	2	3	1	1	2	3	2	3	2	3	1	2	2	1
Eunectes murinus	2	1	2	2	2	1	1	1	2	1	2	NA	2	1	1	1	1
Acrochordus granulatus	1	1	1	3	2	1	1	1	2	1	2	NA	2	3	1	2	1
Enhydris enhydris	3	1	1	2	2	1	1	1	2	2	3	2	3	2	2	2	1
Enhydris punctata	2	1	1	2	2	1	1	1	2	2	3	1	3	1	1	2	1
Cerberus rynchops	2	1	2	2	2	1	1	1	2	2	3	2	3	1	1	2	1
Homalopsis buccata	2	2	1	3	2	1	1	1	2	2	3	2	3	1	1	1	2
Erpeton tentaculum	2	2	1	3	2	1	1	1	2	2	3	2	3	1	2	2	1
Fordonia leucobalia	2	1	1	2	2	1	1	2	2	2	3	1	3	1	1	2	1
Cantoria violacea	1	1	1	2	2	1	1	2	3	1	3	2	2	1	1	2	1
Bitia hydroides	3	1	2	2	1	2	1	1	2	2	3	2	3	1	1	1	1
Aipysurus duboisii	1	1	2	2	1	1	1	1	2	1	3	1	2	1	1	1	2
Aipysurus eydouxii	1	1	2	2	1	1	1	1	2	1	3	1	2	1	1	1	1
Microcephalophis gracilis	1	1	2	2	1	2	1	1	1	1	2	NA	2	1	1	2	1
Hydrophis elegans	1	1	2	2	1	2	1	2	1	1	3	1	2	1	1	1	2
Enhydrina schistosa	1	1	2	2	1	2	1	2	1	1	3	1	2	3	1	2	1
Astrotia stokesii	1	1	2	2	1	1	1	2	1	1	3	1	2	1	1	2	1
Hydrophis major	1	2	2	2	1	2	1	2	1	1	3	1	2	1	1	1	2
Hydrophis ornatus	1	2	2	2	1	2	1	1	1	1	3	1	2	1	1	1	1
Pelamis platurus	2	2	2	3	1	2	1	1	1	1	3	1	3	1	1	1	1

Appendix 5

Distribution of the variables in the principal component analyses performed on the 45 snake specimens

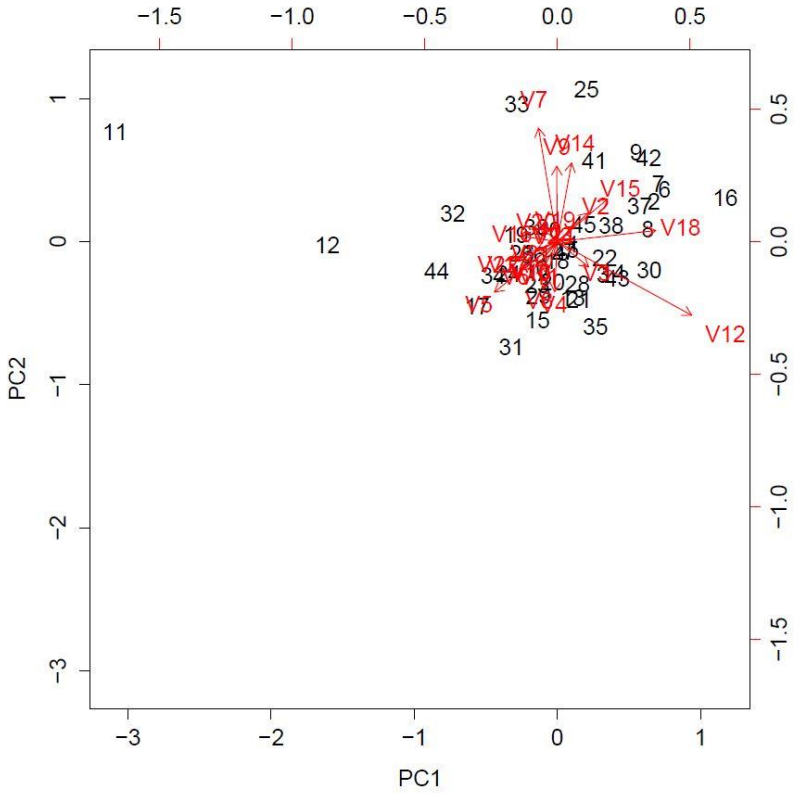

Appendix 6

Table of measurements (in mm) taken on varanid endocasts and *Tethysaurus nopcsai* (SMU 76335) (Chapter 7)

	LE	LOB	LG	HOB	HOP	WOP	WOR	LP	HP	WIE	DWPE	HPE	WPE	WP
V. salvator	24.08	8.93	8.93	2.49	2.3	2.85	10.95	6.88	3.16	3.26	3.98	4.66	7.98	6.45
V. prasinus	24.09	8.4	7.4	2.14	1.57	2.3	10.8	7.02	4.2	2.47	2.78	3.07	6.69	5.3
V. niloticus	24	9.07	9.07	2.28	1.73	2.25	9.7	7.95	4.35	3.34	3.89	3.75	7.1	6.07
V. exanthematicus	20.53	7.98	7.98	1.98	2.69	2.71	9.34	8.01	4.1	3.1	3.33	4.23	6.73	5.43
T. nopcsai	72.1	29.6	26.5	4.20	3.3	5.1	21.2	16.2	17.2	9.5	3.4	7.8	8.3	9.8

Appendix 7

Digital endocasts of the *Tethysaurus nopcsai* specimens GM 1, GM 2, GM 3

These specimens, which consist in the braincase only, are preserved in the collections of the Southern Methodist University of Dallas (USA) and data provided by prof. Michael Polcyn with which collaborations are made. The endocranial reconstructions provided the posterior part of the endocasts presented here in left lateral view. **Abbreviations**: **c**, cartilage between the parietal and supraoccipital; **ic**, internal carotid; **V**, trigeminal nerve; **VI**, abducens nerve; **VII**, facial nerve; **IX**, glossopharyngeal nerve; **X-XI**, vagus and accessory nerves; **XII**, hypoglossal nerves. Scale bar equals 10 mm.

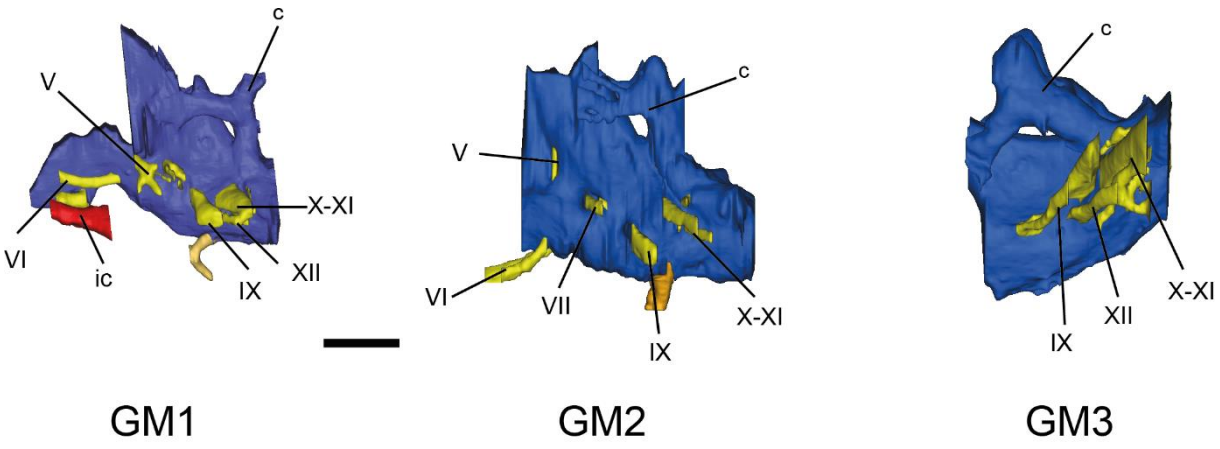

Appendix 8

The character matrix used in Chapter 8.1 is based on that of Benson & Druckenmiller (2014) to which two plesiosaurian taxa were added: SMNS 81783 and the type specimen of *Libonectes atlasense* SMNK-PAL 3978 (see character scores below). Character scores used here for *Libonectes morgani* follow the re-scored proposed by Sachs & Kear (2015).

SMNS 81783

100010?01100?0200??001001??0?0??00??000????0000?0??0??1??????1

?101?1212??01????10122?1?????????0?1?2?130????111100??????????

???0??1010???000????110??

??

??????????????????????

Libonectes atlasense (SMNK-PAL 3978)

00001??0???0????1?0?0??????0?0???0100?????11??????????1???????

????????????????1????????????????????????????????????1??????????

??????1010?0??00????1?0????4?1??1????0????????????1???1??????

??

???????1??1??????????

Appendix 9

Published papers.

Appendix 9.1. Allemand, R., N. Bardet, A. Houssaye and P. Vincent. 2017. Virtual re-examination of a plesiosaurian specimen (Reptilia, Plesiosauria) from the Late Cretaceous (Turonian) of Goulmima (Southern Morocco) thanks to computed tomography. Journal of Vertebrate Paleontology 37: doi:10.1080/02724634.2017.1325894.

Appendix 9.2. Allemand, R., R. Boistel, Z. Blanchet, R. Cornette, N. Bardet, P. Vincent, and A. Houssaye. 2017. Comparative morphology of snake (Squamata) endocasts: evidence of phylogenetical and ecological signals. Journal of Anatomy 2017:doi: 10.1111/joa.12692.

Journal of Vertebrate Paleontology e1325894 (14 pages)

DOI: 10.1080/02724634.2017.1325894

ARTICLE

VIRTUAL REEXAMINATION OF A PLESIOSAURIAN SPECIMEN (REPTILIA, PLESIOSAURIA) FROM THE LATE CRETACEOUS (TURONIAN) OF GOULMIMA, MOROCCO, USING COMPUTED TOMOGRAPHY

RÉMI ALLEMAND,*[,1,2] NATHALIE BARDET,[1] ALEXANDRA HOUSSAYE,[2] and PEGGY VINCENT[1]
[1]Centre de Recherches sur la Paléobiodiversité et les Paléoenvironnements, CR2P-UMR 7207, CNRS, MNHN, UPMC, Sorbonne Universités, 57 rue Cuvier, CP38, F-75005, Paris, France, remi.allemand@edu.mnhn.fr; nathalie.bardet@mnhn.fr; peggy.vincent@mnhn.fr;
[2]UMR 7179, CNRS, MNHN, Département Adaptations du Vivant, 57 rue Cuvier, CP55, F-75005, Paris, France, alexandra.houssaye@mnhn.fr

ABSTRACT—Turonian deposits of the Goulmima area, Er-Rachidia Province in southern Morocco, have yielded a diverse marine vertebrate fauna, including chondrichthyans, bony fishes, and large marine reptiles such as plesiosaurians, mosasauroids, and turtles. These fossils are included in ovoid calcareous nodules that are difficult to prepare. Moreover, bones may be partially or totally dissolved, making their study difficult. Using computed tomography, we have reconstructed the entire skull anatomy of SMNS 81783, one of the rare plesiosaurian specimens found in this locality and more generally in Africa. The digital three-dimensional reconstruction of the skull and the mandible offers for the first time the possibility to describe this specimen exhaustively. The new anatomical characters recorded confirm that SMNS 81783 belongs to Elasmosauridae on the basis of (1) slender and triangular skull; (2) beak index equal to 42%; (3) temporal fossa estimated to occupy about 40% of the skull length; (4) long process of the premaxillae extending posteriorly to meet the parietal above the orbit and separating the frontals; and (5) margin of the temporal fenestra lacking obvious contribution from the frontal. A preliminary phylogenetic analysis confirms its elasmosaurid affinity. The relationships between SMNS 81783, *Libonectes atlasense*, and *Libonectes morgani*, as well as the presence of stapes and pineal foramen, are discussed.

SUPPLEMENTAL DATA—Supplemental materials are available for this article for free at www.tandfonline.com/UJVP

Citation for this article: Allemand, R., N. Bardet, A. Houssaye, and P. Vincent. 2017. Virtual reexamination of a plesiosaurian specimen (Reptilia, Plesiosauria) from the Late Cretaceous (Turonian) of Goulmima, Morocco, using computed tomography. Journal of Vertebrate Paleontology. DOI: 10.1080/02724634.2017.1325894.

INTRODUCTION

Plesiosaurians are extinct predatory marine reptiles that represent one of the longest-persisting groups of Mesozoic marine reptiles, ranging stratigraphically from the Late Triassic to the latest Cretaceous (e.g., Benson et al., 2012; Vincent et al., 2013). Plesiosaurians went extinct during the Cretaceous–Paleogene biotic crisis (Gasparini et al., 2003a; Vincent et al., 2011). However, during the Late Cretaceous, they had a worldwide distribution, including high-latitude seas surrounding Antarctica (Gasparini et al., 2003b; Novas et al., 2015). The fossil record of plesiosaurians is scarcer in Africa than in other continents (Vincent et al., 2011, 2013). Up to now, eight valid taxa have been described from this continent: *Leptocleidus capensis* Andrews, 1911, from the Valanginian (Early Cretaceous) of South Africa (Andrews, 1911; Cruickshank, 1997); *Thililua longicollis* Bardet et al., 2003a, *Manemergus anguirostris* Buchy et al., 2005, *Libonectes atlasense* Buchy, 2005, *Libonectes morgani* Carpenter, 1997, and *Brachauchenius lucasi* Williston, 1903, all from the Turonian (Late Cretaceous) of Morocco (Bardet et al., 2003a; Buchy, 2005; Buchy et al., 2005; Angst and Bardet, 2015; Sachs and Kear, 2017); and *Zarafasaura oceanis* Vincent et al., 2011, as well as *Cardiocorax mukulu* Araújo et al., 2015, from the Maastrichtian (latest Cretaceous) of Morocco (Vincent et al., 2011; Lomax and Wahl, 2013) and Angola (Araújo et al., 2015), respectively. Very fragmentary remains indeterminable at the infrafamilial level also have been described from the Maastrichtian of Morocco, Egypt, and Angola (e.g., Stromer, 1935; for details, see Vincent et al., 2011).

In Morocco, the Goulmima area is on the southern slope of the High Atlas (see Fig. 1A) (Bardet et al., 2003a, 2003b, 2008). Several fossiliferous localities of early Late Cretaceous (Turonian) age in the area have yielded a diverse marine fauna, including ammonites, chondrichthyans (Underwood et al., 2009), bony fishes (Cavin, 1995, 1997, 1999, 2001; Cavin et al., 2001, 2010), and large marine reptiles, such as a turtle, the basal mosasauroid *Tethysaurus nopcsai* Bardet et al., 2003b (Bardet et al., 2003b, 2008), and five plesiosaurian taxa: *Thililua longicollis, Manemergus anguirostris, Libonectes atlasense*, *Libonectes morgani*, and *Brachauchenius lucasi* (Bardet et al., 2003a; Buchy, 2005; Buchy et al., 2005; Angst and Bardet, 2015; Sachs and Kear, 2017). According to Cavin et al. (2010), the vertebrate fossils are contained in ovoid, early diagenetic, calcareous nodules up to 1 m in size. The fossiliferous nodules contain skeletal remains, mainly skulls and vertebral elements, and the marine reptile specimens are sometimes preserved in several distinct nodules (Cavin et al., 2010). Although fossils from this assemblage can sometimes be chemically prepared by dissolving the matrix with formic acid, in many cases the nodule core is composed of siliceous material that prevents complete preparation of the specimens (Cavin

*Corresponding author.

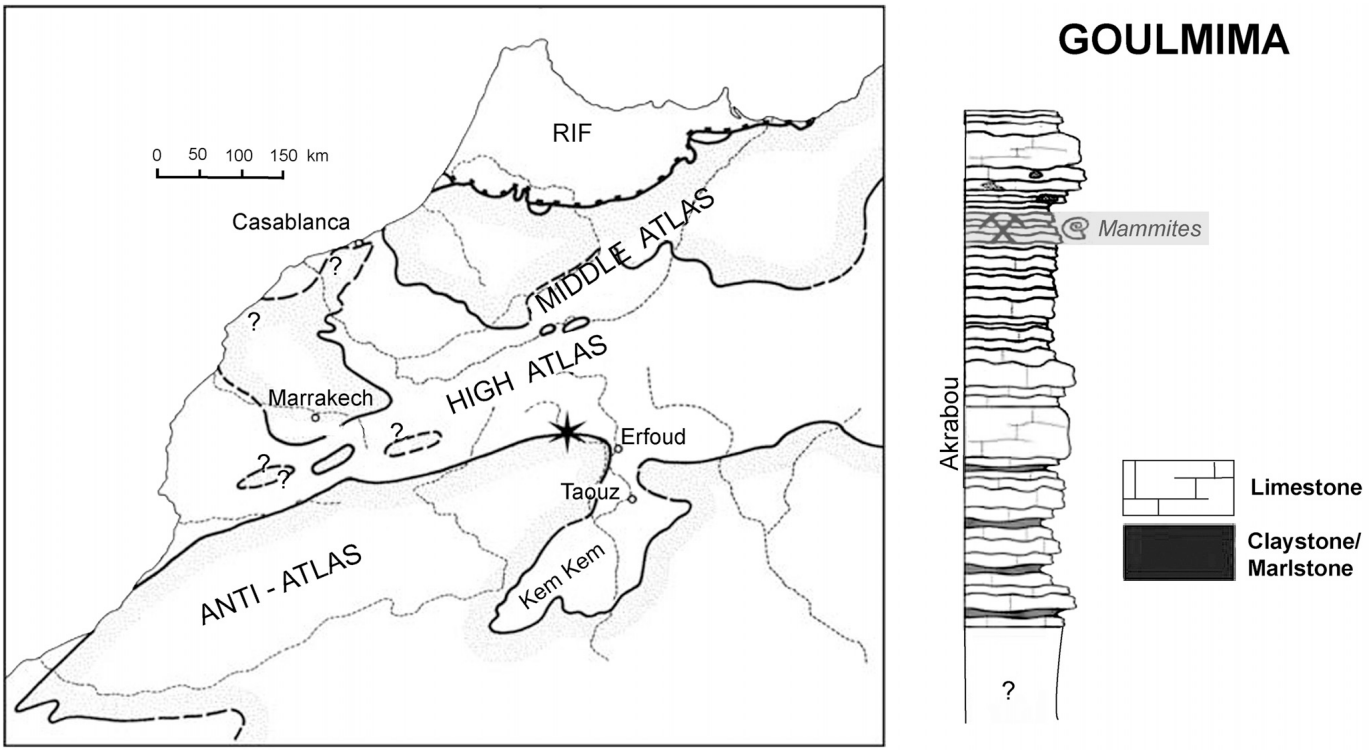

FIGURE 1. Palaeogeographical location of the Goulmima area in southern Morocco and probable stratigraphical range (*Mammites* horizon) of plesiosaurian specimen SMNS 81783 (modified from Angst and Bardet, 2015).

et al., 2010). Moreover, fossilized bones in the nodules are often completely dissolved, making their extraction from the host rock and their study difficult or impossible. This particular preservation can often prevent complete access to the fossil anatomy, and the use of computed microtomography represents a solution to circumvent these technical issues. Here, we used microtomography on a plesiosaurian specimen (SMNS 81783) from this locality. This specimen, poorly preserved in an incompletely prepared nodule (Fig. 1B), was previously referred to *Libonectes atlasense* (Buchy, 2005). This technique reveals details of anatomy that are not otherwise directly observable.

Institutional Abbreviations—MNHN, Muséum National d'Histoire Naturelle, Paris, France; **SMNS**, Staatliches Museum für Naturkunde, Stuttgart, Germany; **SMU SMP**, Shuler Museum of Paleontology, Southern Methodist University, Dallas, Texas, U.S.A.

GEOGRAPHIC AND STRATIGRAPHIC CONTEXT

According to Buchy (2005:6), the specimen comes from "some kilometers around Goulmima" in southern Morocco (Fig. 1), as is the case for the type specimens of *Libonectes atlasense* and *Manemergus anguirostris* (Buchy, 2005; Buchy et al., 2005). Although their exact location remains unknown, the calcareous matrix surrounding these specimens is consistent with the vertebrate-bearing nodules known from the Early Turonian of the Goulmima area (Cavin, 1995, 1997, 1999, 2001; Cavin et al., 2001; Bardet et al., 2003a, 2003b; Buchy, 2005; Buchy et al., 2005). These nodules are concentrated near the top of a Cenomanian–Turonian calcareous succession, in Unit 4 of Ferrandini et al. (1985), previously considered as Early Turonian in age based on the ammonite assemblage (mainly *Mammites*) (Bardet et al., 2003a, 2003b, 2008). The unit was later reappraised as Unit T2a of the Akrabou Formation, Middle Turonian in age, by Ettachfini and Andreu (2004). The Goulmima area was the center of a basin exemplifying large subsidence during the Cenomanian–Turonian transgression. It corresponds to an open marine carbonate platform with influences essentially from the Tethys but also from the central Atlantic (Cavin et al., 2001; Ettachfini and Andreu, 2004; Bardet et al., 2008). The Goulmima deposits surrounding the nodules correspond to marine limestones deposited in dysoxic conditions (Lebedel et al., 2013).

MATERIALS AND METHODS

The specimen is currently housed in the SMNS under collection number SMNS 81783. It is preserved in a nodule about 40 cm long, up to 11 cm wide, and 13 cm high (Fig. 2A, B), which encompasses a skull with mandible in occlusion and the atlas-axis complex. The specimen is incompletely prepared. Its anterior half shows bones incompletely dissolved and exposed, surrounded by a light beige matrix (Fig. 2A, B). The posterior half of the fossil is still embedded in the matrix and thus not observable.

The specimen was scanned at the AST-RX platform of the MNHN (Paris) using a GE Phoenix v|tome|x L240 X-ray scanner with a voxel size of 134 μm (voltage: 230 kV, intensity: 500 μA). A virtual three-dimensional (3D) reconstruction of the skull was then performed at the Palaeontology Imaging Unit of the MNHN Origines et Evolution/UMR 7207 CR2P CNRS/MNHN/UPMC using the MIMICS (Materialise Interactive Medical Image Control System) Innovation Suite software (Materialise, release 18). During segmentation work, bony elements appeared generally with darker grayscale values than the matrix (Fig. 2) due to the different X-ray absorption coefficients. However, no unique threshold value could accurately describe the boundary between bone and the matrix. The reconstruction was thus obtained with the multiple two-dimensional cross-sectional slices edit tool of MIMICS and interpolation between selections on

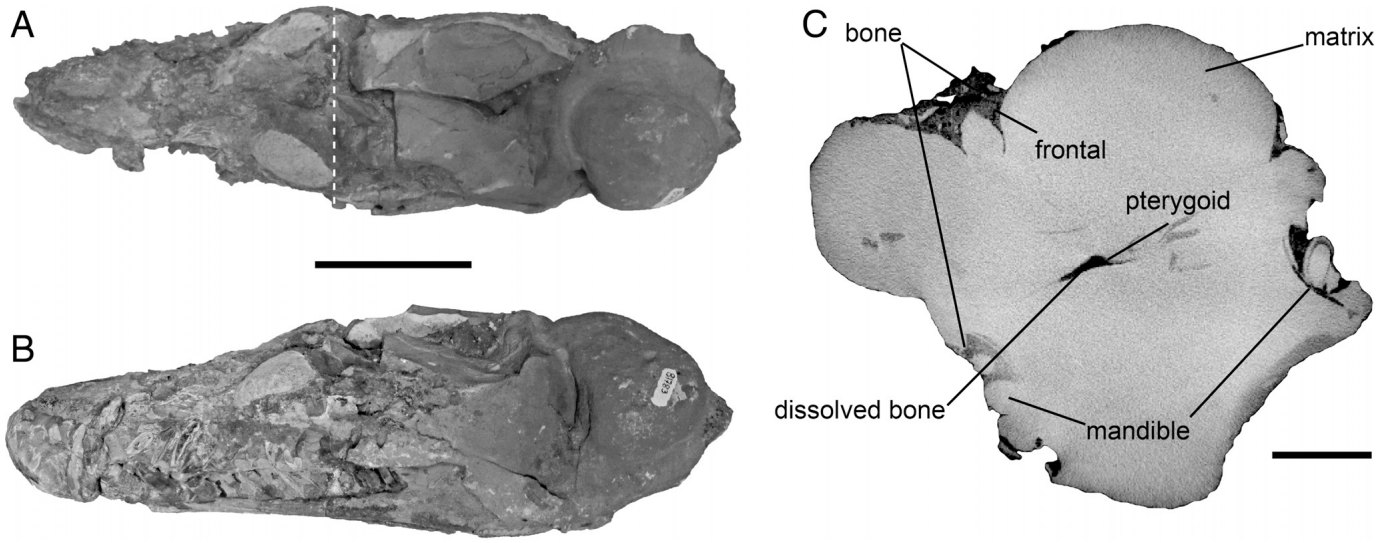

FIGURE 2. **A**, **B**, photographs of SMNS 81783 in dorsal (**A**) and left lateral (**B**) views. The dotted line indicates the location of the transverse section. **C**, transverse section in the middle of the skull of SMNS 81783 showing the general state of preservation. Scale bars equal 10 cm (**A**, **B**) and 2 cm (**C**).

noncontiguous slices. The shape of some bones that appeared completely dissolved at the surface of the nodule has been reconstructed using their natural cast encased in the matrix. This was the case for the mandible, for which only the cast of the medial margin is preserved (Fig. 2C) so that the lateral margin was reconstructed by an approximate extension of its contour (see Fig. 6, hatched area). The same method was used for reconstruction of the lateral margins of the jugal and the squamosal (see Fig. 3, hatched area).

SYSTEMATIC PALEONTOLOGY

SAUROPTERYGIA Owen, 1860
Order PLESIOSAURIA Blainville, 1835
Family ELASMOSAURIDAE Cope, 1869
LIBONECTES MORGANI Carpenter, 1997

Holotype—SMU SMP 69120, skull and mandible, atlas-axis complex, 48 successive cervical vertebrae, fragmentary thoracic ribs, gastralia, and associated gastroliths (Sachs and Kear, 2015); Upper Cenomanian; Britton Formation, Eagle Ford Group, near Cedar Hill, Dallas County, Texas, U.S.A.

Referred Specimens—SMNK-PAL 3978, articulated skull and postcranial skeleton (Buchy, 2005; Sachs and Kear, 2017); SMNS 81783, skull and mandible, atlas-axis complex. Middle Turonian (Upper Cretaceous) Unit T2a (Ettachfini and Andreu, 2004) of the Cenomanian–Turonian limestone bar, north of Goulmima, Er-Rachidia Province, southern Morocco.

DESCRIPTION

General Preservation

The skull of SMNS 81783 is slightly laterally crushed, but most of the bones remain in their natural arrangement and only some parts are missing, including the most dorsal part of the parietal crest, the left lateral margin of the temporal fenestra, and both squamosal arches. The right maxilla is almost dissolved, so that only a small part is preserved. The left part of the palate is broken and disarticulated, but much of the right side, posterior to the internal nares, is well preserved. The identification of the sutures between palatal bones is difficult, and the narial region is crushed and difficult to interpret. The mandible is almost completely preserved except its lateral margin and the posterior part of the right dentary, and it is in occlusion with the cranium.

Skull

We estimate that the original cranial length was about 295 mm from the tip of the premaxilla to the occipital condyle (see measurements and skull proportions in Table 1). The beak index (percentage of the preorbital length to the entire length of the skull; Welles, 1952) is 42%. In most elasmosaurids, this value is close to 40%, whereas it is close to 55% in Polycotylidae (Buchy et al., 2005). The temporal fossae are estimated to have occupied about 40% of the skull length. A similar ratio (35–40%) is observable in Cretaceous Elasmosauridae (Sato et al., 2006).

Premaxillae—Each premaxilla bears five teeth and contributes to the external naris (Fig. 3B), forming its anterior and medial margins. The flat dorsal surface of the premaxilla is slightly pitted and bears a clearly visible suture between the two premaxillae (Fig. 3A). In SMNS 81783 there is a slight transverse 'rostral' constriction between the premaxilla and the maxilla (Fig. 3A), as observed in many large-headed plesiosaurians (e.g., Taylor, 1992; O'Keefe, 2001; Druckenmiller and Russell, 2008; Smith and Dyke, 2008) and in some elasmosaurids (e.g., Vincent et al., 2011). A small diastema forms a concavity between the last premaxillary and the first maxillary teeth (Fig. 3C). The premaxilla-maxilla suture originates posterior to the fifth premaxillary alveolus and extends posterodorsally to a point just anterodorsal to the external naris (Fig. 3C). The posterolateral extension of the premaxilla at the level of the posterior narial border is unclear (Fig. 3A, C), and it is impossible to confirm the presence of a prefrontal and its possible extension. In dorsal view, at the level of the interorbital region, the posterior process of the premaxilla forms a shallow concavity separating the frontals (Fig. 3A). The posterior extension of the premaxillae is long and shows a small contact with the parietal at the level of the last third of the orbital length (Fig. 3A). This feature is seen in many Late Cretaceous elasmosaurids (Sato et al., 2006), polycotylids, and some pliosaurids (Ketchum and Benson, 2010). A small isolated piece of bone, located dorsally in the interorbital region, is preserved dorsally to the concavity of the posterior processes of the premaxillae (Fig. 3A). It is tentatively interpreted as part of the premaxilla, because it matches perfectly with the concavities of the posterior processes of the premaxillae and covers the sutures

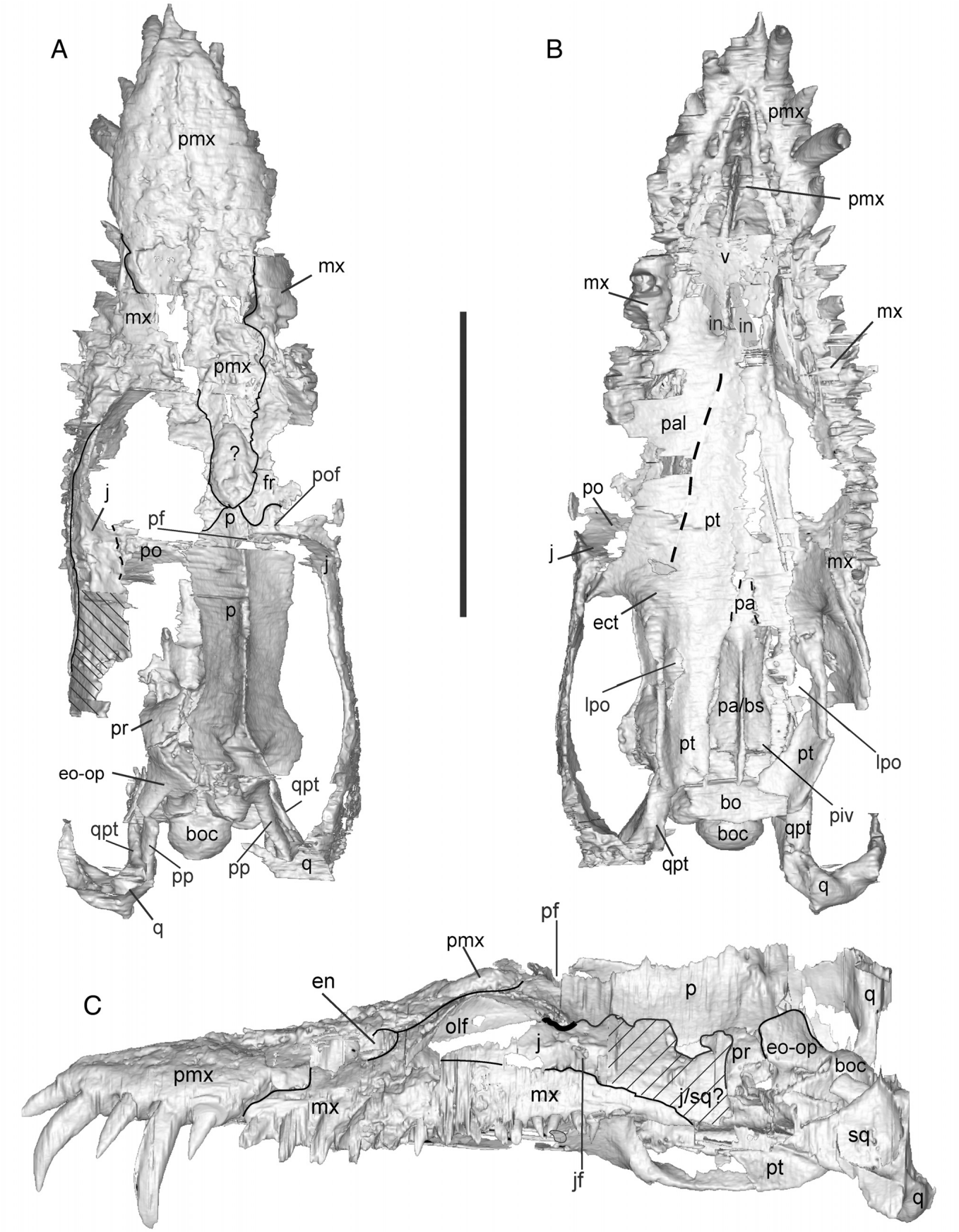
A
pmx
mx
mx
pmx
?
fr
pof
j
pf
p
po
j
p
pr
eo-op
qpt
qpt
boc
pp
pp
q
q
B
pmx
pmx
v
mx
mx
in
in
pal
po
pt
j
mx
pa
ect
lpo
pa/bs
pt
pt
lpo
bo
piv
boc
qpt
qpt
q
C
pf
pmx
en
olf
p
q
j
pr
eo-op
boc
pmx
mx
mx
j/sq?
sq
pt
jf
q

TABLE 1. Measurements (in mm) of the skull and the mandible of SMNS 81783.

Skull length	295
Preorbital length (tip of the snout to anterior margin of orbit)	124
Orbit length (l)	53.4
Temporal fenestra length (r)	128
Paroccipital process length (r)	30
Mandibular symphysis length	44.5

Measurements taken on the left (l) or the right (r) side.

between the premaxillae and the frontal. In ventral view, the palatal surface of the premaxillae exhibits an alveolar channel connecting the replacement alveoli (Fig. 3B).

Maxillae—The right maxilla is severely damaged; only a small piece of its preorbital part is present (Fig. 3C). The left maxilla is well preserved and shows 15 alveoli (Fig. 3C). The maxilla forms the lateral, ventral, and posteroventral margins of the external naris and the anterior corner of the orbit (Fig. 3A, C) as in *Libonectes morgani* (Carpenter, 1997). Anterior to the orbit, the sutures between the maxilla and the frontal-prefrontal are not observable (Fig. 3A, C). Laterally, the maxilla extends beneath the orbit and underlaps the jugal ventrally (Fig. 3C). The maxilla-jugal suture is long and posteroventrally directed as in other elasmosaurids (e.g., *Futabasaurus suzukii*; Sato et al., 2006), and it extends posteriorly to about half the length of the temporal fenestra. Its suture with the squamosal is unclear (Fig. 3C), as is the participation of the maxilla in the margin of the internal naris in palatal view (Fig. 3B).

Nares—The external nares are located above the third to fifth maxillary teeth (Fig. 3C), just anterior to the orbits. The anterior extension of the external nares is difficult to determine (Fig. 3A, C). The internal nares (Fig. 3B) largely overlap the external ones but are located slightly anteriorly to them, as in *Libonectes morgani* (e.g., Carpenter, 1997).

Frontal—The frontal forms the roof of the orbit (Fig. 3A). It contacts the premaxillae medially and the postfrontal posterolaterally (Fig. 3A). It does not seem to contribute to the temporal fenestra, but because of the bad preservation of this area, it is not possible to comment on its contact with the maxillae. The frontals are separated by the long dorsal processes of the premaxillae along their entire length, as in most elasmosaurids (Vincent et al., 2011), but unlike the condition in all Jurassic and a few Cretaceous taxa (*Brancasaurus* and *Callawayasaurus*) that exhibit frontals in contact along their entire length (Carpenter, 1997, 1999; Sato, 2003; Kear, 2005; Brown et al., 2013). Around the posterior orbital margins, the sutural relationships between the frontal, the premaxillae, the parietal, the postfrontal, and the postorbital are difficult to interpret (Fig. 3A). Ventrally, the frontals form the lateral wall of the olfactory sulcus (Fig. 3C).

Orbits—The maxilla forms the anterolateral corner of the orbit (Fig. 3A, C), but it is not clear whether the maxilla or the prefrontal forms the anteromedial corner. The frontal and the jugal form its dorsal and ventral edges, respectively (Fig. 3A, C), as in *Libonectes morgani, Styxosaurus*, and *Thalassomedon* (Carpenter, 1997). The ventral margin formed by the maxillae appears convex in lateral view (Fig. 3C), as in many elasmosaurids (Sato et al., 2006). As in most known elasmosaurid skulls (e.g., *Terminonatator*; Sato, 2003), the sclerotic ring is not preserved.

Postorbital Bar—The postorbital bar is partially preserved on both sides (Fig. 3A). The exact nature of its contacts with the frontal and the postfrontal, as well as its relationships with the posterior rim of the orbits, and its possible contact with the squamosal posteriorly are unclear.

Jugal—The jugal is a plate-like, transversely thin bone that forms the majority of the ventral margin of the orbit (Fig. 3C), as in *Libonectes morgani* and *Futabasaurus* (Carpenter, 1997; Sato et al., 2006). The left jugal is well preserved, unlike the right one, but the suture with the postorbital is not easily observable (Fig. 3A). Posterior to the orbit, a large foramen perforates the lateral surface of the jugal (Fig. 3C), as in *Libonectes morgani* (Welles, 1949). It is not possible to differentiate the squamosal from the posterior part of the jugal (Fig. 3C).

Parietal—The closed parietals form a median dorsal roof over the endocranial cavity, with weakly concave lateral surfaces. The exact height of the parietal crest is unknown because of partial dissolution (Fig. 3C). Anteriorly, the parietal contacts the frontal at the level of the posterior margin of the orbit (Fig. 3A). A small pineal foramen is present anteriorly and is totally enclosed within the parietals at the level of the postorbital bar (Fig. 3A). The pineal foramen is absent in most elasmosaurids (*Futabasaurus suzukii, Libonectes morgani, Styxosaurus snowii, Terminonatator ponteixensis, Tuarangisaurus keyesi*, and *Zarafasaura oceanis*) but present in *Callawayasaurus* (Welles, 1952). Its loss is considered a synapomorphy of Late Cretaceous Elasmosauridae and Polycotylidae by Carpenter (1997), but recent phylogenetic data sets suggest that the pineal foramen was lost independently in some Cretaceous elasmosaurids (e.g., *Eromangasaurus*) and some polycotylids (O'Keefe, 2001; Kear, 2005; Druckenmiller and Russell, 2008; Ketchum and Benson, 2010). The posterior end of the parietal overlaps the supraoccipital.

Squamosal—Both squamosals are partially preserved (Fig. 3A, C); their medial contact is not preserved. The left dorsal ramus has been lost, along with the medial dorsal portion of the right ramus. The anterior and ventral rami are preserved on the right side and show that the suspensorium was only slightly inclined anterodorsally (Fig. 3A), in contrast to the straight suspensorium present in *Terminonatator* (Sato, 2003) or the curved one (posterior margin is convex in lateral view) of *Styxosaurus* and *Thalassomedon* (Carpenter, 1999). The right anterior ramus of the squamosal forms the temporal bar, contacting the jugal anteriorly (Fig. 3A). The sutural relationships of the ventral ramus of the squamosal with the quadrate remain unclear. On the right side, medial to the quadrate, the squamosal is overlain by the quadrate ramus of the pterygoid.

Quadrate—The right quadrate is poorly preserved, but the left one is almost complete (Fig. 3A, C), although its most posterior surface is dissolved. The left quadrate seems to be mediolaterally convex in posterior view and concave in anterior view. It extends anteromedially to contact the quadrate ramus of the pterygoid (Fig. 3A, B). Ventrally, the quadrate extends well ventral to the tooth row (Fig. 3C), being the thickest at the articulation with the mandible to form a large quadrate condyle. The latter is divided into two parts by an oblique, anteroposteriorly oriented intercondylar depression. Both quadrates have a small depression on their medial surface corresponding to the facet of the paroccipital process (Fig. 3A).

Vomer—The vomer is poorly preserved; its anterior-most part is missing (Fig. 3B), and the occurrence of a vomeronasal foramen cannot be determined. The vomer forms the anterior and medial margins of the internal naris (Fig. 3B). Its posterior extension and its sutural relationships with the pterygoid are unclear. The median

←FIGURE 3. Digital reconstruction of the skull of SMNS 81783 in dorsal (**A**), ventral (**B**), and left lateral (**C**) views. **Abbreviations**: **bo**, basioccipital; **boc**, occipital condyle; **ect**, ectopterygoid; **en**, external naris; **eo-op**, exoccipital-opisthotic; **fr**, frontal; **in**, internal nares; **j**, jugal; **jf**, jugal foramen; **lpo**, lateral pterygoid opening; **mx**, maxilla; **olf**, lateral wall of the olfactory canal; **p**, parietal; **pa**, parasphenoid; **pa/bs**, parabasisphenoid; **pal**, palatine; **pf**, pineal foramen; **piv**, posterior interpterygoid vacuities; **pmx**, premaxillae; **po**, postorbital; **pof**, postfrontal; **pp**, paraoccipital process; **pr**, prootic; **pt**, pterygoid; **q**, quadrate; **qpt**, quadrate ramus of the pterygoid; **sq**, squamosal; **v**, vomer; ?, undetermined bone. Scale bar equals 10 cm.

suture between the two vomers is clearly seen in the median sheet of bone separating the internal nares (Fig. 3B).

Palatine—The palatine is well preserved on the right side of the palate (Fig. 3B), although some parts are partially broken and its sutural relationships with the pterygoid are not visible. On the left side the palatine is damaged (Fig. 3B). The anterior extension of the palatine, as well as its participation in the naris margin, is unclear (Fig. 3B).

Pterygoid—The right pterygoid is well preserved, whereas the left one is damaged in a similar manner to the left palatine (Fig. 3B). The pterygoids form the central plate-like portion of the palate, posterior to the vomers and anterior to the posterior interpterygoid vacuities (Fig. 3B). Both pterygoids are broken anterior to the posterior interpterygoid vacuities, obscuring their midline suture. Our interpretation is that there is no anterior interpterygoid vacuity and that the pterygoids are closed along their median suture (Fig. 3B), as in the Jurassic microcleidids, *Microcleidus tournemirensis*, and *Microcleidus homalospondylus* (see Brown et al., 2013), as well as in Cretaceous elasmosaurids (Bardet et al., 1999; Großmann, 2007). Lateral to the narrow and elongated posterior interpterygoid vacuities, the ventral surface of the pterygoid is slightly concave and its lateral margin is projected ventrolaterally, forming a curved prominent flange that contacts posteriorly the quadrate ramus (Figs. 3B, 4). On the right side, the pterygoid bears an anteroposteriorly extended opening located laterally to the posterior interpterygoid vacuities (Figs. 3B, 4). Despite poor preservation of this area on the left side, an opening on the left pterygoid appears present as well. These openings are exactly mirrored on the left and right pterygoids (Fig. 3B), which suggests that they are most likely not taphonomic artifacts. Such openings were reported in *Zarafasaura* as a possible autopomorphy of the taxon (Vincent et al., 2011). Posterior to the interpterygoid vacuities, the bones are dissolved and it is not possible to comment on the medial contact between the pterygoids covering the basioccipital (Fig. 3B).

Epipterygoid—The epipterygoid forms a thin vertical process lateral to the parabasisphenoid (Fig. 4). The epipterygoid seems to extend dorsally from the anterior dorsal edge of the vertical pterygoid process, similarly to that observed in *Libonectes morgani* (Carpenter, 1997).

Ectopterygoid—The ectopterygoid is a 'C'-shaped bone located posterolateral to the palatines and lateral to the pterygoids (Fig. 3B, 4). The suture between the pterygoid and ectopterygoid, although unclear, appears possibly located near the bump formed by the ectopterygoid (Fig. 3B). A facet is visible on the lateral margin of the ectopterygoid and seems to contact the posterior elongation of the maxillary (Fig. 4). At the juncture of the right palatine with the ectopterygoid and the pterygoid, a small fenestra is present that may correspond to the suborbital fenestra (Fig. 3B), as seen in *Libonectes morgani* (see Carpenter, 1997). The poor preservation of the left pterygoid precludes observation of this fenestra on that side.

Braincase

The braincase is formed by the supraoccipital, the fused exoccipital-opisthotics, the basioccipital, the prootic, and the parabasisphenoid. The elements are slightly displaced from their natural position. The foramen magnum is taller than wide and seems to be slightly constricted at the level of the supraoccipital-exoccipital-opisthotic sutures.

Parabasisphenoid—The parasphenoid and the basisphenoid form the anterior floor of the braincase, and there is no trace of a suture between the dorsal part of the parasphenoid and the ventral part of the basisphenoid. Anteriorly, the cultriform process of the parasphenoid is visible on the palatal surface (Fig. 5A–C), where it terminates between the posterior ends of the anterior rami of the pterygoids. The parasphenoid carries a prominent ventral keel that divides the posterior interpterygoid vacuities (Figs. 3B, 5B), as in Cretaceous elasmosaurids and in the Jurassic forms *Microcleidus tournemirensis* and *M. homalospondylus* (Bardet et al., 1999; Brown et al., 2013). The ventral keel continues slightly posterior to the posterior margins of the interpterygoid vacuities and tapers posteriorly along the ventral surface of the basioccipital (Fig. 3B). In dorsal view, just posterior to the cultriform process, the sella turcica is open anteriorly (Fig. 5A). The pituitary fossa occupies about one-third of the braincase floor, which is comparable to the condition in *Tricleidus* Andrews, 1909 (see Sato et al., 2011). The sella turcica posteriorly terminates with the dorsum sellae (Fig. 5A, C). A prominent pila antotica extends anterodorsally from this region, and a pila metoptica is present more anteriorly (Fig. 5A–C), as in *Thalassiodracon* (Benson et al., 2011). In lateral view and ventral to the pila antotica, a process extends from the lateral surface of the basisphenoid (Fig. 5B) and forms a facet that contacts the pterygoid (basipterygoid process). The lateral surface of the parabasisphenoid is pierced by a large foramen for the internal carotid located ventral to the pila antotica

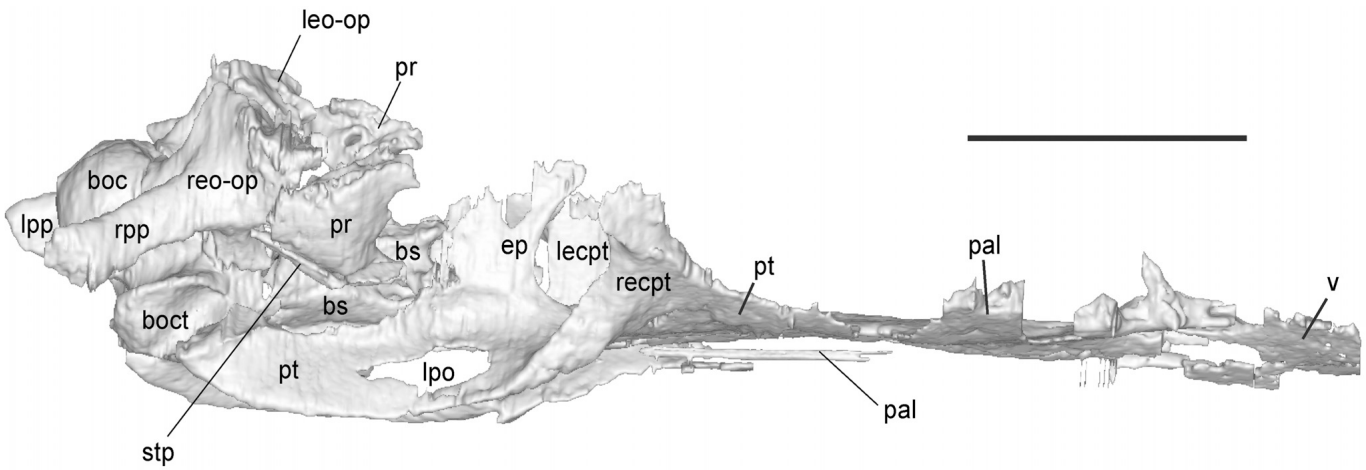

FIGURE 4. Digital reconstruction of the braincase and the palate of SMNS 81783 in right lateral view. **Abbreviations**: **boc**, occipital condyle; **boct**, basioccipital tuber; **bs**, basisphenoid; **ep**, epipterygoid; **lecpt**, left ectopterygoid; **leo-op**, left exoccipital-opisthotic; **lpo**, lateral pterygoid opening; **lpp**, left paraoccipital process; **pal**, palatine; **pr**, prootic; **pt**, pterygoid; **recpt**, right ectopterygoid; **reo-op**, right exoccipital-opisthotic; **rpp**, right paraoccipital process; **stp**, stapes; **v**, vomer. Scale bar equals 5 cm.

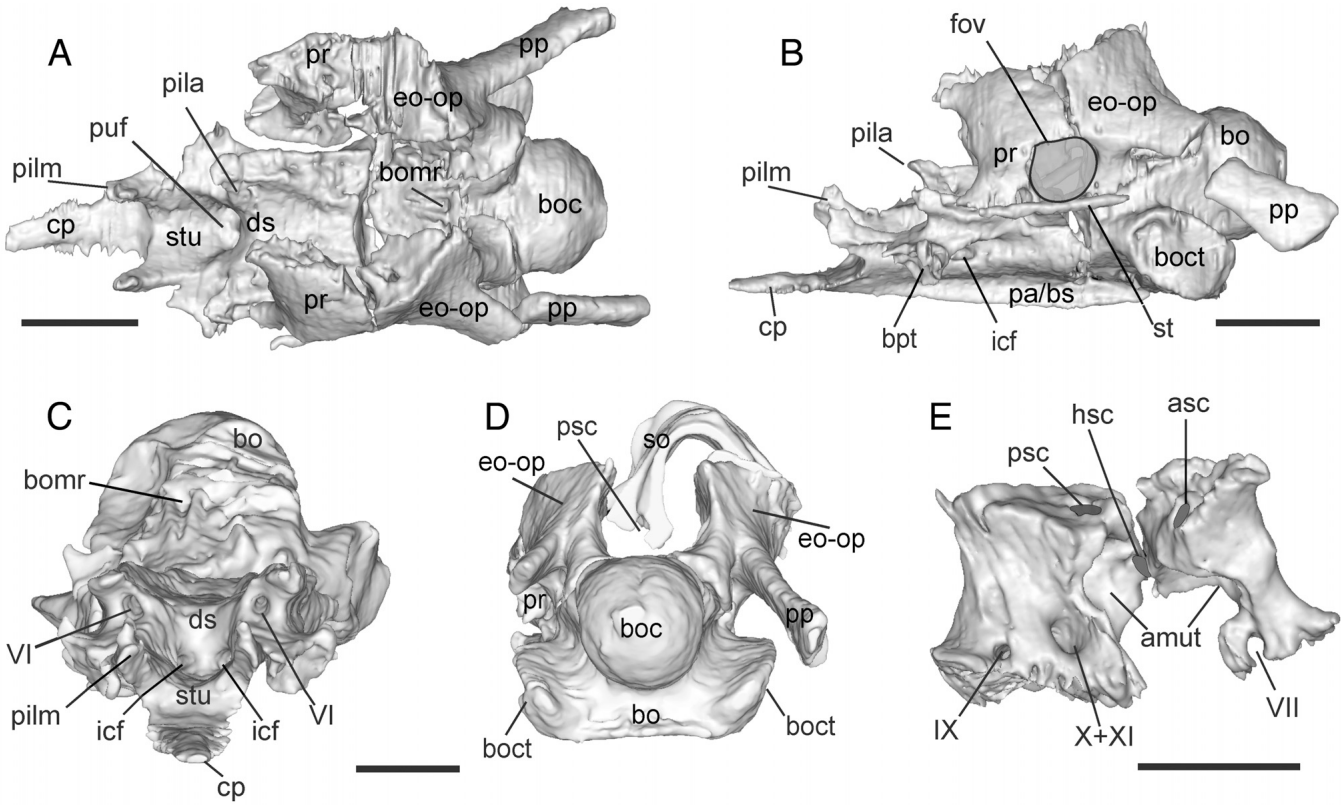

FIGURE 5. Digital reconstruction of the braincase of SMNS 81783 in dorsal (**A**), left lateral (**B**), anterior (**C**), and posterior (**D**) views, and of the left exoccipital-opisthotic and prootic in medial view (**E**). **Abbreviations**: **amut**, chamber for ampulla and utriculus; **asc**, anterior semicircular canal; **bo**, basioccipital; **boc**, occipital condyle; **boct**, basioccipital tuber; **bomr**, basioccipital median ridge; **bpt**, basipterygoid process of the basisphenoid; **cp**, cultriform process; **ds**, dorsum sellae; **eo-op**, exoccipital-opisthotic; **fov**, fenestra ovalis; **hsc**, horizontal semicircular canal; **icf**, internal carotid foramen; **IX**, foramen for glossopharyngeal nerve; **pa/bs**, parabasisphenoid; **pila**, pila antotica; **pilm**, pila metoptica; **pp**, paroccipital process; **pr**, prootic; **psc**, posterior semicircular canal; **puf**, pituitary fossa; **so**, supraoccipital; **st**, stapes; **stu**, sella turcica; **VI**, foramen for the abducens nerve; **VII**, foramen for the facial cranial nerve; **X+XI**, foramen for the vagus and accessory nerves. Scale bars equal 2 cm.

and just posterior to the basipterygoid process of the basisphenoid (Fig. 5B). In anterior view, a pair of internal carotid foramina penetrate the posterior wall of the sella turcica (Fig. 5C), as in *Libonectes morgani* (Carpenter, 1997:fig. 5), differing from *Alexandronectes zealandiensis* in which there is only a single foramen in the floor of the sella turcica (Otero et al., 2016). The dorsolateral side of the pituitary fossa bears a foramen, visible in anterior view (Fig. 5C), that probably carried the abducens nerve (Carpenter, 1997).

Basioccipital—The basioccipital is a stout element. Its dorsal surface bears two facets (Fig. 5C) for articulation with the exoccipitals (otooccipital facets; Evans, 2012). A small portion of the basioccipital median ridge seems to be present in dorsal view (Fig. 5A, C). Ventrolaterally, the basioccipital tubers show two ovoid facets for contact with the pterygoids (Fig. 5B, D). In ventral view, the basioccipital contacts the parabasisphenoid anteriorly and the pterygoids laterally. Contrary to what is reported among pliosaurids and cryptoclidids (e.g., Andrews, 1913; Brown, 1993), in which the exoccipital-opisthotic forms part of the occipital condyle, the basioccipital appears here to form the entire rounded occipital condyle (Fig. 5D). A groove surrounds the occipital condyle, forming a distinct neck ventrally and laterally (Fig. 5D) as in elasmosaurids (Brown, 1993), but differing from the condition of *Thalassiodracon* (Benson et al., 2011) or *Plesiosaurus* (O'Keefe, 2006) in which the occipital condyle is a shallow dome lacking a groove between the condyle and the body of the basioccipital.

Exoccipital-Opisthotics—Both exoccipital-opisthotics are well preserved and are fused, as in most plesiosaurians (e.g., Sato et al., 2011; Sachs et al., 2015). On the anterior surface, a deep chamber for the ampulla and utriculus is visible (Fig. 5E). Dorsally and laterally to these structures, two openings are preserved that correspond to the caudal part of the posterior and horizontal semicircular canals, respectively (Fig. 5E). Two foramina pierce the medial surface of the exoccipital adjacent to its ventral surface (Fig. 5E). The more anterior foramen is larger and might have served for passage of the glossopharyngeal nerve (IX) and possibly also for the perilymphatic duct (Sachs et al., 2015). The smaller one may be considered as a foramen for the vagus and accessory nerves (X + XI) as well as the jugular vein (Sachs et al., 2015). Anteriorly, the opisthotic forms the posterior margin of the fenestra ovalis (Fig. 5B). This character differs from the hypothesis proposed by Maisch (1998) for *Muraenosaurus*, in which the opisthotics do not contribute to the fenestra ovalis. The straight paroccipital process has an anteroposteriorly oval cross-section and is ventrally inclined (Fig. 5A, B, D). Its distal end is a little expanded but does not form a spatulate terminus as observed in pliosaurids and basal plesiosaurians (e.g., Smith and Dyke, 2008; Benson et al., 2011).

Prootic—The prootic is present anterior to the exoccipital-opisthotic and forms the anterior margin of the keyhole-shaped fenestra ovalis seen in lateral view (Fig. 5B). The prootic is a rectangular element, containing the anterior part of the vestibule of the inner ear dorsomedially (Fig. 5E). The facet for the supraoccipital faces posterodorsally and is pierced by an opening for

the anterior semicircular canal (Druckenmiller, 2002; Sato et al., 2011). A much larger foramen on the exoccipital-opisthotic facet (Fig. 5E) is the exit for the horizontal semicircular canal (Sato et al., 2011). A foramen at the posterior part of the prootic base may represent the exit for cranial nerve VII (Carpenter, 1997).

Supraoccipital—The supraoccipital is a small, arch-shaped element lying above the braincase (Fig. 5D) and below the parietal, enclosing the dorsal and dorsolateral margins of the foramen magnum. The supraoccipital contacts the parietal dorsally. Its ventrolateral portions are expanded anteroposteriorly to accommodate part of the semicircular canals, as in *Muraenosaurus* (Maisch, 1998) and *Thalassiodracon* (Benson et al., 2011). It also contacts the prootic anteroventrally and the exoccipital-opisthotic posteroventrally.

Stapes—Two anteroposteriorly oriented rods ventral to the exoccipital-opisthotics and prootics, may correspond to the stapes (Fig. 5B). The two elements are 28 mm in length, but the right one is broken in the middle. Stapes are commonly preserved in Lower Jurassic plesiosaurians (e.g., Brown et al., 2013) but rarely reported among Middle–Upper Jurassic or Cretaceous taxa (Sato et al., 2011), and some authors have hypothesized that these taxa may have lacked stapes (e.g., Carpenter, 1997). Contrary to the stapes identified by Storrs and Taylor (1996) that contacts the anterior surface of the opisthotic (Benson et al., 2011), the stapes in SMNS 81783 does not contact any other element and its anterior end reaches the anterior extremity of the prootic base.

Mandible

Dentary—The dentary is a long and straight bone that occupies most of the lateral surface of the mandible. In dorsal view, the left and right dentaries unite at their anterior ends near alveolus position 4 (Fig. 6A), to form a narrow, gracile, and slightly elongated mandibular symphysis, as observed in *Callawayasaurus* (bearing three to five pairs of teeth) and *Hydrotherosaurus* (bearing three pairs). The symphysis, which represents 15% of the total skull length, is not laterally expanded and is straight in lateral view (Fig. 6C). The dentary seems to be the only component of the symphysis, and it seems that the coronoid extends anteriorly up to the last third of the mandibular ramus. The suture between the dentary and the splenial is only visible anterior to the coronoid (Fig. 6C); however, the anterior extension of the splenial is unclear. The tooth number is difficult to determine because only the medial margin is preserved; however, we estimate the original presence of 16 teeth on the dentary (Fig. 6A). Medial to these teeth, the alveoli for the replacement teeth are visible (Fig. 6A).

Coronoid—The coronoid is preserved on both sides, and each coronoid lies in tight contact with the dentary, on the medial surface of the mandible (Fig. 6A, C). The coronoid is a thin and triangular bone with a large dorsal inflation (Fig. 6C), comparable to that described in *Zarafasaura* (Vincent et al., 2011). It contacts the dentary anteriorly, the prearticular ventrally, and the surangular posteriorly.

Prearticular—The prearticular is a narrow bone that contacts the coronoid dorsally and the dentary ventrally; its anterior end is not preserved (Fig. 6C). Medially, the prearticular covers the posterior part of the Meckelian canal. The cast of the Meckelian canal that is visible in lateral view seems to be narrow anteriorly and to expand posteriorly (Fig. 6C). The mandibular foramen is only visible medially, located between the coronoid and the prearticular (Fig. 6C), where it opens largely posteriorly, although the termination of the foramen cannot be confidently traced posterior to this region due to the poor preservation of the bones in the posterior part of the mandible. The glenoid fossa appears just posterior to the occipital condyle.

Surangular—Only the left surangular is partially preserved (Fig. 6C). Its anterior part is developed dorsoventrally and forms a ridge that becomes flattened posteriorly. In the posterior part of the mandible and posterior to the coronoid, the surangular descends to the glenoid cavity.

Teeth

The teeth (Fig. 3) are slightly flattened and oval in cross-section, as in *Callawayasaurus, Terminonatator, Styxosaurus*, and *Libonectes* (Sachs and Kear, 2015). The two first teeth on the premaxillae are small and procumbent, as in *Libonectes morgani* and *Dolychorhynchops osborni* (Carpenter, 1997). The second and fourth premaxillary teeth are the largest. Several alveoli for replacement teeth are observable on the premaxillae and the left maxilla in palatal view. The maxillary teeth are poorly preserved but appear to diminish in size from anterior to posterior, in contrast to the condition in *Aristonectes* (Gasparini et al., 2003b; Otero et al., 2014) and *Kaiwhekea katiki* (Cruickshank and Fordyce, 2002).

Atlas-Axis Complex

The conjoined atlas-axis centrum (Fig. 7) is cylindrical and distinctly longer than high, as observed in a number of other elasmosaurids (e.g., Welles, 1943; Sachs, 2005; Kubo et al., 2012; Otero et al., 2014; Sachs and Kear, 2015). The atlantal cotyle is circular and deeply concave. The cotylar rim is surrounded by a thin edge that is damaged along its left lateral margin; a posteriorly tapering notch incises its dorsal midline. Ventrally, the atlas intercentrum bears a prominent hypophyseal ridge similar to that reported in *Elasmosaurus platyurus, Eromangasaurus australis, Albertonectes vanderveldei, Libonectes morgani*, and *Vegasaurus molyi* (Kear, 2005; Sachs, 2005; Kubo et al., 2012; Sachs and Kear, 2015; O'Gorman et al., 2015). The anteroventral extremity of the hypophyseal ridge is flattened and elliptical in outline, as recorded in *A. vanderveldei* and *L. morgani* (Kubo et al., 2012; Sachs and Kear, 2015). Posteriorly, the hypophyseal ridge forms a narrow crest merging with the articular face of the axis centrum. The atlas neural spine is oriented posteriorly, narrow at its base and flared dorsally. Only the ventral part of the neural spine is preserved. The exact height is unknown, and the contact between the atlas and axis neural arches seems perforated by a large intervertebral foramen, similar to that depicted in *Libonectes atlasense* and *L. morgani* (Buchy, 2005; Sachs and Kear, 2015), but also in *V. molyi* and *Tuarangasaurus keyesi* (Wiffen and Moisley, 1986; O'Gorman et al., 2015). The atlas ribs, situated at the approximate midsection of the atlas-axis complex, are fused to the axis ribs so that they cannot be distinguished from each other. The rib complex is projected laterally posteroventrally (about 45° from the horizontal), beyond the articular face of the axis centrum. The concave and rounded articular face of the axis is partially preserved. It seems surrounded by a thickened convex rim.

PHYLOGENETIC ANALYSIS

In order to infer the phylogenetic relationships of SMNS 81783 within Plesiosauria, a cladistic analysis was performed using the data sets of Benson and Druckenmiller (2014), plus two additional operational taxonomic units (OTUs): SMNS 81783 and the type specimen of *Libonectes atlasense* (see Appendix 1 and Supplementary Data). The scores of *Libonectes morgani* were modified following Sachs and Kear (2015). *Yunguisaurus liae* Cheng et al., 2006, was specified as the outgroup taxon, and all characters were coded as unordered and unweighted.

A heuristic search for the most parsimonious trees was performed using TNT 1.1 (Goloboff et al., 2008). The search resulted in 100 parsimonious trees; the strict consensus is shown

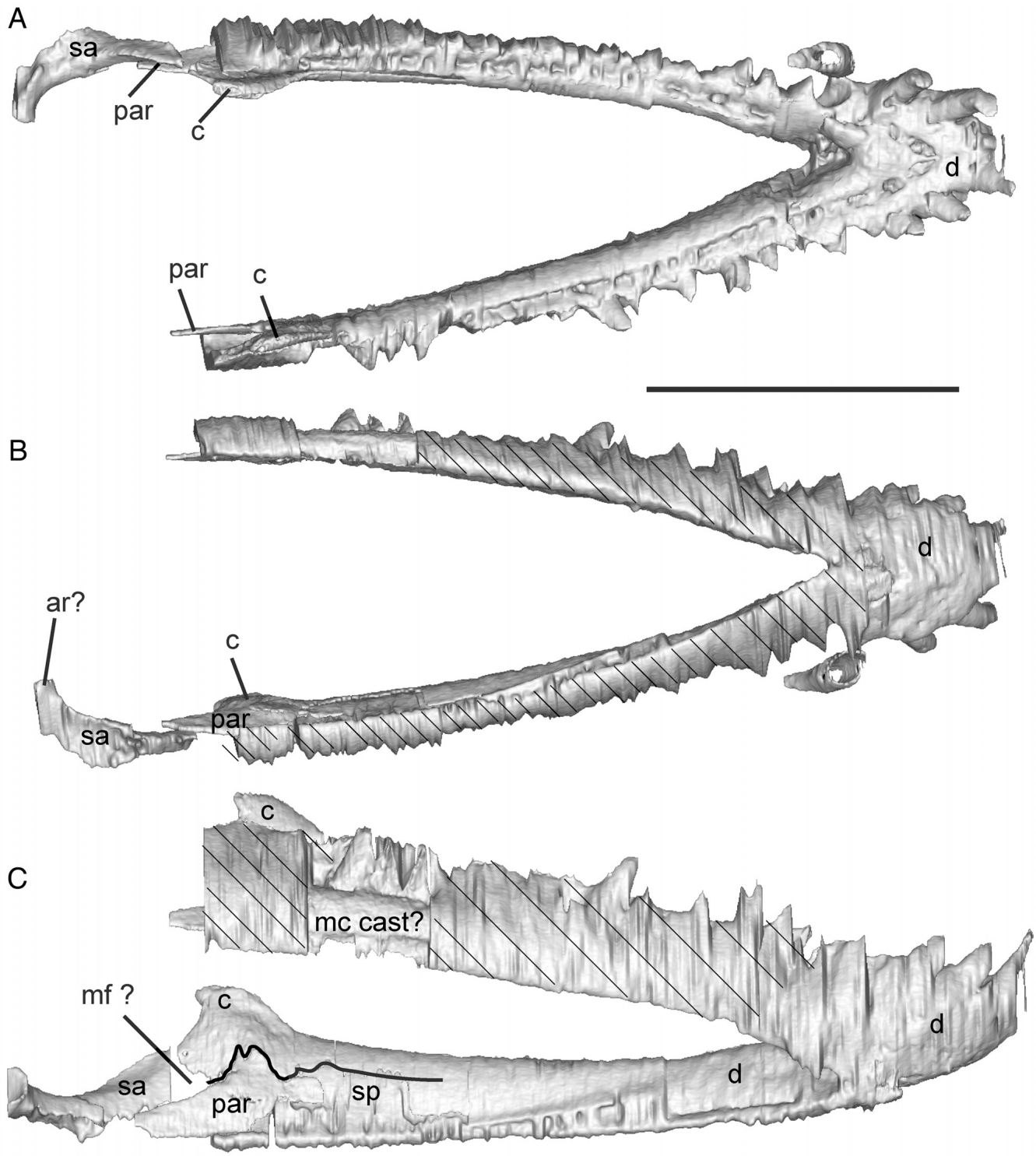

FIGURE 6. Digital reconstruction of the mandible of SMNS 81783 in dorsal (**A**), ventral (**B**), and right ventrolateral (**C**) views. **Abbreviations**: **ar**, articular; **c**, coronoid; **d**, dentary; **mc cast**, cast of the Meckelian canal; **mf**, mandibular foramen; **par**, prearticular; **sa**, surangular; **sp**, splenial. Scale bar equals 10 cm.

in Figure 8. The consensus tree has a tree length of 1345 steps, an ensemble consistency index of 0.24, and an ensemble retention index of 0.62. Bremer indices greater than 1 are indicated for each node shown in Figure 8.

The results of the phylogenetic analysis place SMNS 81783 within the Elasmosauridae (Bremer index = 3), as sister taxon to *Libonectes morgani* and *Libonectes atlasense*. Two synapomorphies (ACCTRAN) unite the three taxa: the posterior extent of maxillary tooth row ventral to the postorbital bar and the heterodont maxillary dentition. Specimen SMNS 81783 presents three autapomorphies (ACCTRAN): the presence of a transverse constriction of the rostrum at the premaxillae-maxilla suture, the absence of a

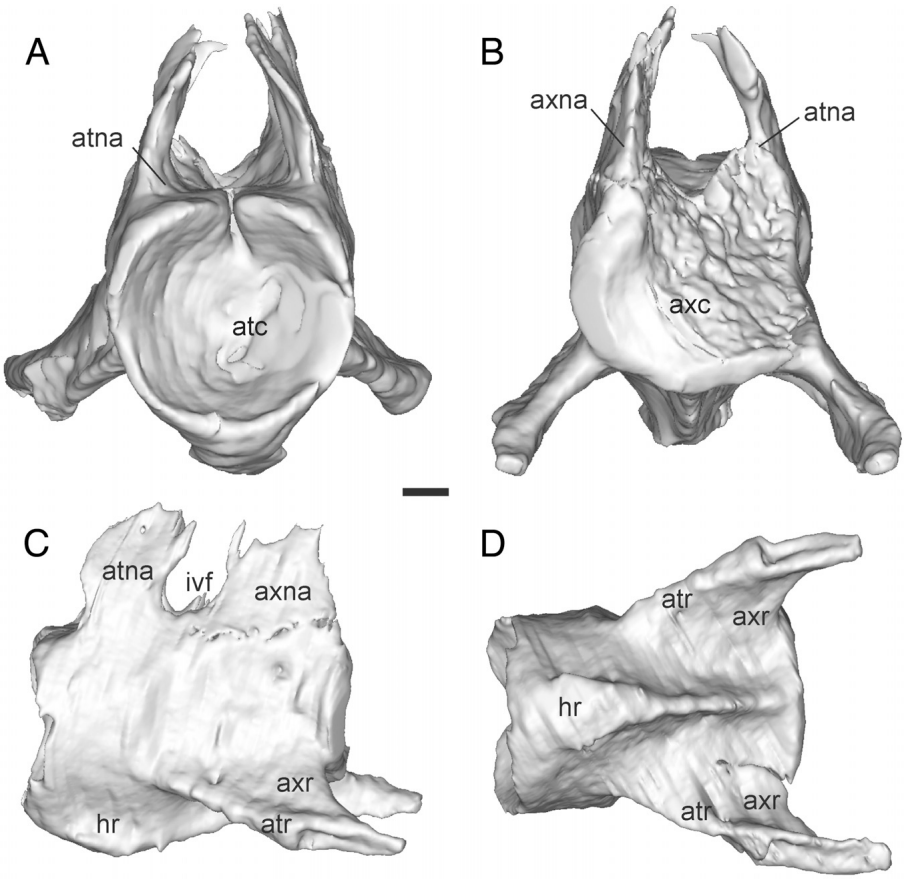

FIGURE 7. Digital reconstruction of the atlas-axis complex of SMNS 81783 in anterior (**A**), posterior (**B**), left lateral (**C**), and ventral (**D**) views. **Abbreviations**: **atc**, atlas centrum; **atna**, atlas neural arch; **atr**, atlas rib; **axc**, axis centrum; **axna**, axis neural arch; **axr**, axis rib; **hr**, hypophyseal ridge; **ivf**, intervertebral foramen. Scale bar equals 1 cm.

dorsomedian ridge on the premaxillae, and the short anterior extension of the parietal to the level of the temporal bar. The clade formed by *L. morgani* and *L. atlasense* is supported by one autapomorphy (ACCTRAN): the absence of a pineal foramen.

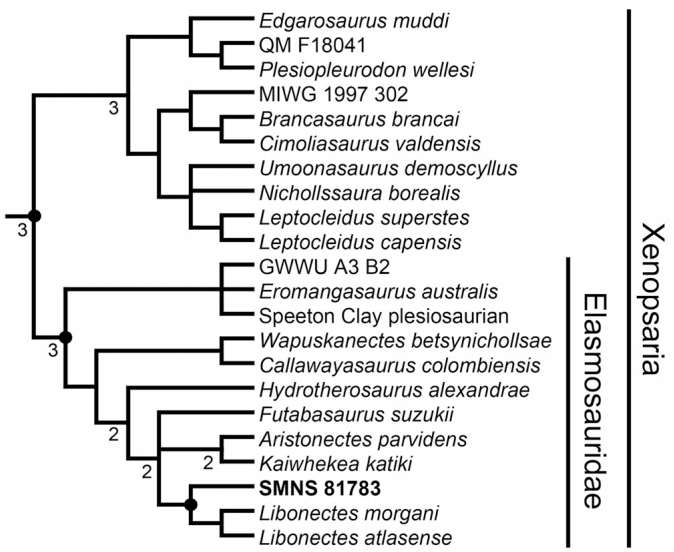

FIGURE 8. Strict consensus tree showing the relationships of specimen SMNS 81783 among xenopsarians. Strict consensus of the 100 most parsimonious trees; tree length = 1345 steps; CI = 0.24; RI = 0.62. Bremer indices greater than 1 are indicated for each node.

DISCUSSION

Comparisons with Other Elasmosaurids

Specimen SMNS 81783 presents several elasmosaurid characters: (1) the anterior tooth with an oval cross-section (Ketchum and Benson, 2010:character 109); (2) absence of an anterior interpterygoid vacuity (Bardet et al., 1999:character 12; Vincent et al., 2011:character 23); (3) high coronoid eminence (Vincent et al., 2011:character 39); and (4) a keyhole-shaped foramen magnum (Druckenmiller and Russell, 2008:character 67). In addition, SMNS 81783 displays a combination of characters variably found in other elasmosaurids: (1) five premaxillary teeth (Brown, 1993; Sato, 2002); (2) a dorsomedial process of the premaxilla contacting the anterior extension of the parietal (Kear, 2005); (3) a pineal foramen present but not bordered by the frontal (Kear, 2005); (4) a convex ventral margin of the orbit (Sachs and Kear, 2015); and (5) a keel on the ventral surface of the parabasisphenoid (Kear, 2005). Comparisons with available elasmosaurid skulls (see Table 2) show that the flat dorsal surface of the premaxillae in SMNS 81783 differs from the prominent dorsomedial bump situated anterior to the orbit in *Futabasaurus, Styxosaurus*, and *Terminonatator* (Sato, 2003; Sato et al., 2006), the prominent dorsomedian ridge present in *Eromangasaurus* (Kear, 2005), or the low keel reported dorsally along the midline of the premaxillae in *Elasmosaurus* (Sachs, 2005). Moreover, in SMNS 81783, the premaxillae bear a total of 10 teeth, contrary to the conditions in *Eromangasaurus* (7 teeth), *Elasmosaurus* (12 teeth), *Terminonatator* (9 teeth), *Kaiwhekea* (7 teeth), or *Aristonectes* (10–13 teeth) (Carpenter, 1999; Cruickshank and Fordyce, 2002; Gasparini et al., 2003b; Sato, 2003; Kear, 2005). In SMNS 81783, the external nares are oval

TABLE 2. Taxa used for comparison, with main references used for each.

Futabasaurus suzukii Sato et al., 2006	Sato et al. (2006)
Styxosaurus snowii (Williston, 1889)	Williston (1889)
Terminonatator ponteixensis Sato, 2003	Sato (2003)
Eromangasaurus australis Kear, 2005	Kear (2005)
Aristonectes parvidens Cabrera, 1941	Gasparini et al. (2003)
Thalassomedon haningtoni Welles, 1943	Welles (1943)
Tuarangasaurus keyesi Wiffen and Moisley, 1986	Wiffen and Moisley (1986)
Zarafasaura oceanis Vincent et al., 2011	Vincent et al. (2011)
Hydrotherosaurus alexandrae Welles, 1943	Welles (1943)
Callawayasaurus colombiensis (Welles, 1962)	Welles (1962), Carpenter (1999)
Elasmosaurus platyurus Cope, 1869	Sachs (2005)
Seeleyosaurus guilelmiimperatoris Dames, 1895	Großmann (2007)

and located above the third to fifth maxillary teeth, just anterior to the orbit. This condition differs from the circular external nares found in *Thalassomedon* (Carpenter, 1999), and from the position of the external nares located above the sixth and seventh maxillary teeth in *Styxosaurus* or above the second and third ones in *Tuarangisaurus* (Carpenter, 1999). The size variability of the maxillary dentition that incorporates teeth with an oval cross-section in SMNS 81783 contrasts with the relatively small and consistently sized dentition present in *Aristonectes* and *Kaiwhekea* (Cruickshank and Fordyce, 2002; Gasparini et al., 2003b) and the rounded tooth cross-sections of *Eromangasaurus* (Kear, 2005) and *Terminonatator* (Sato, 2003). The ventral margin of the orbit in SMNS 81783 is convex and mainly formed by the jugal, in contrast to that reported for *Thalassomedon* and *Zarafasaura*, in which the jugal forms only one-third of the ventral margin of the orbit (Carpenter, 1999; Vincent et al., 2011), or *Hydrotherosaurus*, in which the jugal is excluded from the orbital margin (Welles, 1943), and *Futabasaurus*, which has a straight ventral margin of the orbit (Sato et al., 2006). The pineal foramen present in SMNS 81783 is absent in *Futabasaurus, Hydrotherosaurus, Styxosaurus, Tuarangisaurus, Terminonatator*, and *Zarafasaura* (Welles, 1943; Sato, 2003; Vincent et al., 2011). Moreover, in SMNS 81783, the pineal foramen is totally enclosed by the parietals, contra *Callawayasaurus* where the frontal forms the anterior border of the pineal foramen (Welles, 1952). In SMNS 81783, the anterior margin of the parietal contacts the frontal at the level of the posterior margin of the orbit, differing from the situation in *Aristonectes*, in which the parietal terminates more anteriorly between the orbits (Gasparini et al., 2003b). The mandible of SMNS 81783 presents a Meckelian canal not open for most of its length, contrary to the conditions in *Callawayasaurus* and *Terminonatator* (Welles, 1962; Sato, 2003), and a high coronoid, in contrast to that observed in *Eromangasaurus* (Kear, 2005). The mandibular symphysis in SMNS 81783 reaches the fourth tooth pair, unlike in *Hydrotherosaurus* (three pairs), *Terminonatator, Futabasaurus* (two to three pairs) and *Aristonectes* (one pair). Moreover, the mandibular symphysis represents 15% of the total skull length, contrary to the condition in *Eromangasaurus* (23% of the skull length), *Tuarangisaurus* (6%), and *Zarafasaura* (8%) (Vincent et al., 2011). The characters presented by SMNS 81783 differentiate this specimen from most elasmosaurid taxa, except *Libonectes*, with which many similarities have been found.

Comparison with *Libonectes*

The diagnosis for *Libonectes* established by Carpenter (1997) is principally based on postcranial characters and difficult to apply for SMNS 81783, which preserves only the skull and the atlas-axis complex. The only diagnostic cranial character proposed by Carpenter (1997) concerns the preorbital length/skull length ratio, but according to that author, this character has limited taxonomic utility (Carpenter, 1997:214). Anatomical comparisons between SMNS 81783 and the other elasmosaurids allow its referral to *Libonectes*. Moreover, the phylogenetic result obtained in this study recovers a sister-group relationship with the two species of *Libonectes*, supporting the hypothesis proposed by Buchy (2005).

Comparison with the holotypes of *Libonectes morgani* and *Libonectes atlasense* reveals only a few differences between the three specimens. A pineal foramen is present in SMNS 81783, but not in *L. morgani* and *L. atlasense*. The virtual reconstruction of SMNS 81783 reveals the presence of this structure, but it is hardly visible because of its small size (diameter = 5 mm) as well as its limited depth (4 mm). This structure is possibly not observable in *L. morgani* and *L. atlasense* because of the poor preservation of the interorbital region (see Carpenter, 1997; Buchy, 2005). Lateral to the posterior interpterygoid vacuities, the ventral surface of the pterygoid in SMNS 81783 is dorsally concave and its lateral margin is projected ventrolaterally, forming a curved prominent flange. This contrasts with the description of *L. morgani* given by Carpenter (1997), in which the pterygoids are plate-like structures (Carpenter, 1997:203). However, the illustrations of Welles (1949:pl. 3) and Druckenmiller and Russell (2008:12, fig. 6), as well as the revised character score given by Sachs and Kear (2015:character 100), show that the pterygoids of *L. morgani* are dorsally concave and similar to those of SMNS 81783. The pterygoids are not visible in *L. atlasense* (Buchy, 2005). The openings situated on the pterygoids lateral to the posterior interpterygoid vacuities found in SMNS 81783 are absent in *L. morgani* and not observed in *L. atlasense*. Reasonable doubt remains concerning the real nature of these openings, which could be an artifact of preservation. The dorsomedian ridge found on the dorsal surface of the premaxillae in *L. morgani* (see Sachs and Kear, 2015) and *L. atlasense* (Buchy, 2005:fig. 2) is not present in SMNS 81783, in which the premaxillae appear flattened on their dorsal surface. The dorsomedian ridge found in *L. morgani* was not reported in the description of Carpenter (1997), whereas Welles (1949:8) and Sachs and Kear (2015:696) described the prominent dorsomedian ridge on the premaxillae as a feature distinguishing *L. morgani* from other Elasmosauridea. The ventral emargination between the third premaxillary and the third maxillary teeth is concave in *L. atlasense* (Buchy, 2005) but straight in *L. morgani* (Carpenter, 1997: fig. 2) and SMNS 81783. The mandibular symphysis comprises six teeth in *L. atlasense* (Buchy, 2005) but eight in *L. morgani* (Carpenter, 1997:fig. 2) and SMNS 81783.

It appears difficult to state if SMNS 81783 is more related to *Libonectes morgani* or to *Libonectes atlasense*. Buchy (2005) proposed four diagnostic cranial characters differentiating *L. atlasense* from *L. morgani*: (1) the ventral emargination between the third premaxillary and the third right (fifth on the left) maxillary teeth is concave; (2) the external naris is situated at the level of the fourth to fifth maxillary teeth, which are the largest teeth in the maxillary tooth row; (3) the mandibular symphysis comprises three teeth; and (4) the mandibular symphysis is flat, posteroventrally oriented, and extends to the anterior end of the maxilla. Specimen SMNS 81783 differs from *L. atlasense* in all these characters and is thus more similar to *L. morgani*. Based on the differential diagnosis proposed by Sachs and Kear (2015), SMNS 81783 nevertheless differs from *L. morgani*, based on two characters: the presence of a pineal foramen and the absence of a prominent dorsomedian ridge on the premaxillae. These differences might, however, be related to different states of preservation for the specimens of these taxa, the intraorbital region being poorly preserved in *L. morgani*. Similarly, doubt remains about the prominent dorsomedian ridge on the premaxillae, the absence or

presence of such a structure being possibly due to intraspecific variability (e.g., sexual dimorphism), which is still unknown among plesiosaurians.

The relationships among the different OTUs referred to this genus remain unresolved. Based on the limited differences, we refer SMNS 81783 to *Libonectes morgani*, but the comparison between *L. morgani* and *L. atlasense* is not clear because of the lack of comparative data. The type specimen of *L. morgani* is essentially known from its cranial characters and presents 24% missing cranial data in the phylogenetic analysis of Benson and Druckenmiller (2014). Conversely, *L. atlasense* presents 80% missing cranial data and SMNS 81783 has an intermediate value with 50% missing cranial data. The use of computed tomography on the type specimen of *L. atlasense* would make it possible to obtain new information about its cranial characters, and to clarify the relationships among the specimens referred to *Libonectes*.

Paleobiogeography and Paleoecological Interpretations

The assignment of SMNS 81783, from the Turonian of Morocco, to *Libonectes morgani*, a North American taxon known previously only from the Late Cenomanian of Texas (Sachs and Kear, 2015), greatly enlarges the paleobiogeographical distribution of this species. Some affinities between North American and North African faunas have already been noted for other Turonian vertebrate taxa, more specifically between teleostean fishes (Cavin et al., 2010), but also for a pliosaurid specimen referred to *Brachauchenius lucasi* (e.g., Angst and Bardet, 2015).

Thanks to the particular preservation of the fossil (nodule) and the use of computed microtomography, some structures that are rarely preserved and difficult to observe, such as the pineal foramen and the stapes, could be identified in SMNS 81783. The pineal foramen is considered to be lacking in many derived elasmosaurids (e.g., Wiffen and Moisley, 1986; Carpenter, 1997; Bardet et al., 1999; Sato, 2003). Its condition (small and shallow) in SMNS 81783 raises questions regarding its true or artifactual absence in advanced elasmosaurids. In addition, the absence of the stapes was considered as a synapomorphy of Elasmosauridae (Carpenter, 1997), but its occurrence in the elasmosaurids *Tuarangisaurus keyesi* (see O'Gorman et al., 2017) and SMNS 81783 challenges this hypothesis. According to Sato et al. (2011), it is possible that some plesiosaurians lacked an ossified stapes. However, the morphology of the thin and fragile stapes found in SMNS 81783 suggests that its supposed absence in most elasmosaurid specimens is possibly due to their poor state of preservation.

CONCLUSION

The use of computed microtomography provides new anatomical information on a Moroccan plesiosaurian specimen difficult to study by direct observation because of its particular mode of preservation. The digital reconstruction of SMNS 81783 confirms its position within Elasmosauridae and its assignment to *Libonectes*, as previously suggested by Buchy (2005). The specimen was referred to *Libonectes atlasense* by Buchy (2005), but our study indicates greater similarity to the North American taxon *Libonectes morgani.* A reexamination of the holotype of *Libonectes atlasense* using computed microtomography will help to clarify the morphological disparity with *L. morgani*.

ACKNOWLEDGMENTS

This work was supported by a grant from the Agence Nationale de la Recherche under the LabEx ANR-10-LABX-0003-BCDiv, in the program 'Investissements d'avenir' ANR-11-IDEX-0004-02. We are grateful to the Staatliches Museum für Naturkunde Stuttgart for the loan of the specimen SMNS 81783 and to E. Maxwell for access to the collection of the Stuttgart museum. We thank the AST-RX platform at the MNHN for access to the CT scan, and M. Garcia Sanz (MNHN, UMS 2700 OMSI) for producing the CT scans, and F. Goussard (MNHN, UMR 7207 CR2P) for assistance with 3D digital reconstructions and imaging based on CT scans. We are very grateful to D. Germain (MNHN, UMR 7207 CR2P) for his help with the use of T.N.T. We thank S. Sachs (Naturkundemuseum Bielefeld, Abteilung Geowissenschaften, Germany) and B. Kear (Museum of Evolution, Uppsala University, Sweden) for general discussion. Finally, we thank P. Druckenmiller and both reviewers, Robin O'Keefe and Rodrigo Otero, for helpful comments and suggestions.

LITERATURE CITED

Andrews, C. W. 1909. On some new Plesiosauria from the Oxford Clay of Peterborough. Annals and Magazine of Natural History, London 48:418–429.

Andrews, C. W. 1911. Description of a new plesiosaur (*Plesiosaurus capensis*, sp. nov.) from the Uitenhage Beds of Cape Colony. Annals of the South African Museum 1:309–322.

Andrews, C. W. 1913. A Descriptive Catalogue of the Marine Reptiles of the Oxford Clay. Based on the Leeds Collection in British Museum (Natural History), Part II. British Museum (Natural History), London, 206 pp.

Angst, D., and N. Bardet. 2015. A new record of the pliosaur *Brachauchenius lucasi* Williston, 1903 (Reptilia: Sauropterygia) of Turonian (Late Cretaceous) age, Morocco. Geological Magazine 153:449–459.

Araújo, R., M. J. Polcyn, J. Lindgren, L. L. Jacobs, A. S. Schulp, O. Mateus, A. O. Gonçalves, and M. L. Morais. 2015. New aristonectine elasmosaurid plesiosaur specimens from the Early Maastrichtian of Angola and comments on paedomorphism in plesiosaurs. Netherlands Journal of Geosciences-Geologie en Mijnbouw 94:93–108.

Bardet, N., P. Godefroit, and J. Sciau. 1999. A new elasmosaurid plesiosaur from the Lower Jurassic of Southern France. Palaeontology 42:927–952.

Bardet, N., X. Pereda Suberbiola, and N. E. Jalil. 2003a. A new polycotylid plesiosaur from the Late Cretaceous (Turonian) of Morocco. Comptes Rendus Palevol 2:307–315.

Bardet, N., X. Pereda Suberbiola, and N. E. Jalil. 2003b. A new mosasauroid (Squamata) from the Late Cretaceous (Turonian) of Morocco. Comptes Rendus Palevol 2:607–616.

Bardet, N., A. Houssaye, J. C. Rage, and X. Pereda Suberbiola. 2008. The Cenomanian–Turonian (Late Cretaceous) radiation of marine squamates (Reptilia): the role of the Mediterranean Tethys. Bulletin de la Société Géologique de France 179:605–622.

Benson, R. B. J., and P. S. Druckenmiller. 2014. Faunal turnover of marine tetrapods during the Jurassic–Cretaceous transition. Biological Reviews 89:1–23.

Benson, R. B. J., M. Evans, and P. S. Druckenmiller. 2012. High diversity, low disparity and small body size in plesiosaurs (Reptilia, Sauropterygia) from the Triassic–Jurassic boundary. PLoS ONE 7:e31838. doi: 10.1371/journal.pone.0031838

Benson, R. B. J., K. T. Bates, M. R. Johnson, and P. J. Withers. 2011. Cranial anatomy of *Thalassiodracon hawkinsii* (Reptilia, Plesiosauria) from the Early Jurassic of Somerset, United Kingdom. Journal of Vertebrate Paleontology 31:562–574.

Blainville, H. D. de 1835. Description de quelques espèces de reptiles de la Californie, précédée de l'analyse d'un système général d'Erpétologie et d'Amphibiologie. Nouvelles Annales du Muséum (national) d'Histoire Naturelle de Paris 4:233–296.

Brown, D. S. 1993. A taxonomic reappraisal of the families Elasmosauridae and Cryptoclididae (Reptilia: Plesiosauria). Revue de Paléobiologie 7:9–16.

Brown, D. S., P. Vincent, and N. Bardet. 2013. Osteological redescription of the skull of *Microcleidus homalospondylus* (Sauropterygia, Plesiosauria) from the Lower Jurassic of England. Journal of Paleontology 87:537–549.

Buchy, M. C. 2005. An elasmosaur (Reptilia: Sauropterygia) from the Turonian (Upper Cretaceous) of Morocco. Carolinea 63:5–28.

Buchy, M. C., F. Métayer, and E. Frey. 2005. Osteology of *Manemergus anguirostris* n. gen. et sp., a new plesiosaur (Reptilia, Sauropterygia) from the Upper Cretaceous of Morocco. Palaeontographica, Abteilung A 272:97–120.

Cabrera, A. 1941. Un plesiosaurio nuevo del Cretáceo del Chubut. Revisita del Museo de la Plata (Neuvo Serio) 2:113–130.

Carpenter, K. 1997. Comparative cranial anatomy of two North American Cretaceous plesiosaurs; pp. 191–216 in J. M. Callaway and E. L. Nicholls (eds.), Ancient Marine Reptiles. Academic Press, San Diego, California.

Carpenter, K. 1999. Revision of North American elasmosaurs from the Cretaceous of the Western Interior. Paludicola 2:148–173.

Cavin, L. 1995. *Goulmimichthys arambourgi* n. g., n. sp., un Pachyrhizodontidae (Actinopterygii, Teleostei) d'une nouvelle localité a nodules fossilifères du Turonien inferieur marocain. Comptes Rendus de l'Académie des Sciences, Paris, Série IIa 321:1049–1054.

Cavin, L. 1997. Nouveaux Teleostei du gisement du Turonien inférieur de Goulmima (Maroc). Compte Rendus de l'Académie des Sciences de Paris 325:19–24.

Cavin, L. 1999. Occurrence of a juvenile teleost, *Enchodus* sp., in a fish gut content from the Upper Cretaceous of Goulmima, Morocco. Palaeontology 60:57–72.

Cavin, L. 2001. Osteology and phylogenetic relationships of the teleost *Goulmimichthys arambourgi* Cavin, 1995 from the Upper Cretaceous of Goulmima, Morocco. Eclogae Geologicae Helvetica 133:25–52.

Cavin, L., L. Boudad, S. Duffaud, L. Kabiri, J. Le Loeuff, I. Rouget, and H. Tong. 2001. L'évolution paléoenvironnementale des faunes de poissons du Crétacé supérieur du bassin du Tafilalt et des régions avoisinantes (Sud-Est du Maroc): implications paléobiogéographiques. Compte Rendu de l'Académie des Sciences de Paris, Sciences de la Terre et des planètes 333:677–683.

Cavin, L., H. Tong, L. Boudad, C. Meister, A. Piuz, J. Tabouelle, M. Aarab, R. Amiot, E. Buffetaut, G. Dyke, S. Hua, and J. Le Loeuff. 2010. Vertebrate assemblages from the early Late Cretaceous of southeastern Morocco: an overview. Journal of African Earth Sciences 57:391–412.

Cheng, Y. N., T. Sato, X. C. Wu, and C. Li. 2006. First complete pistosaurid from the Triassic of China. Journal of Vertebrate Paleontology 26:501–504.

Cope, E. D. 1869. Synopsis of the extinct Batrachia and Reptilia of North America. Transactions of the North American Philosophical Society 14:1–252.

Cruickshank, A. R. I. 1997. A Lower Cretaceous pliosauroid from South Africa. Annals of the South African Museum 105:207–226.

Cruickshank, A. R., and R. E. Fordyce. 2002. A new marine reptile (Sauropterygia) from New Zealand: further evidence for a Late Cretaceous austral radiation of cryptoclidid plesiosaurs. Palaeontology 45:557–575.

Dames, W. 1895. Die Plesiosaurier der süddeutschen Liasformation. Abhandlungen der Königliche Preussische Akademie der Wissenschaften zu Berlin 1895:1–83.

Druckenmiller, P. S. 2002. Osteology of a new plesiosaur from the Lower Cretaceous (Albian) Thermopolis Shale of Montana. Journal of Vertebrate Paleontology 22:29–42.

Druckenmiller, P. S., and A. P. Russell. 2008. A phylogeny of Plesiosauria (Sauropterygia) and its bearing on the systematic status of *Leptocleidus* Andrews, 1922. Zootaxa 1863:1–120.

Ettachfini, E. M., and B. Andreu. 2004. Le Cénomanien et le Turonien de la plate-forme Préafricaine du Maroc. Cretaceous Research 25:277–302.

Evans, M. 2012. A new genus of plesiosaur (Reptilia: Sauropterygia) from the Pliensbachian (Early Jurassic) of England, and a phylogeny of the Plesiosauria. Ph.D. dissertation, University of Leicester, Leicester, U.K., 397 pp.

Ferrandini, M., J. Philip, J. F. Babinot, and G. Tronchetti. 1985. La plateforme carbonatée du Cénomano–Turonien de la région d'Erfoud-Errechidia (Sud-Est marocain): stratigraphie et paléoenvironement. Bulletin de la Société Géologique de France 8:559–564.

Gasparini, Z., L. Salgado, and S. Casadi. 2003a. Maastrichtian plesiosaurs from northern Patagonia. Cretaceous Research 14:157–170.

Gasparini, Z., N. Bardet, J. E. Martin, and M. Fernandez. 2003b. The elasmosaurid plesiosaur *Aristonectes* Cabrera from the latest Cretaceous of South America and Antarctica. Journal of Vertebrate Paleontology 23:104–115.

Goloboff, P. A., J. M. Carpenter, J. S. Arias, and D. R. M. Esquivel. 2008. Weighting against homoplasy improves phylogenetic analysis of morphological datasets. Cladistics 24:1–16.

Großmann, F. 2007. Preliminary description and phylogenetic position of a new plesiosaur (Reptilia: Sauropterygia) from the Toarcian of Holzmaden, Germany. Journal of Paleontology 78:973–988.

Kear, B. P. 2005. A new elasmosaurid plesiosaur from the Lower Cretaceous of Queensland, Australia. Journal of Vertebrate Paleontology 25:792–805.

Ketchum, H. F., and R. B. J. Benson. 2010. Global interrelationships of Plesiosauria (Reptilia, Sauropterygia) and the pivotal role of taxon sampling in determining the outcome of phylogenetic analyses. Biological Reviews 85:361–392.

Kubo, T., M. T. Mitchell, and D. M. Henderson. 2012. *Albertonectes vanderveldei*, a new elasmosaur (Reptilia, Sauropterygia) from the Upper Cretaceous of Alberta. Journal of Vertebrate Paleontology 32:557–572.

Lebedel, V., C. Lezin, B. Andreu, M. J. Wallez, E. M. Ettachfini, and L. Riquier. 2013. Geochemical and palaeoecological record of the Cenomanian–Turonian Anoxic Event in the carbonate platform of the Preafrican Trough, Morocco. Palaeogeography, Palaeoclimatology, Palaeoecology 369:79–98.

Lomax, D. R., and W. R. Wahl. 2013. A new specimen of the elasmosaurid plesiosaur *Zarafasaura oceanis* from the Upper Cretaceous (Maastrichtian) of Morocco. Paludicola 9:97–109.

Maisch, M. 1998. Notes on the cranial osteology of *Muraenosaurus* Seeley, 1874 (Sauropterygia, Jurassic), with special reference to the neurocranium and its implications for sauropterygian phylogeny. Neues Jahrbuch für Geologie und Paläontologie, Abhandlungen 207:207–253.

Novas, F. E., J. S. D'Angelo, J. P. O'Gorman, F. L. Agnolín, J. M. Lirio, and M. P. Isasi. 2015. First record of Polycotylidae (Sauropterygia, plesiosauria) from the Upper Cretaceous of Antarctica. Cretaceous Research 56:563–568.

O'Gorman, J. P., L. Salgado, E. B. Olivero, and S. A. Marenssi. 2015. *Vegasaurus molyi*, gen. et sp. nov. (Plesiosauria, Elasmosauridae), from the Cape Lamb Member (lower Maastrichtian) of the Snow Hill Island Formation, Vega Island, Antarctica, and remarks on Wedellian Elasmosauridae. Journal of Vertebrate Paleontology. doi: 10.1080/02724634.2014.931285

O'Gorman, J. P., R. A. Otero, N. Hiller, J. Simes, and M. Terezow. 2017. Redescription of *Tuarangisaurus keyesi* (Sauropterygia; Elasmosauridae), a key species from the Uppermost Cretaceous of the Weddellian province: internal skull anatomy and phylogenetic position. Cretaceous Research 71:118–136.

O'Keefe, R. F. 2001. A cladistic analysis and taxonomic revision of the Plesiosauria (Reptilia: Sauropterygia). Acta Zoologica Fennica 213:1–63.

O'Keefe, R. F. 2006. Morphologic and ontogenetic patterns in elasmosaur neck length, with comments on the taxonomic utility of neck length variables. Paludicola 5:207–229.

Otero, R. A., J. P. O'Gorman, N. Hiller, F. R. O'Keefe, and R. E. Fordyce. 2016. *Alexandronectes zealandiensis* gen. et sp. nov., a new aristonectine plesiosaur from the lower Maastrichtian of New Zealand. Journal of Vertebrate Paleontology. doi: 10.1080/02724634.2015.1054494

Otero, R. A., S. Soto-Acuña, F. R. O'Keefe, J. P. O'Gorman, W. Stinnesbeck, M. E. Suárez, D. Rubilar-Rogers, C. Salazar, and L. A. Quinzio-Sinn. 2014. *Aristonectes quiriquinensis*, sp. nov., a new highly derived elasmosaurid from the upper Maastrichtian of central Chile. Journal of Vertebrate Paleontology 34:100–125.

Owen, R. 1860. On the orders of fossil and Recent Reptilia, and their distribution through time. Report of the British Association for the Advancement of Science 1859:153–166.

Sachs, S. 2005. Redescription of *Elasmosaurus platyurus* Cope 1868 (Plesiosauria: Elasmosauridae) from the Upper Cretaceous (lower Campanian) of Kansas, U.S.A. Paludicola 5:92–106.

Sachs, S., and B. P. Kear. 2015. Postcranium of the paradigm elasmosaurid plesiosaurian *Libonectes morgani* (Welles, 1949). Geological Magazine 152:694–710.

Sachs, S., and B. P. Kear. 2017. Redescription of the elasmosaurid plesiosaurians Libonectes atlasense from the Upper Cretaceous of Morocco. Cretaceous Research 74:205–222.

Sachs, S., J. Lindgren, and M. Siversson. 2015. A partial plesiosaurian braincase from the Upper Cretaceous of Sweden. Geological Society, London, Special Publications 434:293–301.

Sato, T. 2002. Description of plesiosaurs (Reptilia: Sauropterygia) from the Bearpaw Formation (Campanian–Maastrichtian) and a phylogenetic analysis of the Elasmosauridae. Ph.D. dissertation, University of Calgary, Calgary, Alberta, Canada, 391 pp.

Sato, T. 2003. *Terminonatator ponteixensis*, a new elasmosaur (Reptilia: Sauropterygia) from the Upper Cretaceous of Saskatchewan. Journal of Vertebrate Paleontology 23:89–103.

Sato, T., Y. Hasegawa, and M. Manabe. 2006. A new elasmosaurid plesiosaur from the Upper Cretaceous of Fukushima, Japan. Palaeontology 49:467–484.

Sato, T., X. C. Wu, A. Tirabasso, and P. Bloskie. 2011. Braincase of a polycotylid plesiosaur (Reptilia: Sauropterygia) from the Upper Cretaceous of Manitoba, Canada. Journal of Vertebrate Paleontology 31:313–329.

Smith, A. S., and G. J. Dyke. 2008. The skull of the giant predatory pliosaur *Rhomaleosaurus cramptoni*: implications for plesiosaur phylogenetics. Naturwissenschaften 95:975–980.

Storrs, G. W., and M. A. Taylor. 1996. Cranial anatomy of a new plesiosaur genus from the lowermost Lias (Rhaetian/Hettangian) of Street, Somerset, England. Journal of Vertebrate Paleontology 16:403–420.

Stromer, E. 1935. Ergebnisse der Forschungsreisen Prof. E. Stromers in den Wusten Ägyptens. Wirbeltierreste der Baharijestufe (unterstes Cenoman), 15. Plesiosauria: Abhandlungen der Bayerischen Akademie der Wissenschaften, Mathematisch-naturwissenschaftliche Klasse 26:1–56.

Taylor, M. A. 1992. Functional anatomy of the head of the large aquatic predator *Rhomaleosaurus zetlandicus* (Plesiosauria; Reptilia) from the Toarcian (Lower Jurassic) of Yorkshire, England. Philosophical Transactions of the Royal Society of London, Series B 335:247–280.

Underwood, C., K. M. Cleason, and D. J. Ward. 2009. Batoids from the Turonian of SE Morocco; p. 43 in N. E. Jalil (ed.), 1st International Congress on North African Vertebrate Palaeontology, Program and Abstracts, Marrakech, 25–27 May 2009.

Vincent, P., N. Bardet, A. Houssaye, M. Amaghzaz, and S. Meslouh. 2013. New plesiosaur specimens from the Maastrichtian Phosphates of Morocco and their implications for the ecology of the latest Cretaceous marine apex predators. Gondwana Research 24:796–805.

Vincent, P., N. Bardet, X. Pereda Suberbiola, B. Bouya, M. Amaghzaz, and S. Meslouh. 2011. *Zarafasaura oceanis*, a new elasmosaurid (Reptilia: Sauropterygia) from the Maastrichtian Phosphates of Morocco and the palaeobiogeography of latest Cretaceous plesiosaurs. Gondwana Research 19:1062–1073.

Welles, S. P. 1943. Elasmosaurid plesiosaurs with a description of new material from California. Memoirs of the University of California 13:125–254.

Welles, S. P. 1949. A new elasmosaur from the Eagle Ford Shale of Texas. Fordren Science, Series 1:1–28.

Welles, S. P. 1952. A review of the North American Cretaceous elasmosaurs. University of California, Publications in Geological Sciences 29:47–144.

Welles, S. P. 1962. A new species of elasmosaur from the Aptian of Columbia and a review of the Cretaceous plesiosaurs. University of California Publications in Geological Sciences 44:1–96.

Wiffen, J., and W. L. Moisley. 1986. Late Cretaceous reptiles (families Elasmosauridae and Pliosauridae) from the Mangahouga Stream, North Island, New Zealand. Journal of Geology and Geophysics, New Zealand 29:205–252.

Williston, S. W. 1889. A new plesiosaur from the Niobrara Cretaceous of Kansas. Transactions of the Annual Meetings of the Kansas Academy of Science 12:174–178.

Williston, S. W. 1903. North American plesiosaurs. Part I. Field Columbian Museum Publication 2:1–79.

Submitted September 8, 2016; revisions received February 1, 2017; accepted March 27, 2017.

Handling editor: Patrick Druckenmiller.

APPENDIX 1: The character matrix used, based on that of Benson and Druckenmiller (2014), to which two plesiosaurian taxa were added: SMNS 81783 and SMNK-PAL 3978 (SMNK, Staatliches Museum für Naturkunde Karlsruhe, Germany), the type specimen of *Libonectes atlasense* (see character scores below). Character scores used here for *Libonectes morgani* follow those proposed by Sachs and Kear (2015).

SMNS 81783

100010?01100?0200??001001??0?0??00??000????0000?0??0??1??????1?101?1212??01????10122?1??????????
????0?1?2?130????111100?????????????0??1010???000????110???
??

Libonectes atlasense (SMNK-PAL 3978)
00001??0???0????1?0?0??????0?0???0100?????11??????????1?????????????????????1?????????????????
??????????????????1?????????????????1010?0??00????1?0????4?1??1????0????????1???1?????????????????
??1??1??????

Journal of Anatomy

J. Anat. (2017) doi: 10.1111/joa.12692

Comparative morphology of snake (Squamata) endocasts: evidence of phylogenetic and ecological signals

Rémi Allemand,[1,2] Renaud Boistel,[3] Gheylen Daghfous,[4] Zoé Blanchet,[2] Raphaël Cornette,[5] Nathalie Bardet,[1] Peggy Vincent[1] and Alexandra Houssaye[2]

[1]*Centre de Recherche sur la Paléobiodiversité et les Paléoenvironnements, CR2P - UMR 7207 - CNRS, MNHN, UPMC, Muséum National d'Histoire Naturelle, Sorbonne Universités, Paris, France*
[2]*Département Adaptations du Vivant, UMR 7179 – CNRS/Muséum National d'Histoire Naturelle, Paris, France*
[3]*IPHEP-UMR CNRS 6046, UFR SFA, Université de Poitiers, Poitiers, France*
[4]*Groupe de Recherche sur le Système Nerveux Central, Département de Neurosciences, Université de Montréal, Montréal, QC, Canada*
[5]*Institut de Systématique, Evolution, Biodiversité, ISYEB – UMR 7205 – CNRS, MNHN, UPMC, EPHE, Muséum National d'Histoire Naturelle, Sorbonne Universités, Paris, France*

Abstract

Brain endocasts obtained from computed tomography (CT) are now widely used in the field of comparative neuroanatomy. They provide an overview of the morphology of the brain and associated tissues located in the cranial cavity. Through anatomical comparisons between species, insights on the senses, the behavior, and the lifestyle can be gained. Although there are many studies dealing with mammal and bird endocasts, those performed on the brain endocasts of squamates are comparatively rare, thus limiting our understanding of their morphological variability and interpretations. Here, we provide the first comparative study of snake brain endocasts in order to bring new information about the morphology of these structures. Additionally, we test if the snake brain endocast encompasses a phylogenetic and/or an ecological signal. For this purpose, the digital endocasts of 45 snake specimens, including a wide diversity in terms of phylogeny and ecology, were digitized using CT, and compared both qualitatively and quantitatively. Snake endocasts exhibit a great variability. The different methods performed from descriptive characters, linear measurements and the outline curves provided complementary information. All these methods have shown that the shape of the snake brain endocast contains, as in mammals and birds, a phylogenetic signal but also an ecological one. Although phylogenetically related taxa share several similarities between each other, the brain endocast morphology reflects some notable ecological trends: e.g. (i) fossorial species possess both reduced optic tectum and pituitary gland; (ii) both fossorial and marine species have cerebral hemispheres poorly developed laterally; (iii) cerebral hemispheres and optic tectum are more developed in arboreal and terrestrial species.

Key words: brain endocast; computed tomography; ecological signal; morphometrics; sensory information; snakes; squamates.

Introduction

Computed tomography (CT) allows the reconstruction of high-quality 3D models of both hard and soft tissues that can be used for different purposes, such as anatomical and biomechanical studies. It thus constitutes an important exploratory tool in biology and opens a range of new possible investigations (Boistel et al. 2011a; Carril et al. 2015).

Computed tomography is now widely used to visualize the endocranial space with the construction of digital endocasts that may reflect the morphology of the brain and associated tissues (Anderson et al. 2000; Macrini et al. 2007; Olori, 2010; Bienvenu et al. 2011; Smith & Clarke, 2012; Racicot & Colbert, 2013; Ahrens, 2014; Carril et al. 2015; Corfield et al. 2015; Danilo et al. 2015; Gonzales et al. 2015; Kawabe et al. 2015), the inner ear (Chapla et al. 2007; Georgi & Sipla, 2008; Walsh et al. 2009; Ekdale, 2010, 2011,

Correspondence
Rémi Allemand, Centre de Recherche sur la Paléobiodiversité et les Paléoenvironnements, CR2P - UMR 7207 - CNRS, MNHN, UPMC, Muséum National d'Histoire Naturelle, Sorbonne Universités, 57 rue Cuvier, CP38, F-75005 Paris, France. E: remi.allemand@edu.mnhn.fr

Accepted for publication *14 August 2017*

2013; Willis et al. 2013), the vascular system (Porter & Witmer, 2015), the cranial nerves (George & Holliday, 2013) and pneumatic sinuses (Bona et al. 2013). Endocasts are generated at the interface between the skeleton (typically bone or cartilage) and the soft tissues (or fluid) lying immediately near it (Balanoff et al. 2015). In the cranial cavity, the soft tissue forming the interface with the surrounding skeleton is not the brain but the superficial surface of the dural meninges, blood vessels and vasculature enveloping the brain (Walsh & Knoll, 2011). Thus, brain endocasts provide only an overview of the external morphology of the brain itself. They may reflect the relative size of the different regions of the brain and could provide some information about sensory abilities, as well as about the behavior and ecology of the species (Walsh & Knoll, 2011).

The degree to which the brain endocast reflects the morphology of the brain depends on the degree to which the brain fills the cranial cavity. This factor can vary widely between lineages (Jerison, 1973; Hopson, 1979; Witmer et al. 2008; George & Holliday, 2013) and over ontogeny (Macrini et al. 2007; Hurlburt et al. 2013). From different age classes, the brain of the marsupial *Monodelphis domestica* fills between 67.8% and 86.6% of the endocranial volume (Macrini et al. 2007), whereas that of the smallest alligators occupies about 68% of the endocranial space, and about 32% in the largest alligators (Hurlburt et al. 2013). Mammals and birds, which are generally considered as highly encephalized taxa (large brains relative to body size; Balanoff et al. 2015), tend to have brains that nearly fill the cranial cavity, resulting in a strong correlation between the volume and morphology of the brain endocast and those of the brain (Balanoff et al. 2015). Thus, similarly as the brain morphology that may reflect the influence of ecological, behavioral and/or phylogenetic factors (Lefebvre et al. 2004; Walsh & Milner, 2011), the brain endocast of these taxa tends to have both phylogenetic and ecological signals (Lyras & Van Der Geer, 2003; Macrini et al. 2007; Carril et al. 2015; Corfield et al. 2015). Additionally, there is an increasing number of studies performed from brain endocasts of mammals and birds. These studies are generally performed to understand the relation between the mass of the brain and the volume of the cast, but also to consider the intraspecific variability, reflecting either ontogenetic variation, sexual dimorphism, or both (Macrini et al. 2007; Bienvenu et al. 2011; Kawabe et al. 2015), or finally focusing on the interspecific variability (Kawabe et al. 2013).

Among vertebrates other than mammals and birds, it is generally admitted that the brain does not entirely fill the cranial cavity (Balanoff et al. 2015). A commonly cited estimate considers that the brain occupies only 50% of the endocranial space (Hopson, 1979). However, this ratio is only based on the observation of one *Sphenodon* and one *Iguana* brain specimens (Hurlburt et al. 2013), and is probably far from representing a general pattern in non-endotherms. For example, it has been shown that the brain almost entirely fills the endocranial space in some extant chondrichthyans and teleosts (Northcutt, 2002; Balanoff et al. 2015). Within Squamata (lizards, snakes and amphisbaenians), a wide range of brain vs. endocranial cavity proportions were found (Kim & Evans, 2014). The lowest brain–endocranial volume ratio is found in *Gecko gecko* (0.35), whereas the false monitor lizard *Callopistes maculatus* exhibits a brain that nearly fills the endocranial cavity (0.97). Moreover, snakes and amphisbaenians are known to have a brain that fills most of the endocranial space (Starck, 1979; Nieuwenhuys et al. 1998), with a very narrow space between the brain and the cranial wall. The brain may thus fill the intracranial cavity in some squamates, indicating that brain endocasts within these species may reflect the external morphology of the brain with a certain degree of accuracy.

CT (i.e. magnetic resonance imaging and X-ray absorption, as well as X-ray phase-contrast imaging techniques) has already been used on skulls of squamates for different purposes, such as the study of the brain (Anderson et al. 2000), the ear (Walsh et al. 2009; Boistel et al. 2011b; Christensen et al. 2012; Yi & Norell, 2015), the skull morphology (Rowe et al. 1999; Bever et al. 2005; Rieppel & Maisano, 2007; Comeaux et al. 2010), the vascular patterns (Porter & Witmer, 2015), and the lacrimal system (Souza et al. 2015). But to date only a single study has focused on the brain endocast (Olori, 2010). In her study, Olori reconstructed and described the endocast of the burrowing snake *Uropeltis woodmasoni* and thus provided the first description of a snake brain endocast. However, as no comparative data are available within squamates, the results obtained cannot be discussed in detail. To date, there are several studies published about the brain itself or the central nervous system of squamates (Senn, 1966; Senn & Northcutt, 1973; Hoogland, 1982; Smeets et al. 1986; Martinez-Garcia et al. 1991; Reperant et al. 1992; Lanuza & Halpern, 1997; Nieuwenhuys et al. 1998; Atobe et al. 2004; Butler & Hodos, 2005; Powell & Leal, 2014), but the exact relationship between brain endocasts and brain morphology remains currently untested for squamates. In addition, data about the brain endocast morphology in this clade are insufficient to fully interpret this structure.

The present contribution proposes the first brain endocast comparative study in squamates. It will focus on snakes that are of particular interest as they show a great diversity in morphology, and occupy a wide range of ecologies with, for example, fossorial, aquatic and arboreal species (Heatwole, 1999; Greene et al. 2000). Here, we propose to provide a quantitative anatomical description of the brain endocast of a wide sample of snake species using different morphometric approaches in order to: (i) bring new information about this structure, its general traits within snakes and the variation occurring; (ii) test if, as in mammals and birds, the brain endocast of snakes reflects a phylogenetic and/or ecological signal.

Materials and methods

Materials

The material consists of the skull of 45 snake specimens (38 genera and 43 species; Table 1) illustrating the diversity of snakes in both phylogenetic and ecological (i.e. habitat) perspectives (Fig. 1). The dataset is divided into six fossorial, seven arboreal, 13 terrestrial, nine semi-aquatic and 10 marine species (Heatwole, 1999; Houssaye et al. 2013; A. Herrel, personal communication). The semi-aquatic group encompasses species that spend most of their time in freshwater without contact with the sea. Three specimens of a single species, *Python regius*, were analyzed in order to evaluate the intraspecific variation.

Data acquisition

Microtomography was performed in order to non-destructively digitize the brain endocast of the specimens. The skull of the specimens studied were scanned: (i) at the University of Poitiers (France), Institut de Chimie des Milieux et Matériaux of Poitiers (IC2MP, Poitiers, France) using a X8050-16 Viscom model [resolution between 16.7 and 32.3 μm; reconstructions performed using Feldkamp algorithm with DIGICT software, version 1.15 (Digisens SA, France)]; and (ii) at the European Synchrotron Radiation Facility (ESRF, Grenoble, France) using third-generation synchrotron microtomography on beamlines ID19 and BM5 (resolution between 5.0 and 14.9 μm; reconstructions performed using filtered back-projection algorithm with the ESRF PYHST software).

Image segmentation and visualization were performed using VGSTUDIOMAX 2.2 (Volume Graphics, Heidelberg, Germany) at the Palaeontology Imaging Unit of the MNHN/UMR 7207 CR2P and AVIZO 7.0 (VSG, Burlington, MA, USA) at the UMR 7179 MECADEV. The segmentation tools of these software packages were used to select the endocranial space of the specimens thereby allowing separation of the skull from the endocranial space, and to reconstruct the brain endocast.

Institutional abbreviations

IC2MP, Institut de Chimie des Milieux et Matériaux, Poitiers, France; ESRF, European Synchrotron Radiation Facility, Grenoble, France; MCZ, Museum for Comparative Zoology, Harvard University, USA; MNHN, Muséum National d'Histoire Naturelle, Paris, France; ZRC, Zoological Reference Collections, National University of Singapore.

Measurements

For each specimen, 21 measurements were defined and taken to illustrate the whole 3D shape, volume and surface of the brain endocast (Fig. 2B). All the measurements made on the brain endocast were measured point-to-point and obtained with the digital caliper of VGSTUDIOMAX 2.2 and the measuring tool of AVIZO 7.0, both with accuracy of 0.01 mm (see Appendices S1 and S2). The print of the sutures between the different skull bones visible on the brain endocast surface were used to define homologous distances. The following list introduces the measurements taken on the brain endocast. The different parts of the brain endocast are named with the same terms as those used for the brain itself (Fig. 2A), following Butler & Hodos (2005); however, the terms used here do not have a neurological significance and are not related to neural structures.

(1) *Length of the brain endocast* (LE): distance between the anterior-most part of the olfactory bulbs still entirely surrounded by the frontal bone and the tip of the suture left by the contact of the supraoccipital with the two exoccipitals on the dorsal surface of the brain endocast.

(2) *Length of the olfactory bulbs* (LOB): distance between the anterior-most part of the olfactory peduncles still entirely surrounded by the frontal bone and the fronto-parietal suture.

(3) *Length of the groove between the olfactory bulbs* (LG): distance between the anterior-most end of the groove between the olfactory peduncles and the fronto-parietal suture.

(4) *Height of the main olfactory bulb* (HOB): at the level of the anterior-most part of the main olfactory bulb (MOB) still entirely surrounded by the frontal bone.

(5) *Height of the olfactory peduncle* (HOP): at the level of the fronto-parietal suture.

(6) *Width of the olfactory peduncles* (WOP): at the level of the fronto-parietal suture.

(7) *Length of the fissura interhemispherica* (LFI): distance between the fronto-parietal suture and the virtual limit made by the groove between the cerebral hemispheres and the optic tectum.

(8) *Maximal width of the cerebral hemispheres* (WCH).

(9) *Lateral expansion of the cerebral hemispheres* (LCH): distance between the fronto-parietal suture and the posterior end of the lateral margin of the cerebral hemispheres.

(10) *Maximal height of the cerebral hemispheres* (HCH).

(11) *Maximal width of the optic tectum* (WOR).

(12) *Length of the optic tectum* (LOR): distance between the virtual limit made by the groove separating the cerebral hemispheres of the optic tectum (Fig. 2B) and the tip of the V-shaped suture between the parietal and the supraoccipital (Fig. 2A).

(13) *Height of the optic tectum* (HOR): distance between the dorsal surface of the optic tectum and the triple point formed by the suture between the parietal, prootic and basisphenoid (Fig. 2A).

(14) *Length of the pituitary gland* (LP): distance between the fronto-parietal suture and the most posterior point of the pituitary bulb.

(15) *Height of the pituitary gland* (HP): distance between the most ventral point of the pituitary gland and the triple point formed by the sutures between the parietal, prootic and basisphenoid.

(16) *Width of the inner ear region* (WIE): distance between the two triple points formed by the sutures of the supraoccipital, prootic and exoocipital.

(17) *Dorsal width of the posterior end of the brain endocast* (DWPE): distance taken at the level of the suture between the supraoccipital and the two exoccipitals seen on the dorsal surface of the brain endocast.

(18) *Length of the posterior part of the brain endocast* (LPE): distance between the tip of the V-shaped suture between the parietal and the supraoccipital, and the tip of the V-shaped suture between the supraoccipital and the two exoccipitals.

Table 1 List of the material analyzed.

Family	Taxon	Ab.	Ha	Collection reference	Voxel size (in μm)
Boidae	*Rhinotyphlops schlegelii*	Rs	F	AH Unnumb	13.3
Anomalepididae	*Typhlophis squamosus*	Ts	F	MNHN 1997.2042	5.1
Uropeltidae	*Uropeltis pulneyensis*	Up	F	MNHN 1994.0753	5.0
Cylindrophiidae	*Cylindrophis ruffus*	Cy	F	MNHN 1998.0201	20.1
Aniliidae	*Anilius scytale*	An	F	MNHN 1997.2106	10.1
Pythonidae	*Python regius*	P3	T	AH Unnumb	33.3
	Python regius	P2	T	AH Unnumb	28.9
	Python regius	P1	T	AH MS 37	21.6
Boidae	*Boa constrictor*	Bc	A	MNHN 1989.0177	7.6
	Candoia sp.	Cd	T	AH Unnumb	33.3
	Corallus hortulanus	Ch	A	AH MS 62	32
	Eunectes murinus	Em	SA	MNHN 1996.7898	7.6
Acrochordidae	*Acrochordus granulatus*	Ag	SA	ZRC 2.2334	24.2
Pareatidae	*Pareas margaritophorus*	Pm	A	MNHN 1974.1469	7.5
Viperidae	*Crotalus atrox*	Cr	T	AH MS 31	28.5
	Agkistrodon contortrix	Ac	T	AH MS 56	23.4
Homalopsidae	*Enhydris enhydris*	Ee	SA	ZRC 2.5507b	24.2
	Enhydris punctata	Ep	SA	ZRC 2.3554	24.2
	Cerberus rynchops	Ce	SA	MNHN-RA-1998.8583	35.3
	Homalopsis buccata	Hb	SA	ZRC 2.6411	24.2
	Erpeton tentaculatum	Et	SA	GD Unnumb	7.5
	Bitia hydroides	Bh	M	ZRC 2.4374	20.9
	Fordonia leucobalia	Fl	SA	MNHN-RA-1912.26	33.2
	Cantoria violacea	Cv	SA	ZRC 2.3672	20.8
Lamprophiidae	*Mimophis mahfalensis*	Mm	T	MRSN R3171	24.7
	Atractaspis irregularis	Ai	F	MNHN 1999.9129	7.6
Elapidae	*Micrurus lemniscatus*	Ml	T	MNHN 1997.2353	7.6
	Naja nivea	Nn	T	AH MS 68	28.5
	Hydrophis elegans	He	M	MNHN-RA-0.1879	30.7
	Enhydrina schistosa	Es	M	ZRC 2.2043	20.8
	Astrotia stokesii	As	M	ZRC 2.2032	20.8
	Hydrophis major	Hm	M	MNHN 1990 4557	44.8
	Hydrophis ornatus	Ho	M	MNHN-RA-1994.6997	36
	Pelamis platurus	Pp	M	AH MS 64	31.9
	Aipysurus duboisii	Ad	M	MNHN-RA-1990.4519	41
	Aipysurus eydouxii	Ae	M	MNHN-RA-0.7704	40.2
	Microcephalophis gracilis	Mg	M	ZRC 2.2155	20.8
Natricidae	*Thamnophis sirtalis*	Ta	T	GD Unnumb.	7.5
Colubridae	*Chrysopelea ornata*	Co	A	MCZ R-177291	14.9
	Hierophis gemonensis	Hg	T	AH Unnumb	23.4
	Hierophis viridiflavus	Hv	T	AH Unnumb	19.2
	Dispholidus typus	Dt	A	AH Unnumb	32
	Boiga dendrophila	Bd	A	AH MS 102	18.2
	Dasypeltis sp.	Ds	A	MCZ 71877	14.9
	Coronella austriaca	Ca	T	AH MS 51	21.6

Ab. represents the abbreviated names of taxa and Ha represents the categories based on habitat: A, arboreal; F, fossorial; M, marine; T, terrestrial; SA, semi-aquatic; AH, Anthony Herrel personal collections; GD, Gheylen Daghfous personal collections.

(19) *Height of the posterior part of the brain endocast* (HPE): distance between the maximum of concavity of the inner ear region and the ventral margin of the brain endocast.

(20) *Width of the ventral part of the brain endocast* (WPE): distance between the two triple points formed by the suture between the prootic, basisphenoid and basioccipital on the ventral margin.

(21) *Width in the pituitary gland region* (WP): distance taken on the ventral surface of the brain endocast, between the triple points formed by the sutures between the parietal, prootic and basisphenoid.

Quantitative analyses

In order to provide complementary information, three different approaches were used to study the brain endocast variability occurring in snakes.

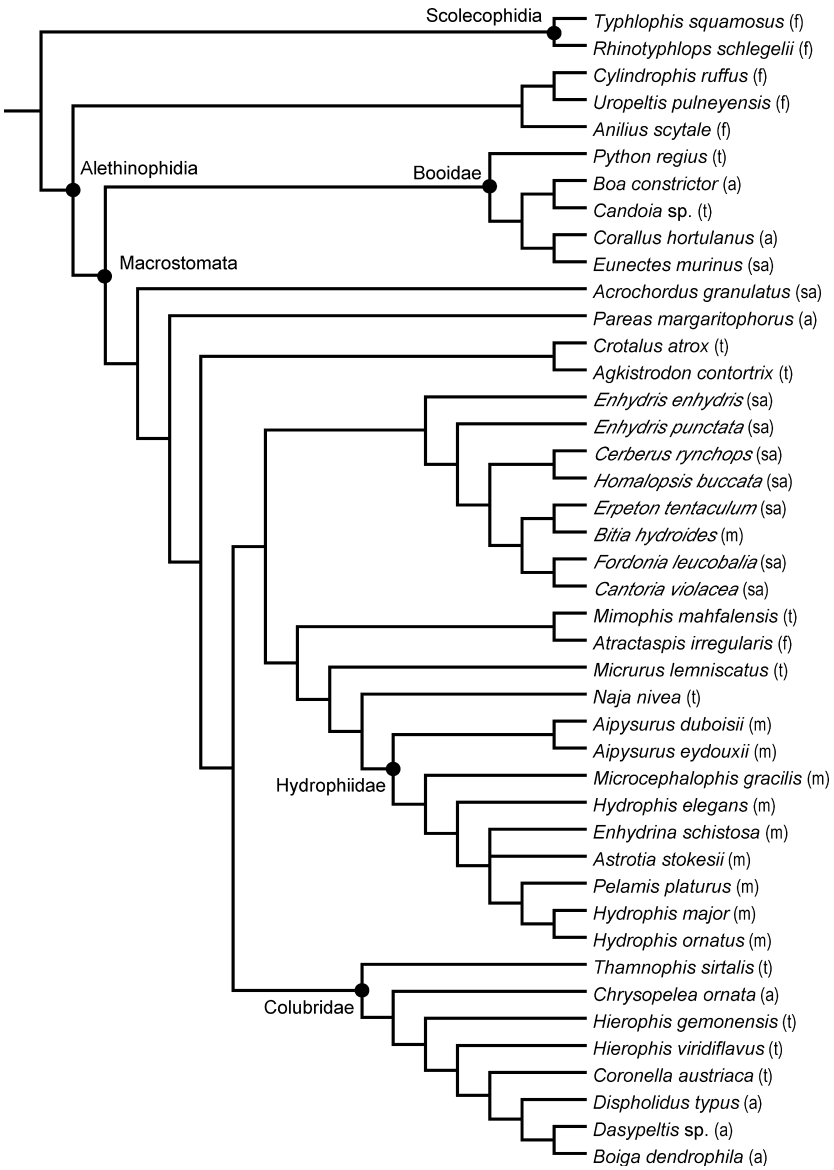

Fig. 1 Schematic phylogenetic relationships of snakes sampled in the study (modified from Lee & Scanlon, 2002; Pyron et al. 2011; Hsiang et al. 2015). Principal ecology/habitat: fossorial (f), terrestrial (t), arboreal (a), semi-aquatic (sa), marine (m).

Descriptive character analysis

The differences observed between the various snake brain endocasts were listed and coded (see Appendix S3: List of the characters and Matrix). We used the coded characters to run a principal coordinate analysis (PCoA) in order to evaluate the distances between the taxa and thus to identify which taxa are similar in brain endocast morphology based on these coded characters: the closer the species, the more similar the brain endocast morphologies.

Measure analysis

All data (see Appendices S1 and S2) were log10-transformed prior to analysis to meet assumptions of normality and homoscedasticity required for parametric analyses. All the analyses were performed using the statistic software R (R Development Core Team, 2008). To analyze shape components independently from size, the log-shape ratios (Mosimann & James, 1979) were calculated based on the raw log10-transformed linear dimensions of the brain endocast.

In order to take into account the biases induced by measurement repeatability, three specimens of *P. regius* showing the lowest shape variation were selected. According to the data published by Aubret et al. (2005), the comparison of their jaw length seems to differentiate a neonate specimen (P1; jaw length = 25.4 mm) from a juvenile (P3; jaw length = 31.4 mm) and an adult (P2; jaw length = 40.3 mm) one. Ten repetitions were performed for each measure on these three specimens. Then, to quantify and visualize the differences between repetitions, a principal component analysis (PCA) was performed. Shape differences between specimens were much higher than shape differences induced by repetitions (see Appendix S2).

To evaluate the phylogenetic signal in the shape of the brain endocast in snakes, we used a multivariate generalization of the *K* statistic of Blomberg et al. (2003): the *K*mult (Adams, 2014). The phylogenetic signal is based on a phylogenetic consensus tree derived from several published phylogenies (Lee & Scanlon, 2002; Pyron et al. 2011; Hsiang et al. 2015; Fig. 1). Adams (2014) demonstrated that values of *K*mult < 1 imply that taxa resemble each other phenotypically less than expected under Brownian motion, whereas values of *K*mult > 1 imply that close relatives are more similar to one another phenotypically than expected under Brownian motion.

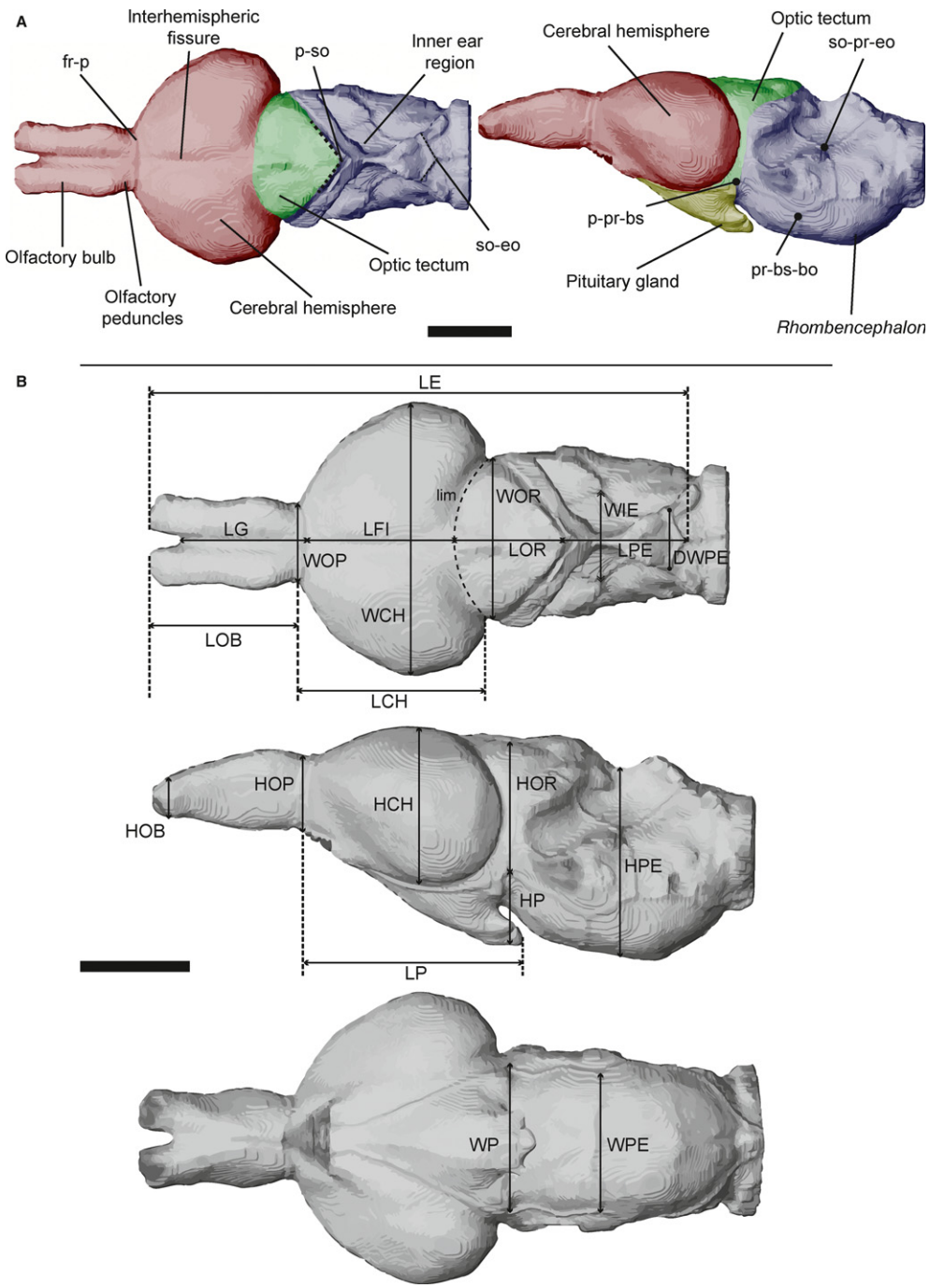

Fig. 2 Reconstructed brain endocast of *Enhydris punctata* (Homalopsidae). (A) Illustration of the major structures seen in dorsal and left lateral views: telencephalon (red), diencephalon (yellow), mesencephalon (green), rhombencephalon (purple). (B) Illustration of the various measurements defined in Materials and methods, and taken in dorsal, left lateral and ventral views. fr-p, fronto-parietal suture; lim, groove between the optic tectum and the cerebral hemispheres; p-pr-bs, triple point formed by the sutures between the parietal, prootic and basisphenoid; p-so, parietal-supraoccipital suture; pr-bs-bo, triple point formed by the suture between the prootic, basisphenoid and basioccipital; so-eo, supraoccipital-exoccipital suture; so-pr-eo, triple point formed by the sutures of the supraoccipital, prootic and exoocipital; DWPE, dorsal width of the posterior end of the brain endocast; HCH, maximal height of the cerebral hemisphere; HOB, height of the main olfactory bulb; HOP, height of the olfactory peduncle; HOR, height of the optic tectum; HP, height of the pituitary bulb; HPE, height of the posterior part of the brain endocast; LCH, lateral expansion of the cerebral hemispheres; LE, length of the brain endocast; LFI, length of the interhemispheric fissure; LG, length of the groove between olfactory bulbs; LOB, length of the olfactory bulbs; LOR, length of the optic tectum; LP, length of the pituitary bulb; LPE, length of the posterior part of the brain endocast; WCH, maximal width of the cerebral hemispheres; WIE, width of the inner ear region; WOP, width of the olfactory peduncles; WOR, maximal width of the optic tectum; WP, width in the pituitary gland region; WPE, width of the ventral part of the brain endocast. Scale bar: 2 mm.

A PCA was also performed on the data obtained from the measurements made on the 45 snake specimens; the mean of the 10 measurements taken on each of the *P. regius* specimens was used.

To test the relationships between the habitat/ecology and the morphology of the brain endocast, the sampled taxa were classified into five habitat categories (Fig. 1): fossorial, terrestrial, arboreal, semi-aquatic and marine (Heatwole, 1999; Houssaye et al. 2013; A. Herrel, personal communication). We performed a standard and phylogenetic MANOVA, to respectively evaluate whether the brain endocast variability could reflect the ecology, taking or not the phylogenetic relationships into consideration.

Outline curve analysis

For each brain endocast, the ventral and lateral views were selected to perform an outline curve analysis using geometric morphometrics (Zelditch et al. 2004). We used 2D sliding semi-landmarks (Gunz & Mitteroecker, 2013) that permit accurate description of homologous anatomical curves devoid of anatomical landmarks. Sliding semi-landmarks are allowed to slide, minimizing the bending energy between each specimen and the mean shape of the dataset. This step creates a geometric homology between specimens that permits all classical geometric morphometric analyses. We performed a General Procrustes Superimposition to work on shape (Rohlf & Slice, 1990) and PCAs for each view.

The dorsal view was not used here because of the difficulty to distinguish homologous outline curves on the posterior part of the structure at the level of the inner ear position. In ventral view, the 45 brain endocasts of our dataset were used. In lateral view, we used the posterior crest formed by the inner ear and three homologous points as landmarks to facilitate the placement of the curve semi-landmarks. The sutures between the different skull bones visible on the posterior part of the brain endocast surface were used to define homologous points. The first point corresponds to the triple point formed by the sutures between the basioccipital, exoccipital and prootic. The second is the triple point formed by the prootic, the basioccipital and the basisphenoid. The last point represents the most ventral point of the suture between the basioccipital and the basisphenoid. In lateral view, we used 38 specimens because the sutures are not visible and did not allow the placement of the same landmarks on *Aipysurus eidouxii*, *Cerebrus rynchops*, *Corallus hortulanus*, *Dispholidus typus*, *Mimophis mahfalensis*, the smallest specimen of *P. regius* and *Uropeltis pulneyensis*.

Results

General description of snake endocast and variability

Here, only a description of the brain endocast will be provided, without considering the cranial nerves or the inner ear (data in Boistel et al. 2011b; Yi & Norell, 2015). The cast of the endocranial space does not only reflect the brain itself: associated tissues (e.g. venous system) are also reconstructed during segmentation and may hide some parts of the brain. The endocast morphology resulting from the segmentation of the endocranial space is described below as a whole. The brain endocast in snakes is surrounded dorsally by the frontal and parietal (anteriorly) and the supraoccipital and exoccipital (posteriorly), laterally by the prootics, and ventrally by the basioccipital and para-basisphenoid (Fig. 3). The surface of the brain endocast of snakes is smooth.

Telencephalon

The telencephalon includes the olfactory bulbs, the olfactory peduncles and the cerebral hemispheres (Fig. 2A). The MOB and accessory olfactory bulbs (AOB) correspond to the

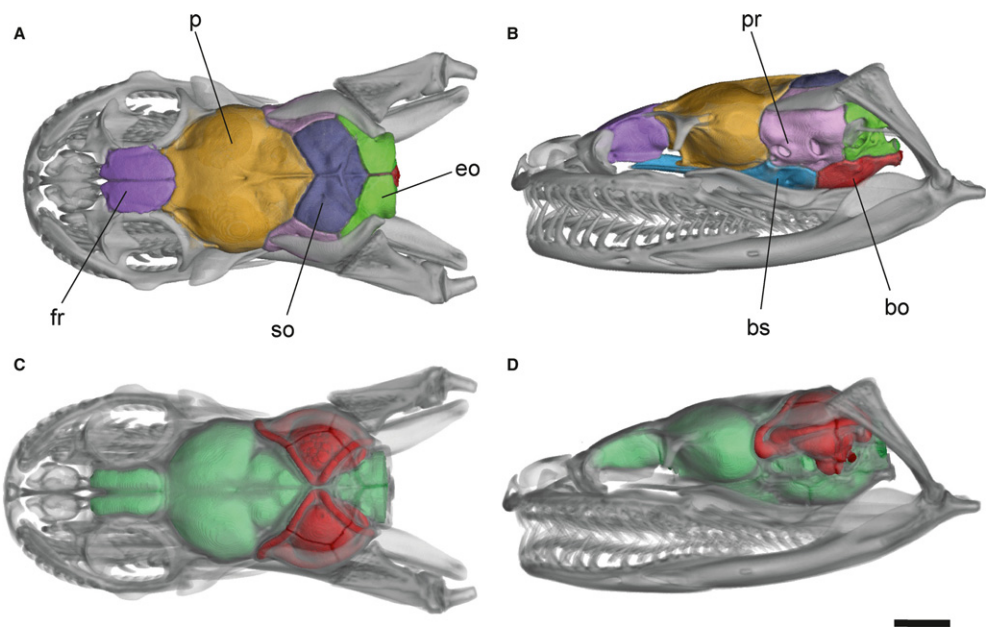

Fig. 3 Skull of *Enhydris punctata* (Homalopsidae) in dorsal (A) and left lateral (B) views showing the bones surrounding the brain endocast; (C,D) with bones rendered transparent to reveal the brain endocast (green) and the inner ear (red). bo, basioccipital; bs, basisphenoid; eo, exoccipitals; fr, frontal; p, parietal; pr, prootics; so, supraoccipitals. Scale bar: 2 mm.

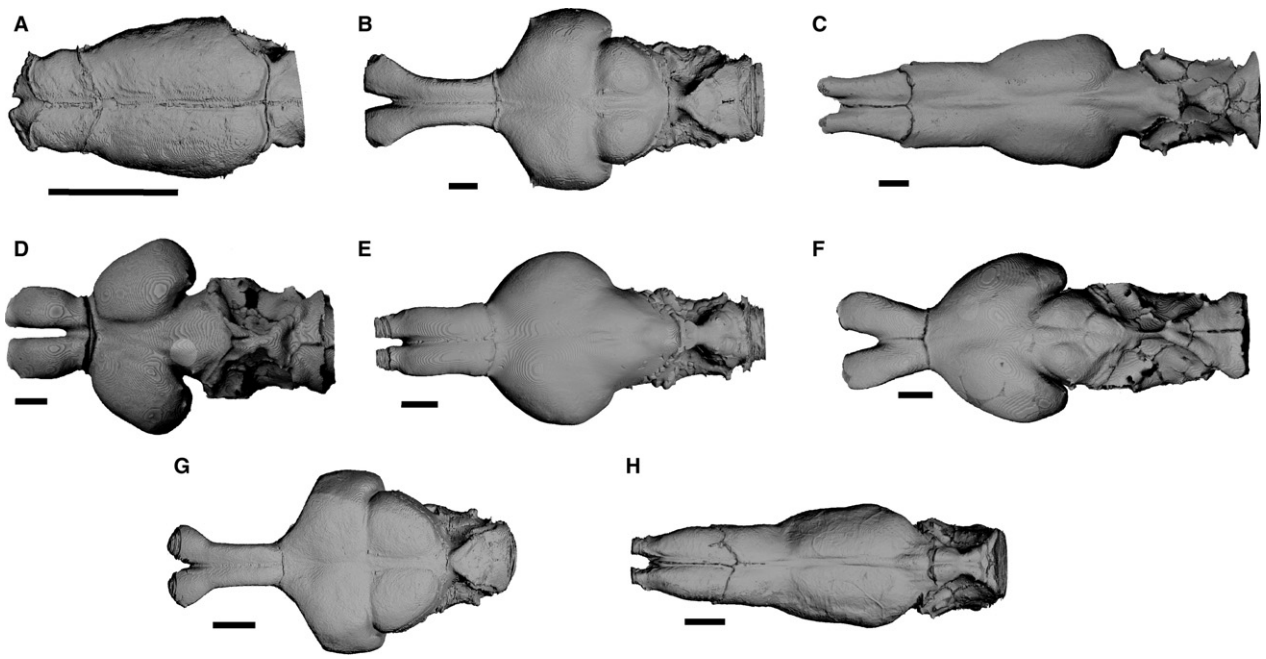

Fig. 4 Brain endocasts in dorsal view of (A) *Typhlophys squamosus* (Typhlopidae); (B) *Hierophis viridiflavus* (Colubridae); (C) *Cylindrophis ruffus* (Cylindrophiidae); (D) *Acrochordus granulatus* (Acrochordidae); (E) *Eunectes murinus* (Boidae); (F) *Homalopsis buccata* (Homalopsidae); (G) *Chrysopelea ornata* (Colubridae); (H) *Anilius scytale* (Aniliidae). Scale bars: 1 mm.

anterior-most structure of the brain endocast (Fig. 2A); however, from the brain endocast only it is not possible to distinguish one from another. They are attached to the rostral pole of the cerebral hemisphere by short olfactory peduncles. In dorsal view, a groove is visible running between the two olfactory bulbs. Posteriorly, the cerebral hemispheres represent the largest part of the brain endocast and gradually widen laterally. An interhemispheric fissure may be visible on the dorsal surface of the brain endocast, as attested by a groove between the cerebral hemispheres. The length of the interhemispheric fissure and the depth of the groove vary according to taxa.

Some taxa may exhibit olfactory bulbs wider than long, giving a short and stout aspect (e.g. width/length aspect ratio superior to one in *Typhlophys squamosus*; Fig. 4A) in dorsal view, while most taxa have an olfactory structure longer than wide (e.g. width/length aspect ratio inferior to one in *Hierophis viridiflavus*; Fig. 4B). The lateral margin of this structure may be mediolaterally convex (e.g. *Acrochordus* granulatus; Fig. 4D), relatively straight (e.g. *Eunectes murinus*; Fig. 4E) or mediolaterally concave (e.g. *H. viridiflavus*; Fig. 4B) in dorsal view. Most species possess in dorsal view a system composed of two parallel olfactory bulbs and peduncles (e.g. *E. murinus*; Fig. 4E). Some others show a projection that diverges laterally from the fronto-parietal suture (e.g. *Homalopsis buccata*; Fig. 4F), whereas others share the two conditions with parallel olfactory bulbs and peduncles diverging laterally at their anterior end (e.g. *H. viridiflavus*; Fig. 4B). In lateral view, the ventral margin may be ventrodorsally concave (e.g. *M. mahfalensis*; Fig. 5D), convex (e.g. *Boiga dendrophila*; Fig. 5B) forming a bulge, or straight (e.g. *H. buccata*; Fig. 5C). Some taxa (e.g. *T. squamosus*; Fig. 4A) do not show any separation over the whole length of the olfactory peduncles in dorsal view. Most taxa have olfactory peduncles diverging only at their anterior end (e.g. *H. viridiflavus*; Fig. 4B). Some species have a large space between the two olfactory structures, separating them along almost their entire length (e.g. *A.* granulatus; Fig. 4D). The width of the olfactory bulbs may vary antero-posteriorly. At the level of the fronto-parietal suture and in dorsal view, some taxa possess a posterior part as wide (e.g. *E. murinus*; Fig. 4E) or wider (e.g. *Cylindrophis ruffus*; Fig. 4C) than the anterior end. However, others have olfactory bulbs with an anterior end wider than the posterior part (e.g. *H. viridiflavus*; Fig. 4B).

The relative size of the cerebral hemispheres varies between taxa. A distinction is seen between those that have hemispheres wider than long (e.g. width/length aspect ratio close to 1.4 in *Chrysopelea ornata*; Fig. 4G) and those that have a structure as long as wide (e.g. width/length aspect ratio close to one in *T. squamosus*; Fig. 4A). A few taxa are exceptions with cerebral hemispheres longer than wide (e.g. width/length aspect ratio close to 0.3 in *C. ruffus*; Fig. 4C). The lateral extension in dorsal view generally begins just posterior to the fronto-parietal suture (e.g. *E. murinus*; Fig. 4E), but two taxa [*C. ruffus* (Fig. 4C) and *Anilius scytale* (Fig. 4H)] exhibit cerebral hemispheres with an anterior part as wide as the fronto-parietal suture, the

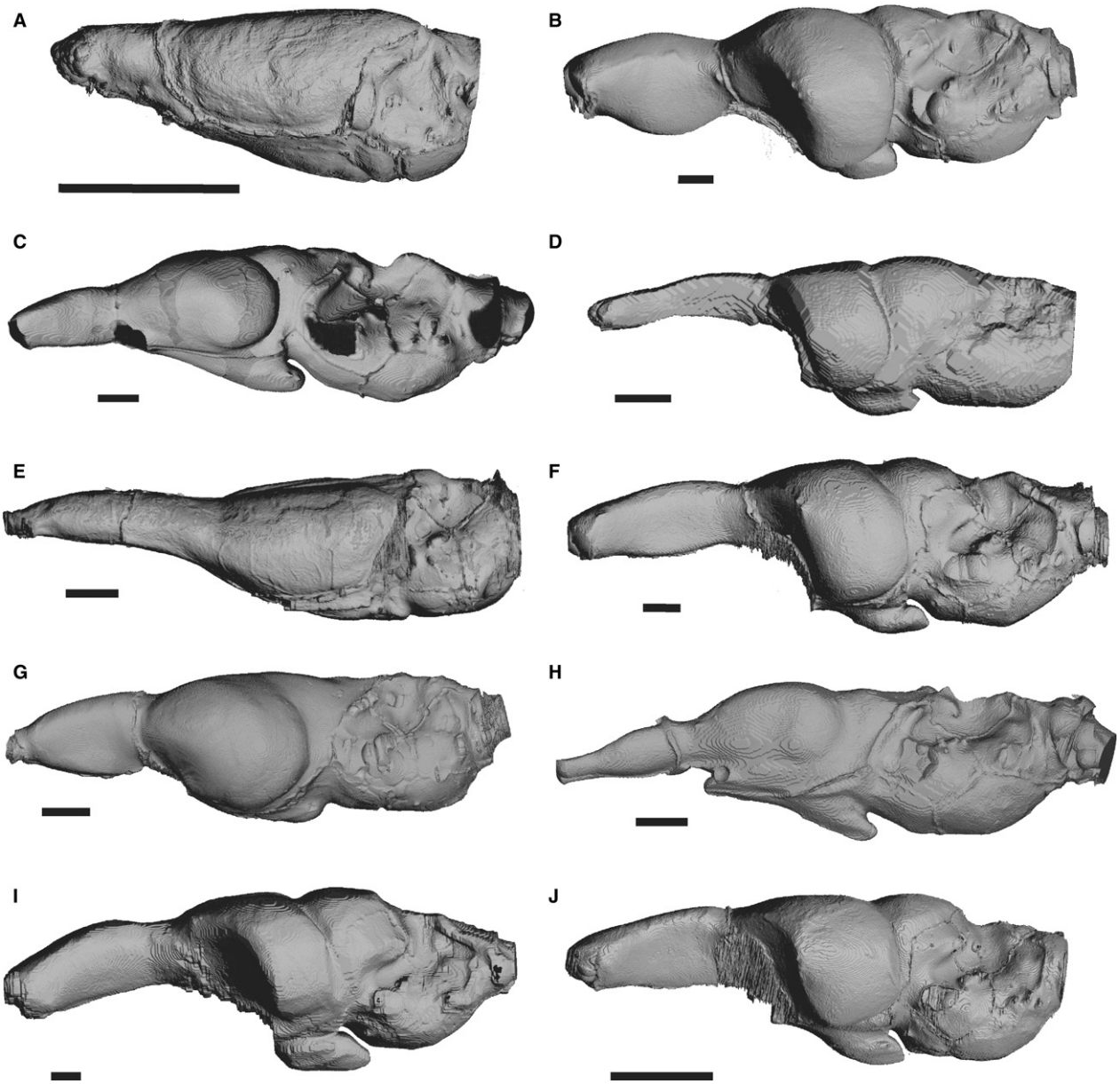

Fig. 5 Brain endocasts in left lateral view of (A) *Typhlophys squamosus* (Typhlopidae); (B) *Boiga dendrophila* (Colubridae); (C) *Homalopsis buccata* (Homalopsidae); (D) *Mimophis mahfalensis* (Lamprophiidae); (E) *Anilius scytale* (Aniliidae); (F) *Hierophis viridiflavus* (Colubridae); (G) *Eunectes murinus* (Boidae); (H) *Enhydrina schistosa* (Elapidae); (I) *Dispholidus typus* (Colubridae); (J) *Thamnophis sirtalis* (Natricidae). Scale bars: 1 mm.

lateral extension occurring more posteriorly. In dorsal view, the lateral margin may be rounded (e.g. *E. murinus*; Fig. 4E) or relatively straight (e.g. *C. ornata*; Fig. 4G), providing a square appearance to the cerebral hemispheres. In lateral view, differences occur between taxa with cerebral hemispheres developed only along the horizontal axis (e.g. *T. squamosus*; Fig. 5A), taxa with cerebral hemispheres developed in the horizontal plane but with a posterior part directed ventrally (e.g. *H. buccata*; Fig. 5C) and taxa with a dorso-ventral extension at least as long as the horizontal one (e.g. *B. dendrophila*; Fig. 5B). The limit between the cerebral hemispheres and the optic tectum depends on the lateral extension of the cerebral hemispheres. Species that do not have an important lateral extension (e.g. *A. scytale*; Fig. 4H) do not show a clear delimitation between the optic tectum and the cerebrum, contrary to those that have a groove between the two structures and have laterally extended cerebral hemispheres (e.g. *C. ornata*; Fig. 4G).

Diencephalon

The pituitary gland, located ventrally to the cerebral hemispheres, is the only structure of the diencephalon seen on the brain endocast (Fig. 2A); the pineal gland is not visible. In addition, the external morphology of the brain endocast

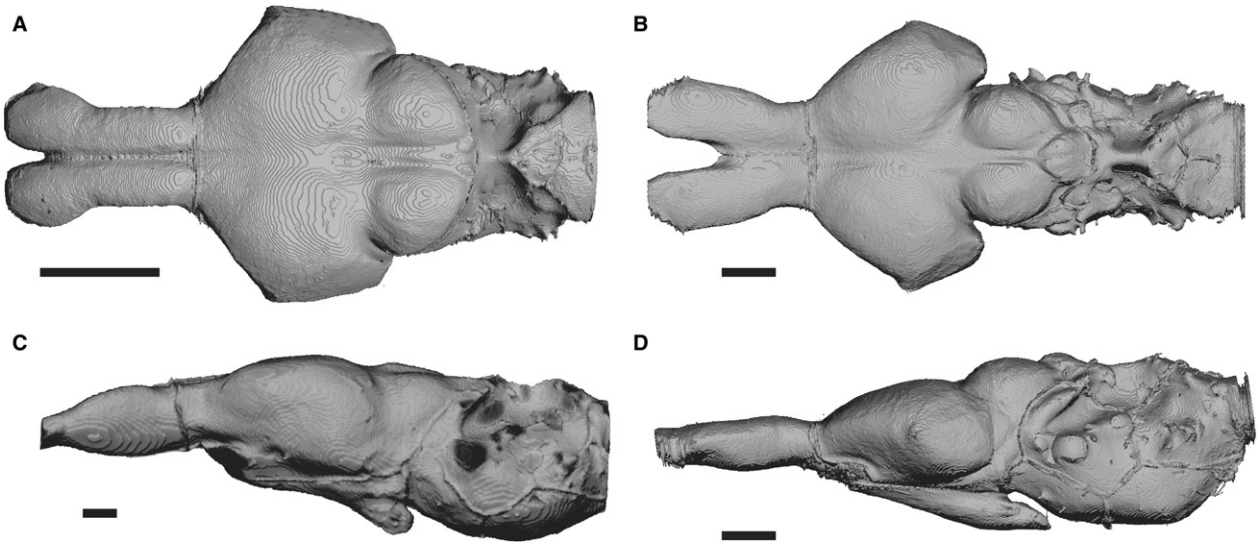

Fig. 6 Brain endocasts in dorsal (upper row) and left lateral (lower row) views of (A) *Thamnophis sirtalis* (Natricidae); (B) *Erpeton tentaculatum* (Homalopsidae); (C) *Hydrophis major* (Elapidae); (D) *Erpeton tentaculatum*. Scale bars: 1 mm.

does not allow the hypothalamus and the hypophysis to be delimited.

The pituitary gland may be marked by the presence in lateral view of a small bulge on the ventral surface of the brain endocast (e.g. *A. scytale*; Fig. 5E). But generally the system shows a structure more developed ventrally, displaying (e.g. *H. viridiflavus*; Fig. 5F) or not (e.g. *E. murinus*; Fig. 5G) a posterior projection. Among those displaying a posterior projection, a distinction is made between those presenting a tilted system (e.g. *Enhydrina schistosa*; Fig. 5H) and those having a posterior projection in the horizontal plane (e.g. *H. viridiflavus*; Fig. 5F). Differences relative to the ventral margin of the posterior projection also occur, between a curved (e.g. *Thamnophis sirtalis*; Fig. 5J) and a flat (e.g. *D. typus*; Fig. 5I) shape.

Mesencephalon

The mesencephalon lies posterior to the cerebral hemispheres. The optic tectum forms the roof of the mesencephalon (Fig. 2A). From the endocast, the distinction between the optic tectum and the tegmentum, which is located more ventrally in the mesencephalon, is not possible. In dorsal view, the mesencephalon is less wide than the cerebral hemispheres.

In a few taxa this structure is not distinguishable from the cerebral hemispheres (e.g. *T. squamosus*; Fig. 4A). In some others, the structure is visible in dorsal view only thanks to its decrease in width as compared with the cerebral hemispheres (e.g. *E. murinus*; Fig. 4E), and its surface appears smooth and flattened. However, in other species, the optic tectum exhibits in dorsal view a pair of domes separated by a median sulcus (e.g. *T. sirtalis*; Fig. 6A). Some taxa show (in dorsal view) a distinct optic tectum as wide as the rhombencephalon (e.g. *H. buccata*; Fig. 4F). The others have an optic tectum wider (e.g. *C. ornata*; Fig. 4G) or narrower (e.g. *A.* granulatus; Fig. 4D) than the ventral margin of the rhombencephalon. In lateral view, most taxa possess a dorsal margin of the optic tectum located at the same height as the cerebral hemispheres (e.g. *E. murinus*; Fig. 5G), except *Erpeton tentaculatum*, in which the margin is located more dorsally (Fig. 6D).

Rhombencephalon

Posterior to the optic tectum, the cerebellum is not visible on the dorsal surface of the brain endocast. According to Aurboonyawat et al. (2008), the dorsal longitudinal vein located on the mid-dorsal surface of the brain endocast must cover it. On the lateral sides of the brain endocast, the large and round impressions indicate the position of the inner ear (Fig. 2A). The *medulla oblongata* is located ventral to the inner ear region, and represents the ventral margin of the posterior part of the brain endocast.

Most species exhibit a rhombencephalon in lateral view with a rounded (e.g. *Boa constrictor*; Fig. 7A) or straight (e.g. *E. tentaculatum*; Fig. 6D) ventral margin, but in some taxa (e.g. *Crotalus atrox*; Fig. 7B) the ventral margin is triangular, pointing ventrally. The ventral extension of the *rhombencephalon* may correspond to the most ventral surface of the brain endocast in lateral view (e.g. *B. constrictor*; Fig. 7A) or not (e.g. *D. typus*; Fig. 5I).

Quantitative analyses

Brain endocasts of snakes show a great variability. This variability is characterized by different relative proportions between the structures visible on the brain endocasts (e.g.

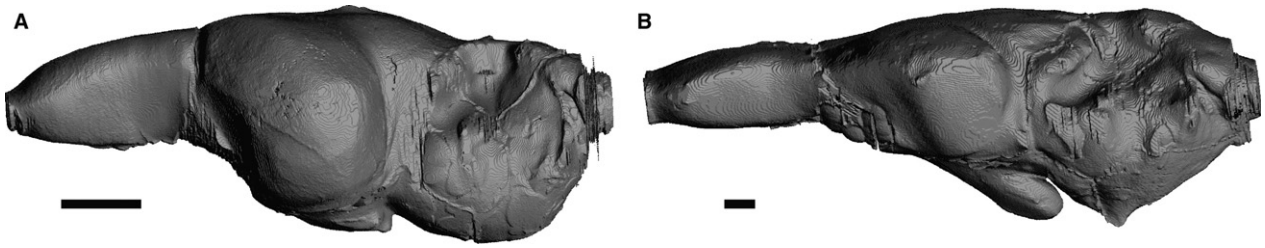

Fig. 7 Brain endocasts in left lateral view of (A) *Boa constrictor* (Boidae); (B) *Crotalus atrox* (Viperidae). Scale bars: 1 mm.

size of the optic tectum compared with that of the cerebral hemispheres), giving a wide range of shapes, from stout (e.g. *T. squamosus*), to elongated and gracile (e.g. *Pelamis platurus*) or elongated and wide (e.g. *B. constrictor*) brain endocasts. Below, this variability is analyzed quantitatively.

Descriptive character analysis

The results obtained (Fig. 8) show that 50.3% of the variance is explained by the two main principal components (29.4% and 20.9%, respectively). The distribution of the taxa indicates that fossorial and marine snakes are both distinct from those with other ecologies. Among the fossorial species, *Atractaspis irregularis* is quite distinct from two groups: the first one including *U. pulneyensis*, *C. ruffus* and *A. scytale*; and the second one made by *T. squamosus* and *Rhinotyphlops schlegelii*. *Micrurus lemniscatus* and *A. granulatus*, a terrestrial and a semi-aquatic snake, respectively, tend toward the brain endocast morphology found in the fossorial taxa. Among the marine species of our dataset, *E. schistosa* and *Microcephalophis gracilis* are close to each other and distinct from other marine snakes. The terrestrial species show a wide distribution. The isolated position of *M. lemniscatus* was already cited above. *Hierophis gemonensis*, *H. viridiflavus* and *T. sirtalis* are close together and located near the two arboreal snakes *D. typus* and *C. ornata*. These species are distinct from *M. mahfalensis*, *C. atrox*, *Agkistrodon contortrix*, *Coronella austriaca* and *Naja nivea*, which are close together and possess a brain endocast morphology similar to the arboreal snakes *B. dendrophila* and *Dasypeltis* sp. In addition, the three specimens of *P. regius* and *Candoia* sp. are distinct from the other terrestrial taxa with a brain endocast morphology tending towards those found in marine ones. Among the arboreal taxa not cited above, *C. hortulanus*, *B. constrictor* and *Pareas margaritophorus* are close to the semi-aquatic snake *Cantoria violacea*. The distribution of the semi-aquatic species overlaps those of the terrestrial and arboreal snakes. The brain endocast of *Enhydris enhydris* is similar to that of *M. mahfalensis* and distinct from those of *E. tentaculum*, *Fordonia leucobalia*, *H. buccata* and *Enhydris punctata,* which are grouped together. The two species *C. rynchops* and *E. murinus* are, respectively, close to *Candoia* sp. and to the three specimens of *P. regius*, and tend towards the marine taxa.

The species distribution suggests the existence of phylogenetic and ecological signals. Phylogenetically close species show more similarities than with other species (e.g. *T. squamosus* and *R. schlegelii*). However, an ecological signal is also perceived, meaning that species sharing the same ecology show more brain endocast similarities than species with a different ecology.

Measure analysis

Intraspecific variability in P. regius. The PCA (Fig. 9) shows that the two main axes explain 93% of the variance (80% and 13%, respectively). The repeatability test is positive as the 10 iterations for each specimen are clearly grouped and the three specimens clearly distinct, indicating that the variability caused by the measurement acquisition is inferior to the variability between the specimens. All variables seem to act on the distribution of the specimens [though the impact of LP (length of the pituitary bulb) on the second axis appears significantly more important than that of the other variables]. The first principal component mostly separates the specimens based on size. The variables principally acting on PCA1 are the height of the olfactory bulbs (HOB), the length of the optic tectum (LOR) and the length of the pituitary gland (LP). The smaller specimen (P1) has the greatest height of the olfactory bulbs, the greatest length of the pituitary bulb, and the smallest length of the optic tectum. The second principal component separates the intermediate specimen (P3) from the two others. The main variable acting along the second axis is still the length of the pituitary gland (LP). The intermediate specimen (P3) shows the smallest height of the olfactory bulb, the greatest length of the optic tectum and an intermediate value for the length of the pituitary gland. Finally, the largest specimen (P2) possesses the greatest length of the pituitary gland, and intermediate values for the height of the olfactory bulb and for the length of the optic tectum.

Interspecific variability. The PCA obtained with all snake specimens (Fig. 10) shows that 60% of the variance is explained by the two-first axes (44.7% and 15.3%, respectively). Fossorial species are clearly distinct from the others, with a great distribution along the first axis, contrary to the snakes with other ecologies, that all display a more limited distribution. The PCA shows some overlap between the snakes with arboreal, terrestrial, semi-aquatic and marine habitats, but a gradation is clearly visible. The arboreal and

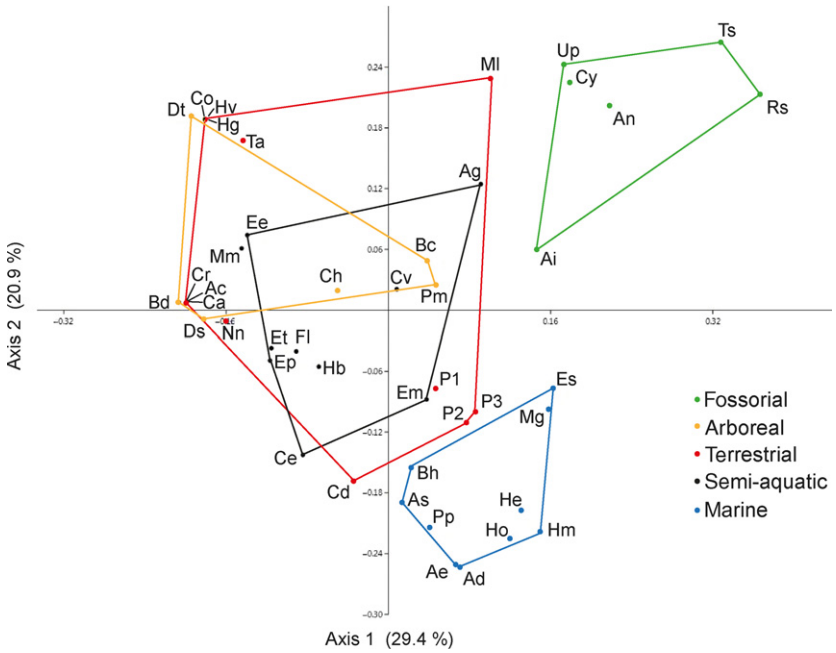

Fig. 8 Results of the PCoA performed on the snake brain endocast characters (Appendix S3). See Table 1 for name abbreviations.

terrestrial taxa appear distinct (with no overlap) from the marine ones. All variables seem to act on the repartition of the species (see Appendix S4). However, along the first axis, two variables mostly act on the distribution of the taxa: the width at the optic tectum level (WOR) and the dorsal width of the posterior end of the brain endocast (DWPE). The first axis seems to separate species that have an optic tectum as wide as the posterior end of the brain endocast (e.g. *T. squamosus*) from the ones in which the optic tectum is much wider than the posterior end of the brain endocast (e.g. *P. platurus*). Along the second axis, the width of the olfactory peduncles (WOP) and the width of the cerebral hemispheres (WCH) explain most of the variability. These variables allow to distinguish species presenting a large difference between the width of the olfactory peduncles and the width of the cerebral hemispheres (e.g. *B. constrictor*), from those that have a smaller difference between these two widths (e.g. *C. ruffus*).

The MANOVA performed on the data indicates significant differences between brain endocasts depending on ecology (MANOVA: Wilks $\lambda = 0.751$, $F_{2,22} = 8.75$, $P = 0.013$). The *K*mult test indicates that brain endocast shape in snakes exhibits a significant phylogenetic signal (*K*mult = 0.814; $P = 0.001$), showing the importance to consider the phylogeny in studies of snake brain endocasts. The phylogenetic MANOVA still indicates significant differences pending on ecology (phylogenetic MANOVA: Wilks $\lambda = 0.0074$, $F_{2,22} = 81.748$, *P*phyl = 0.0087).

Outline curve analysis

The results obtained by the outline curve analyses (Figs 11 and 12) enable to comment on the shape of snake brain endocasts according to the different ecologies.

The first PCA is obtained from the endocast outline curves in ventral view (Fig. 11) and shows that 61.9% of total variance is explained by the two-first axes (44.6% and 17.3%, respectively). The first axis separates proportionally stout brain endocasts, wide at the level of the olfactory bulbs and of the cerebral hemispheres (blue dotted line, Fig. 11, Axis 1), from longer and narrower endocasts (black dotted line, Fig. 11, Axis 1). Thus, brain endocasts of semi-aquatic, arboreal and terrestrial snakes are mostly wide, whereas the fossorial and marine species have an extended distribution along this first axis, encompassing both wide and narrow endocasts. However, the distribution of marine taxa is mainly concentrated towards narrow endocasts and only two species, *Aipysurus duboisii* and *Aipysurus eydouxii*, move towards wide endocasts. Along the second axis, the shape of the forebrain (olfactory bulbs and cerebral hemispheres) principally drives the distribution. Brain endocasts with wide olfactory bulbs have cerebral hemispheres located more anteriorly (dark dotted line, Fig. 11, Axis 2) than those with thinner olfactory bulbs (blue dotted line, Fig. 11, Axis 2). Semi-aquatic, fossorial and marine species all exhibit a brain endocast with wide olfactory bulbs and anteriorly located cerebral hemispheres, contrary to the arboreal and terrestrial snakes that are distributed all along the axis and thus express the two conditions.

The second PCA is obtained from the endocast outline curves in lateral view (Fig. 12) and shows that 65.8% of total variance is explained by the two-first axes (48% and 17.8%, respectively). The first axis illustrates brain endocasts with well dorsoventrally developed and ventrally oriented olfactory bulbs, and a posterior part characterized by a rounded dorsal surface more developed dorsally than the anterior part (blue dotted line in Fig. 12, Axis 1). These

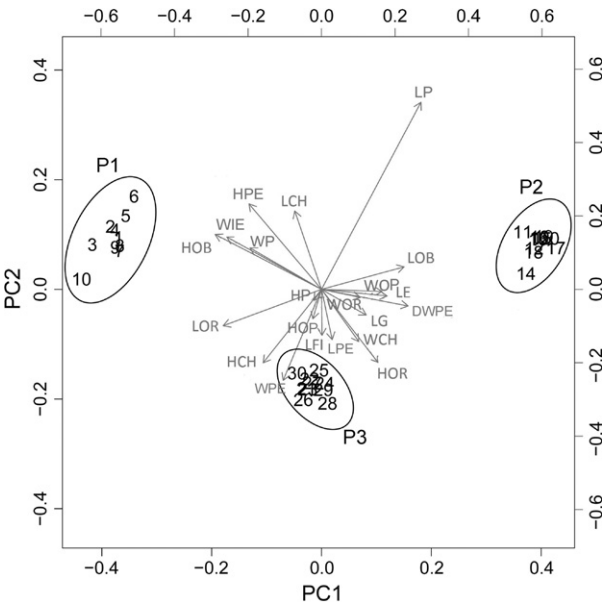

Fig. 9 Results of the PCA performed on the brain endocast variables for three *Python regius* specimens, (P1) smaller specimen, (P3) intermediate specimen, (P2) largest specimen. Scatter plot illustrating the position of the different specimens on the first two principal components. DWPE, dorsal width of the posterior end of the brain endocast; HCH, maximal height of the cerebral hemisphere; HOB, height of the main olfactory bulb; HOP, height of the olfactory peduncle; HOR, height of the optic tectum; HP, height of the pituitary bulb; HPE, height of the posterior part of the brain endocast; LCH, lateral expansion of the cerebral hemispheres; LE, length of the brain endocast; LFI, length of the interhemispheric fissure; LG, length of the groove between olfactory bulbs; LOB, length of the olfactory bulbs; LOR, length of the optic tectum; LP, length of the pituitary gland; LPE, length of the posterior part of the brain endocast; WCH, maximal width of the cerebral hemispheres; WIE, width in the inner ear region; WOP, width of the olfactory peduncles; WOR, maximal width of the optic tectum; WP, width in the pituitary gland region; WPE, width of the ventral part of the brain endocast.

brain endocasts differ from those in which the olfactory bulbs are less developed dorsoventrally and dorsally oriented, and the posterior part presents a flat dorsal surface located at the same level as the anterior part (dark dotted line Fig. 12, Axis 1). The brain endocast of the fossorial species *R. schlegelii* is well distinct from those of other taxa, with a structure very developed dorsoventrally and the posterior region higher than the anterior one. Arboreal and terrestrial species may show a mix between the two morphologies, with a well dorsoventrally developed brain endocast but a flat posterior region located at the same level as the anterior one. Marine snakes tend to have a flat brain endocast, whereas semi-aquatic and fossorial taxa show a large distribution presenting the two brain endocast morphologies. The second axis separates stout brain endocasts well developed dorsoventrally, with a slight dorsal constriction at the limit between the olfactory bulbs and the cerebral hemispheres (blue dotted line Fig. 12, Axis 2) from longer but less dorsoventrally developed brain endocasts (dark dotted line Fig. 12, Axis 2), with a ventral constriction at the limit between the olfactory bulbs and the cerebral hemispheres. The distribution of the taxa seems to indicate that the two morphologies are variably found in all ecologies. However, the dorsoventrally compressed brain endocast found in both marine (*P. platurus*) and terrestrial (*Candoia* sp.) snakes differs from the more dorsoventrally developed brain endocasts found in other taxa sharing their ecologies.

Discussion

Phylogenetic signal

We detected a significant phylogenetic signal in the snake brain endocast variability, meaning that it is at least partly constrained by shared ancestry. Indeed, some patterns or main trends in the brain endocast morphology reflect snakes' systematics. The scolecophidian snakes (*R. schlegelii* and *T. squamosus*; Fig. 1) are the only ones presenting a brain endocast where the optic tectum is not visible (Fig. 4A). Within the Booidae (Fig. 1), the surface of the optic roof is smooth (e.g. *E. murinus*; Fig. 4E), and the pituitary gland is only developed ventrally. The Hydrophiidae (Fig. 1) have cerebral hemispheres poorly developed laterally (e.g. *E. schistosa*; Fig. 5H), contrary to the Colubridae (Fig. 1) that possess cerebral hemispheres very developed both laterally and ventrally (e.g. *H. viridiflavus*; Figs 4B and 5F), as well as an optic roof clearly visible with two distinct domes, and the olfactory bulbs widening on their anterior part. As the multivariate *K* was lower than 1, species resemble each other less than expected under a Brownian motion model of evolution, which shows that, though significant, the phylogenetic signal remains weak. This suggests that other factors, such as ecology, do affect the snake endocast morphology.

Ecological signal

We also detected an ecological signal in the brain endocast of snakes, even when the phylogenetic relationships were taken into account. Though the different ecologies tested here are thus associated with morphological trends of the brain endocast, it nevertheless appears difficult to associate one structure with one ecology. Both standard and phylogenetic MANOVAs indicate significant differences between the ecologies, with an impact of all variables on the distribution of snakes. Thus, fossorial species have a brain endocast with a poor lateral development of the cerebral hemispheres, and not visible or absent optic tectum and pituitary gland. Marine species exhibit an endocast more elongated, with cerebral hemispheres poorly developed laterally and projected only in the antero-posterior plan, but the optic tectum is clearly visible and the pituitary gland is

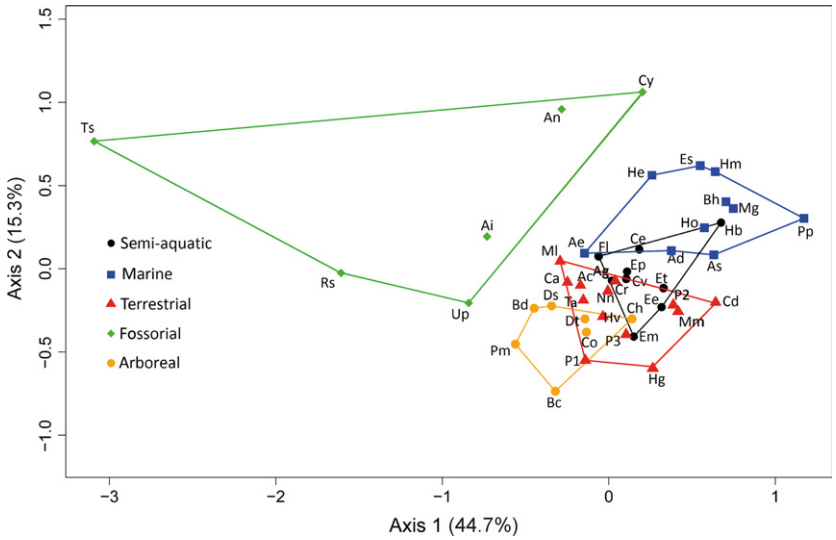

Fig. 10 Results of the PCAs performed on the snake brain endocast variables of the 45 specimens. Scatter plot illustrating the position of the different species on the first and second principal components and figuring the different ecologies. See Table 1 for name abbreviations.

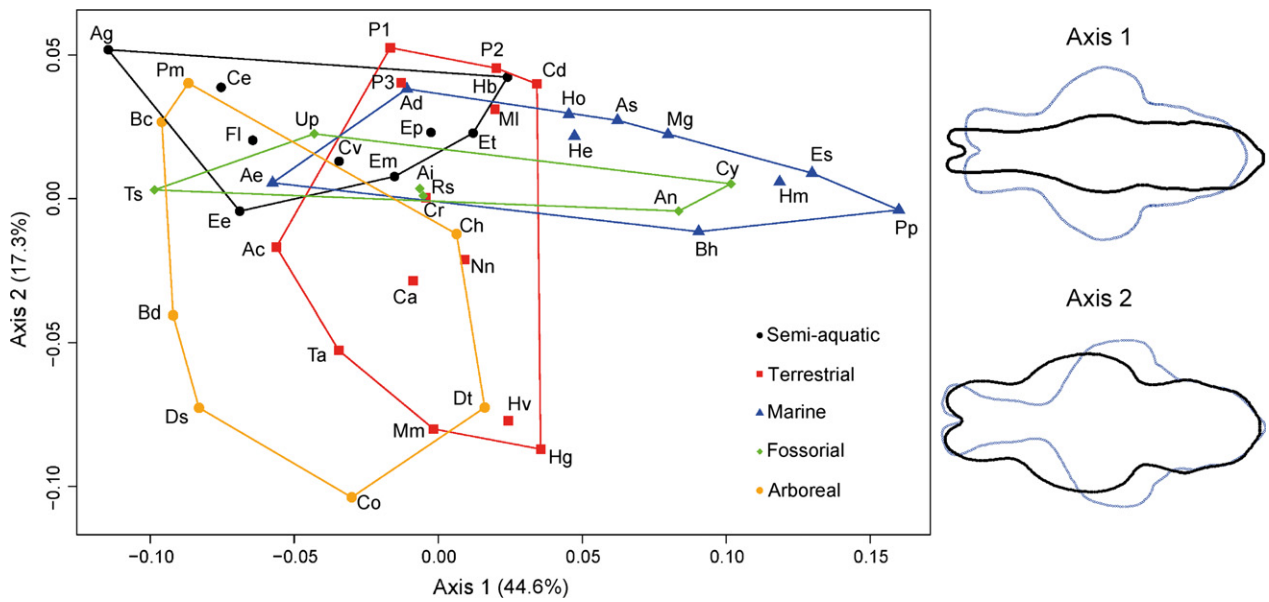

Fig. 11 Results of the PCAs performed on the snake brain endocast outline curves in ventral view. The blue and dark dotted lines indicate, respectively, the low and high values along the two axes. See Table 1 for name abbreviations.

developed ventrally. Brain endocasts of terrestrial and arboreal snakes differ from marine ones' by the great lateral extension of the cerebral hemispheres. Finally, it appears difficult to distinguish a common pattern for semi-aquatic snakes.

Within the same ecology, a great variability in brain endocast morphology can be observed. The results obtained from the outline curve analysis (Figs 11 and 12) provide some examples. The cerebral hemispheres of *A. duboisii* and *A. eydouxii* are wider than long and developed ventrally on their posterior part, whereas in the other marine taxa of our dataset, the cerebral hemispheres are as long as wide and only directed in the horizontal plane. The brain endocasts of *P. platurus* and *Candoia* sp. appear more flattened than those, respectively, found in other marine and terrestrial species. Finally, the morphology, the proportions and the orientation of the brain endocast of *R. schlegelii* appear very distinct from those found in other fossorial snakes. It appears difficult to interpret these differences. It has been demonstrated that constraints imposed by the environment (e.g. habitat) and activity pattern have an impact on snake head shape, irrespective of the phylogenetic relationships (Fabre et al. 2016; Segall et al. 2016). These ecological constraints affect the brain endocast morphology in snakes as well. However, it is difficult to determine with certainty which ecological parameters mostly

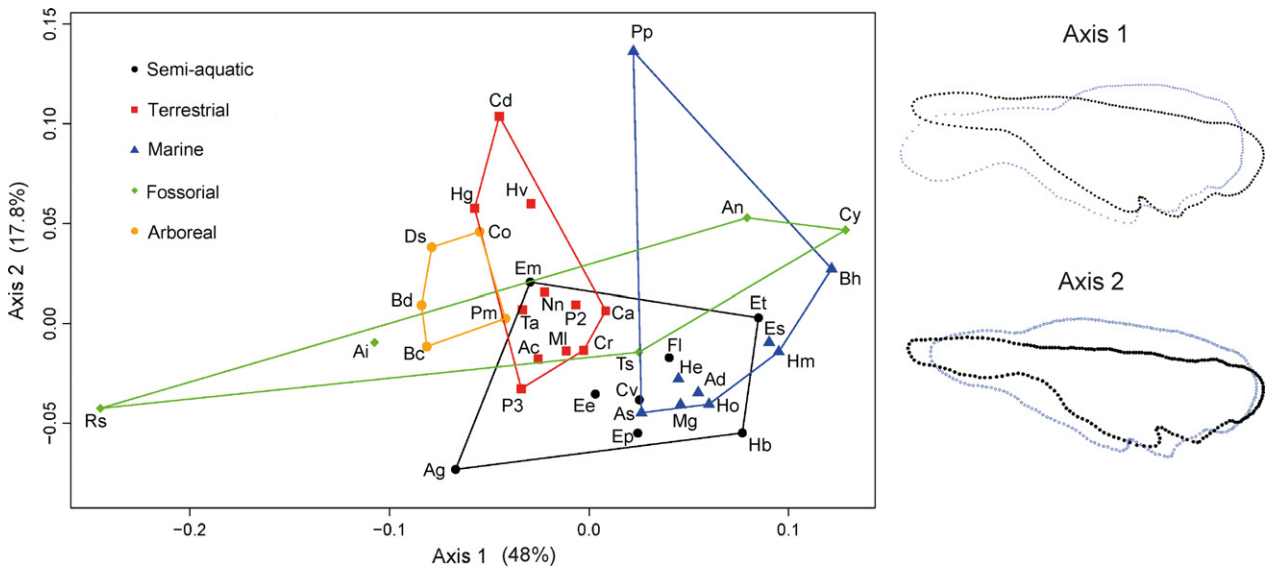

Fig. 12 Results of the PCAs performed on the snake brain endocast outline curves in lateral view. The blue and dark dotted lines indicate, respectively, the low and high values along the two axes. See Table 1 for name abbreviations.

affect the brain endocast morphology. The two marine species, *A. duboisii* and *A. eydouxii,* have a brain endocast quite different from other marine taxa. It is unclear if these differences are related to changes in their skull morphology due to the fish-egg dietary specialization (Sanders et al. 2012), or if the particular morphology of their cerebral hemispheres has a sensory meaning. Similarly, the flattened brain endocast of *P. platurus*, not found in any other marine specimen from our dataset, could be related to modifications in the skull morphology associated with its pelagic condition, only known in this species, or to its unique foraging strategy at the oceanic surface through labile features such as slicks or drift lines (Brischoux & Lillywhite, 2011). It will be interesting to decompose the ecology in different factors (e.g. locomotion, prey capture mode) to determine which parameters mostly influence the snake brain endocast morphology.

Sensory inferences

Studies in mammals and birds have shown that the endocast morphology, like the brain morphology, may give some information about species sensory abilities (Sakai et al. 2011a,b; Corfield et al. 2012, 2015; Carril et al. 2015). Several studies on snake brain have shown a link between structure and function (Kubie et al. 1978; Halpern & Frumin, 1979; Halpern & Kubie, 1980; Friedman & Crews, 1985; Krohmer & Crews, 1987; Crews et al. 1988; Miller & Gutzke, 1999; Wyneken, 2007; Krohmer et al. 2010), but the link between sensory abilities and brain endocasts has never been investigated in snakes. According to Starck (1979) and Nieuwenhuys et al. (1998), the brain of snakes could fill the majority of the endocranial space, and thus reflect the brain anatomy. If it is the case, brain endocasts could provide information about their sensory abilities. The relationships between the brain and the brain endocast are currently untested in snakes (Olori, 2010), and were not the goal of this study.

In snakes, the MOB is responsible for capturing smells at the level of the olfactory epithelium, and transmitting them to the olfactory bulb; the AOB is responsible for pheromone processing related to chemical social communication and prey capture (Bales, 2014). The MOB projects mainly to the lateral cortex and the AOB mainly to the *nucleus sphericus* (Lanuza & Halpern, 1997), two structures localized in the cerebral hemispheres. The MOB and AOB are involved in different behavioral activities, such as predation, mating and courtship (Bales, 2014). It is difficult to clearly identify the two structures and their limits from the brain endocast. However, morphological differences are perceived between the sampled taxa and they may imply differences in their sensory abilities. All snakes have a very developed vomeronasal system (Kubie & Halpern, 1979; Bales, 2014); however, in hydrophiinae sea snakes the MOBs are considered to be functionless and it seems that they use the AOB for smelling underwater (Schwenk, 2008; Shichida et al. 2013). Brain endocasts of hydrophiidae are indeed the only ones to show olfactory bulbs with a width increasing along the antero-posterior axis (e.g. *E. schistosa*; Fig. 5H), which could correspond to a reduced MOB and a more developed AOB.

The cerebral hemispheres of snakes are composed of different structures (e.g. cortex, nucleus sphericus, anterior ventricular ridge, amygdala), each being considered as a link between the sources of sensory information and the brain structures that control and modulate the behavior (Halpern, 1980; Bales, 2014). Different studies about the

lizard brain have shown that the medial dorsal cortices are relatively bigger in active foragers (Day et al. 1999a,b, 2001; Ladage et al. 2009). In snakes, males, which have a larger average territory than females, possess a significantly larger medial cortex than females (Roth et al. 2006). However, all these internal structures are not distinguishable on endocasts. Moreover, no comparative studies on snake brain endocasts have been performed to correlate size variation of these inner neural structures with endocast morphology. It is thus difficult to evaluate whether the different morphologies exhibited by the cerebral hemispheres of snakes involve differences in their sensory abilities.

The optic tectum in snakes is involved in the production of natural orienting movements in response to somatosensory, visual and auditory stimuli (Nieuwenhuys et al. 1998; Wyneken, 2007), and to signals from the infrared sensory system found in some snake families (Boidae, Pythonidae and Crotalinae; Goris, 2011). Several authors have shown that the size of the optic tectum is correlated to some behavioral traits and ecologies (Masai, 1973; Nieuwenhuys et al. 1998). For instance, diurnal species have a larger optic tectum than burrowing species. From snake endocasts, it actually appears that all fossorial species have a reduced optic tectum, (e.g. *C. ruffus*; Fig. 4C), contrary to terrestrial and arboreal taxa, which have a large optic tectum (e.g. *C. ornata*; Fig. 4G). According to Lillywhite (2014), vision is better developed in arboreal snakes, and poorly developed in burrowing species and some aquatic species living in turbid waters. It seems thus possible to connect the size of the optic tectum to the development of vision. According to Masai (1973), the optic tectum of diurnal snakes is, as a rule, larger than that of nocturnal ones. However, the correlation between large optic tectum and diurnal activity is not clear. Some exceptions exist: the endocast of *B. dendrophila* (Fig. 5B), a nocturnal snake (Rodda et al. 1999; Shivik et al. 2000), also shows a large optic tectum. There seems also to be no correlation between the occurrence of an infrared sensory system and the size of the optic tectum on endocasts. Specimens that have infrared organs (e.g. *C. atrox*; Fig. 7B) do not exhibit a larger optic tectum than specimens without infrared organs (e.g. *B. constrictor*; Fig. 7A). There is, however, one exception: *E. tentaculatum* (Fig. 6B–D), the only specimen that has an endocast with the dorsal margin of the optic tectum located more dorsally than the dorsal margin of the cerebral hemispheres. Such features can be correlated to the special nature of *E. tentaculatum*, which is the only snake presenting a pair of appendages that protrude from the face (Catania, 2011, 2012). The tentacles, useful to detect and locate preys, are innervated by trigeminal fibers to the optic tectum and could be responsible for its large size in *E. tentaculatum*.

Snake endocasts also show a great variability in the pituitary gland. This structure is generally considered to be structurally and functionally the most complex organ of the endocrine system (Harris & Donovan, 1966). Among vertebrates, the pituitary of snakes possesses some unique features: an asymmetrical structure flattened dorsoventrally and a pars tuberalis never developed (Schreibman, 1986). From the observation of brain endocasts only, a large variability is observed. However, it is not possible to determine whether this variability has a sensory significance. For example, brain endocasts of fossorial specimens have a clearly reduced pituitary gland but it is not clear whether this morphology is an adaptation reflecting the specialization of the skull due to fossorial activity (Rieppel, 1979; Rieppel & Zaher, 2000) or if this morphology has a sensory implication.

It is tempting to interpret the brain endocast variability in snakes through differences in sensory abilities between species; however, it is necessary to be very careful in the sensory inferences brought by an endocast study, which gives only an overview of the external morphology of the brain, and the complexity of the structure(s) must be taken into account.

Perspectives

The rapidly expanding interest in, and availability of, digital tomography data to visualize casts of the vertebrate endocranial cavity housing the brain (endocasts) represent new opportunities and challenges to the field of comparative neuroanatomy (Balanoff et al. 2015). In snakes, the brain endocast is still poorly known and the information associated with this structure remains untested. The different approaches used here have shown that snake brain endocasts contain both phylogenetic and ecological signals. However, the degree of influence of these two signals on the brain endocast morphology is difficult to interpret. It will be interesting to dissociate the variability due to each signal. Moreover, to fully understand the brain endocast structure and its variability among snakes, it appears necessary to decompose the ecology in different parameters (e.g. locomotion, prey capture mode) in order to test whether one is particularly associated to one brain endocast structure.

Beyond the methodological approaches that we used in this study, the resort to three-dimensional geometric morphometrics (3DGM) would be interesting to improve the amount of shape changes taken into consideration. However, the difficulty of finding homologous anatomical landmarks would impose the use of sliding semi-landmarks on surfaces (Gunz & Mitteroecker, 2013).

Cranial endocasts also represent a potentially large amount of unexplored phylogenetic data. Most morphological data for phylogenetic analyses of vertebrates come from the exterior shape of the skull (Gauthier et al. 2012). Internal cranial morphology is poorly represented in phylogenetic analyses because of the difficulty in visualizing and studying this anatomy. The advent of CT technology provides the potential to incorporate these new data into phylogenetic analyses.

Finally, in the context of the strong debate about the phylogenetic and ecological origin of snakes (Lee et al. 1999; Conrad, 2008; Hsiang et al. 2015; Martill et al. 2015; Reeder et al. 2015; Yi & Norell, 2015), endocranial studies might be of strong interest. Their application on crown snakes and lineages closely related to snakes (i.e. varanids, dibamids, mosasauroids) would provide major complementary information.

Conclusion

We used different methods to describe the brain endocast of snakes: descriptive characters, outline curve analysis, measurement series, and we observed a great variability in the brain endocast morphology of snakes. These methods provided different complementary information but all have shown that the shape of this structure contains, as in mammals and birds, a phylogenetic signal but also an ecological one. The different trends observed in the brain endocast morphology distinguish the different ecologies, notably fossorial and marine snakes. The great diversity observed in the brain endocast of snakes, even within the same ecology, appears difficult to interpret, and further analyses on the relation between brain endocast and ecological and sensory factors will be required. Biological inferences based on this structure should thus be made with caution and it is important to understand the complexity of this structure in order to avoid quick potentially wrong assumptions.

Acknowledgements

This work was supported by a grant from Agence Nationale de la Recherche under the LabEx ANR-10-LABX-0003-BCDiv, in the program 'Investissements d'avenir' n° ANR-11-IDEX-0004-02. The authors thank I. Ineich (MNHN, Paris, France), J. Rosado (MCZ, Harvard, USA), K. Lim (ZRC, National University of Singapore) and A. Herrel (MNHN, Paris, France) for the loan of specimens and already digitized snake data. The authors thank the Steinmann-Institut (Universität Bonn, Bonn, Germany), the UMS 2700 outils et méthodes de la systématique intégrative CNRS-MNHN and AST-RX, Plateau technique d'accès scientifique à la tomographie à rayons X du MNHN, and the ESRF (Grenoble, France; beamline ID17) and Paul Tafforeau for providing beamtime and support. The authors are also thankful to the 3D platform (UMR 7207, CR2P, MNHN) for giving access to the 3D imaging facilities. Finally, the authors want to thank both reviewers for helpful comments and suggestions.

Author contributions

Research conception and design: A. H., N. B., P. V. Data acquisition: A. H., R. A., R. B., G. D. Data analysis and interpretation: A. H., R. A., R.C., Z. B. Drafting of the manuscript: R. A. Critical revision of the manuscript: All authors.

Conflict of interest

The authors declare no conflict of interest.

References

Adams DC (2014) A generalized K statistic for estimating phylogenetic signal from shape and other high-dimensional multivariate data. *Syst Biol* **63**, 685–697.

Ahrens HE (2014) Morphometric study of phylogenetic and ecologic signals in Procyonid (Mammalia: Carnivora) endocasts: morphometrics of Procyonid endocasts. *Anat Rec (Hoboken)* **297**, 2318–2330.

Anderson CL, Kabalka GW, Layne DG, et al. (2000) Noninvasive high field MRI brain imaging of the Garter Snake (*Thamnophis sirtalis*). *Copeia* **2000**, 265–269.

Atobe Y, Nakano M, Kadota T, et al. (2004) Medullary efferent and afferent neurons of the facial nerve of the Pit Viper *Gloydius brevicaudus*. *J Comp Neurol* **472**, 345–357.

Aubret F, Bonnet X, Harris M, et al. (2005) Sex differences in body size and ectoparasite load in the ball python, *Python regius*. *J Herpetol* **39**, 315–320.

Aurboonyawat T, Pereira V, Kring T, et al. (2008) Patterns of the cranial venous system from the comparative anatomy in vertebrates: Part II. The lateral-ventral venous system. *Interv Neuroradiol* **14**, 21–31.

Balanoff AM, Bever GS, Colbert MW, et al. (2015) Best practices for digitally constructing endocranial casts: examples from birds and their dinosaurian relatives. *J Anat* **229**, 173–190.

Bales TB (2014) Proliferation, migration and survival of cells in the telencephalon of the ball python, *Python regius*. PhD Thesis, p. 131.

Bever GS, Bell CJ, Maisano JA (2005) The ossified braincase and cephalic osteoderms of *Shinisaurus crocodilurus* (Squamata, Shinisauridae). *Palaeontol Electronica* **8**, 1–36.

Bienvenu T, Guy F, Coudyzer W, et al. (2011) Assessing endocranial variations in great apes and humans using 3D data from virtual endocasts. *Am J Phys Anthropol* **145**, 231–246.

Blomberg SP, Garland T, Ives AR (2003) Testing for phylogenetic signal in comparative data: behavioral traits are more labile. *Evolution* **57**, 717–745.

Boistel R, Swoger J, Krzic U, et al. (2011a) The future of three-dimensional microscopic imaging in marine biology. *Mar Ecol* **32**, 438–452.

Boistel R, Herrel A, Lebrun R, et al. (2011b) Shake rattle and roll: the bony labyrinth and aerial descent in Squamates. *Integr Comp Biol* **51**, 957–968.

Bona P, Degrange FJ, Fernández MS (2013) Skull anatomy of the bizarre Crocodylian *Mourasuchus nativus* (Alligatoridae, Caimaninae): skull anatomy of *Mourasuchus nativus*. *Anat Rec (Hoboken)* **296**, 227–239.

Brischoux F, Lillywhite HB (2011) Light- and flotsam-dependent 'float-and-wait' foraging by pelagic sea snakes (*Pelamis platurus*). *Mar Biol* **158**, 2343–2347.

Butler AB, Hodos W (2005) *Comparative Vertebrate Neuroanatomy: Evolution and Adaptation*, p. 744, Hoboken, NJ: John Wiley .

Carril J, Tambussi CP, Degrange FJ, et al. (2015) Comparative brain morphology of Neotropical parrots (Aves, Psittaciformes) inferred from virtual 3D endocasts. *J Anat* **229**, 1–13.

Catania KC (2011) The brain and behavior of the tentacled snake. *Ann N Y Acad Sci* **1225**, 83–89.

Catania KC (2012) Tactile sensing in specialized predators – from behavior to the brain. *Curr Opin Neurobiol* **22**, 251–258.

Chapla ME, Nowacek DP, Rommel SA, et al. (2007) CT scans and 3D reconstructions of Florida manatee (*Trichechus*

manatus latirostris) heads and ear bones. *Hear Res* **228**, 123–135.

Christensen CB, Christensen-Dalsgaard J, Brandt C, et al. (2012) Hearing with an atympanic ear: good vibration and poor sound-pressure detection in the royal python, *Python regius*. *J Exp Biol* **215**, 331–342.

Comeaux RS, Olori JC, Bell CJ (2010) Cranial osteology and preliminary phylogenetic assessment of *Plectrurus aureus* Beddome, 1880 (Squamata: Serpentes: Uropeltidae). *Zool J Linn Soc* **160**, 118–138.

Conrad JL (2008) Phylogeny and systematics of Squamata (Reptilia) based on morphology. *Bull Am Mus Nat Hist* **310**, 1–182.

Corfield JR, Wild JM, Parsons S, et al. (2012) Morphometric analysis of telencephalic structure in a variety of Neognath and Paleognath bird species reveals regional differences associated with specific behavioral traits. *Brain Behav Evol* **80**, 181–195.

Corfield JR, Price K, Iwaniuk A, et al. (2015) Diversity in olfactory bulb size in birds reflects allometry, ecology and phylogeny. *Front Neuroanat* **9**, 1–16. https://doi.org/10.3389/fnana.2015.00102.

Crews D, Hingorani V, Nelson RJ (1988) Role of the pineal gland in the control of annual reproductive behavioral and physiological cycles in the Red-Sided Garter Snake (*Thamnophis sirtalis parietalis*). *J Biol Rhythms* **3**, 293–302.

Danilo L, Remy J, Vianey-Liaud M, et al. (2015) Intraspecific variation of endocranial structures in extant Equus: a prelude to endocranial studies in fossil Equoids. *J Mamm Evol* **22**, 561–582.

Day LB, Crews D, Wilczynski W (1999a) Relative medial and dorsal cortex volume in relation to foraging strategy in congeneric lizards. *Brain Behav Evol* **54**, 314–322.

Day LB, Crews D, Wilczynski W (1999b) Spatial and reversal learning in congeneric lizards with different foraging strategies. *Anim Behav* **57**, 395–407.

Day LB, Crews D, Wilczynski W (2001) Effects of medial and dorsal cortex lesions on spatial memory in lizards. *Behav Brain Res* **118**, 27–42.

Ekdale EG (2010) Ontogenetic variation in the bony labyrinth of *Monodelphis domestica* (Mammalia: Marsupialia) following ossification of the inner ear cavities. *Anat Rec (Hoboken)* **293**, 1896–1912.

Ekdale EG (2011) Morphological variation in the ear region of pleistocene elephantimorpha (Mammalia, Proboscidea) from central Texas. *J Morphol* **272**, 452–464.

Ekdale EG (2013) Comparative anatomy of the bony labyrinth (inner ear) of placental mammals. *PLoS One* **8**, e66624.

Fabre A-C, Bickford D, Segall M, et al. (2016) The impact of diet, habitat use, and behaviour on head shape evolution in homalopsid snakes. *Biol J Lin Soc* **118**, 634–647.

Friedman D, Crews D (1985) Role of the anterior hypothalamus–preoptic area in the regulation of courtship behavior in the male Canadian red-sided garter snake (*Thamnophis sirtalis parietalis*): lesion experiments. *Behav Neurosci* **99**, 942–949.

Gauthier JA, Kearney M, Maisano JA, et al. (2012) Assembling the squamate tree of life: perspectives from the phenotype and the fossil record. *Bull Peabody Mus Nat Hist* **53**, 3–308.

George ID, Holliday CM (2013) Trigeminal nerve morphology in *Alligator mississippiensis* and its significance for Crocodyliform facial sensation and evolution. *Anat Rec (Hoboken)* **296**, 670–680.

Georgi JA, Sipla J (2008) Comparative and functional anatomy of balance in aquatic reptiles and birds. In: *Sensory Evolution on the Threshold: Adaptations in Secondarily Aquatic Vertebrates*. (eds Thewissen JMG, Numella S), pp. 233–256. Berkeley: University of California Press.

Gonzales LA, Benefit BR, McCrossin ML, et al. (2015) Cerebral complexity preceded enlarged brain size and reduced olfactory bulbs in Old World monkeys. *Nat Commun* **6**, 1–9.

Goris RC (2011) Infrared organs of snakes: an integral part of vision. *J Herpetol* **45**, 2–14.

Greene HW, Fogden M, Fogden P (2000) *Snakes: The Evolution of Mystery in Nature*, p. 365. Berkeley: University of California Press.

Gunz P, Mitteroecker P (2013) Semilandmarks: a method for quantifying curves and surfaces. *Hystrix* **24**, 103–109.

Halpern M (1980) The telencephalon of snakes. In: *Comparative Neurology of the Telencephalon*. (ed. Ebbesson SOE), pp. 257–295. Plenum Press, New York: Springer US.

Halpern M, Frumin N (1979) Roles of the vomeronasal and olfactory system in prey attack and feeding garter snakes. *Physiol Behav* **22**, 1183–1189.

Halpern M, Kubie JL (1980) Chemical access to the vomeronasal organs of Garter snakes. *Physiol Behav* **24**, 367–371.

Harris GW, Donovan BT (1966) *The Pituitary Gland: Anterior Pituitary*, pp. 444–459. New York: University of California Press.

Heatwole H (1999) *Sea Snakes*, p. 148. Malabar, Florida: Krieger.

Hoogland PV (1982) Brainstem afferents to the thalamus in a lizard, *Varanus exanthematicus*. *J Comp Neurol* **210**, 152–162.

Hopson JA (1979) Paleoneurology. In: *Biology of the Reptilia (Neurology A)*. (eds Gans C, Northcutt RG, Ulinski P), Vol. **9**, pp. 39–146. New York, NY: Academic Press.

Houssaye A, Boistel R, Böhme W, et al. (2013) Jack-of-all-trades master of all? Snake vertebrae have a generalist inner organization. *Naturwissenschaften* **100**, 997–1006.

Hsiang AY, Field DJ, Webster TH, et al. (2015) The origin of snakes: revealing the ecology, behavior, and evolutionary history of early snakes using genomics, phenomics, and the fossil record. *BMC Evol Biol* **15**, 1–22.

Hurlburt GR, Ridgely RC, Witmer LM (2013) Relative size of brain and cerebrum in tyrannosaurid dinosaurs: an analysis using brain-endocast quantitative relationships in extant alligators. In: *Tyrannosaurid Paleobiology*. (eds Parrish JM, Molnar RE, Currie PJ, Koppelhus EB), pp. 1–21. Bloomington: Indiana University Press.

Jerison H (1973) *Evolution of the Brain and Intelligence*, p. 482. New York, NY: Academic Press.

Kawabe S, Shimokawa T, Miki H, et al. (2013) Variation in avian brain shape: relationship with size and orbital shape. *J Anat* **223**, 495–508.

Kawabe S, Matsuda S, Tsunekawa N, et al. (2015) Ontogenetic shape change in the chicken brain: implications for paleontology. *PLoS One* **10**, e0129939.

Kim R, Evans D (2014) Relationships among brain, endocranial cavity, and body sizes in reptiles. *Society of Vertebrate Paleontology 74th Annual Meeting*, Berlin, Germany.

Krohmer RW, Crews D (1987) Temperature activation of courtship behavior in the male red-sided garter snake (*Thamnophis sirtalis parietalis*): role of the anterior hypothalamus-preoptic area. *Behav Neurosci* **101**, 228–236.

Krohmer RW, Boyle MH, Lutterschmidt DI, et al. (2010) Seasonal aromatase activity in the brain of the male red-sided garter snake. *Horm Behav* **58**, 485–492.

Kubie JL, Halpern M (1979) Chemical senses involved in Garter snake prey trailing. *J Comp Physiol Psychol* **93**, 648–667.

Kubie JL, Vagvolgyi A, Halpern M (1978) Roles of the vomeronasal and olfactory systems in courtship behavior of male garter snakes. *J Comp Physiol Psychol* **92**, 627–641.

Ladage LD, Riggs BJ, Sinervo B, et al. (2009) Dorsal cortex volume in male side-blotched lizards (*Uta stansburiana*) is associated with different space use strategies. *Anim Behav* **78**, 91–96.

Lanuza E, Halpern M (1997) Afferent and efferent connections of the nucleus sphericus in the snake *Thamnophis sirtalis*: convergence of olfactory and vomeronasal information in the lateral cortex and the amygdala. *J Comp Neurol* **385**, 627–640.

Lee MS, Scanlon JD (2002) Snake phylogeny based on osteology, soft anatomy and ecology. *Biol Rev* **77**, 333–401.

Lee MS, Bell GL Jr, Caldwell MW (1999) The origin of snake feeding. *Nature* **400**, 655–659.

Lefebvre L, Reader SM, Sol D (2004) Brains, innovations and evolution in birds and primates. *Brain Behav Evol* **63**, 233–246.

Lillywhite HB (2014) *How Snakes Work: Structure, Function, and Behavior of the World's Snakes*, p. 256. Oxford, UK: Oxford University Press.

Lyras GA, Van Der Geer AAE (2003) External brain anatomy in relation to the phylogeny of Caninae (Carnivora: Canidae). *Zool J Linn Soc* **138**, 505–522.

Macrini TE, Rowe T, VandeBerg JL (2007) Cranial endocasts from a growth series of *Monodelphis domestica* (Didelphidae, Marsupialia): a study of individual and ontogenetic variation. *J Morphol* **268**, 844–865.

Martill DM, Tischlinger H, Longrich NR (2015) A four-legged snake from the early cretaceous of Gondwana. *Science* **349**, 416–419.

Martinez-Garcia F, Olucha FE, Teruel V, et al. (1991) Afferent and efferent connections of the olfactory bulbs in the lizard *Podarcis hispanica*. *J Comp Neurol* **305**, 337–347.

Masai H (1973) Structural patterns of the optic tectum in Japanese snakes of the family Colubridae in relation to habit. *J Hirnforsch* **14**, 367–374.

Miller LR, Gutzke WHN (1999) The role of the vomeronasal organ of crotalines (Reptilia: Serpentes: Viperidae) in predator detection. *Anim Behav* **58**, 53–57.

Mosimann JE, James FC (1979) New statistical methods for allometry with application to Florida red-winged blackbirds. *Evolution* **33**, 444–459.

Nieuwenhuys R, ten Donkelaar HJ, Nicholson C (1998) *The Central Nervous System of Vertebrates*, p. 2214. Berlin: Springer.

Northcutt RG (2002) Understanding vertebrate brain evolution. *Integr Comp Biol* **42**, 743–756.

Olori JC (2010) Digital endocasts of the cranial cavity and osseous labyrinth of the burrowing snake *Uropeltis woodmasoni* (Alethinophidia: Uropeltidae). *Copeia* **2010**, 14–26.

Porter WR, Witmer LM (2015) Vascular patterns in Iguanas and other squamates: blood vessels and sites of thermal exchange. *PLoS One* **10**, e0139215.

Powell BJ, Leal M (2014) Brain organization and habitat complexity in Anolis lizards. *Brain Behav Evol* **84**, 8–18.

Pyron RA, Burbrink FT, Colli GR, et al. (2011) The phylogeny of advanced snakes (Colubroidea), with discovery of a new subfamily and comparison of support methods for likelihood trees. *Mol Phylogenet Evol* **58**, 329–342.

R Development Core Team (2008) *R: a Language and Environment for Statistical Computing*. Vienna, Austria: R Foundation for Statistical Computing. ISBN 3-900051-07-0, http://www.R-project.org.

Racicot RA, Colbert MW (2013) Morphology and variation in porpoise (Cetacea: Phocoenidae) cranial endocasts. *Anat Rec (Hoboken)* **296**, 979–992.

Reeder TW, Townsend TM, Mulcahy DG, et al. (2015) Integrated analyses resolve conflicts over squamate reptile phylogeny and reveal unexpected placements for fossil taxa. *PLoS One* **10**, e0118199.

Reperant J, Rio J-P, Ward R, et al. (1992) Comparative analysis of the primary visual system of reptiles. In: *Sensory Integration. Biology of Reptilia, (Neurology C)*. (eds Gans C, Ulinski PS), Vol. **17**, pp. 175–240. Chicago and London: The University of Chicago Press.

Rieppel O (1979) The braincase of Typhlops and Leptotyphlops (Reptilia: Serpentes). *Zool J Linn Soc* **65**, 161–176.

Rieppel O, Maisano JA (2007) The skull of the rare Malaysian snake *Anomochilus leonardi* Smith, based on high-resolution X-ray computed tomography. *Zool J Linn Soc* **149**, 671–685.

Rieppel O, Zaher H (2000) The braincases of mosasaurs and Varanus, and the relationships of snakes. *Zool J Linn Soc* **129**, 489–514.

Rodda GH, Fritts TH, McCoid MJ, et al. (1999) An overview of the biology of the brown treesnake (*Boiga irregularis*), a costly introduced pest on Pacific Islands. In: *Problem Snake Management: the Habu and the Brown Treesnake*. (eds Rodda GH, Sawai Y, Chiszar D, Tanaka H), p. 534. Ithaca, NY: Cornell University Press.

Rohlf FJ, Slice D (1990) Extensions of the Procrustes method for the optimal superimposition of landmarks. *Syst Biol* **39**, 40–59.

Roth ED, Lutterschmidt WI, Wilson DA (2006) Relative medial and dorsal cortex volume in relation to sex differences in spatial ecology of a snake population. *Brain Behav Evol* **67**, 103–110.

Rowe T, Brochu CA, Colbert M, et al. (1999) Introduction to alligator: digital atlas of the skull. *J Vertebr Paleontol* **19**, 1–8.

Sakai ST, Arsznov BM, Lundrigan BL, et al. (2011a) Brain size and social complexity: a computed tomography study in Hyaenidae. *Brain Behav Evol* **77**, 91–104.

Sakai ST, Arsznov BM, Lundrigan BL, et al. (2011b) Virtual endocasts: an application of computed tomography in the study of brain variation among hyenas: Hyena endocasts. *Ann N Y Acad Sci* **1225**, 160–170.

Sanders KL, Rasmussen AR, Elmberg J, et al. (2012) *Aipysurus mosaicus*, a new species of egg-eating sea snake (Elapidae: Hydrophiinae), with a redescription of *Aipysurus eydouxii* (Gray, 1849). *Zootaxa* **3431**, 1–18.

Schreibman MP (1986) The pituitary gland. In: *Vertebrate Endocrinology: Fundamentals and Biomedical Implications*, Vol. I. (eds Pang PKT, Schreibman MP), pp. 11–55. New York, NY: Academic Press.

Schwenk K (2008) Comparative anatomy and physiology of chemical senses in nonavian aquatic reptiles. In: *Sensory Evolution on the Threshold: Adaptations in Secondarily Aquatic Vertebrates*. (eds Thewissen JGM, Nummela S), pp. 65–81. California: University of California Press.

Segall M, Cornette R, Fabre A-C, et al. (2016) Does aquatic foraging impact head shape evolution in snakes? *Proc R Soc B* **283**, 1–7.

Senn DG (1966) Uber das optische System im Gehirn squamater Reptilien. Eine vergleichend-morphologische Untersuchung, unter besonderer Berücksichtigung einiger Wühlschlangen. *Acta Anat Suppl* **52**, 1–87.

Senn DG, Northcutt RG (1973) The forebrain and midbrain of some squamates and their bearing on the origin of snakes. *J Morphol* **140**, 135–152.

Shichida Y, Yamashita T, Imai H, et al. (2013) *Evolution and Senses: Opsins, Bitter Taste, and Olfaction*, p. 46. Berlin, Germany: Springer.

Shivik JA, Wright WG, Clark L (2000) Seasonal variability in brown tree snake (*Boiga irregularis*) response to lures. *Can J Zool* **78**, 79–84.

Smeets WJA, Hoogland PV, Lohman AH (1986) A forebrain atlas of the lizard Gekko gecko. *J Comp Neurol* **254**, 1–19.

Smith NA, Clarke JA (2012) Endocranial anatomy of the charadriiformes: sensory system variation and the evolution of wing-propelled diving. *PLoS One* **7**, e49584.

Souza NM, Maggs DJ, Park SA, et al. (2015) Gross, histologic, and micro-computed tomographic anatomy of the lacrimal system of snakes. *Vet Ophthalmol* **18**, 15–22.

Starck D (1979) Cranio-cerebral relations in recent reptiles. In: *Biology of the Reptilia (Neurology A)*. (eds Gans C, Northcutt RG, Ulinski P), p. 462. London: Academic Press.

Walsh SA, Knoll MA (2011) Directions in palaeoneurology. *Palaeontol Assoc* **86**, 263–279.

Walsh SA, Milner A (2011) Evolution of the avian brain and senses. In: *Living Dinosaurs: the Evolutionary History of Modern Birds*, 1st edn. (eds Dyke G, Kaiser G), pp. 282–305. Chichester, UK: John Wiley & Sons Ltd.

Walsh SA, Barrett PM, Milner AC, et al. (2009) Inner ear anatomy is a proxy for deducing auditory capability and behaviour in reptiles and birds. *Proc R Soc B Biol Sci* **276**, 1355–1360.

Willis KL, Christensen-Dalsgaard J, Ketten DR, et al. (2013) Middle ear cavity morphology is consistent with an aquatic origin for testudines. *PLoS One* **8**, e54086.

Witmer LM, Ridgely RC, Dufeau DL, et al. (2008) Using CT to peer into the past: 3D visualization of the brain and ear regions of birds, crocodiles, and nonavian dinosaurs. In: *Anatomical Imaging: Towards a New Morphology*. (eds Frey R, Endo H), pp. 67–87. Tokyo: Springer.

Wyneken J (2007) Reptilian neurology: anatomy and function. *Vet Clin North Am Exot Anim Pract* **10**, 837–853.

Yi H, Norell MA (2015) The burrowing origin of modern snakes. *Sci Adv* **1**, e1500743.

Zelditch ML, Swiderski DL, Sheets HD, et al. (2004) *Geometric Morphometrics for Biologists: a Primer*, p. 443. New York and London: Academic Press.

Supporting Information

Additional Supporting Information may be found in the online version of this article:

Appendix S1. Table of measurements taken on snake endocasts.

Appendix S2. Table of measurements taken on the three *Python regius* specimens.

Appendix S3. List of characters and matrix used for the PCoA.

Appendix S4. Distribution of the variables in the PCAs performed on the 45 snake specimens.

ABSTRACT

As windows into the deep history of neuroanatomy, endocasts may provide information about the central nervous system of fossil taxa. Based on exceptionally preserved specimens of coeval mosasauroids (Squamata) and plesiosaurians (Sauropterygia), from the Turonian outcrops of Goulmima (Southern Morocco), the aim of this work was to describe for the first time in detail the endocranial anatomy of these two major clades of Mesozoic marine reptiles to provide insights about their sensory abilities, and thus to understand their cohabitation, interactions and niche partitioning. The endocranial anatomy of related extant squamates, mainly snakes but also varanids and amphisbaenians, also almost unknown until now, has been performed for the first time and used for comparative purpose to analyze the form-function relationships associated to endocasts. The analysis of the endocranial variability in extant squamates pointed out that endocasts reflect both phylogenetic and ecological signals, and that the relative size of each endocranial structure can be used to reveal differences in vision and olfaction according to taxa. Among fossil taxa, computed tomography was used to reconstruct in detail the cranial morphology of three unpublished specimens of Plesiosauria. These specimens have been examined and described, two have been referred to the elasmosaurid *Libonectes morgani* and the third one is an indeterminate polycotylid. The 3D morphology of the endocast has been reconstructed for these plesiosaurian specimens and the basal mosasauroid *Tethysaurus nopcsai*. The results show that the endocranial morphology of Plesiosauria differs from that know in other extinct and extant vertebrates. Based on the relative size of the structures composing their endocasts, both the mosasauroid *Tethysaurus* and the plesiosaurians seem to rely more on vision than on olfaction to interact with their environment. However, these new endocast data, added to information already available in the literature suggest different modes of locomotion and hunting techniques, which probably allowed them to coexist in Goulmima as quaternary consumers.

Key words: endocast, mosasauroid, plesiosaurians, Goulmima, sensory abilities, paleoecology.

RÉSUMÉ

En reflétant une image plus ou moins fidèle du cerveau, l'endocrâne permet d'accéder au système nerveux des espèces fossiles. A partir de spécimens exceptionnellement préservés de mosasaures (Squamata) et de plésiosaures (Sauropterygia), provenant des affleurements turoniens de Goulmima (sud du Maroc), ce travail a pour but de décrire, pour la première fois en détail l'anatomie endocrânienne de ces deux grands clades de reptiles marins du Mésozoïque. Cette étude a pour but d'inférer leurs capacités sensorielles permettant de comprendre leur cohabitation, leurs interactions et leur position au sein du réseau trophique. L'anatomie endocrânienne des squamates actuels, principalement des serpents mais aussi des varans et des amphisbènes, presque inconnus jusqu'à présent, a également été étudiée à des fins comparatives afin d'analyser les relations forme-fonction associées aux endocrânes. La variabilité morphologique de l'endocrâne chez les squamates actuel démontre un signal phylogénétique mais également écologique. De plus, la taille relative de chaque structure endocrânienne révèle des différences de vision et d'olfaction selon les espèces. Parmi les taxons fossiles, la microtomographie a été utilisée pour reconstituer en détail la morphologie crânienne de trois nouveaux spécimens de plésiosaures. Deux de ces spécimens ont été assigné à l'élasmosaure *Libonectes morgani* et le troisième à un polycotylidé indéterminé. La morphologie 3D de l'endocrâne a été reconstruite pour ces spécimens ainsi que pour le mosasaure basal *Tethysaurus nopcsai*. La morphologie endocrânienne des plésiosaures diffère de celles retrouvées chez les vertébrés éteints et actuels. En se basant sur la taille relative des structures composant leurs endocrânes, le mosasaure *Tethysaurus* et les plésiosaures semblent davantage utiliser la vision que l'olfaction pour interagir avec leur environnement. Ces nouvelles données endocrâniennes, ajoutées aux informations déjà disponibles dans la littérature, suggèrent différents modes de locomotion et techniques de chasse, ce qui leur a probablement permis de coexister à Goulmima en tant que prédateur.

Mots clés : endocrâne, mosasaure, plésiosaure, Goulmima, capacités sensorielles, paléoécologie.